EVOLUTION AND COMPARATIVE IMMUNOLOGY OF IMMUNE SYSTEMS IN MARINE ORGANISMS

EDITED BY: Gyri T. Haugland, Sissel Jentoft and Monica Hongroe Solbakken
PUBLISHED IN: Frontiers in Immunology

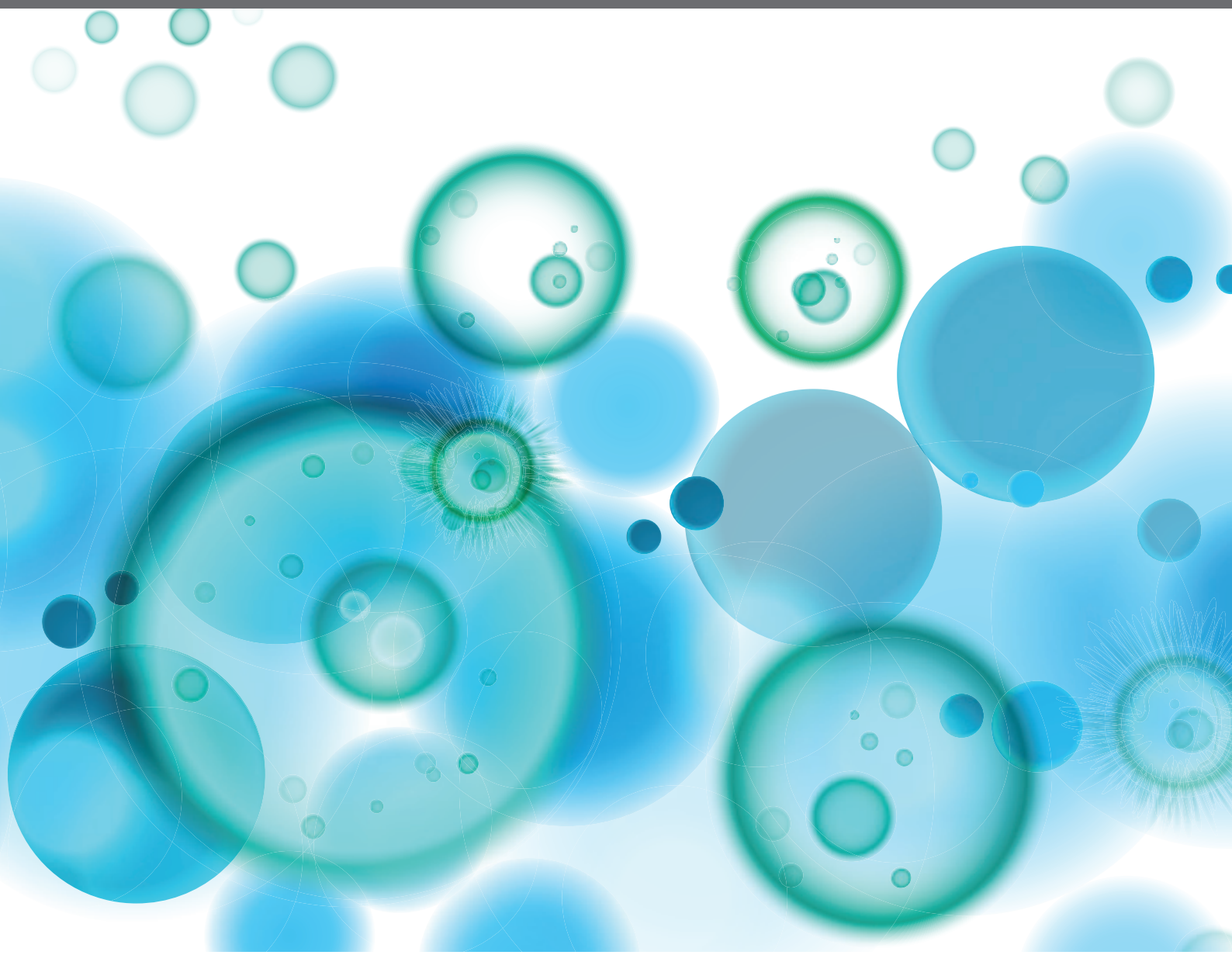

frontiers Research Topics

frontiers

Frontiers eBook Copyright Statement

The copyright in the text of individual articles in this eBook is the property of their respective authors or their respective institutions or funders. The copyright in graphics and images within each article may be subject to copyright of other parties. In both cases this is subject to a license granted to Frontiers.

The compilation of articles constituting this eBook is the property of Frontiers.

Each article within this eBook, and the eBook itself, are published under the most recent version of the Creative Commons CC-BY licence. The version current at the date of publication of this eBook is CC-BY 4.0. If the CC-BY licence is updated, the licence granted by Frontiers is automatically updated to the new version.

When exercising any right under the CC-BY licence, Frontiers must be attributed as the original publisher of the article or eBook, as applicable.

Authors have the responsibility of ensuring that any graphics or other materials which are the property of others may be included in the CC-BY licence, but this should be checked before relying on the CC-BY licence to reproduce those materials. Any copyright notices relating to those materials must be complied with.

Copyright and source acknowledgement notices may not be removed and must be displayed in any copy, derivative work or partial copy which includes the elements in question.

All copyright, and all rights therein, are protected by national and international copyright laws. The above represents a summary only. For further information please read Frontiers' Conditions for Website Use and Copyright Statement, and the applicable CC-BY licence.

ISSN 1664-8714
ISBN 978-2-88974-387-2
DOI 10.3389/978-2-88974-387-2

About Frontiers

Frontiers is more than just an open-access publisher of scholarly articles: it is a pioneering approach to the world of academia, radically improving the way scholarly research is managed. The grand vision of Frontiers is a world where all people have an equal opportunity to seek, share and generate knowledge. Frontiers provides immediate and permanent online open access to all its publications, but this alone is not enough to realize our grand goals.

Frontiers Journal Series

The Frontiers Journal Series is a multi-tier and interdisciplinary set of open-access, online journals, promising a paradigm shift from the current review, selection and dissemination processes in academic publishing. All Frontiers journals are driven by researchers for researchers; therefore, they constitute a service to the scholarly community. At the same time, the Frontiers Journal Series operates on a revolutionary invention, the tiered publishing system, initially addressing specific communities of scholars, and gradually climbing up to broader public understanding, thus serving the interests of the lay society, too.

Dedication to Quality

Each Frontiers article is a landmark of the highest quality, thanks to genuinely collaborative interactions between authors and review editors, who include some of the world's best academicians. Research must be certified by peers before entering a stream of knowledge that may eventually reach the public - and shape society; therefore, Frontiers only applies the most rigorous and unbiased reviews.
Frontiers revolutionizes research publishing by freely delivering the most outstanding research, evaluated with no bias from both the academic and social point of view. By applying the most advanced information technologies, Frontiers is catapulting scholarly publishing into a new generation.

What are Frontiers Research Topics?

Frontiers Research Topics are very popular trademarks of the Frontiers Journals Series: they are collections of at least ten articles, all centered on a particular subject. With their unique mix of varied contributions from Original Research to Review Articles, Frontiers Research Topics unify the most influential researchers, the latest key findings and historical advances in a hot research area! Find out more on how to host your own Frontiers Research Topic or contribute to one as an author by contacting the Frontiers Editorial Office: frontiersin.org/about/contact

EVOLUTION AND COMPARATIVE IMMUNOLOGY OF IMMUNE SYSTEMS IN MARINE ORGANISMS

Topic Editors:
Gyri T. Haugland, University of Bergen, Norway
Sissel Jentoft, University of Oslo, Norway
Monica Hongroe Solbakken, University of Oslo, Norway

Citation: Haugland, G. T., Jentoft, S., Solbakken, M. H., eds. (2022). Evolution and Comparative Immunology of Immune Systems in Marine Organisms. Lausanne: Frontiers Media SA. doi: 10.3389/978-2-88974-387-2

Table of Contents

frontiers in Immunology

ORIGINAL RESEARCH
published: 30 April 2020
doi: 10.3389/fimmu.2020.00711

A Possible Role of Crustacean Cardioactive Peptide in Regulating Immune Response in Hepatopancreas of Mud Crab

Yujie Wei[1], *Dongdong Lin*[1], *Zhanning Xu*[1], *Xiaoman Gao*[1], *Chaoshu Zeng*[2] *and Haihui Ye*[1]*

[1] College of Ocean and Earth Sciences, Xiamen University, Xiamen, China, [2] College of Science and Engineering, James Cook University, Townsville, QLD, Australia

Crustacean cardioactive peptide (CCAP), a cyclic amidated non-apeptide, is widely found in arthropods. The functions of CCAP have been revealed to include regulation of heart rate, intestinal peristalsis, molting, and osmotic pressure. However, to date, there has not been any report on the possible involvement of CCAP in immunoregulation in crustaceans. In this study, a CCAP precursor (designated as *Sp*-CCAP) was identified in the commercially important mud crab *Scylla paramamosain*, which could be processed into four CCAP-associated peptides and one mature peptide (PFCNAFTGC-NH_2). Bioinformatics analysis indicated that *Sp*-CCAP was highly conserved in crustaceans. RT-PCR results revealed that *Sp-CCAP* was expressed in nerve tissues and gonads, whereas the *Sp*-CCAP receptor gene (*Sp-CCAPR*) was expressed in 12 tissues of *S. paramamosain*, including hepatopancreas. *In situ* hybridization further showed that an *Sp-CCAPR*-positive signal is mainly localized in the F-cells of hepatopancreas. Moreover, the mRNA expression level of *Sp-CCAPR* in the hepatopancreas was significantly up-regulated after lipopolysaccharide (LPS) or polyriboinosinic polyribocytidylic acid [Poly (I:C)] challenge. Meanwhile, the mRNA expression level of *Sp-CCAPR*, nuclear transcription factor NF-κB homologs (*Sp-Dorsal* and *Sp-Relish*), member of mitogen-activated protein kinase (MAPK) signaling pathway (*Sp-P38*), pro-inflammatory cytokines factor (*Sp-TNFSF* and *Sp-IL16*), and antimicrobial peptide (*Sp-Lysozyme*, *Sp-ALF*, *Sp-ALF4*, and *Sp-ALF5*) in the hepatopancreas were all up-regulated after the administration of synthetic *Sp*-CCAP mature peptide both *in vivo* and *in vitro*. The addition of synthetic *Sp*-CCAP mature peptide *in vitro* also led to an increase in nitric oxide (NO) concentration and an improved bacterial clearance ability in the hepatopancreas culture medium. The present study suggested that *Sp*-CCAP signaling system might be involved in the immune responses of *S. paramamosain* by activating immune molecules on the hepatopancreas. Collectively, our findings shed new light on neuroendocrine-immune regulatory system in arthropods and could potentially provide a new strategy for disease prevention and control for mud crab aquaculture.

Keywords: neuropeptide, crustacean cardioactive peptide, hepatopancreas, immunoregulation, arthropod

OPEN ACCESS

Edited by:
Gyri T. Haugland, University of Bergen, Norway

Reviewed by:
Ngoc Tuan Tran, Shantou University, China
Yueling Zhang, Shantou University, China

***Correspondence:**
Haihui Ye
haihuiye@xmu.edu.cn

Specialty section:
This article was submitted to Comparative Immunology, a section of the journal Frontiers in Immunology

Received: *15 January 2020*
Accepted: *30 March 2020*
Published: *30 April 2020*

Citation:
Wei Y, Lin D, Xu Z, Gao X, Zeng C and Ye H (2020) A Possible Role of Crustacean Cardioactive Peptide in Regulating Immune Response in Hepatopancreas of Mud Crab. Front. Immunol. 11:711. doi: 10.3389/fimmu.2020.00711

INTRODUCTION

The neuroendocrine-immune (NEI) regulatory system refers to a complex network formed by the interaction of the nervous system, endocrine system, and immune system (1). The nervous and endocrine systems regulate various physiological processes by releasing neuropeptides, neurotransmitters, and hormones (2). The neuropeptides are usually synthesized and secreted by neurons or neuroendocrine cells and composed of 3–100 amino acid residues (3). As an extracellular chemical messenger, neuropeptides regulate a range of physiological functions, including immunity, growth, reproduction, metabolism, food intake, and circadian rhythm, by activating specific receptors (3). Neuropeptide receptors are mostly G protein-coupled receptors (GPCRs), which constitute the largest family of cell surface receptors. They play a vital role in physiological processes by promoting cellular communication *via* recognizing various ligands, including bioactive peptides, nucleosides, and amines (4).

A large number of studies have shown that neuropeptides also interact with the immune system by binding to receptors of immune cells (5–14). For example, it has been reported that in humans, through binding to their respective receptors, vasoactive intestinal peptide (VIP), pituitary adenylate cyclase-activating polypeptide (PACAP), urocortin 1 (UCN), and adrenomedullin (AM) reduced the production of pro-inflammatory factors (5–7). In rainbow trout *Oncorhynchus mykiss*, prolactin has been shown to increase mRNA expression of *MyD88* and *IL-1β* during *in vitro* infection with the pathogen, *Piscirickettsia salmonis* (8), whereas in Japanese pufferfish *Takifugu rubripes*, neuromedin U elevated the mRNA expression of *IL-6*, *IL-18*, and *TNF-α* in peripheral blood leukocytes (9). Similarly, in invertebrates, FMRFamide reportedly regulated the expression of immune effectors and apoptosis-related genes *via* P38 mitogen-activated protein kinase (MAPK) signaling pathway in oyster *Crassostrea gigas* (10). In fruit fly *Drosophila*, allatostatin-C receptor 2 (ASTC-R2) played a crucial role in host survival when infected by the pathogenic bacterium *Photorhabdus luminescens* (11). In crustaceans, it has also been reported that crustacean hyperglycemic hormones (CHHs) promoted the elimination of the pathogen *Vibrio harveyi* in the hemolymph and significantly up-regulated the mRNA levels of antimicrobial peptides (AMPs) (PEN4 and crustin) in Pacific white shrimp *Litopenaeus vannamei* (12, 13). For the same species, the silencing of molt-inhibiting hormone (MIH) also led to significant increases in mortality of the shrimp infected by bacterium *Vibrio parahaemolyticus* and white spot syndrome virus (WSSV) (14).

In recent years, more and more evidence suggested that in addition to hemocytes, the hepatopancreas also plays an important role in the immunity of crustaceans (15–21). In addition to function as a digestive gland, the hepatopancreas is also a crucial organ for immunity in crustaceans (16). Indeed, crustacean hepatopancreas is a major source of immune response molecules, including lectins, nitric oxide (NO), stress proteins, antibacterial and antiviral proteins, enzymes, and apoptotic genes (15). Furthermore, many immune-related signal transduction pathways are also found in crustacean hepatopancreas, including MAPK, PPAR, Rap1, PI3K-Akts, cyclic adenosine monophosphate (cAMP), and NF-κB signaling pathway (15, 16, 22). However, more studies are needed to further clarify the immune mechanisms of the hepatopancreas in crustaceans.

Crustacean cardioactive peptide (CCAP) is a cyclic amidated non-apeptide first isolated from the pericardial organs in shore crab *Carcinus maenas* with a function of regulating heartbeat (23). It has since been derived mainly from the nervous system of various arthropods, with confirmed roles of neurohormone and neurotransmitter (24, 25). In recent studies, CCAP mRNA was found in the midgut of cockroach *Periplaneta americana* and Pacific white shrimp *L. vannamei*, as well as in the gills of oriental river prawn *Macrobrachium nipponense* (26–29). CCAP has been shown to be involved in various physiological processes in insects and crustaceans, such as modulation of heartbeat in fruit fly *Drosophila melanogaster* (30) and marine crabs *C. maenas* and *Callinectes sapidus* (23, 31), stimulation of American cockroach *P. americana* midgut contraction and stick insect *Baculum extradentatum* hindgut contraction (26, 32), regulation of ecdysis in prawn *M. nipponense* (29), modulation of oviduct and spermatheca contraction in grasshopper *Locusta migratoria* (33, 34), and increasing survival of shrimp *L. vannamei* subjected to freshwater stress (27).

Like other neuropeptide receptors, CCAP receptor is a GPCR. So far, CCAP receptor has been identified in various insects and crustaceans and has been shown to be involved with its ligand to regulate physiological processes. For instance, knockdown of CCAP receptor reportedly resulted in the loss of CCAP heartbeat regulation function in blood-suck bug *Rhodnius prolixus* (35), and interfering CCAP and its receptor reduced the success rate of ecdysis in red flour beetle *Tribolium castaneum* (36). In mud crab *Scylla paramamosain*, recently, CCAP partial transcript has been found from the cerebral transcriptome database, and its receptor is identified *via* ligand-receptor binding assay by our laboratory (37, 38).

Mud crab *S. paramamosain* is widely distributed in the Indo-Pacific region, and the species is an important mariculture species along the southeast coastal provinces of China (39). Mud crab in aquaculture is vulnerable to diverse bacterial, fungal, and viral pathogens, which could lead to severe economic losses to the industry. In order to prevent and control disease outbreaks in aquaculture, an increasing number of research has focused on the functions and enhancement of the immune system of cultured species (40–42). In this study, we first obtained and characterized the full-length cDNA of *Sp*-CCAP from the cerebral ganglia of *S. paramamosain*. The tissue distribution of *Sp*-CCAP and its receptor (*Sp*-CCAPR) were detected by semi-quantitative RT-PCR, and the locations of *Sp*-CCAPR in the hepatopancreas were further determined by *in situ* hybridization. Subsequently, we investigated *Sp*-CCAPR expression profiles following immune stimulation, and finally the immunomodulatory mechanisms of *Sp*-CCAP and its receptor were evaluated by *in vivo* and *in vitro* experiments. This is the first report on CCAP involvement in immunomodulation in an arthropod, and it potentially provides a new strategy for disease control based on neuroendocrine immunity for mud crab aquaculture.

MATERIALS AND METHODS

Experimental Animals

The animal study protocol has been approved by the Animal Ethics Committee of Xiamen University.

Healthy mud crabs (36.36 ± 2.31 g) at the intermolt stage were purchased from a fish market in Haicang District, Xiamen City, Fujian Province, China. Prior to the experiments, the crabs were acclimated in small tanks (40 × 40 × 60 cm) filled with seawater with salinity 30 ppt and temperature 26 ± 0.5°C for 7 days. During the acclimation period, the crabs were fed fresh field snail *Cipangopaludina chinensis* Gray once daily, and half of tank water was renewed every day.

Total RNA Extraction and First-Strand cDNA Synthesis

Total RNA from hemocytes and various tissues, that is, eyestalk ganglion, cerebral ganglion, thoracic ganglion, hepatopancreas, gill, stomach, midgut, heart, epidermis, gonad, and muscle, were extracted using TRIzol Reagent (Invitrogen, USA) according to the manufacturer's instructions. The concentrations and quality of RNAs were checked by a Q6000 spectrophotometer (Quawell), and the integrity was assessed by 1.5% (w/v) agarose gel electrophoresis. The first-strand cDNA was synthesized using PrimeScript RT Reagent Kit with gDNA Eraser (TaKaRa) for semi-quantitative RT-PCR and quantitative real-time PCR (qRT-PCR) analyses.

Cloning the Full-Length cDNA of *Sp-CCAP* and Bioinformatics Analysis

Partial cDNA sequence of *Sp-CCAP* was obtained from the transcriptome database of *Scylla paramamosain* (37). The full-length *Sp-CCAP* cDNA with 1 μg of total RNA extracted from cerebral ganglion was amplified with the SMART™ RACE cDNA Amplification Kit (BD Biosciences). The 3′-race and 5′-race PCR amplification was performed with universal primers [Universal Primer Mix (UPM)] and gene-specific primers for touchdown PCR and nested PCR amplification. PCR products were purified and cloned into the pMD19-T plasmids (TaKaRa). The positive colonies were screened and further confirmed by DNA sequencing. The primer sequences are listed in **Table 1**.

The ORF Finder (http://www.ncbi.nlm.nih.gov/gorf/orfig.cgi) was used to predict open reading frames (ORFs) and amino acid sequence of *Sp*-CCAP. The amino acid sequence was submitted to predict protein signal peptide with SignalP 5.0 Server (http://www.cbs.dtu.dk/services/SignalP/). The isoelectric point of *Sp*-CCAP was predicted by ExPASy software. The homology amino acid sequences of *Sp*-CCAP from other species in the National Center for Biotechnology Information (NCBI) database were obtained through the BlastX homology search (http://blast.ncbi.nlm.nih.gov/Blast.cgi). These sequences were used to create the multiple sequence alignment by MEGA 7.0 software. Phylogenic trees were constructed *via* the neighbor-joining (NJ) method using MEGA 7.0 software. Bootstrap sampling was reiterated for 1,000 times.

TABLE 1 | Primers for PCRs.

Name	Sequence (5′-3′)
cDNA cloning	
3′Out-*Sp*-CCAP	GGCAAGGTTATGGGAGCAACT
3′In-*Sp*-CCAP	GCTCTGTGTATCCAAACATGTGTTG
5′Out-*Sp*-CCAP	TTGCTCCCATAACCTTGCCTC
3′In-*Sp*-CCAP	AACGCAAGGAGGAGGATGGTT
UPM (long)	CTAATACGACTCACTATAGGGCAAGCAGT GGTATCAACGCAGAGT
UPM (short)	CTAATACGACTCACTATAGGGC
RT-PCR/qRT-PCR	
Sp-CCAP-qF	CGAGGCAAGGTTATGGGAG
Sp-CCAP-qR	GATACACAGAGCCACTCAAGAAAT
Sp-CCAPR-qF	TCCAAGACTCGCAAATCCA
Sp-CCAPR-qR	ATGTCCGTGAGAACACTGAT
Sp-β-actin-qF	GAGCGAGAAATCGTTCGTGAC
Sp-β-actin-qR	GGAAGGAAGGCTGGAAGAGAG
qRT-PCR	
Sp-IL16-qF (42)	TGGCAGAGGTTACAGGTCACGGTTAT
Sp-IL16-qR (42)	GGAGTCTGGTGTTCGTCACTGTTTCT
Sp-TNFSF-qF (43)	CTGTTGTACGTCAGGTCGACTCT
Sp-TNFSF-qR (43)	GGCTCTTCGTATGGGACCTCTG
Sp-LYZ-qF (44)	TGCCATCAACCACCACAACT
Sp-LYZ-qR (44)	CCCCTTTCCCTTCCACTTCT
Sp-ALF1-qF (41)	AACTCATCACGGAGAATAACGC
Sp-ALF1-qR (41)	CTTCCTCGTTGTTTTCACCCTC
Sp-ALF4-qF (42)	CACTACTGTGTCCTGAGCCGC
Sp-ALF4-qR (42)	GTCCTCGCCTTACAATCTTCTG
Sp-ALF5-qF (42)	CTTGAAGGGACGAGGTGATGAG
Sp-ALF5-qR (42)	TGACCAGCCCATTCGCTACAG
Sp-Relish-qF (42)	AGTGGAACAGTGGTCCAGCTG
Sp-Relish-qR (42)	CACCACCACTTCACAAATC
Sp-Dorsal-qF (42)	TCATCCCCACAATCTGGTGG
Sp-Dorsal-qR (42)	TAAGTGCATCTTCCACGTC
Sp-P38-qF (45)	TTCACTCCGTCCACCACCTT
Sp-P38-qR (45)	GCCCTCGTAACACCTGGTAGAT
***In situ* hybridization**	
T7	TAATACGACTCACTATAGGG
SP6	ATTTAGGTGACACTATAG
Sp-CCAP-IF	CGACTCCTACTACTTCTAC
Sp-CCAP-IR	GATACGGTACTCTTCCAG
PMD19T	
RV-M	GAGCGGATAACAATTTCACACA
M13-47	CGCCAGGGTTTTCCCAGTCACG

Tissue Distribution of *Sp-CCAP* and *Sp-CCAPR* mRNA

Semi-quantitative RT-PCR was used to detect the distribution of *Sp-CCAP* and *Sp-CCAPR* mRNA in hemocytes and tissues from eyestalk ganglion, cerebral ganglion, thoracic ganglion, hepatopancreas, gill, stomach, midgut, heart, epidermis, gonad, and muscle using *Sp-CCAP*-qF, *Sp-CCAP*-qR, *Sp-CCAPR*-qF, and *Sp-CCAPR*-qR as primers (**Table 1**). The PCR was performed

with the Ex-Taq® DNA polymerase (TaKaRa) under the following conditions: pre-denaturation at 94°C for 5 min and 40 cycles consisting of 94°C for 30 s, 58°C for 30 s, and 72°C for 30 s; and the final extension was carried out at 72°C for 10 min. PCR products were resolved on 1.5% agarose gel, and the results were observed and photographed by UV gel imager with water used as a template for negative control and *β-actin* as an internal control. The experiment was repeated three times.

mRNA *in situ* Hybridization

The 217-bp fragment of *Sp-CCAPR* was amplified by PCR and cloned into PGEM-T EASY Vector (Promega) for the subsequent *in situ* hybridization experiment. The riboprobes were synthesized using the DIG RNA Labeling Kit (Roche Diagnostics, Germany) and transcribed by SP6 and T7 polymerases. The hepatopancreas was quickly removed from the crabs and immediately fixed in 4% paraformaldehyde solution for 12 h at 4°C. After being treated with serially diluted ethanol (75, 85, 95, and 100%) and xylene, the sample was embedded in paraffin and sectioned into 0.7-μm continuous sections. Hybridization was subsequently carried out according to the methods reported previously (46) and visualized by the BCIP/NBT Chromogen Kit (Solarbio).

Immune Challenges With Lipopolysaccharide and Polyriboinosinic Polyribocytidylic Acid Injection

Polyriboinosinic polyribocytidylic acid [Poly (I:C)] (Sigma, USA) was dissolved in crustacean physiological saline (1.13×10^{-2} mol/L of KCl, 1.33×10^{-2} mol/L of $CaCl_2$, 0.44 mol/L of NaCl, 1.0×10^{-2} mol/L of Hepes, 2.3×10^{-2} mol/L of Na_2SO_4, and 2.6×10^{-2} mol/L of $MgCl_2$, pH 7.4) at 1 mg/ml; and lipopolysaccharide (LPS) (Sigma, USA) was dissolved in crustacean physiological saline at 0.5 mg/ml. Seventy-five crabs were randomly divided into three groups and injected with 100 μl of Poly (I:C), LPS, or crustacean physiological saline (control). In addition, five untreated crabs were used for the initial measurements. Hepatopancreas tissues of five individuals from each treatment group were subsequently randomly sampled at 3, 6, 12, 24, and 48 h for RNA extraction and qRT-PCR analysis. The qPCR used a QuantStudio™ 6 Flex Real-Time PCR (Applied Biosystems) with SYBR® Select Master Mix (TaKaRa). The total reaction volume was 20 μl containing 10 μl of SYBR® Select Master Mix, 2 μl of the five-fold diluted cDNA, 0.5 μl (1.0×10^{-5} mol/L) each of the forward and reverse primers, and 7 μl of ultrapure water; and the procedure included 50°C for 2 min; 95°C for 2 min; followed by 40 cycles of 95°C for 15 s, 58°C for 30 s, and 72°C for 30 s; and followed by a melting curve analysis at 60–95°C. A relative transcript level was determined using the $2^{-\Delta\Delta Ct}$ algorithm with *β-actin* from *S. paramamosain* as the internal control. The sequences of the primers used are listed in **Table 1**.

Injection of *Sp*-CCAP Mature Peptide

The predicted *Sp*-CCAP mature peptide (PFCNAFTGC-NH2) was synthesized by GL Biochem (Shanghai, China) with a purity of 98% for the subsequent experiments. Forty crabs were randomly divided into two groups: the CCAP treatment group was injected with 100 μl of CCAP mature peptide dissolved in crustacean physiological saline (final concentration in hemolymph about 5×10^{-6} mol/L), whereas the control group was injected with crustacean physiological saline of the same volume. Meanwhile, five untreated crabs were randomly selected for the initial measurement. The hepatopancreas tissues of five crabs from each group were sampled at 3, 6, 12, and 24 h after injection for RNA extraction and gene expression analysis (see *Total RNA Extraction and First-Strand cDNA Synthesis* and *Immune Challenges With Lipopolysaccharide and Polyriboinosinic Polyribocytidylic Acid Injection*).

Hepatopancreas Treated *in vitro* by *Sp*-CCAP Mature Peptide

S. paramamosain at the intermolt stage was anesthetized on ice for 10 min, followed by sterilization in 75% ethanol for 5 min. Hepatopancreas tissues were subsequently dissected and washed with crustacean physiological saline before being cut by a pair of scissors into fragments of ∼20 mg. The fragments were then precultured at 26°C in a 24-well-plate with 200 μl of L15 medium, which contained penicillin (100 U/ml) and streptomycin (100 μg/ml, Sigma). After an hour, the culture was substituted with L15 medium containing *Sp*-CCAP peptide at one of three concentrations of 10^{-6}, 10^{-7}, and 10^{-8} mol/L or without adding any peptide (control), which were based on a previous study from our lab (47). Quadruple treatments were used. After 6 h of culture, tissue fragments were collected from each treatment for total RNA extraction and subsequent qRT-PCR analysis, whereas tissue culture medium was also collected for NO concentration measurement. The NO production was determined using the Total Nitric Oxide Assay Kit (Beyotime, China). Briefly, the absorbance of the nitrite was measured with the Griess reaction at OD_{540nm}, and the nitrite concentration of each tissue culture medium was then calculated according to the standard curve constructed using $NaNO_2$ for the calculation of total NO concentration.

In vitro Antibacterial Assay

The bacterial clearance assay was carried out based on the method described in a previous study (48), with some modifications. That is, after hepatopancreas tissue with *Sp*-CCAP mature peptide was added at three concentrations (10^{-8}, 10^{-7}, and 10^{-6} mol/L) plus a control without adding *Sp*-CCAP being cultured for 6 h, either *Staphylococcus aureus* or *Vibrio parahaemolyticus* suspension (were stored in our laboratory), both pathogenic to the mud crab, was added to culture wells at the final bacterial concentration of $\sim 3 \times 10^4$ cfu/ml per well. After another 3 h of culture, each tissue culture medium was inoculated and cultured on either Luria–Bertani (LB) solid medium (for *S. aureus*) or 2216E solid medium (for *V. parahaemolyticus*) for 12 h at 37°C, and the number of colonies was then observed and recorded. The assay was performed in triplicates for each culture medium.

Statistical Analysis

All data were presented as mean ± SEM. Statistical differences among treatments were analyzed using one-way ANOVA (followed by Duncan's test) or Student's *t*-test (SPSS 18.0). Differences were considered statistically significant at $p < 0.05$ and highly significant at $p < 0.01$.

RESULTS

Molecular Cloning of a cDNA Encoding *Sp-CCAP* Precursor

The complete cDNA sequence of the *Sp-CCAP* precursor was obtained by using 3′/5′ RACE coupled to nested PCR. The full length of *Sp-CCAP* mRNA is 638 bp with a 64-bp 5′ untranslated region (UTR), a 142-bp 3′UTR, and a 432-bp ORF encoding a protein of 143 amino acids with a calculated molecular weight of 15.84 kDa and a theoretical isoelectric point of 9.43 (GenBank Accession MN923209). The deduced precursor peptide contained a signal peptide of 32 amino acids, four putative dibasic (37KR38 and 49KR50), tribasic (61KKR63), and tetrabasic (115RRKR118) cleavage sites, which could give rise to five peptides, including four precursor-related peptides (CCAP AP1: 33-36; CCAP AP2: 39-48; CCAP AP3: 64-114; and CCAP AP4: 115-143) and one mature peptide containing nine amino acids (PFCNAFTGC-NH_2) (**Figure 1**).

Multiple Alignment and Phylogenetic Tree Analysis

Multiple alignment of the amino acid sequences of CCAP precursors from different crustaceans indicated that the CCAP mature peptides were fully identical among the crustacean species used for comparison (**Figure 2**). Phylogenetic analysis of the amino acid sequences of CCAP precursors among different arthropod species showed that *Sp*-CCAP and other crustacean CCAP clustered into one branch, whereas insect CCAP clustered into another branch (**Figure 3**).

Tissue Distribution of *Sp-CCAP*/*Sp-CCAPR*

The expression pattern of *Sp-CCAP* among various tissues was determined by semi-quantitative RT-PCR. The results showed that *Sp-CCAP* was expressed in nerve and gonad tissues (**Figure 4**). To identify the potential target sites of *Sp-CCAP*, the expression pattern of the *Sp-CCAPR* transcript was also determined, and *Sp-CCAPR* was found expressed in 12 tissues, including hemocytes and hepatopancreas (**Figure 4**).

In situ Hybridization of *Sp-CCAPR* in Hepatopancreas

To precisely localize the *Sp-CCAPR* transcript in hepatopancreas, *in situ* hybridization was performed. Histological results showed that hepatopancreatic tubule epithelial cells of *Scylla paramamosain* include E-cells (embryonic), F-cells (fibrillar), B-cells (blisterlike), and R-cells (resorptive) (**Figure 5C**). *In situ* hybridization localized *Sp-CCAPR*-positive signal mainly in the F-cells of hepatopancreas (**Figure 5A**), whereas in the control group, no such positive signal was found (**Figure 5B**).

The Induced mRNA Expression of *Sp-CCAPR* in Response to Lipopolysaccharide and Polyriboinosinic Polyribocytidylic Acid Stimulation

Because involvement of neuropeptides in NEI regulation is mainly by binding to their receptors on immune cells, the temporal patterns of *Sp-CCAPR* mRNA expression in the hepatopancreas after LPS and Poly (I: C) injection were investigated. The results showed that following LPS challenge, a significantly up-regulated mRNA expression level of *Sp-CCAPR* was only observed at 12 h, which was 2.09-fold of that in the control ($p < 0.05$) (**Figure 6A**). However, after Poly (I:C) stimulation, the mRNA expression level of *Sp-CCAPR* was significantly up-regulated at both 3 and 24 h, with 4.16-fold and 2.28-fold increase, respectively, compared with that of the control at the same time point ($p < 0.05$) (**Figure 6B**).

The mRNA Expressions of Immune-Related Genes After *Sp*-CCAP Mature Peptide Injection

To evaluate the potential involvement of *Sp*-CCAP in immune regulation, after being injected with synthetic *Sp*-CCAP mature peptide, the changes in mRNA expression levels of immune-related genes, including *Sp-CCAPR*, nuclear transcription factor NF-κB homologs (*Sp-Dorsal* and *Sp-Relish*), member of MAPK signaling pathway (*Sp-P38*), pro-inflammatory cytokines factor (*Sp-TNFSF* and *Sp-IL16*), and AMP (*Sp-Lysozyme*, *Sp-ALF*, *Sp-ALF4*, and *Sp-ALF5*), in the hepatopancreas were quantified up to 24 h (**Figure 7**). The mRNA expression of *Sp-CCAPR* was shown to increase significantly at 6 and 12 h post-*Sp*-CCAP stimulation, which was 2.69-fold and 2.41-fold of that of the control, respectively ($p < 0.05$) (**Figure 7A**). Similarly, the mRNA expression of *Sp-P38* was significantly up-regulated to 1.45-fold and 1.65-fold of that in the control at 6 and 12 h, respectively ($p < 0.05$) (**Figure 7B**). Likewise, the nuclear transcription factor *Sp-Dorsal* mRNA expression level was significantly up-regulated at 6, 12, and 24 h (**Figure 7C**), whereas the *Sp-Relish* mRNA expression level was significantly up-regulated at 6 and 24 h ($p < 0.05$) (**Figure 7D**). Moreover, pro-inflammatory factor *Sp-TNFSF* and *Sp-IL16* mRNA expression levels were both up-regulated significantly at 6 and 12 h ($p < 0.05$) (**Figures 7E,F**). Additionally, the mRNA expression level of *Sp-lysozyme* and *Sp-ALF4* increased significantly at 12 h ($p < 0.05$) but returned to normal at 24 h ($p > 0.05$) (**Figures 7G,I**). The mRNA expression level of *Sp-ALF1* also increased significantly at 6, 12, and 24 h ($p < 0.05$) (**Figure 7H**). Finally, the *Sp-ALF5* mRNA expression level was sharply up-regulated at 6 h ($p < 0.05$) but dropped back to similar levels to that of the control from 12 h onward ($p > 0.05$) (**Figure 7J**).

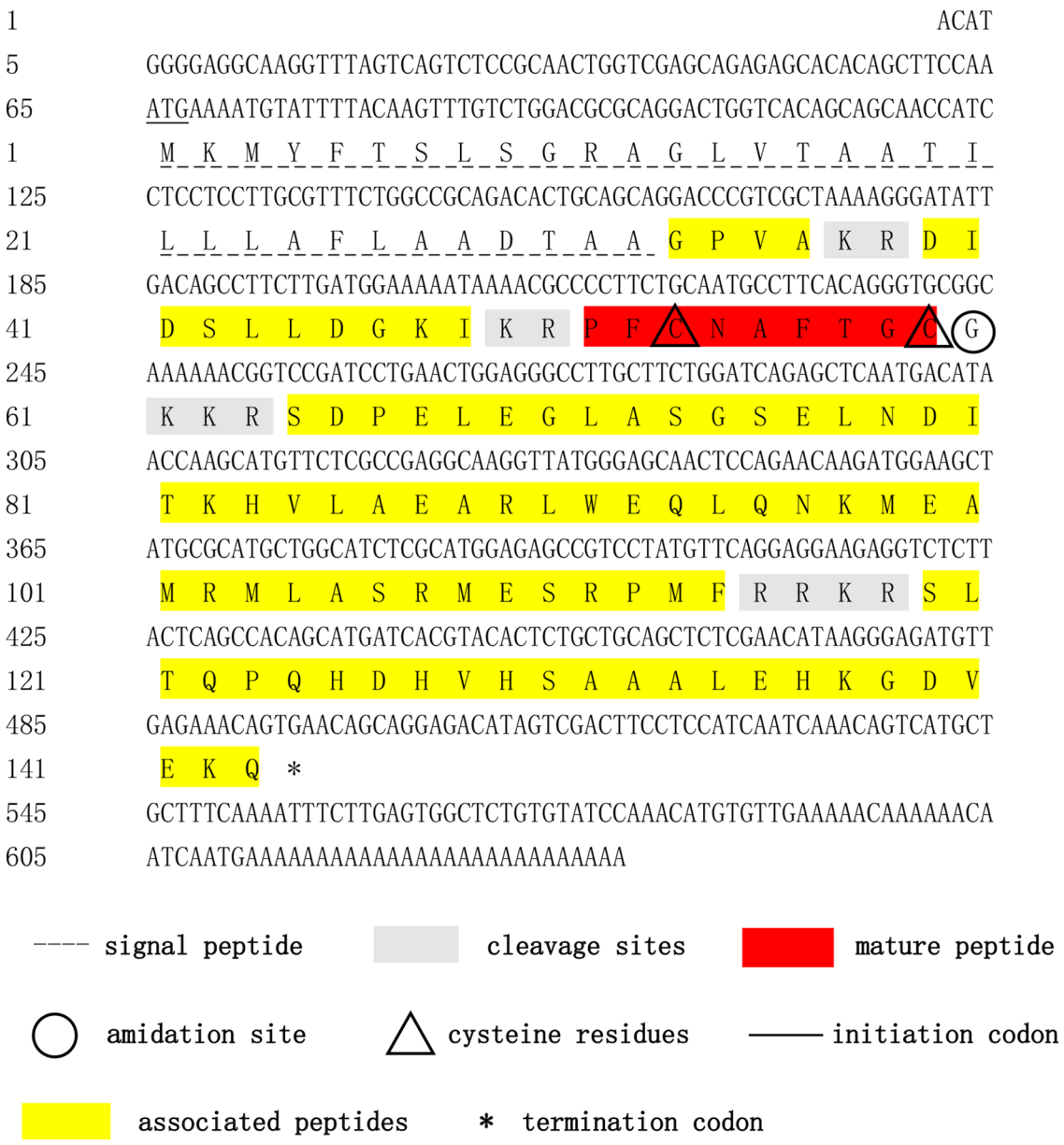

FIGURE 1 | Nucleotide and deduced-amino acid sequences of *Sp-CCAP* cDNA. The initiation codon, termination codon, signal peptide, crustacean cardioactive peptide (CCAP) mature peptide, CCAP-associated peptides, amidation site, cleavage sites, and cysteine residues are marked by different symbols.

The mRNA Expressions of Immune-Related Genes and the NO Concentration After *in vitro Sp*-CCAP Mature Peptide Treatment

To further evaluate the immunoregulation function of *Sp*-CCAP, *Sp*-CCAP mature peptide was added to the hepatopancreatic explant cultures at three different concentrations (10^{-8}, 10^{-7}, and 10^{-6} mol/L), and the expression levels of immune-related genes were measured (**Figure 8**). The mRNA expression level of both *Sp-CCAPR* and *Sp-P38* was both up-regulated following the addition of *Sp*-CCAP mature peptide at all three concentrations, and significant differences were detected at 10^{-8} and 10^{-7} mol/L as compared with those of the control ($p < 0.05$) (**Figures 8A,B**). Moreover, the *Sp-Dorsal* mRNA expression level was significantly up-regulated at all three concentrations ($p < 0.05$) (**Figure 8C**), and the *Sp-Relish* mRNA expression level was significantly up-regulated at 10^{-8} and 10^{-6} mol/L ($p < 0.05$) (**Figure 8D**). Similarly, the *Sp-TNFSF* mRNA expression level was significantly up-regulated at 10^{-8} and 10^{-7} mol/L ($p < 0.05$) (**Figure 8E**), whereas the *Sp-IL16* mRNA expression level was significantly up-regulated at all three concentrations ($p <$

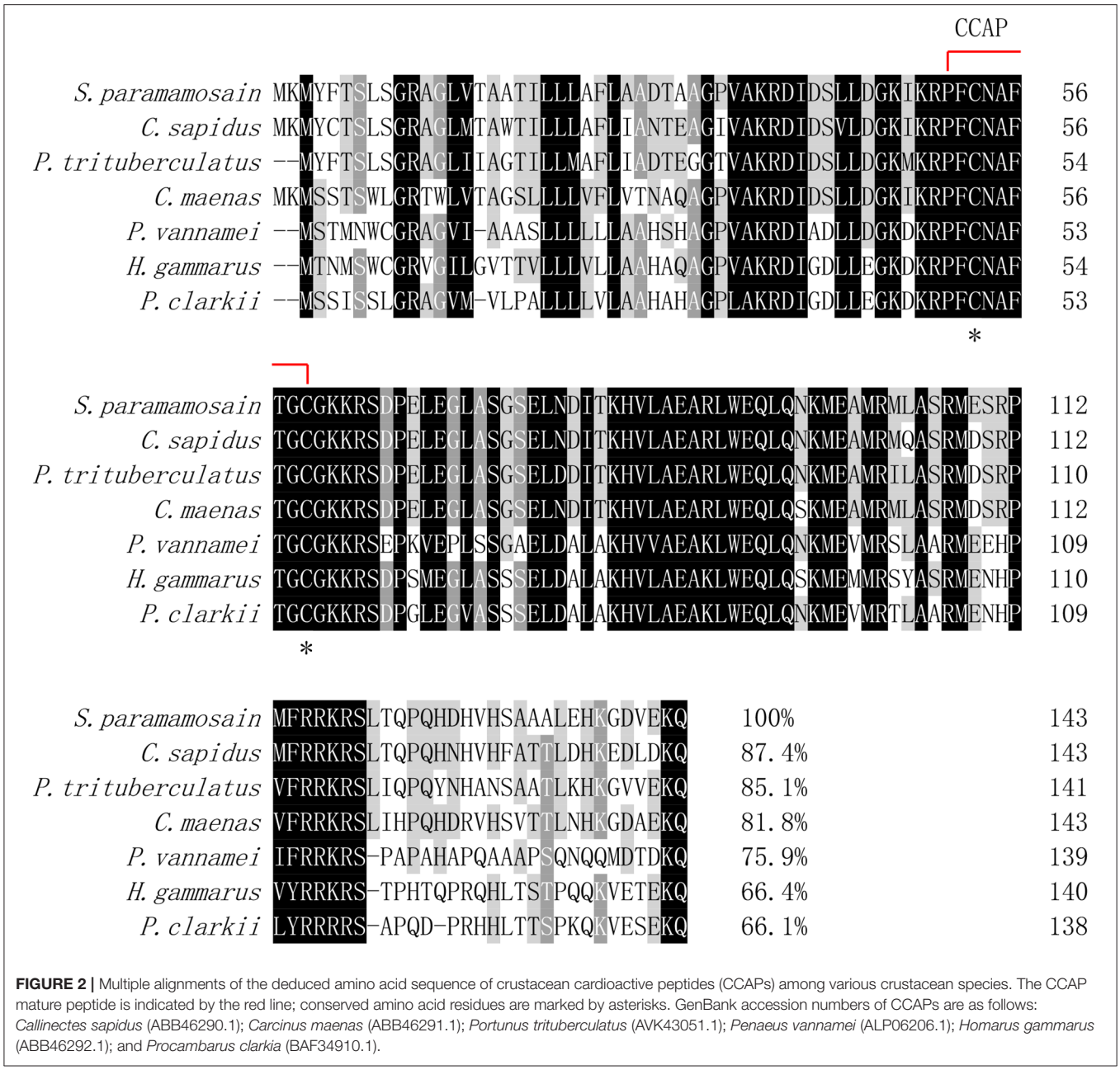

FIGURE 2 | Multiple alignments of the deduced amino acid sequence of crustacean cardioactive peptides (CCAPs) among various crustacean species. The CCAP mature peptide is indicated by the red line; conserved amino acid residues are marked by asterisks. GenBank accession numbers of CCAPs are as follows: *Callinectes sapidus* (ABB46290.1); *Carcinus maenas* (ABB46291.1); *Portunus trituberculatus* (AVK43051.1); *Penaeus vannamei* (ALP06206.1); *Homarus gammarus* (ABB46292.1); and *Procambarus clarkia* (BAF34910.1).

0.05) (**Figure 8F**). Finally, the mRNA expression levels of AMP genes *Sp-lysozyme*, *Sp-ALF1*, and *Sp-ALF5* were significantly up-regulated at 10^{-8} mol/L ($p < 0.05$) (**Figures 8G,H,J**), whereas the mRNA expression level of *Sp-ALF4* was not significantly different from that of the control at all concentrations (**Figure 8I**).

NO is an important gaseous signaling molecule that plays a key role in the innate immune system; NO concentration changes in the hepatopancreas culture media were also determined after adding *Sp*-CCAP mature peptide at different concentrations (**Figure 8J**). It showed that when treated with *Sp*-CCAP at 10^{-8} M, NO concentration in the medium increased significantly ($p < 0.05$); however, NO content did not significantly vary from the control at the concentrations of 10^{-6} and 10^{-7} mol/L (**Figure 8J**).

Clearance of Bacteria Facilitated by *Sp*-CCAP

The bacterial clearance capability of each hepatopancreas culture medium with *Sp*-CCAP mature peptide added at 10^{-8}, 10^{-7}, and 10^{-6} mol/L was evaluated against the control (no *Sp*-CCAP addition) to assess whether up-regulated immune molecules led to enhanced antibacterial capacity. The results showed that based on colony counts, in both cases of *S. aureus* and *Vibrio parahaemolyticus*, bacteria numbers in all tissue culture media

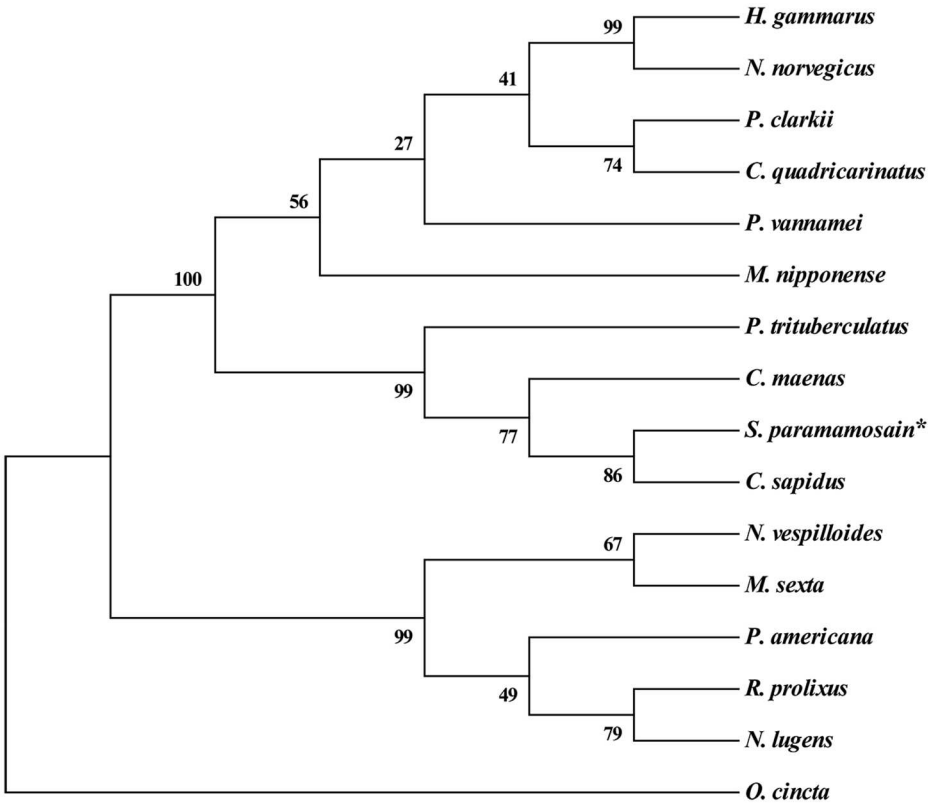

FIGURE 3 | Phylogenetic analysis of crustacean cardioactive peptides (CCAPs) relative to various crustacean and insect species. The sequences used in evolutionary tree analysis include *Callinectes sapidus* (ABB46290.1); *Carcinus maenas* (ABB46291.1); *Portunus trituberculatus* (AVK43051.1); *Homarus gammarus* (ABB46292.1); *Procambarus clarkia* (BAF34910.1); *Nephrops norvegicus* (QBX89037.1); *Cherax quadricarinatus* (AWK57511.1); *Penaeus vannamei* (ALP06206.1); *Macrobrachium nipponense* (ASH96804.1); *Periplaneta Americana* (Q75UG5.1); *Rhodnius prolixus* (ACZ52615.1); *Nilaparvata lugens* (BAO00946.1); *Nicrophorus vespilloides* (XP_017778790.1); and *Orchesella cincta* (ODM98622.1).

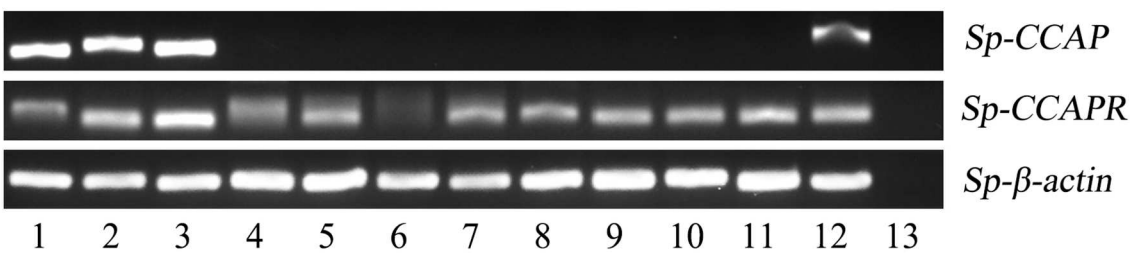

FIGURE 4 | Tissue distribution of *Sp-CCAP* and *Sp-CCAPR* in *S. paramamosain*. 1, eyestalk ganglion; 2, cerebral ganglion; 3, thoracic ganglion; 4, gill; 5, hepatopancreas; 6, hemocytes; 7, stomach; 8, midgut; 9, heart; 10, epidermis; 11, muscle; 12, gonad; and 13, the negative control.

with *Sp*-CCAP mature peptide addition decreased compared with those of the control; and the improvement in bacterial clearance capacity was significant when *Sp*-CCAP mature peptide was added at 10^{-8} and 10^{-7} mol/L ($p < 0.05$) (**Figures 9A–D**).

DISCUSSION

As a multifunctional peptide hormone, CCAP is known to play an important role in the regulation of various physiological processes in arthropods (23, 26–34). Its immunomodulatory function, however, has never been reported previously; the present study hence appears to be the first to report the involvement of CCAP in regulating hepatopancreas immunity in an arthropod.

In this study, a cDNA encoding CCAP precursor was identified from mud crab *Scylla paramamosain*. In the phylogenetic tree constructed, all CCAP precursor peptides could be divided into two branches of crustacean and insect. The *Sp*-CCAP precursor peptide fell into the branch of crustacean, indicating that *Sp*-CCAP shared high similarity with other

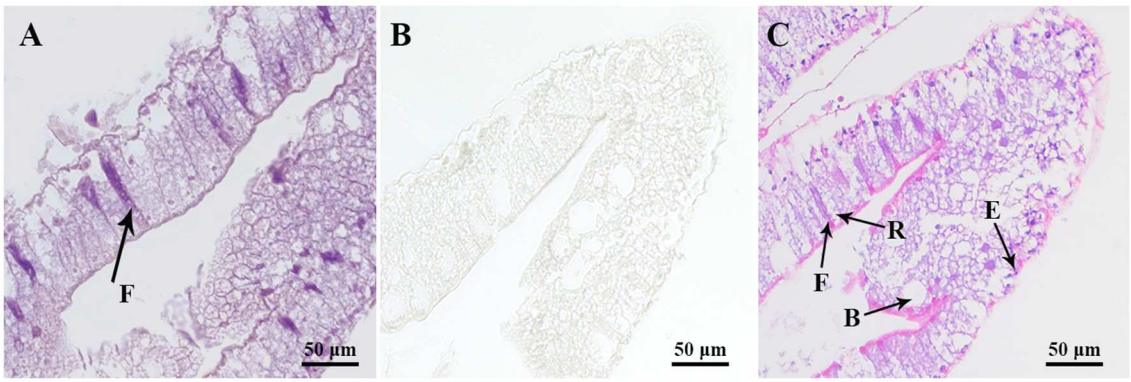

FIGURE 5 | Localization of *Sp-CCAPR* mRNA in the hepatopancreas by *in situ* hybridization. **(A)** Positive signals with the antisense probes. **(B)** Sense probes of *Sp-CCAPR* served as the negative control. **(C)** Histological observation of hepatopancreatic tubule epithelial cells: E, E-cell (E: embryonic); F, F-cell (F: fibrillar); B, B-cell (B: blisterlike); and R-cell (R: resorptive).

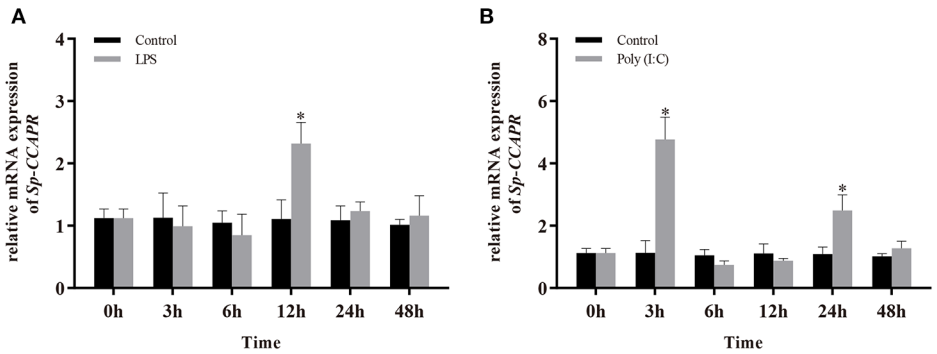

FIGURE 6 | Changes in mRNA expression of *Sp-CCAPR* in the hepatopancreas after lipopolysaccharide (LPS) and polyriboinosinic polyribocytidylic acid [Poly (I:C)] injection. **(A)** After LPS stimulation. **(B)** After Poly (I:C) stimulation. All data are shown as mean ± SEM ($n = 5$); statistical analysis was performed using Student's *t*-test. *indicates significant difference ($p < 0.05$).

crustaceans. By comparing precursor peptides of all sequences from crustaceans, four restriction sites were identified, suggesting that their translation processing modules are highly conserved. CCAP mature peptide sequences (PFCNAFTGC-NH_2) are identical among different species, which indicates essential roles of CCAP to arthropods.

The distribution of genes in different tissues has a guiding role for exploring the physiological functions of neuropeptides (10). RT-PCR results showed that mRNA transcript of *Sp*-CCAP was mainly expressed in the nervous system and gonads of *S. paramamosain*, whereas the *Sp*-CCAPR mRNA was expressed in a wide range of different tissues. However, in American cockroach *Periplaneta americana* and Pacific white shrimp *L. vannamei*, CCAP mRNA was reportedly expressed in the midgut and the nervous system (26, 27), which suggests that likely there are different physiological regulation pathways of CCAP in arthropod species. In the present study, the detection of mRNA expression of both *Sp-CCAP* and *Sp*-CCAPR in gonads suggested that they may act as an autocrine/paracrine factor to regulate ovarian development, similar to that of short neuropeptide F (sNPF) identified in the same crab species (49). Neurohormones have been found to participate in immune regulation through receptors on hemocytes, the well-known immune-related cells that play crucial roles in host immune defense in crustaceans (50). For instance, in insects, 5-HT receptors were found expressed in the hemocytes, and 5-HT has been shown to modulate hemocyte phagocytosis through $5HT_{1B}$ and $5\text{-}HT_{2B}$ receptors (51). Similarly, *Es-GPCR89* mRNA was expressed in the hemocytes of Chinese mitten crab *Eriocheir sinensis* and found to mediate cerebral antimicrobial activity (52). In this study, *Sp*-CCAPR was found expressed in the hemocytes, suggesting that *Sp*-CCAP may be involved in the immune regulation of hemocytes as a neurohormone in *S. paramamosain*. In crustaceans, the hepatopancreas is not only the major organ responsible for digestion but also an important immune organ (16). Indeed, in crayfish *Procambarus clarkii*, a putative GPCR gene, HP1R, was found expressed in the hepatopancreas and was suggested to play a role in protecting the host from bacterial invasion (53). In this study, *in situ* hybridization

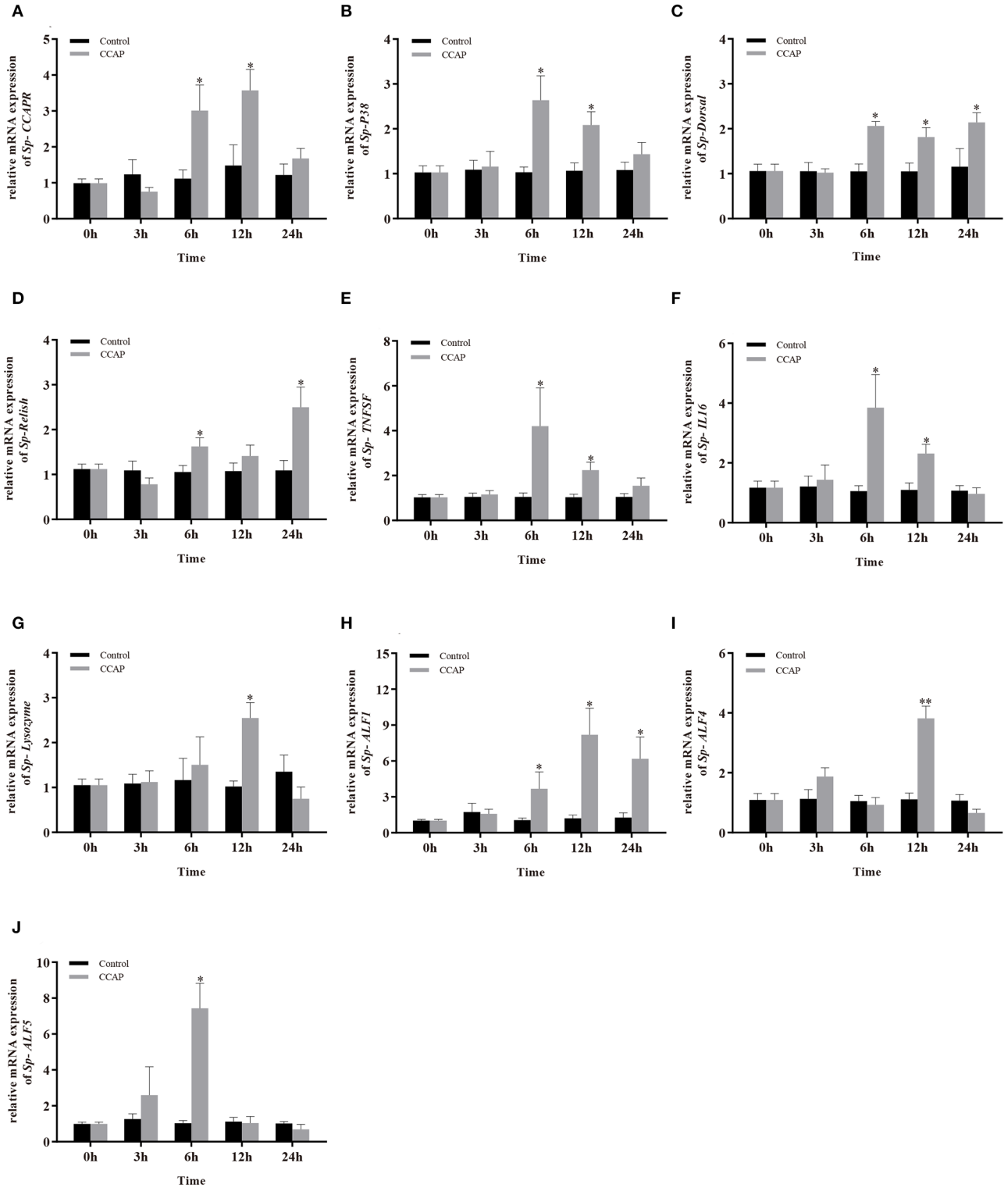

FIGURE 7 | Effects of *Sp*-CCAP injection on the mRNA expressions of immune-related genes in the hepatopancreas. **(A)** *Sp-CCAPR*; **(B)** *Sp-P38*; **(C)** *Sp-Dorsal*; **(D)** *Sp-Relish*; **(E)** *Sp-TNFSF*; **(F)** *Sp-IL16*; **(G)** *Sp-Lysozyme*; **(H)** *Sp-ALF1*; **(I)** *Sp-ALF4*; **(J)** *Sp-ALF5*. All data are shown as mean ± SEM ($n = 5$); statistical analysis by Student's *t*-test. * and **on the top of bars indicate significant ($p < 0.05$) and highly significant differences ($p < 0.01$), respectively.

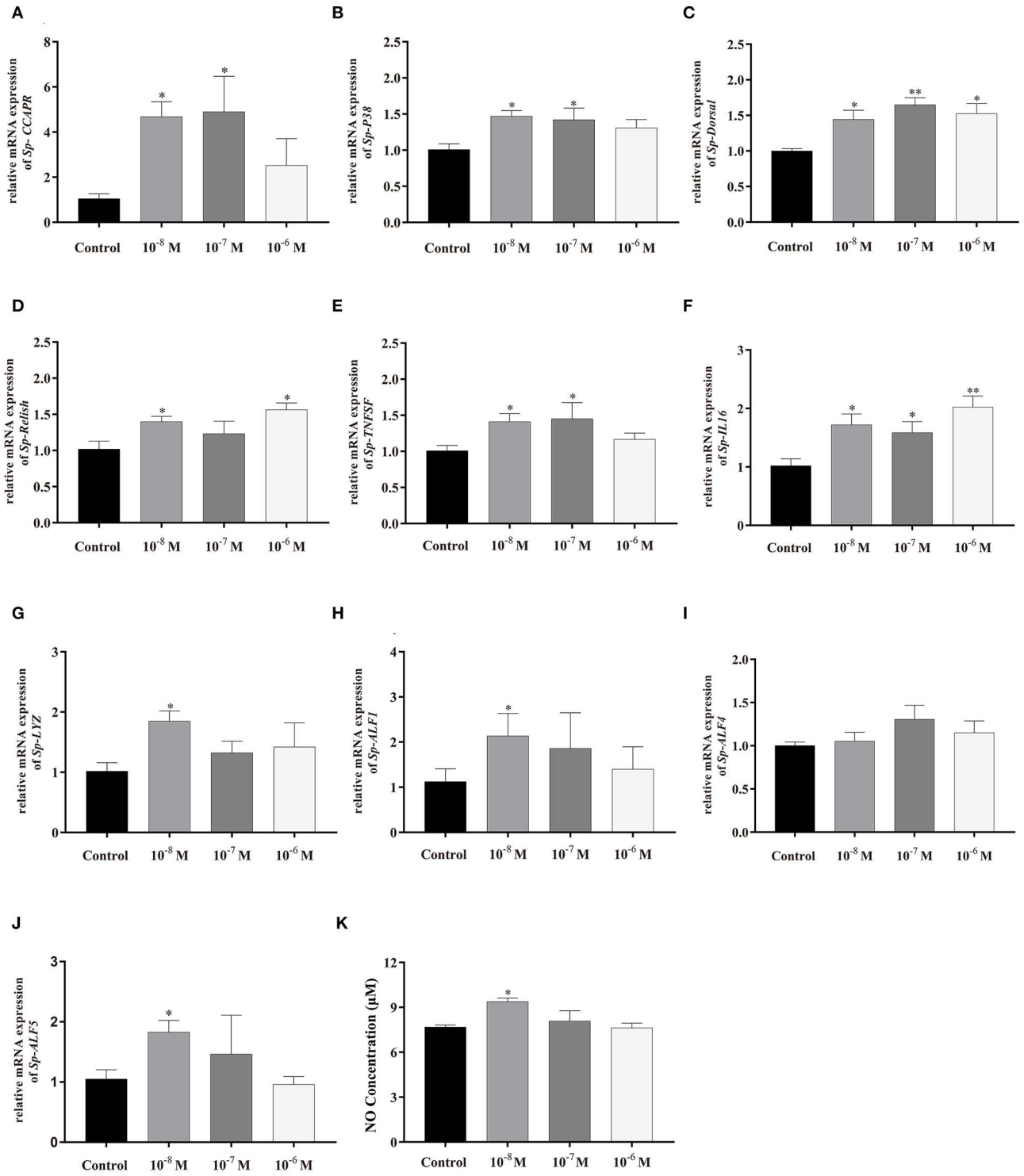

FIGURE 8 | Effects of *Sp*-CCAP addition at different concentrations on mRNA expressions of immune-related genes in *in vitro* cultured hepatopancreas tissues and NO concentration in the culture media. **(A)** *Sp-CCAPR*; **(B)** *Sp-P38*; **(C)** *Sp-Dorsal*; **(D)** *Sp-Relish*; **(E)** *Sp-TNFSF*; **(F)** *Sp-IL16*; **(G)** *Sp-Lysozyme*; **(H)** *Sp-ALF1*; **(I)** *Sp-ALF4*; **(J)** *Sp-ALF5*; and **(K)** the concentration of NO. All data are shown as mean ± SEM ($n = 4$); statistical analysis performed by one-way ANOVA followed by Duncan's test. * and **on top of bars indicate significant ($p < 0.05$) and highly significant differences ($p < 0.01$), respectively.

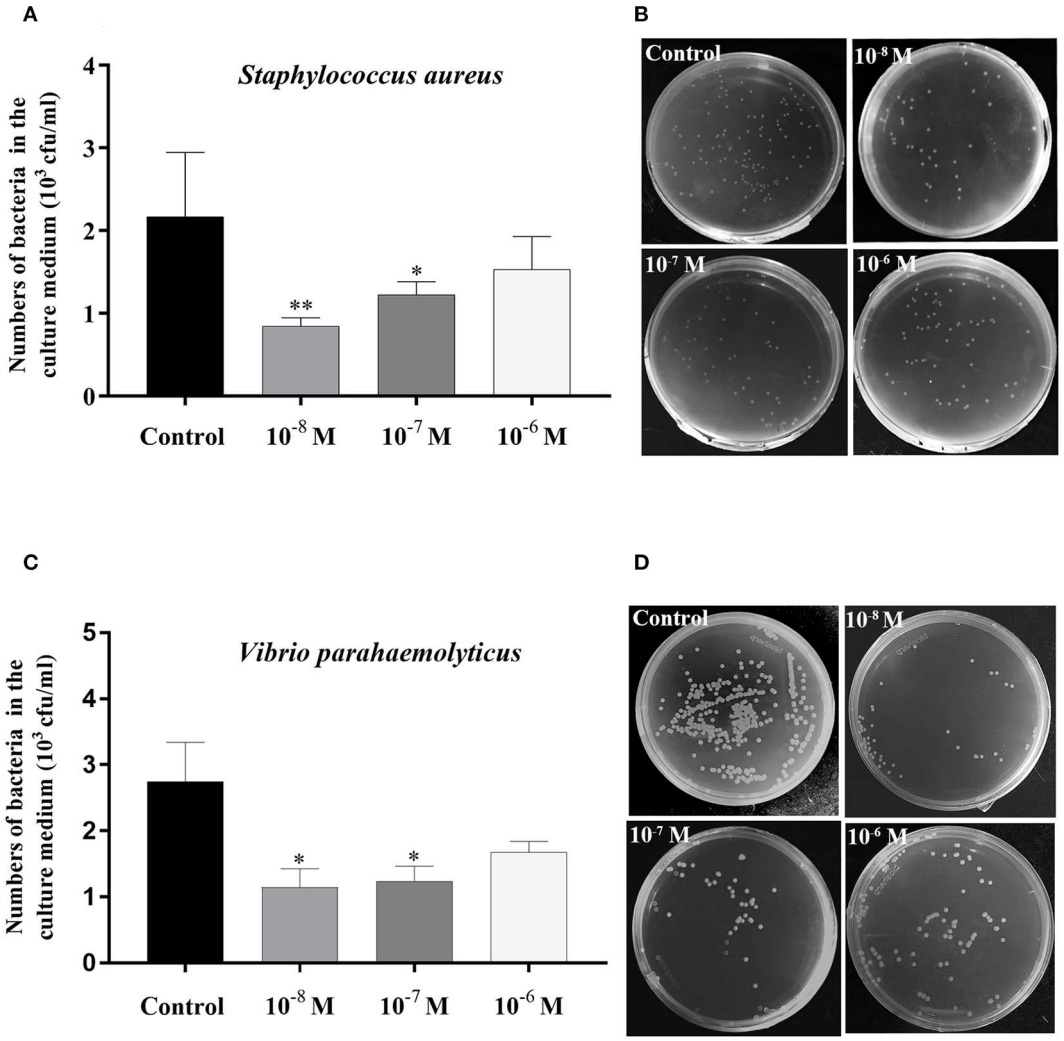

FIGURE 9 | Bacterial clearance capacity of hepatopancreas culture medium treated with different concentrations of *Sp*-CCAP as compared with the no *Sp*-CCAP addition control. **(A)** Results with *Staphylococcus aureus*. **(B)** *S. aureus* colonies grown on Luria–Bertani (LB) plates. **(C)** Results with *Vibrio parahaemolyticus*. **(D)** *S. aureus* colonies grown on 2216E plates. All data are shown as mean ± SEM ($n = 4$); statistical analysis performed by one-way ANOVA followed by Duncan's test. * and **on top of bars indicate significant ($p < 0.05$) and highly significant differences ($p < 0.01$), respectively.

showed that *Sp*-CCAPR mRNA was mainly expressed in F-cells of hepatopancreas, indicating that *Sp*-CCAP may play an immunomodulatory role *via* its receptor on F-cells in *S. paramamosain*.

Increasingly studies have shown that neuropeptides play an important role in the NEI network; typically, they are activated by immune stimuli and bind to their receptors to participate in the innate immune responses (2, 54). In this study, *Sp*-CCAPR was found to distribute in the hepatopancreas of *S. paramamosain*, and its mRNA expression greatly increased after the stimulation of LPS and Poly (I:C), which suggested that both LPS and Poly (I:C) challenges might activate *Sp*-CCAP to bind to its receptor in the hepatopancreas to participate in immune responses. Interestingly, previous studies have reported similar results in other species. For example, HPR1 gene in the hepatopancreas of *P. clarkii* was significantly up-regulated by stimulation with *Aeromonas hydrophila* (53), the mRNA of *LPSenhR-1* was significantly up-regulated after LPS stimulation in rainbow trout *Oncorhynchus mykiss* (55), and Poly (I:C) stimulation induced significantly higher neurokinin-2 receptor mRNA expression in human dendritic cell (56). It is well-known that the neuroendocrine system regulates the immune responses by releasing neuropeptide hormones, whereas the immune system activates the neuroendocrine system by secreting cytokines, thus forming a circular network of neuroendocrine and immune regulation (57). *Sp*-CCAPR showed two expression peaks at 3 and 24 h after Poly (I:C) stimulation; it is speculated that

Sp-CCAP/*Sp*-CCAPR can respond quickly to Poly (I:C) stimulation and be indirectly affected by Poly (I:C)-induced immune factor activation.

In this study, the immunomodulatory effect of *Sp*-CCAP was further studied by *in vivo* injection and *in vitro* culture experiment. In the *in vivo* experiment, *Sp*-CCAP was found to significantly induce the expression of its receptor *Sp-CCAPR*, P38 MAPKs (*Sp-P38*), and nuclear transcription factor NF-κBs (*Sp-Dorsal* and *Sp-Relish*) in the hepatopancreas, which suggested that by stimulating the expression of *Sp*-CCAPR, *Sp*-CCAP likely induced increased amount of *Sp*-CCAPR on the cell membrane in the hepatopancreas, thus greatly enhancing the activity of signaling pathway mediated by *Sp*-CCAP. On the other hand, P38 MAPKs as a member of MAPK superfamily, can associate extracellular signals with intracellular mechanisms (58) and play a crucial role in the inflammatory response and the host defense against pathogen infections (59). The NF-κB pathway is an essential pathway for the innate immune response to pathogen invasion in both vertebrates and invertebrates (60). Therefore, in order to explore the possibility that immune molecules regulated by *Sp*-CCAP and its receptor *Sp*-CCAPR signaling pathway, the mRNA expression levels of several immune molecules with pro-inflammatory and antibacterial properties, that is, *Sp-IL16*, *Sp-TNFSF*, and AMPs, were detected. Of these immune molecules, AMPs are key effector molecules that induce innate immunity in various invertebrates (61). As one of the AMP family, the anti-LPS factor (ALF) is well-known to possess a wide range of antibacterial, antifungal, and antiviral properties (62). Another AMP, lysozyme, reportedly protects organisms by destroying the cell walls of infectious bacterial pathogens (63). Meanwhile, interleukin-16 (IL-16), a pleiotropic cytokine, plays essential roles in the regulation of various innate immune processes (64), and has been reported to play a strong positive role in antibacterial responses in *L. vannamei* (65). Relish and Dorsal are invertebrate NF-κB homologs, they function as essential transcription factors on mediating the activation of AMP genes in crustaceans (66), and the expression of IL-16 is dependent on the NF-κB pathway (67). The P38 MAPK plays a key role in a variety of immune responses by regulating the production of pro-inflammatory cytokines, including TNFs and IFNs (58, 59). In this study, the up-regulation of nuclear transcription factor NF-κBs, pro-inflammatory factor IL-16, and AMP genes suggests that *Sp*-CCAP might influence the expressions of *Sp-IL16* and AMPs by mediating the NF-κB signaling pathway, whereas the up-regulation of *Sp-P38* and *Sp-TNFSF* suggests that *Sp*-CCAP might affect the expression of *Sp-TNFSF* by mediating the P38 MAPK signaling pathway. Together, these results suggest that *Sp*-CCAP possibly activates and induces inflammatory and antimicrobial responses in *S. paramamosain*. Interestingly, the *Sp*-CCAPR expression level was not significantly elevated at 24 h post *Sp*-CCAP mature peptide injection, whereas *Sp-Dorsal*, S*p-Relish*, and *Sp-ALF1* expression levels were still up-regulated. This phenomenon may be explained by the possible accumulation of sufficient receptor proteins on the cell membrane, thus promoting these gene expressions.

The results of the *in vitro* experiment were similar to those of *in vivo* experiment; that is, adding *Sp*-CCAP mature peptide to the hepatopancreas cultures could promote the expressions of signal pathway-related genes and immune effector molecules. They provided further evidence that *Sp*-CCAP was involved in hepatopancreas immunity of *S. paramamosain.* Moreover, NO is an important gaseous signal molecule that plays anti-bacterial and inflammatory roles in invertebrates (68). In the present study, it was found that NO concentration in the hepatopancreas culture medium increased significantly when *Sp*-CCAP mature peptide was added at 10^{-8} mol/L. It provided additional evidence from the point of view of gaseous signal molecules that *Sp*-CCAP likely plays a significant role in the hepatopancreas immunity of *S. paramamosain*.

Finally, the *in vitro* bacterial clearance experiment showed that the up-regulation of immune effector molecules in the hepatopancreas mediated by *Sp*-CCAP signaling pathway could effectively resist bacterial infection. Indeed, the results demonstrated for the first time that neuropeptides play antibacterial roles in the hepatopancreas of a crustacean, likely *via* regulating immune-effector molecules.

In invertebrates, on the one hand, when neuropeptides act on immune cells, neuropeptide receptors on the membrane can activate the G-protein $G\alpha_s/G\alpha_i$ subunit and react with adenylate cyclase to increase or decrease intracellular cAMP concentration (69). On the other hand, when neuropeptides bind to Go/Gq protein-coupled receptors on immune cells, they can activate the activity of phospholipase C, thereby altering intracellular Ca^{2+} concentration (69). The changes of these secondary messengers (cAMP and Ca^{2+}) activate a series of signaling pathways, such as MAPK (JNK, ERK, and P38) and NF-κB signaling pathway, through cascade amplification. They synergistically promote the release of inflammatory factors and immune factors (70). CCAPR was first identified in *Drosophila* but has since been identified in many other insects; it is known that the involvement of CCAPR in various physiological processes, such as molt and heartbeat regulation, is mediated by CCAP (35, 36, 71). A previous study has shown that the binding of *Sp*-CCAP to *Sp*-CCAPR activated the cAMP level and Ca^{2+} signal response in the cytoplasm of *S. paramamosain* (38). Therefore, in this study, activating P38 MAPKs and NF-κB signaling pathways by the binding of *Sp*-CCAP to *Sp*-CCAPR were likely *via* cAMP and Ca^{2+} concentration changes in hepatopancreas cells, which promoted the expression of *Sp-IL16*, *Sp-TNFSF*, *Sp-LYZ*, *Sp-ALF1*, *Sp-ALF4*, and *Sp-ALF5*, hence enhancing the immune responses of *S. paramamosain* to pathogen infection.

In summary, the present study provides the first evidence that CCAP plays an immunomodulatory role in the hepatopancreas in a crustacean. It suggests that CCAP might activate immune effector molecules mediated by the P38 MAPK pathway and NF-κB pathway in the hepatopancreas to resist pathogen infection. This study also potentially provides a new strategy for disease control from the perspective of neuroendocrine immunity for the mud crab aquaculture.

DATA AVAILABILITY STATEMENT

The datasets generated for this study can be found in the National Center for Biotechnology Information GenBank Accession MN923209.

ETHICS STATEMENT

All the animals used in this study have been approved by the Animal Ethics Committee of Xiamen University.

AUTHOR CONTRIBUTIONS

YW and HY designed the experiments. YW and DL performed the experiments. YW and ZX analyzed the data. XG contributed reagents/materials tools. YW and HY contributed to the discussion. YW wrote the manuscript. HY and CZ revised the manuscript. All the authors read and approved the final manuscript.

FUNDING

This study was supported by the Natural Science Foundation of China (Nos. 31972765 and 31772827).

ACKNOWLEDGMENTS

We thank all laboratory members for their constructive suggestions and discussions, as well as the reviewers for their valuable comments.

REFERENCES

1. Besedovsky H, Sorkin E. Network of immune-neuroendocrine interactions. *Clin Exp Immunol.* (1977) 7:1–12.
2. Berczi I, Chalmers IM, Nagy E, Warrington RJ. The immune effects of neuropeptides. *Baillières Clin Rheumatol.* (1996) 10:227–57. doi: 10.1016/S0950-3579(96)80016-1
3. Merighi, A. Neuropeptides and coexistence. In: Squire LR, editor. *Encyclopedia of Neuroscience.* Oxford: Academic Press (2009). p. 843–49. doi: 10.1016/B978-008045046-9.01467-4
4. Bockaert J, Claeysen S, Bécamel C, Pinloche S, Dumuis A. G protein-coupled receptors: dominant players in cell–cell communication. *Int Rev Cytol.* (2002) 212:63–132. doi: 10.1016/S0074-7696(01)12004-8
5. Delgado M, Martinez C, Pozo D, Calvo JR, Leceta J, Ganea D, et al. Vasoactive intestinal peptide (VIP) and pituitary adenylate cyclase-activation polypeptide (PACAP) protect mice from lethal endotoxemia through the inhibition of TNF-α and IL-6. *J Immunol.* (1999) 162:1200–05.
6. Martinez C, Abad C, Delgado M, Arranz A, Juarranz MG, Rodriguez-Henche N, et al. Anti-inflammatory role in septic shock of pituitary adenylate cyclase-activating polypeptide receptor. *Proc Natl Acad Sci USA.* (2002) 99:1053–58. doi: 10.1073/pnas.012367999
7. Gonzalez-Rey E, Chorny A, Varela N, Robledo G, Delgado M. Urocortin and adrenomedullin prevent lethal endotoxemia by down-regulating the inflammatory response. *Am J Pathol.* (2006) 168:1921–30. doi: 10.2353/ajpath.2006.051104
8. Peña B, Isla A, Haussmann D, Figueroa J. Immunostimulatory effect of salmon prolactin on expression of toll-like receptors in *Oncorhynchus mykiss* infected with *Piscirickettsia salmonis. Fish Physiol Biochem.* (2016) 42:509–16. doi: 10.1007/s10695-015-0155-5
9. Kono T, Ida T, Kawahara N, Watanabe F, Biswas J, Sato T, et al. Identification and immunoregulatory function of neuromedin U (Nmu) in the Japanese pufferfish, *Takifugu rubripes. Dev Comp Immunol.* (2017) 73:246–56. doi: 10.1016/j.dci.2017.03.007
10. Li M, Wang M, Wang W, Wang L, Liu Z, Sun J, et al. The immunomodulatory function of invertebrate specific neuropeptide FMRFamide in oyster *Crassostrea gigas. Fish Shellfish Immunol.* (2019) 88:480–88. doi: 10.1016/j.fsi.2019.03.023
11. Bachtel ND, Hovsepian GA, Nixon DF, Eleftherianos I. Allatostatin C modulates nociception and immunity in *Drosophila. Sci Rep.* (2018) 8:7501. doi: 10.1038/s41598-018-25855-1
12. Wanlem S, Supamattaya K, Tantikitti C, Prasertsan P, Graidist P. Expression and applications of recombinant crustacean hyperglycemic hormone from eyestalks of white shrimp (*Litopenaeus vannamei*) against bacterial infection. *Fish Shellfish Immunol.* (2011) 30:877–85. doi: 10.1016/j.fsi.2011.01.014
13. Wang L, Chen H, Xu J, Xu Q, Wang M, Zhao D, et al. Crustacean hyperglycemic hormones directly modulate the immune response of hemocytes in shrimp *Litopenaeus vannamei. Fish Shellfish Immunol.* (2017) 62:164–74. doi: 10.1016/j.fsi.2017.01.007
14. Zuo H, Yuan J, Niu S, Yang L, Weng S, He J, et al. A molting-inhibiting hormone-like protein from Pacific white shrimp *Litopenaeus vannamei* is involved in immune responses. *Fish Shellfish Immunol.* (2018) 72:544–51. doi: 10.1016/j.fsi.2017.11.031
15. Zhou M, Abbas MN, Kausar S, Jiang C, Dai L. Transcriptome profiling of red swamp crayfish (*Procambarus clarkii*) hepatopancreas in response to lipopolysaccharide (LPS) infection. *Fish Shellfish Immunol.* (2017) 71:423–33. doi: 10.1016/j.fsi.2017.10.030
16. Roszer, T. The invertebrate midintestinal gland ("hepatopancreas") is an evolutionary forerunner in the integration of immunity and metabolism. *Cell Tissue Res.* (2014) 358:685–95. doi: 10.1007/s00441-014-1985-7
17. Duan Y, Liu P, Li J, Li J, Chen P. Expression profiles of selenium dependent glutathione peroxidase and glutathione S-transferase from *Exopalaemon carinicauda* in response to *Vibrio* anguillarum and WSSV challenge. *Fish Shellfish Immunol.* (2013) 35:661–70. doi: 10.1016/j.fsi.2013.05.016
18. Cao J, Wang Z, Zhang Y, Qu F, Guo L, Zhong M, et al. Identification and characterization of the related immune-enhancing proteins in crab *Scylla paramamosain* stimulated with rhubarb polysaccharides. *Mol Immunol.* (2014) 57:263–73. doi: 10.1016/j.molimm.2013.10.003
19. Duan Y, Liu P, Li J, Wang Y, Li J, Chen P. Molecular responses of calreticulin gene to *Vibrio anguillarum* and WSSV challenge in the ridgetail white prawn *Exopalaemon carinicauda. Fish Shellfish Immunol.* (2014) 36:164–71. doi: 10.1016/j.fsi.2013.10.024
20. Zheng J, Mao Y, Su Y, Wang J. Effects of nitrite stress on mRNA expression of antioxidant enzymes, immune-related genes and apoptosis-related proteins in *Marsupenaeus japonicus. Fish Shellfish Immunol.* (2016) 58:239–52. doi: 10.1016/j.fsi.2016.08.058
21. Bao S, Zheng Z, Aweya JJ, Yao D, Li S, Sun C, et al. MicroRNA-589-5p modulates the expression of hemocyanin as part of the anti-WSSV immune response in *Litopenaeus vannamei. Dev Comp Immunol.* (2020) 107:103642. doi: 10.1016/j.dci.2020.103642
22. Ren X, Liu P, Li J. Comparative transcriptomic analysis of *Marsupenaeus japonicus* hepatopancreas in response to *Vibrio parahaemolyticus* and white spot syndrome virus. *Fish Shellfish Immunol.* (2019) 87:755–64. doi: 10.1016/j.fsi.2019.02.030
23. Stangier J, Hilbich C, Beyreuther K, Keller R. Unusual cardioactive peptide (CCAP) from pericardial organs of the shore crab *Carcinus maenas. Proc Natl Acad Sci USA.* (1987) 84:575–79. doi: 10.1073/pnas.84.2.575
24. Dircksen H, Homberg U. Crustacean cardioactive peptide-immunoreactive neurons innervating brain neuropils, retrocerebral complex and stomatogastric nervous system of the locust, *Locusta migratoria. Cell Tissue Res.* (1995) 279:495–515. doi: 10.1007/BF00318163
25. Dircksen H, Keller R. Immunocytochemical localization of CCAP, a novel crustacean cardioactive peptide, in the nervous system

of the shore crab, *Carcinus maenas* L. *Cell Tissue Res.* (1988) 254:347–60. doi: 10.1007/BF00225807
26. Matsui T, Sakai T, Satake H, Takeda M. The pars intercerebralis affects digestive activities of the American cockroach, *Periplaneta americana*, *via* crustacean cardioactive peptide and allatostatin-A. *J Insect Physiol.* (2013) 59:33–37. doi: 10.1016/j.jinsphys.2012.06.010
27. Mikani A, Watari Y, Takeda M. Brain-midgut cross-talk and autocrine metabolastat *via* the sNPF/CCAP negative feed-back loop in the American cockroach, *Periplaneta americana*. *Cell Tissue Res.* (2015) 362:481–96. doi: 10.1007/s00441-015-2242-4
28. Chen T, Ren C, Wang Y, Gao Y, Wong NK, Zhang L. Crustacean cardioactive peptide (CCAP) of the Pacific white shrimp (*Litopenaeus vannamei*): molecular characterization and its potential roles in osmoregulation and freshwater tolerance. *Aquaculture.* (2016) 451:405–12. doi: 10.1016/j.aquaculture.2015.10.005
29. Shan D, Fu H, Qiao H, Sun S, Zhang W, Jin S. Molecular cloning, characterization, and expression of crustacean cardioactive peptide in oriental river prawn, *Macrobrachium nipponense*, during acute hypoxia and reoxygenation. *J World Aquacult Soc.* (2018) 49:356–65. doi: 10.1111/jwas.12502
30. Nichols R, Kaminski S, Walling E, Zornik E. Regulating the activity of a cardioacceleratory peptide. *Peptides.* (1999) 20:1153–58. doi: 10.1016/S0196-9781(99)00118-7
31. Fort TJ, Garcia-Crescioni K, Agricola HJ, Brezina V, Miller MW. Regulation of the crab heartbeat by crustacean cardioactive peptide (CCAP): central and peripheral actions. *J Neurophysiol.* (2007) 97:3407–20. doi: 10.1152/jn.00939.2006
32. Lange AB, Patel K. The presence and distribution of crustacean cardioactive peptide in the central and peripheral nervous system of the stick insect, *Baculum extradentatum*. *Regul Pept.* (2005) 129:191–201. doi: 10.1016/j.regpep.2005.02.011
33. Silva RD, Lange AB. The association of crustacean cardioactive peptide with the spermatheca of the African migratory locust, *Locusta migratoria*. *J Insect Physiol.* (2006) 52:399–409. doi: 10.1016/j.jinsphys.2006.01.006
34. Donini A, Lange AB. The effects of crustacean cardioactive peptide on locust oviducts are calcium-dependent. *Peptides.* (2002) 23:683–91. doi: 10.1016/S0196-9781(01)00662-3
35. Lee D, Broeck JV, Lange AB. Identification and expression of the CCAP receptor in the chagas' disease vector, *Rhodnius prolixus*, and its involvement in cardiac control. *PLoS ONE.* (2013) 8:e68897. doi: 10.1371/journal.pone.0068897
36. Arakane Y, Li B, Muthukrishnan S, Beeman RW, Kramer KJ, Park Y. Functional analysis of four neuropeptides, EH, ETH, CCAP and bursicon, and their receptors in adult ecdysis behavior of the red flour beetle, *Tribolium castaneum*. *Mech Dev.* (2008) 125:984–95. doi: 10.1016/j.mod.2008.09.002
37. Bao C, Yang Y, Huang H, Ye H. Neuropeptides in the cerebral ganglia of the mud crab, *Scylla paramamosain*: transcriptomic analysis and expression profiles during vitellogenesis. *Sci Rep.* (2015) 5:17055. doi: 10.1038/srep17055
38. Bao C, Yang Y, Zeng C, Huang H, Ye H. Identifying neuropeptide GPCRs in the mud crab, *Scylla paramamosain*, by combinatorial bioinformatics analysis. *Gen Comp Endocrinol.* (2018) 269:122–30. doi: 10.1016/j.ygcen.2018.09.002
39. Li Y, Xia X, Wu Q, Liu W, Lin Y. Infection with *Hematodinium* sp. in mud crabs Scylla serrata cultured in low salinity water in southern China. *Dis Aquatic Organ.* (2008) 82:145–50. doi: 10.3354/dao01988
40. Li S, Zhang Z, Li C, Zhou L, Liu W, Li Y. Molecular cloning and expression profiles of nitric oxide synthase (NOS) in mud crab *Scylla paramamosain*. *Fish Shellfish Immunol.* (2012) 32:503–12. doi: 10.1016/j.fsi.2011.12.002
41. Wei X, Wang L, Sun W, Zhang M, Ma H, Zhang Y. C-type lectin B (*Sp*CTL-B) regulates the expression of antimicrobial peptides and promotes phagocytosis in mud crab S*cylla paramamosain*. *Dev Comp Immunol.* (2018) 84:213–29. doi: 10.1016/j.dci.2018.02.016
42. Gu WB, Liu ZP, Zhou YL, Li B, Wang LZ, Dong WR. The nuclear factor interleukin 3-regulated (NFIL3) transcription factor involved in innate immunity by activating NF-κB pathway in mud crab *Scylla paramamosain*. *Dev Comp Immunol.* (2019) 101:103452. doi: 10.1016/j.dci.2019.103452
43. Chen B, Fan DQ, Zhu KX, Shan ZG, Chen FY, Wang KJ. Mechanism study on a new antimicrobial peptide Sphistin derived from the N-terminus of crab histone H2A identified in haemolymphs of Scylla paramamosain. *Fish Shellfish Immunol.* (2015) 47, 833–846. doi: 10.1016/j.fsi.2015.10.010
44. Xie JW, Cheng CH, Ma HL, Feng J, Su YL, Guo ZX. Molecular characterization, expression and antimicrobial activities of a c-type lysozyme from the mud crab, Scylla paramamosain. *Dev Comp Immunol.* (2019) 98, 54–64. doi: 10.1016/j.dci.2019.04.002
45. Yu Z, Geng Y, Huang A, Wang K, Huang X, Wang J. Molecular characterization of a p38 mitogen-activated protein kinase gene from Scylla paramamosain and its expression profiles during pathogenic challenge. *J Invertebr Pathol.* (2017) 144, 32–36. doi: 10.1016/j.jip.2017.01.001
46. Wang Y, Chen Y, Han K, Zou Z, Zhang Z. A vasa gene from green mud crab *Scylla paramamosain* and its expression during gonadal development and gametogenesis. *Mol Biol Rep.* (2012) 39:4327–35. doi: 10.1007/s11033-011-1220-5
47. Liu J, Liu A, Liu F, Huang H, Ye H. Role of neuroparsin 1 in vitellogenesis in the mud crab, *Scylla paramamosain*. *Gen Comp Endocrinol.* (2020) 285:113248. doi: 10.1016/j.ygcen.2019.113248
48. An S, Dong S, Wang Q, Li S, Gilbert LI, Stanley D. Insect neuropeptide bursicon homodimers induce innate immune and stress genes during molting by activating the NF-κB transcription factor Relish. *PLoS ONE.* (2012) 7:e34510. doi: 10.1371/journal.pone.0034510
49. Bao C, Yang Y, Huang H, Ye H. Inhibitory role of the mud crab short neuropeptide F in vitellogenesis and oocyte maturation *via* autocrine/paracrine signaling. *Front Endocrinol.* (2018) 9:390. doi: 10.3389/fendo.2018.00390
50. Johansson MW, Keyser P, Sritunyalucksana K, Söderhäll, K. Crustacean haemocytes and haematopoiesis. *Aquaculture.* (2000) 191:45–52. doi: 10.1016/S0044-8486(00)00418-X
51. Qi Y, Huang J, Li M, Wu Y, Xia R, Ye G. Serotonin modulates insect hemocyte phagocytosis *via* two different serotonin receptors. *Elife.* (2016) 5:e12241. doi: 10.7554/eLife.12241
52. Qin X, Jin X, Zhou K, Li H, Wang Q, Li W, et al. EsGPCR89 regulates cerebral antimicrobial peptides through hemocytes in *Eriocheir sinensis*. *Fish Shellfish Immunol.* (2019) 95:151–62. doi: 10.1016/j.fsi.2019.10.015
53. Dong C, Zhang P. A putative G protein-coupled receptor involved in innate immune defense of *Procambarus clarkii* against bacterial infection. *Comp Biochem Physiol Mol Integr Physiol.* (2012) 161:95–101. doi: 10.1016/j.cbpa.2011.09.006
54. Taghert PH, Nitabach MN. Peptide neuromodulation in invertebrate model systems. *Neuron.* (2012) 76:82–97. doi: 10.1016/j.neuron.2012.08.035
55. Kiryu I, Köllner B, Kuroda A, Ototake M, Dijkstra JM. A new putative G-protein coupled receptor gene associated with the immune system of rainbow trout (*Oncorhynchus mykiss*). *Fish Shellfish Immunol.* (2003) 15:117–127. doi: 10.1016/S1050-4648(02)00143-2
56. Kitamura H, Kobayashi M, Wakita D, Nishimura T. Neuropeptide signaling activates dendritic cell-mediated type 1 immune responses through neurokinin-2 receptor. *J Immunol.* (2012) 188:4200–08. doi: 10.4049/jimmunol.1102521
57. Verburg-van Kemenade BML, Van der Aa LM, Chadzinska M. Neuroendocrine-immune interaction: regulation of inflammation via G-protein coupled receptors. *Gen Comp Endocrinol.* (2013) 188:94–101. doi: 10.1016/j.ygcen.2012.11.010
58. Ono K, Han J. The p38 signal transduction pathway activation and function. *Cell Signal.* (2000) 12:1–13. doi: 10.1016/S0898-6568(99)00071-6
59. Sun J, Wang L, Wu Z, Han S, Wang L, Li M. P38 is involved in immune response by regulating inflammatory cytokine expressions in the Pacific oyster *Crassostrea gigas*. *Dev Comp Immunol.* (2019) 91:108–114. doi: 10.1016/j.dci.2018.10.011
60. Jiang M, Tu D, Gu W, Zhou Y, Zhu Q, Guo X. Identification and functional analysis of inhibitor of NF-κB kinase (IKK) from *Scylla paramamosain*: the first evidence of three IKKs in crab species and their expression profiles under biotic and abiotic stresses. *Dev Comp Immunol.* (2018) 84:199–212. doi: 10.1016/j.dci.2018.02.014
61. Diamond G, Beckloff N, Weinberg A, Kisich KO. The roles of antimicrobial peptides in innate host defense. *Curr Pharm Des.* (2009) 15:2377–92. doi: 10.2174/138161209788682325

62. Li J, Zhang Y, Zhang Y, Mao F, Xiang Z, Xiao S. The first invertebrate NFIL3 transcription factor with role in immune defense identified from the Hong Kong oyster, *Crassostrea hongkongensis*. *Dev Comp Immunol.* (2017) 76:1–8. doi: 10.1016/j.dci.2017.05.011
63. Chen T, Ren C, Wang Y, Luo P, Jiang X, Huang W. Molecular cloning, inducible expression and antibacterial analysis of a novel i-type lysozyme (lyz-i2) in Pacific white shrimp, *Litopenaeus vannamei*. *Fish Shellfish Immunol.* (2016) 54:197–203. doi: 10.1016/j.fsi.2016.04.008
64. Center DM, Cruikshank W. Modulation of lymphocyte migration by human lymphokines. I. Identification and characterization of chemoattractant activity for lymphocytes from mitogen-stimulated mononuclear cells. *J Immunol.* (1982) 128:2563–8.
65. Liang Q, Zheng J, Zuo H, Li C, Niu S, Yang L. Identification and characterization of an interleukin-16-like gene from Pacific white shrimp *Litopenaeus vannamei*. *Dev Comp Immunol.* (2017) 74:49–59. doi: 10.1016/j.dci.2017.04.011
66. Li F, Xiang J. Recent advances in researches on the innate immunity of shrimp in China. *Dev Comp Immunol.* (2013) 39:11–26. doi: 10.1016/j.dci.2012.03.016
67. Glas J, Török HP, Unterhuber H, Radlmayr M, Folwaczny C. The- 295T-to-C promoter polymorphism of the IL-16 gene is associated with crohn's disease. *Clin Immunol.* (2003) 106:197–200. doi: 10.1016/S1521-6616(03)00021-4
68. Chen T, Wong NK, Jiang X, Luo X, Zhang L, Yang D. Nitric oxide as an antimicrobial molecule against *Vibrio harveyi* infection in the hepatopancreas of Pacific white shrimp, *Litopenaeus vannamei*. *Fish Shellfish Immunol.* (2015) 42:114–20. doi: 10.1016/j.fsi.2014.10.042
69. Xu G, Wu S, Wu Y, Gu G, Fang Q, Ye G. *De novo* assembly and characterization of central nervous system transcriptome reveals neurotransmitter signaling systems in the rice striped stem borer, *Chilo suppressalis*. *BMC Genomics.* (2015) 16:525. doi: 10.1186/s12864-015-1742-7
70. Gein SV, Baeva TA. Endogenous opioid peptides in regulation of innate immunity cell functions. *Biochemistry*. (2011) 76:309–19. doi: 10.1134/S0006297911030035
71. Cazzamali G, Hauser F, Kobberup S, Williamson M, Grimmelikhuijzen CJ. Molecular identification of a *Drosophila* G protein-coupled receptor specific for crustacean cardioactive peptide. *Biochem Biophys Res Commun.* (2003) 303:146–52. doi: 10.1016/S0006-291X(03)00302-4

Conflict of Interest: The authors declare that the research was conducted in the absence of any commercial or financial relationships that could be construed as a potential conflict of interest.

Copyright © 2020 Wei, Lin, Xu, Gao, Zeng and Ye. This is an open-access article distributed under the terms of the Creative Commons Attribution License (CC BY). The use, distribution or reproduction in other forums is permitted, provided the original author(s) and the copyright owner(s) are credited and that the original publication in this journal is cited, in accordance with accepted academic practice. No use, distribution or reproduction is permitted which does not comply with these terms.

frontiers in Immunology

ORIGINAL RESEARCH
published: 30 June 2020
doi: 10.3389/fimmu.2020.01378

Atlantic Salmon Pre-smolt Survivors of *Renibacterium salmoninarum* Infection Show Inhibited Cell-Mediated Adaptive Immune Response and a Higher Risk of Death During the Late Stage of Infection at Lower Water Temperatures

Marco Rozas-Serri[1,2]*, *Carlos Lobos*[3], *Rodolfo Correa*[1], *Ricardo Ildefonso*[1], *Jorge Vásquez*[1], *Ariel Muñoz*[1], *Lucerina Maldonado*[1], *Victoria Jaramillo*[1], *Darling Coñuecar*[1], *Camila Oyarzún*[1], *Romina Walker*[1], *Carolina Navarrete*[1], *Jorge Gayosa*[1], *Patricio Mancilla*[1], *Andrea Peña*[1], *Carolina Senn*[1] and *Francisco Schwerter*[3]

[1] Laboratorio Pathovet Ltda., Puerto Montt, Chile, [2] Newenko Group SpA., Puerto Montt, Chile, [3] Hendrix Genetics Aquaculture S.A., Puerto Varas, Chile

Bacterial kidney disease (BKD) is widespread in many areas of the world and can cause substantial economic losses for the salmon aquaculture industry. The objective of this study was to investigate the pathophysiological response and gene expression profiles related to the immune response at different water temperatures and to identify the best immunopathological biomarkers to define a phenotype of resistance to BKD. The abundance of *msa* transcripts of *R. salmoninarum* in the head kidney was significantly higher in infected fish at 11°C. *R. salmoninarum* induced significantly more severe kidney lesions, anemia and impaired renal function at 11°C. In addition, the expression pattern of the genes related to humoral and cell-mediated immune responses in infected fish at 11 and 15°C was very similar, although *R. salmoninarum* induced a significantly greater downregulation of the adaptive immune response genes at the lower water temperature. These results could be due to a suppressed host response directly related to the lowest water temperature and/or associated with a delayed host response related to the lowest water temperature. Although no significant differences in survival rate were observed, fish infected at the lowest temperature showed a higher probability of death and delayed the mortality curve during the late stage of infection (35 days after infection). Thirty-three immunopathological biomarkers were identified for potential use in the search for a resistance phenotype for BKD, and eight were genes related specifically to the adaptive cell-mediated immune response.

Keywords: ***Renibacterium salmoninarum*, BKD, cell-mediated, immune response, water temperature**

OPEN ACCESS

Edited by:
Monica Hongroe Solbakken, University of Oslo, Norway

Reviewed by:
Javier Santander, Memorial University of Newfoundland, Canada
Kevin R. Maisey, University of Santiago of Chile, Chile
Mark Polinski, Department of Fisheries and Oceans, Canada

***Correspondence:**
Marco Rozas-Serri
marco.rozas@pathovet.cl

Specialty section:
This article was submitted to Comparative Immunology, a section of the journal Frontiers in Immunology

Received: *04 March 2020*
Accepted: *29 May 2020*
Published: *30 June 2020*

Citation:
Rozas-Serri M, Lobos C, Correa R, Ildefonso R, Vásquez J, Muñoz A, Maldonado L, Jaramillo V, Coñuecar D, Oyarzún C, Walker R, Navarrete C, Gayosa J, Mancilla P, Peña A, Senn C and Schwerter F (2020) Atlantic Salmon Pre-smolt Survivors of Renibacterium salmoninarum Infection Show Inhibited Cell-Mediated Adaptive Immune Response and a Higher Risk of Death During the Late Stage of Infection at Lower Water Temperatures. Front. Immunol. 11:1378. doi: 10.3389/fimmu.2020.01378

INTRODUCTION

Bacterial kidney disease (BKD) or Renibacteriosis is caused by the facultative intracellular bacteria *Renibacterium salmoninarum*, which is widespread in many areas of the world and can cause substantial economic losses for the salmon aquaculture industry (1, 2). *R. salmoninarum* infection is characterized by chronic disease progression and infects both freshwater and saltwater salmonid life stages (3). Chronic BKD is associated with granulomatous lesions and white to gray-white abscesses in internal organs, such as the kidney (4, 5). Periods of stress, such as during smoltification or environmental change, can increase the disease severity and clinical signs (3). Although vaccines against the bacterium exist, BKD is still prevalent in sea cages due to poor efficacy of vaccines and antibiotics (6).

Renibacterium salmoninarum has been shown to be highly clonal with limited phenotypic and genotypic variation (7–11). However, whole-genome single-nucleotide polymorphism-based comparisons identified a deep phylogenetic division of *R. salmoninarum* in the population, which provides evidence for the transatlantic transmission and spread over decadal scales (1). Specific to Chile, multiple introductions of *R. salmoninarum* into the country from global sources over 30 years have been reported based on whole-genome sequencing (2).

Water temperature is one of the most important factors that influence the dynamics of BKD because it strongly regulates the replication rate of the bacteria and the immune response of the fish (12). Fish infected with *R. salmoninarum* can survive and even recover, although whether infected fish can completely eliminate the infection is unknown (12–14). Some studies indicate that higher water temperatures increase BKD mortality (13), while other studies have reported the opposite (12, 15). In addition to the effect of temperature on pathogen replication and host immunity, changes in temperature are an important source of stress that can alter the pathogen-host interaction (12). In addition, *R. salmoninarum* infections are complicated and mortality is only one of the possible outcomes of a chronic infection (12). How *R. salmoninarum* modulates the fish's immune response and what factors contribute to the immunopathology of the disease remain poorly understood.

The systemic nature of the BKD infection has been demonstrated, and the host cytokine and cytokine-related genes are affected during the early stage of *R. salmoninarum* infection in rainbow trout (*Oncorhynchus mykiss*) (16) and Chinook salmon (*Oncorhynchus tshawytscha*) (17). Some studies have examined immune gene expression changes early after *R. salmoninarum* infection or after vaccination and demonstrated the differential regulation of key immune genes related to inflammatory response (16–20). Eslamloo et al. (20) showed that formalin-killed *R. salmoninarum* induced the expression of genes associated with inflammation and cytokine responses but suppressed the expression of genes that have putative roles as a cytokine receptor and kinase regulator. However, no information is available regarding the immunopathological and cell-mediated immune response during the late stage of infection in Atlantic salmon (Salmo salar) kept at different water temperatures (11 and 15°C).

To investigate the late stage of the interaction of *R. salmoninarum* with infected surviving fish, we studied the pathology and kinetics of gene expression related to the innate and adaptive immune response to identify and select the best and most predictive immunopathological biomarkers, with the goal of defining more robust phenotypes of resistance of Atlantic salmon to BKD.

MATERIALS AND METHODS

Renibacterium salmoninarum Isolate

An *R. salmoninarum* strain (Rs2) previously isolated from a commercial farm located in the Magallanes Region of Chile and belonging to Elanco was used. The Rs2 isolate was grown in SKDM medium at 15°C ± 2°C for 15 days. Bacterial colonies were collected from the plates and suspended in 1 ml of 0.9% saline solution. The absorbance at 625 nm (DO_{625}) was measured using a spectrophotometer (Biobase Brand Model BK-UV1000) to quantify the biomass produced. Ten milliliters of inoculum of Rs2 with an OD_{625} of 1.0 each was obtained. This OD_{625} corresponded to approximately 6.84×10^6 u.f.c./mL.

Renibacterium salmoninarum Challenge

The challenge was carried out at the Elanco Animal Health experimental hatchery (Ruta 5 Sur, Km 1012, Puerto Varas, Chile). Non-vaccinated Atlantic salmon, *Salmo salar* L., fry (Hendrix Genetics Aquaculture Chile), with an average size of 25 g, were used for the challenge. Prior to challenge, 30 fish were randomly tested and screened to ensure that they were enzootic pathogen-free using PCR for piscine reovirus (PRv), infectious pancreatic necrosis virus (IPNv), infectious salmon anemia virus (ISAv), *Flavobacterium psychrophilum* and *R. salmoninarum* (21–25). Kidneys from these fish were also histologically examined for microscopic lesions before the challenge.

Two Atlantic salmon stocks were acclimatized at 11 and 15°C for 2 weeks. Then, an intraperitoneal (i.p.) challenge was conducted in two identical independent systems, each with four 100-liter water tanks containing freshwater in which the water flow was regulated to 1.5 changes per hour (Lh^{-1}). All fish were identified using pit-tags and distributed at each treatment randomly. Each system considered three tanks (replicates) with 50 fish each injected by i.p. (0.1 mL) and a control tank with 50 fish inoculated with 0.1 mL of sterile saline (0.9%). Infected fish were kept at 11 and 15°C in the first and second system, respectively.

The fish were fed daily with commercial food. The water temperature, dissolved oxygen concentration, feeding and mortality were recorded daily. The experiment was performed over 55 days, and tissue and blood samples were taken from the surviving fish in each tank. In addition, the weight and length of each fish were recorded at the beginning and end of the study period to calculate the condition factor (k), the specific growth rate (SGR) and the thermal growth coefficient (TGC). Elanco's Animal Welfare Program covers all of Elanco's animal facilities worldwide and ensures the care and use of all animals. Therefore, the study that was completed at the Aquarium Facility in Puerto Varas was reviewed and approved by the Elanco Global Ethical

TABLE 1 | Histopathological criteria and semi-quantitative weighting used to define hsBKD in the kidney.

Histoscore	HT hyperplasia	MMC-hyperplasia	Granulomas	Rs-like	Proliferative GNP
0	No alteration	No alteration	Without granulomas	No bacteria	No alteration
0.1–0.99	Mild hyperplasia (≤10% tissue surface)	Mild hyperplasia (≤10% tissue surface)	≤10% tissue surface	Focal presence, slightly noticeable	Parcial, focal mesangial proliferation
1.0–1.99	Moderate hyperplasia (>10% ≤50% tissue surface)	Moderate hyperplasia (>10% ≤50% tissue surface)	>10% ≤50% tissue surface	Focal presence, very evident	Global, focal mesangial proliferation
2.0–3.0	Severe hyperplasia (>50% tissue surface)	Severe hyperplasia (>50% tissue surface)	>50% tissue surface	Diffuse presence	Global, diffuse mesangial proliferation
Relative ponderation	0.09	0.09	0.54	0.18	0.1

The scoring system considers the mean of the observations of five non-overlapping high-magnitude optical fields (HMOFs, 20X) per kidney sample. GNP: glomerulonephritis; MMC: melano-macrophage centers; HT, hematopoietic tissue; Rs-like, bacteria similar to R. salmoninarum.

Committee (Institutional Animal Care and Use Committee). All efforts were made to provide the best growing conditions and minimize suffering.

Hematological and Biochemical Blood Profile

Whole blood samples were obtained from the caudal vein of each surviving fish and added to 1.5 mL heparin-lithium tubes. One part of each sample was used to perform a complete blood count test or hemogram, and the rest was centrifuged at 5,000 RPM for 5 min to obtain plasma. The concentrations of substrates, enzymes, electrolytes and minerals in the plasma were quantified using photometric, kinetic and colorimetric methods (Hitachi Cobas c311, Roche Diagnostics, Mannheim, Germany).

Histopathological Examination

Samples at 0.5 to 1 cm^3 in volume were collected from the mid-kidney and placed in 10% formalin buffer for at least 24 h. The samples were then dehydrated in a graded alcohol series and processed via a standard histological examination. Sections at 3 μm thick from each tissue were stained with hematoxylin and eosin (H&E) and analyzed by optical microscopy (Leica DM-2000, Hamburg, Germany) using the Leica Application Suite Software (LAS), Image Analysis (Leica, Hamburg, Germany) and a digital camera (Leica DFC-295, Hamburg, Germany). To provide a more unbiased analysis, a semi-quantitative indicator of tissue damage was developed. The BKD histoscore (hsBKD) considered lesions in the kidney according to the criteria described in **Table 1**. The hsBKD of each fish at the end-time sampling point was used to calculate the average histoscore ± standard deviation.

RNA Extraction

Samples at 0.5 cm^3 in volume were obtained from the head kidney, placed in tubes with RNAlater® and stored at −80°C until further analysis. All tissue samples were placed in microtubes with 1 mL TRIzol and ceramic beads and homogenized in a BeadBug® Microtube Homogenizer (Benchmark Scientific, Edison, NJ, USA) at room temperature. Then, 200 μL of chloroform:isoamyl alcohol was added, vigorously mixed and allowed to stand for 2 min before centrifuging at 4°C for 15 min at 12,000 G. The supernatant was transferred to a new tube and mixed with 400 μL of 70% ethanol. This mixture was passed through the columns with the E.Z.N.A.® Tissue RNA Kit (Omega Bio-Tek Inc., Norcross, GA, USA) according to the manufacturer's instructions for RNA extraction. Total RNA was quantified using the fluorimetry method in a Qubit™ 3.0 Fluorometer (Invitrogen™, Thermo Fisher Scientific, Wilmington, DE, USA), and the quality of the total RNA was determined by visualizing the RNA bands separated by electrophoresis in 1% agarose gels using a FlashGel™ System (Lonza Group, Allendale, NJ, USA).

Abundance of msa Transcripts of *R. salmoninarum*

The abundance of msa transcripts was determined using RT-qPCR in a StepOnePlus™ Real-Time PCR system (Applied Biosystems, Life Technologies, Waltham, MA, USA) with the Brilliant III Ultrafast RT-qPCR Master Mix kit (Agilent Technologies, Santa Clara, CA, USA). Relative quantification of mRNA of the major soluble antigen (*msa*, p57) gene of *R. salmoninarum* was performed using RT-qPCR TaqMan® as described in Suzuki and Sakai (23). The amplification was performed in a final volume of 15 μL containing 300 nM primers, 400 nM probe, 300 nM ROX (50 nM) and 100 ng total RNA. The RT-qPCR program consisted of a reverse transcription step at 50°C for 10 min, followed by 3 min of activation and denaturation at 95°C, and 45 cycles of 15 s at 95°C and 30 s at 60°C. The abundance of mRNA transcribed from the *msa* gene mRNA of *R. salmoninarum* is expressed as the relative number of copies of the gene in infected fish compared to the number of copies in the uninfected control group and was calculated as $2^{(CTuninfectedfish - CTinfectedfish)}$. Relative values of the *msa* transcripts of *R. salmoninarum* were expressed as $\log_{10}$ fold (log fold).

RT-qPCR for Immune Response Genes

The RNA extraction and relative quantification of the immune related genes was evaluated in the head kidney of fish at the end-time sampling point by normalized RT-qPCR as described by Rozas-Serri et al. (26, 27) (**Table 2**). Briefly, differential expression

TABLE 2 | Genes, primers, efficiency, correlation coefficients, and optimal annealing temperatures for the reference and target genes.

Gene name	Primers sequence (5'→3')	Accesion number	Tm (°C)	Efficiency	R^2
ifng	CTAAAGAAGGACAACCGCAG	AY795563	56	1.95	0.995
	CACCGTTAGAGGGAGAAATG				
ifga	TGCAGTATGCAGAGCGTGTG	DQ354152	60	1.91	0.999
	TCTCCTCCCATCTGGTCCAG				
il1b	ATCACCATGCGTCACATTGC	NM_001123582	58	2.05	0.997
	GTCCTTGAACTCGGTTCCCA				
il2	CATGTCCAGATTCAGTCTTCTATACACC	AM422779	60	1.95	0.998
	GAAGTGTCCGTTGTGCTGTTCTC				
il4/13	ACCACCACAAAGTGCAAGGAGTTC	FN820501	60	1.89	0.999
	CACCTGGTCTTGGCTCTTCACAAC				
il8	GGCCCTCCTGACCATTACT	NM_001140710	56	2.01	0.997
	ATGAGTCTACCAATTCGTCTGC				
il10	CGCTATGGACAGCATCCT	EF165029	55	2	0.998
	AAGTGGTTGTTCTGCGTT				
il12b	CTGAATGAGGTGGACTGGTATG	BT049114	55	2.1	0.999
	ATCGTCCTGTTCCTCCG				
il17	TGGTTGTGTGCTGTGTGTCTATGC	GW574233	60	1.92	0.99
	TTTCCCTCTGATTCCTCTGTGGG				
tgfβ	AGTTGCCTTGTGATTGTGGGA	EU082211	60	2.04	0.996
	CTCTTCAGTAGTGGTTTGTCG				
mhc1	CTGCATTGAGTGGCTGAAGA	AF508864	60	1.99	0.998
	GGTGATCTTGTCCGTCTTTC				
mhc2	TCTCCAGTCTGCCCTTCACC	BT049430	60	2.03	0.996
	GAACACAGCAGGACCCACAC				
cd4	GAGTACACCTGCGCTGTGGAAT	NM_001124539	60	2.01	0.973
	GGTTGACCTCCTGACCTACAAAGG				
cd8b	CGCACACACCTCAACAACTC	AY693394	56	1.94	0.945
	ATTGATGCGCAGTGTGAAAG				
igm	TCTGGGTTGCATTGCCACTG	CA039888	60	2.09	0.998
	GTAGCTTCCACTGGTTTGGAC				
igt	CAACACTGACTGGAACAACAAGGT	GQ907004	60	2.05	0.998
	CGTCAGCGGTTCTGTTTTGGA				
gata3	CCCAAGCGACGACTGTCT	EU418015	60	1.90	0.999
	TCGTTTGACAGTTTGCACATGATG				
stat1	GAACATGGAGGAGTCCAATGGAAGC	CA343225	60	1.93	0.990
	GGACCCTCATTTGATCTGTTGCCT				
eomes	ACCTCTCGTCGTCAGATACTG	EU418014	56	1.98	0.999
	GGACCGGTGAGTCTTTTCTTC				
tbx21	GGTAACATGCCAGGGAACAGGA	FM863825	58	2.1	0.999
	TGGTCTATTTTTAGCTGGGTGATGTCTG				
gzma	GACATCATGCTGCTGAAGTTG	BT046910	60	1.9	0.992
	TGCCACAGGGACAGGTAACG				
mpeg1	GGCAACATCACCTACTCCATAA	XM_014172502	60	2.09	0.999
	AGGTTGTTCTTGGTGCTCTC				
β-actina	ACGAGAGGTTCCGTTGTCC	BG933897	60	2.1	0.999
	GCAAGACTCCATACCGAGGA				
ELF-1α	CCCCTCCAGGACGTTTACAAA	NM_001123629	60	2	0.997
	CACACGGCCCACAGGTACA				

of selected genes was determined with the Real-Time PCR StepOnePlus^{TM} system (Applied Biosystems, Life Technologies, Waltham, MA, USA) using the Brilliant II SYBR Green qPCR Master Mix kit (Agilent Technologies, Santa Clara, CA, USA). Each amplification reaction was performed in a final volume of 15 μl, which consisted of 7.5 μl of buffer, 250 nM to 750 nM primers

depending on the gene, 300 nM ROX (50 nM) and 2 μl of cDNA diluted 1:10.

The PCR program consisted of a 10-min activation and denaturation step at 95°C, followed by 45 cycles of 15 s at 95°C, 30 s at the annealing temperature of the corresponding primers and an additional 15 s extension at 72°C. Five biological replicates were used, and each qPCR reaction was run in duplicate, including a negative control without reverse transcriptase to check for genomic DNA contamination and a negative control without template to check for primer dimers. The relative expression results were analyzed using amplification efficiencies as described by Pfaffl et al. (28). *ELF1A* and *ß-actin* were selected as housekeeping genes for gene normalization as described by Rozas-Serri et al. (26).

Statistical Analysis

A total of 400 individuals were randomly assigned to the eight experimental groups. The mortality analysis was performed using descriptive statistics and hypothesis testing. Differences in the cumulative mortality rate between groups and their replicates were determined using the chi-squared test, and differences in the meantime to mortality were analyzed using the Mann-Whitney U-test. The cumulative survival function [S(t)] was estimated with the Kaplan-Meier method (29) and separately for each water temperature. Significant differences in S(t) were determined using a Cox proportional hazards model (CPHM). The level of significance was established at $p < 0.05$.

Each variable was descriptively explored based on the time point and water temperature. The level of significance was set at $p < 0.05$. Each variable, including water temperature, was analyzed by an analysis of variance. The association degree between the variables was determined by a correlation matrix, while the dependence degree of each immunopathological variable with the abundance of msa transcripts was explored using simple linear regressions. All analyses were performed using the statistical package Stata, version 13 (StataCorp LP, College Station, TX, USA). Finally, non-parametric principal coordinate analysis (PCO) was used to assess the multivariate association of different variables from the fish response. Euclidean distance matrices for each group of variables and the data set were used. The PCO analysis was performed with the statistical package PRIMER, version 6 (PRIMER-e, Auckland, New Zealand).

RESULTS

Mean Survival Rates at the Different Water Temperatures Did Not Differ, Although the Probability of Death Was Higher, and the Mortality Curve Was Delayed in Infected Fish at Lower Temperatures

The cumulative mortalities and survival study results of fish infected with *R. salmoninarum* and kept at different water temperatures are shown in **Figure 1**. In the group infected at 15°C, the onset of mortality occurred at 15 dpi and the mean days to death was 35.5 dpi. In the stock infected at 11°C, the onset of mortality occurred at 22 dpi and the mean days to death was 38 dpi. The mean survival rates did not differ between infected fish at 11°C (21.5%) and 15°C (21.1%), although a higher probability of death was observed in infected fish at 11°C than at 15°C after 35 days postinfection (**Figure 1**). No mortality was observed in the control group.

Abundance of msa Transcripts of *R. salmoninarum* in the Kidney Is Significantly Higher in Surviving Fish Exposed to Lower Water Temperatures

Infected fish at 11°C showed a significantly higher amount of *msa* transcripts of *R. salmoninarum* in the kidney than infected fish at 15°C at 55 dpi (**Figure 2**). However, water temperature could have modulated the abundance of msa transcripts by changing the magnitude and/or timing of the host response. Thirty-three immunopathological biomarkers were significantly associated with the abundance of *msa* transcripts of *R. salmoninarum* at different water temperatures (**Table 3**). The individual values of the biomarkers analyzed in this study are presented in **Supplementary Table 1**.

R. salmoninarum Induces More Severe Kidney Damage in Surviving Fish Exposed to Lower Water Temperatures

Tissue damage was relatively mild in both groups of infected fish compared to uninfected control fish (hsBKD <1.0), but significantly higher hsBKD was observed in fish infected at 11°C than at 15°C. However, we do not know if the lower water temperature modulated the presentation time and/or the severity of kidney damage. The most frequent microscopic findings in the kidneys were hematopoietic tissue hyperplasia, melano-macrophage centers hyperplasia, granulomas BKD-like and proliferative glomerulonephritis (**Figure 2**). The abundance of msa transcripts in the kidneys was significantly positively correlated with the histopathological lesions expressed as the hsBKD (**Figure 3**).

R. salmoninarum Significantly Deteriorates Growth Indicators in Surviving Fish Exposed to Lower Water Temperatures

R. salmoninarum infection induced a significant reduction in the key productive indicators in infected fish at 11 and 15°C (**Figure 3**). Moreover, infected fish showed a significant high level of association between productive indicators (**Figure 3**). The abundance of msa transcripts showed a more significant association with the condition factor, SGR and TGC than the histoscore BKD (**Figure 3**). Therefore, fish growth would be modulated by the relative abundance of *R. salmoninarum* rather than cell and tissue damage.

R. salmoninarum Induces Anemia and Impaired Renal Function in Surviving Fish Exposed to Lower Water Temperatures

The infected fish at 11°C showed an increase in the serum concentrations of urea and creatinine and a decrease in the

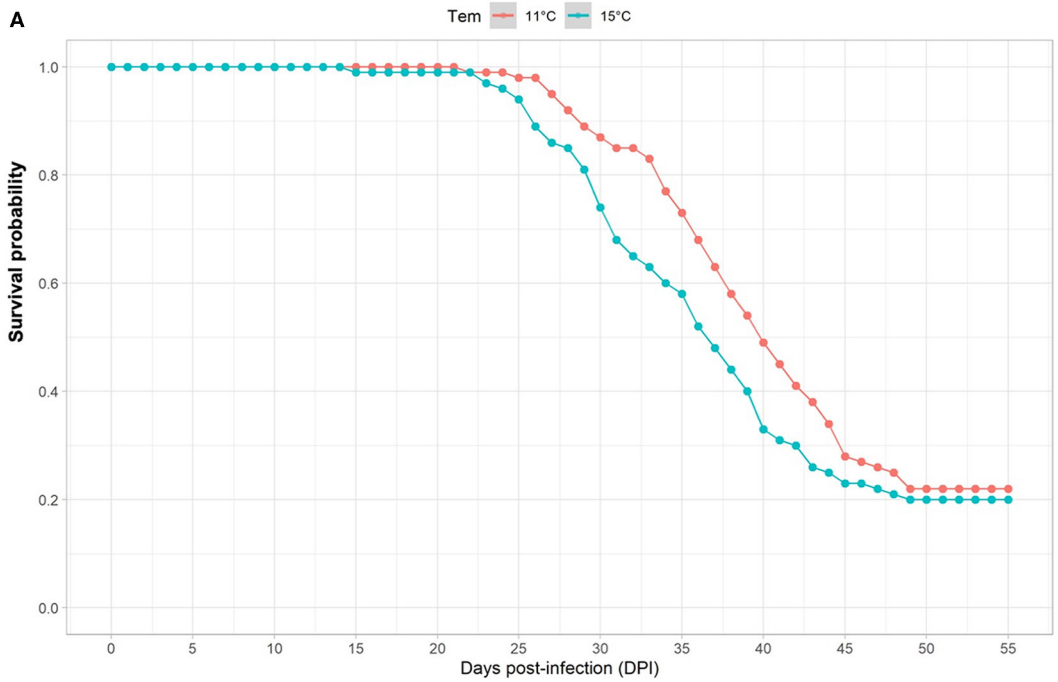

Source of variation	Estimate	Std. Error	t value	Pr(>|t|)
Days	0,054	0,008	6,437	**0,000**
Temperature 11 °C	-2,172	0,353	-6,159	**0,000**
Temperature 15 °C	-2,139	0,351	-6,087	**0,000**

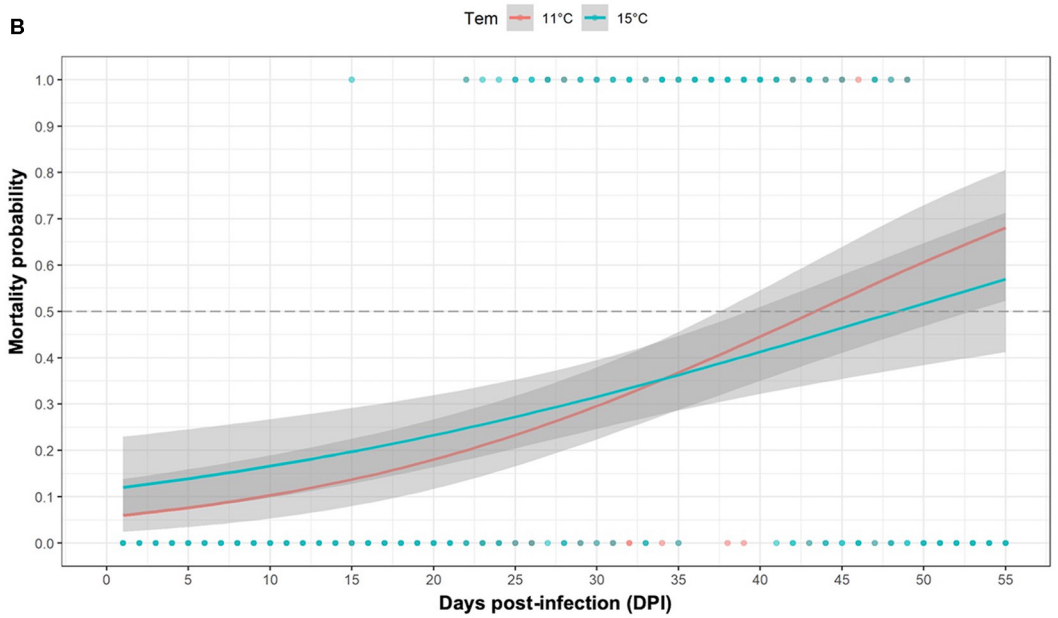

Temperature	Events	Median	0.95 LCL	0.95 UCL	Multiple comparison
11 °C	51	38.0	35	41	[a]
15 °C	52	35.5	32	38	[a]

FIGURE 1 | Survival study and mortality probability model in Atlantic salmon pre-smolts infected with *R. salmoninarum*. **(A)** Kaplan-Meier estimator of the cumulative survival function for fish infected with *R. salmoninarum* at 11 and 15°C considering three replicates. The green and red shaded area represents the 95% confidence interval. **(B)** Multiple comparison logRank test for mortality probability. The gray shaded area represents the 95% confidence interval. Tem, temperature.

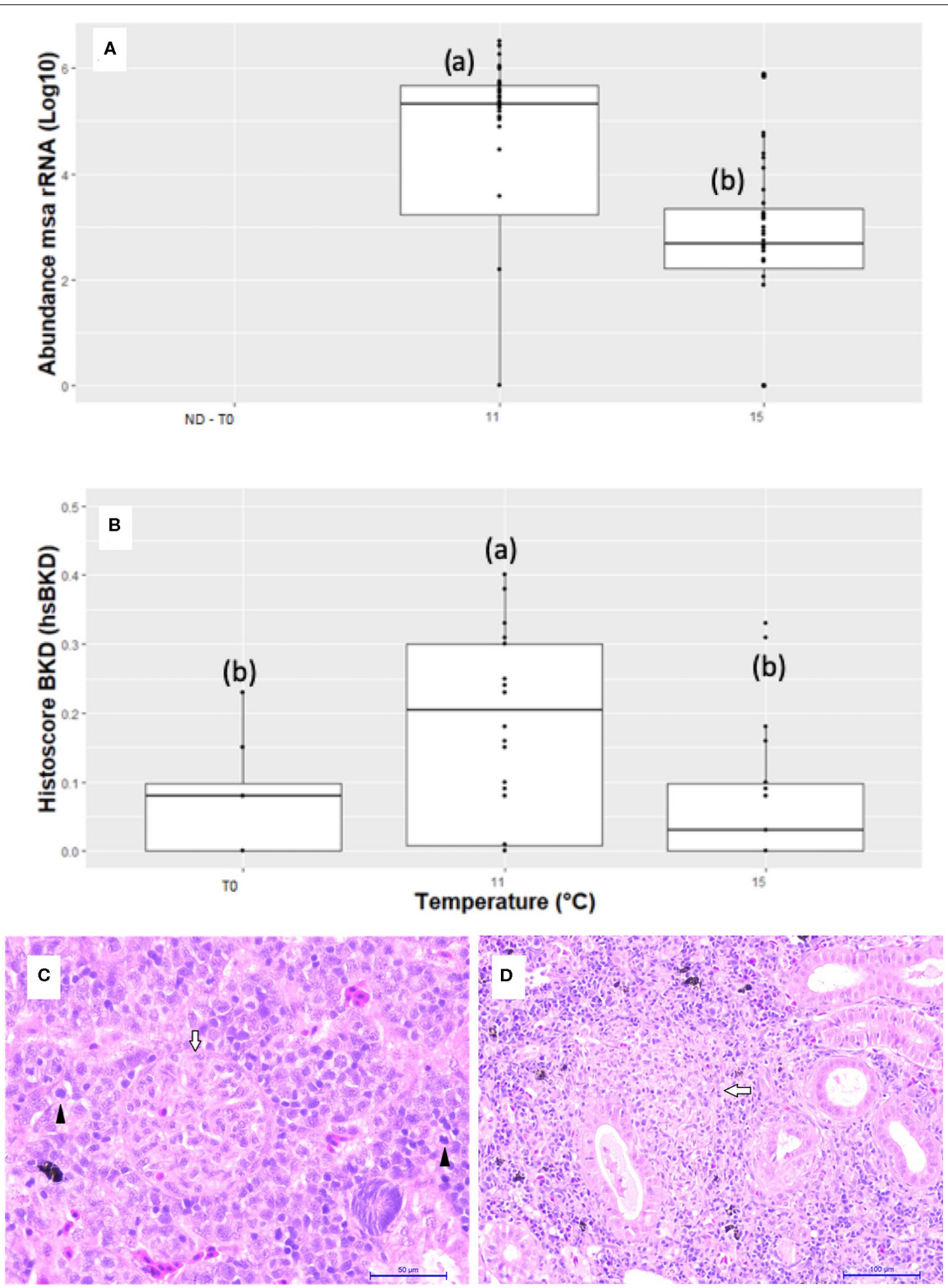

FIGURE 2 | Abundance of msa transcripts of *R. salmoninarum* and BKD histoscore in the head kidneys of Atlantic salmon pre-smolts infected at 11 and 15°C. **(A)** The abundance of msa transcripts of *R. salmoninarum* in infected fish at 11 and 15°C and non-infected fish. The relative quantification of the msa gene in kidneys is expressed as the $\log_{10}$ value of the number of copies of the msa gene of R. salmoninarum in the infected fish group compared to that in the non-infected control group (ND, not detected). **(B)** Histopathological lesions expressed as a BKD histoscore in infected fish at 11 and 15°C and non-infected fish. **(C)** Hyperplasia with mitotic figures (black arrows) in hematopoietic tissue, renal corpuscle with mesangial cell hyperplasia (white arrow) and capillary obliteration (HandE, 40X bar 50 μm). **(D)** Mixed granuloma in the initial stage of formation (white arrow) in kidney of Atlantic salmon pre-smolts infected with *R. salmoninarum* (HandE, 20X bar 100 μm).

TABLE 3 | Goodness-of-fit test results for a simple linear regression between the immunopathological outcomes of fish challenged by *R. salmoninarum* at different water temperatures.

Biomarker group	Abbreviation	Biomarker	Df	SS	MS	*F*-value	Pr(>F)	R^2	R-adjusted
Microscopic lesions	hsBKD	Histoscore BKD	1	0.26927	0.26927	55.886	0.00000	0.381	0.374
Plasma enzymes. substrates and minerals profile	Sodium (mmol/L)	NA	1	1642.8	1642.82	29.712	0.00000	0.287	0.277
	Chloride (mmol/L)	CL	1	650.5	650.47	13.414	0.00047	0.155	0.144
	Potassium (mmol/L)	K	1	0.7644	0.76439	11.268	0.00125	0.132	0.120
	Phosphorus (mmol/L)	P	1	381915	381915	295.54	0.00000	0.846	0.843
	Iron (mmol/L)	FE	1	577417	577417	124.04	0.00000	0.646	0.641
	Magnesium (mmol/L)	MG	1	674.67	674.67	62.068	0.00000	0.466	0.459
	Calcium (mmol/L)	CA	1	1084.9	1084.92	30.556	0.00000	0.301	0.291
	Alcaline phosphatase (U/L)	ALP	1	331208	331208	392.22	0.00000	0.875	0.873
	Pancreatic amilase (U/L)	PAM	1	−1.2237	0.1297	−9.435	0.00000	0.655	0.647
	Lipase (U/L)	LIP	1	−0.23511	0.02741	−8.579	0.00000	0.610	0.602
	Total amilase (U/L)	AMI	1	−1.2319	0.1492	−8.259	0.00000	0.563	0.555
	Creatine kinase (U/L)	CK	1	34.354	34.354	38.502	0.00000	0.407	0.397
	Aspartate aminotransferase (U/L)	AST	1	124928	124928	12.914	0.00065	0.175	0.161
	Alaline aminotransferase (U/L)	ALT	1	0.2764	0.276398	2.8226	0.09823	0.046	0.029
	Lactate dehydrogenase (U/L)	LDH	1	0.0884	0.08843	0.2331	0.63150	0.005	−0.016
	Cholesterol (mmol/L)	CHOL	1	979.86	979.86	391.12	0.00000	0.827	0.825
	Albumin (g/L)	ALB	1	9.096	9.096	126	0.00000	0.612	0.607
	High density lipoprotein (mmol/L)	HDL	1	133.24	133.24	94.498	0.00000	0.578	0.572
	Urea (mmol/L)	URE	1	107.378	107.378	114.53	0.00000	0.566	0.561
	Low density lipoprotein (mmol/L)	LDL	1	22.697	22.6965	57.944	0.00000	0.457	0.449
	Total protein (g/L)	TPO	1	7.4125	7.4125	70.242	0.00000	0.436	0.429
	Glucose (mmol/L)	GLU	1	13.328	13.3282	57.934	0.00000	0.429	0.422
	Globulins (g/L)	GLO	1	5.5818	5.5818	49.639	0.00000	0.353	0.346
	Lactate (mmol/L)	LAC	1	0.47979	0.47979	18.456	0.00004	0.169	0.160
	Uric acid (μmol/l)	UAC	1	1191	1191.04	17.006	0.00008	0.158	0.148
	Creatinine (μmol/l)	CRE	1	1677.4	1677.38	13.779	0.00037	0.144	0.133
	Triglycerides (mmol/L)	TRG	1	0.0002	0.000201	0.0046	0.94640	0.050	−0.011
Hematological profile	Hematocrit (%)	HCT	1	11.6577	11.6577	231.53	0.00000	0.773	0.770
	Red blood cell count (x10e6/Ul)	RBC	1	6.6981	6.6981	221.44	0.00000	0.735	0.731
	Hemoglobin (g/L)	HB	1	7.0518	7.0518	67.127	0.00000	0.438	0.432
	Mean Corpuscular Hemoglobin Concentration (g/L)	MCHC	1	0.37926	0.37926	14.353	0.00028	0.143	0.133
	Mean Corpuscular Hemoglobin (f/L)	MHC	1	0.0439	0.04391	0.9586	0.33050	0.012	−0.001
	Immature red blood cell (N°/mL)	IRBC	1	20175918	20175918	67.026	0.00000	0.626	0.617
	Lymphocytes count (N°/mL)	LYM	1	814043587	814043587	63.828	0.00000	0.477	0.470
	Heterophils count (N°/mL)	HET	1	13530470	13530470	54.819	0.00000	0.450	0.442
	Monocytes count (N°/mL)	MON	1	124.54	124.544	34.336	0.00000	0.389	0.377
	White blood cell count (N°/μL)	WBC	1	739782809	739782809	42.168	0.00000	0.376	0.367
	Blastocytes (N°/mL)	BLA	1	452070	452070	18.157	0.00009	0.275	0.259
	Thrombocytes or Platelet Count (N°/μL)	PLC	1	2.9866	2.98657	11.172	0.00191	0.232	0.211
	Unidentified cells (N°/mL)	UIC	1	196	195.99	1.9546	0.17040	0.050	0.025
Immunological profile (RT–qPCR)	Cluster of differentiation 8	CD8	1	10.9629	10.9629	155.27	0.00000	0.680	0.676
	Eomesodermin	EOMES	1	7.4297	7.4297	113.36	0.00000	0.669	0.663
	Interleukin 12	IL-12	1	6.4925	6.4925	116.23	0.00000	0.663	0.658
	Interleukin 2	IL-2	1	2.561	2.56097	61.368	0.00000	0.600	0.590
	T-bet	TBET	1	2.9251	2.92511	87.005	0.00000	0.596	0.589
	Granzyme A	GZMA	1	23.142	23.1419	49.221	0.00000	0.468	0.458
	Perforin 2	MPEG	1	2.4807	2.48073	38.634	0.00000	0.408	0.398
	Interleukin 10	IL-10	1	18.428	18.4285	38.98	0.00000	0.386	0.376

(Continued)

TABLE 3 | Continued

Biomarker group	Abbreviation	Biomarker	Df	SS	MS	*F*-value	Pr(>F)	R^2	R-adjusted
	Immunoglobulin T	IGT	1	6.058	6.058	33.35	0.00000	0.282	0.273
	GATA-3	GATA3	1	3.6406	3.6406	23.095	0.00001	0.281	0.269
	Interferon gamma	IFNG	1	1.785	1.785	15.894	0.00025	0.265	0.249
	Interleukin 4/13	IL4/13	1	0.85802	0.85802	20.802	0.00003	0.261	0.248
	Interleukin 17	IL-17	1	0.078697	0.078697	11.834	0.00129	0.212	0.194
	Immunoglobulin M	IGM	1	2.155	2.15496	21.669	0.00001	0.192	0.184
	Interleukin 8	IL8	1	0.7799	0.77992	13.9	0.00042	0.183	0.170
	Transforming growth factor beta	TGFB	1	0.37021	0.37021	10.454	0.00201	0.151	0.136
	Interleulin 1 beta	IL-1B	1	0.4017	0.40172	3.5993	0.06270	0.058	0.042
	Cluster of differentiation 4	CD4	1	0.1036	0.103601	2.2298	0.13920	0.026	0.015
	STAT1	STAT1	1	0.1424	0.14238	0.7875	0.37850	0.013	−0.004
	Interferon alpha	IFNA	1	0.0231	0.023098	0.7709	0.38280	0.010	−0.003
	Type I histocompatibility complex	MHCI	1	0.0691	0.069117	0.6599	0.41920	0.009	−0.005
	Type II histocompatibility complex	MHCII	1	0.00711	0.007109	0.1855	0.66800	0.003	−0.011

In black, biomarkers that showed a significant degree of association ($p < 0.0001$; $R^2 > 0,3$) with the abundance of msa transcription of the bacterium in Log_{10} in kidney samples (Df, degree of freedom; SS, sum of squares; MS, mean squares).

serum concentrations of total protein and albumin (**Table 3**). However, the concentrations of the same biomarkers in infected fish at 15°C were within the normal range. These biomarkers are indicators of kidney damage, and alterations in their levels could be linked to the macroscopic and microscopic lesions observed in the kidney that were associated with a high abundance of msa transcripts. Moreover, significant decreases were observed in the plasma concentration of glucose, cholesterol, HDL, LDL, and amylase, which are all indicators of kidney damage, chronic inflammatory process and poor nutritional condition during infection (**Table 3**). The increase in mineral levels, such as magnesium, phosphorus and calcium, are associated with kidney damage. The PCO analysis showed that the abundance of msa transcripts significantly changed the renal function and the overall condition of infected fish at 11°C compared to infected fish at 15°C (**Figure 4**).

Moreover, fish infected at 11°C showed a significant decrease in the total red blood cell count and hematocrit and hemoglobin concentration as well as a significant increase in the immature erythrocyte count (**Table 3**). On the other hand, these biomarkers were within the normal range in infected fish at 15°C. The PCO analysis showed that the abundance of msa transcripts of *R. salmoninarum* generated anemia in infected fish at 11°C compared to infected fish at a higher water temperature and uninfected fish (**Figure 4**). These findings are associated with the significantly high concentration of plasma iron in the same fish.

In contrast, the total white blood cells count was pathologically increased in infected fish at 15°C and showed significant differences with that of fish infected at 11°C, which showed a normal average count that was close to the maximum range. PCO analysis also showed that the abundance of msa transcripts modulated a milder inflammatory response in infected fish at 15°C compared to infected fish at 11°C and uninfected fish (**Figure 4**). The fish infected at 11°C showed monocytosis and lymphopenia.

R. salmoninarum Induces a Significantly Greater Downregulation of the Cell-Mediated Immune Response Genes in Surviving Fish Exposed to Lower Water Temperatures

In the late stage of infection, the abundance of msa transcripts of *R. salmoninarum* in the surviving fish from both groups induced a chronic pro-inflammatory response based on the significant overexpression of the transcripts of *IL-8* and *IFNγ* (**Figure 5**). At the same time, downregulation of Th2 cytokines, such as *IL4/IL13*, as well as *IL10* and *TGFβ*, which are primarily associated with tissue repair and extracellular matrix composition, was observed during the late stage of infection, especially in infected fish at 11°C (**Figure 5**).

The abundance of msa of *R. salmoninarum* promoted the significant decreased the expression of the *T-bet* and *Eomes* transcription factors, cytokines *IL-12* and *IL-2*, *CD8,* and *perforin 2* (**Table 3**, **Figure 5**). Moreover, the load of *R. salmoninarum* showed a significant positive correlation with the downregulation of *IFNγ, Eomes, Tbet, GATA3, IL-2, IL-12, CD8,* and *perforin* (**Table 3**, **Figure 5**). Hence, *R. salmoninarum* did not induce an immune response mediated by $CD8^+$ T-cells in infected fish at 11 or 15°C. The PCO analysis showed that the adaptive cell-mediated immune response was more severely downregulated in infected fish at 11°C (**Figure 4**).

Nevertheless, the infected fish at 15°C showed overexpression of *STAT1, MHCII, CD4, IgT,* and *IgM* transcripts, suggesting that the infection triggered a $CD4^+$ T-cells response and a humoral response. However, this pattern of expression of genes related to humoral immunity was not observed in the infected fish at 11°C (**Figure 5**). Therefore, the best humoral response in infected fish at higher temperatures was not correlated with better protection because no significant differences were observed in the survival rates between both groups of fish. These results are unexpected

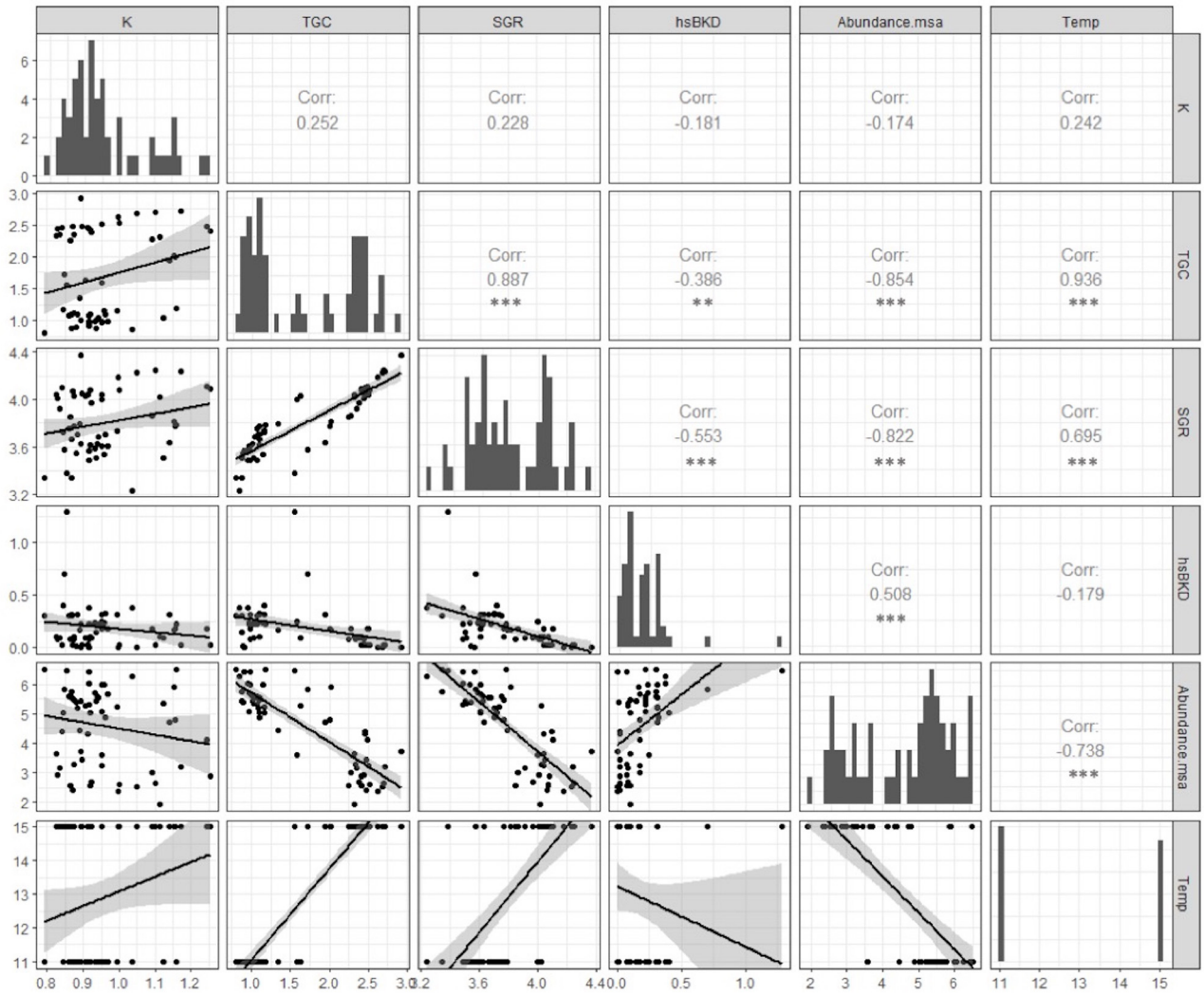

FIGURE 3 | Pearson correlation coefficient (*r*) and *p*-value (*p*) between the abundance of msa transcripts, BKD histoscore and productive growth variables (SGR and TGC) in Atlantic salmon pre-smolts infected with *R. salmoninarum* (**$p < 0.01$, ***$p < 0.001$). The abundance of msa of *R. salmoninarum* induced a significant reduction in the key productive indicators in infected fish at 11 and 15°C. Additionally, infected fish shows a significant high level of association between productive indicators.

in a fish infected with an intracellular bacterium and could partly explain the relative field efficacy of vaccines, although this supposition requires further investigation.

DISCUSSION

Understanding the pathophysiological mechanisms underlying the interaction *in vivo* of *R. salmoninarum* with its host, in this case, the Atlantic salmon, would allow for the development of alternative therapies for the treatment, prevention and control of BKD. We used different immunopathological biomarkers of infection with *R. salmoninarum* to better understand the nature of the host-pathogen interaction during the late stage of infection in Atlantic salmon maintained at different water temperatures. To our knowledge, previous studies have not examined late gene expression associated with the immune response against *R. salmoninarum* in surviving pre-smolts of Atlantic salmon, although previous studies have reported some aspects of the early immunopathological response of rainbow trout (16) and Chinook salmon challenged with *R. salmoninarum* (12), vaccinated Atlantic salmon parr (20) and vaccinated fish, although only *R. salmoninarum* agglutinating antibodies were used (20, 30, 31).

Although several environmental factors influence infectious disease dynamics in aquaculture, water temperature is considered one of the most important because it can determine pathogen and fish biology modulations (12–14). Our results confirmed that there was no significant relationship between water temperature and mean survival rate, although a higher probability of death and delay the mortality curve was observed in infected fish

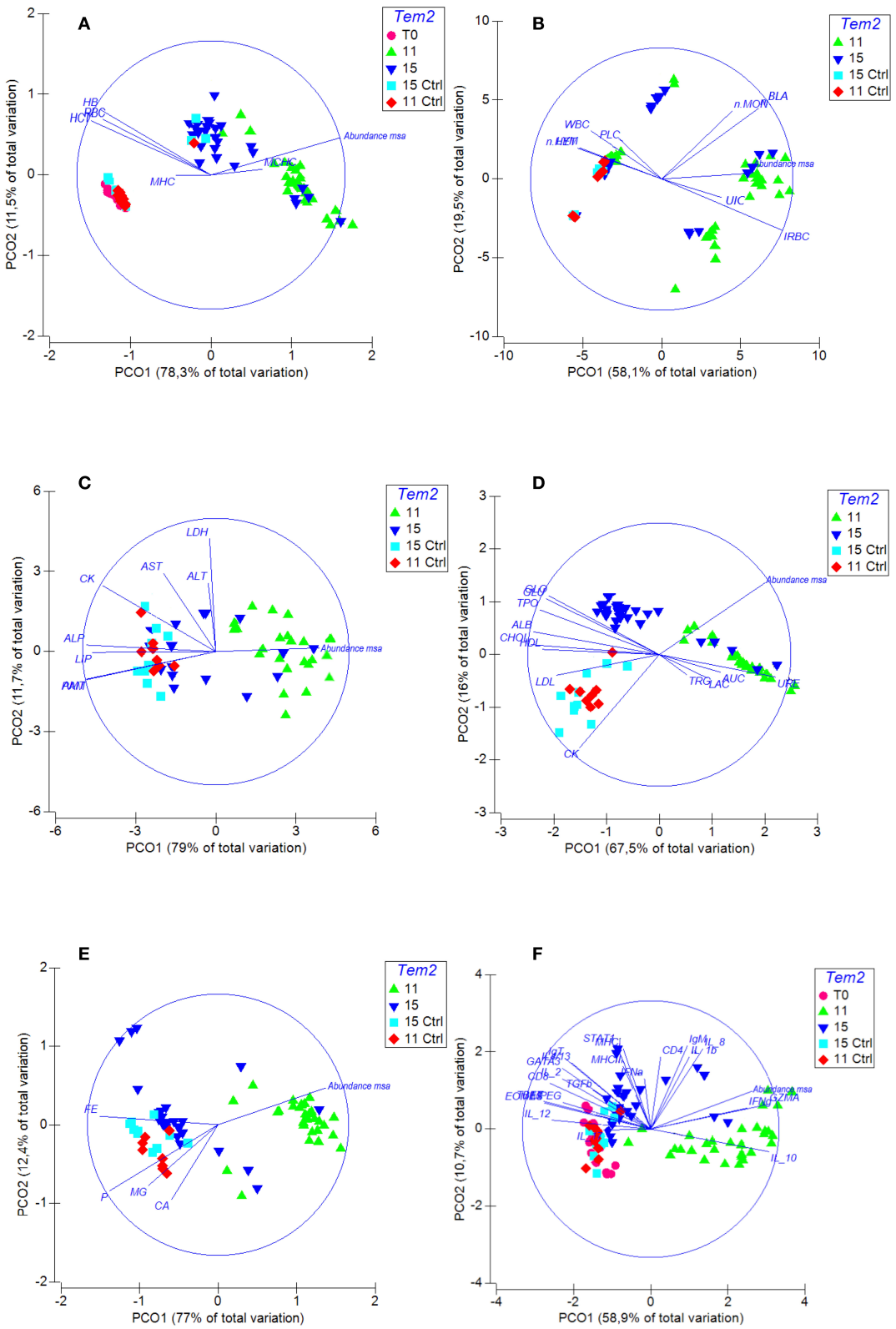

FIGURE 4 | Spatial sorting of the different biomarkers of the immunopathological response of fish challenged with *R. salmoninarum* using a principal coordinate analysis (PCO). Euclidean distance matrices were used before standardization by log (x+1) for all data and independent for each group of variables. The PCOs were

(Continued)

FIGURE 4 | clustered into 5 groups: **(A)** Erythrogram. The abundance of msa transcripts of R. salmoninarum generated anemia in infected fish at 11°C compared to infected fish at a higher water temperature (HCT, RCR, HG, IRBC). **(B)** Leukogram and differential leukocyte count. PCO analysis shows that the abundance of msa transcripts modulated a milder inflammatory response in infected fish at 15°C compared to infected fish at 11°C. The fish infected at 11°C shows monocytosis and lymphopenia. **(C)** Plasma enzymes. Significant decreases were observed in the plasma concentration of different enzymes which are all indicators of poor nutritional condition during infection (AMI, PAM, LIP, ALP). **(D)** Plasma substrates: The infected fish at 11°C shows an increase in the serum concentrations of urea and creatinine and a decrease in the serum concentrations of total protein and albumin. Significant decreases were observed in the plasma concentration of glucose, cholesterol, HDL and LDL, which are all indicators of chronic inflammatory process and poor nutritional condition during infection. **(E)** Plasma minerals. The infected fish at 11°C shows an increase in the serum concentrations of iron. **(F)** Expression of genes involved in the immune response. PCO analysis shows that the cell-mediated immune response is downregulated more severely in infected fish at 11°C. Temp, temperature; Ctrl, control.

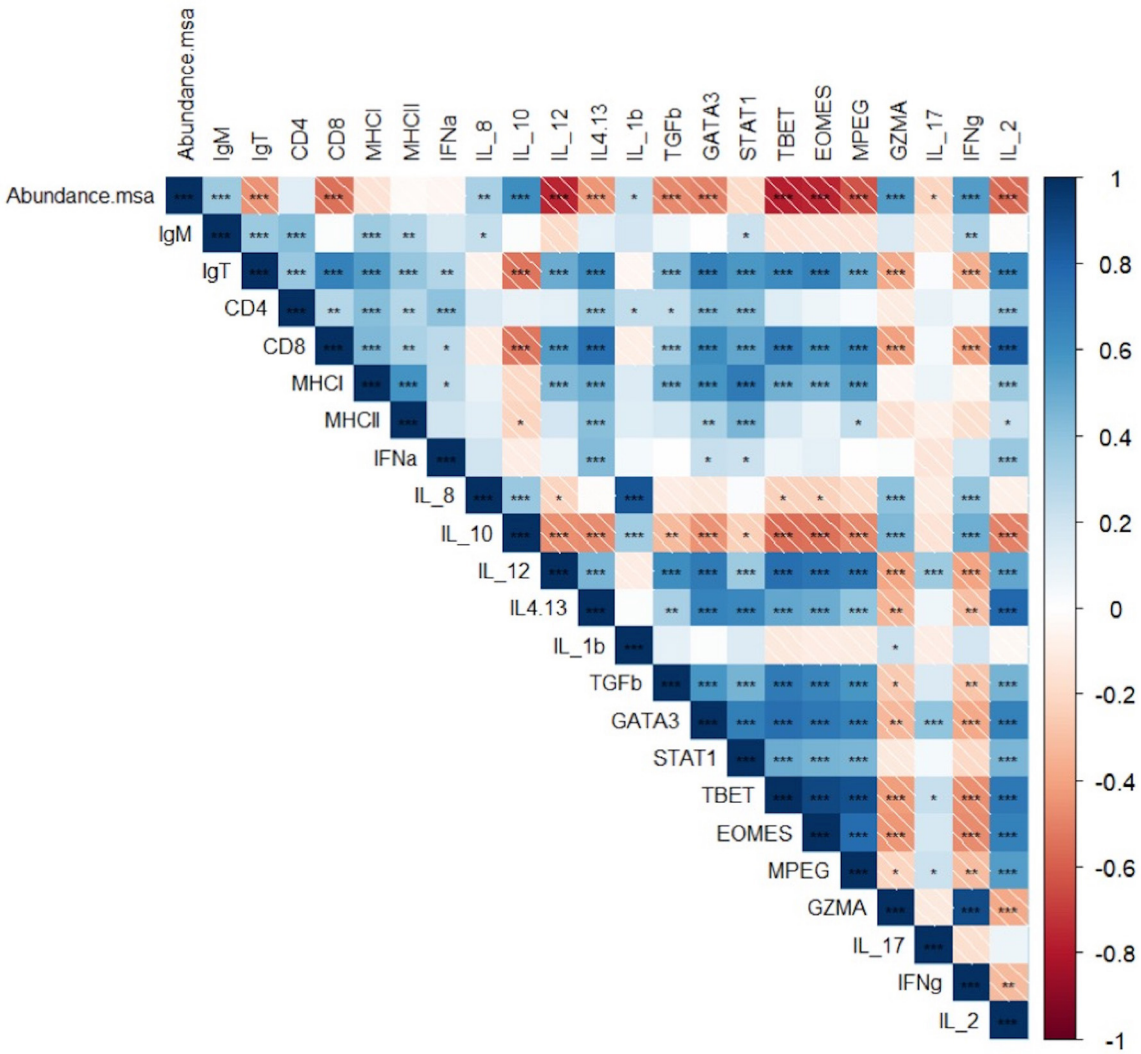

FIGURE 5 | Pearson correlation coefficient (*r*) and *p*-value (*p*) between between the abundance of msa transcripts and the expression of target immune genes and association between the expression of each gene related to the innate and adaptive immune responses in the head kidney of Atlantic salmon pre-smolts infected with *R. salmoninarum* (*$p < 0.05$, **$p < 0.01$, ***$p < 0.001$).

at 11°C than at 15°C after 35 days post-infection. These results are consistent with those reported by Purcell et al. (12), who showed that cold water contributes to greater BKD progression in Chinook salmon and the concomitant increase in bacterial shedding could contribute to greater horizontal transmission of the bacterium. Also, our findings are consistent with those described by Sanders et al. (15), who showed that lower temperatures resulted in higher mortality rates and longer mean times to mortality. However, our findings were not fully consistent with those described by Jones et al.

(13), who showed that higher temperatures resulted in higher mortality rates.

The fish infected with *R. salmoninarum* and kept at 11 or 15°C had a mean survival of 21.5 and 20.1%, respectively. A survival challenge without fish sampling was conducted in Chinook salmon by Purcell et al. (32), and survival was 41% in the Wisconsin (WI) stock and 21% in the Washington (WA) stock. However, our results in Atlantic salmon were not consistent with the average survival rates of 61.3 and 79.8% later reported in Chinook salmon held at 8 and 12°C, respectively (12). One of the limitations of our study was that a low temperature between 6 and 8°C, which is closer to the BKD field conditions, could not be obtained.

Our current research is focused on applying the results of the present study as potential immunopathological biomarkers of a resistance phenotype for BKD to populations of 30 different Atlantic salmon families. Our preliminary results show that there is a clearly higher level of resistance of some families to BKD compared to others at 11°C (range of survival rate between 0 and 76%) (data not yet published). Evolutionary theory predicts that populations with sufficient genetic variation will show adaptive responses to pathogen pressure (33); however, WI and WA Chinook salmon groups challenged with *R. salmoninarum* at 14 and 9°C showed that although the warmer temperature accelerated the time of death in both populations, there was no evidence of phenotypic plasticity or a genotype interaction per environment interaction (14). High h^2 estimates for BKD susceptibility in the WI population, combined with a lack of phenotypic plasticity, predicts that future adaptive gains in BKD resistance are still possible and that these adaptive gains would be stable under the temperature range evaluated (14). Results from the genome-wide association (GWA) studies indicate that BKD resistance has a polygenic genetic architecture with the largest single nucleotide polymorphism (SNP) explaining only 5.3% of the phenotypic variance (34). However, polygenic traits are often not improved greatly through selection based solely on a few significant markers due to the small proportion of variance explained by a single marker (35).

Mortality and survival rates are not the only outcome from *R. salmoninarum* infection. The infected fish at 11°C showed more severe clinical signs and pathological lesions than the infected fish at 15°C, a finding that may be associated with the expression of different virulence factors in the different water temperatures. A microscopic pathology analysis of BKD shows a chronic granulomatous inflammatory response to encapsulate the pathogen (4, 5). Typically, there is extensive tissue damage, a strong cell-mediated response, macrophage proliferation and activation, and probably the deposition of immune complexes in tissues (16, 17, 36). The major soluble antigen of *R. salmoninarum*, p57 (36–41), is produced in the tissues of infected fish, and it may have an important role in the chronic stimulation of TNFα, which could be expected to assist the chronic inflammatory pathology of BKD (16).

Although both groups of fish exhibited similar types of macroscopic kidney responses, the infected fish at 11°C showed a significantly higher BKD histological score, at least for the time period examined and with the infection metrics employed in this study. Purcell et al. (12) showed that changes in water temperature influence disease progression and the elimination of bacteria in Chinook salmon infected with *R. salmoninarum*. Fish held at 8°C showed the highest mortality rate and a higher renal abundance of *msa* transcripts in relation to fish held at 12°C, while fish held at 15°C showed little evidence of the progression of *R. salmoninarum* infection in relation to the group at 12°C.

R. salmoninarum produces abundant quantities of an extracellular, 57-kDa protein called p57 or major soluble antigen is widely known to be an important virulence factor (37, 38). The relative quantification of the abundance of *msa* transcripts in kidneys is expressed as the number of copies of the *msa* gene of *R. salmoninarum* in infected fish compared with that in the non-infected control group. The late stage of infection was characterized by a significantly greater amount of *msa* transcripts in the kidney of infected fish at 11°C than at 15°C. These results could indicate that the infected fish at 15°C appear to have been more successful at controlling the infection, although better protection was not observed because no significant differences were observed in the survival rates between both groups of fish.

Anemia and lymphopenia observed in infected fish at 11°C could be associated with the increased abundance of *msa* transcripts because this virulence factor shows several properties including the ability to bind salmonid erythrocytes (42), hemagglutinate mammalian erythrocytes (37, 39) agglutinate the leucocytes of various salmonid species (43), and adhere to Chinook salmon leucocytes (41). The lymphopenia observed in our study could also determine the typical immunosuppression process described in fish with BKD (43), making these fish more susceptible to opportunistic pathogens.

In salmonids, the development of semiquantitative histological indicators or histoscores has been described for SRS (44), heart disease (HSMI and CMS) (45), pancreas disease (PD) (46) and gill alterations (47), although there are no reports of histoscores for BKD. The severity of the microscopic kidney response expressed as hsBKD showed a significant positive correlation with bacterial growth, which was expressed as the *msa* transcripts of *R. salmoninarum*, and these results are consistent with previous descriptions of SRS pathogenesis in Atlantic salmon (44).

The increased serum level of UAC, CRE and minerals observed in this study indicates significant kidney damage, which is confirmed by the presence of microscopic lesions that suggest important alterations in kidney function. These results are consistent with the increase in CRE reported in sockeye salmon with BKD (48), Atlantic salmon infected with *P. salmonis* (44) and rainbow trout infected with *Serratia liquefaciens* (49).

The decrease in the level of TOP and ALB in fish infected with *R. salmoninarum* could be explained by a reduction in protein synthesis due to liver damage and by the higher excretion of protein or protein loss associated with kidney damage. Protein synthesis can decrease during infection due to the preferential synthesis of specific proteins, and albumin may act as an acute-phase negative protein (50). These results are consistent with reports in sockeye salmon infected with *R. salmoninarum* (48), Atlantic salmon infected with *P. salmonis* (44), tilapia, *Oreochromis* sp. infected with *Edwardsiella*

tarda (51) and Salvelinus fontinalis species infected with *Flavobacterium columnare* (52). In addition, the decrease in the concentration of plasma substrates related to the general state of the fish was based on a decrease in the productive indicators of growth.

An effective antigen-specific $CD8^+$ T-cells response is essential for immune protection against the dominant epitopes of intracellular bacteria and promotes the effective control of these organisms (53). Our results suggest that the abundance of msa transcripts of *R. salmoninarum* showed a significant positive correlation with the downregulation of *IFNγ, Eomes, Tbet, GATA3, IL-2, IL-12, CD8,* and *perforin*; consequently, *R. salmoninarum* did not induce an immune response mediated by $CD8^+$ T-cells in infected fish at 11 or 15°C. These results showed the modulation of the cellular and humoral immune response based on the expression of genes associated with immune response of Atlantic salmon head kidney intraperitoneally infected with *R salmoninarum*, but we must consider that the transcriptomic approach alone is unable to draw conclusions about how bacterial infections affect activation/suppression of CD4 or CD8 T-cells function. Therefore, new studies at protein expression and activity level, immunological reagents and cytotoxic and/or helper T cell clones are essential for further development in the fish immunology.

All T cells possess a T cell receptor (TCR) by which they recognize peptide presented by MHC, along with CD3 and co-stimulatory, e.g., CD28, and co-inhibitory, e.g., CTLA-4, surface molecules (54). T cell associated genes and their encoded proteins with T cell activity in fish, e.g., surface markers, cytokines and transcriptional factors, have been well-documented (55). The presence of cytotoxic T cells (CTLs) and Th cells in fish have been identified as $CD8^+$ and $CD4^+$ T-cells, respectively using monoclonal antibodies (mAbs) (56–58). CD4 and CD8 molecules are expressed not only on T cells but also other cell types, e.g., CD4-1 in melano-macrophages in channel catfish (59). Thereby, multiple markers should be used for the true identification of T cells.

R. salmoninarum induced a significantly greater downregulation of the cell-mediated immune response genes in surviving fish exposed to lower water temperatures. This response could be due to a suppressed host response directly related to the lower water temperature and/or associated with a delayed host response related to the lower water temperature (60). However, acute infections may be resolved as a result of a temperature-dependent T-cell response, although carriers and latency are common (61). As reported for other important intracellular fish bacteria such as *Francisella noatunensis* (62), *P. salmonis* (26, 27, 63) and *Edwardsiella tarda* (64, 65), *R. salmoninarum* would require stimulation of cell-mediated immunity, although the mechanisms of this process in these species of bacteria remain poorly understood and require further investigation.

Yamasaki et al. (64) reported the important role of cellular immunity rather than humoral immunity against *E. tarda* infection in ginbuna cross carp. Bacterial clearance in the kidney and spleen was observed after elevated cytotoxic activity of CTLs and increased numbers of $CD8\alpha^+$ T-cells. However, *E. tarda*-specific antibody titers did not increase until after bacterial clearance, indicating that induction of humoral immunity would be too late to provide protection against infection. Rozas-Serri et al. (26) showed that *P. salmonis* induces the inflammatory and IFN-mediated response, modulation of Th1 polarization, reduced antigen processing and presentation, modulation of the evasion of the immune response mediated by $CD8^+$ T-cells and promotion of the $CD4^+$ T-cell response during the late stage of infection as a mechanism to escape host defenses. Additionally, Rozas-Serri et al. (63) showed several central signatures following infection with *P. salmonis* in Atlantic salmon, including positive regulation of *DC-SIGN* and *TLR5* signaling, which converged at the *NF-kB* level to modulate the pro-inflammatory cytokine response. *P. salmonis* induced an IFN-inducible response, e.g., *IRF-1* and *GBP-1*, but inhibited the humoral and cell-mediated immune responses.

Yamasaki et al. (65) demonstrated the importance of cell-mediated immunity against *E. tarda* infection using vaccine trials comparing the effects of live vs. formalin-killed bacteria. Live cell-vaccinated fish showed high survival rates, high *IFNγ* and *T-bet* gene expression levels, and increased CTLs. On contrary, all bacterin-vaccinated fish died following *E. tarda* infection and induced high *IL4/13a* and *IL-10* expression levels, whereas Th1-like responses were suppressed. Similarly, Rozas-Serri et al. (27) showed that a bacterin *P. salmonis* vaccinated-fish exhibited *MHCI, MHCII,* and *CD4* overexpression but a significant downregulation of *CD8b* and *IgM*, suggesting that the formalin-killed bacteria promoted the $CD4^+$ T-cell response but did not induce an immune response mediated by $CD8^+$ T cells or a humoral response.

Our work shows that infected fish at 15°C presented the overexpression of *STAT1, MHCII, CD4, IgT,* and *IgM* transcripts, suggesting that the infection triggered a $CD4^+$ T-cells response and a humoral response. However, this pattern of expression of genes related to humoral immunity was not observed in infected fish at 11°C. Salmon infected with *R. salmoninarum* produce an antibody response, although it is not necessarily correlated with protection (31, 66). Other studies have shown that p57 suppresses antibody responses and macrophage respiratory burst and renders immunized animals more susceptible to BKD (16, 38, 40).

Underexpression of Th2 cytokines, such as *IL4/IL13*, as well as *IL10* and *TGFβ*, which are primarily associated with tissue repair and extracellular matrix composition, was observed during the late stage of infection, especially in infected fish at 11°C (67, 68). In addition, our results show late underexpression of *IL-1β,* which could induce long-term suppression of cytokine production, phagocyte function, and lymphocyte proliferation and activation, including T-cell-dependent antibody production (69–71). The downregulation of these cytokines during the late stage of infection may affect each of these pathways and facilitate the survival of *R. salmoninarum*.

The chronic higher levels of IFNγ may be implicated in the pathology of BKD and the host-mediated destruction of kidney tissues (16). These results would suggest how *R. salmoninarum* could suppress the host immune response and suggest that the

immune mechanisms for the containment of *R. salmoninarum* infections rely on cell-mediated immune response-dependent pathways. Therefore, prolonged stimulation of IFNγ observed in infected fish at 11°C may contribute to the chronic inflammatory pathology of BKD. There is evidence that *R. salmoninarum* has mechanisms to evade detection by the host's immune system (16), which is also observed for other intracellular bacteria, such as *P. salmonis* (26, 27, 44, 63). The identification of $CD4^+$ and $CD8^+$ T-cell antigens and development of a method to stimulate lasting immunity represent main challenges.

Our results show that the expression patterns of genes related to the humoral and cell-mediated immune response in Atlantic salmon infected with *R. salmoninarum* at 11 and 15°C were very similar; however, *R. salmoninarum* induced a significantly greater downregulation of the adaptive immune response genes at the lower water temperature. A constant suppression of the adaptive immune system is observed in response to colder temperatures, which could be associated with detrimental effects of low temperatures on the innate immune system (60). However, better protection was not observed because the mean survival rates did not show differences between the water temperature groups, although a higher probability of death was observed in infected fish at 11°C than at 15°C after 35 dpi. These results are similar to those reported in different populations of Chinook salmon by Metzger et al. (17), who demonstrated that bacterial load levels positively regulated pro-inflammatory genes expression in fish from both groups despite the higher mortality in the more susceptible Green River stock.

Genetic variability between families of Atlantic salmon and/or the use of different challenge models could show different results than those described here, so further investigation is required. Challenge models using baths and cohabitation more faithfully represent the conditions of natural exposure compared with the i.p. infection (72, 73). This method would bypass any first-barrier defense mechanism that prevents the disease because bacteria are not transferred from the environment to the fish. Our experience with *P. salmonis*, another intracellular bacterium that is of great economic relevance in Chile and modulates the immune response of Atlantic salmon using the same strategy described here for *R. salmoninarum*, indicates that evaluating the host-pathogen interaction using an i.p. challenge model generates different results compared with a cohabitation model (26, 27, 44, 63). Thus, it would be interesting to study the pathogenesis and immune response against BKD and vaccines to BKD using a cohabitation model (73). Thereby, it is important to acknowledge the potential value in performing more comprehensive studies that can strengthen our understanding of the impact of low water temperatures on host-pathogen systems.

Taken together, our results show differences in the immunopathological response of pre-smolts of Atlantic salmon infected with *R. salmoninarum* at different water temperatures, but this differential response could be related to a suppressed host response and/or a delayed host response because they were exposed to a lower water temperature. The virulence of pathogens is affected by water temperature (74), although it may be difficult to separate these effects from those of the host immune system. The effect of water temperature on fish immune systems thus varies depending upon the duration and magnitude of the temperature change. In general, lower temperatures lead to a shutdown or slowing of immune response mechanisms, which is generally reversible upon return to warmer temperatures (60).

At 55 days after infection, the surviving fish kept at 11 and 15°C were carriers of *msa* transcripts of *R. salmoninarum,* which would have downregulated the humoral and cell-mediated adaptive immune genes and persisted chronically in the kidneys. Hence, these carrier fish may have a higher risk of recurrent outbreaks under stress conditions, such as during the transfer of Atlantic salmon smolts to seawater farms with low temperatures. Therefore, more studies are needed to determine the molecular mechanisms underlying the regulation of virulence genes expression in response to temperature in *R. salmoninarum*.

These results provide valuable information on the modulation of the late adaptive immune response in fish after *R. salmoninarum* infection, and we hope that they will be useful for optimizing the health and productive management of farmed fish and designing vaccines to provide long-term protection in fish. In addition, our results supported the identification of 33 immunopathological biomarkers for potential application in the search for a resistance phenotype for BKD, and eight of these genes are related specifically to the adaptive cell-mediated immune response. Finally, our current research is focused on applying the results of the present study as potential immunopathological biomarkers of a resistance phenotype for BKD to populations of 30 different Atlantic salmon families.

DATA AVAILABILITY STATEMENT

Publicly available datasets were analyzed in this study. Requests to access the datasets should be directed to Marco Rozas-Serri at marco.rozas@pathovet.cl.

ETHICS STATEMENT

The animal study was reviewed and approved by Elanco's Animal Welfare Program which covers all of Elanco's animal facilities worldwide and ensures the care and use of all animals. Therefore, the study that was completed at the Aquarium Facility in Puerto Varas was reviewed and approved by the Elanco Global Ethical Committee (Institutional Animal Care and Use Committee). Written informed consent was obtained from the owners for the participation of their animals in this study.

AUTHOR CONTRIBUTIONS

MR-S designed and directed the experiment, fully analyzed the results, and wrote the manuscript. CL designed the experiment and partially analyzed the results. RC, RI, VJ, CO, and DC designed and validated the histoscore BKD and performed the processing and histopathological diagnosis. JV, AM, LM,

and AP validated the molecular analyses and executed the RT-PCRs analysis. RW and CN performed the hematological processing and diagnosis and blood biochemical profiles. JG, PM, and FS carried out the sampling of the fish and taking their respective tissues at the hatchery for the subsequent processing and diagnosis in the laboratory. All authors contributed to the article and approved the submitted version.

FUNDING

This work was supported by the Chilean Economic Development Agency (CORFO) and Hendrix Genetics Aquaculture Chile (18IDAE-90549).

ACKNOWLEDGMENTS

We thank Marilyn Wolter, Astrid Dominguez, and the entire technical team of the Elanco Animal Health experimental hatchery, Puerto Varas, Chile, for their exceptional work in implementing the experimental design.

SUPPLEMENTARY MATERIAL

The Supplementary Material for this article can be found online at: https://www.frontiersin.org/articles/10.3389/fimmu.2020.01378/full#supplementary-material

REFERENCES

1. Brynildsrud O, Feil EJ, Bohlin J, Castillo-Ramirez S, Colquhoun D, McCarthy U, et al. Microevolution of *Renibacterium salmoninarum*: evidence for intercontinental dissemination associated with fish movements. *ISME J.* (2014) 8:746–56. doi: 10.1038/ismej.2013.186
2. Bayliss SC, Verner-Jeffreys DW, Ryder D, Suarez R, Ramirez R, Romero J, et al. Genomic epidemiology of the commercially important pathogen *Renibacterium salmoninarum* within the Chilean salmon industry. *Microb Genomics.* (2018) 4:e000201. doi: 10.1099/mgen.0.000201
3. Evelyn T, Hoskins G, Bell G. First record of bacterial kidney disease in an apparently wild salmonid in British Columbia. *J Fisheries Board Can.* (1973) 30:1578–80. doi: 10.1139/f73-249
4. Bruno DW. Histopathology of bacterial kidney disease in laboratory infected rainbow trout, *Salmo gairdneri* Richardson, and Atlantic salmon, *Salmo salar* L., with reference to naturally infected fish. *J Fish Dis.* (1986) 9:523–37. doi: 10.1111/j.1365-2761.1986.tb01049.x
5. Kent ML, Benda S, St.-Hilaire S, Schreck CB. Sensitivity and specificity of histology for diagnoses of four common pathogens and detection of nontarget pathogens in adult Chinook salmon (*Oncorhynchus tshawytscha*) in fresh water. *J Vet Diagn Investig.* (2013) 25:341–51. doi: 10.1177/1040638713482124
6. Boerlage AS, Stryhn H, Sanchez J, Hammell KL. Case definition for clinical and subclinical bacterial kidney disease (BKD) in Atlantic Salmon (*Salmo salar* L.) in New Brunswick, Canada. *J Fish Dis.* (2017) 40:395–409. doi: 10.1111/jfd.12521
7. Grayson TH, Cooper LF, Atienzar FA, Knowles MR, Gilpin ML. Molecular differentiation of *Renibacterium salmoninarum* isolates from worldwide locations. *Appl Environ Microbiol.* (1999) 65:961–8. doi: 10.1128/AEM.65.3.961-968.1999
8. Grayson TH, Alexander SM, Cooper LF, Gilpin ML. *Renibacterium salmoninarum* isolates from different sources possess two highly conserved copies of the rRNA operon. *Antonie Van Leeuwenhoek.* (2000) 78:51–61. doi: 10.1023/A:1002745129625
9. Grayson TH, Atienzar FA, Alexander SM, Cooper LF, Gilpin ML. Molecular diversity of *Renibacterium salmoninarum* isolates determined by randomly amplified polymorphic DNA analysis. *Appl Environ Microbiol.* (2000) 66:435–8. doi: 10.1128/AEM.66.1.435-438.2000
10. Rhodes LD, Grayson TH, Alexander SM, Strom MS. Description and characterization of IS994, a putative IS3 family insertion sequence from the salmon pathogen, *Renibacterium salmoninarum*. *Gene.* (2000) 244:97–107. doi: 10.1016/S0378-1119(99)00573-9
11. Alexander SM, Grayson TH, Chambers EM, Cooper LF, Barker GA, Gilpin ML. Variation in the spacer regions separating tRNA genes in *Renibacterium salmoninarum* distinguishes recent clinical isolates from the same location. *J Clin Microbiol.* (2001) 39:119–28. doi: 10.1128/JCM.39.1.119-128.2001
12. Purcell MK, McKibben CL, Pearman-Gillman S, Elliott DG, Winton JR. Effects of temperature on *Renibacterium salmoninarum* infection and transmission potential in Chinook salmon, *Oncorhynchus tshawytscha* (Walbaum). *J Fish Dis.* (2016) 39:787–98. doi: 10.1111/jfd.12409
13. Jones DT, Moffitt CM, Peters KK. Temperature-mediated differences in bacterial kidney disease expression and survival in *Renibacterium salmoninarum*-challenged bull trout and other salmonids. *North Am J Fisher Manag.* (2007) 27:695–706. doi: 10.1577/M06-002.1
14. Purcell MK, Hard JJ, Neely KG, Park LK, Winton JR, Elliott DG. Genetic variation in bacterial kidney disease (BKD) susceptibility in Lake Michigan Chinook Salmon and its progenitor population from the Puget Sound. *J Aquat Anim Health.* (2014) 26:9–18. doi: 10.1080/08997659.2013.860061
15. Sanders JE, Pilcher KS, Fryer JL. Relation of water temperature to bacterial kidney disease in Coho Salmon (*Oncorhynchus kisutch*), Sockeye Salmon (*O. nerka)*, and Steelhead Trout (Salmo gairdneri). *J Fisher Res Board Can.* (1978) 35:8–11. doi: 10.1139/f78-002
16. Grayson TH, Cooper LF, Wrathmell AB, Roper J, Evenden AJ, Gilpin ML. Host responses to *Renibacterium salmoninarum* and specific components of the pathogen reveal the mechanisms of immune suppression and activation. *Immunology.* (2002) 106:273–83. doi: 10.1046/j.1365-2567.2002.01420.x
17. Metzger DC, Elliott DG, Wargo A, Park LK, Purcell MK. Pathological and immunological responses associated with differential survival of Chinook salmon following *Renibacterium salmoninarum* challenge. *Dis Aquat Org.* (2010) 90:31–41. doi: 10.3354/dao02214
18. Campos-Perez JJ, Ward M, Grabowski PS, Ellis AE, Secombes CJ. The gills are an important site of iNOS expression in rainbow trout Oncorhynchus mykiss after challenge with the gram-positive pathogen *Renibacterium salmoninarum*. *Immunology.* (2000) 99:153–61. doi: 10.1046/j.1365-2567.2000.00914.x
19. Rhodes LD, Wallis S, Demlow SE. Genes associated with an effective host response by Chinook salmon to *Renibacterium salmoninarum*. *Dev Comp Immunol.* (2009) 33:176–86. doi: 10.1016/j.dci.2008.08.006
20. Eslamloo K, Kumar S, Caballero-Solares A, Gnanagobal H, Santander J, Rise ML. Profiling the transcriptome response of Atlantic salmon head kidney to formalin-killed *Renibacterium salmoninarum*. *Fish Shellfish Immunol.* (2019) 98:937–49. doi: 10.1016/j.fsi.2019.11.057
21. Del Cerro A, Marquez I, Guijarro JA. Simultaneous detection of *Aeromonas salmonicida*, *Flavobacterium psychrophilum*, and *Yersinia ruckeri*, three major fish pathogens, by multiplex PCR. *Appl Environ Microbiol.* (2002) 68:5177–80. doi: 10.1128/AEM.68.10.5177-5180.2002
22. Snow M, McKay P, McBeath AJ, Black J, Doig F, Kerr R, et al. Development, application and validation of a Taqman real-time RT-PCR assay for the detection of infectious salmon anaemia virus (ISAV) in Atlantic salmon (Salmo salar). *Dev Biol.* (2006) 126:133–45.
23. Suzuki K, Sakai DK. Real-time PCR for quantification of viable *Renibacterium salmoninarum* in chum salmon *Oncorhynchus keta*. *Dis Aquat Org.* (2007) 74:209–23. doi: 10.3354/dao074209
24. Palacios G, Lovoll M, Tengs T, Hornig M, Hutchison S, Hui J, et al. Heart and skeletal muscle inflammation of farmed salmon is associated with infection with a novel reovirus. *PLoS ONE.* (2010) 5:e11487. doi: 10.1371/journal.pone.0011487
25. Skjesol A, Skjaeveland I, Elnaes M, Timmerhaus G, Fredriksen BN, Jorgensen SM, et al. IPNV with high and low virulence: host immune

responses and viral mutations during infection. *Virol J.* (2011) 8:396. doi: 10.1186/1743-422X-8-396
26. Rozas-Serri M, Pena A, Arriagada G, Enriquez R, Maldonado L. Comparison of gene expression in post-smolt Atlantic salmon challenged by LF-89-like and EM-90-like Piscirickettsia salmonis isolates reveals differences in the immune response associated with pathogenicity. *J Fish Dis.* (2018) 41:539–52. doi: 10.1111/jfd.12756
27. Rozas-Serri M, Pena A, Maldonado L. Gene expression associated with immune response in Atlantic salmon head-kidney vaccinated with inactivated whole-cell bacterin of Piscirickettsia salmonis and pathogenic isolates. *Fish Shellfish Immunol.* (2019) 93:789–95. doi: 10.1016/j.fsi.2019.08.031
28. Pfaffl MW, Horgan GW, Dempfle L. Relative expression software tool (REST) for group-wise comparison and statistical analysis of relative expression results in real-time PCR. *Nucleic Acids Res.* (2002) 30:e36. doi: 10.1093/nar/30.9.e36
29. Jager KJ, van Dijk PC, Zoccali C, Dekker FW. The analysis of survival data: the Kaplan-Meier method. *Kidney Int.* (2008) 74:560–5. doi: 10.1038/ki.2008.217
30. Paterson WD, Desautels D, Weber JM. The immune response of Atlantic salmon, *Salmo salar* L., to the causative agent of bacterial kidney disease, *Renibacterium salmoninarum*. *J Fish Dis.* (1981) 4:99–111. doi: 10.1111/j.1365-2761.1981.tb01115.x
31. Jansson E, Ljungberg O. Detection of humoral antibodies to *Renibacterium salmoninarum* in rainbow trout *Oncorhynchus mykiss* and Atlantic salmon *Salmo salar* challenged by immersion and in naturally infected populations. *Dis Aquat Org.* (1998) 33:93–9. doi: 10.3354/dao033093
32. Purcell MK, Murray AL, Elz A, Park LK, Marcquenski SV, Winton JR, et al. Decreased mortality of Lake Michigan Chinook salmon after bacterial kidney disease challenge: evidence for pathogen-driven selection? *J Aquat Anim Health.* (2008) 20:225–35. doi: 10.1577/H08-028.1
33. Spielman D, Brook BW, Briscoe DA, Frankham R. Does inbreeding and loss of genetic diversity decrease disease resistance? *Conserv Genet.* (2004) 5:439–48. doi: 10.1023/B:COGE.0000041030.76598.cd
34. Holborn MK, Ang KP, Elliott JAK, Powell F, Boulding EG. Genome wide association analysis for bacterial kidney disease resistance in a commercial North American Atlantic salmon (Salmo salar) population using a 50 K SNP panel. *Aquaculture.* (2018) 495:465–71. doi: 10.1016/j.aquaculture.2018.06.014
35. Bernardo R. Molecular markers and selection for complex traits in plants: learning from the last 20 years. *Crop Sci.* (2008) 48:1649–64. doi: 10.2135/cropsci2008.03.0131
36. Wiens GD, Chien MS, Winton JR, Kaattari SL. Antigenic and functional characterization of p57 produced by *Renibacterium salmoninarum*. *Dis Aquat Org.* (1999) 37:43–52. doi: 10.3354/dao037043
37. Daly JG, Stevenson RMW. Hydrophobic and haemagglutinating properties of *Renibacterium salmoninarum*. *Microbiology.* (1987) 133:3575–80. doi: 10.1099/00221287-133-12-3575
38. Turaga P, Wiens G, Kaattari S. Bacterial kidney disease: the potential role of soluble protein antigen(s). *J Fish Biol.* (1987) 31:191–4. doi: 10.1111/j.1095-8649.1987.tb05312.x
39. Daly JG, Stevenson RMW. Characterization of the *Renibacterium salmoninarum* haemagglutinin. *Microbiology.* (1990) 136:949–53. doi: 10.1099/00221287-136-5-949
40. Brown LL, Iwama GK, Evelyn TPT. The effect of early exposure of Coho salmon (Oncorhynchus kisutch) eggs to the p57 protein of*Renibacterium salmoninarum*on the development of immunity to the pathogen. *Fish Shellf Immunol.* (1996) 6:149–65. doi: 10.1006/fsim.1996.0016
41. Wiens GD, Pascho R, Winton JR. A single Ala139-to-Glu substitution in the *Renibacterium salmoninarum* virulence-associated protein p57 results in antigenic variation and is associated with enhanced p57 binding to chinook salmon leukocytes. *Appl Environ Microbiol.* (2002) 68:3969–77. doi: 10.1128/AEM.68.8.3969-3977.2002
42. Kaattari SL, Irwin MJ, Yui MA, Tripp RA, Parkins JS. Primary *in vitro* stimulation of antibody production by rainbow trout lymphocytes. *Vet Immunol Immunopathol.* (1986) 12:29–38. doi: 10.1016/0165-2427(86)90107-8
43. Wiens GD, Kaattari SL. Monoclonal antibody characterization of a leukoagglutinin produced by *Renibacterium salmoninarum*. *Infect Immun.* (1991) 59:631–7. doi: 10.1128/IAI.59.2.631-637.1991
44. Rozas-Serri M, Ildefonso R, Pena A, Enriquez R, Barrientos S, Maldonado L. Comparative pathogenesis of piscirickettsiosis in Atlantic salmon (*Salmo salar* L.) post-smolt experimentally challenged with LF-89-like and EM-90-like Piscirickettsia salmonis isolates. *J Fish Dis.* (2017) 40:1451–72. doi: 10.1111/jfd.12671
45. Fritsvold C, Kongtorp RT, Taksdal T, Ørpetveit I, Heum M, Poppe TT. Experimental transmission of cardiomyopathy syndrome (CMS) in Atlantic salmon *Salmo salar*. *Dis Aquat Org.* (2009) 87:225–34. doi: 10.3354/dao02123
46. McLoughlin MF, Graham DA, Norris A, Matthews D, Foyle L, Rowley HM, et al. Virological, serological and histopathological evaluation of fish strain susceptibility to experimental infection with salmonid alphavirus. *Dis Aquat Org.* (2006) 72:125–33. doi: 10.3354/dao072125
47. Mitchell S, Baxter E, Holland C, Rodger H. Development of a novel histopathological gill scoring protocol for assessment of gill health during a longitudinal study in marine-farmed Atlantic salmon (Salmo salar). *Aquacult Int.* (2012) 20:813. doi: 10.1007/s10499-012-9504-x
48. Bell GR. Distribution of transaminases (Aminotransferases) in the tissues of pacific salmon (Oncorhynchus), with emphasis on the properties and diagnostic use of glutamic-oxalacetic transaminase. *J Fisher Res Board Can.* (1968) 25:1247–68. doi: 10.1139/f68-108
49. Aydin S, Erman Z, Bilgin ÖC. Investigations of *Serratia liquefaciens* infection in rainbow trout (*Oncorhynchus mykiss* Walbaum). *Turkish J Vet Anim Sci.* (2001) 25:643–50.
50. Braceland M, Bickerdike R, Tinsley J, Cockerill D, McLoughlin MF, Graham DA, et al. The serum proteome of Atlantic salmon, Salmo salar, during pancreas disease (PD) following infection with salmonid alphavirus subtype 3 (SAV3). *J Proteomics.* (2013) 94:423–36. doi: 10.1016/j.jprot.2013.10.016
51. Karasu Benli AC, Yavuzcan Yildiz H. Blood parameters in Nile tilapia (*Oreochromis niloticus* L.) spontaneously infected with *Edwardsiella tarda*. *Aquac Res.* (2004) 35:1388–90. doi: 10.1111/j.1365-2109.2004.01158.x
52. Rehulka J, Minarík B. Blood parameters in brook trout *Salvelinus fontinalis* (Mitchill, 1815), affected by columnaris disease. *Aquac Res.* (2007) 38:1182–97. doi: 10.1111/j.1365-2109.2007.01786.x
53. Jiang J, Fisher EM, Murasko DM. CD8 T cell responses to influenza virus infection in aged mice. *Ageing Res Rev.* (2011) 10:422–7. doi: 10.1016/j.arr.2011.02.001
54. Nakanishi T, Shibasaki Y, Matsuura Y. T Cells in Fish. *Biology.* (2015) 4:640–63. doi: 10.3390/biology4040640
55. Fischer U, Koppang EO, Nakanishi T. Teleost T and NK cell immunity. *Fish Shellfish Immunol.* (2013) 35:197–206. doi: 10.1016/j.fsi.2013.04.018
56. Toda H, Shibasaki Y, Koike T, Ohtani M, Takizawa F, Ototake M, et al. Alloantigen-specific killing is mediated by CD8-positive T cells in fish. *Dev Comp Immunol.* (2009) 33:646–52. doi: 10.1016/j.dci.2008.11.008
57. Takizawa F, Dijkstra JM, Kotterba P, Korytar T, Kock H, Kollner B, et al. The expression of CD8alpha discriminates distinct T cell subsets in teleost fish. *Dev Comp Immunol.* (2011) 35:752–63. doi: 10.1016/j.dci.2011.02.008
58. Toda H, Saito Y, Koike T, Takizawa F, Araki K, Yabu T, et al. Conservation of characteristics and functions of CD4 positive lymphocytes in a teleost fish. *Dev Comp Immunol.* (2011) 35:650–60. doi: 10.1016/j.dci.2011.01.013
59. Saunders HL, Oko AL, Scott AN, Fan CW, Magor BG. The cellular context of AID expressing cells in fish lymphoid tissues. *Dev Comp Immunol.* (2010) 34:669–76. doi: 10.1016/j.dci.2010.01.013
60. Abram QH, Dixon B, Katzenback BA. Impacts of low temperature on the teleost immune system. *Biology.* (2017) 6:39. doi: 10.3390/biology6040039
61. Munro ALS. Vaccination against bacterial kidney disease. In: Evensen E, Lillehaug E, editors. *Fish Vaccination.* London: Academic Press (1988). p. 124–35.
62. Soto E, Brown N, Gardenfors ZO, Yount S, Revan F, Francis S, et al. Effect of size and temperature at vaccination on immunization and protection conferred by a live attenuated Francisella noatunensis immersion vaccine in red hybrid tilapia. *Fish Shellfish Immunol.* (2014) 41:593–9. doi: 10.1016/j.fsi.2014.10.009
63. Rozas-Serri M, Pena A, Maldonado L. Transcriptomic profiles of post-smolt Atlantic salmon challenged with *Piscirickettsia salmonis* reveal a strategy to evade the adaptive immune response and modify cell-autonomous

immunity. *Dev Comp Immunol.* (2018) 81:348–62. doi: 10.1016/j.dci.2017.12.023
64. Yamasaki M, Araki K, Nakanishi T, Nakayasu C, Yoshiura Y, Iida T, et al. Adaptive immune response to Edwardsiella tarda infection in ginbuna crucian carp, *Carassius auratus* langsdorfii. *Vet Immunol Immunopathol.* (2013) 153:83–90. doi: 10.1016/j.vetimm.2013.02.004
65. Yamasaki M, Araki K, Nakanishi T, Nakayasu C, Yamamoto A. Role of CD4(+) and CD8alpha(+) T cells in protective immunity against *Edwardsiella tarda* infection of ginbuna crucian carp, Carassius auratus langsdorfii. *Fish Shellfish Immunol.* (2014) 36:299–304. doi: 10.1016/j.fsi.2013.11.016
66. Bartholomew JL, Arkoosh MR, Rohovec JS. Demonstration of the specificity of the salmonid hurnoral response to *Renibacterium salmoninarum* with a monoclonal antibody against salmonid immunoglobulin. *J Aquat Anim Health.* (1991) 3:254–9.
67. Gordon S. Alternative activation of macrophages. *Nat Rev Immunol.* (2003) 3:23–35. doi: 10.1038/nri978
68. Colton C, Wilcock DM. Assessing activation states in microglia. *CNS Neurol Disord Drug Targets.* (2010) 9:174–91. doi: 10.2174/187152710791012053
69. Hong S, Zou J, Crampe M, Peddie S, Scapigliati G, Bols N, et al. The production and bioactivity of rainbow trout (Oncorhynchus mykiss) recombinant IL-1 beta. *Vet Immunol Immunopathol.* (2001) 81:1–14. doi: 10.1016/S0165-2427(01)00328-2
70. Nakae S, Asano M, Horai R, Iwakura Y. Interleukin-1 beta, but not interleukin-1 alpha, is required for T-cell-dependent antibody production. *Immunology.* (2001) 104:402–9. doi: 10.1046/j.1365-2567.2001.01337.x
71. Nakae S, Asano M, Horai R, Sakaguchi N, Iwakura Y. IL-1 enhances T cell-dependent antibody production through induction of CD40 ligand and OX40 on T cells. *J Immunol.* (2001) 167:90–7. doi: 10.4049/jimmunol.167.1.90
72. Murray C, Evelyn T, Beacham T, Barner L, Ketcheson J, Prosperi-Porta L. Experimental induction of bacterial kidney disease in chinook salmon by immersion and cohabitation challenges. *Dis Aquat Org.* (1992) 12:91–6. doi: 10.3354/dao012091
73. Alcorn S, Murray AL, Pascho RJ, Varney J. A cohabitation challenge to compare the efficacies of vaccines for bacterial kidney disease (BKD) in chinook salmon *Oncorhynchus tshawytscha*. *Dis Aquat Org.* (2005) 63:151–60. doi: 10.3354/dao063151
74. Guijarro JA, Cascales D, Garcia-Torrico AI, Garcia-Dominguez M, Mendez J. Temperature-dependent expression of virulence genes in fish-pathogenic bacteria. *Front Microbiol.* (2015) 6:700. doi: 10.3389/fmicb.2015.00700

Conflict of Interest: MR-S, RC, RI, JV, AM, LM, VJ, DC, CO, RW, CN, JG, PM, AP, and CS are employed by Laboratorio Pethovet Ltda. MR-S is also employed by Newenko Group SpA. CL and FS are employed by Hendrix Genetics Aquaculture S.A.

The authors declare that this study received funding from Hendrix Genetics Aquaculture. The funder had the following involvement in the study: design and decision to submit it for publication.

Copyright © 2020 Rozas-Serri, Lobos, Correa, Ildefonso, Vásquez, Muñoz, Maldonado, Jaramillo, Coñuecar, Oyarzún, Walker, Navarrete, Gayosa, Mancilla, Peña, Senn and Schwerter. This is an open-access article distributed under the terms of the Creative Commons Attribution License (CC BY). The use, distribution or reproduction in other forums is permitted, provided the original author(s) and the copyright owner(s) are credited and that the original publication in this journal is cited, in accordance with accepted academic practice. No use, distribution or reproduction is permitted which does not comply with these terms.

frontiers in Immunology

ORIGINAL RESEARCH
published: 11 August 2020
doi: 10.3389/fimmu.2020.01751

Molecular Evolution of Apolipoprotein Multigene Family and the Original Functional Properties of Serum Apolipoprotein (LAL2) in *Lampetra japonica*

Qing Han[1,2,3†], *Yinglun Han*[1,2,3†], *Hongyan Wen*[1,2,3], *Yue Pang*[1,2,3*] *and Qingwei Li*[1,2,3*]

[1] College of Life Sciences, Liaoning Normal University, Dalian, China, [2] Lamprey Research Center, Liaoning Normal University, Dalian, China, [3] Collaborative Innovation Center of Seafood Deep Processing, Dalian Polytechnic University, Dalian, China

OPEN ACCESS

Edited by:
Gyri T. Haugland,
University of Bergen, Norway

Reviewed by:
Zhihao Jia,
Purdue University, United States
Jing Xing,
Ocean University of China, China

***Correspondence:**
Yue Pang
pangyue01@163.com
Qingwei Li
liqw@263.net

†*These authors have contributed equally to this work*

Specialty section:
This article was submitted to Comparative Immunology, a section of the journal Frontiers in Immunology

Received: *25 February 2020*
Accepted: *30 June 2020*
Published: *11 August 2020*

Citation:
Han Q, Han Y, Wen H, Pang Y and Li Q (2020) Molecular Evolution of Apolipoprotein Multigene Family and the Original Functional Properties of Serum Apolipoprotein (LAL2) in Lampetra japonica. Front. Immunol. 11:1751. doi: 10.3389/fimmu.2020.01751

Apolipoprotein (APO) genes represent a large family of genes encoding various binding proteins associated with plasma lipid transport. Due to the long divergence history, it remains to be confirmed whether these genes evolved from a common ancestor through gene duplication and original function, and how this evolution occurred. In this study, based on the phylogenetic tree, sequence alignment, motifs, and evolutionary analysis of gene synteny and collinearity, APOA, APOC, and APOE in higher vertebrates may have a common ancestor, lamprey serum apolipoprotein LAL1 or LAL2, which traces back to 360 million years ago. Moreover, the results of immunofluorescence, immunohistochemistry, and flow cytometry show that LAL2 is primarily distributed in the liver, kidney, and blood leukocytes of lampreys, and specifically localized in the cytoplasm of liver cells and leukocytes, as well as secreted into sera. Surface plasmon resonance technology demonstrates that LAL2 colocalizes to breast adenocarcinoma cells (MCF-7) or chronic myeloid leukemia cells (K562) associated with lamprey immune protein (LIP) and further enhances the killing effect of LIP on tumor cells. In addition, using quantitative real-time PCR (Q-PCR) and western blot methods, we found that the relative mRNA and protein expression of *lal2* in lamprey leukocytes and sera increased significantly at different times after stimulating with *Staphylococcus aureus*, *Vibrio anguillarum*, and Polyinosinic-polycytidylic acid (Poly I:C). Moreover, LAL2 was found to recognize and bind to gram-positive bacteria (*Staphylococcus aureus* and *Bacillus cereus*) and gram-negative bacteria (*Escherichia coli*) and play an important role in the antibacterial process. All in all, our data reveals a long, complex evolutionary history for apolipoprotein genes under different selection pressures, confirms the immune effect of LAL2 in lamprey sera against pathogens, and lays the foundation for further research regarding biological functions of lamprey immune systems.

Keywords: apolipoprotein, LAL2, lamprey, antibacterial, immune system

INTRODUCTION

As early as 1987, Pontes et al. (1) founded two abundant apolipoproteins in the "high-density lipoprotein fraction" of ultracentrifuged plasma in *Petromyzon marinus*, designated lamprey apolipoproteins LAL1 and LAL2. Their amino acid compositions were similar to portions of apolipoprotein A-IV sequence in mammalian blood. However, the existing database indicates that LAL2 has no apolipoproteinA/E or C domain. Their functions are not fully elucidated, and it remains elusive whether they are the ancestors of vertebrate apolipoproteins. However, it is well-known that apolipoprotein is a protein component of plasma lipoproteins (2, 3). Apolipoproteins of vertebrates are primarily synthesized in the liver and small intestine, which are involved in the transport and redistribution of lipids between different tissues and cells through blood (4, 5). Research shows that several apolipoproteins also play important roles in antibacterial and antiviral processes (6–9). For example, APOA1-containing high-density lipoprotein particles (HDL) exert antibacterial activity by directly affecting the growth of bacteria and promoting the self-defense mechanism of normal and immunocompromised individuals (10). This function is attributed primarily to the ability of APOA1 to bind and neutralize both bacterial endotoxin lipopolysachharide (LPS) and lipoteichoic acid (LTA) (11–14). Moreover, whether it is expressed *in vivo* or injected, APOA1 elictis an antiviral effect on enveloped and non-enveloped DNA and RNA viruses by directly causing viral inactivation. Specifically, APOA1 has been shown to arrest virus-induced cell fusion in the blood during human immunodeficiency virus (HIV) and Herpes virus infection, thereby preventing the virus from penetrating into the cell (15). Additionally, highly conserved alternating cationic/hydrophobic motifs have been identified in the APOC1 sequence that participate in binding to LPS and enhanced biological response to LPS via a mechanism similar to lipopolysaccharide-binding protein (LBP) (16). Meanwhile, APOL-1 has pore-forming microbicidal activity that can cause lysis and death of trypanosome (17).

The lamprey is a member of an ancient lineage of jawless fish that stem ∼550 million years ago and has served as a crucial model for understanding conserved features that are relevant to biomedicine. Lampreys have adaptive immune systems with variable lymphocyte receptors (VLRs) and innate immune systems with complement related molecules to prevent the invasion of various foreign pathogens, such as mannose binding lectin (MBL), complement C1q, C3, etc. (18–20). Lamprey immune protein (LIP), a cytotoxic protein, has a jacalin-like domain and an aerolysin pore-forming domain previously identified in granulocytes of *Lampetra japonica* (21). We demonstrate the crystal structure of LIP and the mode of action involving dual selective recognition and efficient binding dependent on both N-linked glycans on GPI-anchored proteins (GPI-APs) and sphingomyelin (SM) in lipid rafts (22). LIP can kill a panel of human cancer cells yet has minimal effects on normal cells. MCF-7 and K562 cells stimulated with LIP exhibited the generation of chemokines and proinflammatory molecules, and increased the expression of genes in the calcium signaling pathway, ROS signaling pathway, and natural killer cell-mediated cytotoxicity pathways (23, 24). However, it remains unclear whether large amounts of LAL2 in serum interacts with LIP molecule and participates in the immune response.

In the present work, we elucidated the molecular evolution process of LAL2 and LAL1 and determined their relationship with vertebrate orthologs and paralogs. We further investigated LAL2 expression patterns in gill, supraneural body, heart, liver, intestine, and kidney, and also intracellular localization in liver cells and leukocytes. Simultaneously, the potential interaction between LAL2 and LIP was verified, and the addition of LAL2 was found to enhance the killing activity of LIP in lamprey. Moreover, the antibacterial and antiviral activities of LAL2 were examined to shed light on its role in immunity. Exploring the biological function of LAL2 lays the foundation for clarifying antibacterial function in lamprey and provides a reference for the research of innate immune mechanisms of lamprey.

MATERIALS AND METHODS

Animals and Cell Culture

Adult *L. japonica* (length: 36–42 cm, weight: 75–112 g) and *Lampetra morii* (length: 20–25 cm, weight: 18–23 g) were obtained from the Songhua River from Heilongjiang Province, China. The lampreys were housed in fully automatic water purification tanks at 4–6°C. All animals were in good condition before the experiments.

MCF-7 cells and K562 cells, purchased from the American Type Culture Collection (Manassas, VA) were maintained in RPMI 1640 medium (Sigma-Aldrich, USA) supplemented with 10% fetal bovine serum (Sigma-Aldrich, USA), 100 U/mL penicillin (Sigma-Aldrich, USA), and 100 mg/mL streptomycin (Sigma-Aldrich, USA). Cells were cultured in an incubator humidified with 5% CO_2 and 95% air at 37°C.

S. aureus, *B. cereus*, *Vibrio anguillarum*, and *E. coli* strains were isolated from the intestine of the lamprey. *S. aureus* (28°C), *B. cereus* (28°C), and *E. coli* (37°C) strains were cultured in Luria broth liquid medium with 1% peptone, 1% NaCl, and 0.5% yeast extract (Sangon Biotech, Shanghai, China). The *V. anguillarum* (28°C) strain was cultured in 2216E liquid medium with 0.5% peptone, 0.1% yeast extract, and seawater (pH = 8.0). All the strains were supplied by College of Life Science, Liaoning Normal University (Dalian, China).

Sequence Analysis, Sequence Alignments, and Phylogenetic Analysis

The amino acid sequences of lamprey apolipoprotein LAL1 and LAL2 were obtained from the *L. japonica* three-generation sequencing library and *Lethenteron reissneri* database from our laboratory. The amino acid sequences of the corresponding apolipoprotein family genes in other species are from NCBI (https://www.ncbi.nlm.nih.gov/) and Ensembl (http://asia.ensembl.org/index.html) database for sequence alignment by Bioedit 7.0. Two comparisons of syntenic genomic regions, respectively containing *lal1* and *lal2* genes, were completed using *L. reissneri* databases and the Genomicus website (http://www.genomicus.biologie.ens.fr/genomicus-92.01/cgi-bin/search.pl).

Thereafter, a phylogenetic tree was constructed using the neighbor-joining (NJ) method using MEGA 7.0 software and the bootstrap test (1,000 replicates). The tree was drawn to scale, with branch lengths in the same units as those of the evolutionary distances used to infer the phylogenetic tree. Functional domains of the apolipoprotein family genes were analyzed using the NCBI website (https://www.ncbi.nlm.nih.gov/Structure/cdd/wrpsb.cgi). Motif analysis was performed using the MEME website (http://meme-suite.org/) and TB (Toolbox for Biologists) tools software.

Expression of Recombinant LAL2 (rLAL2) Protein and Preparation of Antibodies

The prokaryotic expression vector pET32a-*lal2* was constructed to obtain the recombinant LAL2 (rLAL2) protein as described previously (25). Rabbit anti-LAL2 polyclonal antibody was generated through subcutaneous injection of New Zealand white rabbits with purified rLAL2 protein over 8 weeks, as described previously (26). The antibody titer in the anti-rLAL2 serum was determined via enzyme-linked immunosorbent assay (ELISA) at different dilutions, and the titer increased 640,000-fold over pre-immunization levels (pre-immunized rabbit IgG was used as a negative control). The antibody specificity was confirmed using western blot assays; rLAL2 and lamprey serum were subjected to 12% SDS-PAGE and transferred onto nitrocellulose membranes (Invitrogen, USA). The membranes were blocked with 5% non-fat powdered milk (Sangon Biotech, Shanghai, China) and incubated with rabbit anti-LAL2 (1 μg/mL) antibody overnight at 4°C, followed by incubation with 1.2 μg/mL HRP-conjugated goat anti-rabbit IgG (Sangon Biotech, Shanghai, China). Next, membranes were washed four times with tris-buffered saline Tween-20 (Sangon Biotech, Shanghai, China) and developed with enhanced chemiluminescence (ECL) substrate (Tanon, China) using Alpha FluorChem®Q (Cell Biosciences, USA).

Purification of Natural LAL2 Protein With Anion Exchange Chromatography

Serum from *L. japonica* was dialyzed in buffer A consisting of 20 mM KPB, 0.1 M KCl and 5% glycerol, at pH 7.0 at 4°C. The dialyzed fraction was filtered through a 0.22 μM membrane and was applied to a 10 mL × 2 MacroPrep Ceramic Hydroxyapatite column equilibrated with buffer A. The column was then washed with the same buffer and eluted with a linear gradient from 0 to 250 mM KPB in buffer A. The pooled fractions containing protein activity from the above column were dialyzed in buffer B consisting of 20 mM Tris-HCl and 5% glycerol, at pH 8.0 at 4°C. The dialyzed fraction was applied to a 20 mL Q Sepharose Fast Flow column equilibrated with buffer B. After washing, the sample was eluted with a linear gradient from 0 to 300 mM of KCl in buffer B. During the separation and purification of the active components of lamprey serum (TaKaRa, Dalian, China), we observed an abundance of natural LAL2 protein in the eluted sample No. 46. It was diluted with low-salt buffer (20 mM Tris-HCl, pH = 9.0), passed through the anion exchange column (HiTrap Q HP_1 mL, General Electric Company, USA) at a rate of 0.8 mL/min using ÄKTA pure (General Electric Company, USA), and impure proteins were removed with low-salt buffer at a rate of 1 mL/min. High-salt buffer (20 mM Tris-HCl, 1 M NaCl, pH = 9.0) was gradually added to the low-salt buffer, finally the target protein was eluted at a rate of 1 mL/min using mixed buffer in a time-dose dependent manner. After detection using 15% SDS-PAGE, it was dialyzed using PBS (145.3 mM NaCl, 8.4 mM Na_2HPO_4, and 2 mM NaH_2PO_4). All protein concentrations were measured using the Bicinchoninic acid (BCA) protein assay kit (Sangon biotech, Shanghai, China).

Immunofluorescence and Flow Cytometry Were Used to Detect the Localization of LAL2 and LIP

Lamprey liver cells and blood leukocytes were isolated, fixed, permeabilized, and blocked with fetal bovine serum as previously described (27). Briefly, cells were incubated with rabbit anti-rLAL2 antibody (0.8 μg/mL) at 4°C overnight. The next day, cells were washed twice with PBS (140 mM NaCl, 2.7 mM KCl, 10 mM Na_2HPO_4, and 1.8 mM KH_2PO_4) and incubated with Alexa Fluor 488-labeled donkey anti-rabbit IgG (Thermo Fisher, USA). Following washing with PBS, the cells were stained with 4′,6-diamidino-2-phenylindole (DAPI). After washing twice with PBS, the cover slips were mounted on glass slides with one drop of antifade solution. The immunofluorescence was visualized and captured using LSM 710 Laser Scanning Confocal Microscopy (Carl Zeiss Inc, Germany) and analyzed using Zeiss ZENLE software. The lamprey liver cells and leukocytes were fixed for 15 min in 4% paraformaldehyde with PBS at room temperature. Thereafter, cells were treated according to the method described above to detect the expression of LAL2 in liver cells and leukocytes using flow cytometry (BD Biosciences, USA). The flow cytometer was set at 488 nm (excitation wavelengths) to detect green fluorescence. Cells incubated with normal rabbit IgG were used as isotype controls.

In the same way, MCF-7/K562 cells were observed for 2 h with rLAL2 protein and rLAL2 + LIP protein incubation. When the rLAL2 + LIP incubated group exhibited bubbling, all cells were fixed, blocked using fetal bovine serum, incubated with rabbit anti-rLAL2 antibody (primary antibody), followed by Alexa Fluor 555-labeled donkey anti-rabbit IgG antibody (second antibody) to detect the localization of LAL2 protein on MCF-7/K562 cells. After labeling LIP protein with Alexa Fluor 488 (Microscale Protein Labeling Kit, Invitrogen, USA), four experimental groups: Alexa 488-LIP, rLAL2-1 μg + Alexa 488-LIP, rLAL2-2 μg + Alexa 488-LIP, and rLAL2-3 μg + Alexa 488-LIP, were established to detect the location of LIP protein on the MCF-7/K562 cells. The cells were analyzed on a FACSAria flow cytometer (BD Biosciences, USA), which was set at 488 and 555 nm (excitation wavelengths) to detect green and red fluorescence, respectively.

The Synergistic Effect of rLAL2 on LIP Killing

MCF-7 cells (cultured in 96 well plate) and LIP protein were incubated with rLAL2 for 3 h. According to the experimental sequence in **Figure 4D**, MCF-7 cells were incubated with PBS, 2

μg LIP, 2.5 μg rLAL2, or 5 μg rLAL2, LIP was added to the MCF-7 cells that pre-incubated with 2.5 μg or 5 μg rLAL2, 2.5 μg/5 μg rLAL2, and LIP were pre-incubated and then the mixture was added to MCF-7 cells. Thereafter, cells were stained for 5 min using Hoechst (blue, Beyotime, Shanghai, China) and propidium iodide (PI, red, Thermo fisher, USA), finally analyzed on the Operetta™ High-content machine (PerkinElmer, USA).

MCF-7 and K562 cells were cultured and collected, the cells were divided into five groups with the addition of PBS, 5 μg rLAL2, 2 μg LIP, 2.5 μg rLAL2 + 2 μg LIP, and 5 μg rLAL2 + 2 μg LIP as shown in **Figure 4F**, respectively. Followed by staining with Hoechst and PI for 5 min. Cells were then filtered and analyzed using a flow cytometer set at 560 nm(excitation wavelength), and analyses were performed by using Cell Quest Pro software. The appropriate FSC voltage and threshold were adjusted, inspector-gate, G1 = R1, to regulate the fluorescence voltage to set the negative control and the compensation between the fluorescence. The samples were then loaded in order, and the data files were obtained.

Surface Plasmon Resonance Analysis

LIP or rLAL2 protein were coupled on the second channel of a CM5 chip using buffer (pH = 4.0), while the first channel was used as a reference channel, both chips were activated with NHS/EDC and blocked with ethanolamine. LIP or rLAL2 in HBS-EP solution was flowed through the rLAL2 or LIP chip. The analyte, rLAL2 or LIP protein, was diluted in the same buffer. The Biacore T200 (General Electric Company, USA) was used for the experiment and subsequent analysis. TRX was used as a negative control, using the same experimental method.

Quantitative Real-Time PCR (Q-PCR)

Adult *L. japonica* were divided into three groups (three animals per group), each immunized with 100 μL *S. aureus*, *V. anguillarum* (suspended to 1×10^8 cells/mL in normal saline), or Poly I:C (0.1 mg/mL) for 0 h (immediately following addition of stimulus), 2, 8, 24, 48, and 72 h via intraperitoneal injections, respectively. Adult lamprey blood was collected by cutting the tail, and leukocytes were isolated from blood by Ficoll-Paque gradient centrifugation with lymphocyte separation solution (160 × *g*, 20 min) (TBD, China). *L. morii* were immunized using the same method to collect sera. The gill, supraneural body, heart, liver, intestine, kidney, and leukocytes were obtained from normal adult *L. japonica*. Total RNA was extracted from the tissues and cells using Trizol (Invitrogen, USA), and the RNA was treated with DNase I (TaKaRa, Dalian, China). Reverse transcription that each group of RNA is quantified to 2 μg was performed using gDNA Eraser (PrimeScript™ RT reagent Kit) as described by the manufacturer (TaKaRa, Dalian, China). Real-time quantitative PCR was conducted using a SYBR® PrimeScript™ RT-PCR Kit (TaKaRa, Dalian, China) according to the manufacturer's protocol. The PCR was performed in a 25 μL volume, consisting of 2 μL cDNA (diluting to 50 ng/μL), 12.5 μL SYBR Premix Ex Taq, 1 μL of each primer (10 μM), and ddH_2O. The gene expression in each sample was normalized relative to the *gapdh* gene (GenBank accession no. KU041137.1). The reaction efficiency was tested by gradual dilution of the cDNA template (1, 5, 10, 20, and 40×). The amplification efficiency of all primers was confirmed to be between 0.9 and 1.1, and the specificity of the amplification reaction was analyzed by dissociation curve analyses. The primer sequences used are as follows: *lal2*-F: 5′-ACGGTCCACCTGCACGAAT-3′; *lal2*-R: 5′-TTCACCTCCTTCATCAGTCCAA-3′. L-*gapdh*-F: 5′-AACC AACTGCCTGGCTCCT-3′; L-*gapdh*-R: 5′-GTCTTCTGCGTT GCCGTGT-3′.

Scanning Electron Microscopy (SEM) for Bacterial Morphology

The bacteria were incubated with PBS and 5 μM LAL2 at 4°C for 12 h, fixed with 2.5% glutaraldehyde (Kemiou, China) at 4°C overnight, and dehydrated at various ethanol gradients: 30, 50, 80, and 100%. In 100% ethanol, point samples on tables were sprayed with gold and photographed using scanning electron microscopy.

Enzyme Linked Immunosorbent Assay (ELISA) Analysis of the Interaction Between LAL2 Protein and Microbial Components

Plates were coated with various microbial components (0.2 μg/well) at 4°C overnight, then were washed and incubated with different concentrations of LAL2 (0, 10, 20, 50, 100, 200 nM) at 37°C for 3 h, 1% BSA was added, followed by detection with 100 μL/well rabbit anti-LAL2 antibody (4 μg/mL) and goat anti-rabbit antibody (1.5 μg/mL). ELISA substrate (100 μL/well, Solarbio, USA) was added and incubated for 15 min at 37°C, color development was halted through the addition of 2 M H_2SO_4 (50 μL/well). The plates were washed thrice with PBST (PBS with 0.05% Tween-20) between steps. One representative experiment of three is shown. Background absorbance without LAL2 protein and with anti-LAL2 antibody was subtracted as a negative control (NC).

Statistical Analysis

All calculations were performed using GraphPad Prism 7 (GraphPad Software Inc, USA). The data are presented as the mean ± S.E. The significance of the differences between the mean values was determined using Microsoft Excel 2007. In all cases, $^*P < 0.05$ was considered a statistically significant difference, $^{**}P < 0.01$ was considered a very significant difference, and $^{***}P < 0.001$ was considered an extremely significant difference.

RESULTS

Identification and Purification of Lamprey LAL2

In our previous study, lamprey sera exerted important cytotoxic effects on tumor cells (28). This is evidenced by the morphological changes and cell organelle damage observed in cervical cancer cells (HeLa) and acute promyelocytic leukemia cells (NB4) treated with lamprey serum during a 15 min incubation (28). To identify this cytotoxic protein in the sera (**Figure 1A**), lamprey sera was purified using a hydroxyapatite column and a Q Sepharose Fast Flow column. The fraction of

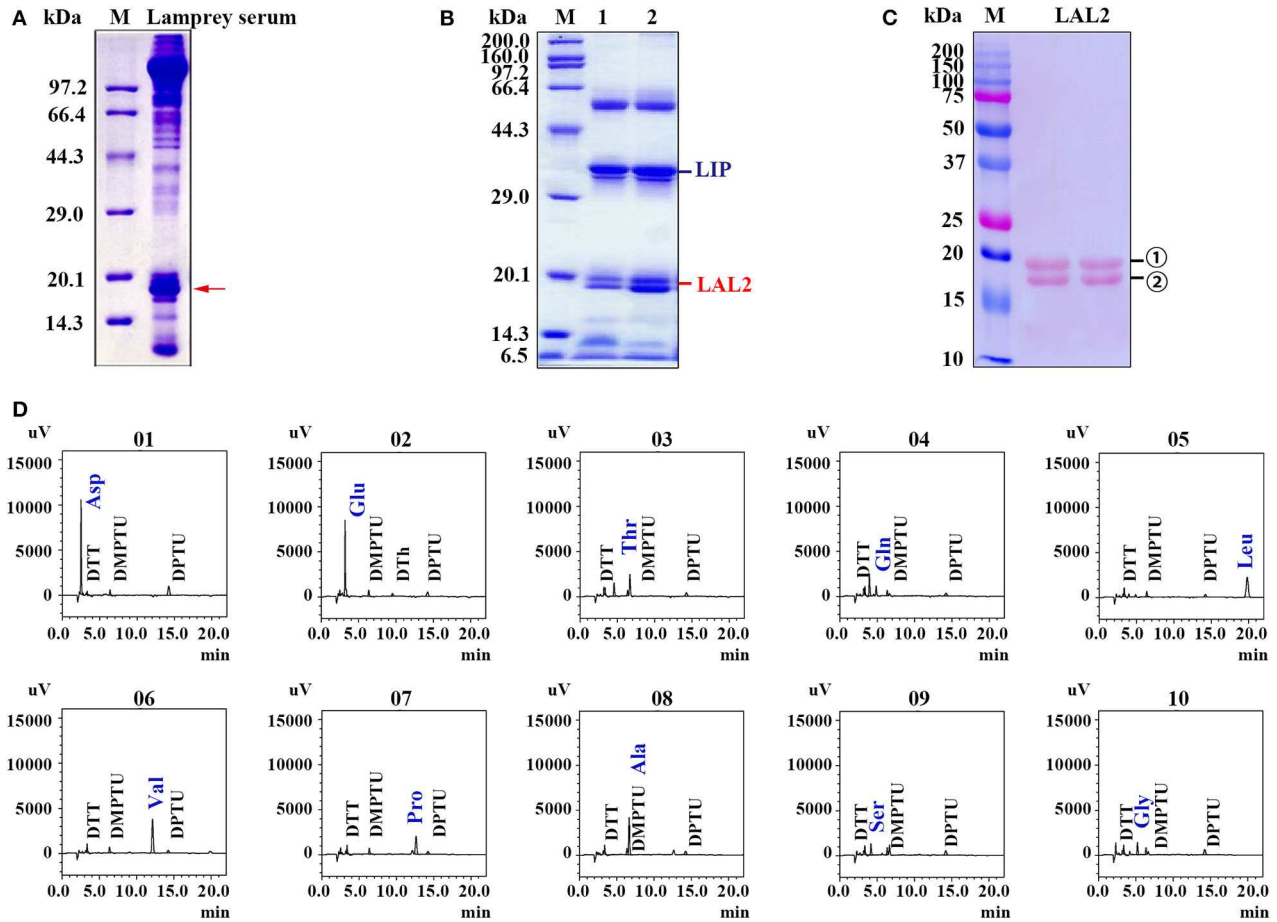

FIGURE 1 | Isolation and identification of LAL2 from lamprey serum. **(A)** Electrophoretic patterns of lamprey serum proteins via 15% SDS-PAGE. M, low molecular-weight protein marker. Red arrow points to apolipoprotein LAL2. **(B)** Detection of killer components in lamprey sera via 12% SDS-PAGE. **(C)** Electrotransfer atlas of LAL2 from lamprey serum that dyed with Ponceau S. M, Dual marker (Bio-Rad), bands for number 1 and 2 both represent LAL2. **(D)** Ten amino acid test maps of LAL2 N-terminal sequence (number 1).

protein activity was determined by the degree of cell membrane disruption. When these fractions with active protein were collected and analyzed via 12% SDS-PAGE, a protein band was observed at ∼34 kDa molecular-weight (**Figure 1B**). According to the liquid chromatography-tandem mass spectrometry (LC/MS/MS) analysis of tryptic-digested peptides, the purified protein was identified as LIP. In addition, we observed two protein bands positioned at ∼15–20 kDa. The two proteins were identified as LAL2 by mass spectrometry (**Tables S1, S2**). To detect the difference between the two LAL2 proteins (①② in **Figure 1C**), N-terminal sequencing was performed by Edman degradation and online analysis of High-Performance Liquid Chromatography at the Shanghai Life Science Research Institute. As shown in **Figure 1D** and **Figure S1**, the first ten amino acids of the two bands were identical (NH2-Asp-Glu-Thr-Gln-Leu-Val-Pro-Ala-Ser-Gly), which may be the result of glycosylation. Of course, it may also be possible that the C-terminal peptide of LAL2 was degraded. The open reading frame (ORF) of LAL2 has 576 bp and encodes a total of 191 amino acid residues. The first 23 amino acids coded after the initiation ATG are characteristic of a signal peptide.

Evolutionary Analyses of LAL1 and LAL2

The LAL2 proteins were purified and identified in the "high-density lipoprotein fraction" of plasma from *Petromyzon marinus* (1). However, high homology in amino acid sequences was not observed between LAL2 and the apolipoproteins of other species, and the domain in LAL2 were not found to be similar to mammalian blood apolipoproteins. In the current study, the amino acid sequence alignment results of LAL2 revealed that LAL2 (*Lampetra japonica*) display more than 90% sequence similarity to blood plasma LAL2 from *Petromyzon marinus*, *Lampetra fluviatilis,* and *Lethenteron reissneri* (**Figure S2**). To better understand the evolution of the *lal2* gene family during the vertebrate evolutionary process, the neighboring gene environment of lamprey *lal2* was compared among fish, amphibian, bird, and mammals. Using the draft genome assemblies of *Lethenteron reissneri*, we were able to assign

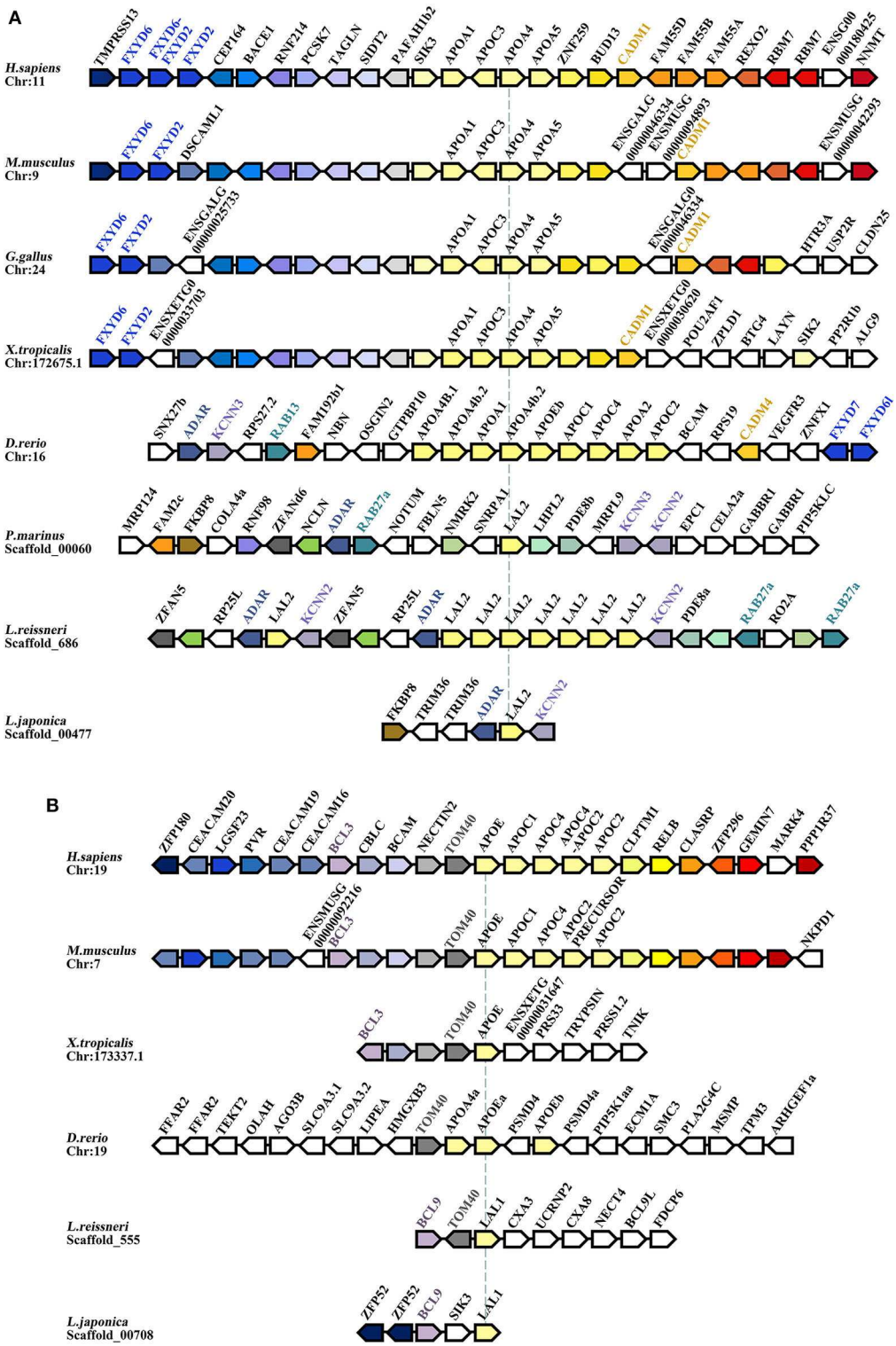

FIGURE 2 | Continued

orthology of the lamprey genes based on conserved synteny for genes directly surrounding the *lal2* gene (**Figure 2A**). A comparison of genomic regions containing *lal2* genes shows that there are eight *lal2* loci on the *L. reissneri* scaffold_686, no introns, and similar gene groups as sea lamprey in its surrounding. Strong syntenic relationships among LAL2 gene

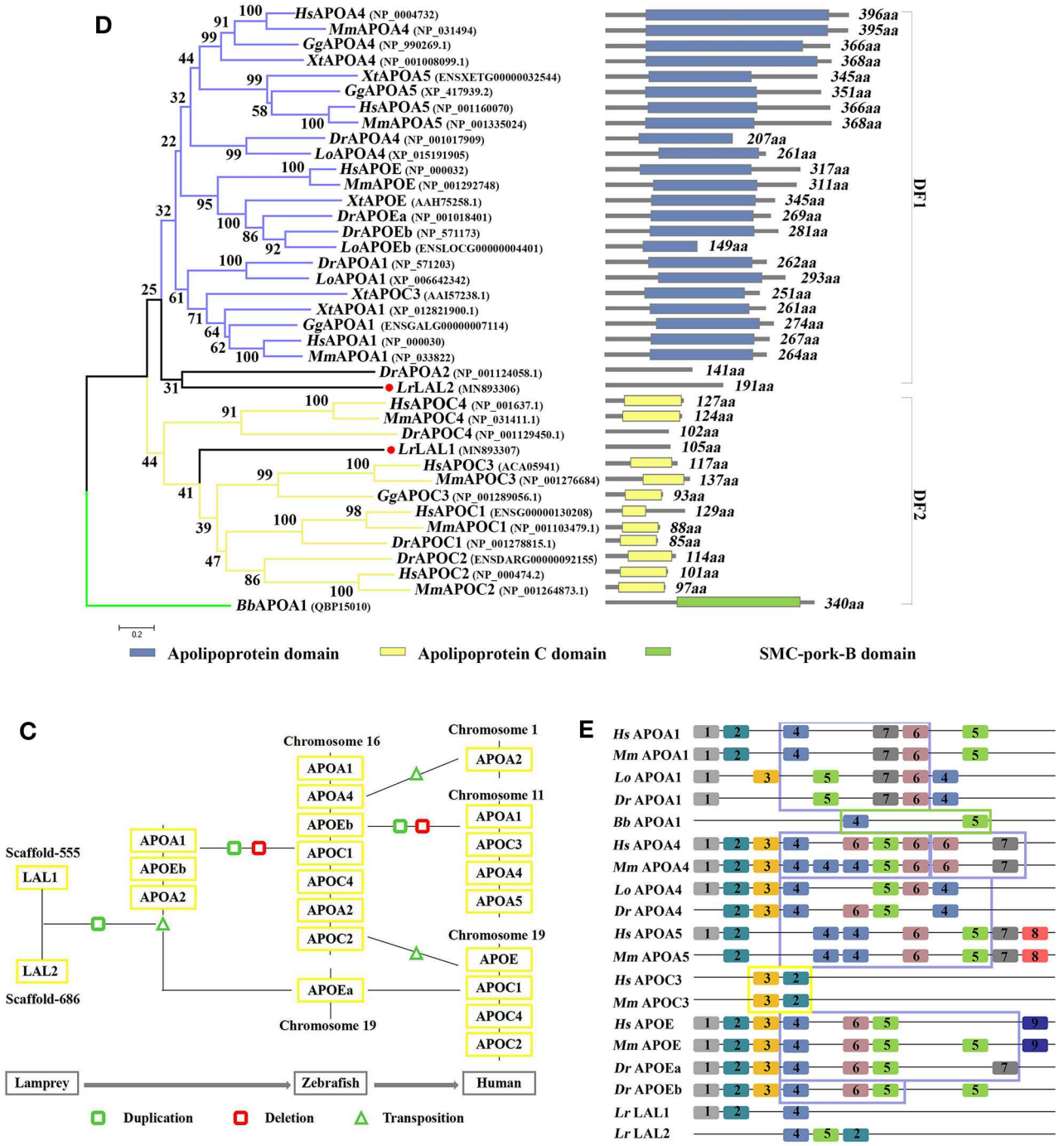

FIGURE 2 | Evolutionary analyses of LAL2. **(A,B)** The conservation of genes neighboring apolipoprotein family genes, the arrowheads pointing in opposite directions indicate genes located on opposite strands. Chr denotes the chromosome. **(C)** Model diagram of vertebrate apolipoprotein evolution. **(D)** The phylogenetic tree was constructed based on the 39 full-length protein sequences of APOA, APOC, APOE, LAL1, and LAL2. The optimal tree with the sum of branch length = 12.09372528 is shown and the percentage of replicate trees in which the associated taxa clustered together in the bootstrap test are shown next to the branches. The section on the right indicates the corresponding domain composition of the sequence in left. **(E)** A motif composition of the apolipoprotein family. The motifs, which are numbered 1–9, are shown in different colored blocks. The regions fenced by blue lines represent "apolipoprotein" domain, similarly the yellow represent "APO-CIII" domain, the green represents "SMC-pork-B" domain.

orthologs were easily detected in three jawless vertebrates (*L. reissneri, P. marinus,* and *L. japonica*) genome sequences that we examined. Three genes (*adar*, *kcnn,* and *rab)* surrounding *lal2* are also found in the neighborhood of zebrafish *apoa1*, *apoa2*, *apoa4*, *apoc1*, *apoc2*, *apoc4*, and *apoe*. In addition, this analysis confirmed that orthologs and paralogs of mammalian

apo are present in birds, amphibians, and bony fishes. Near to the *lal2* gene in the lamprey, the *fxyd* and *cadm* genes, although undetectable, could be examined for syntenic relationship with *apo* neighborhood in other vertebrates. Unfortunately, the tandem LAL2 sequences were unidentified based on the current sea lamprey genome data, thus, it is not possible to define the quantity of LAL2 on the chromosome of sea lamprey. And the adjacent genes of LAL2 are unable to determine perfectly because of poor sequencing and splicing results in *Lampetra japonica* genome. Furthermore, we also found *lal1* and *tom40* to be evolutionarily linked, and located on the *L. reissneri* scaffold_555 (**Figure 2B**). And *lal1* is always accompanied by *bcl* in lamprey, zebrafish, frog, mouse, and human, the chromosome on which it is located is relatively stable. However, we only find *lal1* in scaffold_05301 with no neighboring gene environment from *Petromyzon marinus* Germline Genome. And there is no *apoe* genomic information for reptiles and birds in genomics database. In a word, it is possible that close genomic proximity of *lal2* and *apoa* evolved, while LAL1 is located in close proximity to *apoe* in fish and mammals (**Figure 2C**), *apoc1, 2, 4* were formed by the replication and gene deletion of *apoa* and translocated to the periphery of *apoe* (29).

The phylogenetic tree based on the alignment of *Branchiostoma belcheri* APOA1, and other apolipoprotein amino acid sequences, involved in co-linearity was drawn using the NJ methods. *Lepisosteus oculatus* APOA1, APOA4, and APOEb were added to ensure the stability of the phylogenetic tree. As shown in **Figure 2D**, the BbAPOA1 was placed apart. The overall topology supported two main clusters, which corresponded to APOA/E and APOC vertebrate families, while lamprey LAL2 sequence was considered closer to APOA/E vertebrate family, similar to DrAPOA2 and equivalent to the outgroups of distinct family 1 (DF1). Based on the results of collinear analysis, this suggests that LAL2 is likely a common ancestor of vertebrate APOA1, A4, A5, and E. Lamprey LAL1 sequence was similarly considered closer to the APOC vertebrate family and formed distinct family 2 (DF2) with an improved bootstrap value and compact structure. Notably, the branch of LAL1 is also an outgroup equivalent to DF1. The results of phylogenetic analysis demonstrated that lamprey LAL1 and LAL2 are likely to have common ancestors, and APOA/E and APOC in the vertebrate lineage arose by duplication and reorganization of LAL2 and LAL1, respectively.

Our predicted results using the PSIPRED website show that the α-helix of the LAL2 and LAL1 secondary structures account for 78.01 and 79.05% of the secondary structure, respectively (**Figures S3A,B**). Furthermore, circular dichroism shows the secondary structure of LAL2, similar to APOA1, to be comprised primarily of α-helices (**Figures S3C,D**). To analyze conservation of the amino acid sequence, after searching select representative sequences to predict motif composition (**Figure 2E**, **Table S3**), we observed that when MEME selects nine motifs to analyze the apolipoproteins of each species, amphioxus and lamprey display 2–3 motifs, APOC3 possesses only two motifs, while other apolipoproteins of zebrafish, spotted gar, mouse, and human possess 5–10 motifs. From the types of motifs is was found that LrLAL1 has the same motif 1, 2, and 4 as zebrafish, spotted gar, mouse, and human, while motifs 2, 4, and 5 exist in LrLAL2 and apolipoprotein A and E family sequences of most jaw vertebrates. Furthermore, motifs 3, 6, and 7 evolved from fish apolipoproteins, and motifs 8 and 9 are unique to mammalian APOA5 and APOE, respectively. The apolipoprotein domain of APOA1, APOA4, and APOE from jawed vertebrates, which is associated with lipid particles and may function in lipoprotein-mediated lipid transport, is primarily composed of motifs 4, 5, 6, and 7. These proteins contain several 22 residue repeats which form a pair of α-helices. Meanwhile the APOC3 "APO-CIII apolipoprotein" domain is primarily composed of motifs 2 and 3, which inhibit lipoprotein lipase (LPL) activity and play roles in triglyceride metabolism. It is obvious that LrLAL1 and LrLAL2 retain parts of the same motif as the above-mentioned domain, however, they do not possess the integral apolipoprotein domain. Therefore, it is suggested that the apolipoprotein superfamily from lamprey LAL1 and LAL2 to mammal APOA, APOC, and APOE has acquired most of its structural and functional innovations throughout vertebrate evolution.

The Expression Pattern of LAL2 in Lamprey Tissues and Cells

The relative expression levels of *lal2* gene in the lamprey gill, supraneural body, heart, liver, intestine, kidney, and leukocytes were detected using Q-PCR (**Figure 3A**). LAL2 is expressed in these tissues or cells, and the expression levels in liver, leukocytes, and kidney were relatively high. To detect the distribution of natural LAL2 protein in different tissues of the lamprey, we purified rLAL2 migrated as a single band using a 12% SDS-PAGE gel with a molecular mass of ∼38 kDa (**Figure S4A**), and prepared LAL2 rabbit polyclonal antibody, which specifically recognized rLAL2 and native LAL2 (**Figures S4B,C**). The band around 40 kDa in the serum sample was identified as LAL2-dimer using LC-MS/MS analysis (**Figure S4D**). The localization analysis was performed using immunohistochemistry as described previously (24), and LAL2 was primarily expressed in the epithelial cells and blood cells of the gill, blood cells of the supraneural body, endothelial cell area of the heart, venous areas of the liver, epithelial cells of the intestine, and venous and epithelial cells of the kidney (**Figure 3B**). The expression was relatively high in several tissues, such as liver, kidney, and supraneural body. The lamprey liver cells and leukocytes were fixed separately to further detect LAL2 expression at the protein level. Furthermore, intracellular localization of LAL2 was revealed using flow cytometry. Results showed that LAL2 was expressed in both liver cells and leukocytes (**Figure 3C**, left), which was observed in the cytoplasm using confocal microscopy (**Figure 3C**, right).

LAL2 Can Promote the Localization and Killing Effect of LIP on MCF-7 and K562 Cells

LIP is a cytotoxic lamprey protein, which plays an important role in tumor cell survival and growth (21–24). Previously, during the process of purifying the cytotoxic protein in lamprey serum, it was found that LIP and LAL2 were always present

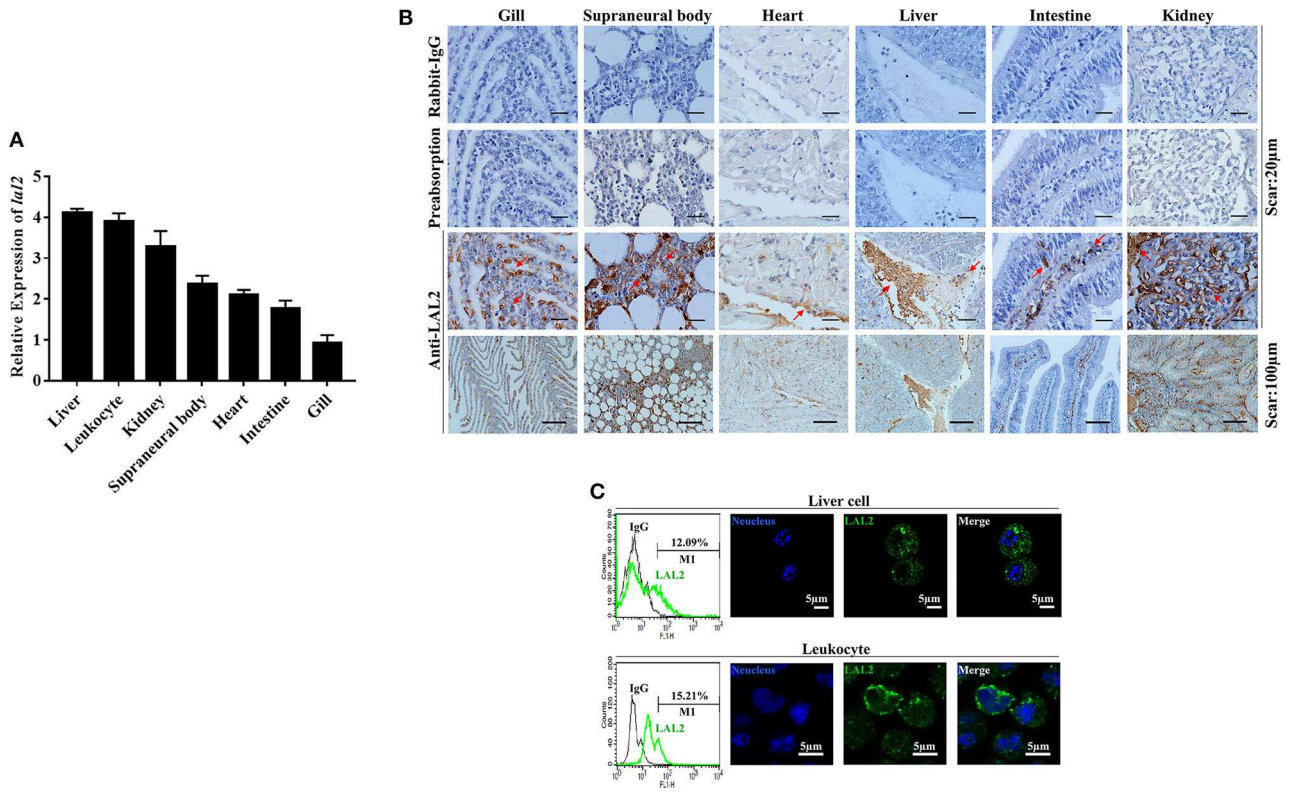

FIGURE 3 | The tissue distribution and cellular localization of LAL2. **(A)** The expression level of *lal2*, which was compared with *gapdh* in various lamprey tissues using Q-PCR. **(B)** Distribution and localization of LAL2 as observed by immunohistochemical staining, in which rabbit IgG is an isotype control, LAL2 with antibody incubating group (preabsorption) was used as a negative control, the upper parts of group anti-LAL2 are the corresponding enlarged view below. **(C)** Flow cytometry and immunofluorescence was used to analyze the localization of LAL2 in lamprey liver cells and leukocytes, as compared to IgG. Images were taken by laser confocal microscopy with the fluorescent cell-labeling dye DAPI (blue) and Alexa Fluor 488 goat anti-rabbit IgG (green). Scale bar: 5 μm.

in an eluted sample (**Figure 1B**). To determine whether there is a certain interaction between LIP and LAL2, rLAL2 or LIP protein were anchored to the surface of the chip using surface plasmon resonance technology, different concentrations of LIP or rLAL2 were used as analytes, and affinity kinetics fitting analysis was performed: rLAL2 protein flowed through the anchored LIP chip, the affinity KD was 5.582E-8M, LIP flowed through the anchored rLAL2 chip, and the affinity KD was 2.11E-8M. Both KD values reflect the same magnitude. This fully demonstrates the strong interaction between rLAL2 and LIP (**Figures 4A,B**), and suggests that LIP has no interaction with TRX (**Figure 4C**).

LIP exerts a specific killing effect on certain tumor cells (23, 24). The selective killing mechanism proposes that LIP could bind to biantennary bi-sialylated non-fucosylated N-glycan of cancer cells, such as MCF-7 and K562 cells, and not affect normal cells (22). It was speculated that the interaction between rLAL2 and LIP may also influence LIP killing activity, the MCF-7 cells sensitive to LIP are plated in 96-well plates for overnight culture, according to the experimental design. Results of PI/Hoechst staining and high-content analysis indicated that rLAL2 treatment alone had no impact on MCF-7 cells. However, rLAL2 significantly promoted the killing effect of LIP on MCF-7 cells in a dose-dependent manner ($^*P < 0.05$, **Figures 4D,E**), regardless of whether rLAL2 protein was incubated with MCF-7 cells alone before LIP protein addition or a mixture of rLAL2 and LIP was added to the cells. In order to further verify the synergy of rLAL2 on the killing activity of LIP, K562 cells were analyzed, showing results identical to those of MCF-7 cells. Furthermore, the effect of rLAL2 on the killing activity of LIP was analyzed using a combination of PI staining and flow cytometry, indicating that the results are consistent with the above results (**Figure 4F**). In summary, our findings show that LAL2 play a major role in assisting LIP to kill tumor cells.

To investigate the localization of LIP on MCF-7 or K562 cells affected by the interaction of LAL2, immunofluorescence assays were performed with LAL2 (labeled with Alexa 555) and LIP (labeled with Alexa 488). Thereafter, MCF-7 or K562 cells were incubated with LAL2 alone, LIP alone, or the combination of LAL2 and LIP. The results revealed that rLAL2 could bind to MCF-7 or K562 cells and was not affected by LIP. When Alexa 555-LAL2 and Alexa 488-LIP were added together to MCF-7/K562 cells, compared with Alexa 488-LIP treated alone, the number of cells located by Alexa 488-LIP increased. As the

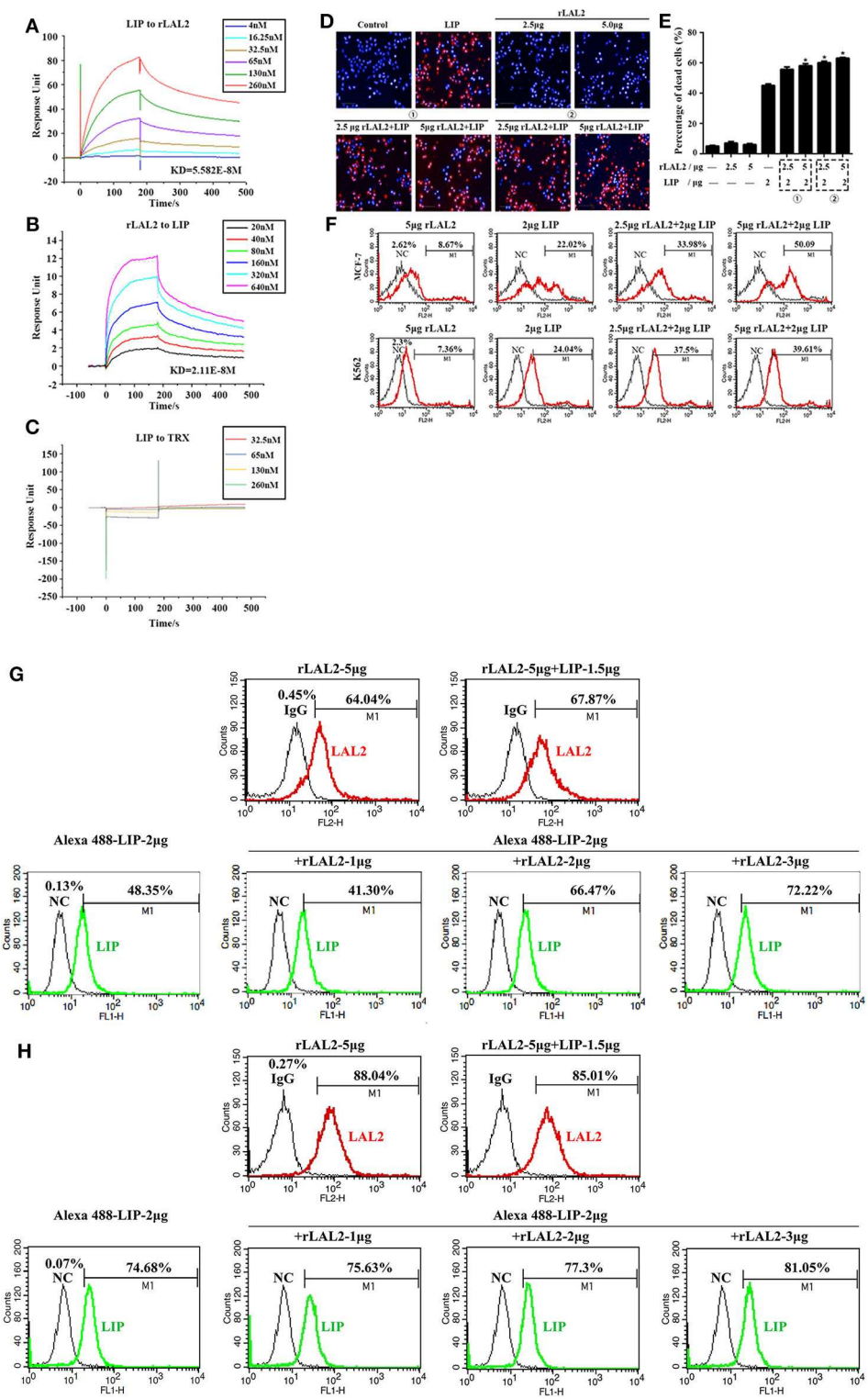

FIGURE 4 | LAL2 plays a synergistic role in LIP killing the tumor cells. **(A)** Biacore analysis of the interactions between different concentrations of rLAL2 and immobilized LIP [in resonance units (RU)]. **(B)** Biacore analysis of different concentrations of LIP and immobilized rLAL2 (in RU). **(C)** Biacore analysis of different TRX concentrations and immobilized LIP. **(D,E)** High-content analyzed the killing effect of LIP on MCF-7 cells after incubation with rLAL2 ($n = 3$), scale bar: 100 μm. The statistical map is calculated from six fields randomly selected for each well. **(F)** Flow cytometry was used to analyze the killing effect of LIP on MCF-7/K562 cells after incubation with rLAL2. **(G,H)** Effect of rLAL2 on the localization of LIP molecule on MCF-7/K562 cells with the Alexa 488-LIP (green) and Alexa 555-goat anti-rabbit IgG (red).

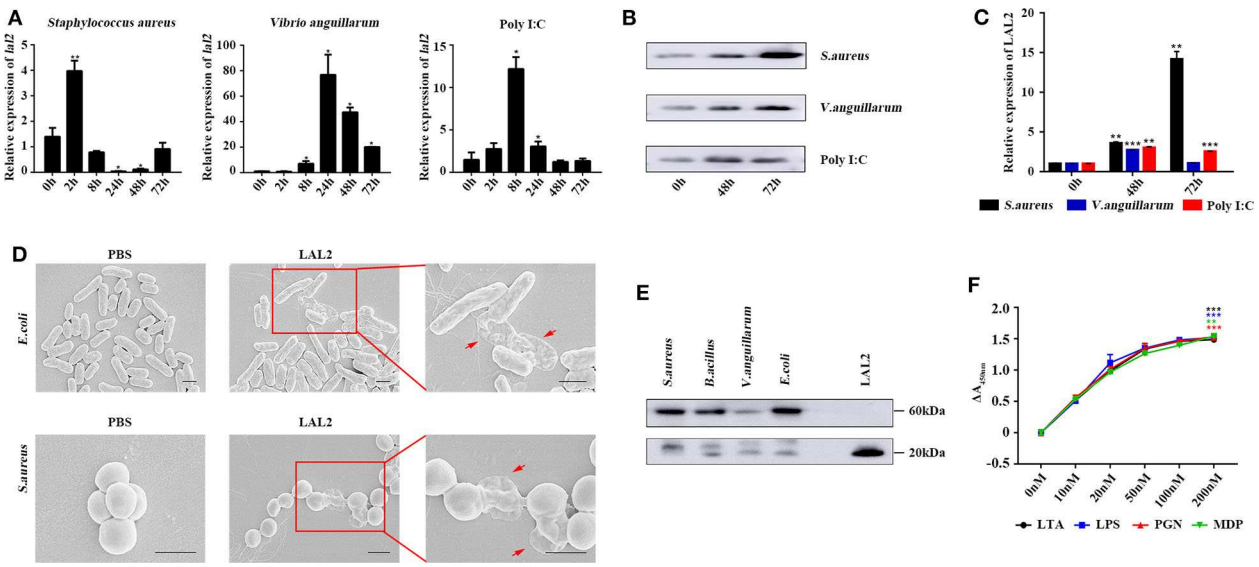

FIGURE 5 | LAL2 plays an important role in the antibacterial and antiviral process. **(A)** Q-PCR was used to determine the relative expression of *lal2* genes after stimulating ($n = 3$). **(B)** After 48 and 72 h stimulation with different immunogens, western blot detected LAL2 protein expression level in lamprey serum ($n = 3$). **(C)** The summary graph of LAL2 relative expression by calculating the ratio of gray values. **(D)** Scanning electron microscope image of bacteria after LAL2 incubation. In the LAL2 treatment group, the right picture is an enlarged view of the left picture. Scale bar: 1 μm. **(E)** The binding of microorganisms by LAL2 proteins. Every living microbial strain was incubated with 10 μg natural LAL2 proteins in PBS buffer for 12 h, and the washed pellets were subjected to 15% SDS-PAGE and detected using western blot with an anti-LAL2 antibody. LAL2 protein 0.5 μg is used as positive control. **(F)** ELISA analysis of the interaction between LAL2 and microbial components ($n = 3$) $^{*}P < 0.05$, $^{**}P < 0.01$, $^{***}P < 0.001$.

concentration of LAL2 increased, the number of cells located by Alexa 488-LIP gradually increased (**Figures 4G,H**).

LAL2 Involved in the Immune Response of Bacteria and Poly I:C

Based on the above experimental results, it is speculated that LAL2 plays a role in the lamprey immune response. To verify this hypothesis, by means of Q-PCR, the temporal expression of *lal2* genes was detected after stimulating lamprey with gram-positive bacterium, gram-negative bacterium, or Poly I:C virus mimic for 0, 2, 8, 24, 48, or 72 h (**Figure 5A**). The results showed that the expression of *lal2* mRNA was up-regulated significantly ($P = 0.0005$) in the *S. aureus* stimulation group, and reached the maximal level at 2 h post-stimulation, which was 4.0-fold compared with the 0 h group. In the *V. anguillarum* stimulation group, the expression of *lal2* was strongly up-regulated ($P = 0.0214$), and reached the maximal level at 24 h, which was 76.8-fold compared with the blank group. The expression of *lal2* was also significantly increased ($P = 0.0134$) with Poly I:C stimulation and reached the maximal level at 8 h, which was 12.2-fold compared with the control group. In the case of the same amount of total serum protein, the protein levels of LAL2 were significantly increased by stimulation of *S. aureus*, *V. anguillarum,* and Poly I:C over 48 and 72 h (**Figures 5B,C**).

Subsequently, we used *S. aureus* and *E. coli* to detect the antibacterial activity of LAL2 (**Figure 5D**). Different bacterial strains were incubated with the purified natural LAL2 proteins in PBS as the experimental group (**Figure S5**), the control group was incubated with PBS. The morphological changes of the bacteria were observed using scanning electron microscopy. After LAL2 incubation, *S. aureus* and *E. coli* had changed in morphology, the cell surface appeared wrinkly and sunken, cell contents were released into the culture media, compared with the control group (areas indicated by red arrow). It was suspected that LAL2 could play a role in antibacterial activity by combining with bacteria to perform bacterial killing and clearance. Thereafter, four different bacterial strains were incubated with natural LAL2 proteins, including *S. aureus*, *B. cereus*, *V. anguillarum*, and *E. coli*, and the bacterial pellets were washed and analyzed using western blot with anti-LAL2 polyclonal antibody, indicating that LAL2 proteins could bind to gram-positive bacteria (*S. aureus* and *B. cereus*) and gram-negative bacteria (*E. coli*) in the form of a trimer. However, the combination with *V. anguillarum* was weak (**Figure 5E**). To explore the mechanism of combination, we used ELISA to evaluate the interaction between the natural LAL2 protein and different bacterial cell wall components (**Figure 5F**). The results showed that LAL2 could interact with soluble peptidoglycan (PGN), LTA, and LPS in a dose-dependent manner, and LAL2 could also bind specifically to minimal PGN motif muramyl dipeptide (MDP).

DISCUSSION

In 1986, M. Pontes et al. suggested that a similar amino acid composition exists for LrLAL1, LrLAL2, and MmAPOA4 (1). Later in 1996, Le Wang et al. performed a practical analysis of the systematic evolution of the apolipoprotein multigene

family and found that the common ancestors of APOA1, APOA2, APOA4, and APOE may have appeared 460 million years ago in an ordovician vertebrate, which may be related to the major apolipoprotein LAL1 and LAL2 in Lamprey (30). Recently, Liu et al. postulated that the ancestral members of apolipoprotein are likely APOA1 and/or APOA4, and that other apolipoproteins emerged subsequently by gene duplication (31). However, our study can trace back to their common vertebrate ancestor, lamprey, indicating that LAL1 and LAL2 are indeed apolipoproteins. Furthermore, LAL2 is located in an evolutionary original position relative to LAL1, with motifs 4 and 5 in LAL2 obtained from amphioxus APOA1, and LAL1 formed by loss of motif 5, inversion, and insertion of the transposon into another scaffold (**Figure 2E**). We, therefore, postulate the following scenario: a series of duplication events beginning from *lal2* and *lal1* (**Figure 2C**), produced on zebrafish chromosome 16, resulting in the following apolipoprotein genes: *apoa1*, *apoa2,* and *apoe*. Subsequently, *apoa1* underwent tandem duplications and produced *apoa4*, while *apoc* is generated by *apoa1*/*apoa4* fragments. A DNA transposition then resulted in the insertion of the *apoc3* gene in between the *apoa1* and *apoa4* genes (28). The *apoa2* gene moved to human chromosome 1 and the genes for *apoa1*, *a4*, and *c3* moved to human chromosome 11. During species evolution, *apoc1*, *apoc2*, and *apoe* were lost in Aves. Eventually the other apolipoprotein genes, *apoe*, *c1*, *c2*, and *c4*, remained as a cluster on human chromosome 19. In the current study, it is speculated that the ancestral apolipoprotein gene may be subjected to different selection pressures at the same time during early differentiation. The order of evolution may be LAL2/LAL1—APOA1/APOA4/APOE—APOA2/APOC1/APOC2—APOC3/APOA5—APOC4 (28, 30–34).

Fitch et al. observed that human APOA1 contains multiple repeats of 22 amino acids (22-mer), each repeat is a tandem array of two 11-mers (28, 33). It is suggested that the repeat unit of 22-mer has been a structural element that builds an amphipathic α-helix. In addition, the existence of a 22-mer periodicity has also been found in other apolipoproteins, including APOA2, A4, C2, C3, and E, and an 11-mer has been found in APOC1. Lamprey LALl has a repeat pattern similar to those in human APOA1 and APOC3, while there is no clear indication for the presence of internal duplication in LAL2 sequence (28). Moreover, since there are a large number of α-helices in LAL1 and LAL2, the segments 79–99 and 100–120 of LAL2 have the potential to form an amphipathic helical structure. The hydrophilic residues on one side of the amphipathic helix keep the apolipoproteins at the surface of the lipoprotein particle to facilitate transfer between lipoprotein particles and interaction with other molecules, such as enzymes and specific cell surface receptors. New motifs are gradually evolved in LAL1 and LAL2 to form the apolipoprotein functional domain and conservative α-helix to ensure better survival, thus producing several types of apolipoproteins with significantly different structures.

Both the mRNA and protein levels of LAL2 were primarily expressed in liver, leukocytes, and kidney of the lamprey, which differed from the tissue distribution observed for apolipoprotein expression in teleost fish. For example, most apolipoprotein genes exhibited tissue-specific expression patterns in intestine, liver, and skin of channel catfish (35). Moreover, human *apoa1*, *apoa4*, and *apoc3* have been cloned in fetal intestine and adult liver but not in fetal liver, kidney, heart, brain, or muscle (36). Hence, with evolution, the distribution of apolipoproteins has gradually become regionalized to further perform unique functions. However, liver, leukocytes, and kidney are important immune tissues, indicating that LAL2 is likely to play a critical role in immune defense. In fact, our previous study demonstrated that LIP is primarily distributed in the supraneural body and leukocytes of the lamprey (21), while LAL2 is abundant in the sera (**Figure 1A**, indicated by the red arrow), suggesting that LAL2 protein acts as a secreted protein and participates extensively in blood circulation to accomplish immune responses. Additionally, the unique recognition mechanism of LIP is dependent on binding with both N-linked glycans on GPI-Aps, and SM in lipid rafts (29). We, therefore, expect that LAL2 can assist LIP in the diagnosis and control of tumor cells via targeted human cancer therapies.

Comprehensive functional analyses revealed the role of lamprey LAL2 and immune responses (**Figure 5**). Insect apolipoproteins were shown to cooperate against pathogens, such as silkworm apolipophorins (13, 37–39). In respect with the immune defense, LAL2 exerts unique biological functions in synergy with LIP. Moreover, *lal2* was up-regulated after stimulating lamprey with gram-positive bacteria, gram-negative bacteria, and Poly I:C virus mimic, respectively. Scanning electron microscope (SEM) images show that LAL2 can destroy the structure of *S. aureus* and *E. coli* and influence bactericidal activity. This is similar to the results highlighting that high-density lipoprotein (HDL) in the carp epidermis is secreted into mucus and performs antibacterial activity (40). This lipoprotein is mainly composed of two major apolipoproteins (APOA1 and APOA2), which correspond to the most abundant plasma proteins in several bony fish and have antibacterial activity. Orange-spotted grouper *E. coioides* APOA1 can inhibit the replication of Singapore grouper iridovirus (SGIV), and up-regulate the expression of its immune-related genes, ISG15 and Mx-I (9).

Microbes express signature molecules known as pathogen-associated molecular patterns (PAMPs), such as LTA, PGN, and MDP in gram-positive bacteria, and LPS in gram-negative bacteria (41). Wang et al. found that *Branchiostoma belcheri* rAPOA1 can bind LPS and LTA of various gram-positive and gram-negative bacteria and exhibits antibacterial activity against gram-negative bacteria *in vitro* (42). Silkworm apolipophorin protein inhibits hemolysin gene expression of *S. aureus* via binding to cell surface LTA (13). Conserved high amphipathic α-helical content between fish and mammal apolipoproteins can neutralize LPS via the CD14/TLR4 (Toll Like Receptor 4) pathway and intercalate into lipid bilayers to resist bacterial invasion (16, 43, 44). To investigate the antibacterial mechanism of lamprey LAL2, ELISA results show LAL2 can bind to LPS, LTA, PGN, and MDP due to highly homologous α-helical content

with human APOA1 (**Figure S4**). In fact, APO-II/I proteins may either shuttle APO-III and other immune proteins to microbial surfaces, contribute to microbial clearance, or detoxify immune-stimulatory cell wall components (40). The lipid particles nucleated by lipid carrier proteins in the hemolymph may serve as platforms for recruiting immunity proteins (45). Future studies are required to elucidate the interaction between molecules in sera with LAL2 and the signaling pathway involving LAL2 in order to further unravel immune defense in lampreys.

In conclusion, this study identified the molecular evolution and tissue distribution of lamprey LAL2. Furthermore, we demonstrate that lamprey LAL2 can serve as an effector molecule in sera for immune responses, pattern recognition, and bactericidal activity. Our studies not only help to expand on the evolutionary history of the vertebrate apolipoprotein multigene family, but also provide new insight into the important and diversified functional properties of apolipoprotein.

DATA AVAILABILITY STATEMENT

Data can be found on Genbank—MN893307 and MN893306. Other raw data supporting the conclusions of this article will be made available by the authors, without undue reservation, to any qualified researcher.

ETHICS STATEMENT

The animal experiments were performed in accordance with the regulations of the Animal Welfare and Research Ethics Committee of the Institute of Dalian Medical University's Animal Care protocol (Permit Number: SCXK2008-0002).

AUTHOR CONTRIBUTIONS

QL, YP, and QH designed the experiments. Flow cytometry and immunohistochemistry were finished by QH. HW, QH, and YH analyzed the experimental results. QH and YP wrote the manuscript. All authors contributed to the article and approved the submitted version.

FUNDING

This work was funded by Chinese National Natural Science Foundation Grant (No. 31772884), The Project of Department of Ocean and Fisheries of Liaoning Province (No. 201805), Program of Science and Technology of Liaoning Province (No. 2019-MS-218), and Science and Technology Innovation Fund Research Project (No. 2018J12SN079).

SUPPLEMENTARY MATERIAL

The Supplementary Material for this article can be found online at: https://www.frontiersin.org/articles/10.3389/fimmu.2020.01751/full#supplementary-material

Figure S1 | Ten amino acid test maps of LAL2 N-terminal sequence (number 2).

Figure S2 | Sequence alignment results of LAL2 in *Lampetra japonica*, *Petromyzon marinus*, and *Lampetra fluviatilis*.

Figure S3 | The secondary structure of LAL2 and LAL1. **(A)** The predicted results on PSIPRED website of LAL2 secondary structures. Alpha helix, extended strand, beta turn, and random coil account for 78.01, 5.76, 3.14, and 13.09%, respectively. **(B)** The predicted results on PSIPRED website of LAL2 secondary structures. Alpha helix, beta turn, and random coil account for 79.05, 5.71, and 15.24%, respectively. **(C)** Circular dichroism shows two negative peaks and one positive peak in LAL2, which conform to the CD spectrum of the α-helix in the secondary structure of the protein (negative peaks at 208 and 222 nm, and positive peaks near 190 nm). **(D)** Sequence alignment analysis of sequence similarity between LrLAL2 and HsAPOA1. LAL2 is highly similar to the APOA1 sequence Helix3 (88–98), and it is also similar to the APOA1 sequence Helix4, 5, and 6 (99–120, 121–142, 143–164).

Figure S4 | Expression and purification of rLAL2 protein and preparation of antibodies. **(A)** Prokaryotic expression and purification of rLAL2. M, low molecular-weight protein marker; *lane 1*, non-induced Rosetta/pET32a-*lal2* cells; *lane 2*, induced Rosetta/pET32a-*lal2* cells using IPTG; *lane 3*, purified LAL2 recombinant protein, black line points at the target protein. **(B)** ELISA assay to assess the serum anti-LAL2 polyclonal antibody titer from two rabbits. **(C)** Analysis of the specificity of the rabbit anti-LAL2 polyclonal antibody using western blot. *lane 1*, LAL2 recombinant protein; *lane 2*, lamprey serum. **(D)** LC-MS/MS analysis trypic-digested peptides of LAL2-Dimer.

Figure S5 | Purification of natural LAL2 protein with anion exchange chromatography. (Left) The map of natural LAL2 protein purification process with anion exchange chromatography from UNICORN 7.0; (Right) Purification of natural LAL2 protein. M, low molecular-weight protein marker; lane 1, No. 46 serum sample; lane 2, Flow-through fluid; lane 3, Equilibrium fluid; lane 4, Eluent 20; lane 5, Eluent 25; lane 6, Eluent 30.

REFERENCES

1. Pontes M, Xu X, Graham D, Riley M, Doolittle RF. cDNA sequences of two apolipoproteins from lamprey. *Biochemistry.* (1987) 26:1611–7. doi: 10.1021/bi00380a019
2. Morita SY. Metabolism and modification of apolipoprotein B-containing lipoproteins involved in dyslipidemia and atherosclerosis. *Biol Pharm Bull.* (2016) 39:1–24. doi: 10.1248/bpb.b15-00716
3. Phillips MC. New insights into the determination of HDL structure by apolipoproteins: thematic review series: high density lipoprotein structure, function, and metabolism. *J Lipid Res.* (2013) 54:2034–48. doi: 10.1194/jlr.R034025
4. Mahley RW, Innerarity TL, Rall SC Jr, Weisgraber KH. Plasma lipoproteins: apolipoprotein structure and function. *J Lipid Res.* (1984) 25:1277–94.
5. Ramasamy I. Recent advances in physiological lipoprotein metabolism. *Clin Chem Lab Med.* (2014) 52:1695–727. doi: 10.1515/cclm-2013-0358
6. Hanada Y, Sekimizu K, Kaito C. Silkworm apolipophorin protein inhibits *Staphylococcus aureus* virulence. *J Biol Chem.* (2011) 286:39360–9. doi: 10.1074/jbc.M111.278416
7. Villarroel F, Bastías A, Casado A, Amthauer R, Concha MI. Apolipoprotein A-I, an antimicrobial protein in *Oncorhynchus mykiss*: evaluation of its expression in primary defence barriers and plasma levels in sick and healthy fish. *Fish Shellfish Immunol.* (2007) 23:197–209. doi: 10.1016/j.fsi.2006.10.008
8. Mohapatra A, Karan S, Kar B, Garg LC, Dixit A, Sahoo PK. Apolipoprotein A-I in *Labeo rohita*: cloning and functional characterisation reveal its broad spectrum antimicrobial property, and indicate significant role during ectoparasitic infection. *Fish Shellfish Immunol.* (2016) 55:717–28. doi: 10.1016/j.fsi.2016.06.045

9. Wei J, Gao P, Zhang P, Guo M, Xu M, Wei S, et al. Isolation and function analysis of apolipoprotein A-I gene response to virus infection in grouper. *Fish Shellfish Immunol.* (2015) 43:396–404. doi: 10.1016/j.fsi.2015.01.006
10. Tada N, Sakamoto T, Kagami A, Mochizuki K, Kurosaka K. Antimicrobial activity of lipoprotein particles containing apolipoprotein Al. *Mol Cell Biochem.* (1993) 119:171–8. doi: 10.1007/978-1-4615-3078-7_23
11. Levine DM, Parker TS, Donnelly TM, Walsh A, Rubin AL. *In vivo* protection against endotoxin by plasma high density lipoprotein. *Proc Natl Acad Sci USA.* (1993) 90:12040–4. doi: 10.1073/pnas.90.24.12040
12. Grunfeld C, Marshall M, Shigenaga JK, Moser AH, Tobias P, Feingold KR. Lipoproteins inhibit macrophage activation by lipoteichoic acid. *J Lipid Res.* (1999) 40:245–52.
13. Omae Y, Hanada Y, Sekimizu K, Kaito C. Silkworm apolipophorin protein inhibits hemolysin gene expression of *Staphylococcus aureus* via binding to cell surface lipoteichoic acids. *J Biol Chem.* (2013) 288:25542–50. doi: 10.1074/jbc.M113.495051
14. Parker TS, Levine DM, Chang JC, Laxer J, Coffin CC, Rubin AL. Reconstituted high-density lipoprotein neutralizes gram-negative bacterial lipopolysaccharides in human whole blood. *Infect Immun.* (1995) 63:253–8. doi: 10.1128/IAI.63.1.253-258.1995
15. Mangaraj M, Nanda R, Panda S. Apolipoprotein A-I: a molecule of diverse function. *Indian J Clin Biochem.* (2016) 31:253–9. doi: 10.1007/s12291-015-0513-1
16. Berbée JF, Coomans CP, Westerterp M, Romijn JA, Havekes LM, Rensen PC. Apolipoprotein CI enhances the biological response to LPS via the CD14/TLR4 pathway by LPS-binding elements in both its N- and C-terminal helix. *J Lipid Res.* (2010) 51:1943–52. doi: 10.1194/jlr.M006809
17. Catapano AL, Pirillo A, Bonacina F, Norata GD. HDL in innate and adaptive immunity. *Cardiovasc Res.* (2014) 103:372–83. doi: 10.1093/cvr/cvu150
18. Wu F, Chen L, Liu X, Wang H, Su P, Han Y, et al. Lamprey variable lymphocyte receptors mediate complement-dependent cytotoxicity. *J Immunol.* (2013) 190:922–30. doi: 10.4049/jimmunol.1200876
19. Nonaka M, Fujii T, Kaidoh T, Natsuume-Sakai S, Nonaka M, Yamaguchi N, et al. Purification of a lamprey complement protein homologous to the third component of the mammalian complement system. *J Immunol.* (1984) 133:3242–9.
20. Pei G, Liu G, Pan X, Pang Y, Li Q. L-C1qDC-1, a novel C1q domain-containing protein from *Lethenteron camtschaticum* that is involved in the immune response. *Dev Comp Immunol.* (2016) 54:66–74. doi: 10.1016/j.dci.2015.08.011
21. Xue Z, Liu X, Pang Y, Yu T, Xiao R, Jin M, et al. Characterization, phylogenetic analysis and cDNA cloning of natterin-like gene from the blood of lamprey, *Lampetra* japonica. *Immunol Lett.* (2012) 148:1–10. doi: 10.1016/j.imlet.2012.08.005
22. Pang Y, Gou M, Yang K, Lu J, Han Y, Teng H, et al. Crystal structure of a cytocidal protein from lamprey and its mechanism of action in the selective killing of cancer cells. *Cell Commun Signal.* (2019) 17:54. doi: 10.1186/s12964-019-0358-y
23. Pang Y, Li C, Wang S, Ba W, Yu T, Pei G, et al. A novel protein derived from lamprey supraneural body tissue with efficient cytocidal actions against tumor cells. *Cell Commun Signal.* (2017) 15:42. doi: 10.1186/s12964-017-0202-1
24. Pang Y, Wang S, Ba W, Li Q. Cell secretion from the adult lamprey supraneural body tissues possesses cytocidal activity against tumor cells. *Springerplus.* (2015) 4:569. doi: 10.1186/s40064-015-1270-6
25. Xu R, Song X, Su P, Pang Y, Li Q. Identification and characterization of the lamprey Flotillin-1 gene with a role in cell adhesion. *Fish Shellfish Immunol.* (2017) 71:286–94. doi: 10.1016/j.fsi.2017.06.061
26. Wang D, Gou M, Hou J, Pang Y, Li Q. The role of serpin protein on the natural immune defense against pathogen infection in *Lampetra japonica*. *Fish Shellfish Immunol.* (2019) 92:196–208. doi: 10.1016/j.fsi.2019.05.062
27. Wang Z, Lu J, Li C, Li Q, Pang Y. Characterization of the LECT2 gene and its protective effects against microbial infection via large lymphocytes in *Lampetra japonica*. *Dev Comp Immunol.* (2018) 79:75–85. doi: 10.1016/j.dci.2017.09.018
28. Han Y, Pang Y, Yu T, Xiao R, Shi B, Su P, et al. Lamprey serum can kill HeLa and NB4 tumor cells. *Acta Biochim Biophys Sin (Shanghai).* (2014) 46:623–6. doi: 10.1093/abbs/gmu039
29. Li WH, Tanimura M, Luo CC, Datta S, Chan L. The apolipoprotein multigene family: biosynthesis, structure, structure-function relationships, and evolution. *J Lipid Res.* (1988) 29:245–71.
30. Wang L, Chai J, Lu Y, Tan CC. Studies on the molecular evolution of apolipoprotein multigene family. *Yi Chuan Xue Bao.* (1994) 21:81–95.
31. Liu JQ, Li WX, Zheng JJ, Tian QN, Huang JF, Dai SX. Gain and loss events in the evolution of the apolipoprotein family in vertebrata. *BMC Evol Biol.* (2019) 19:209. doi: 10.1186/s12862-019-1519-8
32. Huebbe P, Rimbach G. Evolution of human apolipoprotein E (APOE) isoforms: gene structure, protein function and interaction with dietary factors. *Ageing Res Rev.* (2017) 37:146–61. doi: 10.1016/j.arr.2017.06.002
33. Luo CC, Li WH, Moore MN, Chan L. Structure and evolution of the apolipoprotein multigene family. *J Mol Biol.* (1986) 187:325–40. doi: 10.1016/0022-2836(86)90436-5
34. Boguski MS, Birkenmeier EH, Elshourbagy NA, Taylor JM, Gordon JI. Evolution of the apolipoproteins. Structure of the rat apo-A-IV gene its relationship to the human genes for apo-A-I, C-III, E. *J Biol Chem.* (1986) 261:6398–407.
35. Yang Y, Fu Q, Zhou T, Li Y, Liu S, Zeng Q, et al. Analysis of apolipoprotein genes and their involvement in disease response of channel catfish after bacterial infection. *Dev Comp Immunol.* (2017) 67:464–70. doi: 10.1016/j.dci.2016.09.007
36. Karathanasis SK. Apolipoprotein multigene family: tandem organization of human apolipoprotein AI, CIII, and AIV genes. *Proc Natl Acad Sci USA.* (1985) 82:6374–8. doi: 10.1073/pnas.82.19.6374
37. Staczek S, Zdybicka-Barabas A, Mak P, Jasiłek AS, Kedracka-Krok S, Suder P, et al. Studies on localization and protein ligands of *Galleria mellonella* apolipophorin III during immune response against different pathogens. *J Insect Physiol.* (2018) 105:18–27. doi: 10.1016/j.jinsphys.2017.12.009
38. Zdybicka-Barabas A, Cytrynska M. Involvement of apolipophorin III in antibacterial defense of *Galleria mellonella* larvae. *Comp Biochem Physiol B Biochem Mol Biol.* (2011) 158:90–8. doi: 10.1016/j.cbpb.2010.10.001
39. Kamareddine L, Nakhleh J, Osta MA. Functional interaction between apolipophorins and complement regulate the mosquito immune response to systemic infections. *J Innate Immun.* (2016) 8:314–26. doi: 10.1159/000443883
40. Concha MI, Smith VJ, Castro K, Bastías A, Romero A, Amthauer RJ. Apolipoproteins A-I and A-II are potentially important effectors of innate immunity in the teleost fish *Cyprinus carpio*. *Eur J Biochem.* (2004) 271:2984–90. doi: 10.1111/j.1432-1033.2004.04228.x
41. Huang G, Huang S, Yan X, Li J, Xu W, Zhang L, et al. Two apextrin-like proteins mediate extracellular and intracellular bacterial recognition in amphioxus. *Proc Natl Acad Sci USA.* (2014) 111:13469–74. doi: 10.1073/pnas.1405414111
42. Wang W, Qu Q, Chen J. Identification, expression analysis, and antibacterial activity of apolipoprotein A-I from amphioxus (*Branchiostoma belcheri*). *Comp Biochem Physiol B Biochem Mol Biol.* (2019) 238:110329. doi: 10.1016/j.cbpb.2019.110329
43. Brouillette CG, Anantharamaiah GM, Engler JA, Borhani DW. Structural models of human apolipoprotein A-I: a critical analysis and review. *Biochim Biophys Acta.* (2001) 1531:4–46. doi: 10.1016/S1388-1981(01)00081-6
44. Ma J, Liao XL, Lou B, Wu MP. Role of apolipoprotein A-I in protecting against endotoxin toxicity. *Acta Biochim Biophys Sin (Shanghai).* (2004) 36:419–24. doi: 10.1093/abbs/36.6.419
45. Rahman MM, Ma G, Roberts HL, Schmidt O. Cell-free immune reactions in insects. *J Insect Physiol.* (2006) 52:754–62. doi: 10.1016/j.jinsphys.2006.04.003

Conflict of Interest: The authors declare that the research was conducted in the absence of any commercial or financial relationships that could be construed as a potential conflict of interest.

Copyright © 2020 Han, Han, Wen, Pang and Li. This is an open-access article distributed under the terms of the Creative Commons Attribution License (CC BY). The use, distribution or reproduction in other forums is permitted, provided the original author(s) and the copyright owner(s) are credited and that the original publication in this journal is cited, in accordance with accepted academic practice. No use, distribution or reproduction is permitted which does not comply with these terms.

frontiers in Immunology

ORIGINAL RESEARCH
published: 23 September 2020
doi: 10.3389/fimmu.2020.562795

Mediation of Mucosal Immunoglobulins in Buccal Cavity of Teleost in Antibacterial Immunity

Hao-Yue Xu[1,2†], Fen Dong[1†], Xue Zhai[1], Kai-Feng Meng[1], Guang-Kun Han[1], Gao-Feng Cheng[1], Zheng-Ben Wu[1], Nan Li[3] and Zhen Xu[1,2]*

[1] Department of Aquatic Animal Medicine, College of Fisheries, Huazhong Agricultural University, Wuhan, China, [2] Laboratory for Marine Biology and Biotechnology, Qingdao National Laboratory for Marine Science and Technology, Qingdao, China, [3] State Key Laboratory of Freshwater Ecology and Biotechnology, Institute of Hydrobiology, Chinese Academy of Sciences, Wuhan, China

The buccal mucosa (BM) of vertebrates is a critical mucosal barrier constantly exposed to rich and diverse pathogens from air, water, and food. While mammals are known to contain a mucosal associated lymphoid tissue (MALT) in the buccal cavity which induces B-cells and immunoglobulins (Igs) responses against bacterial pathogens, however, very little is known about the evolutionary roles of buccal MALT in immune defense. Here we developed a bath infection model that rainbow trout experimentally exposed to *Flavobacterium columnare* (*F. columnare*), which is well known as a mucosal pathogen. Using this model, we provided the first evidence for the process of bacterial invasion in the fish BM. Moreover, strong pathogen-specific IgT responses and accumulation of IgT^+ B-cells were induced in the buccal mucus and BM of infected trout with *F. columnare*. In contrast, specific IgM responses were for the most part detected in the fish serum. More specifically, we showed that the local proliferation of IgT^+ B-cells and production of pathogen-specific IgT within the BM upon bacterial infection. Overall, our findings represent the first demonstration that IgT is the main Ig isotype specialized for buccal immune responses against bacterial infection in a non-tetrapod species.

Keywords: evolution, mucosal immunoglobulins, B-cells, buccal mucosa, bacterial infection

OPEN ACCESS

Edited by:
Gyri T. Haugland, University of Bergen, Norway

Reviewed by:
David Parra, Hipra Scientific, Spain
Shawna L. Semple, Wilfrid Laurier University, Canada
Fumio Takizawa, Fukui Prefectural University, Japan

***Correspondence:**
Zhen Xu
zhenxu@mail.hzau.edu.cn

[†] These authors have contributed equally to this work

Specialty section:
This article was submitted to Comparative Immunology, a section of the journal Frontiers in Immunology

Received: *16 May 2020*
Accepted: *31 August 2020*
Published: *23 September 2020*

Citation:
Xu H-Y, Dong F, Zhai X, Meng K-F, Han G-K, Cheng G-F, Wu Z-B, Li N and Xu Z (2020) Mediation of Mucosal Immunoglobulins in Buccal Cavity of Teleost in Antibacterial Immunity. Front. Immunol. 11:562795. doi: 10.3389/fimmu.2020.562795

INTRODUCTION

Due to its broad geographic distribution and ability to adhere to mucosal tissues, *Flavobacterium columnare* (*F. columnare*) is considered as one of the most harmful bacterial pathogens that occurs worldwide and causes columnaris disease in most freshwater fish species, including rainbow trout (*Oncorhynchus mykiss*) (1–3). The pathogen is a long Gram-negative rod in the family *Flavobacteriaceae*, one of the main phyletic lines within the *Bacteroidetes* group from the domain (4). Columnaris disease generally begins as an external infection on the skin, fins, gills, or oral cavity (5), resulting in massive mortalities and economic losses. Previous studies have showed that interaction with mucosal surfaces is critical for the pathogenesis and pathological symptoms of *F. columnare* (6, 7). Therefore, it's necessary to understand the mechanisms responsible for mucosal immune responses to columnaris disease.

The buccal cavity (BC) represents the gateway of the gastrointestinal (GI) and respiratory tracts in vertebrates (8), and it is covered by a critical mucosal barrier (buccal mucosa, BM) that separates and protects the underlying tissues from the environment (9). Since the BM is continuously exposed

to a plethora of triggers including diverse commensal microbial communities and dietary and air- or waterborne antigens that may cause infection, vertebrates have evolved an effective innate and adaptive immune system to protect the BM surface (8). In mammals, extensive and organized mucosa-associated lymphoid tissue (MALT) has been characterized in the BM (10), which contains abundant immune cells (macrophages, dendritic cells, natural killer cells, and leukocytes) and effective molecules [immunoglobulins (Igs), cytokines, chemokines, antibacterial peptides, and complement factors] (11). Interestingly, in contrast with mammals, teleost BM lacks keratinization and salivary glands (12). In addition, our previous studies have shown that diffuse MALT appears in teleost BM and contains B-cells and Igs against waterborne antigens (13).

In mammals, secretory IgA (sIgA) is produced by local plasma cells (PCs) in the stroma of the salivary glands and is then transported to the oral mucosal surface mediated by polymeric Ig receptor (pIgR) (14). Moreover, sIgA, one of the principal antibodies present in saliva, could act against cariogenic bacteria and periodontopathic bacteria as well as maintain the homeostasis of the oral microbiota by limiting the colonization of microorganisms and their invasion of the buccal epithelium (11, 15, 16). Therefore, these results indicate that sIgA is the main humoral component involved in immune responses against oral bacterial pathogens (14). Interestingly, as there are many more bacterial pathogens in water than in air, aquatic vertebrates like teleost fish must have evolved an effective mucosal immune system to protect their BC. However, the teleost fish immune response against bacterial infection in the BM remains unknown.

In contrast to mammals (mainly containing IgM, IgG, IgA, IgD, and IgE), only three Ig isotypes have been identified in teleosts (IgM, IgT/IgZ, and IgD) (17). Teleost IgM is the prevalent Ig class in serum and it appears to have strong immune responses in systemic immunity (17, 18). Although secreted IgD (sIgD) has been described coating a low percentage of the bacteria in gill and buccal mucosal surface, and a high percentage in gut of rainbow trout (*O. mykiss*) (13, 19, 20), its function remains unknown. In contrast, teleost IgT (also named IgZ) was identified in 2005 (21, 22), and it was proven to play a predominant role in the mucosal immunity of teleosts, resembling the IgA in mammals (18). Recently, the research has shown the specialization of sIgT in protection of mucosal sites from pathogens and preservation of microbiota homeostasis (23). Notably, our previous studies have shown parasite-specific IgT and IgM titers in teleost buccal mucus and serum, respectively, indicating a specialized role of IgT in BM immune responses (13). However, after bacterial infection, the local responses of mucosal B-cells and specific responses mediated by IgT in teleost BM are thus far unknown. Interestingly, bacteria-specific IgA antibodies have been detected in saliva after bacterial infection in mammalians (24, 25). Since teleost IgT and mammalian IgA have evolved through a process of convergent evolution, we hypothesize that sIgT plays a key role in fish buccal immune responses to bacterial infection. To gain evidence for this hypothesis and further insight into the evolution of buccal B-cell responses, here, we developed a bath infection model with *F. columnare* in rainbow trout, a species often used in the field of evolutionary and comparative immunology. Furthermore, severely pathological changes and pathogen loads were found in trout BM after infection. Importantly, similar to the previous studies on salivary IgA, we showed that IgT is the main buccal Ig class in responses to bacterial pathogens. Moreover, we found that the local proliferation of IgT^+ B-cells and production of IgT occurred in trout BM resistance to bacterial infection, and thus characterized the unrecognized vital role of sIgT antibacterial infection in the BM of teleost fish.

MATERIALS AND METHODS

Fish Maintenance

Rainbow trout (mean weight, 3–5 *g*) were obtained from a fish farm in Shiyan (Hubei, China), and maintained in the aquarium tanks (1 m × 1 m × 1 m) using a water recirculation system involving thermostatic temperature control and extensive biofiltration. Fish were acclimatized for at least 2 weeks at 16°C and fed daily with commercial trout pellets (Efico) at a rate of 0.5–1% body weight during the whole experiment periods. Animal procedures were approved by the Animal Experiment Committee of Huazhong Agricultural University.

F. columnare Strain and Infection

The bacteria used in this study was *F. columnare* G_4 strain that obtained from Professor Pin Nie's lab in the Institute of hydrobiology Chinese academy of sciences. *F. columnare* strain G_4 was streaked from −80°C freezer and routinely cultured in Shieh broth as described previously (7). For *F. columnare* G_4 infection, two types of challenges were performed. In the first challenge, 60 fish (∼3–5 *g*) were challenged with *F. columnare* G_4 via immersion at a final concentration of 1×10^6 CFU ml^{-1} for 4 h at 16°C for each challenge experiment, and then transferred into the aquarium (1 m × 1 m × 1 m) containing new aquatic water. Tissue samples including BM, head kidney and spleen were collected from 6 individuals at days 1, 2, 4, 7, 14, 21, 28, and 75 after infection. Moreover, fluids (serum and buccal mucus) were taken from 12 individuals after 28 days post-infection (28 dpi, infected group). In the second challenge, another 60 fish were infected at 30 and 60 days post primary infection, and samples were taken at 75 days post-infection (75 dpi, immune group). Both experiments were performed at least three independent times. As a control (mock infected), the same number of fish were maintained in a similar tank (1 m × 1 m × 1 m) with the same culture medium without bacteria. The samples from control fish were also collected at days 1, 2, 4, 7, 14, 21, 28, and 75 post the medium culture mock challenge. Throughout this time, the fish were maintained in a flow through aquaria at 16°C, and fed daily with dry pellets at 0.5–1% biomass.

Distribution of *F. columnare* in Trout After Infection

To observe the invasion of *F. columnare* in BM and the distribution in trout tissues, we used green fluorescent protein

(GFP) labeled *F. columnare* G4 strain (with green fluorescent protein, offered by Professor Pin Nie's lab) infected as described above. Tissue samples (BM, gill, skin, and fin) were collected at days 1, 2, and 4 after infection. On the one hand, samples were washed three times with PBS to remove the bacteria on surface. Each sample was placed into sterile sample tube and then diluted with PBS at final concentration of 0.1 g ml^{-1} and homogenized by TissueLyser II (Jingxin Technology) using steel beads and shaking (60 HZ for 1 min) following the manufacturer's instructions. Then the homogenates were diluted tenfold and plated onto Shieh culture containing tetracycline, incubated at 28°C for 48 h. Bacterial counts were done in a double-blind fashion by two independent researchers using the fluorescence microscope as described previously (26). On the other hand, tissue samples (BM, gill, skin, and fin) were dissected and processed for routine histology to detect the localization of *F. columnare* used by fluorescence microscope as described previously (27). All images were acquired and analyzed using an Olympus BX53 fluorescence microscope (Olympus) and the iVision-Mac scientific imaging processing software (Olympus).

Histology, Light Microscopy and Immunofluorescence Microscopy Studies

The tissues of rainbow trout were dissected and fixed in 4% neutral buffered formalin overnight at 4°C, embedded in paraffin, and 4 μm thick sections stained with hematoxylin and eosin (H&E) or alcian blue (AB) as described previously (13). Images were acquired in a microscope (Olympus) using the Axiovision software. For the detection of IgT^+ and IgM^+ B-cells, sections were double stained with polyclonal rabbit anti-trout IgT (pAb; 0.5 μg ml^{-1}) and monoclonal mouse anti-trout IgM (IgG1 isotype; 1 μg ml^{-1}) overnight at 4°C. After washing three times, sections were stained with Alexa Fluor 488-conjugated AffiniPure Goat Anti-Rabbit IgG (H + L) and Cy3-conjugated AffiniPure Goat Anti-Mouse IgG (H + L) (Jackson ImmunoResearch Laboratories Inc.) at 2.5 μg ml^{-1} each for 40 min at room temperature to detect IgT^+ and IgM^+ B-cells, respectively. For detection of $pIgR^+$ cells in trout BM, we used the same methodology described previously by using polyclonal rabbit anti-pIgR antibody (pAb; 0.8 μg ml^{-1}) (18). Before mounting, all sections were stained with DAPI (4', 6-diamidino-2-phenylindole; 1 μg ml^{-1}; Invitrogen). All images were acquired and analyzed using an Olympus BX53 fluorescence microscope (Olympus) and the iVision-Mac scientific imaging processing software (Olympus).

RNA Isolation and Quantitative Real-Time PCR Analysis

Total RNA was extracted by homogenization in 1 ml TRIZol (Invitrogen) using steel beads and shaking (60 HZ for 1 min) following the manufacturer's instructions. A spectrophotometry (NanoPhotometer NP 80 Touch) was used to quantitate the extracted RNA and agarose gel electrophoresis was used to determine the integrity of the RNA. To normalize gene expression levels equivalent amounts of the total RNA (1000 ng), each sample was used for cDNA synthesis with the SuperScript first-strand synthesis system for Quantitative PCR (qPCR; Yeasen) in a 20 μl reaction volume. The synthesized cDNA was diluted 4 times and then used as a template for qPCR analysis. The total volume of qRT-PCR amplification system were 10 μl, containing 5 μl Master mix, 0.25 μl forward primer, and 0.25 μl reverse primer (10 μM), 1 μl diluted cDNA (200 ng), and 3.5 μl nuclease-free water. The internal control gene elongation factor 1α (EF1α) was employed as reference gene. The qPCRs were performed on a 7500 qPCR system (Applied Biosystems) using the EvaGreen 2 × qPCR Master mix (Yeasen). All samples were performed the following conditions: 95°C for 5 min, followed by 40 cycles at 95°C for 10 s and at 58°C for 30 s. A dissociation protocol was carried out after thermo cycling to confirm a band of the correct size was amplified. Ct values determined for each sample were normalized against the values for housekeeping gene (EF1α). The relative expression levels of immune-related genes were shown as $-\Delta\Delta Ct$ while the relative abundance of *F. columnare* were shown as $2^{-\Delta\Delta Ct}$. Primer sequences can be found in **Supplementary Table S1**. The relative expression level of the genes was determined using the Pfaffl's method (28).

DNA Extraction and PCR Amplification

To detect *F. columnare* in trout BM of different time points of experimental group, BM pieces with mucus were collected. About 10 mg BM sample was collected and homogenized by beads beating for 2 min at 60 Hz. DNA was extracted by using the E.Z.N.A.® soil DNA Kit (Omega Bio-tek, Norcross, GA, United States) according to manufacturer's protocols and assessed photometrically using a NanoDrop 2000 UV-vis spectrophotometer (Thermo Scientific, Wilmington, United States). The 16S rRNA specific primer was used to amplify the extracted DNA by thermocycler PCR system (GeneAmp 9700, ABI, United States). PCR reactions were performed in triplicate 20 μl mixture containing 4 μl of 5 × FastPfu Buffer, 2 μl of 2.5 mM dNTPs, 0.8 μl of each primer (5 μM), 0.4 μl of FastPfu Polymerase, and 10 ng of template DNA. The PCR reactions were conducted using the following program: 3 min of denaturation at 95°C, 27 cycles of 30 s at 95°C, 30 s for annealing at 55°C, and 45 s for elongation at 72°C, and a final extension at 72°C for 10 min. The PCR products were extracted from a 2% agarose gel and further purified using the AxyPrep DNA Gel Extraction Kit (Axygen Biosciences, Union City, CA, United States) and quantified using QuantiFluor™-ST (Promega, United States) according to the manufacturer's protocol.

Proliferation of B-Cells in the BM of Trout

For proliferation of B-cells studies, we modified the methodology as previously reported by us (13, 19, 29). Briefly, control and immune fish (∼15 g) were anesthetized with MS-222 and intravenously injected with 200 μg EdU (Invitrogen). After 24 h, the BMs from control and survival fish were dissected, fixed and embedded in paraffin as described above. Subsequently, the paraffin sections of BM were incubated at 4°C overnight with rabbit anti-trout IgT (pAb; 0.5 μg ml^{-1}) and mouse anti-trout IgM (IgG1 isotype; 1 μg ml^{-1}). After washing with PBS, paraffin sections were incubated for 45 min at room

temperature with Alexa Fluor 488-conjugated AffiniPure Goat anti-rabbit IgG and Cy3-conjugated AffiniPure Goat anti-mouse IgG (Jackson ImmunoResearch Laboratories Inc.) at 2.5 μg ml^{-1} each. EdU^+ cell detection was performed according to the manufacturer's instructions (Click-iT EdU Alexa Fluor 647 Imaging Kit, Invitrogen). Cell nuclei were stained with DAPI (1 μg ml^{-1}) before mounting with fluorescent microscopy mounting solution. Images were acquired and analyzed using an Olympus BX53 fluorescence microscope (Olympus) and the iVision-Mac scientific imaging processing software (Olympus).

Collection of Serum and Buccal Mucus

For sampling, trout were anesthetized with MS-222, and serum was collected and stored as described previously (29). To obtain the buccal mucus, we used the method described by Yu et al. (13). Fish BM tissue was excised and rinsed with PBS to remove the remaining blood. Thereafter BM tissue was incubated for 12 h at 4°C, with slightly shaking in protease inhibitor buffer (1 × PBS, containing 1 × protease inhibitor cocktail [Roche], 1 mM phenylmethylsulfonyl fluoride [Sigma]; pH 7.2) at a ratio of 250 mg of BM tissue per ml of buffer. The suspension (buccal mucus) was collected into an Eppendorf tube, and then vigorously vortexed and centrifuged at 400 *g* for 10 min at 4°C to remove trout cells. Then the cell-free supernatant was centrifuged at 10,000 *g* for 10 min at 4°C to remove the buccal bacteria from mucus. The resulting supernatant (containing buccal mucus) was harvested, filtered with 0.45 μm syringe filter (Millipore) and stored at 4°C prior to use.

SDS-PAGE and Western Blot

Buccal mucus and serum samples were resolved on 4–15% SDS-PAGE Ready Gel (Bio-Rad) under non-reducing conditions as described previously (13, 19). For western blot analysis, the gels were transferred onto PVDF membranes (Bio-Rad). Thereafter, the membranes were blocked with 8% skim milk and incubated with anti-trout IgT (rabbit polyclone antibody, pAb), anti-trout IgM (mouse monoclonal antibody, mAb), or biotinylated anti-trout IgD (mouse mAb) antibodies followed by incubating with peroxidase-conjugated anti-rabbit, anti-mouse IgG (Invitrogen) or streptavidin (Invitrogen). Immunoreactivity was detected with an enhanced chemiluminescent reagent (Advansta) and scanned by GE Amersham Imager 600 Imaging System (GE Healthcare). The captured gel images were analyzed by ImageQuant TL software (GE Healthcare). Thereafter, the concentration of IgT, IgM, and IgD were determined by plotting the obtained signal strength values on a standard curve generated for each blot using known amounts of purified trout IgT, IgM, or IgD.

Trout BM Explants Culture

Trout BM explants culture were used the similar method as previously described (13, 19). Briefly, control and immune fish were killed with an overdose of MS-222, and blood was removed through the caudal vein to minimize the blood content in the BM. Thereafter, approximately 20 mg of BM was submerged in 70% ethanol for 1 min to eliminate possible bacteria on their surface and then washed twice with PBS. Thereafter, tissues were placed in a 24-well plate and cultured with 400 μl DMEM medium (Invitrogen), supplemented with 10% FBS, 100 U ml^{-1} penicillin, 100 μg ml^{-1} streptomycin, 200 μg ml^{-1} amphotericin B, and 250 μg ml^{-1} gentamycin sulfate, with 5% CO_2 at 17°C. After 7 days culture, supernatants were harvested, centrifuged and stored at 4°C prior to use the same day, otherwise, stored at −80°C until further analysis.

Binding of Trout Immunoglobulins to *F. columnare*

To access whether infected and immune fish had generated *F. columnare*-specific immunoglobulins, we measured the capacity of IgT, IgM, and IgD from serum, buccal mucus or BM tissue explant supernatants to bind to *F. columnare* using a pull-down assay as described previously (13, 19). Initially, the *F. columnare* suspensions (1×10^8 CFU ml^{-1}) were preincubated with a solution of 0.5% BSA in PBS (pH 7.2) at 4°C for 2 h. Subsequently, 40 μl *F. columnare* were incubated with diluted fluids samples (buccal mucus, serum, or BM tissue explant supernatants) separately from infected, immune and control fish at 4°C for 4 h with continuous shaking in a 300 μl volume with PBS containing 1% BSA (pH 7.2). After incubation, the bacteria were washed three times with PBS and bound proteins were eluted with 2 × Laemmli Sample Buffer (Bio-Rad) and boiled for 5 min at 95°C. The eluted material was resolved on 4–15% SDS-PAGE Ready Gel (Bio-Rad) under non-reducing conditions, and the presence of IgT, IgM, or IgD was detected by western blotting using the anti-trout IgT, IgM, or IgD antibody as described above.

Statistics

An unpaired Student's *t*-test and one-way analysis of variance with Bonferroni correction (Prism version 6.01; GraphPad) were used for analysis of differences between groups. All data were expressed as mean ± SEM. Differences were considered significant when $P < 0.05$.

RESULTS

Pathological Changes in Trout BM After Bacterial Infection

Here, we showed the morphological structure of trout BM containing epithelium and an underlying layer of dense connective tissue (lamina propria; **Supplementary Figure S1**). To observe the invasion and distribution of bacterial pathogens in trout BM, we successfully constructed a bath infection model with *F. columnare* labeled by GFP (**Figure 1** and **Supplementary Figure S2**). At 2 days post-infection, we clearly detected that the classical phenotype of columnaris disease appeared in the trout, characterized by gill necrosis and fin rot, and we saw yellow dots suspected to be *F. columnare* on the surface of the fins and skin (**Figure 1A**). Interestingly, we detected a large number of bacteria with green fluorescence in trout BM from 2-day-infected fish by fluorescence microscope (**Supplementary Figure S2C**). Notably, the tissue homogenates of trout BM from control and 2-day-infected fish were both cultured on Shieh agar, and the bacterial colonies that were rhizoid and flat with yellow centers

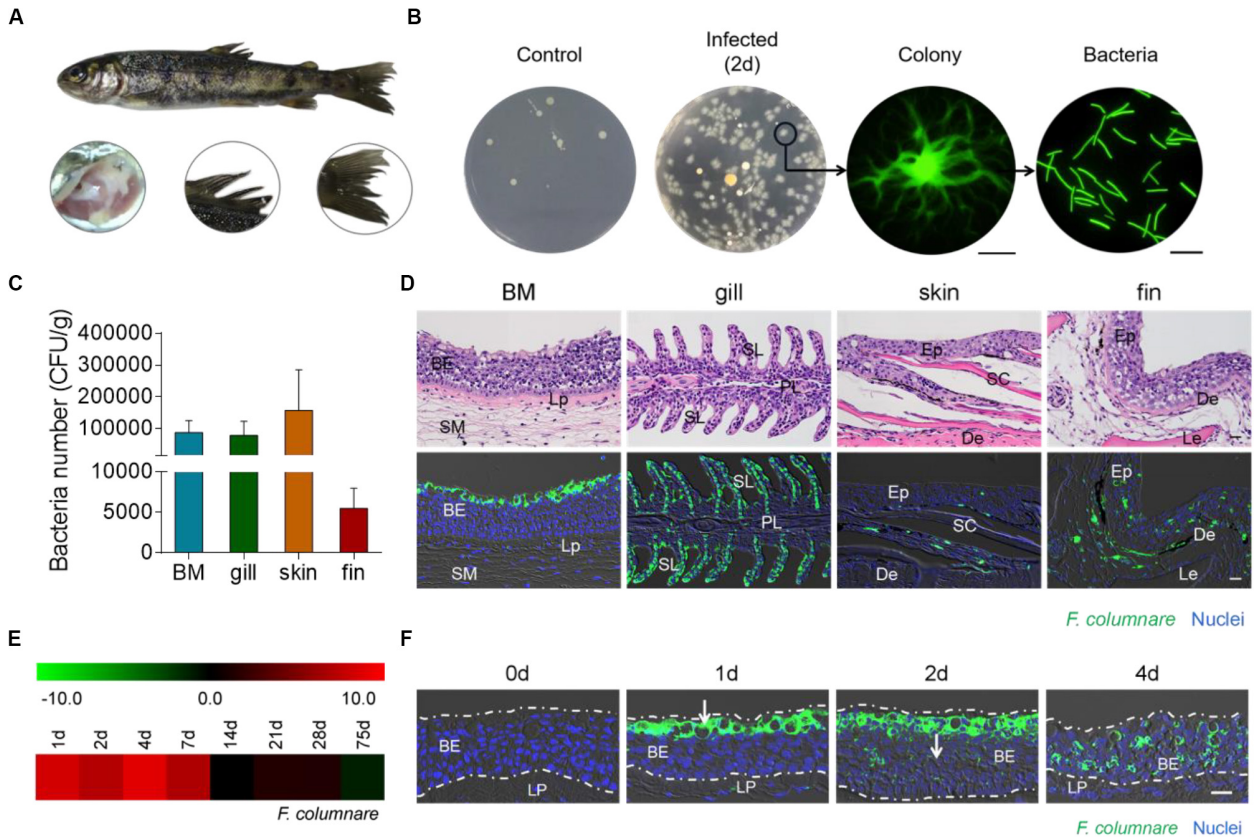

FIGURE 1 | Detection and visualization of *F. columnare* in rainbow trout. **(A)** The phenotype (e.g., gill necrosis and fin rot) of rainbow trout was observed at days 2 after infection with *F. columnare*. **(B)** The culture plates from trout BM of control fish and infected fish at days 2 post-infection. Colony image: a magnified view of circled colony from infected fish by fluorescence microscope (original magnification, ×10), Scale bar, 200 μm. Bacteria image: the observation of bacterial solution obtained by circled colony expansion (original magnification, ×40), Scale bar, 10 μm. **(C)** Numbers of *F. columnare* (CFU g^{-1}) was calculated by plate counting in trout BM, gill, skin, and fin tissue samples of infected fish at days 2 post-infection, respectively ($n = 6$) were 8.73×10^4, 7.83×10^4, 1.57×10^5, and 5.51×10^3 CFU g^{-1}. **(D)** Histological examination by hematoxylin/eosin staining (top) and immunofluorescence staining (bottom) of trout BM, gill, skin and fin paraffinic sections from 2 days infected fish. Differential interference contrast (DIC) images showing merged staining with *F. columnare* (green) and nuclei (blue). **(E)** Heat map demonstrated results from qRT-PCR of mRNAs for *F. columnare* in infected fish versus control fish measured on days 1, 2, 4, 7, 14, 21, 28, and 75 post-infection in BM of rainbow trout ($n = 6$). **(F)** Localization of *F. columnare* in trout BM of control fish and infected fish at days 1, 2, and 4 after infection. The white arrow indicates invasion process of *F. columnare* in BM. BE, buccal epithelium; Lp, lamina propria; SM, submucosa; PL, primary lamellae; SL, secondary lamellae; Ep, epidermis; SC, scales; De, dermis; and Le, lepidotrichia. Scale bar, 20 μm. Data are representative of three independent experiments (mean ± SEM).

were detected only in infected trout. In addition, these single colonies were isolated to grow in pure culture, and characteristic elongated rod-shaped bacteria with green fluorescence were clearly observed by fluorescence microscope (**Figure 1B**), which further verified the successful invasion of *F. columnare* in trout BM after infection.

Next, we measured the amount of *F. columnare* by plate counting in trout BM, gill, skin, and fin tissue samples of 2-day-infected fish. Interestingly, high numbers of bacteria were detected in the BM (8.73×10^4 CFU g^{-1}), gill (7.83×10^4 CFU g^{-1}), skin (1.57×10^5 CFU g^{-1}), and fins (5.51×10^3 CFU g^{-1}; **Figure 1C**). Moreover, using H&E and immunofluorescence microscopy analysis, we observed the *F. columnare* mainly located on the epithelium of trout BM, gill, skin, and fins after infection (**Figure 1D**). By quantitative real-time PCR (qRT-PCR) and PCR, we detected the expression of *F. columnare* 16S rRNA in the BM of both trout after bacterial infection and control fish (**Figure 1E** and **Supplementary Figure S2B**). A time-series study of *F. columnare* 16S rRNA expression showed that the bacteria accumulated in trout BM mainly in the first 7 days after challenge. Importantly, we observed that *F. columnare* gathered especially on the mucus cells of the buccal epithelium on the first day after challenge, and the localization of this bacterial pathogen gradually moved down to the middle layer of the buccal epithelium over time (**Figure 1F**), suggesting the invasion pathway of *F. columnare* in trout BM.

Bacterial Infection Elicits Strong Immune Responses in Trout BM

To assess the immune responses in trout BM after infection with *F. columnare*, we detected morphological changes and analyzed the expression of immune-related genes at each sampling time point. By AB staining, morphological changes were easily

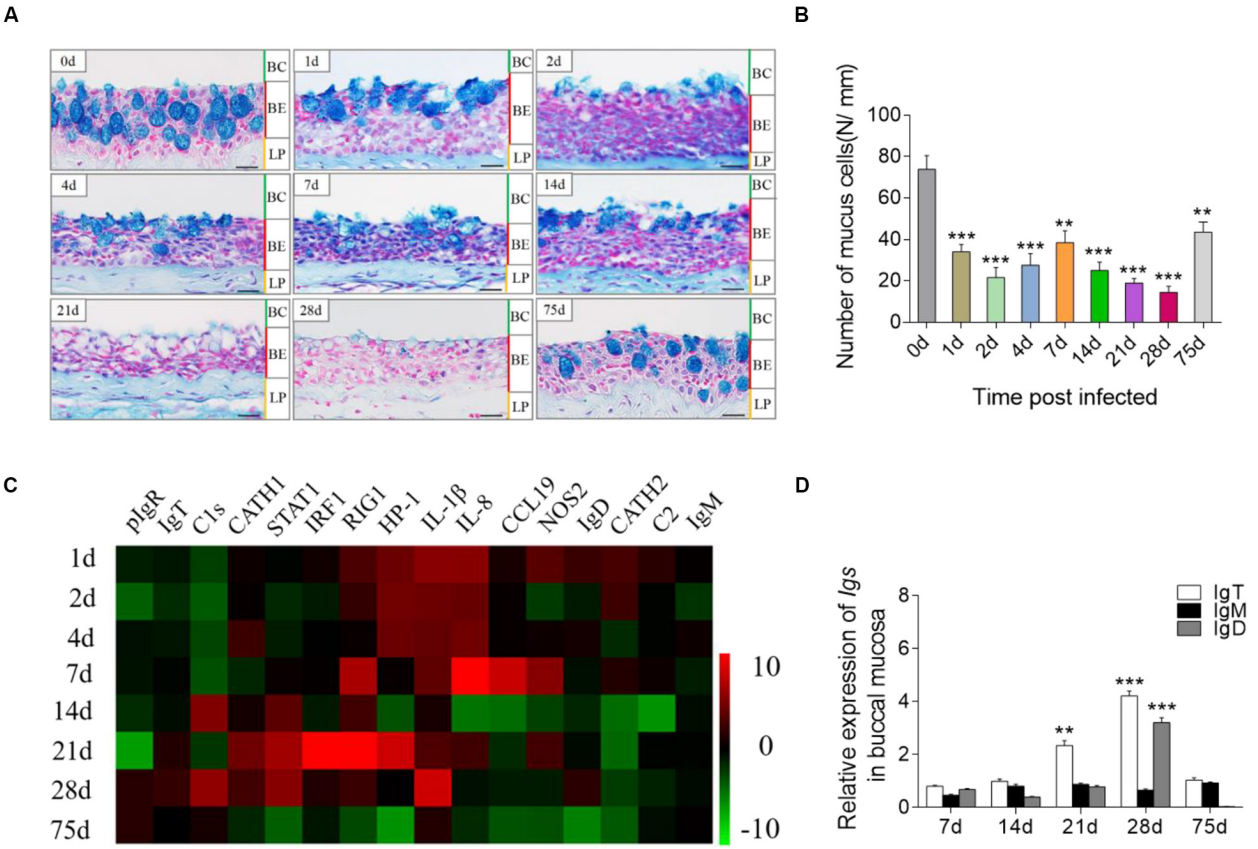

FIGURE 2 | Pathological changes and immune response in the trout BM after infection with *F. columnare*. **(A)** Histological examination by AB staining of BM from trout infected with *F. columnare* after 1, 2, 4, 7, 14, 28, and 75 days and uninfected control fish (n = 6 fish per group). **(B)** The number of mucus cells per millimeter in the buccal epithelium of *F. columnare*-infected rainbow trout at 1, 2, 4 7, 14, 21, 28, and 75 days and control fish (n = 6 fish per group), counted in 25 fields from **(A)**. **(C)** Heat map illustrates results from quantitative real-time PCR of mRNAs for selected immune markers in *F. columnare*-infected fish versus control fish measured at days 1, 2, 4, 7, 14, 21, 28, and 75 post-infection (n = 6 per group) in the BM of rainbow trout. Data are expressed as mean fold increase in expression. **(D)** Relative expression of IgT, IgM, and IgD at days 1, 7, 28, and 75 post-infection with *F. columnare* in trout BM (n = 6 fish per group). BC, buccal cavity; BE, buccal epithelium; and LP, lamina propria. Scale bars, 20 μm. $^{**}P < 0.01$, $^{***}P < 0.001$ (unpaired Student's t-test). Data are representative of three independent experiments (mean ± SEM).

observed in the BM epithelium (**Figure 2A**), and the number of mucus cells decreased significantly at different time points post-infection, particularly at 28 days (**Figure 2B**). To study the mRNA expression levels of immune-related genes and cell markers in trout BM after infection, we measured 16 immune-related genes, including the cytokines [interleukin (IL) 8 and 1β], chemokine gene (chemokine-like 19), antimicrobial peptides [cathelicidin (CATH) 1 and 2], complement factors (C2 and C1s), signal transducer and activator of transcription 1 (STAT1), retinoic acid inducible gene 1 (RIG1), heterochromatin protein 1 (HP1), nitric oxide synthase 2 (NOS2), pIgR, and Ig heavy chain genes (IgT, IgM, and IgD; **Figure 2C** and **Supplementary Figures S3A,B**; primers used in this study are shown in **Supplementary Table S1**) by qRT-PCR. Importantly, through our studies, we characterized that strong immune responses occurred in trout BM, head kidney and spleen after challenge with *F. columnare*. Notably, in agreement with the highest level of *F. columnare* in the BM, the significantly upregulated mRNA expression of immune-related genes (e.g., CATH-2, HP1, IL-8, IL-1β, and RIG1) was detected at days 1, 2, 4, and 7 post-infection (**Figure 2C**). Interestingly, the expression of IgT (∼4-fold) and IgD (∼3-fold) was upregulated significantly at 28 days post-infection (**Figure 2D**). Moreover, in the trout head kidney and spleen, the similar expression regulation of immune-related genes was seen in the early stages of infection, while the expression of IgM was upregulated significantly at days 28 and 75 post-infection (**Supplementary Figures S3A,B**).

Responses of B-Cells and Igs in Trout BM After Bacterial Infection

By immunofluorescence microscopy analysis, we observed few IgT^+ and IgM^+ B-cells in the buccal epithelium of control fish (**Figure 3A**; isotype-matched control antibodies, **Supplementary Figure S4A**). Interestingly, in the *F. columnare*-infected group, a moderate increase (∼4-fold) in the number of IgT^+ B-cells was observed in the trout buccal epithelium at day 28 post-infection (**Figures 3A,B**). Notably, we detected substantially

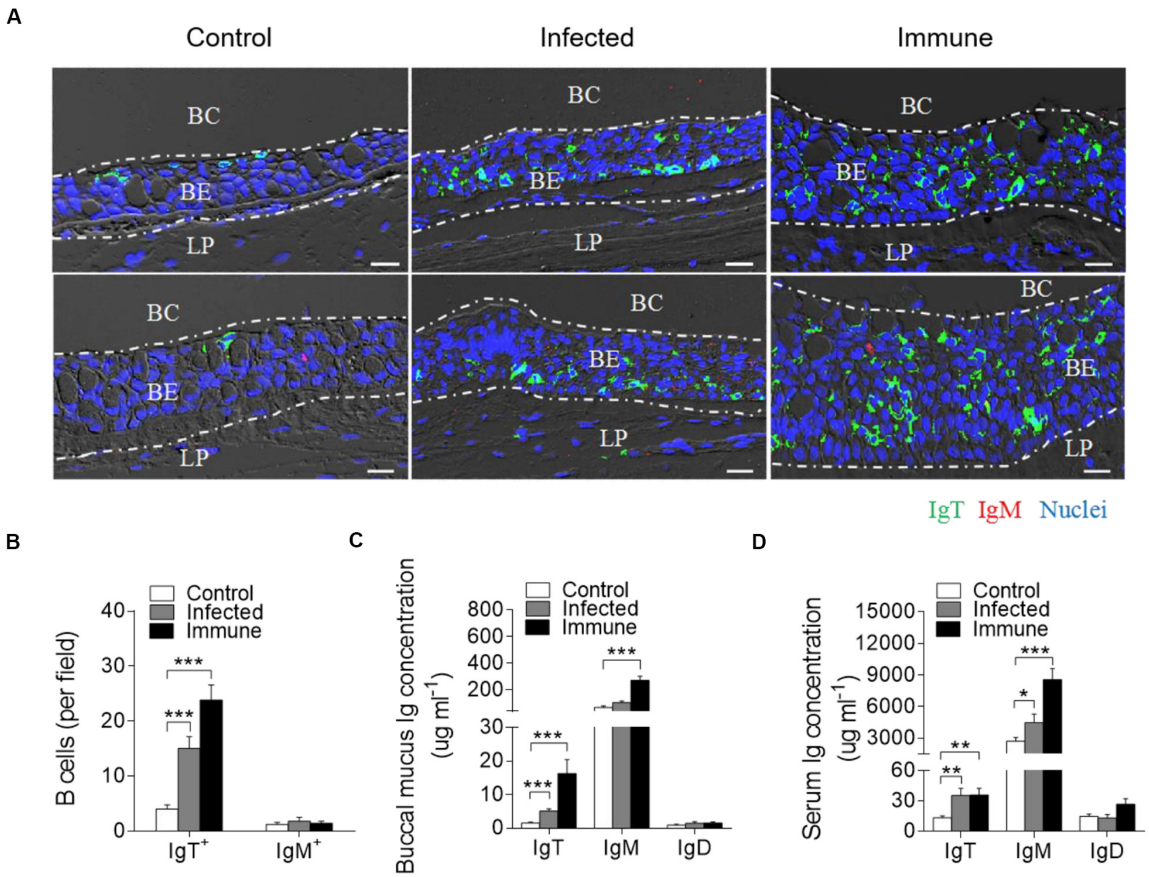

FIGURE 3 | Accumulation of IgT$^+$ B-cells in the BM of trout infected with *F. columnare*. **(A)** Representative DIC images of immunofluorescence staining on paraffinic sections of BM from uninfected control fish (left), infected fish (28 dpi, middle), and immune fish (75 dpi, right). IgT$^+$ and IgM$^+$ B-cells were stained with rabbit anti-trout IgT (green) and mouse anti-trout IgM (red), respectively; nuclei were stained with DAPI (blue; isotype-matched control antibody staining, **Supplementary Figure S4** in Supporting Information). **(B)** The number of IgT$^+$ and IgM$^+$ B-cells in paraffinic sections of BM from uninfected control fish, infected fish, and immune fish (n = 6 per group), counted in 20 fields from **(A)** (original magnification, × 20). **(C,D)** Concentration of IgT, IgM, and IgD in buccal mucus **(C)** and serum **(D)** of control, infected, and immune fish (n = 12 per group). BC, buccal cavity; BE, buccal epithelium; and LP, lamina propria. Scale bar, 20 μm. *P < 0.05, **P < 0.01, and ***P < 0.001 (one-way ANOVA with Bonferroni correction). Data in **(B–D)** are representative of at least three independent experiments (mean ± SEM).

more accumulation (∼6-fold) of IgT$^+$ B-cells on the trout buccal epithelium of immune fish (75 dpi) when compared with those of control fish (**Figures 3A,B**). However, the abundance of IgM$^+$ B-cells did not change significantly in the infected and immune fish when compared with the controls (**Figures 3A,B**).

The high accumulation of IgT$^+$ B-cells in trout BM after *F. columnare* challenge led us to hypothesize a critical role of IgT protein in BM. To address this hypothesis, by immunoblot analysis, we found that the IgT concentration in the buccal mucus of infected and immune fish increased by ∼3-fold and ∼11-fold when compared with control fish, respectively, which is consistent with the results of immunofluorescence. However, the concentration of IgM increased by ∼4-fold only in the immune group (**Figure 3C**). In serum, ∼3-fold increases of IgT concentration were detected in both infected and immune fish. Conversely, in serum, ∼ 2-, and 3-fold increases of IgM concentration were detected in infected and immune fish, respectively, when compared with control fish (**Figure 3D**). In contrast, the IgD protein concentration did not change significantly in either the buccal mucus or serum of the same fish groups (**Figures 3C,D**).

Bacteria-Specific Ig Responses in Trout BM

The results of large increases of IgT protein levels in the buccal mucus of infected and immune fish led us to hypothesize a key role of bacteria-specific IgT in trout BM. To verify this hypothesis, we measured the capacity of Igs from buccal mucus and serum to bind to *F. columnare* with a pull-down assay (**Figure 4**). In buccal mucus, we detected a significant increase in bacteria-specific IgT binding in up to 1/40 dilution from both infected (∼2.9-fold) and immune fish (∼4.8-fold) when compared to control fish (**Figures 4A–C**). Interestingly, we did not find any bacteria-specific IgM binding in the buccal mucus (**Figures 4A–C**). In serum, we found a significant increase in bacteria-specific IgT binding only in the 1/10 dilution (∼4.3-fold) and only in immune fish (**Figures 4D–F**).

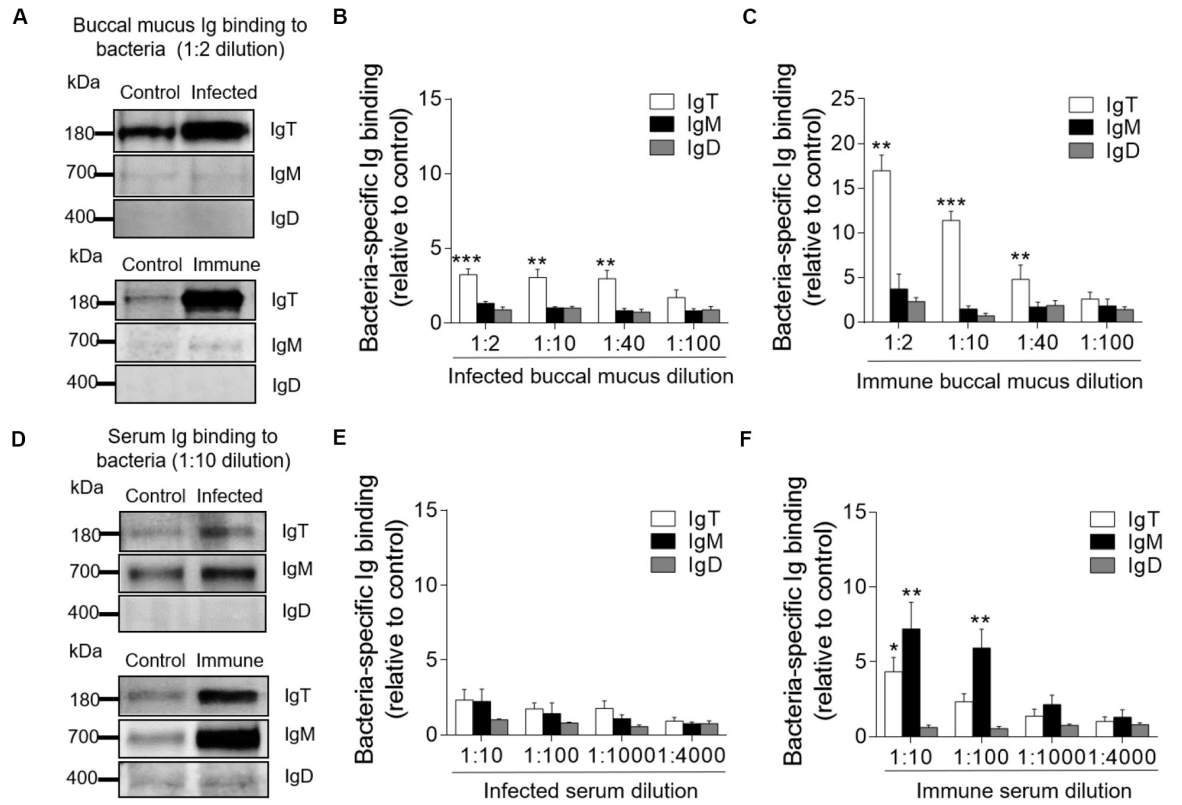

FIGURE 4 | Immunoglobulin responses in the buccal mucus and serum from infected and immune trout. **(A)** Western blot analysis of IgT-, IgM-, and IgD- specific binding to *F. columnare* in buccal mucus (dilution 1:2) from infected and immune fish. **(B,C)** IgT-, IgM-, and IgD- specific binding to *F. columnare* in dilutions of buccal mucus from infected **(B)** and immune **(C)** fish, evaluated by densitometric analysis of immunoblots and presented as relative values to those of control fish (n = 12 per group). **(D)** Western blot analysis of IgT-, IgM-, and IgD- specific binding to *F. columnare* in serum (dilution 1:10) from infected and immune fish. **(E,F)** IgT-, IgM-, and IgD- specific binding to *F. columnare* in dilutions of serum from infected **(E)** and immune **(F)** fish, evaluated by densitometric analysis of immunoblots and presented as relative values to those of control fish (n = 12 per group). $^{*}P < 0.05$, $^{**}P < 0.01$, and $^{***}P < 0.001$ (unpaired Student t-test). Data are representative of three independent experiments (mean ± SEM).

In contrast, bacteria-specific IgM binding was found in up to 1/100 dilution (∼5.9-fold) of the diluted serum from immune fish (**Figures 4D–F**). However, bacteria-specific IgD binding was not detected in buccal mucus or serum from infected or immune fish (**Figure 4**).

Local Proliferation of B-Cells and Ig Responses in Trout BM After Bacterial Infection

To evaluate whether there was an increase of IgT^+ B-cells in the trout BM of immune fish, we performed *in vivo* proliferation studies of B-cells stained with 5-Ethynyl-2'-deoxyuridine (EdU), which can incorporate into DNA during cell division. Immunofluorescence microscopy analysis showed a significant increase in the percentage of proliferating cells in the trout BM of immune fish (∼5.88 ± 0.70%) when compared with that of control animals (∼3.49 ± 0.85%; **Figures 5A,B**). Interestingly, we detected a significant increase in the proliferation of EdU^+ IgT^+ B-cells in immune fish (∼5.76 ± 0.96%) when compared with that of control fish (∼2.29 ± 1.32%; **Figures 5A,C**). However, no difference was detected in the percentage of EdU^+ IgM^+ B-cells of control fish and immune fish (**Figures 5A,C**). Next, we measured bacteria-specific Igs titers from the medium of cultured BM (**Figures 5D,E**). We detected a significant increase in bacteria-specific IgT binding in up to 1/10 diluted medium (∼3.1-fold) of cultured trout BM explants of immune fish when compared to control fish (**Figures 5D,E**). Interestingly, negligible bacteria-specific IgM and IgD titers were detected in the medium of cultured trout BM explants from control and immune fish (**Figures 5D,E**). Together, our results of the proliferation of IgT^+ B-cells and production of IgT suggest that bacteria-specific IgT in trout BM is locally generated after bacterial challenge.

Responses of pIgR in Trout BM After Bacterial Infection

Our previous studies have shown that pIgR exists in trout BM and mediates the transepithelial transport of secretory Igs (13). Thus, we hypothesized that pIgR might conduct the transportation of sIgs to the buccal mucus during the immune responses to *F. columnare*. Using immunofluorescence analysis, we observed that few of the buccal epithelial cells from naïve

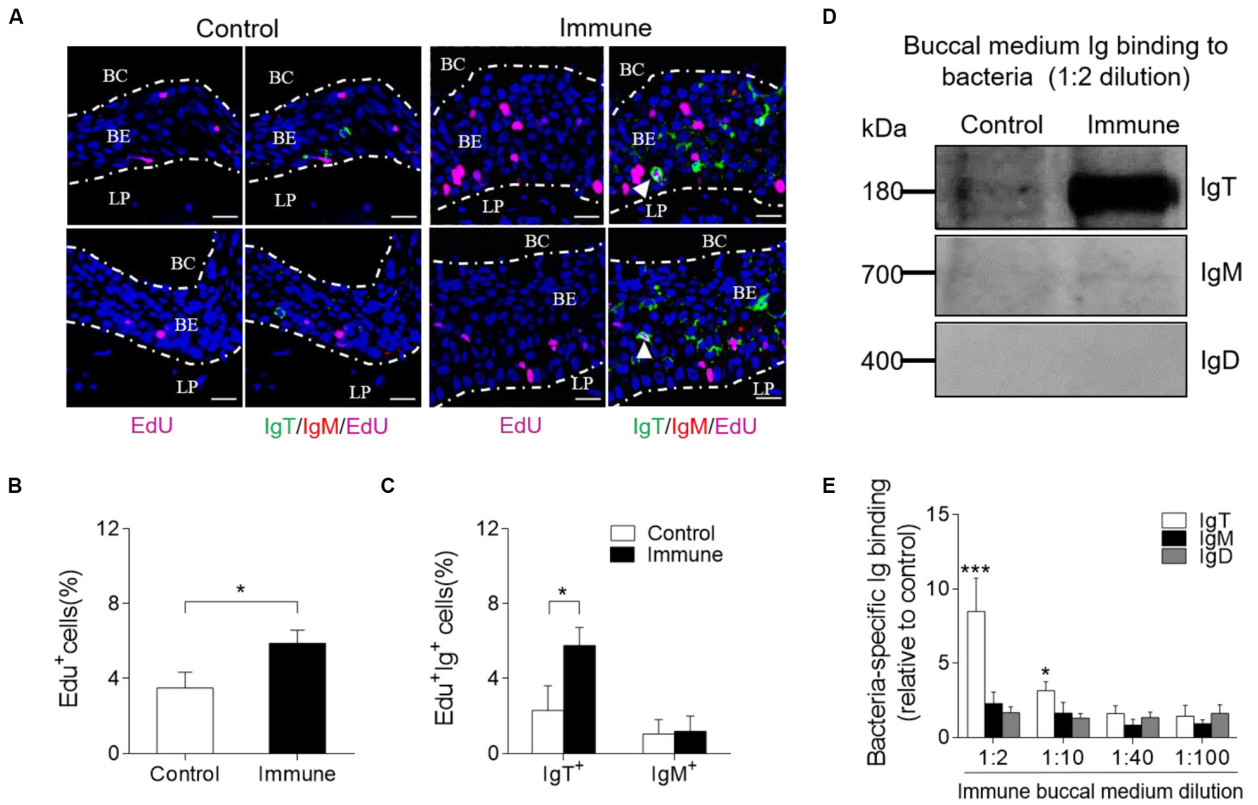

FIGURE 5 | Local Igs-specific responses in BM explants and proliferative responses of IgT^+ and IgM^+ B-cells in the BM from immune fish. **(A)** Immunofluorescence analysis of EdU incorporation by IgT^+ or IgM^+ B-cells in the BM of control and immune fish. Paraffinic sections of BM were stained for EdU (magenta), trout IgT (green), trout IgM (red), and nuclei (blue) detection. White arrowheads point to cells double stained for EdU and IgT. BC, buccal cavity; BE, buccal epithelium; and LP, lamina propria. Scale bars, 20 μm. **(B)** Percentage of EdU^+ cells from total BM cells in control or immune fish (n = 12 per group), counted in 20 fields from **(A)**. **(C)** Percentage of EdU^+ cells from the total BM IgT^+ and IgM^+ B-cell populations in control and immune fish (n = 12 per group), counted in 20 fields from **(A)**. **(D)** The BM explants (~20 mg each) from control and immune fish were cultured in medium (400 μl) for 7 days. Immunoblot analysis of IgT-, IgM-, and IgD-specific binding to *F. columnare* in the culture medium of buccal mucosa (dilution 1:2) from control and immune fish. **(E)** IgT-, IgM-, and IgD-specific binding to *F. columnare* in dilutions of buccal culture medium from control and immune fish, evaluated by densitometric analysis of immunoblots and presented as relative values to those of uninfected control fish (n = 12 per group). $^*P < 0.05$ and $^{***}P < 0.001$ (unpaired Student t-test). Data in **(B,C,E)** are representative of at least three independent experiments (mean ± SEM).

fish were stained by the anti-trout pIgR polyclonal antibody (**Figure 6A**). Interestingly, a significantly increased number of $pIgR^+$ cells was observed in the epidermis of trout BM from infected (28 dpi, ~1.7-fold) and immune (75 dpi, ~2.0-fold) fish (**Figures 6A,B**; isotype-matched control antibodies, **Supplementary Figure S4B**), respectively, when compared with those of control fish. Moreover, using qRT-PCR, the expression of pIgR was found to be significantly upregulated in the trout BM of infected (~2.9-fold) and immune fish (~2.9-fold), respectively, when compared with that of control fish (**Figure 6C**).

DISCUSSION

The BM is a critical first line of defense in terrestrial vertebrates (8, 11, 30). While mammals' BC is known to contain a MALT, which plays a key role in the control of bacterial pathogens (10, 31), very little is known about the evolutionary origins of buccal MALT and its primordial roles in immune defense. Here, we report for the first time that *F. columnare* can infect the BM of rainbow trout when the fish are exposed to this type of bacteria by bath, the natural route of exposure, and elicit local mucosal immune responses in trout BM. Moreover, we show the critical role of sIgT and B-cell responses in response to *F. columnare* infection in trout BM, which indicates the evolutionary conserved functions of mucosal Igs in the BM of vertebrates.

Previous studies have shown that columnaris disease is caused by the Gram-negative bacterium *F. columnare* and severely affects the global production of many fish species (2, 32). As a mucosal bacterial pathogen, *F. columnare* infection results in the damage of mucosal tissues, with a high degree of mortality (2, 5, 32). In the present study, we successfully conducted a waterborne challenge model of rainbow trout with *F. columnare* G_4. Notably, after 2 days of infection, clinical signs (frayed fins, depigmented lesions on the skin, and necrotic gill lesions) of columnaris disease were easily recognized, and rod-shaped bacteria that form rhizoid colonies with green fluorescence on

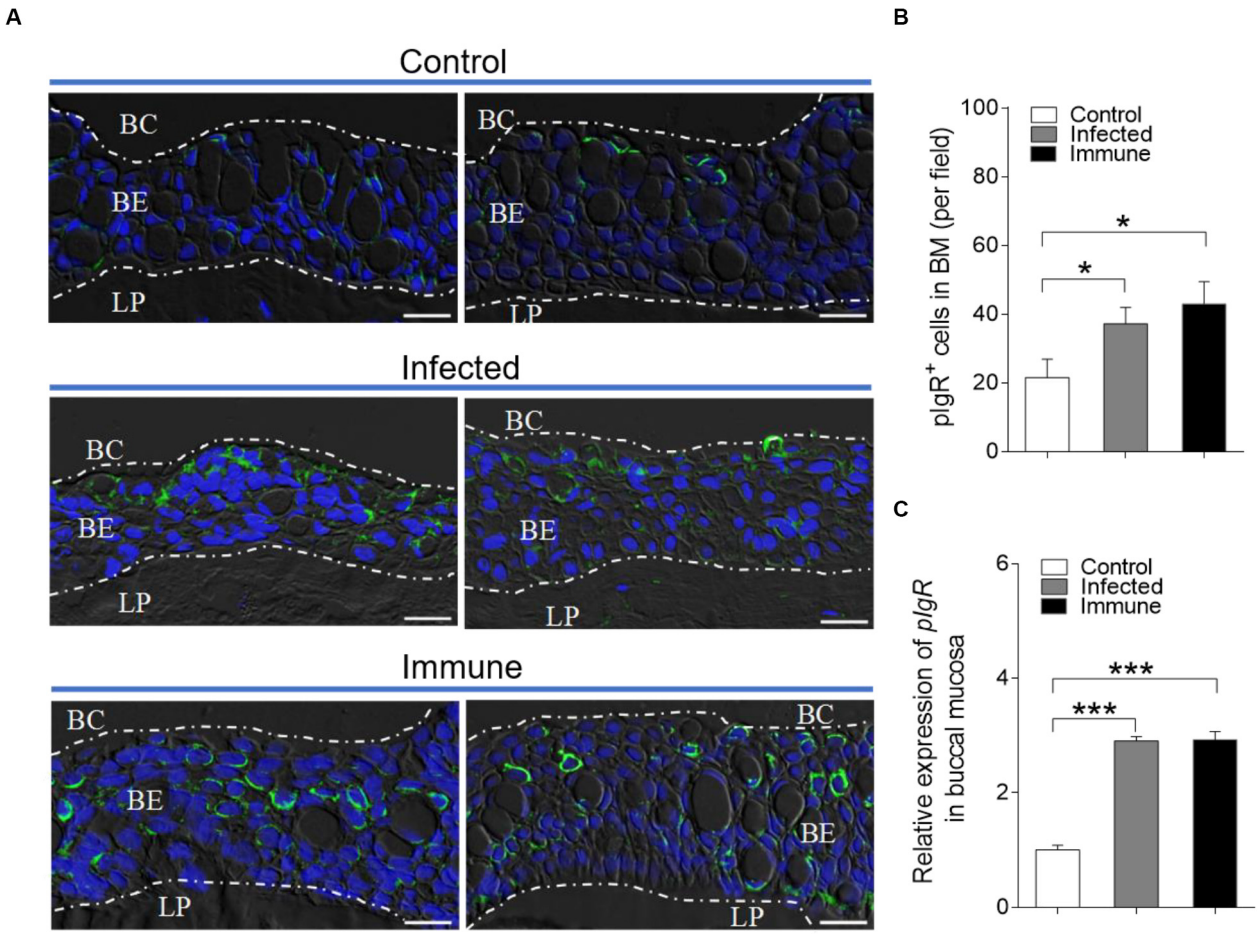

FIGURE 6 | Accumulation of pIgR$^+$ cells in the BM of trout after infected with *F. columnare*. **(A)** DIC images of immunofluorescence staining on trout BM paraffinic sections from control (top), infected (28 dpi, middle), and immune (75 dpi, bottom) fish, stained for pIgR (green) and nuclei with DAPI (blue; n = 12 fish per group; isotype-matched control antibody staining, **Supplementary Figure S4** in Supporting Information). **(B)** The number of pIgR$^+$ cells in trout BM paraffin sections of control, infected (28 dpi), and immune (75 dpi) fish (n = 12 fish per group), counted in 20 fields from **(A)**. **(C)** Relative mRNA expression of pIgR in the BM of control, infected and immune fish were detected by qRT-PCR (n = 6 fish per group). BC, buccal cavity; BE, buccal epithelium; and LP, lamina propria. Scale bar, 20 μm. $^*P < 0.05$ and $^{***}P < 0.001$ (one-way ANOVA with Bonferroni correction). Data in **(B,C)** are representative of at least three independent experiments (mean ± SEM).

solid growth medium could only be seen in the infected group. Moreover, by culture plate counting and histological observation, we found that the quantity and localization of *F. columnare* were different in trout BM, gills, skin, and fins, suggesting that the infection capacity and invasion rate of this bacterium vary in different mucosal tissues. These results are in agreement with the finding in mammalian BM after infection with bacterial periodontal pathogens (*Aggregatibacter actinomycetemcomitans*, *Porphyromonas gingivalis*, *Tannerella forsythia*, and *Treponema denticola*), which can induce inflammatory responses that lead to attachment loss and periodontal destruction (33, 34). Strikingly, we described that bacteria loads were highest in the BM along with the skin and similar to gill, which strongly indicates that the buccal route of infection may be one of the main targets of *F. columnare*, like skin and gill. It is interesting to note that *F. columnare* gathered especially on the mucus cells of the buccal epithelium on the first day after challenge, and the localization of this bacterial pathogen gradually moved down to the middle layer of the buccal epithelium over time. Moreover, with the occurrence of infection, significantly decreased numbers of mucus cells were observed in trout BM. These findings parallel those obtained in a former study in which the membranes of mucus cells ruptured and then the vesicle content was released, forming mucus holding antimicrobial activity and offering defense against bacterial pathogens (35–37). Overall, our results represent a unique example of a bacterial pathogen that could enter the BM of non-tetrapods.

In mammals, the buccal epithelium forms part of an intercommunicating network of the immune system, in which signals are regularly exchanged in dynamic interactions (11). However, the immune responses against bacterial pathogens in the BM of teleost fish have not yet been investigated. Here, we showed that 16 immune-related genes, including antibacterial peptides, cytokines, chemokines and complement factors, were significantly upregulated in trout BM at the early stages following *F. columnare* infection. These results correlated

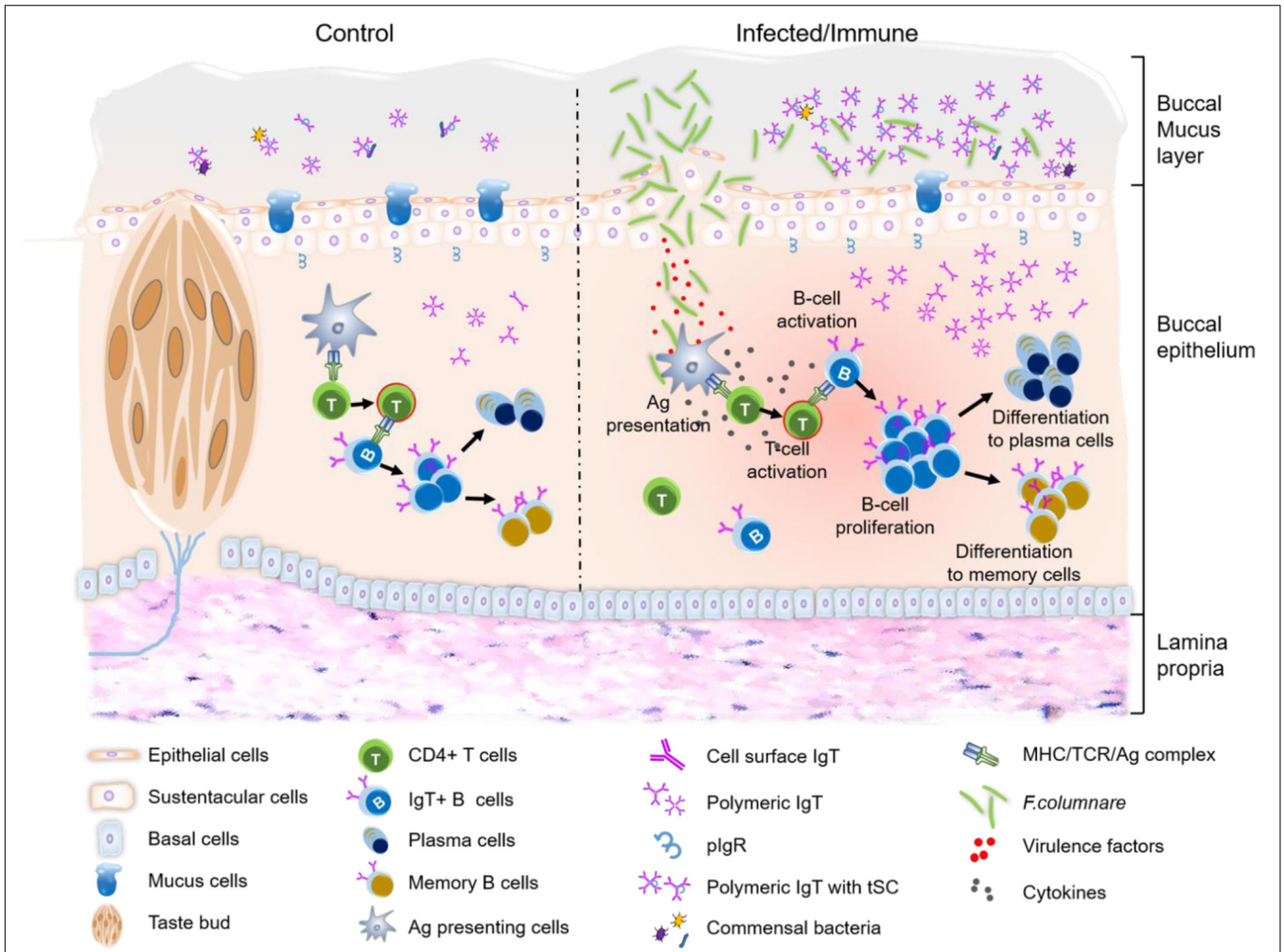

FIGURE 7 | Proposed model of local IgT and IgT$^+$ B-cell induction in the BM after *F. columnare* infection. The trout BM contains mucus layer, epithelium layer and lamina propria. The proposed model contains two partitions: control (left) and infected/immune (right). Induction of local IgT responses in the trout BM based on our findings. The number of IgT$^+$ B-cells in control fish BM is low. IgT are produced by IgT-secreting B cells and transported from the epithelium into the mucus layer via pIgR. And the secreted IgT coats the majority of commensal bacteria in the BM surface (5). When *F. columnare* invaded the BM, antigen (Ag) can be taken up by antigen-presenting cells (APC) and presented to naive CD4$^+$ T-cells. Ag-specific CD4$^+$ T-cells then produce cytokines to activate B cells. Activated B cells start proliferating and may differentiation to plasma cells to locally produce *F. columnare*-specific IgT, which will be transported by pIgR into buccal mucus where can specially binding to the *F. columnare*. Alternatively, some IgT$^+$ plasma cells may differentiate into memory IgT$^+$ B-cells. When *F. columnare* invade the host again, the memory IgT$^+$ B-cells would directly proliferate and differentiate into plasma cells, and then rapidly produce specific-IgT to bind *F. columnare*.

with the noteworthy histopathological changes in the BM of the same animals. Importantly, we found significantly increased mRNA expression levels of antimicrobial peptides, CATH-1 and CATH-2, in trout BM immediately after *F. columnare* infection, which form the first line of host defense against infectious microorganisms prior to stimulating animals' adaptive immune systems (38–40). In addition, we described that the mRNA expression levels of proinflammatory cytokines IL-8 and IL1-β increased significantly after bacterial infection, which were induced similarly in mammal gingival epithelial cells against bacterial pathogens, *P. gingivalis* and *Lactobacillus acidophilus* (41). Combined with those of previous studies, our results indicate that *F. columnare* infection induces drastic inflammatory reactions as well as strong immune responses in the trout buccal epidermis, which is similar to what happens in the mammalian BM (10).

It has been well established that mammalian sIgA is the predominant Ig in saliva and is considered the main specific defense molecule in the BM. Notably, previous studies have shown a positive relationship between the concentration of salivary IgA and periodontal disease, which is caused by bacterial pathogens (14, 15). Interestingly, our previous report proved the presence of a diffuse MALT in trout BM, which is characterized by an epithelial layer containing a higher percentage of IgT$^+$ B-cells than IgM$^+$ B-cells, similar to what was previously described in other mucosa tissues of teleost (18, 19, 42–44). However, whether the IgT$^+$ B-cells and sIgT play predominant roles in the BM of fish after bacterial infection is presently unknown. In

this study, we found significant increases in the concentration of IgT but not IgM or IgD in the buccal mucus of infected and immune fish exposed to *F. columnare*, in accordance with the large accumulation of IgT^+ but not IgM^+ B-cells in the trout BM of the same individuals. Our results parallel those obtained in a previous study that indicated that trout surviving infection with the parasite *Ichthyophthirius multifiliis* exhibited large accumulations of IgT and IgT^+ B-cells in the trout BM (13). Interestingly, similar dramatic increases of IgA secretion as well as IgA-positive cells in the salivary glands have been described in mammals following infection with the bacteria *Streptococcus mutans* (45). Interestingly, we found that the protein levels and mRNA expression of Igs were inconsistent and showed poor correlations, especially at days 75 post infection (the protein levels of IgT and IgM increased significantly while the mRNA expression not changed), this result might due to different infection methods. A constant stimulation for fish (75 dpi) made them obtain high immunity, performed as increased protein levels of Igs. However, the detection of mRNA expression was based on challenge once. Since there were many complicated and varied post-transcriptional mechanisms involved in turning mRNA into protein that were not yet sufficiently well-defined to be able to compute protein concentrations from mRNA. In addition, proteins might differ substantially in their *in vivo* half-lives (46), and these reasons caused different performance between protein and mRNA expression. Importantly, our study for the first time showed the detection of bacteria-specific titers of all three-existing teleost Igs in the buccal mucus and found pathogen-specific IgT titers mainly in the buccal mucus and to a much lesser degree in the serum of immune fish. In contrast, pathogen-specific IgM titers were detected only in the serum. Similarly, it was shown that *P. gingivalis* infection elicited *P. gingivalis*-specific IgA responses in saliva as well as IgG and IgA in serum (47). Moreover, experiments with animal models have also shown that salivary IgA specific to *Candida albicans* has an inhibitory effect on the adherence of *C. albicans* yeast cells to oral surfaces (24, 25). Overall, our results indicate that mucosal Ig (sIgT) play a key role in the BM immunity against bacterial pathogens of fish.

By *in vivo* proliferation assays, we found significant proliferative IgT^+ B-cell responses in trout BM, suggesting that the accumulation of IgT^+ B-cells in the BM after bacterial infection is due to local proliferation, although this remains to be fully demonstrated. In addition, the production of high titers of bacteria-specific IgT in buccal explant cultures confirmed the local production of bacteria-specific IgT and further demonstrated the presence of specific PCs in the local BM. These results parallel our previous findings on the trout gills and olfactory organ (19, 44) and suggest that trout BM acts as both an inductive and effector site of IgT responses. In contrast, mammalian BM works only as an effector site (48, 49), and most activated B-cells in the salivary glands of mammalians mainly migrate from gut-associated lymphoid tissue (GALT) and nasopharynx-associated lymphoid tissue (NALT), and the sIgA is produced by local PCs in the stroma of the salivary glands (14, 50). Hence, based on the results from previous studies in mammals and our study in trout, it suggested that although there are different molecules (sIgT versus sIgA) and cell types/glands (mucus-secreting cells versus salivary glands) in the BM of fish and mammals, functionally analogous strategies can be used to fight bacterial pathogens under evolutionary selective force.

It is well established that the transepithelial transport of secretory Igs into the mucosal surfaces is mediated by pIgR in both mammals and teleosts (17, 19, 51). Previous studies have shown that the putative trout secretory component (tSC) of pIgR is associated with sIgT in buccal mucus (13). However, the contribution of pIgR to the bacterial infection is unclear. Here, we found that trout pIgR (tpIgR) was mainly expressed in the epithelial layer of the trout BM, and we detected significantly increased numbers of $pIgR^+$ cells and transcript levels of pIgR in the BM from bacterial-infected trout when compared with that in the control group. Interestingly, in a study of germ-free mice implanted with Bacteroides *thetaiotaomicron*, the expression of pIgR was upregulated (52). Thus, together with previous studies, our results strongly suggest an important role of pIgR in the transport of Igs into the buccal mucus in both mammals and teleosts after bacterial infection.

In conclusion, our results provide the first evidence for the process of bacterial invasion in trout BM. Moreover, following bacterial infection, pathological changes, immune-related gene upregulation, as well as B-cell proliferation and bacteria-specific IgT production events occur within trout BM (**Figure 7**). Thus, from an evolutionary viewpoint, our results not only expand our view of buccal immune systems from a novel perspective but also reinforce the idea of mucosal Igs (sIgT and sIgA) specialized in fish and mammalian mucosal immunity through primordially conserved principles. In addition, since many pathogens invade fish through the BM, our findings suggest that buccal vaccination may be an effective way to prevent aquatic bacterial diseases.

DATA AVAILABILITY STATEMENT

The original contributions presented in the study are included in the article/**Supplementary Material**, further inquiries can be directed to the corresponding author.

ETHICS STATEMENT

The animal study was reviewed and approved by The Animal Experiment Committee of Huazhong Agricultural University.

AUTHOR CONTRIBUTIONS

ZX designed the research. H-YX and FD performed most of the experiments and contributed to conduct the infection model. XZ and G-KH contributed to the immunofluorescence analysis. K-FM contributed to western blot analysis. G-FC and Z-BW contributed to real-time analysis. H-YX, FD, NL, and ZX wrote the manuscript. All authors contributed to the article and approved the submitted version.

FUNDING

This work was supported by grants from National Key Research and Development Program of China (2018YFD0900400) and the National Natural Science Foundation of China (31873045).

ACKNOWLEDGMENTS

We thank Dr. J. Oriol Sunyer (University of Pennsylvania) for his generous gift of anti-trout IgM, anti-trout IgD, anti-trout IgT mAbs, anti-trout IgT and anti-trout pIgR pAbs, and Dr. Pin Nie for his generous gift of the GFP-labeled *F. columnare* G_4.

SUPPLEMENTARY MATERIAL

The Supplementary Material for this article can be found online at: https://www.frontiersin.org/articles/10.3389/fimmu.2020.562795/full#supplementary-material

Supplementary Figure 1 | An overview of rainbow trout buccal area. **(A)** The image representing the anatomical location and morphology of trout buccal area. **(B,C)** Histological examination by Hematoxylin/eosin (H&E) staining of trout BM **(B)** and enlarged images **(C)** of the areas outlined. BE, buccal epithelium; LP, lamina propria; and SM, submucosa. Scale bar, 20 μ m.

Supplementary Figure 2 | Successful infection with *F. columnare* in BM of trout. **(A)** Percentage survival of control and fish infected with *F. columnare* (n = 60 fish per group). **(B)** Detection of *F. columnare* by PCR in trout BM at days 1, 2, 4, 7, 14, 21, 28, and 75 after infection. **(C)** Representative DIC images of trout BM tissues isolated from infected fish at days 2 post-infection. The respective images were obtained and merged as illustrated. Scale bars, 100 μm. $P < 0.01$ (unpaired Student's t-test). Data are representative of three independent experiments (mean ± SEM).

Supplementary Figure 3 | Kinetics of the immune response in head kidney and spleen of trout after infected with *F. columnare*. **(A,B)** Heat map illustrates results from qRT-PCR of mRNAs for selected immune markers in *F. columnare*-infected fish versus control fish measured at days 1, 2, 4, 7, 14, 21, 28, and 75 post-infection in trout head kidney **(A)** and spleen (**B**; n = 6 fish per group) Data are representative of three different independent experiments (mean ± SEM).

Supplementary Figure 4 | Isotype control staining for anti-IgT, anti-IgM, and anti-pIgR antibodies in trout BM paraffin-sections. DIC images of buccal paraffin-sections from control fish, with merged staining of isotype control antibodies for anti-trout IgT pAb (green) and anti-trout IgM (red) mAb **(A)**, or anti-trout pIgR (green) mAb **(B)**. Nuclei were stained with DAPI (blue). BC, buccal cavity; BE, buccal epithelium; LP, lamina propria. Scale bars, 20 μm. Data are representative of three independent experiments.

Supplementary Table 1 | Primers used in this study.

REFERENCES

1. Suomalainen LR, Bandilla M, Valtonen ET. Immunostimulants in prevention of columnaris disease of rainbow trout, *Oncorhynchus mykiss* (Walbaum). *J Fish Dis.* (2009) 32:723–6. doi: 10.1111/j.1365-2761.2009.01026.x
2. Declercq AM, Chiers K, Haesebrouck F, Van den Broeck W, Dewulf J, Cornelissen M, et al. Gill infection model for columnaris disease in common carp and rainbow trout. *J Aquat Anim Health.* (2015) 27:1–11. doi: 10.1080/08997659.2014.953265
3. Evenhuis JP, LaPatra SE, Marancik D. Early life stage rainbow trout (Oncorhynchus mykiss) mortalities due to *Flavobacterium columnare* in Idaho, USA. *Aquaculture.* (2014) 418–419:126–31. doi: 10.1016/j.aquaculture.2013.09.044
4. Bernardet J, Segers P, Vancanneyt M, Berthe F, Kersters K, Vandamme P. Cutting a gordian knot: emended classification and description of the genus Flavobacterium, emended description of the family Flavobacteriaceae, and proposal of *Flavobacterium hydatis* nom nov (basonym, *Cytophaga* aquatilis Strohl and Tait 1978). *Int J Syst Bacteriol.* (1996) 46:128–48. doi: 10.1099/00207713-46-1-128
5. Dumpala PR, Gülsoy N, Lawrence ML, Karsi A. Proteomic analysis of the fish pathogen *Flavobacterium columnare*. *Proteome Sci.* (2010) 8:26. doi: 10.1186/1477-5956-8-26
6. Almeida GMF, Laanto E, Ashrafi R, Sundberg LR. Bacteriophage adherence to mucus mediates preventive protection against pathogenic bacteria. *mBio.* (2019) 10:e01984-19. doi: 10.1128/mBio.01984-19
7. Li N, Zhu Y, LaFrentz BR, Evenhuis JP, Hunnicutt DW, Conrad RA, et al. The type IX secretion system is required for virulence of the fish pathogen *Flavobacterium columnare*. *Appl Environ Microbiol.* (2017) 83:e01769-17. doi: 10.1128/aem.01769-17
8. Moutsopoulos NM, Konkel JE. Tissue-specific immunity at the oral mucosal barrier. *Trends Immunol.* (2018) 39:276–87. doi: 10.1016/j.it.2017.08.005
9. Groeger S, Meyle J. Oral mucosal epithelial cells. *Front Immunol.* (2019) 10:208. doi: 10.3389/fimmu.2019.00208
10. Walker DM. Oral mucosal immunology: an overview. *Ann Acad Med Singapore.* (2004) 33:27–30.
11. Feller L, Altini M, Khammissa RAG, Chandran R, Bouckaert M, Lemmer J. Oral mucosal immunity. *Oral Surg Oral Med Oral Pathol Oral Radiol.* (2013) 116:576–83. doi: 10.1016/j.oooo.2013.07.013
12. Abbate F, Germanà GP, De Carlos F, Montalbano G, Laurà R, Levanti MB, et al. The oral cavity of the adult zebrafish (Danio rerio). *Anat Histol Embryol.* (2006) 35:299–304. doi: 10.1111/j.1439-0264.2006.00682.x
13. Yu YY, Kong WG, Xu HY, Huang ZY, Zhang XT, Ding LG, et al. Convergent evolution of mucosal immune responses at the buccal cavity of teleost fish. *iScience.* (2019) 19:821–35. doi: 10.1016/j.isci.2019.08.034
14. Brandtzaeg P. Secretory immunity with special reference to the oral cavity. *J Oral Microbiol.* (2013) 5:20401. doi: 10.3402/jom.v5i0.20401
15. Sood LI, Alezzy MYH, Diajil AR. Correlation between *Streptococci mutans* and salivary IgA in relation to some oral parameters in saliva of Children. *J Bagh Coll Dentistry.* (2014) 26:71–9. doi: 10.12816/0015168
16. Costalonga M, Herzberg MC. The oral microbiome and the immunobiology of periodontal disease and caries. *Immunol Lett.* (2014) 162:22–38. doi: 10.1016/j.imlet.2014.08.017
17. Salinas I, Zhang YA, Sunyer JO. Mucosal immunoglobulins and B cells of teleost fish. *Dev Comp Immunol.* (2011) 35:1346–65. doi: 10.1016/j.dci.2011.11.009
18. Zhang YA, Salinas I, Li J, Parra D, Bjork S, Xu Z, et al. IgT, a primitive immunoglobulin class specialized in mucosal immunity. *Nat Immunol.* (2010) 11:827–35. doi: 10.1038/ni.1913
19. Xu Z, Takizawa F, Parra D, Gómez D, von Gersdorff JL, LaPatra SE, et al. Mucosal immunoglobulins at respiratory surfaces mark an ancient association that predates the emergence of tetrapods. *Nat Commun.* (2016) 7:10728. doi: 10.1038/ncomms10728
20. Perdiguero P, Martín-Martín A, Benedicenti O, Díaz-Rosales P, Morel E, Muñoz-Atienza E, et al. Teleost IgD(+)IgM(-) B Cells mount clonally expanded and mildly mutated intestinal IgD responses in the absence of lymphoid follicles. *Cell Rep.* (2019) 29:4223–35.e4225. doi: 10.1016/j.celrep.2019.11.101
21. Hansen JD, Landis ED, Phillips RB. Discovery of a unique Ig heavy-chain isotype (IgT) in rainbow trout: Implications for a distinctive B cell developmental pathway in teleost fish. *Proc Natl Acad Sci USA.* (2005) 102:6919–24. doi: 10.1073/pnas.0500027102
22. Danilova N, Bussmann J, Jekosch K, Steiner LA. The immunoglobulin heavy-chain locus in zebrafish: identification and expression of a previously unknown

isotype, immunoglobulin Z. *Nat Immunol.* (2005) 6:295–302. doi: 10.1038/ni1166
23. Xu Z, Takizawa F, Casadei E, Shibasaki Y, Ding Y, Sauters TJC, et al. Specialization of mucosal immunoglobulins in pathogen control and microbiota homeostasis occurred early in vertebrate evolution. *Sci Immunol.* (2020) 5:3254. doi: 10.1126/sciimmunol.aay3254
24. van der Wielen PA, Holmes AR, Cannon RD. Secretory component mediates Candida albicans binding to epithelial cells. *Oral Dis.* (2016) 22:69–74. doi: 10.1111/odi.12397
25. Silva C, Oliveira L, Leão M, Jorge A. Candida spp. adherence to oral epithelial cells and levels of IgA in children with orthodontic appliances. *Braz Oral Res.* (2013) 28:28–32. doi: 10.1590/S1806-83242013005000031
26. Chu WH, Lu CP. In vivo fish models for visualizing *Aeromonas hydrophila* invasion pathway using GFP as a biomarker. *Aquaculture.* (2008) 277:152–5. doi: 10.1016/j.aquaculture.2008.03.009
27. O'Toole R, von Hofsten J, Rosqvist R, Olsson PE, Wolf-Watz H. Visualisation of Zebrafish infection by GFP-labelled Vibrio *anguillarum*. *Microb Pathogenesis.* (2004) 37:41–6. doi: 10.1016/j.micpath.2004.03.001
28. Pfaffl MW. A new mathematical model for relative quantification in real-time RT-PCR. *Nucleic Acids Res.* (2001) 29:e45–45. doi: 10.1093/nar/29.9.e45
29. Kong WG, Yu YY, Dong S, Huang ZY, Ding LG, Cao JF, et al. Pharyngeal immunity in early vertebrates provides functional and evolutionary insight into mucosal homeostasis. *J Immunol.* (2019) 203:3054–67. doi: 10.4049/jimmunol.1900863
30. Groeger SE, Meyle J. Epithelial barrier and oral bacterial infection. *Periodontology.* (2015) 69:46–67. doi: 10.1111/prd.12094
31. Moor K, Slack E. What makes a bacterial oral vaccine a strong inducer of high-affinity IgA responses? *Antibodies.* (2015) 4:295–313. doi: 10.3390/antib4040295
32. Declercq AM, Haesebrouck F, Van den Broeck W, Bossier P, Decostere A. Columnaris disease in fish: a review with emphasis on bacterium-host interactions. *Vet Res.* (2013) 44:27–27. doi: 10.1186/1297-9716-44-27
33. Tatakis DN, Kumar PS. Etiology and pathogenesis of periodontal diseases. *Dent Clin North Am.* (2005) 49:491–516. doi: 10.1016/j.cden.2005.03.001
34. van Winkelhoff AJ, Loos BG, van der Reijden WA, van der Velden U. Porphyromonas gingivalis, *Bacteroides* forsythus and other putative periodontal pathogens in subjects with and without periodontal destruction. *J Clin Periodontol.* (2002) 29:1023–8. doi: 10.1034/j.1600-051x.2002.291107.x
35. Yashpal M, Kumari U, Mittal S, Mittal AK. Histochemical characterization of glycoproteins in the buccal epithelium of the catfish, Rita rita. *Acta Histochemica.* (2007) 109:285–303. doi: 10.1016/j.acthis.2007.03.002
36. Yashpal M, Kumari U, Mittal S, Mittal AK. Morphological specializations of the buccal cavity in relation to the food and feeding habit of a carp *Cirrhinus mrigala*: a scanning electron microscopic investigation. *J Morphol.* (2009) 270:714–28. doi: 10.1002/jmor.10713
37. Yashpal M, Mittal AK. Serous goblet cells: the protein secreting cells in the oral cavity of a catfish, Rita rita (Hamilton, 1822) (Bagridae, Siluriformes). *Tissue Cell.* (2014) 46:9–14. doi: 10.1016/j.tice.2013.08.001
38. Yeaman MR, Yount NY. Mechanisms of antimicrobial peptide action and resistance. *Pharmacol Rev.* (2003) 55:27. doi: 10.1124/pr.55.1.2
39. Kościuczuk EM, Lisowski P, Jarczak J, Strzałkowska N, Jóźwik A, Horbańczuk J, et al. Cathelicidins: family of antimicrobial peptides. A review. *Mol Biol Rep.* (2012) 39:10957–70. doi: 10.1007/s11033-012-1997-x
40. Zasloff M. Antimicrobial peptides of multicellular organisms. *Nature.* (2002) 415:389–95. doi: 10.1038/415389a
41. Zhao JJ, Feng XP, Zhang XL, Le KY. Effect of Porphyromonas gingivalis and *Lactobacillus acidophilus* on secretion of IL1B, IL6, and IL8 by gingival epithelial cells. *Inflammation.* (2012) 35:1330–7. doi: 10.1007/s10753-012-9446-5
42. Xu Z, Parra D, Gómez D, Salinas I, Zhang Y-A, von Gersdorff JL, et al. Teleost skin, an ancient mucosal surface that elicits gut-like immune responses. *Proc Natl Acad Sci USA.* (2013) 110:13097–102. doi: 10.1073/pnas.1304319110
43. Tacchi L, Musharrafieh R, Larragoite ET, Crossey K, Erhardt EB, Martin SAM, et al. Nasal immunity is an ancient arm of the mucosal immune system of vertebrates. *Nat Commun.* (2014) 5:5205. doi: 10.1038/ncomms6205
44. Yu YY, Kong W, Yin YX, Dong F, Huang ZY, Yin GM, et al. Mucosal immunoglobulins protect the olfactory organ of teleost fish against parasitic infection. *PLoS Pathog.* (2018) 14:e1007251. doi: 10.1371/journal.ppat.1007251
45. Colombo NH, Pereira JA, da Silva ME, Ribas LF, Parisotto TM, Mattos-Graner Rde O, et al. Relationship between the IgA antibody response against Streptococcus mutans GbpB and severity of dental caries in childhood. *Arch Oral Biol.* (2016) 67:22–7. doi: 10.1016/j.archoralbio.2016.03.006
46. Greenbaum D, Colangelo C, Williams K, Gerstein M. Comparing protein abundance and mRNA expression levels on a genomic scale. *Genome Biol.* (2003) 4:117–117. doi: 10.1186/gb-2003-4-9-117
47. Shimizu Y, Iwasaki T, Tajima T, Yuba E, Kono K, Watarai S. Induction of antibody response in the oral cavity of dogs following intraocular (eye drop) immunization with Porphyromonas gingivalis cell lysate incorporated in pH-sensitive fusogenic polymer-modified liposomes. *J Vet Med Sci.* (2017) 79:290–8. doi: 10.1292/jvms.16-0338
48. Brandtzaeg PER. Do salivary antibodies reliably reflect both mucosal and systemic immunity? *Ann N Y Acad Sci.* (2007) 1098:288–311. doi: 10.1196/annals.1384.012
49. Novak N, Haberstok J, Bieber T, Allam JP. The immune privilege of the oral mucosa. *Trends Mol Med.* (2008) 14:191–8. doi: 10.1016/j.molmed.2008.03.001
50. Hashizume-Takizawa T, Shibata N, Kurashima Y, Kiyono H, Kurita-Ochiai T, Fujihashi K. Distinct roles for Peyer's patch B cells for induction of antigen-specific IgA antibody responses in mice administered oral recombinant *Salmonella*. *Int Immunol.* (2019) 31:531–41. doi: 10.1093/intimm/dxz029
51. Proctor GB, Carpenter GH. Neural control of salivary S-IgA secretion. *Int Rev Neurobiol.* (2002) 52:187–212. doi: 10.1016/s0074-7742(02)52010-9
52. Hooper LV, Wong MH, Thelin A, Hansson L, Falk PG, Gordon JI. Molecular analysis of commensal host-microbial relationships in the intestine. *Science.* (2001) 291:881–4. doi: 10.1126/science.291.5505.881

Conflict of Interest: The authors declare that the research was conducted in the absence of any commercial or financial relationships that could be construed as a potential conflict of interest.

The reviewer, FT, declared a past co-authorship with one of the author, ZX, to the handling editor.

Copyright © 2020 Xu, Dong, Zhai, Meng, Han, Cheng, Wu, Li and Xu. This is an open-access article distributed under the terms of the Creative Commons Attribution License (CC BY). The use, distribution or reproduction in other forums is permitted, provided the original author(s) and the copyright owner(s) are credited and that the original publication in this journal is cited, in accordance with accepted academic practice. No use, distribution or reproduction is permitted which does not comply with these terms.

frontiers in Immunology

REVIEW
published: 02 October 2020
doi: 10.3389/fimmu.2020.567941

Immunoglobulins, Mucosal Immunity and Vaccination in Teleost Fish

Yongyao Yu[1†], *Qingchao Wang*[1†], *Zhenyu Huang*[1†], *Liguo Ding*[1†] *and Zhen Xu*[1,2,3*]

[1] Department of Aquatic Animal Medicine, College of Fisheries, Huazhong Agricultural University, Wuhan, China, [2] Laboratory for Marine Biology and Biotechnology, Qingdao National Laboratory for Marine Science and Technology, Qingdao, China, [3] Key Laboratory of Marine Biotechnology of Fujian Province, Institute of Oceanology, Fujian Agriculture and Forestry University, Fuzhou, China

Due to direct contact with aquatic environment, mucosal surfaces of teleost fish are continuously exposed to a vast number of pathogens and also inhabited by high densities of commensal microbiota. The B cells and immunoglobulins within the teleost mucosa-associated lymphoid tissues (MALTs) play key roles in local mucosal adaptive immune responses. So far, three Ig isotypes (i.e., IgM, IgD, and IgT/Z) have been identified from the genomic sequences of different teleost fish species. Moreover, teleost Igs have been reported to elicit mammalian-like mucosal immune response in six MALTs: gut-associated lymphoid tissue (GALT), skin-associated lymphoid tissue (SALT), gill-associated lymphoid tissue (GIALT), nasal-associated lymphoid tissue (NALT), and the recently discovered buccal and pharyngeal MALTs. Critically, analogous to mammalian IgA, teleost IgT represents the most ancient Ab class specialized in mucosal immunity and plays indispensable roles in the clearance of mucosal pathogens and the maintenance of microbiota homeostasis. Given these, this review summarizes the current findings on teleost Igs, MALTs, and their immune responses to pathogenic infection, vaccination and commensal microbiota, with the purpose of facilitating future evaluation and rational design of fish vaccines.

Keywords: evolution, immunoglobulins, mucosal immunity, mucosa-associated lymphoid tissues, teleost

OPEN ACCESS

Edited by:
Monica Hongroe Solbakken, University of Oslo, Norway

Reviewed by:
Jorge Galindo-Villegas, Nord University, Norway
David Parra, Hipra Scientific, Spain

***Correspondence:**
Zhen Xu
zhenxu@mail.hzau.edu.cn

[†]These authors have contributed equally to this work

Specialty section:
This article was submitted to Comparative Immunology, a section of the journal Frontiers in Immunology

Received: *31 May 2020*
Accepted: *16 September 2020*
Published: *02 October 2020*

Citation:
Yu Y, Wang Q, Huang Z, Ding L and Xu Z (2020) Immunoglobulins, Mucosal Immunity and Vaccination in Teleost Fish. Front. Immunol. 11:567941. doi: 10.3389/fimmu.2020.567941

INTRODUCTION

Aquatic environments, which are inhabited by teleost fish, provide more nutrients to microbes than land ecosystems and therefore are more conducive to bacterial growth (1). Therefore, potential pathogens mostly enter the bodies of fish across their mucosal epithelial barriers including the gills, gastrointestinal system or skin lesions (2). Unlike invertebrates, teleost fish has evolved both innate and adaptive immunity to protect themselves against pathogens residing in their aquatic environment. Similar to mammals, teleost fish also produce B- and T-cells, which constitute the first adaptive immunity mechanisms in all bony vertebrates. Particularly, B-cells and immunoglobulins (Igs) in mucosal-associated lymphoid tissues (MALTs) are thought to mediate mucosal homeostasis, given that secretory Igs (sIgs; i.e., antibodies) are known to neutralize pathogens or promote their elimination in the mucosa, thereby preventing further infection (3). Recent studies have demonstrated that B-cells within the mucosal tissues, including the gills, buccal mucosa (BM), pharyngeal mucosa (PM), and olfactory organ, exhibit potent local proliferation (4–6). Additionally,

the large commensal microbiota populations that colonize fish mucosal surfaces can be recognized by Igs (7). So far, three main Ig isotypes have been identified in teleosts including IgM, IgD, and IgT/Z (8, 9), of which IgT/Z is thought to be specialized in mucosal immunity. The predominant roles of IgT/Z antibodies and IgT^+ B-cells have been elucidated in six different teleost MALTs, including GALT (10), SALT (11), GIALT (4), NALT (12), and buccal (5) and pharyngeal MALT (6).

The present review aims to summarize the regulatory functions of Igs in teleost mucosal immunity. First, we will review the basic current information on the three known teleost Igs at both the gene and protein levels. Afterward, we will describe the six different MALTs in teleosts. We will then discuss teleost Ig responses to pathogens and microbiota in mucosal surfaces and finally teleost Ig responses to immunization. Altogether, the information compiled herein will provide insights into the fundamental mechanisms of Igs in fish mucosal tissues and aid in the development of novel teleost mucosal vaccines.

IMMUNOGLOBULINS

Igs are highly specialized recognition glycoproteins that can recognize a great variety of antigens from bacteria, viruses, and other disease-causing organisms and recruit other cells and molecules to destroy these pathogens (13). Igs are composed of two heavy (H) chains and two light (L) chains, with the exception of certain antibodies in camelids and nurse shark that lack L chains (14). The constant region within the heavy chain determines the effector function of a specific antibody, which in teleosts includes Cμ, Cδ, and Cτ/Cζ, encoding IgM, IgD, and IgT/IgZ, respectively (8, 9). Four L chain types have been identified in bony fish, of which Igκ and Igσ are found in most teleost species, Igλ has been lost in most teleost lineages during species divergence (cod, catfish, and rainbow trout are notable exceptions), and Igσ-2 was also recently identified in the coelacanth (15).

In tetrapods, naïve B-cells tend to produce IgM before any other isotype, but the germinal centers of secondary lymphoid tissues can induce B-cells to express a different antibody isotype *via* class switching when activated by antigens (16). However, class switching does not exist in any fish species including teleosts and cartilaginous fish, as there are no distinct switch regions in the gene locus (17) despite the identification of an activation-induced cytidine deaminase (AID) (18). Two forms of Igs are reported in both teleosts and tetrapods, a membrane-bound form of Igs, also known as the B-cell receptor (BCR), which serves as the cell's antigen receptor, and the secreted form of Igs, which is produced by terminally differentiated B-cells, plasmablasts, and plasma cells, and functions as the main effector of B-cells in adaptive immunity (19). Here, we mainly focus on the secreted teleost forms IgM, IgD, and IgT/Z.

IgM

IgM is nearly universal in all jawed vertebrates, with only the exception of the African coelacanth that carries exclusively IgW H chain loci (20). In teleosts harbouring IgZ/T, the Cμ domain is not the first constant region after the VDJ domain, and additional Dτ-Jτ-Cτ/ζ domains are located before the Dμ/δ-Jμ/δ-Cμ-Cδ domains in the gene locus of the teleost IgH chain (8, 9). During V(D)J rearrangement in teleosts, the upstream VH could merge with the aforementioned Dμ/δ-Jμ/δ-Cμ-Cδ domains *via* Dτ-Jτ-Cτ/ζ domain deletion, which results in IgM synthesis.

Tetrameric IgM is widely accepted as the prevalent serum Ig type in most teleosts (13). Teleost IgM lacks the J chain, and its monomers are mainly associated by covalent (disulfide) bonds. Increased disulfide polymerization has been reported to correlate with a greater affinity of trout IgM to antigens, and this trout IgM was also reported to remain active for longer periods (21). Teleost serum IgM concentration may vary (0.6–16 mg/ml) depending on water temperature and quality, as well as fish species, size, stress, stimulation, and immunization (22). During parasitic infection, both the total serum IgM concentration and parasite-specific IgM binding capacity of trout were significantly increased, in addition to an increased IgM^+ B-cell proliferation in head kidney (5, 6), which demonstrated the regulatory functions of IgM in teleost systemic immunity. IgM has also been shown to occur as a tetramer in the different mucus types of rainbow trout at different concentrations, including gut mucus (~0.075mg/ml), skin mucus (~0.0046 mg/ml), gill mucus (~0.02mg/ml), pharyngeal mucus (~0.072mg/ml), and nasal mucus (~0.28mg/ml), all of which exhibited lower IgM concentrations than serum (~2.5mg/ml). Nonetheless, IgM still comprises the largest fraction among all three Igs in all teleost mucus, and parasite-specific IgM binding in pharyngeal mucus has been shown to increase after parasitic infection. IgM has also been found to coat bacteria in different mucus types, albeit at a lower rate than IgT (4–7, 11). Moreover, IgM expression exhibits some general features in teleosts. For instance, cytoplasmic IgM is normally expressed earlier than surface IgM, and Ig-producing cells appear in different tissues in the following order: head kidney, spleen, and finally MALT (23). In zebrafish, ontogenic IgM expression patterns occur in the following order: surface Ig transcript [7 days post-fertilization (dpf)], IgH chain transcript in the pancreas (10 dpf), sIg transcript (13 dpf), IgH chain transcript in the head kidney (19 dpf), and detectable humoral Ig (28 dpf) (8, 24).

IgD

Compared to the limited (i.e., normally two or three) Cδ domains in mammals, the number of Cδ domains varies widely in different fish species (25). Unlike eutherian δ chains, in which two domains are connected by a hinge, the higher number of Cδ domains in teleosts may provide a wider variety of structural options to synthesize more flexible H chain products. Moreover, δ in bony fish was found to be uniquely formed by splicing Cμ1 between rearranged VDJ and Cδ1, producing a chimeric H chain sequence (26). Notably, this inclusion of Cμ1 has been observed in almost every teleost Igδ transcript (27). In channel catfish, membrane bound and secreted IgD is transcribed from two different IgH genes. Interestingly, the secreted delta form is encoded by an IgH transcript lacking a V-region (25). A germline-recombined VDJ is present in the second gene, but the signal sequence is directly spliced to Cδ1 in

the mRNA, indicating that the secreted δ form may not perform antigen recognition functions (17).

In teleosts, IgD was found to be to co-expressed with IgM in rainbow trout B-cells (4); however, an IgM^-/IgD^+ B-cell population was also identified in channel catfish (28) and a European trout line (29). In channel catfish, IgM^-/IgD^+ B-cells isolated from peripheral blood lymphocytes (PBLs) likely expand in response to certain pathogens, functioning as pattern recognition molecules. And a recent intriguing study in the trout identified a preponderant IgT^- B cells, i.e. IgD^+ IgM^- cells, to secrete IgDs which were reactive to the commensal microbiota in both gut and gills but not skin (29). However, the immunoprotective role of IgD in teleosts remains largely unknown. Although some reports have hypothesized the role of IgD in teleost gills (26), this antibody is known to be uninvolved in specific immunity in the gills and PM of rainbow trout during parasitic infection (4, 6). Additionally, teleost sIgD can coat a subset of commensal microbiota in mucosal tissues, including the gut mucosa, gill mucosa, BM, and PM. Nonetheless, mucosal bacteria coating by sIgD occurs significantly less than sIgT coating (4–6). These results suggest that teleost sIgD may also be involved in mucosal homeostasis.

IgT

IgT acts as a mucosal-associated Ig in bony fish, similar to IgA in mammals and IgX in frogs (10). Besides the salmonids fish (8, 9, 30, 31), IgT subclasses are also reported in other teleosts such as stickleback (*Gasterosteus aculeatus*) (32, 33) and carp (*Cyprinus carpio*). Differential immune responses have been observed which may vary depending on both species and the route of pathogens/vaccination used in the study. Similar results have been observed for other ig isotypes (34). In teleost B cells, the IgH V domain is known to rearrange either to Dτ-Jτ-Cτ/ζ to encode a τ/ζ chain or to Dμ/δ-Jμ/δ-Cμ-Cδ to encode μ and δ chains (19). Similar to IgD, the number of τ/ζ domains varied in different teleost species. For instance, four domains have been identified in most analyzed species (35); three domains in stickleback (33) and Antarctic fish (36); and two domains in fugu (37). Two separate IgZ loci encoding IgZ1 and IgZ2 have been identified in zebrafish (38) and common carp (39). IgZ1 represents a typical teleost IgHτ/ζ feature, whereas the Cμ 1 and Cζ 4 domains constitute a chimeric transcript of IgZ2. Moreover, very recent study has reported that multiple independent rounds of duplication and deletion of the teleost-specific antibody class IGHZ in the cyprinodontiform lineage, demonstrating the extreme volatility of IGH evolution (40).

In rainbow trout serum, IgT mainly occurs in monomeric form and is eluted at ~180 kDa, as determined from standard curve analysis. Within the multiple types of mucus, a great portion of IgT is present in polymeric form, whereas a small portion of IgT is still present in monomeric form during elution. Unlike the tetrameric IgM which is associated by covalent (i.e., disulfide) bonds, gut polymeric IgT is composed of non-covalent associated monomeric subunits. The concentration of IgT in the serum of rainbow trout is 4–10 mg/ml, whereas it is ~7 μg/ml, ~0.31 μg/ml, ~1.55μ g/ml, ~1.7 μg/ml, and ~3.46 μg/ml in the gut mucus, skin mucus, gill mucus, nasal mucus, and pharyngeal mucus, respectively. It is important to note that teleost mucus possesses a much higher ratio of IgT/IgM than serum. Moreover, mucosal microbiota is mainly coated with IgT in the gut, skin, gills, and olfactory organ (4–7, 10–12). Among the different mucosal tissues, it was also observed that, compared to the gills and gut, skin mucosa showed lower IgT concentrations, lower IgT titers, and a lower percentage of coated microbiota which were correlated with lower percentages of IgT^+ B-cells in the skin of the same fish (4, 10). The abundance of IgT^+ B-cells within a specific mucosal surface may be driven by its commensal microbiota, which then modulates humoral immune response potency (7).

MUCOSA-ASSOCIATED LYMPHOID TISSUE (MALT)

So far, six different MALTs (classified based on their localization in the body) have been identified in teleost fish (**Figure 1**), which contain diffuse MALTs (D-MALTs) but lack the organized MALTs (O-MALTs) such as Peyer's patches and tonsils that are found in mammals. These organized structures are the inductive sites for the selection of high-affinity B-cells and are

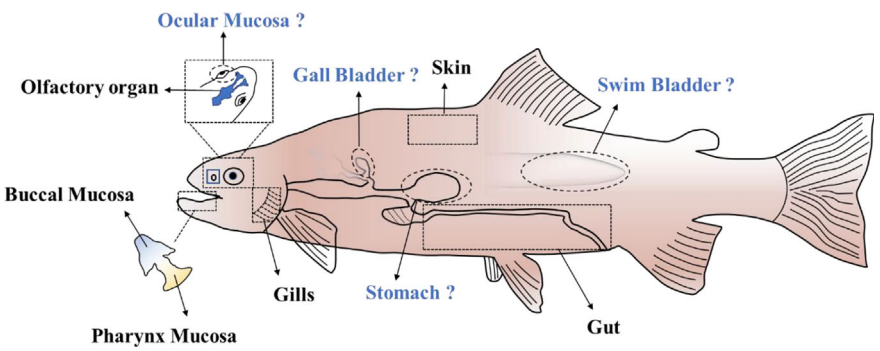

FIGURE 1 | The MALTs in teleost. "?" indicates the potential MALTs in teleost fish which remain to be clearly delineated.

believed to facilitate antibody response maturation (41). Teleost MALTs harbor abundant myeloid and diffuse lymphoid cells, which can work together to initiate both innate and adaptive immunity to maintain mucosa homeostasis.

Gut-Associated Lymphoid Tissue (GALT)

The digestive tract is directly connected with the external environment and could be a main portal of pathogen entry in both mammals and teleost fish, among which gut is the largest part (42). As a crucial component of the mucosal immune system in teleost fish, GALT constitutes a local immune response environment for protection against pathogens. Although the gut structure varies in different teleost species, it can be generally divided into three main segments (43). The enterocytes of the first segment act as absorptive cells for dietary protein uptake. The second segment is involved in macromolecule and enterocyte uptake. The third segment is thought to have osmoregulatory functions. In addition to the digestive function of the teleost gut, studies have shown that the posterior segment of the teleost intestine contains several immune cell types (10, 17, 44), which suggests that this section is involved in immune responses against pathogen invasion. Research on gut-associated immune responses in fish have been primarily investigated in the study of T-cell function (45); Moreover, three B-cell populations (IgM^+IgD^+, IgM^-IgD^+, and IgT^+ B-cells) in the intestine of rainbow trout have been described (10, 29). Particularly, IgM^+ and IgT^+ B-cells have mostly been located in the lamina propria (LP), whereas some studies have shown that IgT^+ B-cells in carp and sea bass are primarily localized in intraepithelial lymphocytes (IELs) (10). This suggests that due to the privileged population of IgT^+ B-cells, differential immune responses can be effortlessly generated upon infection or vaccination.

Gill-Associated Lymphoid Tissue (GIALT)

Unlike terrestrial animals that acquire oxygen from the air and possess invaginated breathing structures (i.e., lungs), aquatic organisms possess evaginated gas-exchange structures. In the case of teleost fish, four pairs of gill arches consisting of many gill filaments constitute a highly efficient way to increase contact surface to acquire oxygen from water. However, in addition to the respiratory function of the gills, they also possess osmoregulation, pH balance regulation, ammonia excretion, hormone regulation, and detoxification functions (46). Notably, because of their direct exposure to water, teleost gills are continuously challenged with environmental pollutants/toxins and pathogens, both of which trigger an immune response in the teleost GIALT (47). Moreover, several studies have demonstrated that numerous innate and adaptive immune molecules or cells involved in immune-related pathways are present in teleost gills, such as Igs and antibody-secreting cells (4, 48). It has been noted that the IgT^+ B-cell locus on the epithelial layer plays an essential role in the defense against pathogens (4). Moreover, unlike IgM^+IgD^+ B-cells, IgM^-IgD^+ B-cell populations are also present in the gills of rainbow trout (29), but the function of these cells remains to be clearly characterized.

Skin-Associated Lymphoid Tissue (SALT)

The skin of teleost fish also acts as the first line of defense against invading pathogens and it contains SALT, which can elicit gut-like immune responses against pathogen infection/antigen stimulation (11, 49). Compared with GALT, SALT might play a key role in defense against pathogens during the earlier developmental period of the teleost fish. Recently, a model of a germ-free zebrafish embryo challenged with osmotic stress showed that the embryo skin acts as the first organ to protect the organism from bacterial infection during the early developmental period when GALT was not yet functional (50). In general, all vertebrates possess two main skin layers: the epidermis and the dermis. However, unlike mammals, teleost skin is not keratinized and therefore their epithelial cells with abundant mucus-producing cells are in direct contact with the water medium (13, 51). Additionally, the skin surface of teleosts generates numerous molecules including lysozymes, complements, lectins, and Igs, all of which attach to the skin mucus to protect the host (52). Skin mucus in most fish contains numerous innate immune components, which can be produced continuously to prevent the entry of pathogens to the underlying tissues. Importantly, fewer IgT^+ and IgM^+ B-cells are found in teleost SALT than in GALT. However, teleost skin B cells are dominantly located in the epidermis, and almost none of them are found in the basal dermis layer (11).

Nasal-Associated Lymphoid Tissue (NALT)

Olfaction is an essential ancient sensory system prevalent in all animals. Interestingly, the olfactory systems of teleost fish resemble those of land-based animals in terms of anatomical features (53). Given their distinctive environment, teleosts have developed different mechanisms to discriminate odors. Terrestrial vertebrates breathe and sense their environment through inhalation, whereas teleost fish actively draw water containing dissolved gases into their olfactory organs (54). Additionally, teleost olfactory organs are continually stimulated with pollutants/toxins or pathogens in the water (55). Therefore, teleost NALTs are similar to other teleost MALTs, containing diffuse lymphoid cells without organized structures, and IgT^+-B cells play a crucial role in pathogenic invasion defense.

Buccal Mucosa-Associated Lymphoid Tissue

The buccal cavity, located between the gastrointestinal and respiratory tracts, is a vital mucosal surface in vertebrates. In mammals, the BM contains numerous salivary glands to produce saliva, which subsequently translocates into the salivary layer (SL). Moreover, the buccal cavity (BC) is covered with a keratinized stratified epithelium associated with the gingiva, hard palate, and outer lips and a non-keratinized stratified epithelium in other areas (56). Conversely, the BC of teleost fish is lined with abundant mucus-secreting cells that replace the function of the salivary glands in mammals to produce the mucus to coat their buccal epithelium (57). Furthermore, only non-keratinized buccal epithelia have been observed in teleost fish, which exhibit similar characteristics to those of the

mammals. Specifically, this epithelium consists of two main layers: the stratified squamous epithelium and the LP (58, 59). Given that aquatic environments are far more complex than air, teleost fish are subject to more stimuli. A recent study reported that fish BC also contains MALTs as in other mucosal tissues such as skin and has evolved an effective mucosal immune system to protect itself from parasite infection (5).

Pharyngeal Mucosa-Associated Lymphoid Tissue

The pharynx is connected with the digestive and respiratory tracts in vertebrates (60). In mammals, the pharyngeal cavity (PC) contains a choana which is connected with the nasal cavity (NC). However, in teleost fish, the PC (which is located between the mouth and esophagus) is a separate compartment from the NC and does not contain a choana. The PC of teleosts is coated with mucosa, and contains the stratified squamous epithelium and the LP (61). Unlike the PC of mammals, which possesses both mucus-secreting cells and mucus glands to secrete mucus into the mucus layer (62), aquatic animals lack mucus glands and instead possess numerous mucus-secreting cells in the PM. Similar to the buccal MALT, IgT^+ B-cells are chiefly located in the pharyngeal epithelium (PE), where their numbers increase significantly upon pathogenic invasion (6).

The Potential Mucosa-Associated Lymphoid Tissues Which Might Present in Teleosts

In addition to the six MALTs mentioned above, four potential extra MALTs might be present in the teleosts. Ocular mucosa of the teleost fish is directly exposed to the water medium. As one of the mucosa-associated lymphoid tissues in mammals, ocular mucosa plays an important role in defense against the pathogen invasion. From an evolutionary perspective, ocular mucosa in teleost fish might also have a role in protecting the individual from environmental pathogens. The stomach is another component of the digestive tract that has a potential role as MALT. Recent research has shown that IgA plays an important role in maintaining homeostasis of the stomach mucosa in mammals (63). In contrast, whether IgT/IgZ in teleosts perform a similar role as IgA in stomach remains to be demonstrated. The gallbladder is also an accessory organ of the digestive tract, and it greatly influences bile inflow into the intestine and thereby the enterohepatic circulation of bile acids. Therefore, it is closely connected to the intestine and might defense against pathogen invasion together with the intestine. Finally, the swim bladder which connects with the esophagus *via* the pneumatic duct is a homologous structure to the tetrapod lung (64). Its primary function is to control whole-body density and buoyancy. Recently, swim bladder-associated microbiota in rainbow trout was investigated and the result showed that *Arthrobacter* and *Cellulosimicrobium* were the major genera located in the swim bladder mucosa (65). The cross-talk between resident bacteria and host, and whether a connection exists between the swim bladder and the gut microbiota, is a highly interesting hypothesis.

IMMUNOGLOBULIN RESPONSES TO PATHOGENS IN MUCOSAL SURFACES

Fish are continuously exposed to an aquatic environment that contains abundant pathogens such as bacteria, viruses, and parasites, all of which can break through the immune barrier of the body. The mucosal immune system of fish is highly efficient and plays a critical role in resisting various pathogens, as previously reported in mammals. Many functions of mammalian IgA in mucosal secretions have been confirmed, such as preventing pathogens from adsorbing to the mucosal epithelium, mediating virus neutralization in infected cells, and promoting the death of pathogens by activating the alternative complement system pathway (66). To date, IgM, IgD, and IgT/IgZ have been identified in teleost fish and IgT/Z are the main immunoglobulin isotypes specialized in mucosal immunity (4, 7, 10).

Immunoglobulin Responses to Pathogens in the Gut

The Igs in the teleost gut play an important role in resisting the invasion of potential pathogens through its epithelium (67). In 2010, Zhang et al. identified IgT as the most ancient known Ig specialized in mucosal immunity (10). In their report, more IgT^+ B-cells were detected in the GALT of fish infected with *Ceratomyxa shasta* (a gut parasite) than that of control fish; however, the percentage of IgM^+ B-cells was not higher than that of control fish. Importantly, the authors identified parasite-specific IgM titers in serum, whereas IgT-specific responses to the parasite were confined to the gut mucus, which demonstrated that IgT might play a major role in pathogen inhibition in the fish gut. The above results suggest that teleost IgT contributes exclusively to gut mucosal immune responses, which is similar to the role of mammalian IgA, whereas IgM plays a major role in systemic immunity. In mammals, the secondary lymphoid follicles in the gut (e.g., Peyer's patches; PP) are responsible for the proliferation and enrichment of IgA^+ B-cells (68). However, unlike mammals, teleosts lack PP, suggesting that the proliferation of IgT in the GALT of trout occurs through other pathways. In a later study on gilthead seabream (*Sparus aurata*), increased IgM expression in the posterior intestine was found in fish infected with *Enteromyxum leei*. Additionally, an increased number of IgM^+ B-cells was also detected in the intestine of infected fish (69). Natalia et al. described that after rainbow trout were orally infected with infectious pancreatic necrosis virus (IPNV), the transcript levels of many immune-related genes significantly changed and the gene expressions of IgM and IgT were higher in the pyloric ceca than that in kidneys (70). So far, reports on Ig responses in intestinal mucosa after viral infection are still scarce. To further clarify the critical role of Igs against pathogens in the intestine of fish, additional bacterial and viral studies should be conducted.

Immunoglobulin Responses to Pathogens in Gills

Previous studies have demonstrated that gill tissues contain abundant immune cells, which are regulated by several

immune genes and pathways (71–73). A later study examined the specific Ig responses to pathogens in fish gills (4). In this study, *Ichthyophthirius multifiliis* (Ich) trophonts in the gills were overwhelmingly coated with IgT and slightly coated with IgM at 25 days post-infection (dpi), whereas parasites coated with IgD could not be detected. Moreover, a significantly increased number of IgT^+ B-cells in the gills could be detected in infected and survivor fish compared to control fish. In contrast, IgM^+ B-cell numbers did not show obvious changes. Additionally, at the protein level, IgT protein concentration also increased significantly in the gill mucus of infected and survivor fish, whereas the IgM and IgD protein concentrations remained unchanged. Conversely, the concentration of IgM in serum showed a significant increase (unlike IgT). Moreover, high titers of parasite-specific IgT and parasite-specific IgM were detected in gill mucus and serum, respectively. Similar results were obtained when detecting the titers of bacteria-specific IgT/IgM in gill mucus of fish infected with *Flavobacterium columnare*. More details about the Ig responses in trout gills infected with *F. columnare* were provided in that study (74). Additionally, significant upregulation of genes encoding IgM and IgT was induced by immunization and challenge with Ich in teleost fish gills (75). Moreover, upon bath immunization, the expression of the IgT gene in the gills could be induced by treating *Epinephelus coioides* with a nervous necrosis virus vaccine (34). To elucidate the roles of Igs against different pathogens in fish gills, further studies should be conducted to provide insights into the gill responses in virus-infected fish.

Immunoglobulin Responses to Pathogens in Skin

Previous studies have found that IgT protein concentration significantly increases in skin mucus upon Ich infection and coats the surface of the invasive parasite (Ich), suggesting the critical function of IgT in skin infection resistance (11). In this study, rainbow trout infected with Ich presented a significant increase in IgT^+ B-cells in the skin at 3 months post-infection. However, IgM^+ B-cell numbers remained largely unchanged in infected groups. Additionally, all parasites localized within the skin epidermis were largely covered with anti-IgT antibodies. At the protein level, the IgT protein concentration in the skin mucus of infected and survivor fish was significantly higher, whereas IgM levels remained unchanged. Similar to the results in fish gut, the presence of parasite-specific Igs was discovered in skin mucus and serum. Moreover, when fish treated with mucosal vaccination were bath-challenged with pathogens, the IgM titers in serum and IgT responses in skin mucus were strongly induced (34). Furthermore, in Ich-infected fish, a significant upregulation of IgT, IgM, and IgD levels was observed in the skin at 24 h post-infection (76).

Immunoglobulin Responses to Pathogens in the Olfactory Organ

The nasal mucosa is known to inhibit and neutralize pathogens and participates in both local innate and adaptive immune responses (12, 77). In Ich-infected trout, parasites in the olfactory organ were mostly coated with IgT, slightly coated with IgM, and hardly coated with IgD. The nasal epithelium also produced notable IgT^+ B-cell accumulation when the fish survived the parasite. Moreover, in agreement with the results that nasal IgT^+ B-cells increased in infected fish, the IgT protein concentration in the nasal mucosa of these fish was also noticeably increased, whereas IgM and IgD protein concentrations did not show any significant changes. Contrary to the results in the nasal mucosa, the IgM concentration in the serum of infected fish significantly increased. A later study determined that parasite-specific IgT was secreted in the nasal mucosa in response to Ich infection. Additionally, Magadan et al. reported that enteric red mouth (ERM) intranasal administration resulted in a significant perturbation of the IgM (IgH μ) repertoire in trout spleen, and the IgT repertoire showed a lower diversity and higher relative IGHV2 usage compared with the controls. However, no ERM-specific IgT was detected in serum after intranasal immunization, suggesting a lower capacity to activate plasmatic B-cell differentiation or to stimulate their migration to the head kidney (78). Interestingly, Sepahi et al. reported that the percentage of IgT^+ B cells markedly decreased in the olfactory organ of IHNV-treated trout, whereas IgM^+ B cells did not change significantly (79). Therefore, to further our knowledge of Ig responses to pathogens in fish nasal mucosa, immune responses induced by bacterial and viral infections in the nasal mucosa should be further studied.

Immunoglobulin Responses to Pathogens in BC

In tetrapod species, sIgA plays a critical role in adaptive immune responses to prevent the invasion of oral pathogens as a pivotal humoral component (80). Recently, studies of Ig responses to pathogens in the BM of fish have also been conducted (5). The highest innate immune response intensity in fish was detected at days 14 and 28 post-Ich infection, including the expression of IgM, IgT, and IgD heavy chain genes. Moreover, similar to other fish MALTs, the accumulation of IgT^+ B-cells could also be observed in the buccal epithelium of surviving fish and, similar to previous studies, the number of IgM^+ B-cells did not change significantly. In line with the increased number of IgT^+ B-cells in the buccal epithelium, a significantly increased IgT protein concentration was detected in the buccal mucus of infected and surviving fish. In contrast, the concentrations of IgM and IgD did not significantly change in the buccal mucus of the infected group. However, the concentration of IgM increased significantly in the serum of infected fish. Moreover, compared to the Igs concentration of control fish, the titers of parasite-specific IgT were much higher in the buccal mucus of infected fish, as demonstrated by a pull-down assay, whereas the titers of parasite-specific IgM increased mainly in the serum. However, no parasite-specific IgD was detected in either the buccal mucus or the serum.

Immunoglobulin Responses to Pathogens in PC

B cells and Ig are present in the PM of teleost fish (6). In fish challenged with Ich for 28 days, IgT^+ B-cells increased

dramatically in the PE and were found to secrete IgT. In contrast, the number of IgM$^+$ B-cells in the pharynx of the infected group remained at the same level as that of the controls. Moreover, the IgT concentration in the pharyngeal mucus was also obviously upregulated, whereas the protein concentrations of IgM and IgD in the pharyngeal mucus remained unchanged after Ich infection. However, in the serum, higher IgM and IgT but not IgD concentrations were detected in infected fish. Upon further pull-down experiments, the titers of parasite-specific IgT and IgM were tested in both pharyngeal mucus and serum. The titers of parasite-specific IgT were higher in pharyngeal mucus, whereas the titers of parasite-specific IgM were mainly detected in serum.

IMMUNOGLOBULIN RESPONSES TO MICROBIOTA AT MUCOSAL SITES

Commensal microbes are very important to overall fish healthy, some of which have been demonstrated to be involved in the protection of fish against infectious agents (81). Fish MALTs have developed a complex immune system to interact with microbiota at mucosal sites, and the relationship between them provides mutual benefits at homeostatic conditions. Maintaining the mucosal microbial homeostasis is critical for the maintenance of the mucosa and ultimately whole-body health. Thus, understanding the mechanisms by which teleosts MALTs are involved is of critical importance. In the teleost experiments described above, three Igs have been characterized in their mucosal secretions (IgM, IgD, IgT), where IgT is the most ancient antibody class specialized in mucosal immunity (10). Interestingly, it has been found that the interaction between teleost Igs and microbiota *via* coating (**Figure 2**) is similar to that in mammals (80), whereas the percentage of Ig-coated bacteria varies at individual mucosa sites. This demonstrates that microbiota control at mucosal sites has emerged early in the evolution of vertebrates and is conserved. Here, we review some current studies on teleost fish Ig immune responses to microbiota.

Immunoglobulin Responses to Microbiota in the Gut

The intestinal mucosal surface interfaces of vertebrates, including teleost fish, are colonized with large and complex microbial populations. Although microbiota composition in teleost intestines is influenced by the aquatic environment or the diet, microbial content is generally maintained at approximately 10^7–10^8 bacteria per gram, among which aerobic and facultative anaerobic organisms are dominant (17). In some cases, the teleost-gut-associated microbiota is also essential for body health, as zebrafish devoid of microbiota showed impaired innate immune functions when compared to normal fish (82). Alternatively, under the effects of a stressor, symbiotic bacteria can also turn into pathogenic bacteria, thereby causing disease or even death (83). Therefore, the role of GALT in the control of homeostasis of commensal microorganisms is crucial to support fish health (84, 85).

In mammals, the involvement of IgA in the coating of both beneficial bacteria and opportunists promote the preservation of microbiota homeostasis on mucosal surfaces (84, 86). Given that IgT appears to be a dedicated mucosal Ig in teleosts, IgT not only plays a key role in pathogen response but is also implicated in intestinal homeostasis by recognizing and coating bacterial microbiota (10). In a previous study, almost half of the microbiota present on the intestinal surface were found to be coated with IgT, whereas IgM and IgD could only bind to a small and similar percentage of bacteria (10, 29). As the Ig-bacteria interaction in teleosts is currently unclear, further studies are needed to shed light on the function og IgT, IgM and IgD with respect to bacterial coating and gut homeostasis.

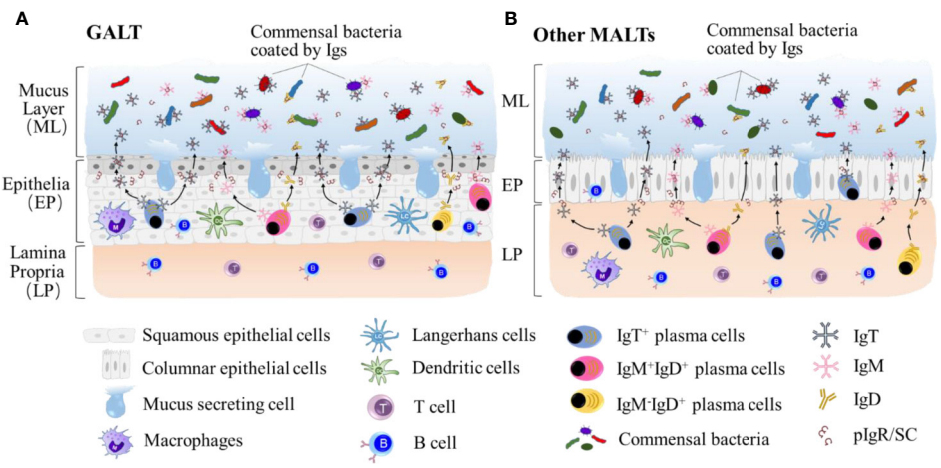

FIGURE 2 | Teleost IgT, IgM and IgD are produced by IgT$^+$, IgM$^+$IgD$^+$ and IgM$^-$IgD$^+$ B-cells mainly located in lamina propria in GALT **(A)** and epithelial layer other MALTs, such as GIALT, SALT, NALT, PM and buccal MALT **(B)**. Igs are transported from the epithelium into the mucus layer by the teleost pIgR to maintain the homestasis of microbiota at mucosal sites. The symbiotic bacteria in the mucus is predominantly coated by sIgT.

Immunoglobulin Responses to Microbiota in Gills

Similar to the function of sIgs in mammal lungs (87), Igs in gill mucus can maintain immune homeostasis by limiting microbial antigen access to the fish body, thereby keeping the epithelial barrier's integrity and shaping the composition of the symbiotic microbiota (4, 7, 74). One study demonstrated a large population of bacteria in the gill mucosa was predominately coated by sIgT and to a much lesser degree by IgM and IgD, indicating the conserved role of a specialized mucosal Ig in vertebrates that recognize commensal bacteria on the gas-exchange surface (4). Upon IgT depletion, it was clearly observed that the percentage of IgT-coated microbiota decreased significantly and recovered when IgT was re-produced in the fish gill mucosa. Moreover, a set of microbes translocated from the mucus layer across the gill epithelium and invaded the systemic circulation in sIgT-depleted fish. IgT-seq demonstrated that IgT coats a broad but well-defined range of bacteria with both beneficial and pathogenic characteristics and microbiota composition changed significantly, which demonstrated the loss of potentially beneficial bacteria that produce short-chain fatty acids (SCFAs) and pathobiont expansion after IgT depletion. Interestingly, when the level of IgT was restored to its original state, the balance of microbiota was reestablished in the gill surfaces (7). Thus, these observations strongly imply that teleost IgT is essential to maintain microbiota homeostasis in the gills.

Additionally, *Flectobacillus major*, a bacterial species that dominates trout gill, can induce specific IgT secretion in the gills of healthy rainbow trout (55). It is assumed that *F. major* modulates Igs and then regulates the symbiotic homeostasis in the gill surface. However, its specific mechanisms still need to be determined. Thus, future studies should investigate not only the functional mechanisms by which Igs regulate the commensal microbiota and the role of IgT/IgZ in targeting specific bacteria in teleost fish gills, but also the mechanisms by which certain components of the commensal microbiota affects mucosal and systemic immunity.

Immunoglobulin Responses to Microbiota in Skin

The skin of teleosts contains a layer of live cells covered by a rich mucous layer with high densities of bacterial microbiota (88, 89). Under normal circumstances, the skin mucosal immune system of teleosts is in a dynamic equilibrium with symbiotic microorganisms, and skin homeostasis is critical to preserve teleost health in vertebrates. However, once the original balance is disturbed by external factors such as parasitic infection, bacterial community composition changes significantly, thereby leading to pathobiont proliferation and secondary infection (76). Thus, an understanding of the mechanism by which microbial homeostasis is maintained is necessary for the study of skin immunity in teleosts. So far, it has been demonstrated that teleost sIgs, especially sIgT, play a significant role in the control of skin symbiotic flora homeostasis. In a study on rainbow trout, IgT was found to be bound to a large fraction of skin bacteria (~38%), whereas only a small proportion (~12%) was coated with IgM (11), which is consistent with the mammalian sIgA coating of skin bacterial microbiota (90). The targeting of skin microbes by mammalian sIgA plays a key role in immune exclusion (90); however, mucosal Ig can promote the colonization of certain bacteria on the skin surface (91). Therefore, considering that teleost skin is a unique mucosal surface that elicits gut-like immune responses, future research should determine whether teleost sIgT is involved in immune exclusion or assists with bacterial colonization.

Immunoglobulin Responses to Microbiota in the Olfactory Organ

The olfactory organs of vertebrates are extraordinary chemosensory structures that harbor a variety of symbiotic microorganisms in the NC (12). In mammals, nasal symbiotic bacteria play an important role in controlling immunological development *via* different mechanisms including inhibiting pathogen colonization on the mucosal surface and stimulating the host immune system (92). In contrast, the function of microbiota in the NC of teleost fish has not been determined in the olfactory organ of teleost fish; however, the bacterial community in NC of rainbow trout is dominated by *Proteobacteria*, *Actinobacteria*, *Bacteroidetes*, and *Firmicutes* (93), among which *Proteobacteria* and *Firmicutes* may be the most conserved taxa in the olfactory organ of vertebrates (55).

The nasal bacteria of teleosts are also anchored by sIgs, similar to those in the gul, gill and skin, to the mucus layer through a mechanism known as immune exclusion (12, 55). However, sIgT and sIgM in the olfactory organ coat equal proportions of microbiota in contrast to skin, gut and gills where IgT is specialized in coating, and IgM coats significantly lower numbers of bacteria (10, 11). This may be because the isotypes of Ig coating mucosal bacteria on MALTs are different due to the diversity of local microbiota (93). Alternatively, as the percentage of nasal commensal bacteria coated with both IgM and IgT is much higher than that of other mucosal sites, it is possible that the extent of Ig binding-microbiota varies in trout depending on genetic lines or ages, and some of the bacterial taxa coated by sIgM are those bacteria found initially coated by sIgT. Thus, a future Ig-seq study of the species of microbiota coated by IgT/IgZ and IgM may confirm the aforementioned possibilities.

Immunoglobulin Responses to Microbiota in BC

The BC is covered with a critical layer of mucus that is constantly exposed to microorganisms from air, water, and food in vertebrates. Similar to humans, *Proteobacteria* and *Actinobacteria* are dominant in the BC of teleosts (94, 95). However, the bacterial communities differed post-infection when challenged with hematopoietic necrosis virus (IHNV); that is, the abundance of *Pseudomonas* significantly decreased, while the abundance of *Clostridiales*, *Bacteroidales*, and *Escherichia-Shigella* increased, all of which are related to human intestinal diseases (96–98). As previously described for skin sites, pathogenic infection may break the homeostasis of microbiota in the BM, facilitate the colonization of opportunistic bacteria, and then cause secondary bacterial infections in the BC (95). Thus, the

microbial homeostasis of the teleost BM is necessary for buccal health.

It is important to point out that the BMs of vertebrates have evolved an efficient immune system to maintain homeostasis (5). Moreover, the mucosal molecular responses of fish and mammals (i.e., sIgT versus sIgA) utilize different but functionally analogous strategies to initiate a response to microbiota in the BC (5). Due to its constant interaction with the water environment, the homeostasis of fish BM microbiota may be prone to frequent adverse effects. Among the three teleost Igs, sIgT is also the main Ig class that binds to BM-associated bacteria, and significantly lower percentages of the microbiota are coated by sIgM and sIgD, similar to those in the gut, skin, and gills of trout (4, 5, 10, 11). So far, previous studies have demonstrated that some salivary sIgA predominantly coating commensal bacteria, such as *Streptococcus mutans*, *Actinobacillus actinomycetemcomitans*, and *Porphyromonas gingivalis*, are associated with mammalian buccal diseases (99, 100). However, the type of buccal microbiota species coated by IgT/IgZ, IgM, and IgD is still unknown, which is critical to gain insights into the role of Igs in the homeostasis of the BM in teleosts.

Immunoglobulin Responses to Microbiota in PC

The PM, as well as the ML covering the teleost PC, contains D-MALT with abundant symbiotic bacteria, but without the tonsils found in mammals (6, 101). Microbial community compositions were analyzed *via* 16S rRNA sequencing, and it was found that *Proteobacteria* and *Actinobacteria* were dominant in the pharynx of naive fish (95). However, although many studies have demonstrated the role of pharyngeal sIgA in pathogen elimination in vertebrates, limited studies have elucidated the interaction between mucosal Igs and PM microbiota. Our previous study on rainbow trout showed that pharyngeal Igs occur in response to commensal bacteria in PC, demonstrating that pharyngeal IgT coated a large population of bacteria while IgM and IgD do so to a lesser degree. Moreover, the study showed that sIgT is generated by IgT^+ B-cells located in the PM, transferred by pIgR secreted by pIgR-expressing epithelium cells onto the pharyngeal surface, and finally binds to the microbiota (6). This fascinating similarity of IgT microbiota targeting in different MALTs may corroborate the notion that teleost MALTs form an interactive network structure and communicate with each other (4, 5, 10, 11).

IMMUNOGLOBULIN RESPONSES FOLLOWING MUCOSAL IMMUNIZATION

Compared to systemic immunization, mucosal immunization efficiently induces a local mucosal immune response (102), which can induce "frontline immunity" with local Igs production in the MALT, neutralizing pathogens and finally preventing infection (103). Additionally, mucosal vaccines are superior to systemic vaccines from a production and regulatory standpoint (104). Mucosal immunization is simple and suitable for farmed fish immunization. Additionally, immunization *via* injection inflicts minor trauma on the body through which pathogens may easily break through and induce an inflammatory response. In contrast, mucosal immunization does not have this potential drawback. Therefore, understanding the Igs response in teleosts following mucosal immunization will be helpful for the design and development of novel fish vaccines.

Immunoglobulin Responses Following Oral Immunization

In mammals, sIgA plays an important role in humoral immunity, which participates in adaptive immune responses to inhibit oral pathogens (80); recently, the BM of fish was proven to be a type of MALT (5). However, compared to oral immunization in mammals, oral vaccination methods in fish are still in development. Many new attempts to develop new fish immunization strategies such as the use of pathogen-coding DNA and pathogen recombinant proteins have established the basis for the potential development of oral immunization in the future (105–107). After orally treating trout with an alginate-encapsulated antigen (i.e., oral vaccination), increased numbers of IgT^+ and IgM^+ B-cell were observed in the pyloric caeca, which correlated with an increased expression of IgT and IgM in the same area (108). Later on, Iván et al. demonstrated that high levels of specific IgM antibodies could be detected in fish serum when oral immunizations were administered (109). Importantly, it has been proved that recombinant tumor necrosis factor a (rTNFa) could significantly improve a commercial sea bass oral vaccine against *V. anguillarum*. And during the response, gut IgT transcripts were detected to increase (110). Overall, future studies should characterize Ig responses following oral immunization in more detail.

Immunoglobulin Responses Following Immersion Immunization

Immersion immunization is considered to be the simplest and most practical method of vaccination in aquaculture. Amend and Fender first described the method of immersion immunization in small fish, and they found that when the fish were exposed to a bovine serum albumin (BSA) solution with hyperosmotic treatment, the BSA would penetrate the juvenile trout blood, highlighting the effectiveness of immersion immunization (111). Although abundant studies on immersion immunization have been reported in different fish species, the involvement of Ig responses is relatively limited. In one study, after the fish were immersion-vaccinated with a Danish strain of *Y. ruckeri* serotype O1, biotype 2, the concentration of *Y. ruckeri* -specific IgM hardly changed compared to that of unvaccinated fish. However, after 3 weeks of exposure to live bacteria, the antibody level in vaccinated fish increased significantly (112). Similarly, another study also detected significantly increased IgM antibody levels in vaccinated rainbow trout challenged with 1×10^9 CFU mL^{-1} *Y. ruckeri* bacterin for 1 h (113). Moreover, the titers of bacteria-specific antibody in rainbow trout increased when immersion vaccinated with a 2.0×10^8 CFU mL^{-1} live *F. psychrophilum* suspension (114). These results suggest that immersion immunization can induce the adaptive immune response to

protect the body. Additionally, upregulated mRNA expression of IgM and pIgR could be detected in vaccinated fish after *V. anguillarum* bacterin exposure and the pIgR expression levels were higher in some mucosal tissues (gills, skin, and hindgut) (115). Importantly, the delivery of live attenuated vaccines can improve the immune ability of fish (116). For instance, after fish fry were bath vaccinated with a live *F. columnare* vaccine, the survival rate of channel catfish (*Ictalurus punctatus*) increased between 57% and 94% (117). Moreover, another study reported that zebrafish vaccinated with live attenuated *Vibrio anguillarum* possessed more strong mucosal immune responses (118). However, despite these observations, further studies on teleost IgT/IgZ response and IgM and IgD response in fish lacking IgT following immersion immunization are still needed.

Immunoglobulin Responses Following Anal Immunization

The presentation of M-like cells in the intestine suggest that antigens could be uptaken (119), thereby inducing strong immunity in the infected or vaccinated fish. A recent study showed that, compared with oral vaccination, single-dose anal bacterin intubation following bath challenge with *Y. ruckeri* rendered a high survival rate in teleost fish, suggesting that immunizing antigens might have been destroyed in the stomach of the oral vaccination group. However, in the same study, no significant differences in the IgM antibody levels were detected in the plasma of the two vaccination groups at any of the sampling time points (120). A later study also demonstrated that there were no significant differences in IgM levels of anally-intubated fish, yet the expression of sIgD and IgT were upregulated in both the intestines of fish immunized *via* anal intubation and in the gills of fish immunized by immersion (121). Recently, the anal administration of thymus-independent (TI) antigens without additional adjuvants was investigated in rainbow trout. An efficient B-cell response was induced, which facilitated the production of specific IgM in serum and the differentiation of antigen-specific ASCs (122).

Immunoglobulin Responses Following Nasal Immunization

Compared with other vaccination types, nasal vaccination, which is an accessible method to control infectious diseases (123), has the advantages of using a needle-free delivery system and a lower dosage of antigen to elicit an immune response. Nasal vaccines are widely used in many animals such as cats, dogs, and cattle. Nasal vaccination in mammals induces IgA-specific responses in O-NALT and D-NALT (124). Recently, the discovery of NALT in rainbow trout prompted studies concerning nasal vaccines for use in aquaculture (12). Thereafter, it was found that nasal vaccination can effectively protect fish against viral and bacterial pathogens (125). Furthermore, the nasal vaccinated group with live attenuated IHNV could significantly reduce mortalities of the trout after the IHNV infection, whereas nasal vaccinated group with formalin killed *Y. ruckeri* appear to fully protect fish against enteric red mouth (ERM) disease (126). Moreover, nasal vaccination with ERM bacterin also generated different IgM and IgT repertoire dynamics at systemic and mucosal levels and induced striking IgT responses in the spleen of rainbow trout (78).

CONCLUDING REMARKS

This review sought to gather recent advances that have shed some light on the immune responses of Igs in teleost fish to microorganisms or immunization, including mucosal pathogens, vaccines and microbiota. Teleost sIgM, sIgT, and sIgD coexist at all mucosal sites, including the gut, gills, olfactory organ, skin, BC, and PC. During pathogenic infection, specific sIgT can be locally produced in mucosal secretions, and mucosal sensitivity increases in IgT-depleted fish, while large quantities of specific sIgM are generated in the serum. These findings suggest that the IgT-mediated immune response is crucial in all mucosal sites, whereas IgM responses are typically systemic in all teleosts and also functional in mucosal sites of teleosts which lack IgT/Z (7, 77). Considering that IgM has the highest protein concentration among teleost Igs on mucosal surfaces and that the specific IgM also can be induced in the mucosal surfaces by parasites as in the serum, it is worth investigating whether sIgM has an auxiliary effect on sIgT to eliminate pathogens at mucosal sites. Additionally, mucosal responses of Igs in fish, mainly trout, have been demonstrated after parasitic and bacterial infection (4, 5, 10, 11, 74, 77), but fish mucosal responses after infection by other pathogens such as virus or fungi are still unclear. In vertebrates, the common mucosal immune system (CMIS), which means that antigens administration induces humoral immune responses not only at the mucosal site of antigen application but also in other external mucosal tissues due to the dissemination of antigen-sensitized cells, is vitally important. Specifically, mammalian has been found to produce specific IgA or IgM responses in other MALTs upon stimulation of one mucosal site (127); however, data on the CMIS in teleosts remains currently limited. Therefore, our current understanding of the mechanisms underlying teleost Ig responses at mucosal sites remains nascent. Especially, the humoral immune responses in teleosts which lack IgT/Z remain much unknown. Future studies need to consider the role of IgT, IgM, and IgD in mucosal immunity to different pathogens by infection or immunization and explore the CMIS in teleosts, which will contribute to the development of fish vaccines.

Another very important point is that the mucosal microbiota is predominantly coated by teleost IgT at mucosal sites. IgT depletion induces a profound dysbiosis, the expansion of pathobionts, tissue damage, the translocation of mucosal bacteria, and inflammation. These findings demonstrate the previously unrecognized ability of IgT in immune exclusion to protect the mucosa from microbiota (7). However, information on the role of teleost sIgT in bacterial colonization remains scarce. Understanding how sIgT coating of bacteria mediates bacterial colonization under homeostatic conditions may improve the efficiency of aquatic probiotics. Moreover, it is worth noting that teleost IgM can bind a subset of microbiota, especially in the

teleost olfactory organ, and the percentage of IgM-coating bacteria in fish is notably higher than that in mammals (10, 12, 96). Importantly, in fish devoid of IgT, the percentage of microbiota coated by IgM is significantly higher, suggesting that compensatory sIgM might then coat microbiota that was originally coated by sIgT (7). Thus, the function of sIgM in teleost commensal homeostasis has not yet been determined, and future studies based on IgM depletion experiments may provide important insights into this matter. Additionally, mammalian IgA-derived antibodies are commonly polyreactive and show low-affinity to numerous microbial antigens. Although teleost mucosal Ig (IgT) has been found to target a taxonomically distinct subset of microbiota at the gill surface (7), the extent of the microbe recognition capacity of IgT as well as its mucosal-specific pathogen-binding capacity during infection are still unknown.

Overall, it seems clear that Igs in teleosts, similar to those of mammals, can defend mucosa against pathogens for elimination and interact with microbiota to maintain commensal homeostasis; however, many aspects of their responses remain poorly understood. Thus, the inner mechanisms of Igs regulating both the pathogenic clearance and commensal homeostasis should be determined in the future research.

AUTHOR CONTRIBUTIONS

All authors contributed to the article and approved the submitted version.

FUNDING

This work was supported by grants from the National Natural Science Foundation of China (U1905204, 31873045) and the Key Laboratory of Marine Biotechnology of Fujian Province (2020MB03).

REFERENCES

1. Cossins AR, Crawford DL. Fish as models for environmental genomics. *Nat Rev Genet* (2005) 6:324–33. doi: 10.1038/nrg1590
2. Koppang EO, Kvellestad A, Fischer U. 5-Fish mucosal immunity: gill. *Mucosal Health Aquaculture* (2015) 93–133. doi: 10.1016/B978-0-12-417186-2.00005-4
3. Mantis NJ. Role of B cells and antibodies in controlling bacterial pathogens. *Encyclopedia Microbiol* (2019) 194–200. doi: 10.1016/B978-0-12-801238-3.66120-2
4. Xu Z, Takizawa F, Parra D, Gómez D, Gersdorff Jørgensen L, LaPatra SE, et al. Mucosal immunoglobulins at respiratory surfaces mark an ancient association that predates the emergence of tetrapods. *Nat Commun* (2016) 7:10728. doi: 10.1038/ncomms10728
5. Yu YY, Kong WG, Xu HY, Huang ZY, Zhang XT, Ding LG, et al. Convergent evolution of mucosal immune responses at the buccal cavity of teleost fish. *iScience* (2019) 19:821–35. doi: 10.1016/j.isci.2019.08.034
6. Kong WG, Yu YY, Dong S, Huang ZY, Ding LG, Cao JF, et al. Pharyngeal immunity in early vertebrates provides functional and evolutionary insight into mucosal homeostasis. *J Immunol* (2019) 203:3054–67. doi: 10.4049/jimmunol.1900863
7. Xu Z, Takizawa F, Casadei E, Shibasaki Y, Ding Y, Sauters T, et al. Specialization of mucosal immunoglobulins in pathogen control and microbiota homeostasis occurred early in vertebrate evolution. *Sci Immunol* (2020) 5:3254. doi: 10.1126/sciimmunol.aay3254
8. Danilova N, Bussmann J, Jekosch K, Steiner LA. The immunoglobulin heavy-chain locus in zebrafish: identification and expression of a previously unknown isotype, immunoglobulin Z. *Nat Immunol* (2005) 6:295–302. doi: 10.1038/ni1166
9. Hansen JD, Landis ED, Phillips RB. Discovery of a unique Ig heavy-chain isotype (IgT) in rainbow trout: implications for a distinctive B cell developmental pathway in teleost fish. *Proc Natl Acad Sci U S A* (2005) 102:6919–24. doi: 10.1073/pnas.0500027102
10. Zhang YA, Salinas I, Li J, Parra D, Bjork S, Xu Z, et al. IgT, a primitive immunoglobulin class specialized in mucosal immunity. *Nat Immunol* (2010) 11:827–35. doi: 10.1038/ni.1913
11. Xu Z, Parra D, Gómeza D, Salinas I, Zhang YL, Jørgensen L, et al. Teleost skin, an ancient mucosal surface that elicits gut-like immune responses. *Proc Natl Acad Sci U S A* (2013) 110:13097–102. doi: 10.1073/pnas.1304319110
12. Tacchi L, Musharrafieh R, Larragoite ET, Crossey K, Erhardt EB, Martin SAM, et al. Nasal immunity is an ancient arm of the mucosal immune system of vertebrates. *Nat Commun* (2014) 5:5205. doi: 10.1038/ncomms6205
13. Salinas I, Zhang YA, Sunyer JO. Mucosal immunoglobulins and B cells of teleost fish. *Dev Comp Immunol* (2011) 35:1346–65. doi: 10.1016/j.dci.2011.11.009
14. Conrath KE, Wernery U, Muyldermans S, Nguyena VK. Emergence and evolution of functional heavy-chain antibodies in *Camelidae*. *Dev Comp Immunol* (2003) 27:87–103. doi: 10.1016/S0145-305X(02)00071-x
15. Saha NR, Ota T, Litman GW, Hansen J, Parra Z, Hsu E, et al. Genome complexity in the coelacanth is reflected in its adaptive immune system. *J Exp Zool B Mol Dev Evol* (2014) 322:438–63. doi: 10.1002/jez.b.22558
16. Roco J, Mesin L, Binder S, Nefzger C, Gonzalez-Figueroa1 P, Canete1 P, et al. Class-switch recombination occurs infrequently in germinal centers. *Immunity* (2019) 51:337–50. doi: 10.1016/j.immuni.2019.07.001
17. Parra D, Korytar T, Takizawa F, Sunyer J. B cells and their role in the teleost gut. *Dev Comp Immunol* (2016) 64:150–66. doi: 10.1016/j.dci.2016.03.013
18. Zhao Y, Pan-Hammarstrom Q, Zhao Z, Hammarstrom L. Identification of the activation-induced cytidine deaminase gene from zebrafish: an evolutionary analysis. *Dev Comp Immunol* (2005) 29:61–71. doi: 10.1016/j.dci.2004.05.005
19. Mashoof S, Criscitiello MF. Fish Immunoglobulins. *Biology* (2016) 5:1–23. doi: 10.3390/biology5040045
20. Amemiya C, Alföldi J, Lee A, Fan S, Philippe H, MacCallum I, et al. The African coelacanth genome provides insights into tetrapod evolution. *Nature* (2013) 496:311–6. doi: 10.1038/nature12027
21. Ye J, Bromage ES, Kaattari SL. The strength of B cell interaction with antigen determines the degree of IgM polymerization. *J Immunol* (2010) 184:844–50. doi: 10.4049/jimmunol.0902364
22. Solem ST, Stenvik J. Antibody repertoire development in teleosts–a review with emphasis on salmonids and *Gadus morhua* L. *Dev Comp Immunol* (2006) 30:57–76. doi: 10.1016/j.dci.2005.06.007
23. Rombout JH, Huttenhuis HB, Picchietti S, Scapigliati G. Phylogeny and ontogeny of fish leucocytes. *Fish Shellfish Immunol* (2005) 19:441–55. doi: 10.1016/j.fsi.2005.03.007
24. Lam SH, Chua HL, Gong Z, Lam TJ, Sin YM. Development and maturation of the immune system in zebrafish, *Danio rerio*: a gene expression profiling, in situ hybridization and immunological study. *Dev Comp Immunol* (2004) 28:9–28. doi: 10.1016/s0145-305x(03)00103-4
25. Edholm ES, Bengten E, Wilson M. Insights into the function of IgD. *Dev Comp Immunol* (2011) 35:1309e1316. doi: 10.1016/j.dci.2011.03.002
26. Bengtén E, Quiniou S, Hikima J, Waldbieser G, Warr GW, Miller NW, et al. Structure of the catfish IGH locus: analysis of the region including the single functional IGHM gene. *Immunogenetics* (2006) 58:831–44. doi: 10.1007/s00251-006-0139-9
27. Srisapoome P, Ohira T, Hirono I, Aoki T. Genes of the constant regions of functional immunoglobulin heavy chain of Japanese flounder, *Paralichthys*

olivaceus. *Immunogenetics* (2004) 56:292–300. doi: 10.1007/s00251-004-0689-7
28. Edholm ES, Bengtén E, Stafford JL, Sahoo M, Taylor EB, Miller NW, et al. Identification of two IgD^+ B cell populations in channel catfish, *Ictalurus punctatus*. *J Immunol* (2010) 185:4082–94. doi: 10.4049/jimmunol.1000631
29. Perdiguero P, Martín-Martín A, Benedicenti O, Díaz-Rosales P, Morel E, Muñoz-Atienza E, et al. Teleost IgD^+IgM^- B Cells Mount Clonally Expanded and Mildly Mutated Intestinal IgD Responses in the Absence of Lymphoid Follicles. *Cell Rep* (2019) 29:4223–35. doi: 10.1016/j.celrep.2019.11.101
30. Yasuike M, de Boer J, von Schalburg KR, Cooper GA, McKinnel L, Messmer A, et al. Evolution of duplicated IgH loci in Atlantic salmon, *Salmo salar*. *BMC Genomics* (2010) 11:486. doi: 10.1186/1471-2164-11-486
31. Zhang N, Zhang XJ, Chen DD, Oriol Sunyer J, Zhang YA. Molecular characterization and expression analysis of three subclasses of IgT in rainbow trout (*Oncorhynchus mykiss*). *Dev Comp Immunol* (2017) 70:94–105. doi: 10.1016/j.dci.2017.01.001
32. Bao Y, Wang T, Guo Y, Zhao Z, Li N, Zhao Y. The immunoglobulin gene loci in the teleost *Gasterosteus aculeatus*. *Fish Shellfish Immunol* (2010) 28 (1):40–8. doi: 10.1016/j.fsi.2009.09.014
33. Gambón-Deza F, Sánchez-Espinel C, Magadán-Mompó S. Presence of an unique IgT on the IGH locus in three-spined stickleback fish (Gasterosteus aculeatus) and the very recent generation of a repertoire of VH genes. *Dev Comp Immunol* (2010) 34(2):114–22. doi: 10.1016/j.dci.2009.08.011
34. Piazzon MC, Galindo-Villegas J, Pereiro P, Estensoro I, Calduch-Giner JA, Gómez-Casado E, et al. Differential Modulation of IgT and IgM upon Parasitic, Bacterial, Viral, and Dietary Challenges in a Perciform Fish. *Front Immunol* (2016) 7:637. doi: 10.3389/fimmu.2016.00637
35. Fillatreau S, Six A, Magadan S, Castro R, Sunyer JO, Boudinot P. The astonishing diversity of Ig classes and B cell repertoires in teleost fish. *Front Immunol* (2013) 4:28. doi: 10.3389/fimmu.2013.00028
36. Giacomelli S, Buonocore F, Albanese F, Scapigliati G, Gerdol M, Oreste U, et al. New insights into evolution of IgT genes coming from Antarctic teleosts. *Mar Genomics* (2015) 24:55–68. doi: 10.1016/j.margen.2015.06.009
37. Savan R, Aman A, Sato K, Yamaguchi R, Sakai M. Discovery of a new class of immunoglobulin heavy chain from fugu. Eur. *J Immunol* (2005) 35:3320–31. doi: 10.1002/eji.200535248
38. Hu YL, Xiang LX, Shao JZ. Identification and characterization of a novel immunoglobulin Z isotype in zebrafish: Implications for a distinct B cell receptor in lower vertebrates. *Mol Immunol* (2010) 47:738–46. doi: 10.1016/j.molimm.2009.10.010
39. Ryo S, Wijdeven RH, Tyagi A, Hermsen T, Kono T, Karunasagar I, et al. Common carp have two subclasses of bonyfish specific antibody IgZ showing differential expression in response to infection. *Dev Comp Immunol* (2010) 34:1183–90. doi: 10.1016/j.dci.2010.06.01
40. Bradshaw WJ, Valenzano DR. Extreme genomic volatility characterizes the evolution of the immunoglobulin heavy chain locus in cyprinodontiform fishes. *Proc R Soc B* (2020) 287:20200489. doi: 10.1098/rspb.2020.0489
41. Salinas I. The Mucosal Immune System of Teleost Fish. *Biology* (2015) 4:525–39. doi: 10.3390/biology4030525
42. Arena ET, Campbell-Valois FX, Tinevez JY, Nigro G, Sachse M, Moya-Nilges M, et al. Bioimage analysis of Shigella infection reveals targeting of colonic crypts. *Proc Natl Acad Sci U S A* (2015) 112:3282–90. doi: 10.1073/pnas.1509091112
43. Rombout JH, Abelli L, Picchietti S, Scapigliati G, Kiron V. Teleost intestinal immunology. *Fish Shellfish Immunol* (2011) 31:616–26. doi: 10.1016/j.fsi.2010.09.001
44. Tafalla C, Leal E, Yamaguchi T, Fischer U. T cell immunity in the teleost digestive tract. *Dev Comp Immunol* (2016) 64:167–77. doi: 10.1016/j.dci.2016.02.019
45. Rombout JH, Yang G, Kiron V. Adaptive immune responses at mucosal surfaces of teleost fish. *Fish Shellfish Immunol* (2014) 40:634–43. doi: 10.1016/j.fsi.2014.08.020
46. Maina JN. Structure, function and evolution of the gas exchangers: comparative perspectives. *J Anat* (2002) 201:281–304. doi: 10.1046/j.1469-7580.2002.00099
47. Gómez D, Bartholomew J, Sunyer JO. Biology and mucosal immunity to myxozoans. *Dev Comp Immunol* (2014) 43:243–56. doi: 10.1016/j.dci.2013.08.014
48. Maki JL, Dickerson HW. Systemic and cutaneous mucus antibody responses of channel catfish immunized against the protozoan parasite *Ichthyophthirius multifiliis*. *Clin Diagn Lab Immunol* (2003) 10:876–81. doi: 10.1128/cdli.10.5.876-881.2003
49. Parra D, Reyes-Lopez FE, Tort L. Mucosal Immunity and B Cells in Teleosts: Effect of Vaccination and Stress. *Front Immunol* (2015) 6:354 doi: 10.3389/fimmu.2015.00354
50. Galindo-Villegas J, Montalban-Arques A, Liarte S, de Oliveira S, Pardo-Pastor C, Rubio-Moscardo F, et al. TRPV4-Mediated Detection of Hyposmotic Stress by Skin Keratinocytes Activates Developmental Immunity. *J Immunol* (2016) 196(2):738–49. doi: 10.4049/jimmunol.1501729
51. Schempp C, Emde M, Wolfle U. Dermatology in the Darwin anniversary. Part 1: Evolution of the integument. *J Dtsch Dermatol Ges* (2009) 7:750–7. doi: 10.1111/j.1610-0387.2009.07193.x
52. Nigam AK, Kumari U, Mittal S, Mittal AK. Comparative analysis of innate immune parameters of the skin mucous secretions from certain freshwater teleosts, inhabiting different ecological niches. *Fish Physiol Biochem* (2012) 38:1245–56. doi: 10.1007/s10695-012-9613-5
53. Ache BW, Young JM. Olfaction: diverse species, conserved principles. *Neuron* (2005) 48:417–30. doi: 10.1016/j.neuron.2005.10.022
54. Agbesi MP, Naylor S, Perkins E, Borsuk HS, Sykes D, Maclaine JS, et al. Complex flow in the nasal region of guitarfishes. *Comp Biochem Physiol A Mol Integr Physiol* (2016) 193:52–63. doi: 10.1016/j.cbpa.2015.12.007
55. Sepahi A, Cordero H, Goldfine H, Esteban MÁ, Salinas I. Symbiont-derived sphingolipids modulate mucosal homeostasis and B cells in teleost fish. *Sci Rep* (2016) 6:39054. doi: 10.1038/srep39054
56. Squier CA, Kremer MJ. Biology of oral mucosa and esophagus. *J Natl Cancer Inst Monogr* (2001) 29:7–15. doi: 10.1093/oxfordjournals.jncimonographs.a003443
57. Yashpal M, Kumari U, Mittal S, Mittal AK. Histochemical characterization of glycoproteins in the buccal epithelium of the catfish, Rita rita. *Acta Histochem* (2007) 109:285–303. doi: 10.1016/j.acthis.2007.03.002
58. Winning TA, Townsend GC. Oral mucosal embryology and histology. *Clin Dermatol* (2000) 18:499–511. doi: 10.1016/s0738-081x(00)00140-1
59. Abbate F, Germanà GP, De Carlos F, Montalbano G, Laurà R, Levanti MB, et al. The oral cavity of the adult zebrafish (*Danio rerio*). *Anat Histol Embryol* (2006) 35:299–304. doi: 10.1111/j.1439-0264.2006.00682.x
60. Graham A, Richardson J. Developmental and evolutionary origins of the pharyngeal apparatus. *Evodevo* (2012) 3:24. doi: 10.1186/2041-9139-3-24
61. Chatchavalvanich K, Marcos R, Poonpirom J, Thongpan A, Rocha E. Histology of the digestive tract of the freshwater stingray *Himantura signifer* Compagno and Roberts. *Anat Embryol* (2006) 211:507–18. doi: 10.1007/s00429-006-0103-3
62. Suzuki T, Sato T, Kano M, Ichikawa H. The distribution of galanin-immunoreactive nerve fibers in the rat pharynx. *Neuropeptides* (2013) 47:231–6. doi: 10.1016/j.npep.2013.05.001
63. Satoh-Takayama N, Kato T, Motomura Y, Kageyama T, Taguchi-Atarashi-Giner N, Kinoshita-Daitoku R, et al. Bacteria-Induced Group 2 Innate Lymphoid Cells in the Stomach Provide Immune Protection through Induction of IgA. *Immunity* (2020) 52(4):635–49.e4. doi: 10.1016/j.immuni.2020.03.002
64. Smith FM, Croll RP. Autonomic control of the swimbladder. *Auton Neurosci* (2011) 165(1):140–8. doi: 10.1016/j.autneu.2010.08.002
65. Villasante A, Ramirez C, Catalán N, Romero J. First Report of Swim Bladder-Associated Microbiota in Rainbow Trout (Oncorhynchus mykiss). *Microbes Environ* (2017) 32(4):386–9. doi: 10.1264/jsme2.ME17071
66. Rodríguez A, Tjärnlund A, Ivanji J, Singh M, Garcia I, Williams A, et al. Role of IgA in the defense against respiratory infections IgA deficient mice exhibited increased susceptibility to intranasal infection with *Mycobacterium Bovis* BCG. *Vaccine* (2005) 23:2565–72. doi: 10.1016/j.vaccine.2004.11.032
67. Sommer F, Bäckhed F. The gut microbiota–masters of host development and physiology. *Nat Rev Microbiol* (2013) 11:227–38. doi: 10.1038/nrmicro2974
68. Cerutti A, Rescigno M. The biology of intestinal immunoglobulin A responses. *Immunity* (2008) 28:740–50. doi: 10.1016/j.immuni.2008.05.001
69. Estensoro I, Calduch-Giner JA, Kaushik S, Pérez-Sánchez J, Sitjà-Bobadilla A. Modulation of the IgM gene expression and IgM immunoreactive cell

distribution by the nutritional background in gilthead sea bream (*Sparus aurata*) challenged with *Enteromyxum leei* (Myxozoa). *Fish Shellfish Immunol* (2012) 33:401–10. doi: 10.1016/j.fsi.2012.05.029
70. Ballesteros NA, Saint-Jean SS, Encinas PA, Perez-Prieto SI, Coll JM. Oral immunization of rainbow trout to infectious pancreatic necrosis virus (Ipnv) induces different immune gene expression profiles in head kidney and pyloric ceca. *Fish Shellfish Immunol* (2012) 33:174–85. doi: 10.1016/j.fsi.2012.03.016
71. Aquilino C, Castro R, Fischer U, Tafalla C. Transcriptomic responses in rainbow trout gills upon infection with viral hemorrhagic septicemia virus (VHSV). *Dev Comp Immunol* (2014) 44:12–20. doi: 10.1016/j.dci.2013.11.006
72. Pennacchi Y, Leef MJ, Crosbie PB, Nowak BF, Bridle AR. Evidence of immune and inflammatory processes in the gills of AGD-affected Atlantic salmon, *Salmo salar* L. *Fish Shellfish Immunol* (2014) 36:563–70. doi: 10.1016/j.fsi.2013.12.013
73. Shi M, Huang R, Du F, Pei Y, Liao L, Zhu Z, et al. RNA-seq profiles from grass carp tissues after reovirus (GCRV) infection based on singular and modular enrichment analyses. *Mol Immunol* (2014) 61:44–53. doi: 10.1016/j.molimm.2014.05.004
74. Tongsri P, Meng K, Liu X, Wu Z, Yin G, Wang Q, et al. The predominant role of mucosal immunoglobulin IgT in the gills of rainbow trout (*Oncorhynchus mykiss*) after infection with *Flavobacterium columnare*. *Fish Shellfish Immunol* (2020) 99:654–62. doi: 10.1016/j.fsi.2020.01.044
75. Olsen MM, Kania PW, Heinecke RD, Skjoedt K, Rasmussen KJ, Buchmann K. Cellular and humoral factors involved in the response of rainbow trout gills to *Ichthyophthirius multifiliis* infections: molecular and immunohistochemical studies. *Fish Shellfish Immunol* (2011) 30:859–69. doi: 10.1016/j.fsi.2011.01.010
76. Zhang XT, Ding LG, Yu YY, Kong WG, Yin YM, Huang ZY, et al. The change of teleost skin commensal Microbiota is associated with skin mucosal transcriptomic responses during parasitic infection by *Ichthyophthirius multifillis*. *Front Immunol* (2018) 9:2972. doi: 10.3389/fimmu.2018.02972
77. Yu YY, Kong W, Yin YX, Dong F, Huang ZY, Yin GM, et al. Mucosal immunoglobulins protect the olfactory organ of teleost fish against parasitic infection. *PLoS Pathog* (2018) 14:1007251. doi: 10.1371/journal.ppat.1007251
78. Magadan S, Jouneau L, Boudinot P, Salinas I. Nasal Vaccination Drives Modifications of Nasal and Systemic Antibody Repertoires in Rainbow Trout. *J Immunol* (2019) 203:1480–92. doi: 10.4049/jimmunol.1900157
79. Sepahi A, Kraus A, Casadei E, Johnston CA, Galindo-Villegas J, Kelly C, et al. Olfactory sensory neurons mediate ultrarapid antiviral immune responses in a TrkA-dependent manner. *Proc Natl Acad Sci U S A* (2019) 116(25):12428–36. doi: 10.1073/pnas.1900083116
80. Brandtzaeg P. Secretory immunity with special reference to the oral cavity. *J Oral Microbiol* (2013) 5:1–24. doi: 10.3402/jom.v5i0.20401
81. Galindo-Villegas J, García-Moreno D, de Oliveira S, Meseguer J, Mulero V. Regulation of immunity and disease resistance by commensal microbes and chromatin modifications during zebrafish development. *Proc Natl Acad Sci U S A* (2012) 109(39):E2605–14. doi: 10.1073/pnas.1209920109
82. Kanther M, Rawls JF. Host-microbe interactions in the developing zebrafish. *Curr Opin Immunol* (2010) 22:10–9. doi: 10.1016/j.coi.2010.01.006
83. Kelly C, Salinas I. Under Pressure: Interactions between Commensal Microbiota and the Teleost Immune System. *Front Immunol* (2017) 8:559. doi: 10.3389/fimmu.2017.00559
84. Bunker JJ, Bendelac A. IgA Responses to Microbiota. *Immunity* (2018) 49(2):211–24. doi: 10.1016/j.immuni.2018.08.011
85. Pérez T, Balcázar JL, Ruiz-Zarzuela I, Halaihel N, Vendrell D, de Blas I, et al. Host-microbiota interactions within the fish intestinal ecosystem. *Mucosal Immunol* (2010) 3:355–60. doi: 10.1038/mi.2010.12
86. Palm NW, de Zoete MR, Flavell RA. Immune-microbiota interactions in health and disease. *Clin Immunol* (2015) 159:122–27. doi: 10.1016/j.clim.2015.05.014
87. Robak OH, Heimesaat MM, Kruglov AA, Prepens S, Ninnemann J, Gutbier B, et al. Antibiotic treatment-induced secondary IgA deficiency enhances susceptibility to Pseudomonas aeruginosa pneumonia. *J Clin Invest* (2018) 128:3535–45. doi: 10.1172/JCI97065
88. Austin B. The bacterial microflora of fish. *Sci World J* (2002) 2:558–72. doi: 10.1100/tsw.2002.137
89. Reid KM, Patel S, Robinson AJ, Bu L, Jarungsriapisit J, Moore LJ, et al. Salmonid alphavirus infection causes skin dysbiosis in Atlantic salmon (*Salmo salar* L.) post-smolts. *PLoS One* (2017) 12:e0172856. doi: 10.1371/journal.pone.0172856
90. Metze D, Kersten A, Jurecka W, Gebhart W. Immunoglobulins coat microorganisms of skin surface: a comparative immunohistochemical and ultrastructural study of cutaneous and oral microbial symbionts. *J Invest Dermatol* (1991) 96:439–45. doi: 10.1111/1523-1747.ep12469908
91. Maynard CL, Elson CO, Hatton RD, Weaver CT. Reciprocal interactions of the intestinal microbiota and immune system. *Nature* (2012) 489:231–41. doi: 10.1038/nature11551
92. Buffie CG, Pamer EG. Microbiota-mediated colonization resistance against intestinal pathogens. *Nat Rev Immunol* (2013) 13(11):790–801. doi: 10.1038/nri3535
93. Lowrey L, Woodhams DC, Tacchi L, Salinas I. Topographical Mapping of the Rainbow Trout (*Oncorhynchus mykiss*) Microbiome Reveals a Diverse Bacterial Community with Antifungal Properties in the Skin. *Appl Environ Microbiol* (2015) 81:6915–25. doi: 10.1128/AEM.01826-15
94. Contreras M, Costello EK, Hidalgo G, Magris M, Knight R, Dominguez-Bello MG. The bacterial microbiota in the oral mucosa of rural Amerindians. *Microbiology* (2010) 156:3282–7. doi: 10.1099/mic.0.043174-0
95. Dong S, Ding LG, Cao JF, Liu X, Xu HY, Meng KF, et al. Viral-Infected Change of the Digestive Tract Microbiota Associated With Mucosal Immunity in Teleost Fish. *Front Immunol* (2019) 10:2878. doi: 10.3389/fimmu.2019.02878
96. Xu J, Chen N, Wu Z, Song Y, Zhang Y, Wu N, et al. 5-aminosalicylic acid alters the gut bacterial microbiota in patients with ulcerative colitis. *Front Microbiol* (2018) 9:1274. doi: 10.3389/fmicb.2018.01274
97. Sears CL. Enterotoxigenic Bacteroides fragilis: a rogue among symbiotes. *Clin Microbiol Rev* (2009) 22:349–69. doi: 10.1128/CMR.00053-08
98. Ciarán P, Kelly M, Thomas J, LaMont M. Clostridium difficile infection. *Ann Rev Med* (1998) 49:375–90. doi: 10.1146/annurev.med.49.1.375
99. Mikuls TR, Payne JB, Reinhardt RA, Thiele GM, Maziarz E, Cannella AC, et al. Antibody responses to *Porphyromonas gingivalis* (*P. gingivalis*) in subjects with rheumatoid arthritis and periodontitis. *Int Immunopharmacol* (2009) 9:38–42. doi: 10.1016/j.intimp.2008.09.008
100. Nogueira RD, Alves AC, Napimoga MH, Smith DJ, Mattos-Graner RO. Characterization of salivary immunoglobulin A responses in children heavily exposed to the oral bacterium Streptococcus mutans: influence of specific antigen recognition in infection. *Infect Immun* (2005) 73:5675–84. doi: 10.1128/IAI.73.9.5675-5684.2005
101. Yokoyama Y, Harabuchi Y. Intranasal immunization with lipoteichoic acid and cholera toxin evokes specific pharyngeal IgA and systemic IgG responses and inhibits streptococcal adherence to pharyngeal epithelial cells in mice. *Int J Pediatr Otorhinolaryngol* (2002) 63:235–41. doi: 10.1016/s0165-5876(02)00021-6
102. Neutra MR, Kozlowski PA. Mucosal vaccines: the promise and the challenge. *Nat Rev Immunol* (2006) 6:148–58. doi: 10.1038/nri1777
103. Rose MA. Mucosal immunization in perspective. *Hum Vaccin Immunother* (2014) 10:2115–7. doi: 10.4161/hv.29609
104. Levine MM. Immunogenicity and efficacy of oral vaccines in developing countries: lessons from a live cholera vaccine. *BMC Biol* (2010) 8:129. doi: 10.1186/1741-7007-8-129
105. De las Heras AI, Rodríguez Saint-Jean S, Pérez-Prieto SI. Immunogenic and protective effects of an oral DNA vaccine against infectious pancreatic necrosis virus in fish. *Fish Shellfish Immunol* (2010) 28:562–70. doi: 10.1016/j.fsi.2009.12.006
106. Tian JY, Yu J, Sun XQ. Chitosan microspheres as candidate plasmid vaccine carrier for oral immunisation of Japanese flounder (Paralichthys olivaceus). *Vet Immunol Immunopathol* (2008) 126(3-4):220–9. doi: 10.1016/j.vetimm.2008.07.002
107. Gomez-Casado E, Estepa A, Coll JM. A comparative review on European-farmed finfish RNA viruses and their vaccines. *Vaccine* (2011) 29:2657–71. doi: 10.1016/j.vaccine.2011.01.097
108. Ballesteros NA, Castro R, Abos B, Rodríguez Saint-Jean SS, Pérez-Prieto SI, Tafalla C, et al. The pyloric caeca area is a major site for IgM(+) and IgT(+) B cell recruitment in response to oral vaccination in rainbow trout. *PLoS One* (2013) 8:e66118. doi: 10.1371/journal.pone.0066118

109. Tobar I, Arancibia S, Torres C, Vera V, Soto P, Carrasco C, et al. Successive Oral Immunizations Against *Piscirickettsia Salmonis* and Infectious Salmon Anemia Virus are Required to Maintain a Long-Term Protection in Farmed Salmonids. *Front Immunol* (2015) 6:244. doi: 10.3389/fimmu.2015.00244
110. Galindo-Villegas J, Mulero I, García-Alcazar A, Muñoz I, Peñalvez-Mellado M, Streitenberger S, et al. Recombinant TNFα as oral vaccine adjuvant protects European sea bass against vibriosis: insights into the role of the CCL25/CCR9 axis. *Fish Shellfish Immunol* (2013) 35(4):1260–71. doi: 10.1016/j.fsi.2013.07.046
111. Amend DF, Fender DC. Uptake of bovine serum albumin by rainbow trout from hypersmotic solutions: a model for vaccinating fish. *Science* (1976) 192:793–4. doi: 10.1126/science.1265480
112. Jaafar RM, Al-Jubury A, Chettri JK, Dalsgaard I, Kania PW, Buchmann K. Secondary immune response of rainbow trout following repeated immersion vaccination. *J Fish Dis* (2018) 41:117–23. doi: 10.1111/jfd.12682
113. Raida MK, Nylén J, Holten-Andersen L, Buchmann K. Association between plasma antibody response and protection in rainbow trout *Oncorhynchus mykiss* immersion vaccinated against *Yersinia ruckeri*. *PLoS One* (2011) 6: e18832. doi: 10.1371/journal.pone.0018832
114. Lorenzen E, Brudeseth BE, Wiklund T, Lorenzen N. Immersion exposure of rainbow trout (*Oncorhynchus mykiss*) fry to wildtype *Flavobacterium psychrophilum* induces no mortality, but protects against later intraperitoneal challenge. *Fish Shellfish Immunol* (2010) 28:440–4. doi: 10.1016/j.fsi.2009.11.025
115. Sheng X, Qian X, Tang X, Xing J, Zhan W. Polymeric immunoglobulin receptor mediates immune excretion of mucosal IgM-antigen complexes across intestinal epithelium in flounder (*Paralichthys olivaceus*). *Front Immunol* (2018) 9:1562. doi: 10.3389/fimmu.2018.01562
116. Huising MO, Guichelaar T, Hoek C, Verburg-van Kemenade BM, Flik G, Savelkoul HF, et al. Increased efficacy of immersion vaccination in fish with hyperosmotic pretreatment. *Vaccine* (2003) 21:4178–93. doi: 10.1016/s0264-410x(03)00497-3
117. Shoemaker CA, Klesius PH, Drennan JD, Evans JJ. Efficacy of a modified live *Flavobacterium columnare* vaccine in fish. *Fish Shellfish Immunol* (2011) 30 (1):304–8. doi: 10.1016/j.fsi.2010.11.001
118. Liu X, Wu H, Chang X, Tang Y, Liu Q, Zhang Y. Notable mucosal immune responses induced in the intestine of zebrafish (*Danio rerio*) bath-vaccinated with a live attenuated *Vibrio anguillarum* vaccine. *Fish Shellfish Immunol* (2014) 40:99–108. doi: 10.1016/j.fsi.2014.06.030
119. Fuglem B, Jirillo E, Bjerkås I, Kiyono H, Nochi T, Yuki Y, et al. Antigen-sampling cells in the salmonid intestinal epithelium. *Dev Comp Immunol* (2010) 34(7):768–74. doi: 10.1016/j.dci.2010.02.007
120. Villumsen KR, Neumann L, Ohtani M, Strøm HK, Raida MK. Oral and anal vaccination confers full protection against enteric redmouth disease (ERM) in rainbow trout. *PLoS One* (2014) 9:e93845. doi: 10.1371/journal.pone.0093845
121. Makesh M, Sudheesh PS, Cain KD. Systemic and mucosal immune response of rainbow trout to immunization with an attenuated *Flavobacterium psychrophilum* vaccine strain by different routes. *Fish Shellfish Immunol* (2015) 44:156–63. doi: 10.1016/j.fsi.2015.02.003
122. Martín-Martín A, Simón R, Abós B, Díaz-Rosales P, Tafalla C. Rainbow trout mount a robust specific immune response upon anal administration of thymus-independent antigens. *Dev Comp Immunol* (2020) 109:103715. doi: 10.1016/j.dci.2020.10371
123. Birkhoff M, Leitz M, Marx D. Advantages of Intranasal Vaccination and Considerations on Device Selection. *Indian J Pharm Sci* (2009) 71:729–31.
124. Yanagita M, Hiroi T, Kitagaki N, Hamada S, Ito HO, Shimauchi H, et al. Nasopharyngeal-associated lymphoreticular tissue (NALT) immunity: fimbriae-specific Th1 and Th2 cell-regulated IgA responses for the inhibition of bacterial attachment to epithelial cells and subsequent inflammatory cytokine production. *J Immunol* (1999) 162:3559–65.
125. LaPatra S, Kao S, Erhardt EB, Salinas I. Evaluation of dual nasal delivery of infectious hematopoietic necrosis virus and enteric red mouth vaccines in rainbow trout (*Oncorhynchus mykiss*). *Vaccine* (2015) 33:771–76. doi: 10.1016/j.vaccine.2014.12.055
126. Salinas I, LaPatra SE, Erhardt EB. Nasal vaccination of young rainbow trout (*Oncorhynchus mykiss*) against infectious hematopoietic necrosis and enteric red mouth disease. *Dev Comp Immunol* (2015) 53:105–11. doi: 10.1016/j.dci.2015.05.015
127. Brandtzaeg P, Pabst R. Let's go mucosal: communication on slippery ground. *Trends Immunol* (2004) 25(11):570–7. doi: 10.1016/j.it.2004.09.005. Erratum in: Trends Immunol. 2005 Jan;26(1):12.

Conflict of Interest: The authors declare that the research was conducted in the absence of any commercial or financial relationships that could be construed as a potential conflict of interest.

Copyright © 2020 Yu, Wang, Huang, Ding and Xu. This is an open-access article distributed under the terms of the Creative Commons Attribution License (CC BY). The use, distribution or reproduction in other forums is permitted, provided the original author(s) and the copyright owner(s) are credited and that the original publication in this journal is cited, in accordance with accepted academic practice. No use, distribution or reproduction is permitted which does not comply with these terms.

frontiers in Immunology

ORIGINAL RESEARCH
published: 06 October 2020
doi: 10.3389/fimmu.2020.559332

Polyunsaturated Fatty Acids Influence LPS-Induced Inflammation of Fish Macrophages Through Differential Modulation of Pathogen Recognition and p38 MAPK/ NF-κB Signaling

Qingfei Li[1], *Kun Cui*[1], *Mengjiao Wu*[1], *Dan Xu*[1], *Kangsen Mai*[1,2] *and Qinghui Ai*[1,2]*

[1] Key Laboratory of Aquaculture Nutrition and Feed (Ministry of Agriculture) & Key Laboratory of Mariculture (Ministry of Education), College of Fisheries, Ocean University of China, Qingdao, China, [2] Laboratory for Marine Fisheries Science and Food Production Processes, Qingdao National Laboratory for Marine Science and Technology, Qingdao, China

OPEN ACCESS

Edited by:
Gyri T. Haugland,
University of Bergen, Norway

Reviewed by:
Chenghua Li,
Ningbo University, China
Mark D. Fast,
University of Prince Edward Island, Canada

***Correspondence:**
Qinghui Ai
qhai@ouc.edu.cn

Specialty section:
This article was submitted to Comparative Immunology, a section of the journal Frontiers in Immunology

Received: 05 May 2020
Accepted: 17 August 2020
Published: 06 October 2020

Citation:
Li Q, Cui K, Wu M, Xu D, Mai K and Ai Q (2020) Polyunsaturated Fatty Acids Influence LPS-Induced Inflammation of Fish Macrophages Through Differential Modulation of Pathogen Recognition and p38 MAPK/NF-κB Signaling. Front. Immunol. 11:559332. doi: 10.3389/fimmu.2020.559332

Polyunsaturated fatty acids (PUFAs) not only serve as essential nutrients but also function as modulators of the immune response in marine fish. However, their immunomodulatory mechanism is poorly understood given that the underlying regulation of the innate immune response in fish has not been fully elucidated. Hence, study of the innate immunity of fish could help elucidate the mechanism by which PUFAs affect the fish immune response. Here, we used combined transcriptome analysis and *in vitro* experimentation to study the mechanism of LPS-induced inflammation. Transcriptome profiling indicated that LPS elicited strong pro-inflammatory responses featuring high expression levels of pathogen recognition receptors (PRRs) and cytokines along with the activation of NF-κB and MAPK signaling pathways. The transcription factor p65 alone could increase the transcription of *IL1β* by binding to the promoter of *IL1β*, and this promoting effect disappeared after mutation or deletion of its binding sites. We then examined the effects of PUFAs on the levels of gene expression and the abundance of proteins of critical kinases associated with LPS-induced inflammation. We found that LA exerts pro-inflammatory response while ALA, EPA, and DHA induced anti-inflammatory effects by modulating the expression of PRRs, phosphorylation of IKK and p38, and the nuclear translocation of p65. Overall, this study advances our understanding of the regulatory mechanisms by which PUFAs regulate LPS-induced inflammation in a non-model fish species.

Keywords: large yellow croaker, LPS, polyunsaturated fatty acids (PUFAs), inflammatory responses, signaling transduction, immunomodulatory effects

INTRODUCTION

Currently, the aquaculture industry is facing global shortfalls in the supply of fish oil. With its relatively considerable output, lower price, and relatively high content of polyunsaturated fatty acids (PUFAs), vegetable oil is a promising alternative to fish oil (rich in ω-3 PUFAs). However, replacing fish oil with vegetable oil in fish diets can result in substantial variation in the dietary composition of fatty acids, altering the immunological responses of fish to infections (1). Because of the potency and economic benefits of PUFAs, study of the immunomodulatory effects of PUFAs has become a major focus of research, and a central goal of this research is to improve the health of fish and their resistance to pathogens. ω-6 PUFAs are widely known to exert pro-inflammatory effects, while ω-3 PUFAs are known to have anti-inflammatory properties through a wide range of mechanisms, including (i) differential modulation of the expression of pathogen recognition receptors (PRRs) (2); (ii) regulation of signaling pathway activities; and (iii) production of lipid mediators that modify the functions of immune cells. Despite an abundance of seemingly robust data, a majority of studies have only demonstrated "associations" but not "cause and effect," and in some cases, results are even "confliction" (3). As a result, the mechanism by which individual fatty acids affect fish inflammation remains unclear.

Generally, elucidating the detailed mechanism governing fish immune responses is important, as the establishing mechanisms lay the molecular foundation for understanding the immunomodulatory roles of PUFAs (4). Recently, advances in genomic research in fish have benefited studies of the molecular mechanisms of fish immunity, as new genomic techniques have been widely applied in fish immune studies (5, 6). Nevertheless, few experimental validations have been made to support the raised working model. An *in vitro* approach is considered a promising tool for exploring the molecular events related to immunity for advantages including its simplification, convenience, and specificity together with exclusion of cell-cell interactions and environmental interference (7). Macrophages are the major immune effector cells in fish and are capable of detecting and responding robustly to various pathogen-associated molecular patterns (PAMPs) to execute protective functions against intruding pathogens (8). Functional immune responses can be recapitulated *in vitro* using macrophages derived from fish, and these results have been validated through observation of a "highly directed response and more generalized state of activation" (9–11). Hence, the combination of transcriptome sequencing and *in vitro* assays should provide sensitive and efficient analyses for exploring how pathogen recognition, signaling transduction, and gene expression are orchestrated during the response of fish to specific stimuli.

Large yellow croaker is an economically important marine fish in China, but its susceptibility and vulnerability to bacterial disease is considered a main constricting factor for its expansion in the aquaculture industry. In aquatic environments, infectious bacteria with the capacity to reproduce independently of their host can cause severe inflammation, increased morbidity, and even mortality (5, 12). Moreover, the ubiquitous replacement of fish oil in the diets of large yellow croaker negatively alters their immune capacity against disease and their resilience to stress (13). In addition, the availability of the draft genome of large yellow croaker permits study of gene function and the molecular mechanisms underlying biological responses. Thus, large yellow croaker could serve as an excellent model for studying the immunity-PUFA interactions in fish. The objective of this present study was to elucidate the mechanism by which the innate immune system of fish responds to bacterial infection. In doing so, this study sheds light on the mechanism underlying PUFAs-mediated inflammation in the macrophages of large yellow croaker. These insights advance our understanding of host-pathogen relationships in fish and contribute to the development of nutritional strategies mediated by PUFAs for treatment against bacterial infections.

MATERIALS AND METHODS

Fish, Macrophage Culture, and Treatments

Large yellow croaker (weight 750 ± 50 g) of the Daiqu strain were purchased from a commercial fish farm in Ningbo, China, and were kept in a flow-through water system at 20–22°C. Macrophages were isolated from fish head kidney and maintained according to a modified procedure described previously (14). Macrophage-rich cells were adjusted to 2.0×10^5 cells/mL and seeded in cell culture plates (Nunc, Denmark). After overnight incubation at 26°C, unattached cells were removed after two vigorous washes, and the resultant macrophage monolayer was primed in DMEM/F12 medium supplemented with 5% FBS (Gibco, USA) for the experiments described below.

Experiment 1: In transcriptome sequencing, macrophages were stimulated by LPS (from *Escherichia coli* O55:B5, Sigma, USA) for 2 h, and cells cultured in DMEM/F12 medium were used as controls. Cells were prepared in triplicate for sequencing. **Experiment 2:** In kinetics of gene expression and protein synthesis associated with LPS-induced innate immune response, macrophages were exposed to LPS stimulation for 1, 3, 6, and 18 h before harvest for RNA or protein extraction. **Experiment 3:** In inhibition assay, macrophages were exposed to 30 min of incubation with 2.5 μM NF-κB inhibitor BAY11-7082 (InvivoGen, USA), 5 μM MEK inhibitor PD98059 (Sigma, USA), p38 MAPK inhibitors SB3580 (Sigma, USA), or JNK inhibitor SP600125 (MCE, USA) prior to 6 h of stimulation with LPS. Cells were then later sampled for RT-PCR analyses. **Experiment 4:** In immunomodulatory effects of PUFAs on the LPS-induced inflammatory response in macrophage, macrophages were incubated with 100 μM PUFAs, namely linoleic acid (LA), linolenic acid (ALA), eicosapentaenoic acid (EPA), and docosahexaenoic acid (DHA), for 12 h before LPS stimulation for 3 h (for western blot analysis) and 6 h (for gene expression). Notably, the final working concentrations of LPS, PUFAs, and inhibitors were determined when significant changes in the expression of representative genes were observed and when cell

viability was not compromised through time and dose-dependent assays.

RNA Extraction, cDNA Library Construction, and Sequencing

TRIzol reagent (Takara, Japan) was used for RNA extractions as per the manufacturer's instructions. RNA integrity and purity were assessed by 1% agarose gel electrophoresis and NanoDrop UV spectrophotometry analysis, respectively. According to the NEBNext Ploy(A) mRNA Magnetic Isolation Module (NEB) protocol provided by Novogene, RNA samples were used to construct RNA-seq libraries followed by quantification with a Qubit 2.0 Fluorometer and Agilent 2100 bio-analyzer. Then libraries were sequenced on an Illumina NovaSeq6000 platform and 150bp pair-end reads were generated.

Differential Gene Expression Analysis

After removing reads containing adaptor sequences, reads with an N, and low-quality reads (> 50% of bases with a quantity score Q-phred ≤ 20), clean reads were subsequently aligned to the genome and mapped to the coding sequences of the large yellow croaker genome using Hisat2 (v2.0.5). The DESeq2 R and edgeR R package were used to perform DEGs analysis, respectively. Gene expression levels were calculated based on the FPKM method (expected number of Fragments Per Kilobase of transcript sequence per Millions base pairs sequenced). Differences between the LPS treatment and the control were assessed by a strict Poisson distribution algorithm. DEGs were defined when the adjusted P-value ≤0.05 determined by DESeq2 and edgeR, and absolute value of $\log_2$ (fold change) ≥ 1.5 were obtained.

Gene Ontology (GO) and Kyoto Encyclopedia of Genes and Genomes (KEGG) Analysis

All DEGs were mapped to the GO database (http://www.geneontology.org) (15). For GO enrichment analysis, all P-values were Bonferroni corrected. A corrected P-value of 0.05 was used as the threshold for determining the significant enrichment of gene sets. The large-scale molecular datasets generated by genome sequencing were processed by the KEGG database (http://www.genome.jp/kegg). We used the clusterProfiler R package to test for the statistical enrichment of DEGs in KEGG pathways.

Quantitative RT-PCR

RT-PCR was performed using a Roche LightCycler® 96 system (USA) and SYBR Premix Ex Taq (Tli RNaseH Plus) (Takara, Japan) as described previously (16). The sequence-specific primer sets were designed based on the coding sequences of identified genes in the large yellow croaker genome (**Supplementary Table 1**). In the current study geNorm algorithm was used to determine the most stable reference genes (17). We found that the most stable genes in the samples determined by geNorm analysis with an acceptable M value < 0.5 were β-actin = 18S rRNA < ubiquitin < GAPDH.Validation of the geNorm reference gene rankings for each sample type was confirmed following the re-analysis of data using BestKeeper software (18). Hence, β-actin was the most stable transcript across all of the samples and was used as the internal control. Each sample was run in triplicate, and the fold change was calculated using the comparative 2-ΔΔCT method (19).

Western Blot Analysis

Cells were harvested by adding RIPA reagent (Solarbio, China) along with supplementation of protease inhibitors (Thermo Fisher Scientific, USA). Nuclear protein was extracted using NE-PER Nuclear and Cytoplasmic Extraction Reagents (Thermo) per the instruction manual. Protein concentration was evaluated by BCA protein assays (Beyotime Biotechnology, China) for adjustments. Western blot experiments were performed as described previously (20). Denatured protein was separated by 10% sodium dodecyl sulfate polyacrylamide gel electrophoresis (SDS-PAGE) and was then transferred to polyvinylidene fluoride membranes (Millipore, USA). After blocking with 5% skimmed milk at room temperature for 2 h, the membrane was incubated with primary antibodies overnight at 4°C. Finally, the membrane was incubated with secondary antibodies for 2 h, which were then visualized by an Electrochemiluminescence kit (Beyotime Biotechnology). Signals generated on the western blot were recorded using a densitometer to scan the film. Image J software (USA) was then used to quantify the generated bands. The rabbit polyclonal antibodies targeting IKKβ (Cell Signaling Technology, Cat# 2678, RRID : AB_2122301) and lamin B1 (Santa Cruz Biotechnology, Cat# sc-374015, RRID : AB_10947408) as well as rabbit p-IKKα/β mAb (Cell Signaling Technology, Cat# 2697, RRID : AB_2079382) were diluted at 1:1000. Rabbit monoclonal antibodies against p65 (Cell Signaling Technology, Cat# 8242, RRID : AB_10859369), p38 (Cell Signaling Technology, Cat# 8690, RRID : AB_10999090), p-p38 (Cell Signaling Technology, Cat# 9215, RRID : AB_331762), JNK (Cell Signaling Technology, Cat# 9252, RRID : AB_2250373), and p-JNK (Cell Signaling Technology, Cat# 4668, RRID : AB_823588) were diluted at 1:2000. Rabbit ERK mAb (Cell Signaling Technology, Cat# 4695, RRID : AB_390779) and p-ERK mAb (Cell Signaling Technology, Cat# 4370, RRID : AB_2315112) were diluted at 1:4000. Mouse anti-GAPDH mAb (ZSGB-Bio, Cat# TA-08, RRID : AB_2747414), secondary antibodies including HRP-labeled goat anti-rabbit IgG polyclonal antibody (ZSGB-Bio, Cat# ZB-2301, RRID : AB_2747412) and HRP-labeled goat anti-mouse IgG polyclonal antibody (Beyotime Biotechnology, #A0216, RRID : AB_2860575) were diluted at 1:5000.

Plasmid Construction and Luciferase Reporter Assays

Specific primers were designed based on large yellow croaker genomic data to construct luciferase reporters and expression plasmids (**Supplementary Table 2**). The primers for truncated promoters were designed to amplify the shortened sequences extending from ATG translation start codon to different sites upstream of IL1β. Primers for the mutant Luc-IL1β promoters

were designed using a site-directed mutagenesis method (Takara, Japan). All generated PCR products were inserted into pGL3-basic plasmid (Promega, USA) as reporter plasmids using the homologous recombination method provided by ClonExpress II One Step Cloning Kit (Vazyme Biotech, China). To construct expression plasmids of transcription factors (TFs), including P50, P65, C-JUN, C-FOS, and STAT4, PCR products were ligated into pcDNA3.1 plasmids (Invitrogen, USA) using the method described above. All plasmids for transfection were prepared using the EasyPure HiPure Plasmid MiniPrep Kit (TransGen Biotech, China) and were verified by sequencing at Sangon Biotech Co., Ltd. (Shanghai, China).

For luciferase assays, reporter plasmids, expression plasmids, and pRT-TK renilla luciferase plasmids were co-transfected into HEK293T cells. After 24 h of transfection, cells were harvested and detected by the Dual-Luciferase Reporter Assay System (TransGen Biotech, China). The firefly and Renilla luciferase activities were read by a SpectraMax i3x multifunctional detection station (Molecular Devices, USA). Transfections were performed in triplicate.

Chromatin Immunoprecipitation Assay

To determine the *in vitro* DNA-binding activity of p65 with IL1β promoter, HEK293T cells were transfected with plasmids containing IL1β promoter and plasmids containing FLAG (as vector control) or p65-Flag followed by 36 h of culture at 37°C. Next, cells were harvested after cross-linking of the target protein and genomic DNA in 1% formaldehyde. Immunoprecipitation of chromatin (ChIP) assay was performed according to the protocol provided by a commercial ChIP kit (Thermo). TheDYKDDDDK Tag (D6W5B) rabbit mAb (Cell Signaling Technology, Cat# 14793, RRID : AB_2572291) was used to immunoprecipitate and isolate the target from other nuclear components, and rabbit mAb IgG (Cell Signaling Technology, Cat# 3900, RRID : AB_1550038) served as the control in this study. The resultant purified chromatin was amplified by PCR for 40 cycles with specific primer pairs for the detection of genomic regions corresponding to the promoter and the control.

Statistical Analysis

All raw data were subjected to one-way ANOVAs followed by Tukey's multiple-range tests, and the results were presented as means ± SEM. The threshold for statistically significant difference between means was $P < 0.05$.

RESULTS

Transcriptome Analysis of LPS-Treated Macrophages

Illumina pair-end sequencing technology generated two transcriptomes for the control group and the LPS-treated group, resulting in a total of 75,241,451 and 69,006,809 clean reads, respectively. Data were then mapped to the L. crocea genome with mapping coverage falling within 85%–86%. Raw sequencing reads data have been deposited in NCBI under the accession number SRX7427103–SRX7427108. Two well-established statistical analysis methods (DESeq2 and edgeR) were applied to identify DEGs. Compared with the control group, a total of 465 DEGs consisting of 415 up-regulated genes and 50 down-regulated genes were identified by DEseq2 method, while 554 up-regulated genes and 84 down-regulated genes totaling 638 DEGs were found by edgeR method in the LPS-treated group (**Supplementary Figure 1**).

GO analysis showed that DEGs were highly enriched into two major functional categories: biological process and molecular function. The biological category was characterized by immune responses and immune system process terms. The molecular function category was abundant in cytokine receptor binding, receptor binding, tumor necrosis factor receptor binding, chemokine activity, and chemokine receptor binding (**Supplementary Figure 1**). KEGG analysis revealed that LPS-stimulated DEGs were associated with the following pathways: C-type lectin receptor signaling pathway, Toll-like receptor signaling pathway, Cytokine-cytokine receptor interaction, RIG-I-like receptor signaling pathway, etc. (**Supplementary Figure 1**).

Annotation of DEGs Associated With the Innate Immune Response

Functional annotation further classified DEGs into three clusters: pattern recognition receptor; adaptors and signal transduction protein; and chemokines, cytokines, and receptors **(Supplementary Table 3**).

Expression Kinetics of Innate Immunity-Related Genes in Response to LPS

Several genes were selected for further analysis based on their functional annotations. Following exposure to LPS, the mRNA expressions of *TLR2*, *TLR5*, and *NOD1* increased significantly up to 18 h relative to the control group (**Figures 1A–C**). Increase in the expression of *TLR13*, CD209, and *peptidoglycan recognition protein 5* (*PGLYRP5*) were sustained up to 6 h, followed by a marked drop at 18 h (**Figures 1D–F**). LPS promoted a significant increase in *myeloid differentiation factor 88* (*MyD88*) expression (**Figure 1G**), but not in *TIR-domain-containing adapter-inducing interferon-β* (*TRIF*) transcription (data not shown). LPS markedly increased the expression of *P65* and *JUN* (**Figures 1H, I**). In addition, LPS significantly up-regulated the expression of *IL1β*, *IL6*, and *CCL2* compared with the control group (**Figures 1J–L**).

Activation of NF-κB and MAPK Signaling Pathways Induced by LPS

BAY11-7082, the NF-κB pathway inhibitor, significantly down-regulated IL1β and IL6 transcription by~ 90% and ~80%, respectively, relative to the LPS positive treatment. ERK inhibitor PD98059 showed no inhibitory effects, whereas SB23580, the p38 inhibitor, was able to reduce LPS-induced expression of *IL1β* and *IL6* substantially. The expression-promoting effects of LPS were partially attenuated by JNK inhibitor SP600125, which had a less pronounced effect than BAY11-7082 and SB23580 in decreasing *IL1β* expression (**Figure 2A**).

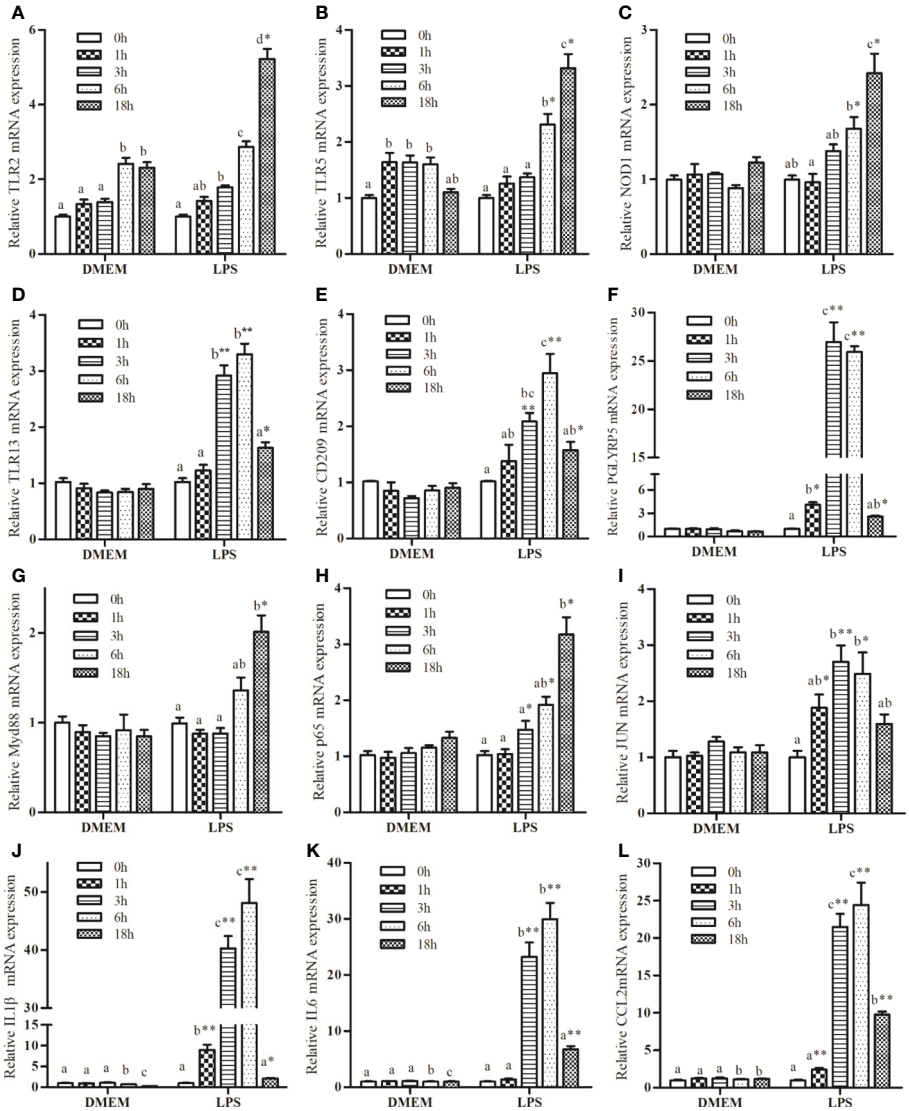

FIGURE 1 | Kinetics expression of *TRL2* **(A)**, *TRL5* **(B)**, *NOD1* **(C)**, *TLR13* **(D)**, *CD209* **(E)**, *PGLYRP5* **(F)**, *MyD88* **(G)**, *P65* **(H)**, *JUN* **(I)**, *IL1β* **(J)**, *IL6* **(K)**, and *CCL2* **(L)** in macrophages of large yellow croaker following 50 μg/mL LPS stimulation. Values are presented as mean ± SEM (n=4). Means with different superscript letters are significantly different ($P < 0.05$, Tukey's test) relative to the 0 h time point within the same treatment. *P <0.05 and **P <0.01 indicate significant difference compared with the control at each time point.

LPS could significantly upregulate the activity of the NF-κB pathway, as levels of phosphorylated-IKK increased 1 h and 3 h post-stimulation and then declined gradually thereafter. Despite this slight increase, no significant differences were noted in either ERK or JNK pathway after LPS stimulation, whereas levels of phosphorylated-p38 protein were significantly increased (**Figure 2B**). Overall, LPS strongly activated NF-κB and MAPK signaling pathways featuring phosphorylation cascades.

p65 Alone Controls Transcription of IL1β by Binding to Its Promoter

IL1β was chosen as the representative effector for the pro-inflammatory response because of its high expression upon LPS stimulation. Dual-luciferase reporter assays showed that p65 alone could significantly activate *IL1β* luciferase activities, which was highlighted by the significant increase (~10 fold) in *IL1β* promoter activity compared with the control group (**Figure 3A**).

To locate the putative binding sites of the critical transcriptional factor p65 in the promoter of *IL1β*, we constructed luciferase plasmids containing truncated sequences and mutated putative binding sites in the promoters according to the computational prediction made by the Jasper (21) and Promo (22) algorithms. Truncated promoter analyses revealed that the binding sites of p65 were located from 494 to 1384 bp upstream from the start codon ATG of *IL1β* (**Figure 3B**). Furthermore, a significant

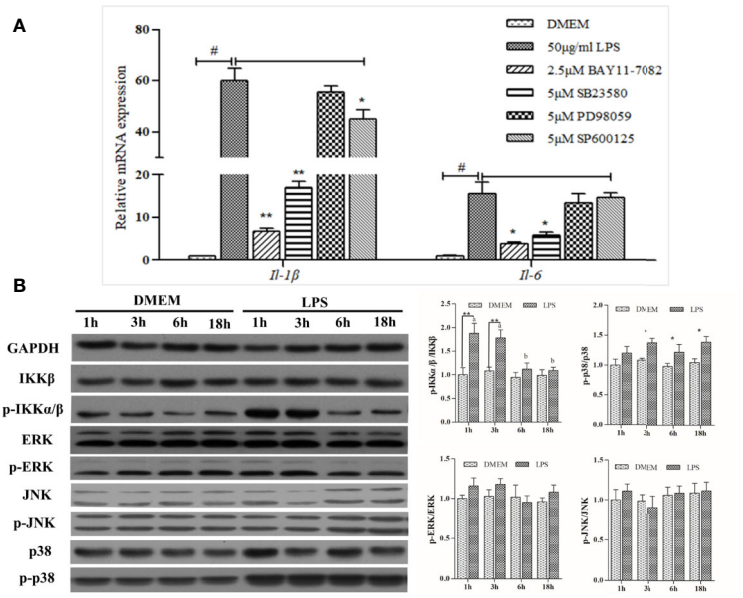

FIGURE 2 | Analysis of NF-κB and MAPK signaling activation. **(A)** Effects of various inhibitors on mRNA expression of LPS-induced inflammation related genes in large yellow croaker head kidney macrophages. Data are expressed as mean ± SEM (n=4). $^{\#}P < 0.05$ indicates significant differences relative to the DMEM group as the negative control; $^{*}P < 0.05$ and $^{**}P < 0.01$ indicate significant differences compared with the LPS treatment as the positive control. **(B)** Western blot analysis of relevant protein expression in the macrophages. Data are expressed as A.U. of the western blots, and signaling activation is depicted as the ratio of phosphorylated protein to total protein. Data are presented as mean ± SEM (n = 3). $^{*}P < 0.05$, $^{**}P < 0.01$ when compared with the control group at each time point. Means with different superscript letters are significantly different ($P < 0.05$, Tukey's test) within the same treatment.

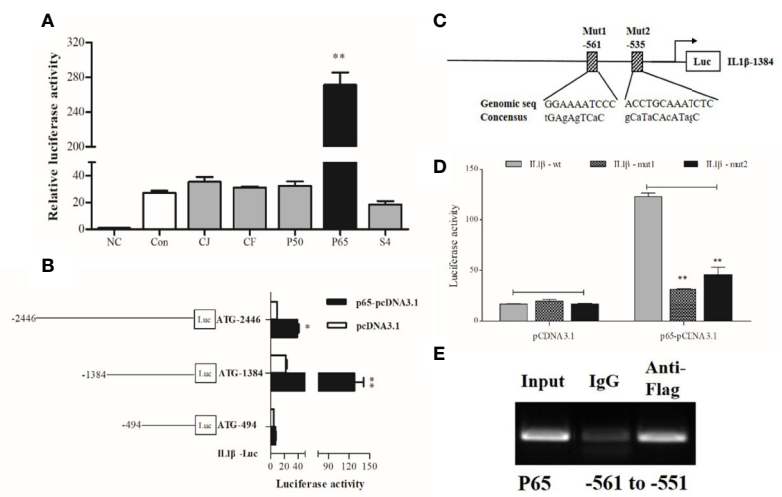

FIGURE 3 | Transcriptional analysis of large yellow croaker IL1β. **(A)** HEK293T cells were co-transfected with *IL1β* promoter construct plasmids, pRL-TK renilla luciferase plasmid, and with expression plasmids of transcription factors, including C-JUN (CJ), C-FOS (CF), P50, P65, STAT4 (S4). The negative control (NC) consisted of empty plasmids (pGL3-basic), and cells transfected with *IL1β* luciferase reporter plasmids were the control (Con). **(B)** A series of truncated promoter plasmids containing various lengths of the promoter regions starting from ATG and **(C)** mutant promoter reporters with specific site-directed mutagenesis in the *IL1β* promoter (ATG-1384) were constructed. **(D)** HEK293 cells were co-transfected with truncated or mutant promoter plasmids and p65-pcDNA3.1 expression plasmids, cells transfected with luciferase reporter and empty vector pcDNA3.1 represented the control. At 36 h post-transfection, luciferase activity was measured. **(E)** ChIP assay identified p65 binding sites in the promoter of *IL1β*. The luciferase activities are normalized to the NC group and presented as means ± SEM (n = 3). $^{*}P < 0.05$; $^{**}P < 0.01$ when compared with the control.

decline in promoter activity was observed after the predicted binding sites were mutated, indicating that the distant p65 binding site (p65 site 1, -561) in the *IL1β* luciferase reporter ATG-1384 was essential for transcriptional activity (**Figures 3C, D**). Next, ChIP assays coupled with PCR data showed that fragments of DNA sequences amplified by specific primers contained the binding site of p65 in the *IL1β* promoter (**Figure 3E**).

Fatty Acids Differentially Regulated LPS-Induced Inflammation through MAPK and NF-κB Pathways in Macrophages

LA had pro-inflammatory effects by increasing LPS-induced expression of pro-inflammatory cytokines, including *IL1β* and *CCL2* (**Figure 4A**). ALA, EPA, and DHA appeared to possess anti-inflammatory functions; DHA exerted the strongest inhibitory effects followed by EPA and ALA. Patterns of expression of cytokines correlated well with those of PRRs genes, namely *TLR2*, *TLR5*, and *PGLYRP5* (**Figure 4B**). Furthermore, western blot analysis indicated that LA treatment increased the abundance of phosphorylated p38 and IKKα/β with concomitant increases in nuclear p65 content. Conversely, ALA, EPA, and DHA had pronounced inhibitory effects, and the inhibitory effect of DHA on the LPS-induced phosphorylation of IKKα/β and the unclear translocation of p65 was stronger than that of EPA and ALA. Specifically, DHA appeared to exert its inhibitory effect on the synthesis of phosphorylated p38 induced by LPS, while ALA and EPA showed no effects of phosphorylated p38 synthesis (**Figures 4C, D**).

DISCUSSION

Bacterial diseases are one of the most important problems in current aquaculture; fish tend to rely more on their innate responses to combat invading bacteria because of their evolutionarily less-well-developed adaptive immune function (23). Innate immunity is the first line of defense against microbial pathogens, and the study of innate immunity to bacteria has focused heavily on the mechanisms by which immune cells deal with LPS, the conserved PAMP of Gram-negative bacteria (24). In mammals, LPS can be well recognized by toll-like receptor 4 (TLR4) (25). Immune signals are then transmitted downstream through MyD88 dependent and TRIF-dependent pathways, which activates a series of key TFs including NF-κB, interferon regulatory factors (IRFs), and mitogen-activated protein kinases (MAPKs), leading to the induction of pro-inflammatory cytokines, chemokines, and antimicrobial responses (20, 26). Fish share similar components of the immune system as mammals and thus possess innate immune responses similar to mammals. However, given that fish occupy a different portion of the evolutionary tree from mammals, accumulating evidence suggests that some detailed mechanisms are specific to fish (23). Unlike mammals, most fish lack TLR4 receptors according to the genomic data; even though TLR4 has been found in some fish, such as zebrafish, the function of LPS recognition is missing because of the absence of the costimulatory molecules MD2 and CD14-like constituents in mammals (27, 28). Overall, fish immunology is less well studied compared with mammals; consequently, the general principles

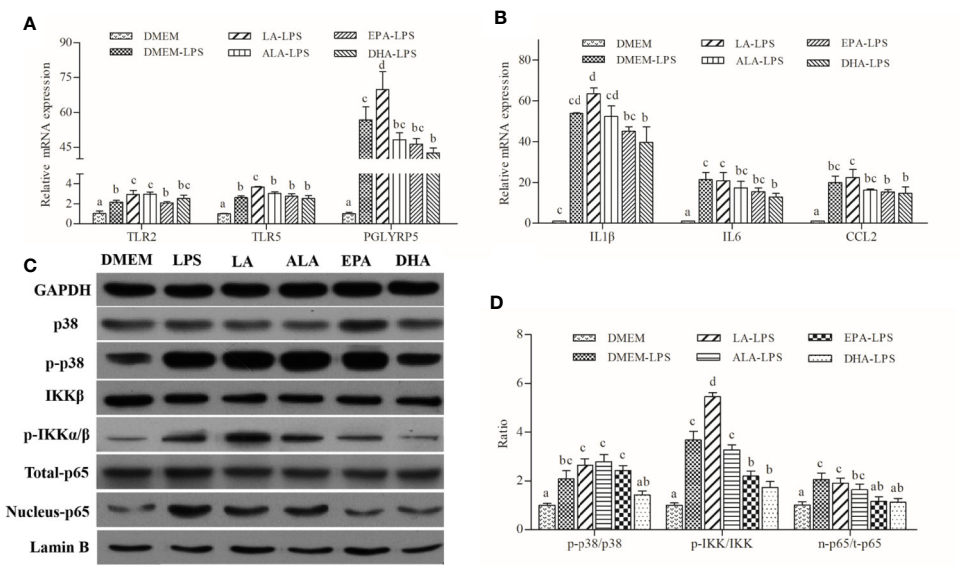

FIGURE 4 | Effects of PUFAs on the innate immune response of large yellow croaker macrophages. **(A, B)** Expression of *TLR2*, *TRL5*, *PGLYRP5*, *IL1β*, *IL6*, and *CCL2* in macrophages of large yellow croaker by LPS (50 μg/mL) stimulation after incubation with PUFAs for 12 h. **(C, D)** The ratios of p-IKKα/β to IKKβ, p-p38 to p38, nucleus p65 to total p65 were determined; GAPDH or Lamin B were used as the total and nucleus reference protein, respectively. Data are expressed as A.U. of the western blots and are depicted as the ratio of target protein to reference protein. All data are presented as mean ± SEM (n= 3). Means with different superscript letters are significantly different ($P < 0.05$, Tukey's test).

underlying signal generation and the mediation of downstream signaling cascades in the immune regulatory network have yet to be fully elucidated.

Cytokines are biologically potent immune molecules secreted by stimulated immune cells that act to protect against pathogens (29). Irrespective of the type of immune cells, cytokine profiles released from activated cells primarily depend on the type of stimulus (30). In the current study, large yellow croaker head kidney macrophages could respond strongly to LPS stimulation, resulting in an increase in the mRNA transcripts of *IL1β*, *IL6*, and *CCL2*. Similar patterns of gene expression have also been described in rainbow trout (*Oncorhynchus mykiss*) (10) and Atlantic cod (*Gadus morhua* L.) (31). The impacts of PUFAs on the inflammation of macrophages have been extensively investigated both *in vitro* and *in vivo*, and these studies have generally shown that LA is the typical n-6 PUFA eliciting pro-inflammatory effects while ALA, EPA, and DHA possess anti-inflammatory properties (13, 32, 33). These findings are consistent with the results of the present study. We found that the reduction in the expression of pro-inflammatory genes in cells pretreated with DHA was more pronounced than that observed in other groups following LPS exposure. This finding is consistent with data obtained from human macrophages (34) and fish hepatocytes by our team (unpublished data).

The initiation of the innate immune response depends on the ability of the host to sense various PAMPs in pathogens through PRRs. Previous *in vivo* studies have suggested that the transcriptional levels of TLRs are increased after flagellin, poly (I:C), peptidoglycan (PGN), and pure LPS challenge in large yellow croaker, and flagellin and peptidoglycan had the strongest ability to stimulate *TLR2* (35). This observation is roughly similar to the present result showing that LPS induced higher levels of *TLR2* and P*GLYRP5* mRNA expression in large yellow croaker head kidney macrophages. One possibility is that the crude LPS used in the present experiment was contaminated with the TLR2 and PGRPs ligands flagellin and PGN from bacteria (5, 10). In addition, a recent study has shown that NOD1 was able to identify LPS (36); thus, the NLRs in teleost were considered partially responsible for LPS recognition. Here, LPS appeared to stimulate the transcription of NLRs, suggesting the role of fish NLRs in interactions with LPS. Given that fatty acids can affect the immune response by altering TLRs in large yellow croaker (20), we examined whether PUFAs could affect inflammation by PRR-mediated pathways. Pretreatment of LPS-induced macrophages with LA induced the expression of *TLR2*, *TLR5*, and *PGLYRP5*, whereas ALA, EPA, and DHA decreased these mRNA transcripts. Accumulating evidence in mammals has revealed that PUFAs can modulate PRR-mediated inflammation through a variety of strategies (37). However, existing literature on teleost PRRs has primarily focused on transcriptional responses to dietary factors, but few studies examined the function of signaling transduction. Further research is needed to fill this gap.

Typically, the transcription of target genes stems from the specific transduction of signaling cascades (38). Teleost NF-κB and MAPK pathways have been shown to govern the transcription of a variety of cytokine genes induced by LPS (25, 39, 40). Our results were consistent with these observations, as a cohort of signal transducers consisting of NF-κB pathways components, mitogen-activated protein kinase kinase kinase 8 (MAP3K8) were activated upon LPS stimulation. We next identified the roles of both pathways in pro-inflammatory responses and found that the inhibition of NF-κB and p38MAPK dampened the expression of *IL1β* and *IL6*. Furthermore, increased levels of phosphorylated IKKα/β and p38 MAPK proteins induced by LPS were also indicative of activation of the NF-κB and MAPK pathways, respectively. LPS did not increase the level of phosphorylated ERK at any of the assayed time, which was comparable to the results obtained on macrophages of salmon (41) and trout (42). Although no significant difference in phosphorylated JNK was detected, the expression of *IL1β* and *IL6* mRNA was suppressed after treatment with the JNK inhibitor SP600125. These observations altogether reinforce the previous conclusion that the p38 module plays an important role in inflammatory responses, that JNK can regulate the transcription of inflammatory genes directly or indirectly, and that ERK activity favors, but is not strictly necessary for, LPS-induced cytokine transcription in fish (42).

Activation of signaling pathways results in the nuclear translocation of central TFs that control gene expression through their direct or indirect interactions with binding sites in the promoters of target genes (43). As the downstream target of the NF-κB pathway, p65 is an important subunit of NF-κB, and the ap1 complex consisting of the TFs C-JUN and C-FOS is the downstream target of MAPK signaling. Here, we focused the regulatory predictions of TFs on the expression of *IL1β*, which was selected to be the representative target gene for its responsiveness (i.e., high levels of expression) to LPS stimulation. In mammals, both p65 and p50 appear to function as positive regulators in the transcriptional expression of *IL1β* (44). However, our study in fish suggested that p65 alone could trigger the transcription of *IL1β*, which was confirmed by a ChIP assay that confirmed the binding of p65 to DNA sequences of *IL1β* promoter. AP1 was reported unlikely to be effective because of the absence of its binding sites within *IL1β* promoter regions; nevertheless, AP1 might contribute by interacting with other TFs (45). This is supported by the present observation that the AP1 complex failed to affect the promoter activity of *IL1β*. Thus, the transcription of *IL1β* in fish might be a consequence of the synergistic actions of NF-κB and p38MAPK signaling combined with the nuclear translocation of p65.

Fatty acids appear to partially affect the inflammatory response *via* their capacities to modulate the activities of pivotal signaling pathways and the nuclear translocation of certain TFs (46). Pretreatment of ALA, EPA, and DHA had a promoting effect on the LPS-induced phosphorylation of IKKα/β and the impaired nuclear translocation of p65, whereas pretreatment of cells with LA had an opposite effect. Notably, DHA was the only PUFA that could also suppress the phosphorylation of p38, which might reflect the fact that it possessed the strongest anti-inflammatory properties among the PUFAs tested in this study. This finding is consistent with

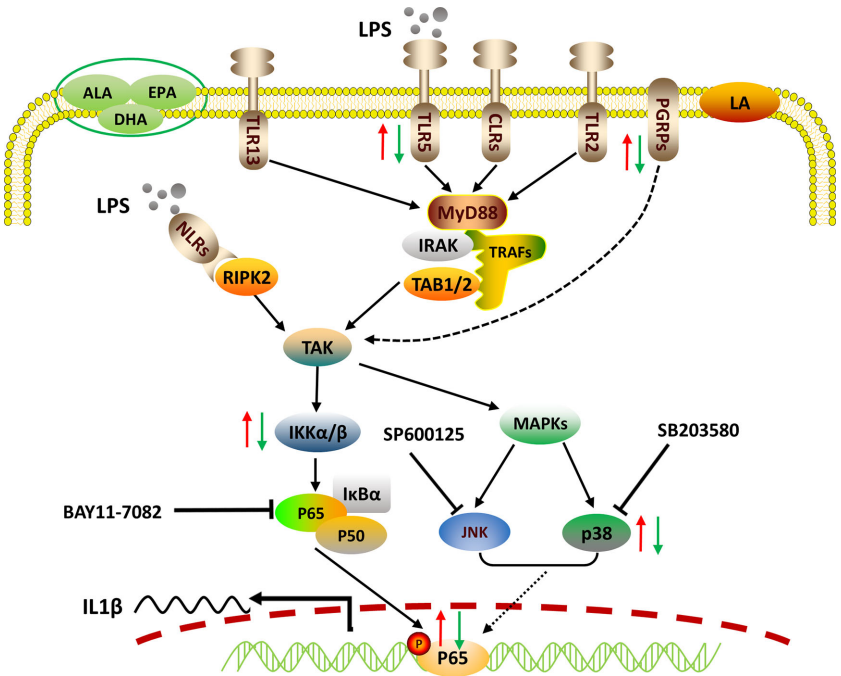

FIGURE 5 | Proposed working model of how PUFAs regulate mRNA expression of the representative pro-inflammatory gene *IL1β*. Crude LPS is recognized by specific PRRs, including TLRs, NLRs, and PGRPs of fish macrophages. Triggered immune signals are transmitted downstream to activate NF-κB and MAPK pathways, leading to the nuclear translocation of p65, which controls the transcription of *IL1β* by binding to its promoter. PUFAs can differentially regulate the LPS-induced pro-inflammatory responses *via* pathogen recognition, signaling activation, and pro-inflammatory gene expression. The red arrows indicate the enhancing effects by LA and the green arrows show the suppressing effects exerted by ALA, EPA, and DHA.

our previous study on the hepatocytes of large yellow croaker (unpublished data). However, the more specific mechanism underlying the immunomodulatory effects of fatty acids remains unclear. Numerous mammal studies have shown that PUFAs can affect the expression of inflammatory genes in a variety of manners, including post-transcriptional (47) and post-translational modifications (48), protein-to-protein interactions (49), macrophage polarization (20), and the production of lipid mediators (50). The immunology of fish has been traditionally less well understood compared with the immunology of mammals because there have been fewer studies conducted in fish. Therefore, these areas will likely be the focus of future research.

In sum, we reported the LPS-stimulated transcriptome of large yellow croaker using an *in vitro* macrophage model. LPS induced the transcription of pro-inflammatory cytokines through pathogen recognition and activation of MAPK and NF-κB signaling pathways. We also confirmed that p65 alone could up-regulate the transcription of *IL1β* by targeting the specific response elements within its promoter. Grounded in those findings, PUFAs were found to differentially regulate the gene expression of PRRs, the activities of MAPK and NF-κB signaling, as well as the nuclear translocation of p65, thereby exerting differential immunomodulatory effects (**Figure 5**). Our findings advance our understanding of fish innate immunity against bacterial infections and contribute to the development of nutritional strategies for improving the health of cultured fish.

DATA AVAILABILITY STATEMENT

The datasets presented in this study can be found in online repositories. The names of the repository/repositories and accession number(s) can be found in the article/**Supplementary Material**.

ETHICS STATEMENT

The animal study was reviewed and approved by Institutional Animal Care and Use Committee of Ocean University of China.

AUTHOR CONTRIBUTIONS

QA and QL designed the experiment. QL and KC conducted the research. QL, MW, and DX analyzed the data. QL wrote the manuscript. KM and QA revised the article. All authors contributed to the article and approved the submitted version.

FUNDING

This research was supported by the National Science Fund for Distinguished Young Scholars of China (Grant NO. 31525024), Key Program of National Natural Science Foundation of China

(Grant NO. 31830103), Ten-thousand Talents Program (Grant NO. 2018-29), and the Agriculture Research System of China (Grant NO. CARS-47-11).

ACKNOWLEDGMENTS

We thank Jikang Shentu and Lin Huang for providing experimental animals and facilities. We also appreciate Xiang Xu for his assistance in gene clone and plasmid preparation. Great thanks are due to Yongnan Li for his assistance in ChIP experimentation.

SUPPLEMENTARY MATERIAL

The Supplementary Material for this article can be found online at: https://www.frontiersin.org/articles/10.3389/fimmu.2020.559332/full#supplementary-material

REFERENCES

1. Eslamloo K, Xue X, Hall JR, Smith NC, Caballero-Solares A, Parrish CC, et al. Transcriptome profiling of antiviral immune and dietary fatty acid dependent responses of Atlantic salmon macrophage-like cells. *BMC Genomics* (2017) 18 (1):706. doi: 10.1186/s12864-017-4099-2
2. Zuo R, Ai Q, Mai K, Xu W, Wang J, Xu H, et al. Effects of dietary docosahexaenoic to eicosapentaenoic acid ratio (DHA/EPA) on growth, nonspecific immunity, expression of some immune related genes and disease resistance of large yellow croaker (*Larmichthys crocea*) following natural infestation of parasites (*Cryptocaryon irritans*). *Aquaculture* (2012) 334–337:101–9. doi: 10.1016/j.fsi.2011.11.005
3. Tocher DR. Omega-3 long-chain polyunsaturated fatty acids and aquaculture in perspective. *Aquaculture* (2015) 449:94–107. doi: 10.1016/j.aquaculture.2015.01.010
4. Pohlenz C, Gatlin DM. Interrelationships between fish nutrition and health. *Aquaculture* (2014) 431:111–7. doi: 10.1016/j.aquaculture.2014.02.008
5. Zhang X, Mu Y, Mu P, Ao J, Chen X. Transcriptome Analysis Reveals Comprehensive Insights into the Early Immune Response of Large Yellow Croaker (*Larimichthys crocea*) Induced by Trivalent Bacterial Vaccine. *PLoS One* (2017) 12(1):e0170958. doi: 10.1371/journal.pone.0170958
6. Mu Y, Li M, Ding F, Ding Y, Ao J, Hu S, et al. De novo characterization of the spleen transcriptome of the large yellow croaker (*Pseudosciaena crocea*) and analysis of the immune relevant genes and pathways involved in the antiviral response. *PLoS One* (2014) 9(5):e97471. doi: 10.1371/journal.pone.0097471
7. Li Q, Ai Q, Mai K, Xu W, Zheng Y. A comparative study: In vitro effects of EPA and DHA on immune functions of head-kidney macrophages isolated from large yellow croaker (*Larmichthys crocea*). *Fish Shellfish Immunol* (2013) 35(3):933–40. doi: 10.1016/j.fsi.2013.07.004
8. Magnadottir B. Innate immunity of fish (overview). *Fish Shellfish Immunol* (2006) 20(2):137–51. doi: 10.1016/j.fsi.2004.09.006
9. MacKenzie S, Iliev D, Liarte C, Koskinen H, Planas JV, Goetz FW, et al. Transcriptional analysis of LPS-stimulated activation of trout (*Oncorhynchus mykiss*) monocyte/macrophage cells in primary culture treated with cortisol. *Mol Immunol* (2006) 43(9):1340–8. doi: 10.1016/j.molimm.2005.09.005
10. MacKenzie SA, Roher N, Boltaña S, Goetz FW. Peptidoglycan, not endotoxin, is the key mediator of cytokine gene expression induced in rainbow trout macrophages by crude LPS. *Mol Immunol* (2010) 47(7):1450–7. doi: 10.1016/j.molimm.2010.02.009
11. Pijanowski L, Scheer MH, Kemenade BMLV, Chadzinska M. Production of inflammatory mediators and extracellular traps by carp macrophages and neutrophils in response to lipopolysaccharide and/or interferon-γ2. *Fish Shellfish Immunol* (2015) 42(2):473–82. doi: 10.1016/j.fsi.2014.11.019
12. Ben Hamed S, Tavares Ranzani-Paiva MJ, Tachibana L, de Carla Dias D, Ishikawa CM, Esteban MA. Fish pathogen bacteria: Adhesion, parameters influencing virulence and interaction with host cells. *Fish Shellfish Immunol* (2018) 80:550–62. doi: 10.1016/j.fsi.2018.06.053
13. Mu H, Shen H, Liu J, Xie F, Zhang W, Mai K. High level of dietary soybean oil depresses the growth and anti-oxidative capacity and induces inflammatory response in large yellow croaker *Larimichthys crocea*. *Fish Shellfish Immunol* (2018) 77:465–73. doi: 10.1016/j.fsi.2018.04.017
14. Li Q, Ai Q, Mai K, Xu W, Zheng Y. In vitro effects of arachidonic acid on immune functions of head kidney macrophages isolated from large yellow croaker (*Larmichthys crocea*). *Aquaculture* (2012) 330–333:47–53. doi: 10.1016/j.aquaculture.2011.11.045
15. Mortazavi A, Williams BA, McCue K, Schaeffer L, Wold B. Mapping and quantifying mammalian transcriptomes by RNA-Seq. *Nat Methods* (2008) 5 (7):621–8. doi: 10.1038/nmeth.1226
16. Zhu S, Xiang X, Xu X, Gao S, Mai K, Ai Q. TIR Domain-Containing Adaptor-Inducing Interferon-β (TRIF) Participates in Antiviral Immune Responses and Hepatic Lipogenesis of Large Yellow Croaker (*Larimichthys Crocea*). *Front Immunol* (2019) 10:2506. doi: 10.3389/fimmu.2019.02506
17. Vandesompele J, De Preter K, Pattyn F, Poppe B, Van Roy N, Paepe De, et al. Accurate normalization of real-time quantitative RT-PCR data by geometric averaging of multiple internal control genes. *Genome Biol* (2002) 3: research0034–research0034.11. doi: 10.1186/gb-2002-3-7-research0034
18. Pfaffl MW, Tichopad A, Prgomet C, Neuvians TP. Determination of stable housekeeping genes, differentially regulated target genes and sample integrity: BestKeeper—Excel-based tool using pair-wise correlations. *Biotechnol Lett* (2004) 26:509–15. doi: 10.1023/b:bile.0000019559.84305.47
19. Livak KJ, Schmittgen TD. Analysis of relative gene expression data using real-time quantitative PCR and the 2(-Delta Delta C(T)) Method. *Methods* (2001) 25(4):402–8. doi: 10.1006/meth.2001.1262
20. Tan P, Dong X, Mai K, Xu W, Ai Q. Vegetable oil induced inflammatory response by altering TLR-NF-κB signalling, macrophages infiltration and polarization in adipose tissue of large yellow croaker (*Larimichthys crocea*). *Fish Shellfish Immunol* (2016) 59:398–405. doi: 10.1016/j.fsi.2016.11.009
21. Khan A, Fornes O, Stigliani A, Gheorghe M, Castro-Mondragon JA, van der Lee R, et al. JASPAR 2018: update of the open-access database of transcription factor binding profiles and its web framework. *Nucleic Acids Res* (2018) 46:260–6. doi: 10.1093/nar/gkx1126
22. Messeguer X, Escudero R, Farre D, Nunez O, Martinez J, Alba MM. PROMO: detection of known transcription regulatory elements using species-tailored searches. *Bioinf (Oxford England)erinarni* (2002) 18(2):333–4. doi: 10.1093/bioinformatics/18.2.333
23. Uribe C, Folch H, Enríquez R, Moran G. Innate and adaptive immunity in teleost fish: a review. *Vet Med* (2011) 56(10):486–503. doi: 10.17221/3294-VETMED
24. Li Y, Xu X, Zhao D, Pan L, Huang C, Guo L, et al. TLR3 ligand Poly I:C attenuates reactive astrogliosis and improves recovery of rRats after focal cerebral ischemia. *CNS Neurosci Ther* (2015) 21(11):905–13. doi: 10.1111/cns.12469
25. Freudenberg MA, Tchaptchet S, Keck S, Fejer G, Huber M, Schütze N, et al. Lipopolysaccharide sensing an important factor in the innate immune response to Gram-negative bacterial infections: Benefits and hazards of LPS hypersensitivity. *Immunobiology* (2008) 213(3):193–203. doi: 10.1016/j.imbio.2007.11.008
26. Wang T, Yan J, Xu W, Ai Q, Mai K. Characterization of Cyclooxygenase-2 and its induction pathways in response to high lipid diet-induced inflammation in *Larmichthys crocea*. *Sci Rep* (2016) 6(1):19921. doi: 10.1038/srep19921
27. Matsuo A, Oshiumi H, Tsujita T, Mitani H, Kasai H, Yoshimizu M, et al. Teleost TLR22 recognizes RNA duplex to induce IFN and protect cells from birnaviruses. *J Immunol (Baltimore Md 1950)* (2008) 181(5):3474–85. doi: 10.4049/jimmunol.181.5.3474
28. Kasamatsu J, Oshiumi H, Matsumoto M, Kasahara M, Seya T. Phylogenetic and expression analysis of lamprey toll-like receptors. *Dev Comp Immunol* (2010) 34(8):855–65. doi: 10.1016/j.dci.2010.03.004

29. Salazar-Mather T, Hokeness K. Cytokine and chemokine networks: pathways to antiviral defense. *Curr Top Microbiol Immunol* (2006) 303:29–46. doi: 10.1007/978-3-540-33397-5_2
30. Muñoz-Carrillo JL, Cordero JFC, Gutiérrez-Coronado O, Villalobos-Gutiérrez PT, Ramos-Gracia LG, Hernández-Reyes VE. Cytokine profiling plays a crucial role in activating immune system to clear infectious pathogens. In: *Immune Response Activation and Immunomodulation*. London, UK: IntechOpen (2018). doi: 10.5772/intechopen.80843
31. Seppola M, Larsen AN, Steiro K, Robertsen B, Jensen I. Characterisation and expression analysis of the interleukin genes, IL-1beta, IL-8 and IL-10, in Atlantic cod (*Gadus morhua* L.). *Mol Immunol* (2008) 45(4):887–97. doi: 10.1016/j.molimm.2007.08.003
32. Wang T, Yang B, Ji R, Xu W, Mai K, Ai Q. Omega-3 polyunsaturated fatty acids alleviate hepatic steatosis-induced inflammation through Sirt1-mediated nuclear translocation of NF-κB p65 subunit in hepatocytes of large yellow croaker (*Larmichthys crocea*). *Fish Shellfish Immunol* (2017) 71:76–82. doi: 10.1016/j.fsi.2017.09.064
33. Zuo R, Mai K, Xu W, Turchini GM, Ai Q. Dietary ALA, but not LNA, increase growth, reduce inflammatory processes, and increase anti–oxidant capacity in the marine finfish *Larimichthys crocea*. *Lipids* (2015) 50(2):149–63. doi: 10.1007/s11745-014-3970-z
34. Allam-Ndoul B, Guénard F, Barbier O, Vohl MC. Effect of different concentrations of omega-3 fatty acids on stimulated THP-1 macrophages. *Genes Nutr* (2017) 12:7. doi: 10.1186/s12263-017-0554-6
35. Fan ZJ, Jia QJ, Yao CL. Characterization and expression analysis of Toll-like receptor 2 gene in large yellow croaker, *Larimichthys crocea*. *Fish Shellfish Immunol* (2015) 44(1):129–37. doi: 10.1016/j.fsi.2015.01.037
36. Bi D, Wang Y, Gao Y, Li X, Chu Q, Cui J, et al. Recognition of lipopolysaccharide and activation of NF-kappaB by cytosolic sensor NOD1 in teleost fish. *Front Immunol* (2018) 9:1413. doi: 10.3389/fimmu.2018.01413
37. Lee JY, Zhao L, Hwang DH. Modulation of pattern recognition receptor-mediated inflammation and risk of chronic diseases by dietary fatty acids. *Nutr Rev* (2010) 68(1):38–61. doi: 10.1111/j.1753-4887.2009.00259.x
38. Kawasaki T, Kawai T. Toll-Like Receptor Signaling Pathways. *Front Immunol* (2014) 5:461. doi: 10.3389/fimmu.2014.00461
39. Romo MR, Perezmartinez D, Ferrer CC. Innate immunity in vertebrates: an overview. *Immunology* (2016) 148(2):125–39. doi: 10.1111/imm.12597
40. Saeij JP, de Vries BJ, Wiegertjes GF. The immune response of carp to trypanoplasma borreli: kinetics of immune gene expression and polyclonal lymphocyte activation. *Dev Comp Immunol* (2003) 27(10):859–74. doi: 10.1016/s0145-305x(03)00083-1
41. Iliev DB, Hansen T, Jørgensen SM, Krasnov A, Jørgensen JB. CpG- and LPS-activated MAPK signaling in in vitro cultured salmon (*Salmo salar*) mononuclear phagocytes. *Fish Shellfish Immunol* (2013) 35(4):1079–85. doi: 10.1016/j.fsi.2013.07.014
42. Roher N, Callol A, Planas JV, Goetz FW, MacKenzie SA. Endotoxin recognition in fish results in inflammatory cytokine secretion not gene expression. *Innate Immun* (2011) 17(1):16–28. doi: 10.1177/1753425909348232
43. Heisig J, Weber D, Englberger E, Winkler A, Kneitz S, Sung W-K, et al. Target gene analysis by microarrays and chromatin immunoprecipitation identifies HEY proteins as highly redundant bHLH repressors. *PLoS Genet* (2012) 8(5): e1002728. doi: 10.1371/journal.pgen.1002728
44. Hiscott J, Marois J, Garoufalis J, D'Addario M, Roulston A, Kwan I, et al. Characterization of a functional NF-kappa B site in the human interleukin 1 beta promoter: evidence for a positive autoregulatory loop. *Mol Cell Bio* (1993) 13(10):6231–40. doi: 10.1128/mcb.13.10.6231
45. Fontana MF, Baccarella A, Pancholi N, Pufall MA, Herbert DBR, Kim CC. JUNB Is a key transcriptional modulator of macrophage activation. *J Immunol* (2015) 194(1):177. doi: 10.4049/jimmunol.1401595
46. Zhao Y, Chen LH. Eicosapentaenoic acid prevents lipopolysaccharide-stimulated DNA binding of activator protein-1 and c-Jun N-terminal kinase activity. *J Nutr Biochem* (2005) 16(2):78–84. doi: 10.1016/j.jnutbio.2004.09.003
47. Roessler C, Kuhlmann K, Hellwing C, Leimert A, Schumann J. Impact of Polyunsaturated Fatty Acids on miRNA Profiles of Monocytes/Macrophages and Endothelial Cells-A Pilot Study. *Int J Mol Sci* (2017) 18(2):284. doi: 10.3390/ijms18020284
48. Raphael W, Sordillo LM. Dietary polyunsaturated fatty acids and inflammation: the role of phospholipid biosynthesis. *Int J Mol Sci* (2013) 14 (10):21167–88. doi: 10.3390/ijms141021167
49. Xue B, Yang Z, Wang X, Shi H. Omega-3 polyunsaturated fatty acids antagonize macrophage inflammation via activation of AMPK/SIRT1 pathway. *PLoS One* (2012) 7(10):e45990. doi: 10.1371/journal.pone.0045990
50. Norris PC, Dennis EA. Omega-3 fatty acids cause dramatic changes in TLR4 and purinergic eicosanoid signaling. *Pro Natl Acad Sci* (2012) 109(22):8517–22. doi: 10.1073/pnas.1200189109

Conflict of Interest: The authors declare that the research was conducted in the absence of any commercial or financial relationships that could be construed as a potential conflict of interest.

Copyright © 2020 Li, Cui, Wu, Xu, Mai and Ai. This is an open-access article distributed under the terms of the Creative Commons Attribution License (CC BY). The use, distribution or reproduction in other forums is permitted, provided the original author(s) and the copyright owner(s) are credited and that the original publication in this journal is cited, in accordance with accepted academic practice. No use, distribution or reproduction is permitted which does not comply with these terms.

frontiers in Immunology

ORIGINAL RESEARCH
published: 08 October 2020
doi: 10.3389/fimmu.2020.581070

Plasma Proteome Responses in Salmonid Fish Following Immunization

Fiona K. Bakke[1], Milena M. Monte[1], David A. Stead[2], Dwight R. Causey[1], Alex Douglas[1], Daniel J. Macqueen[3†] and Helen Dooley[4*†]*

[1] School of Biological Sciences, University of Aberdeen, Aberdeen, United Kingdom, [2] Aberdeen Proteomics, The Rowett Institute, University of Aberdeen, Aberdeen, United Kingdom, [3] The Roslin Institute and Royal (Dick) School of Veterinary Studies, University of Edinburgh, Edinburgh, United Kingdom, [4] Department of Microbiology and Immunology, Institute of Marine and Environmental Technology (IMET), University of Maryland School of Medicine, Baltimore, MD, United States

Vaccination plays a critical role in the protection of humans and other animals from infectious diseases. However, the same vaccine often confers different protection levels among individuals due to variation in genetics and/or immunological histories. While this represents a well-recognized issue in humans, it has received little attention in fish. Here we address this knowledge gap in a proteomic study of rainbow trout (*Oncorhynchus mykiss*, Walbaum), using non-lethal repeated blood sampling to establish the plasma protein response of individual fish following immunization. Six trout were immunized with adjuvanted hen egg-white lysozyme (HEL) and peripheral blood sampled at ten time points from day 0 to day 84 post-injection. We confirm that an antigen-specific antibody response to HEL was raised, showing differences in timing and magnitude among individuals. Using label-free liquid chromatography-mass spectrometry, we quantified the abundance of 278 plasma proteins across the timecourse. As part of the analysis, we show that this approach can distinguish many (but not all) duplicated plasma proteins encoded by paralogous genes retained from the salmonid-specific whole genome duplication event. Global variation in the plasma proteome was predominantly explained by individual differences among fish. However, sampling day explained a major component of variation in abundance for a statistically defined subset of 41 proteins, representing 15% of those detected. These proteins clustered into five groups showing distinct temporal responses to HEL immunization at the population level, and include classical immune (e.g. complement system members) and acute phase molecules (e.g. apolipoproteins, haptoglobins), several enzymes and other proteins supporting the immune response, in addition to evolutionarily conserved molecules that are as yet uncharacterized. Overall, this study improves our understanding of the fish plasma proteome, provides valuable marker proteins for different phases of the immune response, and has implications for vaccine development and the design of immune challenge experiments.

Keywords: plasma, salmonid, immunity, proteome, liquid chromatography-mass spectrometry, trout, immunoglobulin M

OPEN ACCESS

Edited by:
Monica Hongroe Solbakken, University of Oslo, Norway

Reviewed by:
Kim Dawn Thompson, Moredun Research Institute, United Kingdom
Bo Peng, Sun Yat-sen University, China

***Correspondence:**
Daniel J. Macqueen
daniel.macqueen@roslin.ed.ac.uk
Helen Dooley
hdooley@som.umaryland.edu

†These authors have contributed equally to this work

Specialty section:
This article was submitted to Comparative Immunology, a section of the journal Frontiers in Immunology

Received: *07 July 2020*
Accepted: *21 September 2020*
Published: *08 October 2020*

Citation:
Bakke FK, Monte MM, Stead DA, Causey DR, Douglas A, Macqueen DJ and Dooley H (2020) Plasma Proteome Responses in Salmonid Fish Following Immunization. Front. Immunol. 11:581070. doi: 10.3389/fimmu.2020.581070

INTRODUCTION

Vaccination plays a critical role in protecting humans and other animals from infectious diseases (e.g. (1–4)). While a perfect vaccine will impart full protection to every member of a targeted population, in reality this is limited by the inherent variability among individuals, including genetics and distinct environmental and/or immunological histories. Indeed, it is well recognized that humans show high variability in immune phenotypic parameters (e.g. serum protein levels) and responses (e.g. cytokine induction), which can largely be explained by non-heritable environmental influences (5, 6). However, the extent of individual-level variation in the immune response remains poorly defined in most species. This includes fishes used in aquaculture, an industry that plays a crucial role in global food provision and economic security, yet remains threatened by infectious disease outbreaks (e.g. (7)).

Vaccination is applied broadly in aquaculture (4), and there remains a need to develop new and improved vaccines for many species and diseases, along with less labor-intensive modes of administration (3). An important part of the development pipeline is vaccine efficacy testing, which can be assessed directly *via* the extent of protection (e.g. using disease challenge tests), or indirectly, by studying changes in immune parameters, for example by confirming an antigen-specific antibody response (8, 9) or recording changes in the expression of immune molecules (e.g. (10, 11)). Such work usually relies on the terminal sampling of tissues from large numbers of fish, at different time points, to adequately capture the response dynamic. However, underlying such studies is the assumption that individuals in a population will show similar immune responses (12). A step towards testing this assumption in salmonid species was the development of methods for repeated non-lethal sampling of blood from the same fish (12, 13). This approach can help elucidate immunological variation between individuals, either in their constitutive state or following immunization/disease challenge.

The current study tests the hypothesis that rainbow trout, a commercially important salmonid fish, shows a high degree of individual variation in response to immunization. By combining non-lethal blood sampling with high-throughput proteomics, we sought to document global changes in plasma protein abundance in individual fish following a common immunization protocol. The plasma proteome provides a strong index of biological status (14), including in fish (e.g. (15, 16)), and can be analysed using liquid chromatography-mass spectrometry (LC-MS) using small blood samples (e.g. (17)). Recent work has applied such approaches in salmonids (18), including to document changes in plasma protein abundance during sea water adaptation in rainbow trout (19). Such approaches require a comprehensive protein database for the target species and enable simultaneous identification and quantification of hundreds to thousands of proteins per experiment (20–23).

Our study design involved the immunization of a small cohort of rainbow trout with adjuvanted hen egg-white lysozyme (HEL) followed by sequential blood sampling of every individual at ten points across a 12-week timecourse. After verifying an antigen-specific antibody response was generated by each individual, high-throughput LC-MS proteomics was used to monitor changes in plasma protein abundance in the same animals. Our analyses revealed the extent of individual versus population-wide responses to the same immunization protocol, as well as providing a detailed characterization of a salmonid plasma proteome.

MATERIALS AND METHODS

Immunization Protocol and Plasma Sampling

All procedures were conducted following the UK Home Office 'Animals and Scientific Procedures Act 1986; Amendment Regulations 2012' on animal care and use, with prior ethical approval from the University of Aberdeen's Animal Welfare and Ethical Review Body (AWERB). Rainbow trout (245.6 ± 0.64 g; 27.6 ± 0.19 cm; mixed sex) were purchased from Almondbank Hatchery, Perthshire. The size of fish was chosen to ensure we could collect enough plasma per animal to perform technical optimization and data acquisition without exceeding 10% blood volume taken from any individual per month (13). The fish were maintained in 1-metre diameter tanks containing continuously circulating fresh water at 14±1°C in the aquarium facility of the School of Biological Sciences, University of Aberdeen, and were fed twice daily with standard commercial pellets (EWOS, Scotland). Fish were sedated with 2-phenoxyethanol (Sigma Aldrich) prior to any experimental procedure and daily monitoring undertaken for the duration of the experiment. Following PIT tagging fish were allowed 1 week to recover prior to immunization. Six fish were immunized intraperitoneally (IP) with hen egg-white lysozyme (HEL) emulsified in an equal volume of Complete Freund's Adjuvant (CFA), and one control fish was immunized with CFA only. HEL is a model antigen that has been used for immunization studies in several other vertebrate species (e.g. (24–26)). We can be certain that our study animals have no prior exposure to this antigen and know from other species the response to HEL is T-dependent and therefore a good proxy for the response we would wish to raise when developing an effective vaccine. Blood samples were drawn on days 0, 7, 14, 21, 28, 35, 42, 56, 70, and 84 post-immunization into syringes containing 100µl porcine heparin reconstituted to 1,000 U/ml in PBS. Plasma was aliquoted into low protein binding tubes, flash frozen, and stored at -80°C prior to analysis.

Measurement of Antigen-Specific IgM

ELISA plates were coated for 48 h at 4°C with 100 µl/well of HEL diluted in 0.05 M carbonate-bicarbonate (pH 9.6) buffer to 10 µg/ml. Wells were emptied, washed once with 200 µl PBS containing 0.05% Tween20 (PBST), and blocked with 200 µl 3% fat-free milk solution (MPBS) for 3 h at room temperature. Plasma samples were pre-diluted 1/10 in PBS then three-fold dilutions performed so that titration curves could be obtained for each sample. Wells were washed with PBST x3, plasma samples

added at 100 µl/well then incubated overnight at 4°C. Wells were washed three times with PBST then 4C10 anti-salmonid IgM monoclonal supernatant (27), diluted 1:1 in PBS, was added at 100 µl/well and the plates incubated overnight at 4°C. After three washes with PBST, anti-mouse HRP-conjugated antibody (Sigma Aldrich), diluted 1:1000 in MPBS, was added at 100 µl/well and incubated for 2 h at room temperature. Following three further washes with PBST, binding was detected by the addition of 100 µl/well TMB solution; the reaction was stopped by the addition of 50 µl/well 1M H_2SO_4, and the plate read at 450 nm. Data were normalized across the plates, and titration curves plotted for each timepoint for each animal. To illustrate the data more easily we picked a dilution where signal was subsaturated for all samples, in this case the 1/270 dilution, and used this to plot absorbance at 450nm against time (as shown in **Figure 1**). Plasma from our CFA-only immunized animal was used as the negative control. The following technical controls were also performed; plasma samples on an irrelevant target (i.e. ELISA wells both coated and blocked with MPBS), PBS in place of plasma, and monoclonal antibodies raised against irrelevant targets in place of the 4C10 monoclonal.

LC-MS Analysis

Plasma samples were prepared for proteomic analysis at Aberdeen Proteomics (University of Aberdeen) for the same n=6 trout individuals assayed by ELISA (as above). 1 µl of plasma was diluted with 99 µl 50mM ammonium bicarbonate and proteins were reduced in 2mM dithiothreitol for 25 min at 60°C, S-alkylated in 4mM iodoacetamide for 30 min at 25°C in the dark, digested with porcine trypsin (sequencing grade, Promega) overnight at 37°C, then freeze-dried. The protein pellets were dissolved in 40 µl 0.1% TFA and desalted using ZipTip µ-C18 stage tips (Merck Millipore) following the manufacturer's instructions. The eluted peptide solutions were dried and dissolved in 10 µl LC-MS loading solvent (98 parts UHQ water: 2 parts acetonitrile: 0.1 parts formic acid). Samples were transferred to a 96-well microtitre plate ready for injection into an UltiMate 3000 RSLCnano LC system (Thermo Scientific Dionex) coupled to a Q-Exactive Hybrid Quadrupole Orbitrap MS system (Thermo Scientific). The LC was configured for pre-concentration onto a PepMap RSLC C18 50 µm x 25 cm column (Thermo Scientific P/N ES802) fitted to an EASY-Spray ion source (Thermo Scientific). The loading pump solvent was UHQ water: acetonitrile: formic acid (98: 2: 0.1) at a flow rate of 10 µl/min; nano pump solvent A was UHQ water: formic acid (100: 0.1); nano pump solvent B was acetonitrile: UHQ water: formic acid (80: 20: 0.1). The LC gradient was programmed to increase the proportion of solvent B from 3% to 10% between 5 and 15 min, from 10% to 40% between 15 and 95 min, from 40% to 80% from 95 to 100 min and hold for 10 min before re-equilibration of the nano-column in 3% solvent B for 25 min. MS data acquisition was started at 10 min into the LC gradient, 5 min after switching the flow through the pre-column, and continued for a total of 100 min.

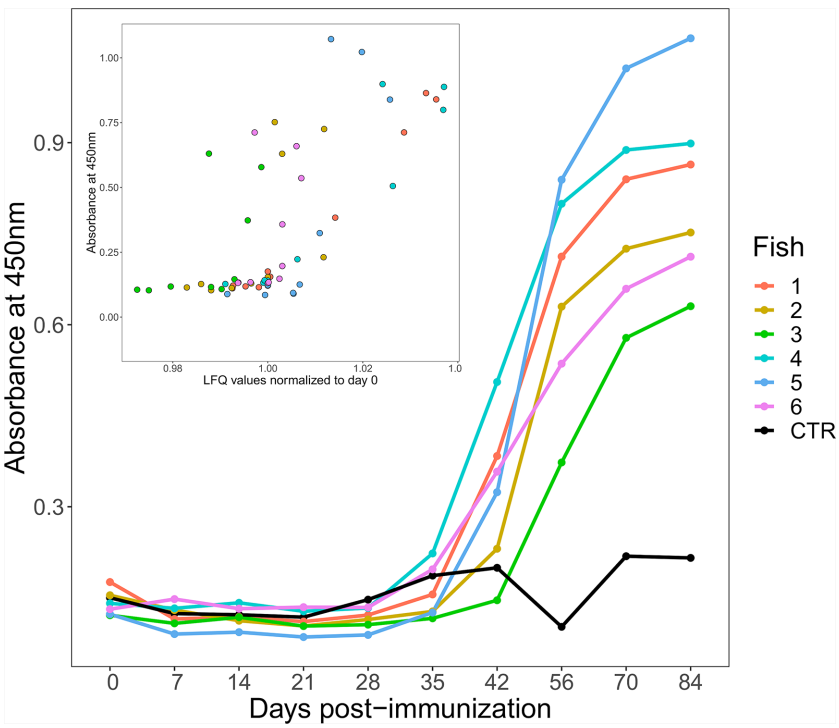

FIGURE 1 | Changes in antigen-specific IgM levels following immunization of six rainbow trout (coloured lines) to HEL-CFA as compared to the CFA-only control fish (black line). The data shown are representative of duplicate technical replicates. The insert shows a positive correlation between antigen-specific and total IgM levels estimated by ELISA and label free proteomics, respectively (Spearman's Rho = 0.71, P <0.001).

Computational Proteomics

MS data were uploaded to MaxQuant v1.5.3.30 (28) together with a reference database containing all protein sequences (n=71,625) predicted in the current rainbow trout RefSeq genome assembly (NCBI accession: GCA_002163495.1) (29). Despite representing a comprehensive annotation of proteins, we noted a poor representation of immunoglobulin (Ig) M (IgM) proteins. As we were interested in quantifying total IgM in addition to antigen-specific IgM, we supplemented the reference database with 317 *O. mykiss* IgM proteins downloaded from the NCBI nr protein database. The Andromeda peptide search engine within MaxQuant (21) was used to match the mass spectra of all detected peptides against the reference protein database, using the label-free quantification method. Digestion type was set to "trypsin" and two missed cleavages were permitted to maximize peptide detection if tryptic digestion was incomplete. Variable modifications of methionine oxidation and N-terminal acetylation were allowed. To increase quantitative accuracy, the Fast LFQ option was not selected. "Match between runs" was used to maximise peptide detection; any features with retention times within 0.7 min and mass within the mass tolerance of peptides identified during previous runs (30) were assigned the same peptide identity. The false discovery rate was set at 0.01, using a target-decoy based search applied at both peptide and protein group levels, which calculated the probability that identified peptides and proteins were false hits (31).

The Andromeda platform within MaxQuant generated protein groups and majority protein groups (MPGs) comprising all proteins sharing at least 50% of their peptides (31). This additional filter increases confidence in the identifications, and only MPGs were considered in subsequent statistical analyses. Proteins identified as contaminants and false positives were removed. Hereafter, where possible we use the term protein in exchange of MPG, as it provides a more intuitive biological description. Protein abundance values for each sample were generated using the label-free quantification (LFQ) method (32).

Statistical Analyses

Among 604 unique proteins initially identified by MaxQuant (**Table S1**), we retained those with abundance (LFQ) values in at least seven out of ten samples across the post-immunization timecourse for all six individuals (278 MPGs; **Table S2**). Our rationale for this cut-off was to filter the analysis to only consistently measured proteins, allowing reliable downstream inferences. After filtering, just 130 missing values remained in the dataset (0.78% of 16,680 data-points) across individuals. LFQ values for the remaining proteins were $\log_2$-transformed and missing values imputed using a random forest-based method (33). Subsequent statistical analyses were performed on transformed imputed values using Minitab v.19 and R v3.6.2.

Principal component analyses (PCA) were performed in R using the *prcomp* function and visualized in ggplot2 v3.2.1 (34). One-way analysis of variance (ANOVA) was performed in Minitab on abundance levels for each of the 278 proteins separately, using sampling day as a fixed factor. The Anderson-Darling test was performed to verify that the residuals were normally distributed and Levene's test used to assess homogeneity of variance. We recorded the R^2 value for each analysis, defining the proportion of variance in protein abundance explained by sampling day. We classified proteins of interest as markers for population responses to immunization as those showing a Benjamini-Hochberg corrected P-value ≤0.05 (corrected at the level of 278 separate analyses), indicating an effect of sampling day. The relationship between P-value and R^2 is shown in **Figure S1**, where a Benjamini-Hochberg corrected P-value ≤0.05 corresponds to R^2 >0.34. The ANOVA data are provided in **Table S3**. For 41 proteins meeting the cut-off, differences in abundance across days were assessed using Tukey's test. Hierarchical clustering analysis was performed in PermutMatrix (35) using abundance data for the 41 proteins, in addition to the mean total IgM abundance (mean $\log_2$ transformed imputed values for all fish, at each time point, for proteins in the dataset annotated as IgM) and antigen-specific Ig titres assessed by ELISA. Clustering and seriation were based on Pearson's correlation coefficient dissimilarity z-scores. The multiple-fragment heuristic seriation method was used with complete linkage (furthest neighbour) aggregation to obtain hierarchical clusters.

Annotation of Trout Plasma Proteins

We used STRING (36) to annotate the 278 proteins in the filtered rainbow trout plasma proteome set on the basis of identifiable orthologues in human, testing for statistical enrichment in protein-protein interaction (PPI) networks, done using default parameters, and recording enrichment (P<0.0001) for Biological Processes within the Gene Ontology (37) and Reactome Pathway (38) frameworks (**Table S4**). We also used the GO FEAT (39) webserver to summarize the annotation of GO Biological Processes for the same protein set.

Analysis of Duplicated Proteins

The common ancestor to salmonid fishes underwent a whole genome duplication (WGD) event (Ss4R) ~88–103 million years ago (40) and consequently, approximately half of the functional genes are found in duplicated pairs (41, 42). Duplicated proteins retained from Ss4R share identities ranging from ~75% to >99% (41). Previous LC-MS studies in salmonids have not tested how analysis platforms using the protein group approach handle the presence of duplicated proteins. We thus aimed to establish how MaxQuant organizes duplicated proteins into MPGs using the current dataset on the basis of protein similarity (**Table 1**; **Figure S2; Tables S5, S6**).

The analysis was performed using the unfiltered high-confidence 604 MPGs and compared the number of MPGs containing duplicated proteins ("scenario i") with the number of duplicated proteins classified into unique MPGs ("scenario ii"). The analysis was informed by BLASTp searches (43) using one representative protein per MPG as the query versus all other proteins within the full set of MPGs. For each MPG, we checked if the proteins present were translated from distinct NCBI RefSeq genes (i.e. duplicated genes), as opposed to representing isoforms of the same gene. For MPGs solely comprised of proteins translated from the same gene, BLASTp was used to record any duplicated proteins within other MPGs (cut-off: >70%

TABLE 1 | Comparison of amino acid sequence identity and shared peptide content between Ss4R and other duplicates classified into the same or different MPGs.

	% Similarity *Mean*	% Similarity *S.D.*	% Similarity *Range*	% Shared peptides *Mean*	%Shared peptides *S.D.*	% Shared peptides *Range*
Duplicates in same MPG (Scenario i)						
Ss4R duplicates	95.28	4.65	80.34 - 100	92.91	11.36	46.47 - 100
Other duplicates	94.66	7.17	73.21 - 100	91.12	12.93	53.13 - 100
Duplicates in different MPGs (Scenario ii)						
Ss4R duplicates	90.40	6.10	70.20 - 98.58	34.49	28.76	0 - 100
Other duplicates	92.16	5.89	77.34 - 98.86	43.65	33.43	0 - 100

identity/coverage). We used ClustalW sequence alignment (44) within BioEdit (v.7.0.5) (45) to align putative duplicated proteins within MPGs and between MPGs. The alignments were trimmed to the shortest protein present, and the mean pairwise identity between duplicated proteins was recorded. Chromosomal locations of genes encoding duplicated proteins were recorded to record duplications resulting from Ss4R (after (29, 42)). Finally, the number of detected peptides shared by duplicated proteins was recorded.

Phylogenetic Analysis

Phylogenetic analyses were used to clarify the evolution of several proteins detected in the trout plasma proteome. For the analysis of apolipoprotein proteins we used human A-I, A-IV, and E protein sequences (NCBI accession numbers: AAA35545, AAA96731, and NP_000032, respectively) as BLASTp queries (43) against the NCBI nr protein database and collected the highest scoring homologues (e-value $<1e^{-10}$) from coelacanth (*Latimeria chalumnae*), spotted gar (*Lepisosteus oculatus*), zebrafish (*Danio rerio*), northern pike (*Esox lucius*), Atlantic salmon (*Salmo salar*) and rainbow trout. We also performed phylogenetic analysis for two plasma proteins with 'uncharacterized' annotations (XP_021436350 and XP_021423950). For this analysis, the trout proteins were used as the query for BLASTp searches against the following taxa in NCBI: invertebrates, jawless fish, Chondrichthyes, Teleostei, Amphibia, Reptilia, Aves, and Mammalia. Hits for these 'uncharacterized' proteins were filtered to proteins showing >40/30% sequence coverage/identity to the query (e-value $<1e^{-04}$). BLAST data are provided in **Table S7**.

For each analysis, sequence alignment was performed using Mafft v.7 with default parameters (46) and trees were built using the IQ-TREE maximum likelihood method (47, 48), which estimated and employed the best fitting amino acid substitution model (49). Ultra-fast bootstrapping (50) was used to generate branch support values. Consensus trees were visualised and rendered in Mega X (51). All used sequence alignments are given in **Supplementary Data 1**.

RESULTS AND DISCUSSION

Antigen-Specific and Total IgM Response

ELISA demonstrated that an antigen-specific IgM response was generated by all six fish injected with HEL-CFA, however the timing and magnitude of the response varied considerably between individuals (**Figure 1**). While antigen-specific IgM levels began to increase in four of the six HEL-immunized fish between 28 and 35 days post-immunization, fish 2 and fish 3 did not show antigen-specific IgM binding appreciably above that of the CFA-only control fish even at day 42 (**Figure 1**). While all six HEL-immunized fish showed antigen-specific IgM levels significantly (3–5 fold) higher than the CFA-only control by day 84, there was an approximately 2-fold difference in ELISA signal between some of the antigen exposed individuals (**Figure 1**).

In mammals, primary antigen exposure causes a rapid increase in both total and antigen-specific IgM levels. This contrasts with sharks (i.e. cartilaginous fish), where total IgM levels remain relatively constant and it is only the monomeric antigen-specific portion that increases in concentration upon immunization (26). We were curious to establish if the HEL-specific IgM responses observed in trout were coupled to changes in total IgM, as in mammals, or were largely uncoupled, as in sharks. As the IgM proteins in our database were present as 11 distinct, closely related proteins, we took their average values at each time point to approximate the total IgM response. Antigen-specific IgM response and total IgM levels were significantly correlated for each of our 60 samples (Spearman's Rho = 0.71, $P < 0.001$; **Figure 1**).

Overview of Trout Plasma Protein Functions

Biological processes and molecular pathways overrepresented among the 278 trout plasma proteins are shown in **Table S4**. These plasma proteins are highly biologically connected, showing 8.42 times more protein-protein interactions than expected by chance ($P < 1.0e^{-16}$; visualized in **Figure S3**). The overrepresented Biological Processes (GO framework) and Reactome pathways reflect the large number of proteins from, or involved in the regulation of, the complement system (e.g. 24 annotated with Reactome term 'complement cascade', $P = 1.83e^{-30}$), diverse immune functions (e.g. 53 annotated with Reactome term 'immune system', $P = 8.88e^{-17}$, 29 annotated with GO term 'humoral immune response', $P = 4.88e^{-23}$, and 23 annotated with GO term 'adaptive immune response', $P = 1.52^{e-15}$), a range of blood, blood clotting/coagulation and platelet functions (e.g. 34 annotated with Reactome term "hemostasis", $P = 7.78e^{-19}$), in addition to metabolic functions (e.g. 5 annotated with Reactome term 'gluconeogenesis', $P = 8.14e^{-05}$). GO FEAT analysis highlighted similar terms, but also emphasised representation of proteins involved in lipid transport and metabolism, largely apolipoproteins (see later section).

Analysis of Duplicated Proteins

In LC-MS proteomics, it is common to collapse proteins that share identical or highly similar peptides into single protein groups. This method aims to capture protein isoforms derived from the same gene, but also creates potential for proteins translated from highly similar duplicated genes to be grouped together. Logically, this situation will arise most commonly for proteins sharing high similarity, such as those translated from gene duplicates retained from Ss4R (41, 42). On these grounds, we predicted that the classification of duplicated proteins into distinct MPGs or a common MPG by MaxQuant would be a product of paralogous sequence divergence.

Among the 604 MPGs available for analysis, 46.5% were comprised of proteins without identifiable duplicates in the dataset (**Figure S2**). Among the remaining 286 MPGs, 31% included duplicated proteins translated from distinct genes ("scenario i"), whereas for the other 69%, any duplicated proteins in the dataset were in unique MPGs ("scenario ii") (**Tables S5, S6**). Under scenarios i and ii, ~70% and ~85% of the proteins were retained from the Ss4R event, respectively (**Figure S2**). On average, duplicated proteins classified into the same MPG shared higher amino acid sequence identity and a higher percentage of shared peptides than duplicated proteins classified into two or more MPGs (**Table 1**). Under both scenarios we observed a significant positive correlation between the proportion of shared peptides and % identity between duplicated proteins (**Figure S4**; Pearson's R=0.62 and 0.70; P=0.006 and P<0.0001 for scenario i and ii, respectively). MaxQuant classified many duplicated proteins sharing >95% amino acid level into distinct MPGs, despite sharing >50% common peptides (**Figure S4**). Overall, these data indicate that MaxQuant often distinguishes protein duplicates across a range of sequence divergence levels relevant to the detection of Ss4R duplicates (40, 41). However, the results advocate for a careful approach when drawing conclusions about duplicated proteins using the protein group concept in LC-MS proteomics, requiring a protein-by-protein investigation of the make-up of protein groups.

Individual-Level Variation Dominates the Plasma Proteome

We used PCA to visualise groupings among the 60 sampled plasma proteomes according to fish individual and the ten post-immunization time points (**Figure 2**). We did this twice, firstly with the overall plasma protein abundance levels (**Figure 2A**), and secondly using the same values normalized to day 0 values (i.e. day 7/day 0, day 14/day 0, etc.) in order to remove the effect of variability in starting abundances, thus focusing on the response dynamic (**Figure 2B**). For the first analysis, PC1 and PC2 together explained around a third of the total variation and showed largely fish-specific groupings (**Figure 2A**). For the second analysis, a similar amount of total variation was explained by PC1 and PC2, and while there was a more substantial overlap among fish individuals (**Figure 2B**), this was not clearly explained by differences among days. Overall, a substantial proportion of total variation in our dataset is explained by overarching differences in plasma protein abundance and responses among the six trout individuals.

Proteins Showing Similar Population Responses to Immunization

We next classified proteins according to the extent of variation in abundance levels explained by sampling day using one-way ANOVA (**Table S3**). We recorded R^2 to describe the variance explained by differences among sampling days. The relationship between P-value and R^2 is shown in **Figure S4**, which highlights the cut-off we employed (corrected $P \leq 0.05$) to identify 41 proteins showing an overall population effect of sampling day. These proteins represent approximately 15% of all detected plasma proteins, and within our dataset are characterized by the most similar overall abundances within days, and most similar responses to immunization across the six individuals between days. We grouped these proteins according to commonalities in their average response to immunization using hierarchical clustering, also including mean total Ig and antigen-specific IgM levels (**Figure 3**). This revealed two major clades ("A" and "B"), separating proteins showing highest abundances during the early or late part of the timecourse (**Figure 3**). In the following sections, we outline the responses and characteristics of proteins grouped into five sub-clusters, two within clade A (clusters A1 and A2) and three within clade B (clusters B1, B2, and B3).

Cluster A1: IgM and Neuropilin-2

Mean total IgM and antigen-specific IgM clustered closely, together with a single IgM heavy chain protein (**Figure 3**), which showed large variation between fish individuals, such that abundance levels were not significantly different between any time points (**Figure 4A**). The other protein in this cluster, neuropilin-2, showed a significantly higher abundance at day 56 compared to days 14–21 (**Figure 4B**). Neuropilin-2 is a transmembrane glycoprotein that is abundantly expressed in immune cells, and supports multiple immune functions, including antigen presentation (52, 53).

Cluster A2: Diverse Molecules With Immune Functions; From Complement to Metabolic Enzymes

Members of the A2 cluster showed lowest abundance during the earliest days in the timecourse (**Figure 3**) and included complement system proteins annotated as C1q-like, C3, C6, and factor H (**Figure 5**). For instance, a C3 protein (XP_021469459.1), which is a central component of the complement system, showed significantly higher levels on days 21–84 than day 0 (**Figure 5A**). Similarly, complement C6, part of the membrane attack complex (54), was significantly higher on days 28–70 than day 0 (**Figure 5B**). Similar abundance profile changes were observed for complement C1q-like protein 2 and two distinct factor H proteins (**Figure S5**). Several additional proteins with known immune functions were present in cluster A2, including C type lectin receptor B (**Figure 5C**), a pattern recognition receptor, precerebellin-like protein, a known acute

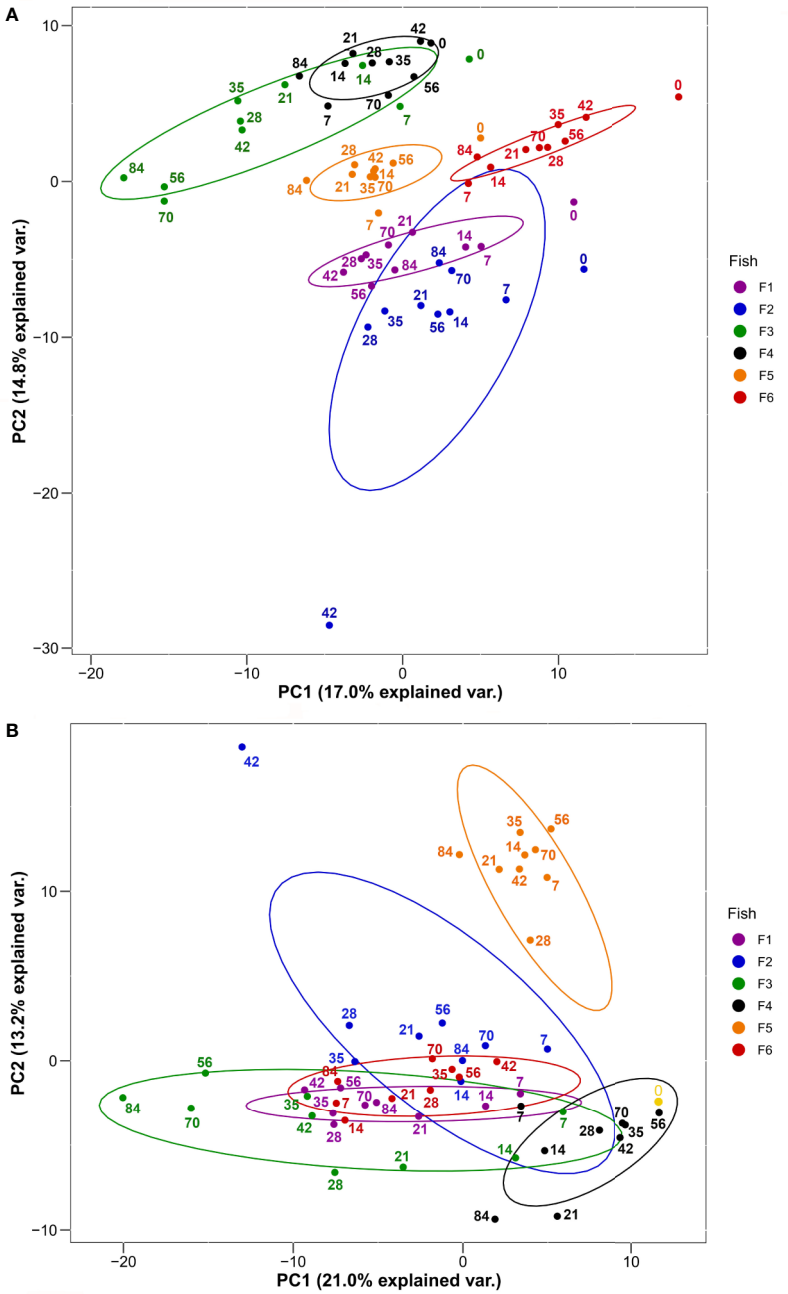

FIGURE 2 | PCA of 278 plasma proteins derived from the six HEL-immunized fish shown in **Figure 1** using **(A)** log_2-transformed imputed values and **(B)** log_2-transformed imputed values normalized to Day 0 values. Normalized Day 0 value common to all fish is shown in yellow. Ellipses are 95% confidence intervals around the centroid. Sampling days are shown by numbering within the plots.

phase protein showing regional similarity to C1q (**Figure 5D**) (55, 56) and the antibacterial enzyme lysozyme (57) (**Figure 5E**). Two separate microfibril-associated glycoprotein 4 proteins also grouped within cluster A2 (**Figure S5**), and may act as soluble pathogen recognition molecules (58). Cluster A2 also included a protein annotated 'uncharacterized' (XP_0214236350; detailed further below) that showed significantly higher abundance at days 21-84 compared to day 0 (**Figure 5**).

Within cluster A2, glucose-6-phosphate isomerase (GPI) levels increased steadily during the timecourse, and reached peak levels at day 84, which was significantly higher than days 0-42 (**Figure 6A**). While best known for its role in glycolysis and gluconeogenesis, in mammals a secreted form of GPI ("neuroleukin") induces maturation of B cells into plasma cells, thereby increasing Ig production (59). Thus, the increasing levels of GPI may have been supporting the development of the

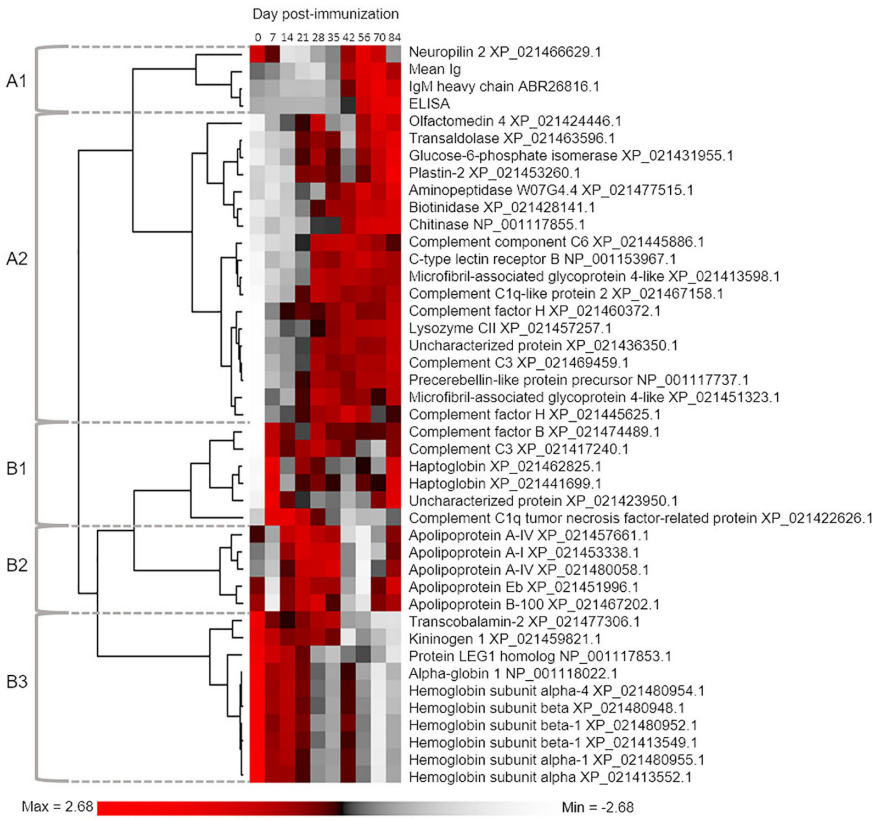

FIGURE 3 | Hierarchical clustering analysis used to group proteins according to similar mean abundance profiles across the sampling timecourse. The 41 included proteins were defined by One-way ANOVA defining an overall population effect of sampling day (see **Table S3**). For comparison, we also included data for mean total Ig levels and antigen-specific IgM levels. The five defined clusters are referred to in the main text.

observed antigen-specific IgM response. Like GPI, plastin-2 (LCP1 or L-plastin) increased during the timecourse to show highest levels at day 84, with days 70 and 84 each showing significantly higher levels than days 0–14 (**Figure 6B**). Plastin-2 is an actin-regulating protein expressed specifically in leucocytes, and in humans is among the most abundant of all monocyte and T-cell proteins, with key immune functions including lymphocyte migration and T-cell activation (60, 61). The metabolic enzyme transaldolase showed a similar abundance profile (**Figure S5**), and is involved in the pentose phosphate pathway; its increasing levels during the time course may help support the high metabolic demands of an adaptive immune response (62).

Olfactomedin-4 showed a significant increase in abundance at days 28 and days 56–84 compared to day 0 (**Figure S5**). The secreted form of olfactomedin-4 can interact with many proteins, such as NOD1/NOD2, lectins, cadherins, and cathepsins, all of which regulate immune functions (63). The enzymes chitinase (**Figure 6C**), biotinidase (**Figure S5**), and aminopeptidase W07G4.4 (**Figure S5**), all increased steadily in abundance across the timecourse, with chitinase and biotinidase reaching significantly higher levels than day 0 by days 35–42. Chitinase has well established roles in innate immune protection, providing antifungal and antihelminthic activity (64). While no direct immune functions have been attributed to biotinidase, this enzyme may support immune function indirectly, e.g. biotin is an essential cofactor for enzyme functioning in many cell types, including maturing and proliferating lymphocytes (65, 66). Upregulation of biotinidase should increase the supply of biotin, perhaps supporting the production of antigen-specific Ig in the adaptive phase.

Cluster B1: Including Haptoglobins and Complement Proteins

Cluster B1 contained proteins that tended to show highest levels from day 7 onwards (**Figure 3**). This included two complement proteins, a second C3 molecule (XP_021417240) along with factor B (Bf), an integral component of the alternative pathway C3 convertase (67). Both molecules showed a dramatic increase in abundance between day 0 and 7 and remained at elevated levels across the remainder of the timecourse (**Figures 7A, B**). Cluster B1 contained two haptoglobin (Hp) molecules, also showing large increases in abundance from day 0 to 7, consistent with Hp being an acute-phase protein, before dropping back to levels not significantly different from 0 between days 14–70, and increasing again on day 84

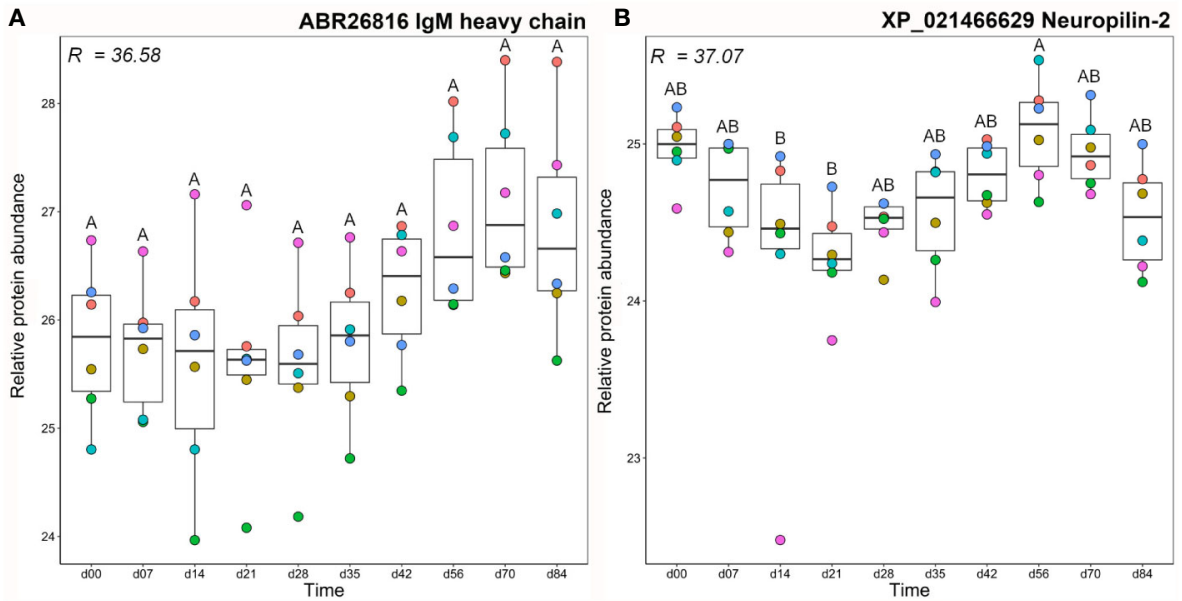

FIGURE 4 | Abundance profiles for all proteins in cluster A1 (**Figure 3**); **(A)** IgM heavy chain and **(B)** neuropilin-2. R^2 values describe the proportion of variance in abundance explained by differences in sampling day according to one-way ANOVA (**Table S3**). Different letters shown on the plots indicate days with significantly different protein abundance values (Tukey's test). Relative protein abundance represents log2 transformed imputed values. The different colour dots represent different fish.

(**Figures 7C, D**). Hp is best known for sequestering haemoglobin released by haemolysis in mammals (68). However, it has recently been shown that Hp is a divergent member of the complement-activating MASP family (69) and possesses various immunoregulatory functions (70, 71). The adipokine C1q TNF-related protein (CTPR3) showed a similar mean profile, but with larger variation among individuals, and only showed a significant difference in abundance between days 14 and 42 (**Figure 7E**). Given the wide-ranging effects ascribed to CTPR3, including roles in metabolism and inflammation (reviewed in (72)), it is difficult to predict the consequences of these changes. A second uncharacterized protein (XP_0211423950; detailed further below) was contained in cluster B1. This protein increased significantly in abundance between day 0 and day 7, dropped to a slightly lower level from days 14–70, then increased in abundance again at day 84 (**Figure 7F**), an abundance profile remarkably similar to the Hp proteins, with which it clustered (**Figure 3**).

Cluster B2: Apolipoproteins

Cluster B2 was comprised of five apolipoproteins (**Figure 3**), among 17 unique apolipoproteins detected in our dataset (**Table S2**). Each of the five apolipoproteins showed related changes in abundance during the timecourse, but with distinct levels of individual variation within days (**Figure 8**). Two of these proteins showed among the highest R^2 values reported in our dataset (**Table S3**; **Figures 8A, B**). Apolipoprotein A-I (XP_021453338) showed highest levels at days 21–35 (significantly higher than days 0–7 and days 42–70) and lowest levels at day 56 (significantly lower than all days except days 42 and 70) (**Figure 8A**), which was highly similar to apolipoprotein A-IV (**Figure 8B**). A distinct protein annotated as apolipoprotein A-I (XP_021480058) showed a similar profile, but with greater individual variation within days, showing a significantly lower abundance at day 56 compared to days 21–35 (**Figure 8C**). Apolipoprotein B-100 was unique in showing a significant decrease from day 0 to day 7, before significantly increasing by day 21, and significantly decreasing again by day 56 (**Figure 8D**). Apolipoprotein Eb showed significantly lower abundance at day 56 compared to days 21–35 and day 84 (**Figure 8E**).

The similar annotations and abundance profiles of multiple apolipoprotein A family members led us to question their evolutionary relationships. A phylogenetic analysis was performed for all annotated apolipoprotein A proteins in our dataset, within a broader background of orthologs from additional vertebrate species (**Figure 9**). Note, we included the apolipoprotein E family in this analysis as the sister group to the apolipoprotein A family, but excluded apolipoprotein B molecules, which are more evolutionarily divergent (73). This analysis provides a different, and more well supported evolutionary history of apolipoprotein AI and IV than existing scenarios (73). Specifically, our tree strongly supports a scenario where the ancestor to ray-finned fish and lobe-finned fish had separate genes encoding three distinct proteins related to apolipoprotein AI and IV, all of which are retained in coelacanth (**Figure 9**). Included among these three proteins, humans retain apolipoprotein AI and IV while ray-finned fish

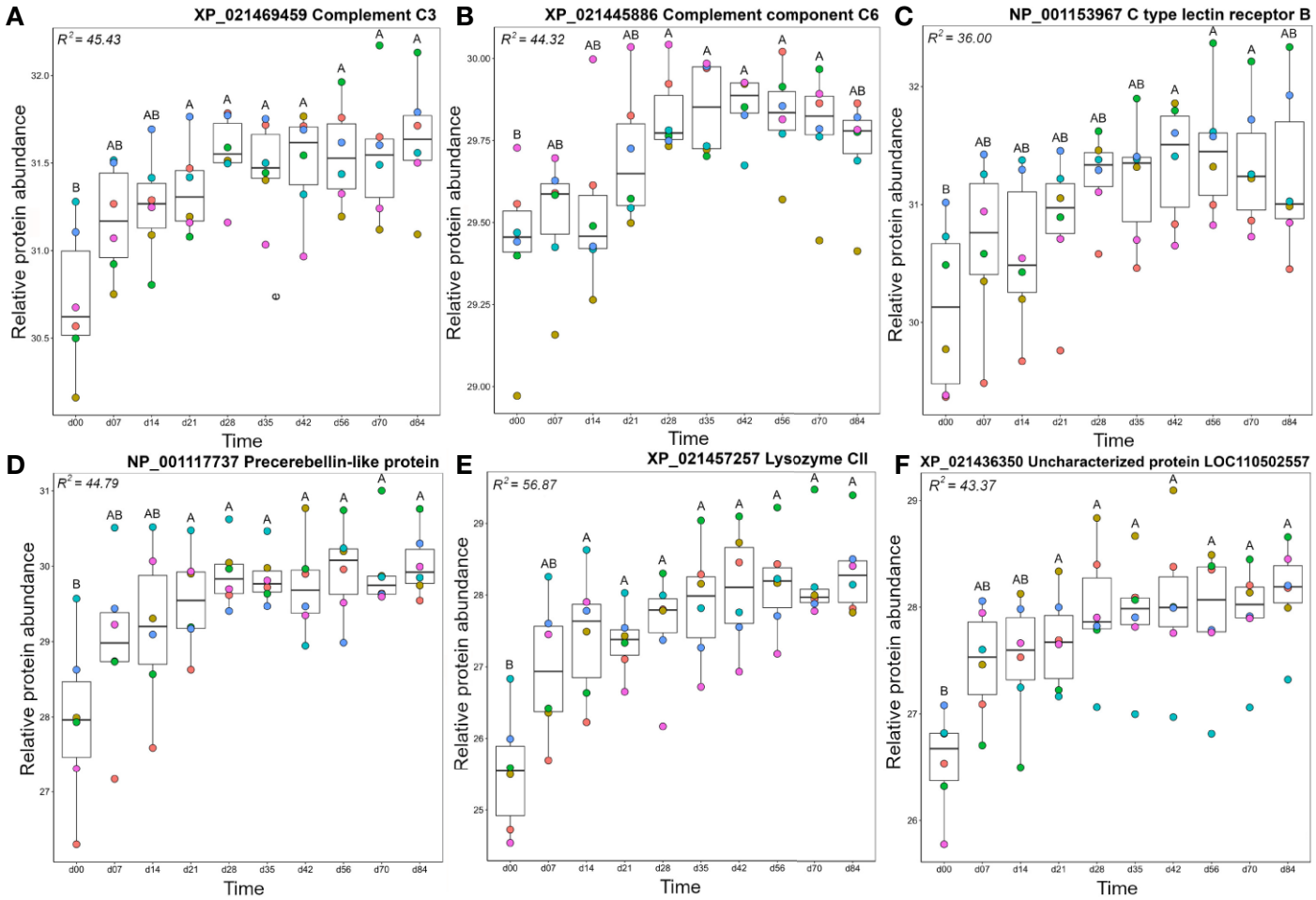

FIGURE 5 | Abundance profiles for representative proteins in cluster A2 (**Figure 3**); **(A)** complement C3, **(B)** complement C6, **(C)** C type lectin receptor B, **(D)** precerebellin-like protein, **(E)** Lysozyme CII, and **(F)** uncharacterized protein XP_021436350. Other details as in the **Figure 4** legend. Additional proteins represented in cluster A2 are plotted in **Figure S5**.

only retain orthologues of AI (**Figure 9**). However, ray-finned fish and coelacanth retain a distinct paralogue of apolipoprotein AI, absent in humans (**Figure 9**). Three rainbow trout representatives of this clade are grouped within Cluster B2, with two representing salmonid-specific duplicates (i.e. XP_021453338 and XP_021457661) (**Figure 9**) showing highly correlated abundance changes (**Figure 3**). The third protein (XP_021480058) is a more ancient paralogue that arose in the common ancestor to salmonids and zebrafish after the split from spotted gar, which is consistent with the teleost-specific WGD event (74). The current annotation of apolipoprotein A-like proteins in salmonids is thus not supported by phylogenetic analysis, and future work might expand the phylogenetic analysis of the apolipoprotein A family to achieve an evolutionarily-supported nomenclature.

When interpreting the changes in abundance of apolipoproteins in our data, it is important to note that while classically associated with lipid transport and metabolism (75) these molecules also modulate innate and adaptive immune processes (reviewed in (76)). Recent data from amphioxus (77) suggest at least some of these immune roles are evolutionarily ancient. Apolipoprotein B-100 has been shown to inhibit *Staphylococcus aureus* colonization (78), while class A apolipoproteins can bind and neutralize bacterial LPS (79) and have bactericidal (80–82) and viricidal (83) activity in teleosts, including salmonids. They also kill pathogens indirectly, acting as immunostimulants to enhance respiratory burst responses in innate immune cells (84). Class A and E apolipoproteins also modulate many adaptive immune processes. Generally these immune functions tend towards regulation, e.g. inhibiting the production of pro-inflammatory cytokines by disrupting contact between stimulated T cells and monocytes (85), stimulating regulatory T cell expansion (86), and inhibiting T cell activation through the downregulation of antigen-presentation by dendritic cells (87). Thus, the complex changes in abundance observed across the timecourse may reflect the multifaceted regulatory roles of rainbow trout apolipoproteins at different phases of the immune response.

Cluster B3: Including Haemoglobin and Proteins With Blood Functions

Proteins in cluster B3 showed highest levels on day 0, then decreased in abundance over the timecourse (**Figure 10**, **Figure S6**). Seven haemoglobin (Hb) proteins fell within this cluster and reached lowest levels on day 70. The presence of Hb in plasma is due to red blood cell (RBC) lysis, occurring biologically *in vivo* or during sample processing *ex vivo*. The drop in abundance of Hb subunits may simply reflect improvement in our sampling and processing technique over the experiment, however, there are several biological processes that could cause or contribute to this drop. For example, repeated blood sampling could reduce RBC counts and consequently reduce free Hb. However, Collet and colleagues (12) recorded no significant drop in haematocrit using the same approach with more regular bleeding (taken every 4 days). While we did not measure haematocrit, the fish in our study were sampled every 7 days using the same volume criteria

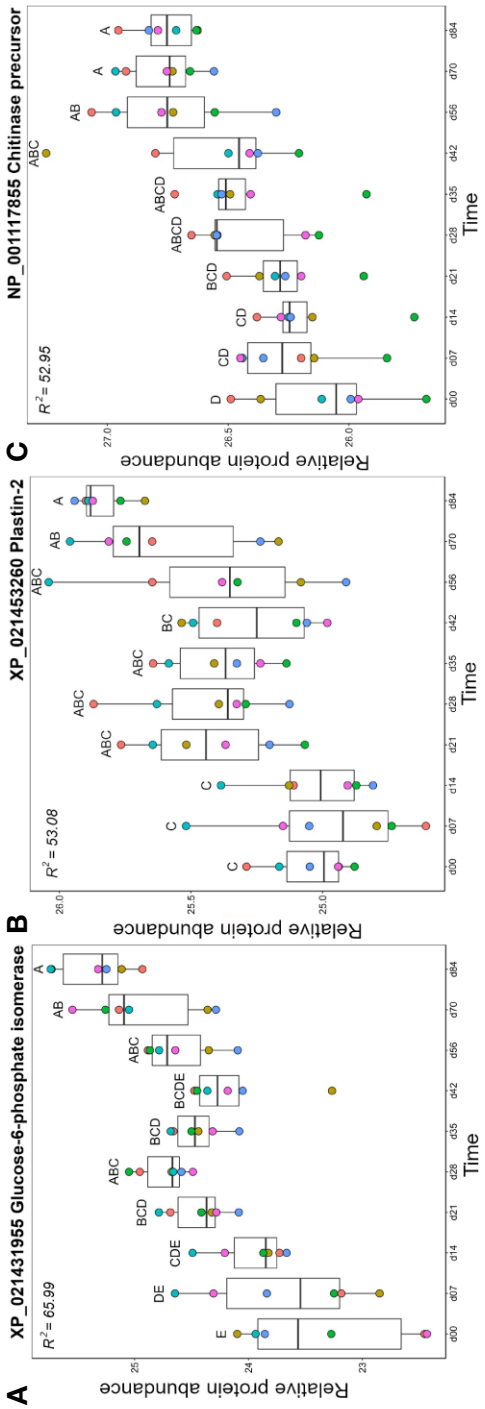

FIGURE 6 | Abundance profiles for representative proteins in cluster A2 (**Figure 3**); **(A)** Glucose-6-phosphate isomerase, **(B)** Plastin-2, and **(C)** Chitinase precursor. Other details as in the **Figure 4** legend. Additional proteins represented in cluster A2 are plotted in **Figure S5**.

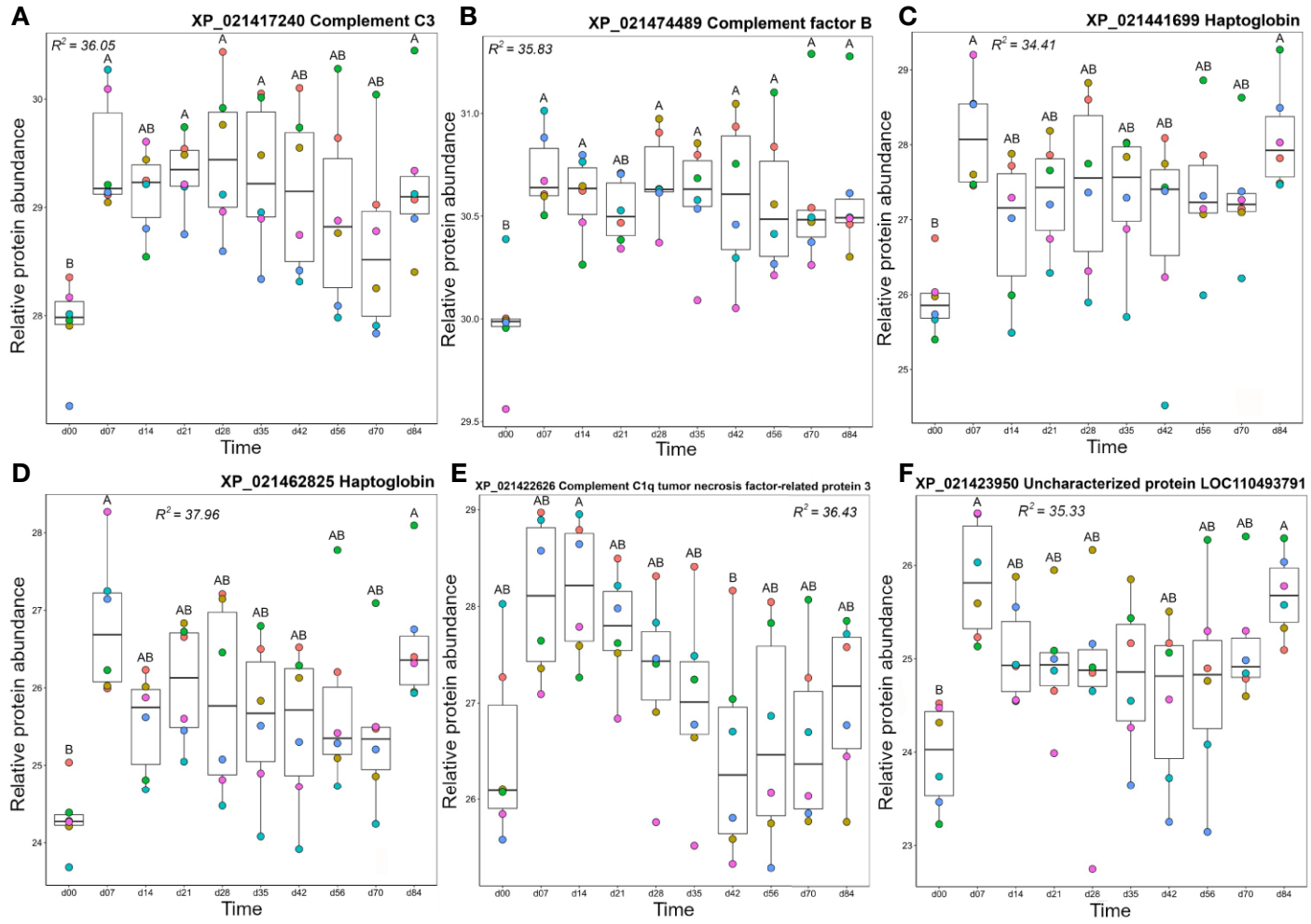

FIGURE 7 | Abundance profiles for all proteins in Cluster B1 (**Figure 3**); **(A)** complement C3, **(B)** complement factor B, **(C)** haptoglobin, **(D)** haptoglobin, **(E)** complement C1q tumor necrosis factor-related protein 3, and **(F)** uncharacterized protein XP_021423950. Other details as in the **Figure 4** legend.

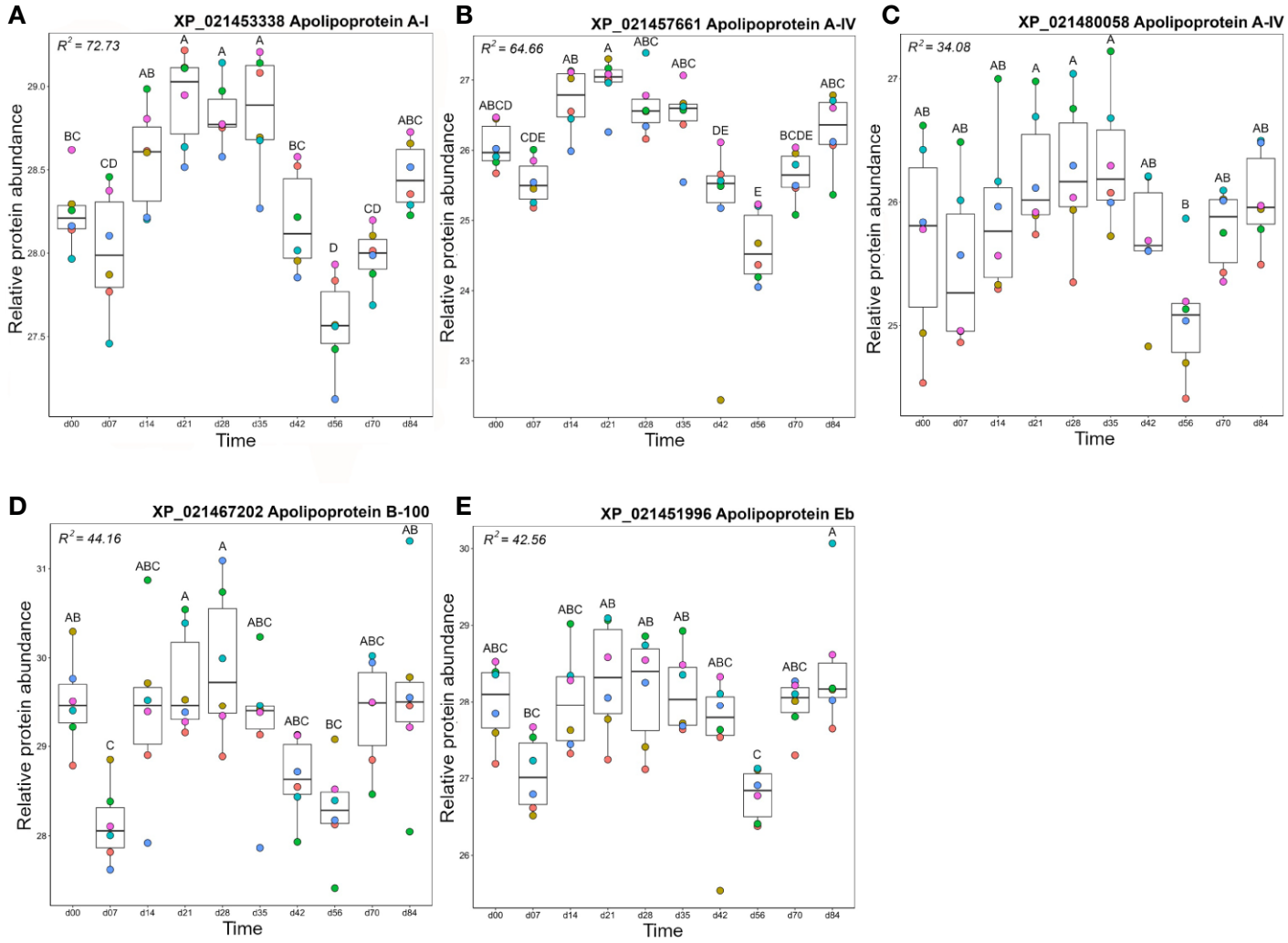

FIGURE 8 | Abundance profiles for all proteins in Cluster B2 (**Figure 3**); **(A)** apolipoprotein A-I, **(B)** apolipoprotein A-IV, **(C)** apolipoprotein A-IV, **(D)** Apolipoprotein B-100, and **(E)** apolipoprotein Eb. Other details as in the **Figure 4** legend.

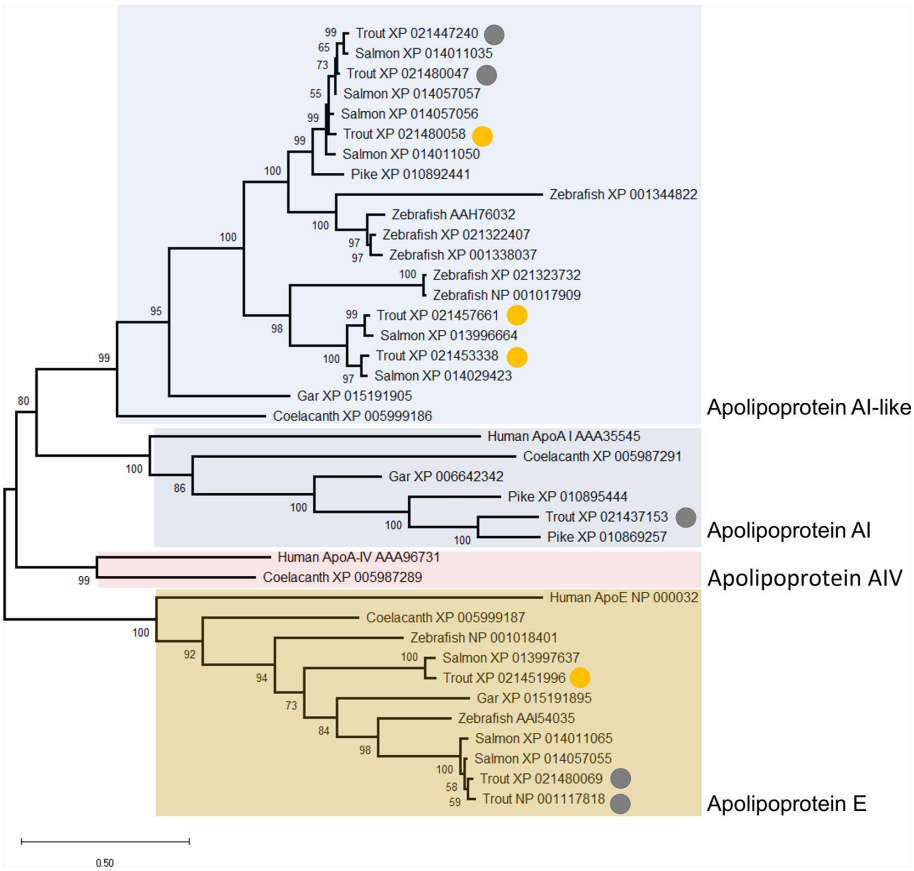

FIGURE 9 | Maximum likelihood consensus tree of apolipoprotein A and E proteins detected in the rainbow trout plasma proteome, alongside putative orthologues from human, coelacanth, spotted gar, zebrafish, Atlantic salmon, and northern pike. The tree, which is rooted to the ApoE clade, was generated using the best fitting amino acid substitution model (LG+G4) and includes branch support values from 1,000 ultrafast bootstrap replicates. The circles highlight nine distinct apolipoprotein A and E family members detected in our dataset. The yellow circles highlight proteins included in Cluster B2 (**Figure 3**) with specific abundance profiles plotted in **Figure 8**.

(<10% blood volume from each animal in any 4-week period). Thus, it would be surprising if reduced Hb was caused by reduced haematocrit. Replacement of removed RBCs with newer, more robust, cells could partly explain the drop in free Hb. Finally, there is known to be a slow turn-over of RBCs *in vivo* due to formation of the alternative pathway C3 convertase (formed from fragments of C3 and Bf) of the complement system on their surface. It is worth noting that free Hb levels drop around the time that the levels of one C3 and Bf decrease, while the two molecules of factor H, a regulatory protein which accelerates the decay of the C3 convertase and thus would protect host RBCs from lysis, show an increase. Further study is required to ascertain which, if any, of these mechanisms explain our data.

Transcobalamin-2, which is required to bind and transport vitamin B12 for red blood cell production (88, 89), also decreased over the timecourse, with highest abundance levels between day 0 and day 35, dropping at day 42 and remaining at this level until day 84 (**Figure 10C**). Kininogen-1 is a multi-functional protein with a major role in blood clotting and blood pressure regulation but is also a mediator of immune inflammation (90). Kininogen-1 levels decreased steadily over the experimental timecourse such that there was a significant drop between day 0 and day 84 (**Figure 10D**). Protein LEG1 homolog, a structural protein necessary for liver development and function (91), also decreased in abundance over the study timecourse, showing lower levels at days 70–84 than at day 0 (**Figure 10E**).

Evolutionary Conservation of "Uncharacterized" Trout Plasma Proteins

The presence of two proteins annotated as 'uncharacterized' within the group of 41 proteins included in **Figure 3** (**Figures 5F**, **8F**), led us to question their annotations and evolutionary origins. We determined if these molecules show homology to proteins in other taxa using BLASTp (**Table S7**). Despite not being detected in any mammal, both proteins are conserved across multiple vertebrate classes (**Table S7**). The protein in cluster A2 (XP_021436350) is a 22 kDa cysteine-rich glycoprotein containing no known conserved domains,

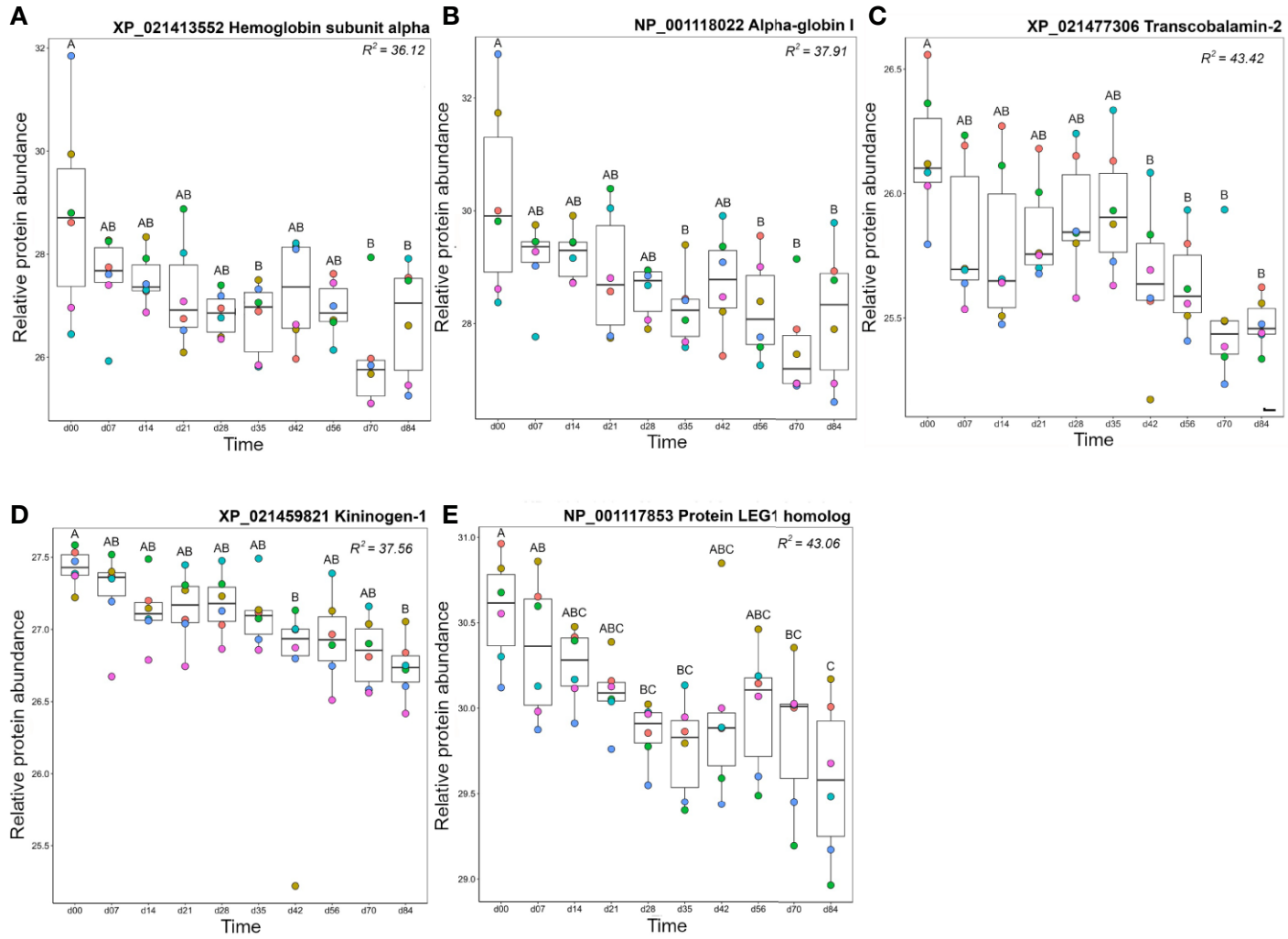

FIGURE 10 | Proteins in Cluster B3 (**Figure 3**); **(A)** hemoglobin subunit alpha, **(B)** alpha-globin I, **(C)** transcobalamin-2, **(D)** kininogen-1, and **(E)** protein LEG1 homolog. Other details are as in the **Figure 4** legend.

conserved in teleosts, amphibians and reptiles (**Figure 11A**). The protein in cluster B1 (XP_021423950) is a 24 kDa cysteine-rich protein with no known conserved domains, and conserved in cartilaginous fish, birds, and teleosts (**Figure 11B**). The identification of conserved uncharacterized proteins showing temporal changes in abundance highly correlated to known immune molecules highlights a strength of the "discovery" approach enabled by LC-MS proteomics; specifically, the scope for revealing novel molecules with putative immune functions, which clearly warrant further attention.

CONCLUSIONS, PERSPECTIVES, AND CAVEATS

This is the first study to apply label-free proteomics to quantify long-term changes in plasma protein abundance in a salmonid fish following immunization, capturing different phases in the immune response. By keeping samples from each individual separate, we were able to explore the variation in humoral response between individuals as well as population-level responses. It is well-established that vaccination does not induce comparable protective responses in individual fish (92–94), however the extent of individual variation we observed here was nevertheless surprising. For example, although all fish produced antigen-specific IgM, the kinetics and magnitude of the response varied markedly between individuals. Importantly, now we have proved antigen-specific IgM levels as measured by antigen-binding ELISA correlate highly with total IgM as measured by LC-MS/MS, future studies would require much smaller plasma volumes (i.e. only 1 µl of plasma is required for LC-MS analysis compared to ≥10 µl for ELISA) thus permitting study of immune responses in much smaller fish (e.g. fingerlings of usual vaccination size).

Mirroring the data on the IgM response, we found that the overall plasma proteome response to HEL immunization was predominantly explained by differences between fish individuals. Due to the small number of individuals in our study we did not attempt to explore the factors contributing to this variation in response. However, given the importance of consistent, population-wide protection to the eventual success of aquaculture vaccines, this is certainly something that should be explored in future studies. The power of our study comes from our ability to compare each time point from an individual animal to its own day 0 sample. We cannot rule out that some changes in protein abundance are linked to the repeated sampling protocol rather than immune challenge, the globin proteins being a possible example. However, it seems unlikely this would be the case for all the proteins showing similar abundance profiles across fish individuals, especially as many have previously established immune functions. Following additional validation, at least some of these molecules may provide useful new immune biomarkers that can be utilized in future vaccine trials in salmonids. Of note is our discovery of two uncharacterized plasma proteins with putative immune functions. Our phylogenetic analyses indicate these proteins are absent from placental mammals, including humans and mice, so likely would not have been identified using standard comparative approaches. It will be interesting to discover what role these new molecules play in immune protection in trout and, where present, other species. As yet we are unable to correlate any specific proteins with high production of antigen-specific antibody, however, as data from other proteomic studies is accrued and new markers are utilized, we are confident such information will eventually be forthcoming.

Finally, our study highlights how LC-MS is an enabling technology for the study of non-mammalian species where large sequence datasets are often available, but species-specific monoclonal antibodies are in short supply. Indeed, the power of LC-MS is illustrated by our ability to differentiate proteins with high amino acid identity, such as those expressed from recently

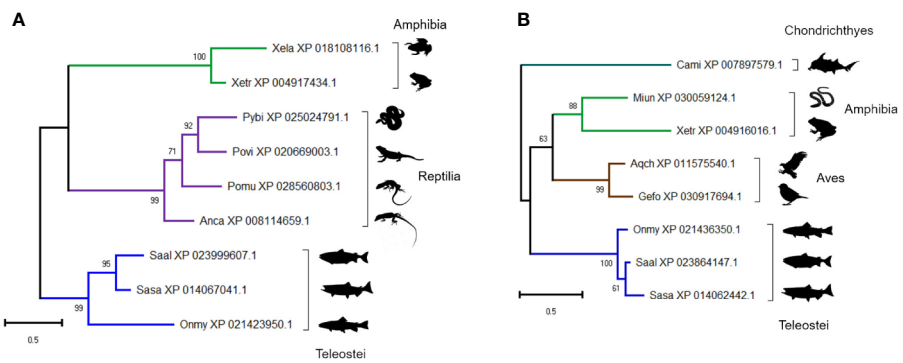

FIGURE 11 | Maximum likelihood consensus trees for two trout proteins annotated as 'uncharacterized': **(A)** XP_021436350 and **(B)** XP_021423950, including putative orthologues in other taxa. The trees were generated using the best fitting amino acid substitution model and includes branch support values from 1,000 ultrafast bootstrap replicates. Species abbreviations: Anca, Anolis carolinensis (green anole); Aqch, Aquila chrysaetos (Golden eagle); Cami, Callorhinchus milii (elephant shark); Gefo, Geospiza fortis (medium ground finch); Miun, Microcaecilia unicolor (caecilian spp.); Onmy, Oncorhynchus mykiss (rainbow trout); Pomu, podarcis muralis (common wall lizard); Povi, Pogona vitticeps (bearded dragon); Pybi, Python bivittatus (Burmese python); Saal, Salvelinus alpinus (Arctic charr); Sasa, Salmo salar (Atlantic salmon); Xela, Xenopus laevis (African clawed frog); Xetr, Xenopus tropicalis (Western clawed frog).

duplicated genes. These may have different functional roles/response kinetics but would be difficult to raise discriminatory antibodies against. Even if such antibodies were available, the research effort and sample volumes required to monitor abundance changes of >250 plasma proteins renders the use of classical methods such as ELISA or Western blots impractical. However, we also recognize there is room to further improve our approach; for example, although we detected over 600 unique proteins in our samples, only 278 proteins were detected in at least seven out of ten samples for all six individuals and thus retained following filtering. This issue could perhaps be overcome through application of an isobaric labelling strategy, whereby the peptides generated following trypsin treatment of each sample are tagged with chemical groups of identical mass but differing in their distribution of stable heavy isotopes. Tagged samples are pooled then analyzed simultaneously by MS. While tagging kits can be costly, such strategies should reduce the number of missing observations and consequentially improve the number of unique proteins retained for subsequent analyses. Alternatively, another recently developed label free MS method called sequential window acquisition of all theoretical mass spectra (SWATH) can be used to increase precision across the detectable proteome [e.g. (95)]. The application of such methods would also facilitate the detection of important but low abundance proteins, such as cytokines, that were not picked up during this study. Even with such limitations, the in-depth information obtained *via* LC-MS studies such as ours will undoubtedly improve our understanding of fish immune responses and the immunological variation between individuals, hopefully accelerating the testing of new aquaculture vaccines and improved administration methods.

DATA AVAILABILITY STATEMENT

The datasets presented in this study can be found in online repositories. The names of the repository/repositories and accession number(s) can be found in the article/**Supplementary Material**.

ETHICS STATEMENT

The animal study was reviewed and approved by UK home office and University of Aberdeen's Animal Welfare and Ethical Review Body (AWERB).

AUTHOR CONTRIBUTIONS

Study conception and design: DM and HD. Animal work: MM and HD. Proteomics lab work: DS. Proteomic data analysis: FB, DC, AD. Data interpretation: FB, DM, and HD. Drafted figures and tables: FB and DM. Drafted manuscript: FB, DM, and HD. All authors contributed to the article and approved the submitted version.

FUNDING

This work was supported by the Biotechnology and Biological Sciences Research Council (BBSRC) grant numbers: BB/M010996/1, BB/M026345/1, BBS/E/D/20002174, and BBS/E/D/10002071.

ACKNOWLEDGMENTS

Our thanks to Prof. Chris Secombes (University of Aberdeen) for the 4C10 anti-salmonid IgM mAb used in our ELISAs and for his valuable intellectual contributions during the planning of this project. We also gratefully acknowledge the supervisory support given by Prof. Sam Martin (University of Aberdeen) to FB.

SUPPLEMENTARY MATERIAL

The Supplementary Material for this article can be found online at: https://www.frontiersin.org/articles/10.3389/fimmu.2020.581070/full#supplementary-material

REFERENCES

1. Crane M, Hyatt A. Viruses of fish: an overview of significant pathogens. *Viruses* (2011) 3:2025–46. doi: 10.3390/v3112025
2. Centers for Disease Control and Prevention (CDC). *A CDC framework for preventing infectious diseases: Sustaining the essentials and innovating for the future* (2011). Available at: https://www.cdc.gov/ddid/docs/ID-Framework.pdf (Accessed May 17, 2020).
3. Plant KP, Lapatra SE. Advances in fish vaccine delivery. *Dev Comp Immunol* (2011) 35:1256–62. doi: 10.1016/j.dci.2011.03.007
4. Gudding R, Van Muiswinkel WB. A history of fish vaccination: science-based disease prevention in aquaculture. *Fish Shellfish Immun* (2013) 35:1683–8. doi: 10.1016/j.fsi.2013.09.031
5. Brodin P, Jojic V, Gao T, Bhattacharya S, Lopez Angel CJ, Furman D, et al. Variation in the human immune system is largely driven by non-heritable influences. *Cell* (2015) 160:37–47. doi: 10.1016/j.cell.2014.12.020
6. ter Horst R, Jaeger M, Smeekens SP, Oosting M, Swertz MA, Li Y, et al. Host and environmental factors influencing individual human cytokine responses. *Cell* (2016) 167:1111–24. doi: 10.1016/j.cell.2016.10.018
7. Stentiford GD, Sritunyalucksana K, Flegel TW, Williams BAP, Withyachumnarnkul B, Itsathitphaisarn O, et al. New paradigms to help solve the global aquaculture disease crisis. *PloS Pathog* (2017) 13:e1006160. doi: 10.1371/journal.ppat.1006160
8. Ballesteros NA, Rodriguez Saint-Jean S, Perez-Prieto SII. Food pellets as an effective delivery method for a DNA vaccine against infectious pancreatic necrosis virus in rainbow trout (Oncorhynchus mykiss, Walbaum), Fish. Shellfish. *Immunol* (2014) 37:220–8. doi: 10.1016/j.fsi.2014.02.003
9. Hoare R, Jung S-J, Ngo TPH, Bartie KL, Thompson KD, Adams A. Efficacy of a polyvalent injectable vaccine against Flavobacterium psychrophilum administered to rainbow trout (Oncorhynchus mykiss L.). *J Fish Dis* (2018) 42:229–36. doi: 10.1111/jfd.12919
10. Skov J, Chettri JK, Jaafar RM, Kania PW, Dalsgaard I, Buchmann K. Effects of soluble immunostimulants on mucosal immune responses in rainbow trout immersion-vaccinated against Yersinia ruckeri. *Aquaculture* (2018) 492:237–46. doi: 10.1016/j.aquaculture.2018.04.011
11. Wangkahart E, Secombes CJ, Wang T. Dissecting the immune pathways stimulated following injection vaccination of rainbow trout (*Oncorhynchus mykiss*) against enteric redmouth disease (ERM). *Fish Shellfish Immun* (2019) 85:18–30. doi: 10.1016/j.fsi.2017.07.056

12. Collet B, Urquhart K, Monte M, Collins C, Perez SG, Secombes CJ, et al. Individual monitoring of immune response in Atlantic salmon Salmo salar following experimental infection with Infectious Salmon Anaemia Virus (ISAV). *PloS One* (2015) 10:e0137767. doi: 10.1371/journal.pone.0137767
13. Monte M, Urquhart K, Secombes CJ, Collet B. Individual monitoring of immune responses in rainbow trout after cohabitation and intraperitoneal injection challenge with Yersinia ruckeri. *Fish Shellfish Immun* (2016) 55:469–78. doi: 10.1016/j.fsi.2016.05.041
14. Anderson NL, Anderson NG. The Human Plasma Proteome: History, character, and diagnostic prospects. *Mol Cell Proteomics* (2002) 1:845–67. doi: 10.1074/mcp.R200007-MCP200
15. Veiseth-Kent E, Grove H, Færgestad EM, Fjæra SO. Changes in muscle and blood plasma proteomes of Atlantic salmon (*Salmo salar*) induced by crowding. *Aquaculture* (2010) 309:272–9. doi: 10.1016/j.aquaculture.2010.09.028
16. Braceland M, Bickerdike R, Tinsley J, Cockerill D, Mcloughlin MF, Graham DA, et al. The serum proteome of Atlantic salmon, Salmo salar, during pancreas disease (PD) following infection with salmonid alphavirus subtype 3 (SAV3). *J Proteomics* (2013) 94:423–36. doi: 10.1016/j.jprot.2013.10.016
17. Babaei F, Ramalingam R, Tavendale A, Liang Y, Yan LSK, Ajuh P, et al. Novel blood collection method allows plasma proteome analysis from single zebrafish. *J Proteome Res* (2013) 12:1580–90. doi: 10.1021/pr3009226
18. Nynca J, Arnold G, Fröhlich T, Ciereszko A. Proteomic identification of rainbow trout blood plasma proteins and their relationship to seminal plasma proteins. *Proteomics* (2017) 17:1600460. doi: 10.1002/pmic.201600460
19. Morro B, Doherty MK, Balseiro P, Handeland SO, MacKenzie S, Sveler H, et al. Plasma proteome profiling of freshwater and seawater life stages of rainbow trout (*Oncorhynchus mykiss*). *PloS One* (2020) 15:e0227003. doi: 10.1371/journal.pone.0227003
20. Aebersold R, Mann M. Mass spectrometry-based proteomics. *Nature* (2003) 422:198–207. doi: 10.1038/nature01511
21. Cox J, Neuhauser N, Michalski A, Scheltema RA, Olsen JV, Mann M. Andromeda: a peptide search engine integrated into the maxquant environment. *J Proteome Res* (2011) 10:1794–805. doi: 10.1021/pr101065j
22. Causey DR, Pohl MAM, Stead DA, Martin SAM, Secombes CJ, Macqueen DJ. High-throughput proteomic profiling of the fish liver following bacterial infection. *BMC Genomics* (2018) 19:719. doi: 10.1186/s12864-018-5092-0
23. Causey DR, Kim J-H, Stead DA, Martin SAM, Devlin RH, Macqueen DJ. Proteomic comparison of selective breeding and growth hormone transgenesis in fish: unique pathways to enhanced growth. *J Proteomics* (2019) 192:114–24. doi: 10.1016/j.jprot.2018.08.013
24. Tasumi S, Velikovsky CA, Xu G, Gai A, Wittrup KD, Flajnik MF, et al. High-affinity lamprey VLRA and VLRB monoclonal antibodies. *PNAS* (2009) 31:12891–6. doi: 10.1073/pnas.0505379103
25. De Genst E, Silence K, Decanniere K, Conrath K, Loris R, Kinne R, et al. Molecular basis for the preferential cleft recognition by dromedary heavy-chain antibodies. *PNAS* (2006) 103:4586–91. doi: 10.1073/pnas.0505379103
26. Dooley H, Flajnik MF. Shark immunity bites back: Affinity maturation and memory response in the nurse shark, Ginglymostoma cirratum. *Eur J Immunol* (2005) 35:936–45. doi: 10.1002/eji.200425760
27. Thuvander A, Fossum C, Lorenzen N. Monoclonal antibodies to salmonid immunoglobulin: characterization and applicability in immunoassays. *Dev Comp Immunol* (1990) 14:415–23. doi: 10.1016/0145-305X(90)90034-C
28. Cox J, Mann M. MaxQuant enables high peptide identification rates, individualized p.p.b.-range mass accuracies and proteome-wide protein quantification. *Nat Biotechnol* (2008) 26:1367–72. doi: 10.1038/nbt.1511
29. Pearse DE, Barson NJ, Nome T, Gao G, Campbell MA, Abadía-Cardoso A, et al. Sex-dependent dominance maintains migration supergene in rainbow trout. *Nat Ecol Evol* (2019) 3:1731–42. doi: 10.1038/s41559-019-1044-6
30. Beer LA, Pengyuan L, Ky B, Barnhart KT, Speicher DW. Efficient Quantitative comparisons of plasma proteomes using label-free analysis with MaxQuant. In: D Greening, R Simpson, editors. *Methods in molecular biology*, vol. 1619 . New York, NY: Humana Press (2017). p. 339–52. doi: 10.1007/978-1-4939-7057-5_23
31. Tyanova S, Temu T, Cox J. The MaxQuant computational platform for mass spectrometry-based shotgun proteomics. *Nat Protoc* (2016) 11:2301–2319. doi: 10.1038/nprot.2016.136
32. Cox J, Hein MY, Luber CA, Paron I, Nagaraj N, Mann M. Accurate proteome-wide label-free quantification by delayed normalization and maximal peptide ratio extraction, termed MaxLFQ. *Mol Cell Proteomics* (2014) 13:2513–26. doi: 10.1074/mcp.M113.031591
33. Stekhoven DJ, Bühlmann P. MissForest - non-parametric missing value imputation for mixed-type data. *Bioinformatics* (2012) 28:112–8. doi: 10.1093/bioinformatics/btr597
34. Wickham H. *ggplot2: elegant graphics for data analysis*. New York: Springer (2016).
35. Caraux G, Pinloche S. PermutMatrix: a graphical environment to arrange gene expression profiles in optimal linear order. *Bioinformatics* (2005) 21:1280–1. doi: 10.1093/bioinformatics/bti141
36. Szklarczyk D, Gable AL, Lyon D, Junge A, Wyder S, Huerta-Cepas J, et al. STRING v11: protein-protein association networks with increased coverage, supporting functional discovery in genome-wide experimental datasets. *Nucleic Acids Res* (2018) 47:607–13. doi: 10.1093/nar/gky1131
37. Ashburner M, Ball CA, Blake JA, Botstein D, Butler H, Cherry M, et al. Gene ontology: tool for the unification of biology. *Nat Genet* (2000) 25:25–29. doi: 10.1038/75556
38. Joshi-Tope G, Gillespie M, Vastrik I, d'Eustachio P, Schmidt E, de Bono B, et al. Reactome: a knowledgebase of biological pathways. *Nucleic Acids Res* (2005) 33:D428–32. doi: 10.1093/nar/gki072
39. Araujo FA, Barh DB, Silva A, Guimarães L, Ramos RTJ. GO FEAT: a rapid web-based functional annotation tool for genomic and transcriptomic data. *Sci Rep* (2018) 8:1–4. doi: 10.1038/s41598-018-20211-9
40. Macqueen DJ, Johnston IA. A well-constrained estimate for the timing of the salmonid whole genome duplication reveals major decoupling from species diversification. *Proc R Soc B* (2014) 281:20132881. doi: 10.1098/rspb.2013.2881
41. Berthelot C, Brunet F, Chalopin D, Juanchich A, Bernard M, Noël B, et al. The rainbow trout genome provides novel insights into evolution after whole-genome duplication in vertebrates. *Nat Commun* (2014) 5:1–10. doi: 10.1038/ncomms4657
42. Lien S, Koop BF, Sandve SR, Miller JR, Kent MP, Nome T, et al. The Atlantic salmon genome provides insights into rediploidization. *Nature* (2016) 533:200–5. doi: 10.1038/nature17164
43. Altschul SF, Gish W, Miller W, Myers EW, Lipman DJ. Basic local alignment search tool. *J Mol Biol* (1990) 215:403–10. doi: 10.1016/S0022-2836(05)80360-2
44. Thompson JD, Higgins DG, Gibson TJ. CLUSTAL W: improving the sensitivity of progressive multiple sequence alignment through sequence weighting, position-specific gap penalties and weight matrix choice. *Nucleic Acids Res* (1994) 22:4673–80. doi: 10.1093/nar/22.22.4673
45. Hall T. BioEdit: a user-friendly biological sequence alignment editor and analysis program for Windows 95/98/NT. *Nucleic Acids Symp Ser* (1999) 41:95–8. doi: 10.14601/Phytopathol_Mediterr-14998u1.29
46. Katoh K, Rozewicki J, Yamada KD. MAFFT online service: multiple sequence alignment, interactive sequence choice and visualization. *Brief Bioinform* (2019) 20:1160–1166. doi: 10.1093/bib/bbx108
47. Nguyen LT, Schmidt HA, von Haeseler A, Minh BQ. IQ-TREE: A fast and effective stochastic algorithm for estimating maximum-likelihood phylogenies. *Mol Biol Evol* (2015) 32:268–74. doi: 10.1093/molbev/msu300
48. Trifinopoulos J, Nguyen L-T, von Haeseler A, Minh BQ. W-IQ-TREE: a fast online phylogenetic tool for maximum likelihood analysis. *Nucleic Acids Res* (2016) 44:W232–W5. doi: 10.1093/nar/gkw256
49. Kalyaanamoorthy S, Minh BQ, Wong TKF, von Haeseler A, Jermiin LS. ModelFinder: fast model selection for accurate phylogenetic estimates. *Nat Methods* (2017) 14:587–9. doi: 10.1038/nmeth.4285
50. Hoang DT, Chernomor O, von Haeseler A, Minh BQ, Vinh LS. UFBoot2: Improving the ultrafast bootstrap approximation. *Mol Biol Evol* (2018) 35:518–22. doi: 10.1093/molbev/msx281
51. Kumar S, Stecher G, Li M, Knyaz C, Tamura K. MEGA X: Molecular Evolutionary Genetics Analysis across Computing Platforms. *Mol Biol Evol* (2018) 35:1547–9. doi: 10.1093/molbev/msy096
52. Roy S, Bag AK, Singh RK, Talmadge JE, Batra SK, Datta K. Multifaceted role of neuropilins in the immune system: potential targets for immunotherapy. *Front Immunol* (2017) 8:1228. doi: 10.3389/fimmu.2017.01228

53. Schellenburg S, Schulz A, Poitz DM, Muders MH. Role of neuropilin-2 in the Immune System. *Mol Immunol* (2017) 90:239–44. doi: 10.1016/j.molimm.2017.08.010
54. Boshra H, Li J, Sunyer O. Recent advances on the complement system of teleost fish. *Fish Shellfish Immun* (2005) 20:239–62. doi: 10.1016/j.fsi.2005.04.004
55. Gerwick L, Reynolds WS, Bayne CJ. A precerebellin-like protein is part of the acute phase response in rainbow trout, *Oncorhynchus mykiss*. *Dev Comp Immunol* (2017) 24:597–607. doi: 10.1016/S0145-305X(00)00016-1
56. Raida MK, Buchmann K. Innate immune response in rainbow trout (*Oncorhynchus mykiss*) against primary and secondary infections with *Yersinia ruckeri* O1. *Dev Comp Immunol* (2009) 33:35–45. doi: 10.1016/j.dci.2008.07.001
57. Saurabh S, Sahoo PK. Lysozyme: an important defence molecule of fish innate immune system. *Aquac Res* (2008) 39:223–39. doi: 10.1111/j.1365-2109.2007.01883.x
58. Niu D, Peatman E, Liu H, Lu J, Kucuktas H, Liu S, et al. Microfibrillar-associated protein 4 (MFAP4) genes in catfish play a novel role in innate immune responses. *Dev Comp Immunol* (2011) 35:568–79. doi: 10.1016/j.dci.2011.01.002
59. Gurney ME, Apatoff BR, Spear GT, Baumel MJ, Antel JP, Bania MB, et al. Neuroleukin: a lymphokine product of lectin-stimulated T cells. *Science* (1986) 234:574–81. doi: 10.1126/science.3020690
60. Morley SC. The actin-bundling protein L-plastin supports T-cell motility and activation. *Immunol Rev* (2013) 256:48–62. doi: 10.1111/imr.12102
61. Freeley M, O'Dowd F, Paul T, Kashanin D, Davies A, Kelleher D, et al. L-plastin regulates polarization and migration in chemokine-stimulated human T lymphocytes. *J Immunol* (2012) 188:6357–70. doi: 10.4049/jimmunol.1103242
62. Ganeshan K, Chawla A. Metabolic Regulation of Immune Responses. *Annu Rev Immunol* (2014) 32:609–34. doi: 10.1146/annurev-immunol-032713-120236
63. Liu W, Rodgers GP. Olfactomedin 4 expression and functions in innate immunity, inflammation, and cancer. *Cancer Metastasis Rev* (2016) 35:201–12. doi: 10.1007/s10555-016-9624-2
64. Lee CG, Da Silva CA, Dela Cruz CS, Ahangari F, Ma B, Kang M-J, et al. Role of chitin and chitinase/chitinase-like proteins in inflammation, tissue remodelling and injury. *Annu Rev Physiol* (2011) 73:479–501. doi: 10.1146/annurev-physiol-012110-142250
65. Zempleni J, Mock DM. Utilization of biotin in proliferating human lymphocytes. *J Nutr* (2000) 130:335S–7S. doi: 10.1093/jn/130.2.335S
66. Báez-Saldaña A, Díaz G, Espinoza B, Ortega E. Biotin deficiency induces changes in subpopulations of spleen lymphocytes in mice. *Am J Clin Nutr* (1998) 67:431–7. doi: 10.1093/ajcn/67.3.431
67. Li X-P, Sun L. A teleost complement factor Ba possesses antimicrobial activity and inhibits bacterial infection in fish. *Dev Comp Immunol* (2017) 71:49–58. doi: 10.1016/j.dci.2017.01.021
68. Wicher KB, Fries E. Haptoglobin, a hemoglobin-binding plasma protein, is present in bony fish and mammals but not in frog and chicken. *Proc Natl Acad Sci* (2006) 103:4168–73. doi: 10.1073/pnas.0508723103
69. Redmond AK, Ohta Y, Criscitiello MF, Macqueen DJ, Flajnik MF, Dooley H. Haptoglobin is a divergent MASP family member that neofunctionalized to recycle hemoglobin via CD163 in mammals. *J Immunol* (2018) 201:2483–2491. doi: 10.4049/jimmunol.1800508
70. Arredouani M, Matthijs P, Van Hoeyveld E, Kasran A, Baumann H, Ceuppens JL, et al. Haptoglobin directly affects T cells and suppresses T helper cell type 2 cytokine release. *Immunology* (2003) 108:144–51. doi: 10.1046/j.1365-2567.2003.01569.x
71. Arredouani MS, Kasran A, Vanoirbeek JA, Berger FG, Baumann H, Ceuppens JL. Haptoglobin dampens endotoxing-induced inflammatory effects both *in vitro* and *in vivo*. *Immunology* (2005) 114:263–71. doi: 10.1111/j.1365-2567.2004.02071.x
72. Li Y, Wright GL, Peterson JM. C1q/TNF-related protein 3 (CTRP3) Function and regulation. *Compr Physiol* (2107) 7:863–78. doi: 10.1002/cphy.c160044
73. Otis JP, Zeituni EM, Thierer JH, Anderson JL, Brown AC, Boehm ED, et al. Zebrafish as a model for apolipoprotein biology: comprehensive expression analysis and a role for ApoA-IV in regulating food intake. *Dis Model Mech* (2015) 8:295–309. doi: 10.1242/dmm.018754
74. Jaillon O, Aury J-M, Brunet F, Petit J-L, Stange-Thomann N, Mauceli E, et al. Genome duplication in the teleost fish *Tetraodon nigroviridis* reveals the early vertebrate proto-karyotype. *Nature* (2004) 431:946–57. doi: 10.1038/nature03025
75. Dominiczak MH, Caslake MJ. Apolipoproteins: metabolic role and clinical biochemistry applications, Ann. *Clin Biochem* (2011) 48:498–515. doi: 10.1258/acb.2011.011111
76. Kaji H. High-density lipoproteins and the immune system. *J Lipids* (2013) 2013:684903. doi: 10.1155/2013/684903
77. Wang W, Qu Q, Chen J. Identification, expression analysis, and antibacterial activity of Apolipoprotein A-I from amphioxus (Branchiostoma belcheri). *Comp Biochem Physiol B Biochem Mol Biol* (2019) 238:110329. doi: 10.1016/j.cbpb.2019.110329
78. Peterson MM, Mack JL, Hall PR, Alsup AA, Alexander SM, Sully EK, et al. Apolipoprotein B is an innate barrier against invasive *Staphylococcus aureus* infection. *Cell Host Microbe* (2008) 4:555–66. doi: 10.1016/j.chom.2008.10.001
79. Wurfel MM, Kunitake ST, Lichenstein H, Kane JP, Wright SD. Lipopolysaccharide (LPS)-binding protein is carried on lipoproteins and acts as a cofactor in the neutralization of LPS. *J Exp Med* (1994) 180:1025–35. doi: 10.1084/jem.180.3.1025
80. Concha MII, Smith VJ, Castro K, Bastías A, Romero A, Amthauer RJ. Apolipoproteins A-I and A-II are potentially important effectors of innate immunity in the teleost fish Cyprinus carpio. *Eur J Biochem* (2004) 271:2984–90. doi: 10.1111/j.1432-1033.2004.04228.x
81. Villarroel F, Bastías A, Casado A, Amthauer R, Concha M. Apolipoprotein A-I, an antimicrobial protein in *Oncorhynchus mykiss*: evaluation of its expression in primary defence barriers and plasma levels in sick and healthy fish. *Fish Shellfish Immun* (2007) 23:197–209. doi: 10.1016/j.fsi.2006.10.008
82. Johnston LD, Brown G, Gauthier D, Reece K, Kator H, van Veld P. Apolipoprotein A-I from striped bass (*Morone saxatilis*) demonstrates antibacterial activity in vitro. *Comp Biochem Phys B* (2008) 151:167–75. doi: 10.1016/j.cbpb.2008.06.011
83. Wei J, Gao P, Zhang P, Guo M, Xu M, Wei S, et al. Isolation and function analysis of apolipoprotein A-I gene response to virus infection in grouper. *Fish Shellfish Immun* (2015) 43:396–404. doi: 10.1016/j.fsi.2015.01.006
84. Pridgeon JW, Klesius PH. Apolipoprotein A1 in channel catfish: transcriptional analysis, antimicrobial activity, and efficacy as plasmid DNA immunostimulant against Aeromonas hydrophila infection. *Fish Shellfish Immun* (2013) 35:1129–37. doi: 10.1016/j.fsi.2013.07.028
85. Hyka N, Dayer J-M, Modoux C, Kohno T, Edwards III CK, Roux-Lombard P, et al. Apolipoprotein A-I inhibits the production of interleukin-1β and tumor necrosis factor-α by blocking contact-mediated activation of monocytes by T lymphocytes. *Blood* (2001) 97:2381–9. doi: 10.1182/blood.V97.8.2381
86. Wilhelm AJ, Zabalawi M, Owen JS, Shah D, Grayson JM, Major AS, et al. Apolipoprotein A-I modulates regulatory T Cells in autoimmune LDLr -/-, ApoA-I -/- Mice. *J Bio Chem* (2010) 285:36158–69. doi: 10.1074/jbc.M110.134130
87. Bonacina F, Coe D, Wang G, Longhi MP, Baragetti A, Moregola A, et al. Myeloid apolipoprotein E controls dendritic cell antigen presentation and T cell activation. *Nat Commun* (2018) 9:1–15. doi: 10.1038/s41467-018-05322-1
88. Brada N, Gordon MM, Wen J, Alpers DH. Transfer of cobalamin from intrinsic factor to transcobalamin II. *J Nutr Biochem* (2001) 12:200–6. doi: 10.1016/S0955-2863(00)00129-7
89. Benoit CR, Stanton AE, Tartanian AC, Motzer AR, McGaughey DM, Bond SR, et al. Functional and phylogenetic characterization of noncanonical vitamin B12-binding proteins in zebrafish suggests involvement in cobalamin transport. *J Biol Chem* (2018) 293:17606–21. doi: 10.1074/jbc.RA118.005323
90. Wong MK-S, Takei Y. Lack of plasma kallikrein-kinin system in teleosts. *PloS One* (2013) 8:e81057. doi: 10.1371/journal.pone.0081057
91. Chang C, Hu M, Zhu Z, Lo LJ, Chen J, Peng J. Liver-enriched gene 1a and 1b encode novel secretory proteins essential for normal liver development in zebrafish. *PloS One* (2011) 6:e22910. doi: 10.1371/journal.pone.0022910
92. Kaattari SL, Zhang HL, Khor IW, Kaattari IM, Shapiro DA. Affinity maturation in trout: Clonal dominance of high affinity antibodies late in the immune response. *Dev Comp Immunol* (2002) 26:191–200. doi: 10.1016/S0145-305X(01)00064-7
93. Cain KD, Jones DR, Raison RL. Antibody–antigen kinetics following immunization of rainbow trout (Oncorhynchus mykiss) with a T-cell dependent antigen. *Dev Comp Immunol* (2002) 26:181–90. doi: 10.1016/S0145-305X(01)00063-5
94. Costa G, Danz H, Kataria P, Bromage E. A holistic view of the dynamisms of teleost IgM: A case study of Streptococcus iniae vaccinated rainbow trout (Oncorhynchus mykiss). *Dev Comp Immunol* (2012) 36:298–305. doi: 10.1016/J.DCI.2011.04.011

95. Huang Q, Yang L, Luo J, Guo L, Wang Z, Yang XJ, et al. SWATH enables precise label-free quantification on proteome scale. *Proteomics* (2015) 15:1215–23. doi: 10.1002/pmic.201400270

Conflict of Interest: The authors declare that the research was conducted in the absence of any commercial or financial relationships that could be construed as a potential conflict of interest.

Copyright © 2020 Bakke, Monte, Stead, Causey, Douglas, Macqueen and Dooley. This is an open-access article distributed under the terms of the Creative Commons Attribution License (CC BY). The use, distribution or reproduction in other forums is permitted, provided the original author(s) and the copyright owner(s) are credited and that the original publication in this journal is cited, in accordance with accepted academic practice. No use, distribution or reproduction is permitted which does not comply with these terms.

frontiers in Immunology

ORIGINAL RESEARCH
published: 09 October 2020
doi: 10.3389/fimmu.2020.559555

Single-Cell Transcriptome Profiling of Immune Cell Repertoire of the Atlantic Cod Which Naturally Lacks the Major Histocompatibility Class II System

Naomi Croft Guslund[1,2]*, *Monica Hongrø Solbakken*[1], *Marine S. O. Brieuc*[1], *Sissel Jentoft*[1], *Kjetill S. Jakobsen*[1] *and Shuo-Wang Qiao*[2]*

[1] Centre for Ecological and Evolutionary Synthesis, Department of Biosciences, University of Oslo, Oslo, Norway,
[2] Department of Immunology, Institute of Clinical Medicine, University of Oslo, Oslo, Norway

OPEN ACCESS

Edited by:
Linsheng Song,
Dalian Ocean University, China

Reviewed by:
Jing Xing,
Ocean University of China, China
Jianmin Ye,
South China Normal University, China

***Correspondence:**
Naomi Croft Guslund
naomi.croft@gmail.com
Shuo-Wang Qiao
s.w.qiao@medisin.uio.no

Specialty section:
This article was submitted to Comparative Immunology, a section of the journal Frontiers in Immunology

Received: *06 May 2020*
Accepted: *16 September 2020*
Published: *09 October 2020*

Citation:
Guslund NC, Solbakken MH, Brieuc MSO, Jentoft S, Jakobsen KS and Qiao S-W (2020) Single-Cell Transcriptome Profiling of Immune Cell Repertoire of the Atlantic Cod Which Naturally Lacks the Major Histocompatibility Class II System. Front. Immunol. 11:559555. doi: 10.3389/fimmu.2020.559555

The Atlantic cod's unusual immune system, entirely lacking the Major Histocompatibility class II pathway, has prompted intriguing questions about what mechanisms are used to combat bacterial infections and how immunological memory is generated. By single-cell RNA sequencing we here report an in-depth characterisation of cell types found in immune tissues, the spleen and peripheral blood leukocytes of Atlantic cod. Unbiased transcriptional clustering revealed eleven distinct immune cell signatures. Resolution at the single cell level enabled characterisation of the major cell subsets including the cytotoxic T cells, B cells, erythrocytes, thrombocytes, neutrophils, and macrophages. Additionally, to our knowledge we are the first to uncover cell subsets in Atlantic cod which may represent dendritic cells, natural killer-like cells, and a population of cytotoxic cells expressing *GATA-3*, a master transcription factor of T helper 2 cells. We further identify putative gene markers for each cluster and describe the relative proportions of each cell type in the spleen and peripheral blood leukocytes. Of the major haematopoietic cell populations, the lymphocytes make up 55 and 68% of the spleen and peripheral blood leukocytes respectively, while the myeloid cells make up 45 and 32%. By single-cell analysis, this study provides the most detailed molecular and cellular characterisation of the immune system of the Atlantic cod so far.

Keywords: Atlantic cod (*Gadus morhua*), single-cell sequencing, *GATA-3*, immune system, gene marker

INTRODUCTION

Teleosts, accounting for nearly half of all extant vertebrates (1), demonstrate an extraordinary level of diversity within their habitat, morphology, physiology, behaviour, and in the genetic repertoire of their immune system (2–4). Whole genome sequencing of the Atlantic cod (*Gadus morhua*) and other Gadiform species revealed that genes encoding Major Histocompatibility class II (MHCII) were missing, along with the absence of the entire CD4+ T cell component of the adaptive immunity (5, 6). For the first time, it was demonstrated that this classical immune pathway can no longer be considered the hallmark

of vertebrate immunity (4, 6, 7). Why Atlantic cod and its relatives have lost the MHCII pathway is not known; however, several putative past biological scenarios have been suggested (4, 8). Additional peculiarities mark the Atlantic cod immune system, including extreme expansion of MHC class I (MHCI) genes as well as gene losses and expansions within the innate immune system (3, 5, 9, 10). Further, Atlantic cod studies have reported a low to modest response by specific antibodies following pathogen exposure but a consistently high level of natural IgM (11, 12). Since the Atlantic cod and codfishes demonstrate such an interesting immune system, understanding the workings of an immune system that naturally lacks CD4+ T cells is an evolutionary intriguing question, as well as providing insights into the flexibility of the vertebrate immune system. Moreover, a better grasp of the Atlantic cod immune system would also be beneficial for improved management of cod stock and potential cod aquaculture where infectious disease is a challenge (13, 14).

Traditionally, immune cells are characterised using the unique combination of cell markers present on the cell surface, but for non-model organisms a lack of specific antibody-based reagents makes this approach difficult. Advances in next-generation sequencing technologies allow for a closer examination of biological systems without the need for existing antibodies. The use of single-cell RNA sequencing (scRNA-seq) enables examination of the global mRNA content of thousands of individual cells, and thus facilitates a more detailed characterisation without the need of any pre-existing knowledge. Cell types can be clustered computationally using bioinformatic tools according to their transcriptional activity, and by analysing the transcriptional fingerprint in comparison to an annotated genome cell types and functions can be assigned (15).

A combination of microscopy and *in vitro* functional studies has already identified some immune cell types in Atlantic cod, while whole genome and transcriptome sequencing have led to the identification of putative cell markers. The functional assignment and cell markers of cytotoxic CD8+ T cells (CD8, TRGC1, TNFSF11, EOMES, TCR, CD3), B cells (IGLC2, IgM, CD79), natural killer (NK)-like cells (LITR/NITR, B3GAT1), cells with granules and perforin activities (PERF1, UNC13D), monocytes/macrophages (IL34), and neutrophils (MPO) have been described to some extent within the Atlantic cod (5, 16–19). Additional cell types found in the blood and organs of related teleost species might also be expected in the Atlantic cod, including thrombocytes (20), non-specific cytotoxic cells (NCCs) (21–23) and dendritic cells (DCs) (24, 25). However, the relative proportion of these verified and putative immune cell subsets and an overall assessment of the cellular functions are still lacking. Further, cell type characterisation by means of single-cell RNA sequencing will reveal candidate markers for each cell type which in turn could be used in the development of Atlantic cod antibodies.

In this study, we report an in-depth characterisation of cell types found in immune tissues and organs (*i.e.* spleen and blood) of Atlantic cod by using single-cell RNA sequencing. Gene expression profiling of over 8,000 individual peripheral blood leukocytes (PBLs) and spleen cells combined with conventional morphological microscope studies resulted in the characterisation of 13 distinct cell subsets, of which 11 are likely immune cell populations. Additionally, we identify putative gene markers for each of these cell clusters and provide for the first time, as far as we know, a systematic overview of the relative frequencies of these cell populations in the blood and spleen. Six major cell populations, including the T cells, B cells, erythrocytes, thrombocytes, neutrophils, and macrophages, are shown to make up 94 and 98% of haematopoietic cells in the spleen and PBLs respectively. From these six groups, the lymphocytes make up the majority of cells at 55 and 68% of the spleen and PBLs respectively, while the myeloid cells make up 45 and 32%. In addition, we describe less abundant cell populations which may represent dendritic cells and natural killer cells, as well as a population of cytotoxic cells expressing *GATA-3* which we propose to be a type of innate lymphocyte cell. Our study clearly demonstrates the power of using single-cell RNA sequencing for molecular and cellular characterisation of the immune system in non-model organisms and is a valuable resource for development of antibodies towards the specific Atlantic cod immune cell subsets for future functional studies.

METHODS AND MATERIALS

Atlantic Cod Sampling

The Atlantic cod specimens used in this study originate from the NOFIMA national breeding programme of Atlantic cod (Norway, Tromsø). They all come from one single breeding family (bred from one female and two males) and supplied as juveniles to the NIVA Research Facility at Solbergstrand (near Oslo), Norway where they were reared for approximately one year. The water temperature was kept at an average of 8°C (*e.g.* following the seasonality of the water temperature in this region), with salinity at 34 PSU, and the light conditions were 12:12 h light:dark (L:D) throughout the year. The fish were fed with Skretting cod pellets and checked twice a day. Blood and spleen samples were taken from two specimens of non-vaccinated, 2-year-old Atlantic cod; one male (fish 1, 47 cm, 0.99 kg) and one female (fish 2, 52 cm, 1.77 kg). Tissue sampling was conducted after the fish were killed, which took place within seconds of capture by cranial concussion. Neither fish showed visible signs of infection on skin, gills, fins or internally. Blood samples were collected from the *vena caudalis* with heparinised syringes. The spleens were removed and placed in Leibovitz L-15þ [L-15 (BioWhittaker) adjusted to 370 mOsm by adding 5% (v/v) of a solution consisting of 0.41 M NaCl, 0.33 M NaHCO3, and 0.66% (w/v) D-glucose] and transported on ice. Spleen cell suspensions were obtained by gently forcing the tissue through a cell strainer (Falcon, 100 µm). Blood samples of 0.7 ml were diluted in L-15þ to a total volume of 5 ml. The blood cell suspensions were placed on discontinuous Percoll gradients (3 ml 1.070 g/ml overlaid with 2.5 ml 1.050 g/ml) and centrifuged for 40 min at 400×g and 4°C. A peripheral blood leukocyte (PBL) fraction was collected from the interface of the two Percoll densities, including the downward density layer, and washed twice by diluting the

suspension in L-15þ and centrifuging at 300×g for 7 min at 4°C. All cells were kept in regular microcentrifuge tubes to minimise any cell loss and kept on ice at all times.

The rearing and sampling are performed according to animal welfare regulations and approved by the Norwegian authorities (FOTS ID 12336).

Sorting of Cell Populations by Flow Cytometry

Spleen, blood, and PBL suspensions were further separated into sub-populations on a FACS Aria II flow cytometer (Flow Cytometry Core facility at Oslo University Hospital) gated on the forward scatter (FSC, cell size) *vs* side scatter (SSC, granularity) plot. The sorted populations were examined by microscopy after cytospin and staining.

Staining of Sorted Cell Populations

Immediately after sorting, 10,000 cells in 15 µl PBS buffer were added to a Cytospin carrier and subjected to centrifugation onto glass slides (80 g for 3 min). Slides were then air-dried and stained either next day or stored at −20 C until fixation and staining. The slides were subjected to routine haematoxylin-eosin (HE) staining. In short, slides of cells were briefly stained with haematoxylin and then by eosin solution, followed by alcohol dehydration. Some cells were also stained for peroxidase activity with the iVIEW DAB detection kit (Roche) according to the manufacturer's instructions.

Cell Populations Sent for scRNA-Seq

An overview of the sample origin and the cell populations sent for scRNA-seq using the droplet based scRNA-sequencing (Drop-seq) protocol (15) can be seen in **Supplementary Table 1**. From fish 1 and fish 2, we sequenced unsorted spleen and sub-populations of potential interest from flow-sorted spleen (S3, containing a large myeloid cell population) and the blood (B1, containing a large lymphocyte population). In fish 2 we further extended our investigation into additional populations, including PBLs and flow-sorted populations from PBL: P1 (containing mostly lymphocytes), P2 (containing mostly lymphocytes and thrombocytes), and P3 (containing mostly myeloid cells).

scRNA-Seq With Drop-Seq

The protocol and reagents used closely followed the protocol written by the McCarroll laboratory, which is an amended version of the method used by Macosko et al., 2015. Briefly, the cell suspension was fed through a droplet generator (Dolomite, UK) that encapsulated a single cell and a barcoded bead in a water-in-oil droplet with a diameter of approximately 80 µm. All the beads contain a primer with a common "PCR handle" sequence to enable PCR amplification. Each individual bead contains 10^8 primers with the same "cell barcode" but also contains unique molecular identifiers (UMIs), thus enabling the transcripts to be digitally counted at a later stage. A 30-bp oligo dT sequence for the capture of mRNAs is incorporated at the end of the primer. When a cell and bead are enclosed in a droplet the cell is lysed and the poly-dT sequences capture the released mRNA, forming single-cell transcriptomes attached to microparticles (STAMPs). The STAMPs are reverse-transcribed to make cDNA, amplified, and barcoded fragments generated by Tn5-mediated tagmentation. During the post-tagmentation PCR, unique sample barcodes were introduced in the adaptor primers so that samples from different cell populations could be multiplexed in the same sequencing library.

Quantification of Genes

The libraries were sequenced at the Norwegian Sequencing Centre (Oslo University Hospital), on the NextSeq500 platform with a 75 bp kit, high output mode, with paired end reads. 20 bp was sequenced in Read 1 using a custom sequencing primer (GCCTGTCCGCGGAAGCAGTGGTATCAACGCAGAGTAC) and 60 bp in Read 2 with the regular Illumina sequencing primer. We used the Drop-seq Core Computational Protocol using STAR alignment to map the raw sequencing data to the most recent version of the Atlantic cod genome, gadMor3 (RefSeq accession GCF_902167405.1). A gene of interest, *GATA-3*, was present in gadMor2 (26) but missing in gadMor3, so the *GATA-3* gene sequence was manually added to the gadMor3 assembly fasta file. Reads were then grouped by cell barcode and the unique molecular identifiers (UMIs) for each gene counted, resulting in a digital expression matrix showing the number of transcripts per gene per cell. From each sample, reads from the first 600–5,000 STAMPs (depending on sample size) in decreasing number of reads were included into the next steps for filtering (**Supplementary Figure 2**). Further analysis was performed using R version 3.4.4.

Cell and Gene Selection

We followed the unsupervised clustering analysis tutorial (27) on the R package Seurat 3.0.2. The data matrix from all samples was merged to create one Seurat object. Cells with a gene count of fewer than 150 or a gene count of more than 1,500 and cells with a total number of molecules of more than 4,000 were filtered away in order to remove low-quality cells and possible cell multiplets (**Supplementary Figure 3**). By excluding genes expressed in less than five cells (among the cells having passed the quality control), 15,273 genes across 8,180 cells were used in the study. An overview of the sample origin, average mapping percentages, included cells, mapped transcripts and genes are shown in **Supplementary Table 1**.

Cell Clustering and Visualisation

After "LogNormalize" and scaling (with a scale factor 10,000), we ran a principal component analysis (PCA) on the expression of the top 2,000 variable genes. We then used the FindCluster function in Seurat in order to cluster cells based on a shared nearest neighbour (SNN) modularity optimisation result on the top 30 principal components (PCs) (**Supplementary Figure 4**). The resolution for clustering was 0.35. The cell clusters were visualised by the non-linear dimensional reduction method uniform manifold approximation and projection (UMAP).

Differentially Expressed Genes

All differential expression analyses in this study were performed using FindMarkers embedded in the Seurat package, which performs differential expression based on the non-parameteric Wilcoxon rank sum test. Adjusted p-values were calculated based on Bonferroni correction. In order to be counted as a differentially expressed gene, the gene must be expressed by a minimum of 25% of cells in the cluster. The most significantly differentially expressed genes for each cluster are listed in order of significance (**Supplementary Excel Sheet**).

Additional Data From Three Wild-Caught Cod

In addition, similar analyses were carried out on unsorted blood and spleen samples from three other Atlantic cod in pilot studies. These samples were taken from wild-caught Atlantic cod from Oslo fjord, taken by direct sampling alongside the project "Monitoring cod health in the inner Oslo fjord". Data from this pilot experiment accounts for an additional 15,758 genes across 3,744 cells (**Supplementary Excel Sheet** and **Supplementary Figure 5**).

RESULTS

Following stringent quality control filtering, we derived a gene expression matrix of 15,273 genes across 8,180 cells (**Supplementary Table 1**). Visualisation of cell types in two dimensions using Uniform Manifold Approximation and Projection (UMAP) (**Figure 1A**) reveals 13 cell clusters with distinct gene expression signatures, with cell cluster sizes ranging from 1,463 cells to the smallest cluster with only

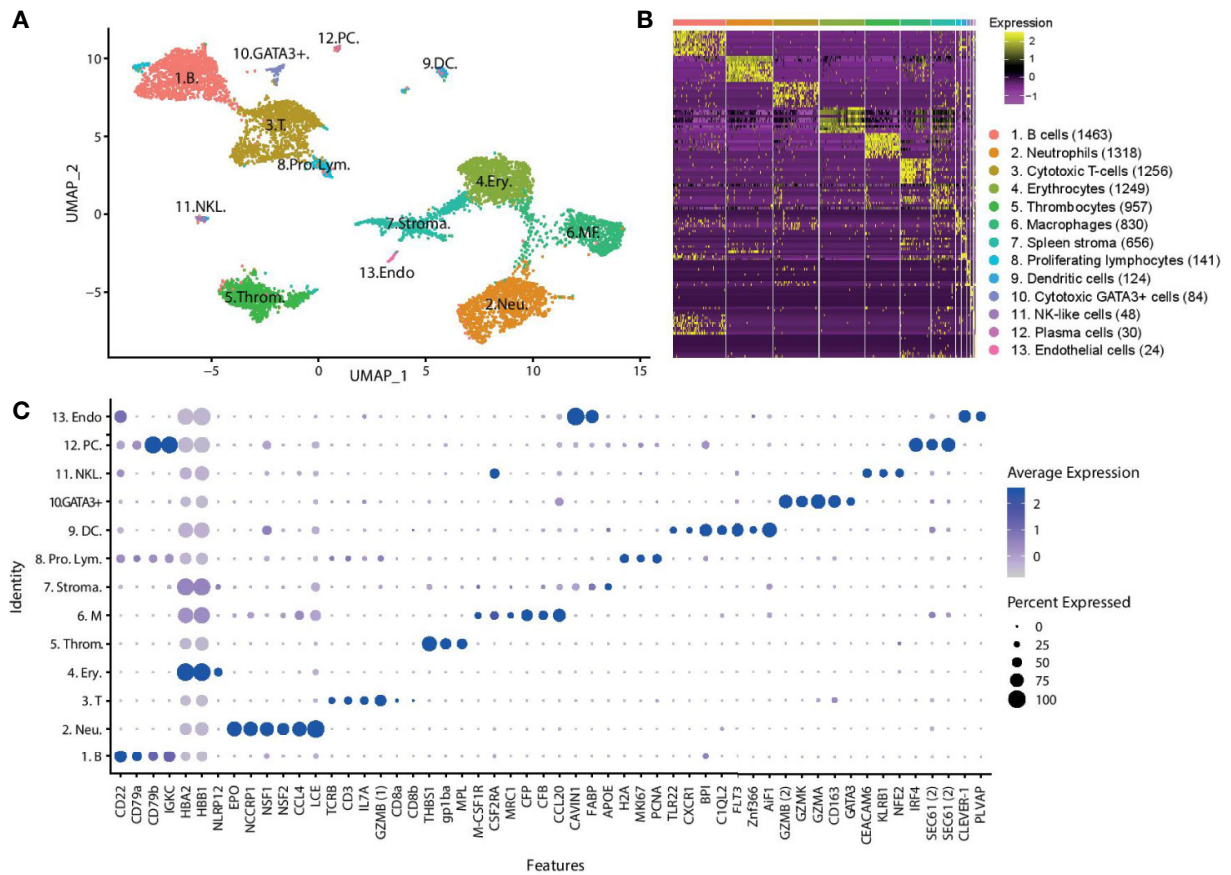

FIGURE 1 | Unsupervised clustering of transcriptomic profiles of Atlantic cod immune cells demonstrates distinct cell populations. **(A)** Visualisation of cell types in two dimensions using UMAP. Putative cell cluster labels are based upon the differential gene expression of known markers in mammals, overall expression pattern and microscopy. **(B)** Heatmap showing differential gene expression, with top 10 differentially expressed genes for each cluster shown (**Supplementary Excel Sheet**). Each row represents a gene, while each column represents a cell. The clusters are shown in descending population size, from B cells to endothelial cells respectively. The size of each cell population is shown in brackets. **(C)** Dot plot showing the putative marker genes across the cell clusters. The size of the dot encodes the percentage of cells within a cluster expressing the gene, while the colour intensity encodes the average expression level of 'expressing' cells. *Two *GZMB* and *SEC61* genes are identified (denoted $_1$ and $_2$ for clarity). **(Key)** 1. B. are B cells, 2. Neu. are neutrophils, 3. T. are T cells, 4. Ery. are erythrocytes, 5. Throm. are thrombocytes, 6. MΦ. are macrophages, 7. Stroma. are spleen stromal cells, 8. Pro. Lym. are proliferating lymphocytes, 9. DC. are dendritic cells, 10. GATA3+. are cytotoxic GATA3+ cells, 11. NKL. are natural-killer like cells, 12. PC. are plasma cells, 13. Endo. are endothelial cells.

24 cells. Overlapping distribution of cells from the two fish (**Supplementary Figure 6**) supports the robustness of the clusters. Additionally, the clusters formed (**Supplementary Figure 5**), and the top differentially expressed genes expressed by each cluster (**Supplementary Excel Sheet**), are similar to those produced in the pilot study.

To assign a cell identity to each cell cluster we performed differential gene expression analysis. Identified populations include a lymphocyte lineage, with B cells and plasma cells, T cells, cytotoxic GATA3$^+$ cells, and putative NK-like cells and a myeloid lineage that includes erythrocytes, thrombocytes, neutrophils, and macrophages (**Figure 1C**). A putative DC population is also described. Additionally, some cells have been classified as spleen stroma and endothelial cells.

The largest cell cluster was identified as the B cell population based on *CD22*, *CD79*, and immunoglobulin genes such as Immunoglobulin Kappa Constant (*IGKC*). A small population of B cells, also expressing immunoglobulin genes and *CD79*, were identified as plasma cells or plasmablasts due to the expression of the transcription factor interferon regulatory factor 4 (*IRF4*) which controls plasma cell differentiation (28). These cells also show high expression of the transport protein *SEC61*, which mediates the transport of proteins across the endoplasmic reticulum. The T cells express the classical T cell genes *TCR*, *CD3*, and Interleukin-7 receptor (*Il7r*). Expression of the cytotoxic protease granzyme B ($GZMB_1$) and CD8α and CD8β confirm this population as cytotoxic CD8$^+$ T cells. *CD8*α and *CD8*β are lowly expressed by only a small percentage of cells suggesting that the transcription of these genes may occur in short bursts, or there is a low cell surface expression level. A small group of lymphocytes were differentially clustered from the majority of T and B cells. These cells highly differentially expressed many histone genes, such as histone *H2A*, marker of proliferation Ki-67 (*MKI67*) and proliferating cell nuclear antigen (*PCNA*). This set of genes has greatest expression in actively proliferating cells, and we therefore named these cells proliferating lymphocytes. Some proliferating lymphocytes are more closely aligned to T cells (97 cells), while others are more closely aligned with the B cells (44 cells).

Two additional lymphocyte-related populations were found. Cluster 10, a rare population found in both the PBL and the spleen, is characterized by the expression of *GATA-3* and several cytotoxic enzymes, including granzyme (*GZM*) B_2, K, and A. *GATA-3* is a transcriptional activator that is shown to play a crucial role in the development of T cells, where it acts as a master regulator of T helper 2 (Th2) differentiation in mammalian species (29, 30), as well as a role in the maturation of innate lymphoid cells (31). We named this population cytotoxic GATA3+ cells.

The cluster labelled as NK-like cells express a somewhat unclear pattern of genes, and it is hard to confidently assign an identify based on classical mammalian markers. These cells differentially express carcinoembryonic antigen-related cell adhesion molecule 6 (*CEACAM6*), killer cell lectin-like receptor subfamily B (*KLRB1*), nuclear factor erythroid 2 (*NFE2*), Colony Stimulating Factor 2 Receptor Alpha Subunit (*CSF2RA*), and the *CD163* molecule. *CEACAM6* is involved in cell adhesion, *KLRB1* is a well-known NK receptor (32, 33), *NFE2* is a transcription factor, *CSF2RA* is a cytokine receptor, and *CD163* is a haemoglobulin scavenger receptor. Collectively, these markers have been affiliated with a range of mammalian cell populations including neutrophils, T cells, NK cells, macrophages, and granulocytes (34, 35). Considering the combined expression profile of these genes, we putatively have named them NK-like cells.

The neutrophils represent the second largest cell population and were identified by the expression of the cytotoxic genes eosinophil peroxidase (*EPO*) and non-specific cytotoxic cell receptor protein 1 (*NCCRP1*), genes involved in phagocytosis, neutrophil cytosolic factors 1 and 2 (*NSF1*, *NSF2*), and chemoattractant genes such as C-C motif chemokine 4 (*CCL4*). The gene classified as *EPO* has a sequence similar to both that of myeloperoxidase, the classic marker of neutrophils, and *EPO*. The most highly expressed gene of the neutrophils is low choriolytic enzyme (*LCE*), a proteolytic enzyme most commonly associated with egg hatching. Zebrafish neutrophils have been shown to express high choriolytic enzyme (*HCE*, also known as *nephrosin*) (36), a related protein with high sequence similarity.

Erythrocytes were identified by the high expression of multiple haemoglobin genes (*HBB*). Erythrocytes also expressed immune related genes, such as NACHT, LRR, and PYD domain-containing protein 12 (*NLRP12*), a potent mitigator of inflammation (37). Expression of thrombospondin-1 (*THBS1*), platelet glycoprotein Ib alpha chain (*GP1BA*), and thrombopoietin receptor (*MPL*) genes was used to identify the thrombocytes.

Macrophages were identified by the marker genes macrophage colony-stimulating factor 1 receptor (M-*CSF1R*), *CSF2RA*, and macrophage mannose receptor 1-like (*MRC1*). This cell population expresses many genes involved in the complement system, such as properdin (*CFP*) and complement factor B (*CFB*), and chemotactic genes, such as C-C motif chemokine 20 (*CCL20*).

Cluster 9 is a small population of cells found mostly in the spleen which express many innate immune genes including toll-like receptor 22 (*TLR22*), the chemokine receptor chemokine XC receptor 1 (*CXCR1*), bactericidal permeability-increasing proteins (*BPI*) and complement genes such as complement C1q-like protein 2 (*C1QL2*). We also observe the expression of the cytokine receptor fms like tyrosine kinase 3 (*FLT3*) and the transcription factor zinc finger 366 (*ZNF366*, also known as *DC-SCRIPT*), which have both been linked to differentiation of DCs in mammalian systems as well as in other teleost species (38). Another highly expressed gene in this cluster is allograft inflammatory factor 1 (*AIF1*), a gene which has recently been described in DCs (39). Based on these markers, we have putatively named cells in this cluster DCs.

The cells tentatively named spleen stromal cells express many genes involved in fat metabolism and tissue structure, such as caveolae-associated protein 1 (*CAVIN1*), fatty acid-binding protein (*FABP*), apolipoprotein E (*APOE*). These cells are almost exclusively found in the spleen (94%). The expression profile of these cells is not as clearly differentiated as other clusters, as demonstrated in the heatmap (**Figure 1B**), with a variable expression of genes also found in other clusters. It is possible this cluster of cells is not a 'true' cell population and is merely an artefact of ambient RNA captured by beads in empty

droplets. A small population of cells branching off from the spleen stroma, population 13, express markers for cell endothelium, including common lymphatic endothelial and vascular endothelial receptor-1 (*CLEVER-1*), a protein that is primarily expressed on high endothelial venules and lymphatic vessels (40) where it supports the adhesion and transmigration of lymphocytes (41), and plasmalemma vesicle associated protein (*PLVAP*), an endothelial cell-specific membrane protein (42).

The cells from the unsorted spleen and the PBL samples are found in each cell cluster (**Figure 2**). The largest cell population of the unsorted spleen sample are the spleen stroma cells (27%), classified within the 'other cells' in the pie chart, followed by the cytotoxic T cells (22%), the B cells (16%), and then the erythrocytes (13%). In the PBL sample, B cells are the largest cell population (42%), followed by the T cells (25%) and neutrophils (18%). Cells from the sorted spleen S3 sample are populated mostly by neutrophils (35%), macrophages (28%), and erythrocytes (26%). The sorted blood B1 sample contains mostly thrombocytes (34%) and erythrocytes (23%), followed by cytotoxic T cells (19%) and B cells (19%).

The six largest haematopoietic cell populations, including the T cells, B cells, erythrocytes, thrombocytes, neutrophils, and macrophages, make up 94 and 98% in the spleen and PBL respectively. From these major populations, the lymphocytes (including the B cells, plasma cells, T cells, and proliferating lymphocyte populations) make up the majority of immune cells at 55 and 68% of the spleen and PBL respectively, while the myeloid cells make up 45 and 32%.

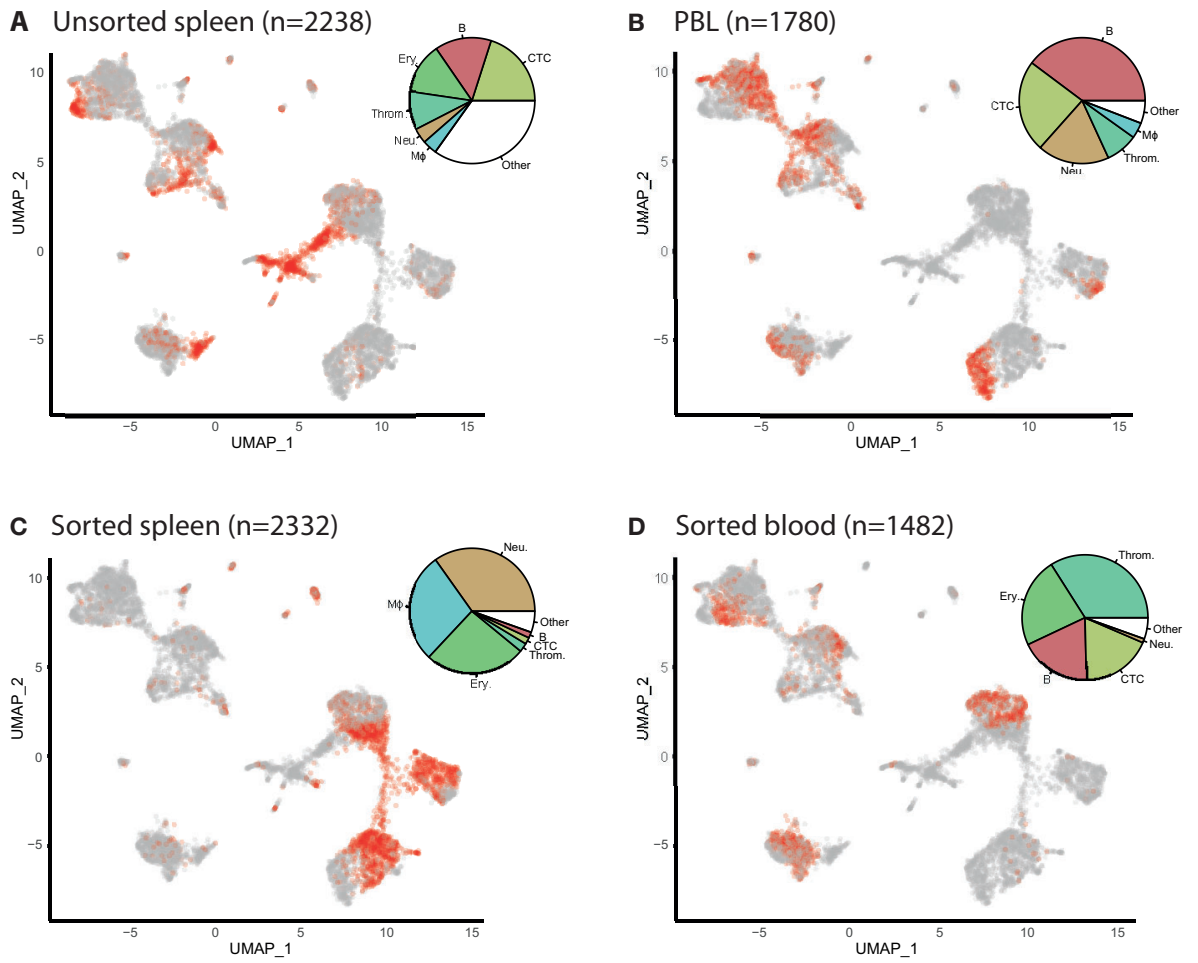

FIGURE 2 | UMAP feature plots show the distribution of cells from Atlantic cod unsorted spleen, peripheral blood leukocytes (PBLs) and flow sorted sub-populations. **(A)** Cells from unsorted spleen. **(B)** Cells from PBL. **(C)** Spleen cells which have been flow-sorted to contain mostly myeloid cells (S3). **(D)** Cells from the blood which have been flow-sorted to contain mostly lymphocytes and thrombocytes (B1). The number of cells per sample is given in brackets (n=). The cells from the named sample are shown in red. The pie charts show the distribution of each cell type in the sample. Resting and proliferating T cells are grouped together, whereas resting and proliferating B cells as well as plasma cells are grouped as B cells. **(Key)** 1. B. are B cells, 2. Neu. are neutrophils, 3. T. are T cells, 4. Ery. are erythrocytes, 5. Throm. are thrombocytes, 6. MΦ. are macrophages, 7. Stroma. are spleen stromal cells, 8. Pro. Lym. are proliferating lymphocytes, 9. DC. are dendritic cells, 10. GATA3+. are cytotoxic GATA3+ cells, 11. NKL. are natural-killer like cells, 12. PC. are plasma cells, 13. Endo. are endothelial cells.

Identification of cells by their transcriptional fingerprint is consistent with the characterisation of the major cell populations by microscopy (**Figure 3**). HE stained S3 sample, which was sorted as a relatively large and granulated population of spleen cells, revealed an apparent maturation of monocytes into macrophages, with a development from a lobed nucleus and few vacuoles to larger nuclei and more vacuoles. Vacuoles could also be seen in the erythrocytes, neutrophils, and in some of the lymphocytes, supporting previous assertations that these are phagocytic cell types. Peroxidase staining of S3 sample revealed peroxidase positive myeloid cells, the neutrophils, and some peroxidase negative myeloid cells, the monocytes/macrophages. The ratio of peroxidase positive and peroxidase negative myeloid cells observed in the S3 population is similar to the ratio of neutrophils and macrophages seen in **Figure 2**.

We next looked at the overall transcriptional activities of the different cell clusters (**Figure 4A**). The average number of transcripts per cell was noticeably high (1,915 transcripts per cell) in the plasma cell group, whereas it was markedly low in the thrombocyte cluster (<500 transcripts per cell). DCs and macrophages also demonstrate a high transcriptional activity (1,200–1,300 transcripts per cell). **Figure 4B** shows the differential expression of cathepsin genes (*CTSB* and *CTSL1*) and an Fc-receptor gene (*FCGR1a*) in these two cell types. MHCI expression is present in all of the cell types as expected; however, poor mapping has resulted in an inconclusive pattern across the cell clusters (**Supplementary Figure 7**).

DISCUSSION

Despite its lack of MHC-II and CD4+ T cells, the Atlantic cod is able to mount a protective and specific immunity after vaccination (12, 43–46). Interestingly, this protective immunity is poorly correlated with specific antibody responses (46, 47). Indeed, based on these and other molecular observations, it was hypothesised that cod could lack functional MHCII molecules (48) before it was definitely shown by the first assembly of the Atlantic cod genome (5). Despite major genetic losses within the CD4+ pathway and the limited response of specific antibody upon immunisation, in its natural environment cod is not particularly prone to infectious diseases (48). How cod fights bacterial infections and how it acquires immunological memory are puzzling questions that are both interesting biologically and important practically for the cod aquaculture industries. With the near complete lack of antibody-based reagents and immortalised cod immune cell lines these mechanisms have not been fully understood, although some insights have been gained by genome data and transcriptome analyses at the whole organism or organ level (18, 19). To find the exact immune cell composition and the steady-state gene expression of each cell subset is the first step toward a more detailed molecular mapping of the cod immune system.

This study presents an overview of the immune cells found in the Atlantic cod peripheral blood and spleen, using single-cell RNA sequencing and microscopy of both unfractionated and sorted cell populations based on size and granularity. By using unbiased clustering of global transcriptomics, we find 13 different cell populations, with cell identity assigned to these populations based on their unique transcriptional profiles compared with known profiles from mammalian systems. Given the limited number of genes detected in each cell, we restricted our analyses to assign cell population identities, without a more in-depth exploration of the cellular functions of these cell subsets. We identified the most well-known major cell populations such as: the cytotoxic T cells, B cells, erythrocytes, thrombocytes, neutrophils, and macrophages. Overall, these six major cell populations make up 94 and 98% of haematopoietic cells in the spleen and PBL respectively. In the lymphoid lineage, we identified sub-populations of both B and T cells that are actively dividing. In addition, we identified

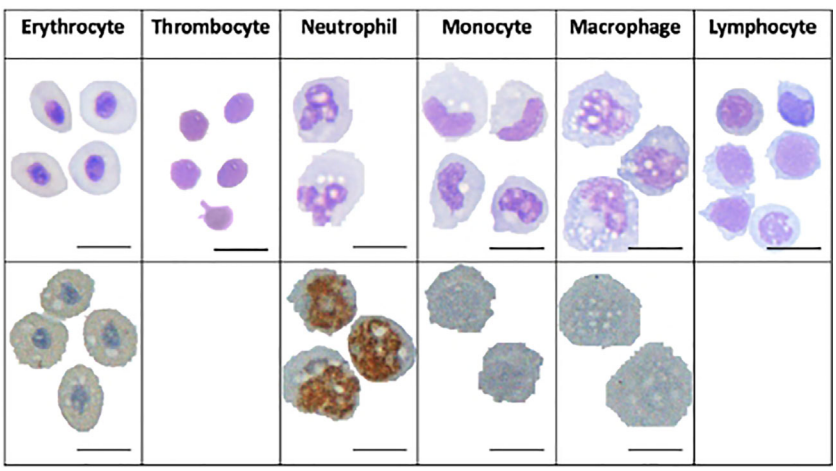

FIGURE 3 | Microscopy images of Atlantic cod immune cells. Cells in the top panel are HE-stained and the cells in the bottom panel are stained with peroxidase. Scale bars 10 μm.

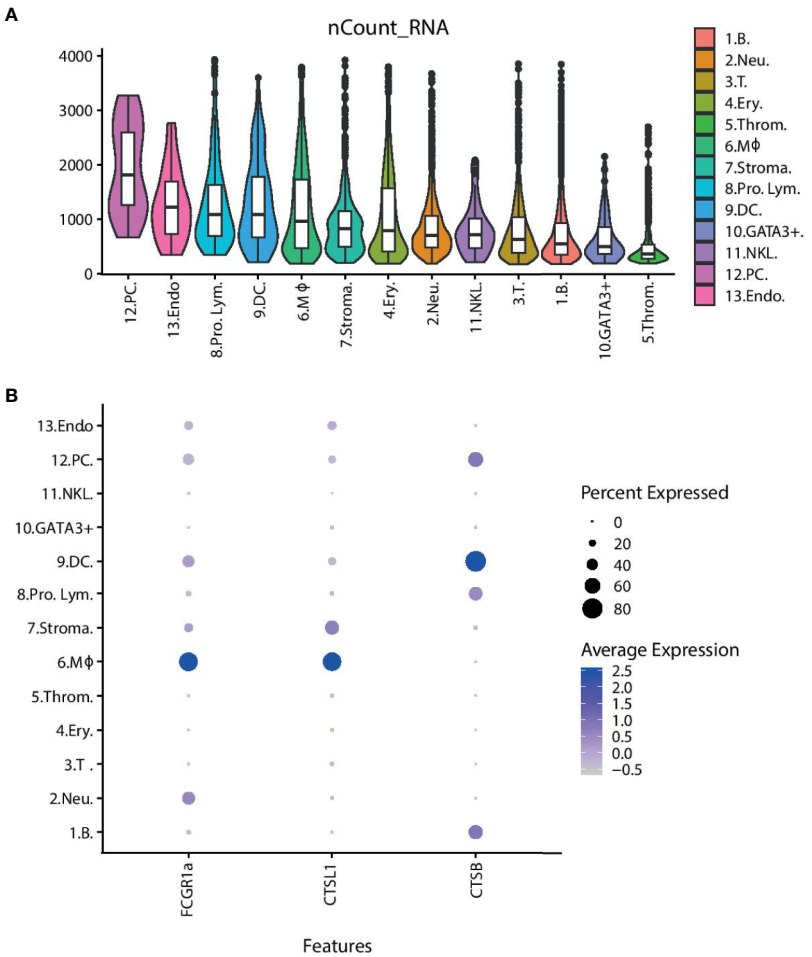

FIGURE 4 | The overall transcriptional activity of each cell type and differential expression of selected genes. **(A)** Violin plots showing the average number of transcripts per cell within the cluster. The overlaid boxplots show the mean and the 25 and 75% percentile of transcripts. **(B)** Dot plot showing the expression of selected genes across the cell clusters. The size of the dot displays the percentage of cells within a class expressing the gene, while the colour intensity encodes the average expression level of 'expressing' cells. **(Key)** 1. B. are B cells, 2. Neu. are neutrophils, 3. T. are T cells, 4. Ery. are erythrocytes, 5. Throm. are thrombocytes, 6. MΦ. are macrophages, 7. Stroma. are spleen stromal cells, 8. Pro. Lym. are proliferating lymphocytes, 9. DC. are dendritic cells, 10. GATA3+. are cytotoxic GATA3+ cells, 11. NKL. are natural-killer like cells, 12. PC. are plasma cells, 13. Endo. are endothelial cells.

plasma cells as a separate subset in Atlantic cod, supporting previous findings where the presence of plasma cells was suggested by *in situ* hybridisation with immunoglobulin probes (49). To note, a small subset of cells in this cluster were from PBL samples, therefore it is possible that this cluster also contains plasmablasts. Terminally differentiated plasma cells are rarely found in circulation, unlike the more immature plasmablasts (50). This data indicates that Atlantic cod B cells have the capability of end-differentiation into plasma cells despite the lack of CD4+ T helper cells. Future studies are needed to clarify the signalling pathways that are involved in B cell differentiation in cod.

Besides erythrocytes and thrombocytes, based on the top differentially expressed genes, we could clearly delineate the two major phagocytic and cytotoxic subsets within the myeloid lineage; namely macrophages and neutrophils. In mammalian systems, macrophages are important producers of cytokines as well as being antigen-presenting cells, especially in the spleen and lymph nodes (51). However, we could only find a handful of chemokines and no cytokine transcripts in our data. The low sensitivity of detecting transcript for single gene in any given single cell, combined with cytokines being expressed in short bursts only upon activation (52), could explain this particular pattern in our study.

The average number of transcripts that a cell cluster expresses may indicate, with a broad brushstroke, how active the cells are in steady state. Cells which are producing a lot of proteins, proliferating or carrying out multiple tasks, for example phagocytosis and antigen presentation, may be expected to have a higher transcript count than cell populations with fewer "tasks". Unsurprisingly plasma cells are the most transcriptionally active cell population, with an average transcript count of 1,915 detected

transcripts, as this population of cells will be actively producing antibodies. The erythrocytes, neutrophils, NK-like cells, T cells, B cells, and cytotoxic GATA3+ cells have medium levels of transcriptional activity, with approximately 650–1,070 transcripts per cell. These levels represent most likely the steady-state transcriptional activity. The low level of transcriptional activity in thrombocytes is in accordance with the largely absent cytoplasm of these cells. Meanwhile, the DCs and macrophages have a recorded transcript number of roughly 1,200–1,300 per cell. A higher transcript number in these cells compared to the other known phagocytes—the neutrophils, erythrocytes, and B cells—suggest that they may have additional tasks. The macrophages and the DCs are shown to express cathepsin genes (*CTSB* and *CTSL1*) and high affinity immunoglobulin gamma Fc receptor I A (*FCGR1a*). The gene annotation of *FCGR1a* is somewhat misleading since teleost does not have IgG (53). However, as the annotation is based on sequence similarity to annotated genes in other organisms, it is more likely that this gene represents an Ig-Fc binding receptor that could play a role in antibody-mediated uptake of antigens. Cathepsin B and L1 are lysosomal cysteine proteases that play a major role in catabolism of proteins and thus a function in the processing and presentation of antigens *via* MHC (54, 55). The expression of genes involved in antigen presentation coupled with a high transcript number suggests the DCs and the macrophages may act as antigen presenting cells (APCs) in the Atlantic cod. It would be interesting to see if MHCI gene expression is higher in these cell populations and if the expression increases following immune challenge. An initial analysis of MHCI expression in our data is inconclusive, mainly due to the low mapping efficiency. Dedicated efforts using longer reads and tailored bioinformatical tools that can deal with the complexities of MHCI are needed.

Interestingly, the Atlantic cod has evolved MHCI expansion and an unusual repertoire of TLR receptors (3, 5). In addition, novel combination of endosomal sorting motifs was suggested to facilitate a more versatile use of MHCI through cross-presentation and a potential MHCII-like functionality (5, 56). Whether the Atlantic cod is able to mount a cellular immune response that functionally resembles the T helper cells is unknown and remains an intriguing issue for the large group of Gadiform species—all lacking MHCII (6). In our data, the expression of *GATA-3* in a small subset of cells, with an expression profile that indicates close resemblance to the cytotoxic T cells, is an interesting finding. *GATA-3* has been identified and isolated from several species of teleost fish, including zebrafish (57), carp (58), salmonids (59), and in Atlantic cod (60). *GATA-3* expression was detected in surface-IgM-negative lymphocytes in carp (61). Interestingly, the expression of *GATA-3* in Atlantic cod was shown to be increased following stimulation by the T cell-stimulant phorbol 12-myristate 13-acetate (PMA) (60), suggesting the presence of *GATA-3* in activated T cells. In mammals, the transcription factor *GATA-3* plays an essential role in CD4+ T cell development and survival and is necessary for the differentiation of naive CD4+ T cells to T helper (Th) 2 cells (62–64). However, classical T helper cells are absent in Atlantic cod, and this cytotoxic GATA3$^+$ cluster lacks the cytotoxic T cell markers that was demonstrated in our data-set (*TCR*, *CD3*, *Il7r*, *GZMB*$_1$, *CD8α* and *CD8β*), suggesting that this population may belong to a different lineage than T cells. In mammals *GATA-3* is also central to the development of innate lymphoid cells (ILCs), chiefly the ILC2 lineage (34, 65). Recently, it was shown that *GATA-3* expression was also important for ILC2 in zebrafish (66). ILC2 cells are also known as innate helper 2 cells (67) based on similar cytokine secretion profile. Thus, in summary, the cells described here possibly represent a form of helper ILC. At the same time, these cells also show granzyme expression; indicating possible dual cytotoxic and helper functions. Future studies should look into how this small but intriguing cell subset behaves during immune perturbation, such as immunisation and infection.

In conclusion, using state-of-the-art single-cell sequencing technology on a non-model system, we performed a detailed molecular and cellular characterisation of the Atlantic cod immune system. In addition to describing in more detail the major cell subsets, we also describe for the first time in Atlantic cod, as far as we know, cells that may represent dendritic cells, natural killer-like cells and innate lymphoid cells, as well as suggest that macrophages and dendritic cells may act as antigen presenting cells. Further functional characterisation of these cells is needed to delineate their role in antigen presentation. This work provides an expression profile baseline of the Atlantic cod in a steady state, which lays a foundation for future work with immune system challenge experiments. Future challenge experiments may show how the different cod immune cell subsets respond to immunological challenge, in particular whether the GATA3+ cells could be involved in the B-cell differentiation process. The acquired knowledge will be highly beneficial for the development of antibodies towards cod-specific cell markers, our understanding of alternative vertebrate immune systems and potentially aid cod aquaculture and stock management.

DATA AVAILABILITY STATEMENT

The sequencing data is available at the ENA repository with project number PRJEB39706.

ETHICS STATEMENT

The rearing and sampling are performed according to animal welfare regulations and approved by the Norwegian authorities (FOTS ID 12336).

AUTHOR CONTRIBUTIONS

NG—Data collection and analysis and writing of paper. MS and MB—Data analysis and paper review. SJ and KJ—Intellectual contribution to direction of study and paper review. S-WQ—Intellectual contribution to direction of study, data collection and writing of the paper. All authors contributed to the article and approved the submitted version.

FUNDING

This study was funded by the University of Oslo.

ACKNOWLEDGMENTS

We thank Kjetil Hylland for providing cod, Ole Tørresen for bioinformatic support and Espen Bækkevold for help with histology. This manuscript has been released as a pre-print at bioRxiv, Single-cell transcriptome profiling of the Atlantic cod immune system Naomi Guslund, Monica Hongrø Solbakken, Kjetill S. Jakobsen, Shuo-Wang Qiao bioRxiv 2020.01.31.926410; doi: https://doi.org/10.1101/2020.01.31.926410.

SUPPLEMENTARY MATERIAL

The Supplementary Material for this article can be found online at: https://www.frontiersin.org/articles/10.3389/fimmu.2020.559555/full#supplementary-material

REFERENCES

1. Ravi V, Venkatesh B. The Divergent Genomes of Teleosts. *Annu Rev Anim Biosci* (2018) 6:47–68. doi: 10.1146/annurev-animal-030117-014821
2. Zhu LY, Nie L, Zhu G, Xiang LX, Shao JZ. Advances in research of fish immune-relevant genes: a comparative overview of innate and adaptive immunity in teleosts. *Dev Comp Immunol* (2013) 39(1-2):39–62. doi: 10.1016/j.dci.2012.04.001
3. Solbakken MH, Torresen OK, Nederbragt AJ, Seppola M, Gregers TF, Jakobsen KS, et al. Evolutionary redesign of the Atlantic cod (Gadus morhua L.) Toll-like receptor repertoire by gene losses and expansions. *Sci Rep* (2016) 6:25211. doi: 10.1038/srep25211
4. Solbakken MH, Voje KL, Jakobsen KS, Jentoft S. Linking species habitat and past palaeoclimatic events to evolution of the teleost innate immune system. *P Roy Soc B-Biol Sci* (2017) 284(1853):20162810. doi: 10.1098/rspb.2016.2810
5. Star B, Nederbragt AJ, Jentoft S, Grimholt U, Malmstrøm M, Gregers TF, et al. The genome sequence of Atlantic cod reveals a unique immune system. *Nature* (2011) 477:207–10. doi: 10.1038/nature10342
6. Malmstrom M, Matschiner M, Torresen OK, Star B, Snipen LG, Hansen TF, et al. Evolution of the immune system influences speciation rates in teleost fishes. *Nat Genet* (2016) 48(10):1204–10. doi: 10.1038/ng.3645
7. Parham P. How the codfish changed its immune system. *Nat Genet* (2016) 48 (10):1103–4. doi: 10.1038/ng.3684
8. Star B, Jentoft S. Why does the immune system of Atlantic cod lack MHC II? *Bioessays* (2012) 34(8):648–51. doi: 10.1002/bies.201200005
9. Solbakken MH, Rise ML, Jakobsen KS, Jentoft S. Successive Losses of Central Immune Genes Characterize the Gadiformes' Alternate Immunity. *Genome Biol Evol* (2016) 8(11):3508–15. doi: 10.1093/gbe/evw250
10. Torresen OK, Brieuc MSO, Solbakken MH, Sorhus E, Nederbragt AJ, Jakobsen KS, et al. Genomic architecture of haddock (Melanogrammus aeglefinus) shows expansions of innate immune genes and short tandem repeats. *BMC Genomics* (2018) 19(1):240. doi: 10.1186/s12864-018-4616-y
11. Solem ST, Stenvik J. Antibody repertoire development in teleosts—a review with emphasis on salmonids and Gadus morhua L. *Dev Comp Immunol* (2006) 30(1):57–76. doi: 10.1016/j.dci.2005.06.007
12. Magnadottir B, Gudmundsdottir S, Gudmundsdottir BK, Helgason S. Natural antibodies of cod (Gadus morhua L.): Specificity, activity and affinity. *Comp Biochem Phys B* (2009) 154(3):309–16. doi: 10.1016/j.cbpb.2009.07.005
13. Murray AG, Peeler EJ. A framework for understanding the potential for emerging diseases in aquaculture. *Prev Vet Med* (2005) 67(2-3):223–35. doi: 10.1016/j.prevetmed.2004.10.012
14. Bostock J, McAndrew B, Richards R, Jauncey K, Telfer T, Lorenzen K, et al. Aquaculture: global status and trends. *Philos Trans R Soc Lond B Biol Sci* (2010) 365(1554):2897–912. doi: 10.1098/rstb.2010.0170
15. Macosko EZ, Basu A, Satija R, Nemesh J, Shekhar K, Goldman M, et al. Highly Parallel Genome-wide Expression Profiling of Individual Cells Using Nanoliter Droplets. *Cell* (2015) 161(5):1202–14. doi: 10.1016/j.cell.2015.05.002
16. Fischer U, Utke K, Somamoto T, Köllner B, Ototake M, Nakanishi T. Cytotoxic activities of fish leucocytes. *Fish Shellfish Immun* (2006) 20 (2):209–26. doi: 10.1016/j.fsi.2005.03.013
17. Øverland HS, Pettersen EF, Rønneseth A, Wergeland HI. Phagocytosis by B-cells and neutrophils in Atlantic salmon (Salmo salar L.) and Atlantic cod (Gadus morhua L.). *Fish Shellfish Immun* (2010) 28(1):193–204. doi: 10.1016/j.fsi.2009.10.021
18. Solbakken MH, Jentoft S, Reitan T, Mikkelsen H, Gregers TF, Bakke O, et al. Disentangling the immune response and host-pathogen interactions in Francisella noatunensis infected Atlantic cod. *Comp Biochem Phys D* (2019a) 30:333–46. doi: 10.1016/j.cbd.2019.04.004
19. Solbakken MH, Jentoft S, Reitan T, Mikkelsen H, Jakobsen KS, Seppola M. Whole transcriptome analysis of the Atlantic cod vaccine response reveals subtle changes in adaptive immunity. *Comp Biochem Phys D* (2019b) 31:100597. doi: 10.1016/j.cbd.2019.100597
20. Nagasawa T, Nakayasu C, Rieger AM, Barreda DR, Somamoto T, Nakao M. Phagocytosis by Thrombocytes is a Conserved Innate Immune Mechanism in Lower Vertebrates. *Front Immunol* (2014) 5:445. doi: 10.3389/fimmu.2014.00445
21. Evans DL, Leary JH3rd, Jaso-Friedmann L. Nonspecific cytotoxic cell receptor protein-1: a novel (predicted) type III membrane receptor on the teleost equivalent of natural killer cells recognizes conventional antigen. *Cell Immunol* (1998) 187(1):19–26. doi: 10.1006/cimm.1998.1310
22. Shen L, Stuge TB, Zhou H, Khayat M, Barker KS, Quiniou SM, et al. Channel catfish cytotoxic cells: a mini-review. *Dev Comp Immunol* (2002) 26(2):141–9. doi: 10.1016/S0145-305X(01)00056-8
23. Shen L, Stuge TB, Bengten E, Wilson M, Chinchar VG, Naftel JP, et al. Identification and characterization of clonal NK-like cells from channel catfish (Ictalurus punctatus). *Dev Comp Immunol* (2004) 28(2):139–52. doi: 10.1016/S0145-305X(03)00119-8
24. Lugo-Villarino G, Balla KM, Stachura DL, Banuelos K, Werneck MB, Traver D. Identification of dendritic antigen-presenting cells in the zebrafish. *Proc Natl Acad Sci U S A* (2010) 107(36):15850–5. doi: 10.1073/pnas.1000494107
25. Bassity E, Clark TG. Functional identification of dendritic cells in the teleost model, rainbow trout (Oncorhynchus mykiss). *PLoS One* (2012) 7(3):e33196. doi: 10.1371/journal.pone.0033196
26. Torresen OK, Star B, Jentoft S, Reinar WB, Grove H, Miller JR, et al. An improved genome assembly uncovers prolific tandem repeats in Atlantic cod. *BMC Genomics* (2017) 18(1):95. doi: 10.1186/s12864-016-3448-x
27. Butler A, Hoffman P, Smibert P, Papalexi E, Satija R. Integrating single-cell transcriptomic data across different conditions, technologies, and species. *Nat Biotechnol* (2018) 36(5):411–20. doi: 10.1038/nbt.4096
28. Klein U, Casola S, Cattoretti G, Shen Q, Lia M, Mo T, et al. Transcription factor IRF4 controls plasma cell differentiation and class-switch recombination. *Nat Immunol* (2006) 7(7):773–82. doi: 10.1038/ni1357
29. Lee GR, Fields PE, Flavell RA. Regulation of IL-4 Gene Expression by Distal Regulatory Elements and GATA-3 at the Chromatin Level. *Immunity* (2001) 14(4):447–59. doi: 10.1016/S1074-7613(01)00125-X
30. Yagi R, Zhu J, Paul WE. An updated view on transcription factor GATA3-mediated regulation of Th1 and Th2 cell differentiation. *Int Immunol* (2011) 23(7):415–20. doi: 10.1093/intimm/dxr029
31. Tindemans I, Serafini N, Di Santo JP, Hendriks RW. GATA-3 Function in Innate and Adaptive Immunity. *Immunity* (2014) 41(2):191–206. doi: 10.1016/j.immuni.2014.06.006
32. Bennett IM, Zatsepina O, Zamai L, Azzoni L, Mikheeva T, Perussia B. Definition of a natural killer NKR-P1A(+)/CD56(-)/CD16(-) functionally immature human NK cell subset that differentiates in vitro in the presence of interleukin 12. *J Exp Med* (1996) 184(5):1845–56. doi: 10.1084/jem.184.5.1845

33. Konjevic G, Martinovic KM, Vuletic A, Jurisic V, Spuzic I. Distribution of Several Activating and Inhibitory Receptors on CD3(-)CD16(+) NK Cells and Their Correlation with NK Cell Function in Healthy Individuals. *J Membrane Biol* (2009) 230(3):113–23. doi: 10.1007/s00232-009-9191-3
34. Lanier LL, Chang CW, Phillips JH. Human Nkr-P1a - a Disulfide-Linked Homodimer of the C-Type Lectin Superfamily Expressed by a Subset of Nk and T-Lymphocytes. *J Immunol* (1994) 153(6):2417–28.
35. Skubitz KM, Skubitz AP. Interdependency of CEACAM-1, -3, -6, and -8 induced human neutrophil adhesion to endothelial cells. *J Transl Med* (2008) 6:78. doi: 10.1186/1479-5876-6-78
36. Di Q, Lin Q, Huang Z, Chi Y, Chen X, Zhang W, et al. Zebrafish nephrosin helps host defence against Escherichia coli infection. *Open Biol* (2017) 7 (8):170040. doi: 10.1098/rsob.170040
37. Normand S, Waldschmitt N, Neerincx A, Martinez-Torres RJ, Chauvin C, Couturier-Maillard A, et al. Proteasomal degradation of NOD2 by NLRP12 in monocytes promotes bacterial tolerance and colonization by enteropathogens. *Nat Commun* (2018) 9(1):5338. doi: 10.1038/s41467-018-07750-5
38. Zoccola E, Delamare-Debouteville J, Barnes AC. Identification of Barramundi (Lates calcarifer) DC-SCRIPT, a Specific Molecular Marker for Dendritic Cells in Fish. *PLoS One* (2015) 10(7):e0132687. doi: 10.1371/journal.pone.0132687
39. Elizondo DM, Andargie TE, Yang DZ, Kacsinta AD, Lipscomb MW. Inhibition of Allograft Inflammatory Factor-1 in Dendritic Cells Restrains CD4(+) T Cell Effector Responses and Induces CD25(+)Foxp3(+) T Regulatory Subsets. *Front Immunol* (2017) 8:1402. doi: 10.3389/fimmu.2017.01502
40. Irjala H, Elima K, Johansson EL, Merinen M, Kontula K, Alanen K, et al. The same endothelial receptor controls lymphocyte traffic both in vascular and lymphatic vessels. *Eur J Immunol* (2003) 33(3):815–24. doi: 10.1002/eji.200323859
41. Salmi M, Koskinen K, Henttinen T, Elima K, Jalkanen S. CLEVER-1 mediates lymphocyte transmigration through vascular and lymphatic endothelium. *Blood* (2004) 104(13):3849–57. doi: 10.1182/blood-2004-01-0222
42. Stan RV. Endothelial stomatal and fenestral diaphragms in normal vessels and angiogenesis (vol 11, pg 621, 2007). *J Cell Mol Med* (2008) 12(1):355–60. doi: 10.1111/j.1582-4934.2007.00075.x
43. Lund V, Bordal S, Schroder MB. Specificity and durability of antibody responses in Atlantic cod (Gadus morhua L.) immunised with Vibrio anguillarum O2b. *Fish Shellfish Immun* (2007) 23(4):906–10. doi: 10.1016/j.fsi.2007.04.006
44. Caipang CMA, Brinchmann MF, Kiron V. Profiling gene expression in the spleen of Atlantic cod, Gadus morhua upon vaccination with Vibrio anguillarum antigen. *Comp Biochem Phys A* (2009) 153(3):261–7. doi: 10.1016/j.cbpb.2009.03.005
45. Gudmundsdottir S, Magnadottir B, Bjornsdottir B, Arnadottir H, Gudmundsdottir BK. Specific and natural antibody response of cod juveniles vaccinated against Vibrio anguillarum. *Fish Shellfish Immun* (2009) 26(4):619–24. doi: 10.1016/j.fsi.2008.09.017
46. Mikkelsen H, Lund V, Larsen R, Seppola M. Vibriosis vaccines based on various sero-subgroups of Vibrio anguillarum O2 induce specific protection in Atlantic cod (Gadus morhua L.) juveniles. *Fish Shellfish Immun* (2011) 30 (1):330–9. doi: 10.1016/j.fsi.2010.11.007
47. Magnadottir B, Jonsdottir H, Helgason S, Bjornsson B, Solem ST, Pilstrom L. Immune parameters of immunised cod (Gadus morhua L.). *Fish Shellfish Immun* (2001) 11(1):75–89. doi: 10.1006/fsim.2000.0296
48. Pilström L, Warr GW, Strömberg S. Why is the antibody response of Atlantic cod so poor? The search for a genetic explanation. *Fish Sci* (2005) 71(5):961–71. doi: 10.1111/j.1444-2906.2005.01052.x
49. Stenvik J, Schroder MB, Olsen K, Zapata A, Jorgensen TO. Expression of immunoglobulin heavy chain transcripts (VH-families, IgM, and IgD) in head kidney and spleen of the Atlantic cod (Gadus morhua L.). *Dev Comp Immunol* (2001) 25(4):291–302. doi: 10.1016/S0145-305X(00)00056-2
50. Minges Wols HA. Plasma Cells. In: *Encyclopedia of Life Sciences* (2006).
51. Arango Duque G, Descoteaux A. Macrophage cytokines: involvement in immunity and infectious diseases. *Front Immunol* (2014) 5:491. doi: 10.3389/fimmu.2014.00491
52. Fang MQ, Xie HM, Dougan SK, Ploegh H, van Oudenaarden A. Stochastic Cytokine Expression Induces Mixed T Helper Cell States. *PLoS Biol* (2013) 11 (7):e1001618. doi: 10.1371/journal.pbio.1001618
53. Mashoof S, Criscitiello MF. Fish Immunoglobulins. *Biol (Basel)* (2016) 5 (4):45. doi: 10.3390/biology5040045
54. Hsieh CS, deRoos P, Honey K, Beers C, Rudensky AY. A role for cathepsin L and cathepsin S in peptide generation for MHC class II presentation. *J Immunol* (2002) 168(6):2618–25. doi: 10.4049/jimmunol.168.6.2618
55. Chapman HA. Endosomal proteases in antigen presentation. *Curr Opin Immunol* (2006) 18(1):78–84. doi: 10.1016/j.coi.2005.11.011
56. Malmstrom M, Jentoft S, Gregers TF, Jakobsen KS. Unraveling the Evolution of the Atlantic Cod's (Gadus morhua L.) Alternative Immune Strategy. *PLoS One* (2013) 8(9):e74004. doi: 10.1371/journal.pone.0074004
57. Neave B, Rodaway A, Wilson SW, Patient R, Holder N. Expression of zebrafish GATA 3 (gta3) during gastrulation and neurulation suggests a role in the specification of cell fate. *Mech Dev* (1995) 51(2-3):169–82. doi: 10.1016/0925-4773(95)00351-7
58. Wang L, Shang N, Feng H, Guo Q, Dai H. Molecular cloning of grass carp (Ctenopharyngodon idellus) T-bet and GATA-3, and their expression profiles with IFN-gamma in response to grass carp reovirus (GCRV) infection. *Fish Physiol Biochem* (2013) 39(4):793–805. doi: 10.1007/s10695-012-9741-y
59. Kumari J, Bogwald J, Dalmo RA. Transcription factor GATA-3 in Atlantic salmon (Salmo salar): molecular characterization, promoter activity and expression analysis. *Mol Immunol* (2009) 46(15):3099–107. doi: 10.1016/j.molimm.2009.06.008
60. Chi H, Zhang Z, Inami M, Bogwald J, Zhan W, Dalmo RA. Molecular characterizations and functional assessments of GATA-3 and its splice variant in Atlantic cod (Gadus morhua L.). *Dev Comp Immunol* (2012) 36(3):491–501. doi: 10.1016/j.dci.2011.09.004
61. Takizawa F, Mizunaga Y, Araki K, Moritomo T, Ototake M, Nakanishi T. GATA3 mRNA in ginbuna crucian carp (Carassius auratus langsdorfii): cDNA cloning, splice variants and expression analysis. *Dev Comp Immunol* (2008) 32(8):898–907. doi: 10.1016/j.dci.2008.01.004
62. Murphy KM, Reiner SL. The lineage decisions of helper T cells. *Nat Rev Immunol* (2002) 2(12):933–44. doi: 10.1038/nri954
63. Bosselut R. CD4/CD8-lineage differentiation in the thymus: from nuclear effectors to membrane signals. *Nat Rev Immunol* (2004) 4(7):529–40. doi: 10.1038/nri1392
64. Ho IC, Pai SY. GATA-3 - not just for Th2 cells anymore. *Cell Mol Immunol* (2007) 4(1):15–29.
65. Hoyler T, Klose CSN, Souabni A, Turqueti-Neves A, Pfeifer D, Rawlins EL, et al. The Transcription Factor GATA-3 Controls Cell Fate and Maintenance of Type 2 Innate Lymphoid Cells. *Immunity* (2012) 37(4):634–48. doi: 10.1016/j.immuni.2012.06.020
66. Hernandez PP, Strzelecka PM, Athanasiadis EI, Hall D, Robalo AF, Collins CM, et al. Single-cell transcriptional analysis reveals ILC-like cells in zebrafish. *Sci Immunol* (2018) 3(29):eaau5265. doi: 10.1126/sciimmunol.aau5265
67. Moro K, Yamada T, Tanabe M, Takeuchi T, Ikawa T, Kawamoto H, et al. Innate production of T(H)2 cytokines by adipose tissue-associated c-Kit(+)Sca-1(+) lymphoid cells. *Nature* (2010) 463(7280):540–4. doi: 10.1038/nature08636

Conflict of Interest: The authors declare that the research was conducted in the absence of any commercial or financial relationships that could be construed as a potential conflict of interest.

Copyright © 2020 Guslund, Solbakken, Brieuc, Jentoft, Jakobsen and Qiao. This is an open-access article distributed under the terms of the Creative Commons Attribution License (CC BY). The use, distribution or reproduction in other forums is permitted, provided the original author(s) and the copyright owner(s) are credited and that the original publication in this journal is cited, in accordance with accepted academic practice. No use, distribution or reproduction is permitted which does not comply with these terms.

frontiers in Immunology

ORIGINAL RESEARCH
published: 20 October 2020
doi: 10.3389/fimmu.2020.565958

Enhanced Immune Protection of Mud Crab *Scylla paramamosain* in Response to the Secondary Challenge by *Vibrio parahaemolyticus*

Xin Zhang[1,2,3], *Xinyang Zeng*[3], *Yulong Sun*[1], *Yilei Wang*[2,3]* *and Ziping Zhang*[1,4]*

[1] College of Animal Science, Fujian Agriculture and Forestry University, Fuzhou, China, [2] Fujian Engineering Research Center of Aquatic Breeding and Healthy Aquaculture, Jimei University, Xiamen, China, [3] Key Laboratory of Healthy Mariculture for the East China Sea, Ministry of Agriculture, Fisheries College, Jimei University, Xiamen, China, [4] Key Laboratory of Marine Biotechnology of Fujian Province, College of Animal Science, Institute of Oceanology, Fujian Agriculture and Forestry University, Fuzhou, China

"Immune priming" plays a vital part in the immune system of invertebrates, protecting against recurrent infections by pathogens, and can provide some ideas for the prevention and treatment of invertebrate diseases. Many invertebrates have been demonstrated recently to have immune priming, but the relevant mechanisms are not known. Expression of immune system–related genes in the hemocytes and hepatopancreas of the mud crab (*Scylla paramamosain*) before and after repeated stimulation with *Vibrio parahaemolyticus* were analyzed by real-time fluorescence quantitative polymerase chain reaction. Some molecules that may participate in the immune priming of *S. paramamosain* were screened out, and their possible roles in immune priming were interpreted. Crabs injected first with heat-killed *V. parahaemolyticus* (HkVp group) or physiologic (0.9%) saline (PS group) were rechallenged at 168 h with live *V. parahaemolyticus* (HkVp+Vp group and PS+Vp group, respectively). The log-rank test shows a significant difference in survival rate between the HkVp+Vp group and the other groups after the ICH ($p < 0.05$). Expression of genes involved in the toll-like receptor (TLR) signaling pathway and some antimicrobial peptide genes were detected. By, respectively, comparing gene quantification at different time points in hemocytes and the hepatopancreas, the molecules that may play a part in the early stage of the immune priming of *S. paramamosain* in the hemocytes are found to be down syndrome cell adhesion molecule (Dscam), Hyastatin, Cactus, Arasin, antilipopolysaccharide factor 3 (ALF3), ALF4, ALF5, and ALF6 as well as later acting molecules, such as Crustin, Dorsal, Pelle, and myeloid differentiation factor 88 (MyD88). The molecules that functioned throughout the entire period are TLR and Spaetzle. In the hepatopancreas, the molecules that may play a part in the early stages of immune priming are Dscam, Hyastatin, Arasin, ALF6, Pelle, Spaetzle, Dorsal and, in the later stage, ALF4. The molecules that functioned throughout the entire period are TLR, Crustin, Cactus, MyD88, ALF3, and ALF5. In summary, the immune function of *S. paramamosain* is enhanced after it receives the same repetitive stimulation by *V. parahaemolyticus*, indicating immune priming in *S. paramamosain*. Our study enriches research on

OPEN ACCESS

Edited by:
Monica Hongroe Solbakken, University of Oslo, Norway

Reviewed by:
Yueling Zhang, Shantou University, China
Ngoc Tuan Tran, Shantou University, China

***Correspondence:**
Yilei Wang
ylwang@jmu.edu.cn
Ziping Zhang
zhangziping@fafu.edu.cn

Specialty section:
This article was submitted to Comparative Immunology, a section of the journal Frontiers in Immunology

Received: *26 May 2020*
Accepted: *12 August 2020*
Published: *20 October 2020*

Citation:
Zhang X, Zeng X, Sun Y, Wang Y and Zhang Z (2020) Enhanced Immune Protection of Mud Crab Scylla paramamosain in Response to the Secondary Challenge by Vibrio parahaemolyticus. Front. Immunol. 11:565958. doi: 10.3389/fimmu.2020.565958

immune priming in invertebrates and lays the foundation for further studies revealing the molecular mechanism of immune priming in crabs.

Keywords: antimicrobial peptides, toll-like receptor signaling pathway, *Scylla paramamosain*, immune priming, gene expression

INTRODUCTION

Since the clonal-selection and gene-rearrangement theories were first proposed, significant progress has been achieved in the research of adaptive immunity (1, 2). It is considered that invertebrates lack the "true" memory B/T lymphocytes and antigen-specific immunoglobulin (Ig) molecules, which are the prerequisites and most striking features of the adaptive immune system of vertebrates (3, 4). Hence, it is a popular view that there is no adaptive immune response in invertebrates (5). Invertebrates can survive infection from various environmental pathogens and continue to have offspring, mainly by relying on their complex innate immune system.

The immune system of invertebrates has been considered to be nonspecific. However, increasing numbers of studies show that, if invertebrates are infected repeatedly by pathogenic microorganisms, a phenomenon similar to the immune memory found in vertebrates is observed (3, 4, 6–8), but the priming effect is not universal across all bacterial strains (9). The improved survival and immune responses observed after secondary exposure to a pathogen encountered previously in invertebrates is defined as "the ability to store and recall information on previously encountered microbial communities or their components" (10) and is called "immune priming" (11), "specific immune priming" (12), or "quasi-immune response" (13).

Initially, the immune memory of invertebrates was found only in starfish (*Dermasterias imbricata*), ribbon worm (*Lineus sanguineus*), earthworm (*Lymbricus terrestris*), and cockroach (*Periplaneta americana*) (14–17). However, often the results were controversial because the genotypes of animals used in the experiments could not be determined. This problem hindered the progress of research on the immune memory of invertebrates at that time.

Later, the study of the immune memory of invertebrates focused on the interaction between the host and parasites/bacteria. It was found that the immune memory of *Macrocyclops albidus* could be induced by *Schistocephalus solidus* (18). Since then, similar experimental conclusions have been reported in *Bombus terrestris* and *Paenibacillus species*, *Daphnia magna*, and *Pasteuria ramosa* (19, 20). Subsequently, some researchers questioned if this type of immune priming was overly dependent on the experimental conditions (21, 22). They note that most studies evaluate only the survival rate and fecundity of the host instead of measuring the expression of immune system–related genes or the infection rate of parasites/pathogens (8, 23, 24).

In recent years, "omics" research in invertebrates has revealed that some highly variable receptor molecules might be involved in the specific immune priming of invertebrates: scavenger receptor cysteine-rich proteins and immune-response proteins (25–27), down syndrome cell adhesion molecule (Dscam) (28–31), and fibrinogen-related proteins (FREPs) (32–34). In particular, the FREPs of *Biomphalaria glabrata* have been shown to interact with the mucin (SmPoMucs) of *Schistosoma mansoni* to form an immune complex, which is important evidence of the interaction between diverse immune receptors and antigen variation in the invertebrate host/pathogen (35). In 2015, Coustau and colleagues showed that the interaction between *B. glabrata* and *S. mansoni* is an extremely complex immune process in which a large number of antigens, immune receptors, effectors, and antieffector systems are involved (36).

Dubief and colleagues demonstrate that the hemolymph phagocytosis of *Haliotis tuberculata* is enhanced after reinfection by *Vibrio harveyi* (37). De Melo and colleagues demonstrate that secondary infection by *Schistosoma japonicum* caused a significant increase in the number of granulocytes in hemolymph in *B. glabrata* and *Biomphalaria straminea* (38). Research into *Eriocheir sinensis* indicates that the survival rate of individuals immunized with inactivated *Aeromonas hydrophila* for 7 days was significantly higher than that of untreated individuals when they were infected with live *A. hydrophila*. The phagocytosis of hemocytes in the inactivated *A. hydrophila*-immunized group was significantly greater than that in the *Micrococcus luteus*-immunized group and could be maintained for a long time compared with that after the first immunization with *A. hydrophila*. The serum of the *A. hydrophila*–immunized group had stronger antibacterial activity against the same bacteria than against different bacteria and showed a certain specificity (39). Moreover, research into oysters shows that the toll-like receptor (TLR) pathway participated in enhanced immune protection for hemocytes defending against second stimulation by *Vibrio splendidus* (40). Therefore, enhanced immune protection is a universal phenomenon shared by all species and not provided exclusively by adaptive immunity in vertebrates. Also, Ig molecules or lymphocytes might not be the essential prerequisites for enhanced immune protection in all organisms.

The mud crab, *Scylla paramamosain*, is distributed widely throughout the Indo-Pacific region. It is found commonly in estuaries and mangrove areas. It has also been cultured along the southeast coasts of China. Recently, mass mortality occurred due to an outbreak of diseases caused by viruses, bacteria, and parasites (41). *V. parahaemolyticus* is a primary bacterial pathogen of *S. paramamosain*. It has been reported to cause "milky disease" with high mortality and has led to major losses in the mud-crab aquaculture industry (42–44). However, due to a lack of research into disease prevention, the culture of *S. paramamosain* has been hampered by infection by various pathogens, which has restricted the development of the breeding industry.

During disease control/prevention, the use of antibiotics and immune enhancers can cause an excessive immune response and

environmental pollution, so it does not constitute an ideal strategy. Immune priming, if present in *S. paramamosain*, could be an essential defense against *V. parahaemolyticus*. Antimicrobial peptides (AMPs) have been reported to be important components of the host immune defense system against pathogen infection. In crab species, even in *S. paramamosain*, several AMPs have been discovered and characterized (45–47). In addition to AMPs, classical immune-related processes, such as the TLR signaling pathway, are also reported to be involved in the immunity of *S. paramamosain* against Gram-negative and -positive bacteria (48–50). Taken together, these observations indicate that AMPs and the TLR signaling pathway have vital roles in recognizing and eliminating *V. parahaemolyticus* during immune protection of *S. paramamosain*, which may also induce enhanced immune protection.

Hence, the main objectives of the present study were to (i) examine the different experimental treatments of *S. paramamosain* resistant to *V. parahaemolyticus* infection, (ii) compare the immune responses of different tissues (hemocytes and the hepatopancreas) during successive exposures to the pathogen and thereby explain differences in tolerance to the disease, and (iii) investigate if AMPs and the TLR signaling pathway take part in the immune priming of *S. paramamosain* against *V. parahaemolyticus*.

MATERIALS AND METHODS

Animals, Ethics Statement, and Bacterial Strains

Healthy *S. paramamosain* (bodyweight 69.07 ± 23.99 g) were purchased from the Tulou Putou farm (Zhangpu, Zhangzhou, Fujian Province, China) in June 2018. Crabs were maintained in a self-built recycling cultivation system (seawater temperature at 26°C, salinity at 18‰–20‰, and fed with clams or oysters once a day at night) for 10 days to acclimatize to their new environment before experimentation. In all subsequent experiments, ≥6 individuals were sampled at different times. All of the study design and animal experiments were conducted following the guidelines of Fujian Agriculture and Forestry University's Animal Care and Use Committee.

V. parahaemolyticus (isolated from diseased mud crab and preserved in our laboratory) was cultured in LB media (containing 10 g/L peptone, 5 g/L yeast extract, and 10 g/L NaCl) at 37°C for 24 h and harvested *via* centrifugation (6000 × *g*, 10 min, 4°C). The pellet was washed and resuspended in sterilized physiologic (0.9%) saline for crabs (PS), which comprises (in g/L), NaCl (26.00), KCl (0.85), $CaCl_2$ (1.50), $MgCl_2$ (2.33), H_3BO_3 (0.55), NaOH (0.02), and Na_2SO_4 (3.00). The suspension was adjusted to a final concentration of 3.1×10^7 CFU/mL and termed the "live *V. parahaemolyticus* suspension." Heat-killed *V. parahaemolyticus* was acquired by autoclaving the suspension for 30 min at 60°C. Subsequently, the plate coating was used to determine whether all the bacteria had been killed.

Bacterial Challenge

The experiment was split into the immune priming phase (IPP) and immune challenge phase (ICP). For the IPP, 250 crabs received an injection of PS (100 μL) and were employed as the PS group. Another 250 crabs received the heat-killed *V. parahaemolyticus* suspension at an effective CFU per gram of crab of 10^4 and were employed as the HkVp group. At 6, 9, and 72 h of the IPP, 36 crabs from the PS grup and HkVp groups had their hemolymph and hepatopancreas collected, respectively (N = 6). After 168 h of the IPP, in the ICP, all the remaining crabs from the PS group received an injection of live *V. parahemolyticus* (5.0×10^3 CFU/g) and were employed as the PS+Vp group. Meanwhile, the remaining crabs from the HkVp group were again divided into the HkVp+Vp group (received an injection of live *V. parahaemolyticus* with the effective CFU per gram of crab of 5.0×10^3) and HkVp+PS group (received an injection of 100 μL of PS). All the concentrations of *V. parahaemolyticus* mentioned above were determined by the mortality of mud crabs after injection of *V. parahaemolyticus* in the pre-experimental stage. Six crabs from each group had hemolymph and hepatopancreas collected at 6, 9, and 72 h of the ICP. The experimental design is illustrated in **Figure 1**.

Survival Rate

The survival rate of crabs was measured at different time points after challenge with live *V. parahaemolyticus* (5.0×10^3 CFU/g) after crabs had been pretreated with heat-killed *V. parahaemolyticus*. Survival was followed daily, and dead crabs were removed from tanks. Survival rates were analyzed for statistical differences between treatments by log-rank test on Kaplan-Meier survival curves using the computer software package GraphPad Prism v. 7.0.

Isolation of Total RNA and Reverse Transcription

Hepatopancreas samples were stored immediately in liquid nitrogen and RNAlater, respectively, until used for RNA isolation. Hemocytes were isolated rapidly by centrifugation at 2000 × g for 10 min at 4°C from the hemolymph. The latter was harvested from the last walking leg with an equal volume of ice-cold anticoagulant buffer (contains 0.45 M NaCL, 0.1 M glucose, 30 mM trisodium citrate, 26 mM citric acid, and 10 mM EDTA) and frozen immediately in liquid nitrogen until used for RNA isolation.

Total RNA was extracted from different tissues of unchallenged and challenged samples using TRIzol® Reagent (Invitrogen, Carlsbad, CA, USA) according to manufacturer protocols. The quality of total RNA was assessed by agarose gel electrophoresis and quantified by spectrophotometry using a NanoDrop™ 1000 (Thermo Fisher, Waltham, MA, USA). Then, 2 μg of total RNA and 2 μL of random primers (10 μM) were used to synthesize cDNA by M-MLV reverse transcriptase (Invitrogen, Carlsbad, CA, USA). Then, synthesized complementary (c)DNA was diluted 10-fold and 100-fold and stored at −20°C until use.

Quantitative Real-Time Polymerase Chain Reaction (qRT-PCR) and Statistical Analyses

Fourteen pairs of gene-specific primers for the genes of members of the TLR signaling pathway and AMPs (**Additional File 1: Table S1**) were designed to amplify products of 150–250 bp from

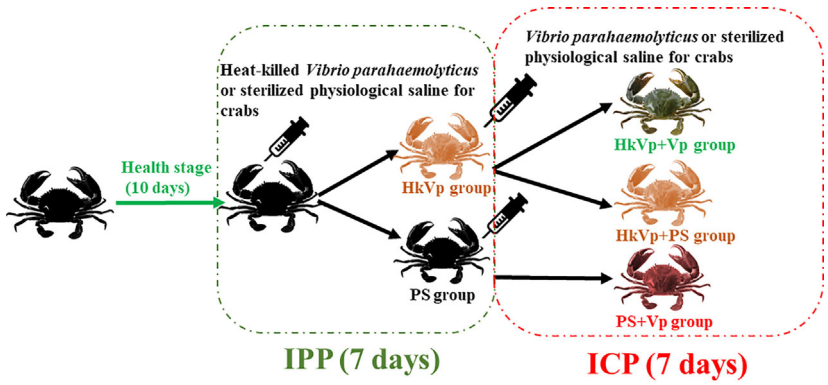

FIGURE 1 | Experimental design of *S. paramamosain* receiving heat-killed *V. parahaemolyticus* (IPP) and live *V. parahaemolyticus* (ICP).

cDNA, respectively. To compare the relative expression of these 14 genes in the samples, the housekeeping gene *EF1a* (GenBank ID: JQ824130) was also amplified with the same cDNA samples (**Additional File 1: Table S1**). The PCR was carried out in a LightCycler™ 480 Real-time Thermal Cycler (Roche, Basel, Switzerland) following manufacturer instructions with a total reaction volume of 20 μL [10 μL of 10× SYBR Green Master Mix (Yeasen Biotechnology, Shanghai, China), 9 μL of original cDNA (1:100 dilution), and 0.5 μL of each primer (10 μM)]. The thermal profile for RT-PCR was 1 min at 95°C, followed by 40 cycles at 95°C for 15 s and 60°C for 1 min. Melting curves were also plotted (60°C–90°C) to ensure that a single PCR product was amplified for each pair of primers. The comparative CT method (ΔCT = CT of target gene − CT of *EF1a* and ΔΔCT = ΔCT of any sample − the calibrator sample) was used to calculate the relative expression of all 14 genes (51). Then, the data were subjected to a Student's *t*-test to determine the difference in the mean values among the treatments, and the significant difference in expression was shown at $P < 0.05$.

Violin plots were created using OmicShare tools, a free online platform for data analyses (www.omicshare.com/tools), to measure the expression of the genes related to the TLR signaling pathway and AMPs in each tissue at different time points under dissimilar conditions. Heat maps were created using R Programming Language v3.5.3 (R Center for Statistical Computing, Vienna, Austria) to visualize gene-expression data graphically. The intermolecular interaction network of TLR signaling pathway-related genes was constructed using String v11.0 (https://string-db.org/) and Cytoscape 3.7.1 (https://cytoscape.org/).

RESULTS

Increased Survival Rate of *S. paramamosain* After the ICP With Live *V. parahaemolyticus*

To understand the immune effect of *V. parahaemolyticus* during the IPP and ICP, we counted the number of *S. paramamosain* that survived. After the IPP, the mortality of the PS group was not significantly different to that of the HkVp group. At 7 days after the IPP, animals entered the ICP with a lethal dose of live *V. parahemolyticus*. There was a difference in the survival rate between the HkVp+Vp group and PS+Vp group from 9 h, and it became greater and more significant with increasing time, and the log-rank test shows a significant difference in survival rate between HkVp+Vp group and the other groups after the ICH ($p < 0.05$) (**Figure 2**). The contrast in the survival rate between the HkVp+Vp and PS+Vp groups indicates that the immune protection of *S. paramamosain* was enhanced when they were infected again by *V. parahaemolyticus* (**Figure 2**).

Changes in mRNA Expression of Genes Involved in the TLR Signaling Pathway

In hemocytes, mRNA expression of *MyD88* in the HkVp+Vp and PS+Vp groups was upregulated 6 h after the ICP, and it peaked significantly at 72 h in the PS+Vp group compared with that in the HkVp+Vp and HkVp+PS groups ($p < 0.05$). After the IPP, the expression of *Dorsal* in the HkVp group was upregulated at first and peaked significantly at 72 h ($p < 0.05$). After the ICP, the HkVp+Vp and PS+Vp groups seemed to adopt two immune modes. *Dorsal* expression in the HkVp +Vp group showed a downregulation trend that was significantly lower than that in the HkVp+PS group at 9 and 72 h, whereas mRNA expression in the PS+Vp group peaked at 72 h and was significantly more upregulated than that in the HkVp+PS and HkVp+Vp groups ($p < 0.05$). Similar to the expression pattern of *Dorsal*, we found that the expression of *TLR* and *Pelle* also showed a downregulation trend after the ICP ($p < 0.05$). Conversely, the expression of *Spaetzle* and *Cactus* showed a significantly upregulated pattern at almost all time points after the ICP ($p < 0.05$). Expression of *Dscam* in the HkVp+Vp group peaked 9 h after the ICP and was upregulated significantly compared with that in the HkVp +PS and PS+Vp groups. The significant difference was still present at 72 h ($p < 0.05$) (**Figure S1**).

In the hepatopancreas, mRNA expression of *MyD88* in the HkVp group was upregulated significantly 9 h after the IPP

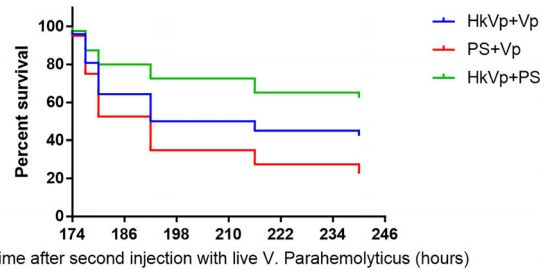

FIGURE 2 | Cumulative survival using the Kaplan-Meier method following the ICP with live *V. parahaemolyticus* after previous IPP with heat-killed *V. parahaemolyticus* (HkVp group) or physiologic (0.9%) saline (PS group) in *S. paramamosain*. "168–240 h" denotes the time started after the ICP. This survival experiment was repeated three times.

($p < 0.05$) and showed a significant downregulation trend at 6 and 9 h in the HkVp+Vp group ($p < 0.05$). Expression of *Dscam* in the HkVp+Vp group peaked 9 h after the ICP and was upregulated considerably more than that in the HkVp+PS and PS+Vp groups ($p < 0.05$). The expression of *TLR* and *Dorsal* in the HkVp+Vp group was significantly weaker than that in the PS +Vp group ($p < 0.05$). After the IPP, *Pelle* expression in the HkVp group was significantly upregulated at 6 and 72 h ($p < 0.05$), whereas it was also upregulated significantly 6 and 9 h after the ICP in the HkVp+Vp group. Analogous to the expression pattern of *Pelle*, the expression of *Spaetzle* and *Cactus* also showed a considerably upregulated trend at different time points after the ICP ($p < 0.05$) (**Figure S2**).

Changes of mRNA Expression of AMPs Genes

In hemocytes, mRNA expression of *Arasin* was upregulated significantly at 6 h in the HkVp+Vp group and at 72 h in the PS+Vp group after the ICP. Compared with the HkVp+PS and PS+Vp groups, expression of *Crustin*, *ALF3*, and *ALF4* in the HkVp+Vp group after the ICP peaked at 72, 6, and 9 h, respectively. The expression pattern of *ALF6* was identical to that of *ALF3* and was upregulated significantly 6 h after the ICP in the HkVp+Vp group ($p < 0.05$). *ALF5* maintained a high level of expression at all time points after the ICP in the HkVp+Vp group compared with that in the HkVp+PS and PS +Vp groups ($p < 0.05$). Slightly different from the expression pattern of *ALF5*, *Hyastatin* showed significantly high expression 6 and 9 h after the ICP in the HkVp+Vp group ($p < 0.05$) (**Figure S3**).

In the hepatopancreas, mRNA expression of *Arasin* was maintained at a significantly high level at all time points after the ICP in the HkVp+Vp group ($p < 0.05$). *ALF3*, *ALF5*, and *ALF6* also had the same pattern of expression as that of *Arasin*. *Crustin* expression in the HkVp+Vp group was upregulated significantly 9 and 72 h after the ICP than that in the HkVp +PS and PS+Vp groups ($p < 0.05$). Nine hours after the ICP, *ALF4* and *Hyastatin* in the HkVp+Vp group showed significantly high expression. However, *ALF4* expression at 6 and 72 h was much lower than that in the PS+Vp group, and *Hyastatin* expression was also upregulated significantly 9 and 72 h after the IPP ($p < 0.05$) (**Figure S4**).

Visualization of the Expression Data of Genes of the TLR Signaling Pathway and AMPs

After standardizing all the data, heat maps exhibit the different expression of genes of the TLR pathway or AMPs in the hepatopancreas and hemocytes after injection at different time points. Some of the same genes in the two tissues show different expression patterns. This result suggests that different regulatory modes of expression of genes in the TLR signaling pathway and AMP genes were activated in the hepatopancreas and hemocytes in the IPP and ICP (**Figure 3**).

Violin plots are used to summarize the differences in gene expression in hemocytes and the hepatopancreas, respectively. All genes of the TLR signaling pathway or AMPs at different time points (6, 9, 72, 174, 177, and 240 h) show that the different expression (i) was higher in hemocytes than that in hepatopancreas, (ii) became more significant in the hepatopancreas from 9 h in the ICP, (iii) became more significant in hemocytes at all time points of the ICP, and (iv) was greater at 9 h of the ICP in the hepatopancreas and hemocytes (**Figures 4A, B**).

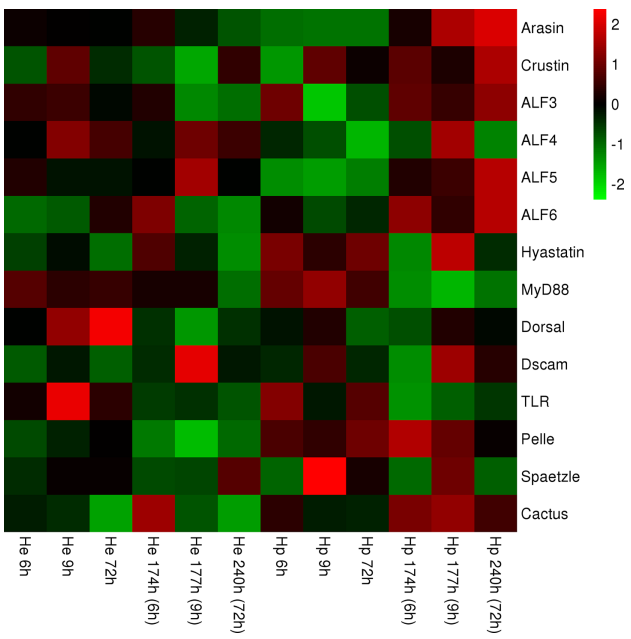

FIGURE 3 | Heat map representing expression of genes of members of the TLR signaling pathway and AMPs in hemocytes and the hepatopancreas, respectively, containing continuous time points [IPP (6, 9, and 72 h) and ICP (174, 177, and 240 h)]. The color scale at the far right of the heat map represents expression, whereby red, green, and black indicate upregulated, downregulated, and unaltered expression, respectively.

The Molecular Network of the TLR Signaling Pathway Constructed by Cytoscape

The molecular network of the related genes in the TLR signaling pathway created using Cytoscape indicates gene interactions at a discrete time point after injection (**Figure 5**). In terms of expression of different genes, there are considerable differences between the hepatopancreas (**Figure 5A**) and hemocytes (**Figure 5B**) according to this interaction network.

DISCUSSION

In mammals, health maintenance and disease prevention are promoted owing to studies of enhanced immune protection and their underlying immune mechanisms. Based on numerous studies in vertebrates, researchers are driven to explore the origin, evolution, and underlying mechanism of enhanced immune protection in invertebrates. Nevertheless, exploration of its evolution is limited (52).

Early studies on adaptive immunity focus mainly on the identification of lymphocytes and their receptors as well as molecules in the major histocompatibility complex. However, since the discovery of alternative mechanisms of adaptive immunity based on variable lymphocyte receptor in jawless vertebrates, Ig-dependent adaptive immunity ceased to be regarded as the only solution to enhance immune protection (53). In recent years, increasing attention has been paid to the long-neglected role of immune protection in invertebrates.

It is reported that immune protection after identical stimulation is significantly stronger in invertebrates than that in an unvaccinated group and that the effect is similar to that of a vaccine (3, 37, 38, 54–56). A mechanism of enhanced immune protection is demonstrated, but it is also reported to be associated with several factors: the interaction between

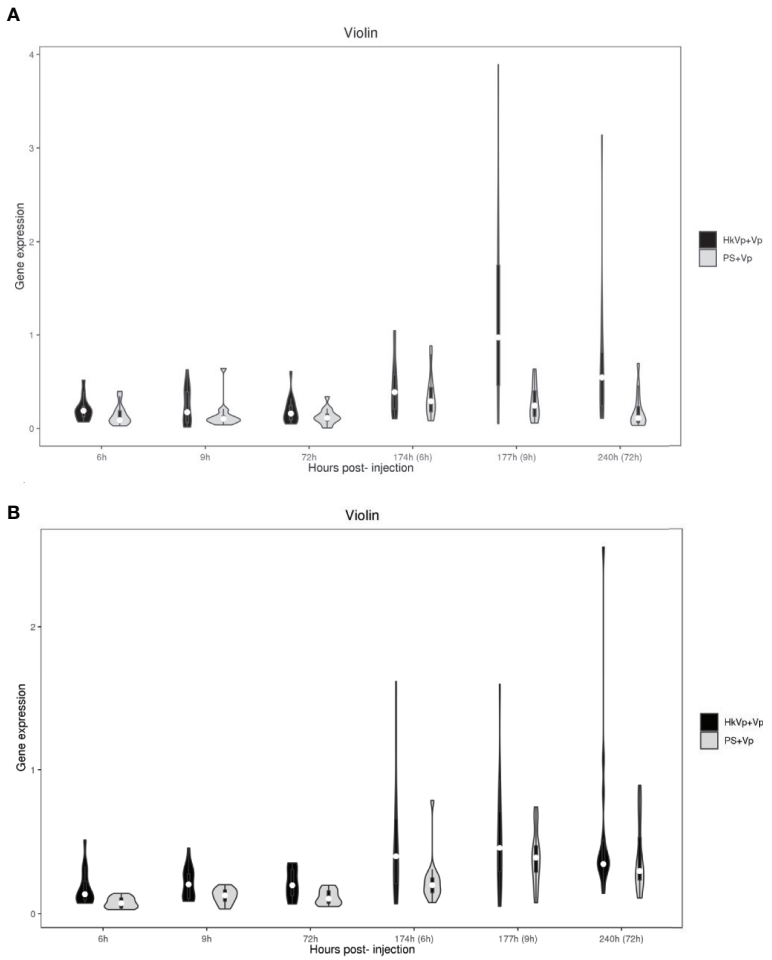

FIGURE 4 | Violin plots representing mRNA expression of genes of members of the TLR signaling pathway and AMPs. **(A)** mRNA expression of genes in the hepatopancreas in the HkVp+Vp group compared with that in the PS+Vp group. **(B)** mRNA expression of genes in hemocytes in the HkVp+Vp group compared with that in the PS+Vp group. The *x*-axis denotes the hours after bacterial injection [IPP (6, 9, and 72 h) and the ICP (174, 177, and 240 h)]. The *y*-axis represents expression of genes of members of the TLR signaling pathway and AMPs.

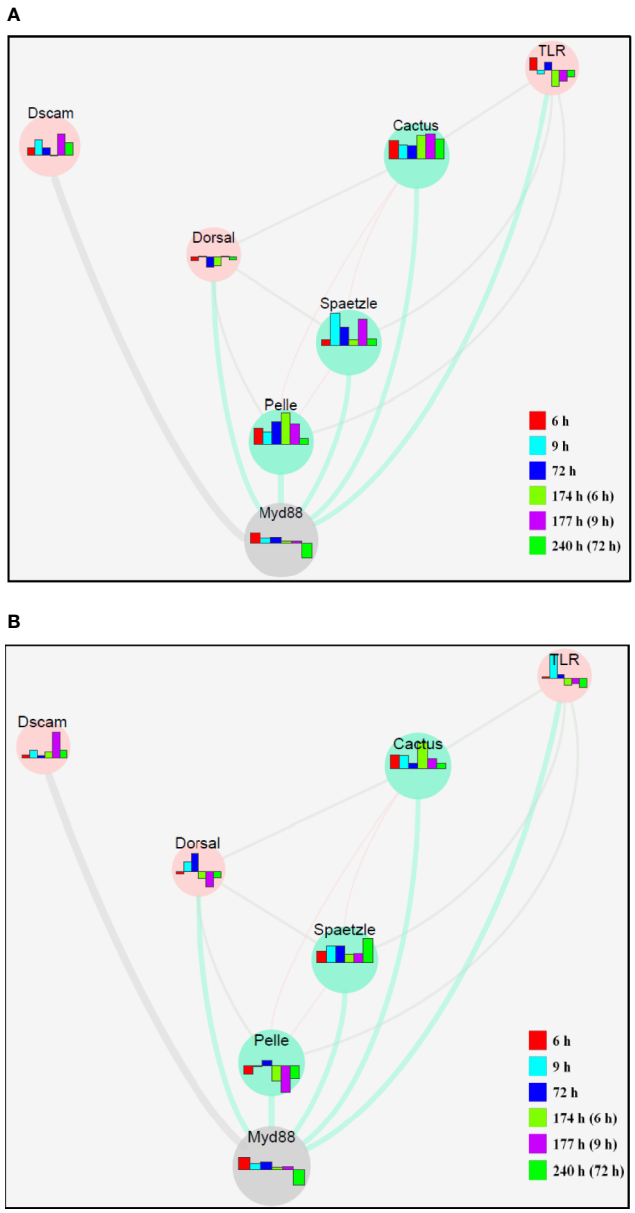

FIGURE 5 | The molecular network of related genes in the TLR signaling pathway in response to secondary challenge by *V. parahaemolyticus* in the hepatopancreas **(A)** and hemocytes **(B)** of *S. paramamosain* constructed by Cytoscape. The bar chart represents the different expression patterns of each gene, and the different colors of the bar chart represent different time phases.

different hosts and pathogens, the induced dose, and the duration (57).

Initially, crabs were immune-primed (IPP) with heat-killed *V. parahaemolyticus*. Then, they were immune challenged (ICP) with live *V. parahaemolyticus* with a lethal dose 7 days after the IPP. The survival rate of crabs after the ICP was the most direct evidence to judge the existence of immune priming in crabs. The difference in the survival rate between the HkVp+Vp and PS+Vp groups began to appear 9 h after the ICP, and it built up gradually over time. At 72 h, the difference between the two groups reached 20%. This result suggests (i) enhanced immune protection was initiated after the primary exposure to the same strain of *V. parahaemolyticus* and (ii) the existence of immune priming in *S. paramamosain*. Our finding of an enhanced immune response is in agreement with data from other studies showing a higher immune response could be induced by stimulation with inactivated pathogens in shrimps and crabs (39, 58). In other invertebrates, the upregulation of the immune response after repeated infection by the same pathogen is widespread, and it is considered to denote immune priming (56, 59, 60).

AMPs are vital components of the host innate immune response against microbial invasion (46). Pathogen infection can activate the TLR signaling pathway and its downstream signaling molecules; then the signal is translocated to the nucleus to induce the release of AMPs. AMPs, such as ALF3–6, Crustin, Arasin, and Hyastatin, are reported to be effectors of the immune response against infection by Gram-positive and Gram-negative bacteria in *S. paramamosain*. In the present study, expression of these AMP genes was also measured to ascertain if they were involved in the immune priming of *S. paramamosain*. We note significantly high expression of *Arasin*, *ALF3*, *ALF4*, *ALF6*, and *Hyastatin* in the hemocytes of the HkVp+Vp group in the initial stage after ICP. Simultaneously, *Crustin* expression peaked 72 h after the ICP. In the hepatopancreas of crabs in the HkVp+Vp group, the expression patterns of *ALF4* and *Hyastatin* were similar to those in hemocytes.

Interestingly, expression of *Arasin*, *Crustin*, *ALF3*, and *ALF6* was activated at the initial stage after the ICP and was upregulated significantly throughout the period. Moreover, *ALF5* expression was upregulated markedly throughout the ICP in hemocytes and in the hepatopancreas. Taken together, these results suggest that AMP genes participate in the immune priming of *S. paramamosain*, but in different tissues, the regulation mode is not identical.

The TLR signaling pathway is vital for the immune system of organisms due to its regulatory effect upon bacterial infection: It positively regulates the expression of downstream innate immune-related genes (48, 61). In the TLR signaling pathway of *Drosophila*, a platform is provided for Pelle to permit incorporation and form a trimeric complex by MyD88 recruiting its upstream-activated TLR and downstream cytosolic adaptor Tube. Meanwhile, the complex can also allow further activation of Pelle and then induce activation of Dorsal expression (62). Studies of various bacterial-induced Dscam isoforms in arthropods have focused on assays of gene silencing, bacterial binding assays, and pathogen clearance (29, 63, 64). The speed and intensity of the response of Dscam to pathogen infection after a previous encounter suggest specific immune priming (65, 66). Several studies have centered on Dscam and its involvement in immune priming in invertebrates, but those studies are on only a few species (31, 64, 67, 68).

We measured expression of seven genes associated with the TLR signaling pathway by qRT-PCR after pre-exposure of

V. parahaemolyticus to evaluate whether these genes are involved in enhanced immune protection. Unlike the expression pattern of AMP genes, which were upregulated in the hepatopancreas and hemocytes, the expression pattern of genes in the TLR signaling pathway was quite different after the ICP. In hemocytes of the HkVp+Vp group, *Spaetzle* was activated in the early stage after *V. parahaemolyticus* infection and showed high expression throughout the ICP. *MyD88* had high transient expression 6 h after infection and then showed a stable expression pattern. However, expression of genes, such as *TLR*, *Pelle*, and *Dorsal*, was inhibited after the ICP, especially in the advanced stage of infection. *Cactus* was activated at the early stage after infection, and in the later stage, the effect was weakened. *Dscam* expression reached its peak at 9 h. In the hemocytes of the PS+Vp group, *Spaetzle* was activated in the early stage after infection, whereas *TLR* and *Pelle* were activated in the later stage. *MyD88* and *Dorsal* were activated through the ICP, and expression of *Cactus* and *Dscam* was relatively unchanging. In the hepatopancreas, the expression and regulation patterns of the genes stated above were different from those in hemocytes. Similar to results in *Drosophila*, in studies of *S. paramamosain*, TLR, Pelle, and MyD88-mediated antibacterial models are reported, and in those models, toll-associated downstream signaling molecules (such as Spaetzle, TLR, Cactus, and Dorsal) participated in the immune response to Gram-negative bacteria (50, 69). Also, studies have shown that at least 36,736 isoforms of Dscam could potentially be generated in *S. paramamosain* and that the pathogen-induced Dscam isoforms could enhance self-protection upon pathogen infection (70).

Interestingly, the expression patterns of most genes in the PS +Vp group after the ICP were similar to those reported previously, which were upregulated significantly after infection by Gram-negative bacteria. Hence, the classical TLR signaling pathway was the main way to resist infection by *V. parahaemolyticus* in the PS +Vp group. However, after pre-exposure to *V. parahaemolyticus*, expression of these genes in the HkVp+Vp group suggests that, whether in hemocytes or the hepatopancreas, the classic TLR signaling pathway could not be activated by *V. parahaemolyticus* (or other compensatory mechanisms were activated simultaneously), which led to inhibition of expression of TLR, Pelle, and Dorsal after the ICP. In addition, irrespective of which type of pathway is activated, Spaetzle played a major part in this process. More importantly, expression of most genes of the TLR pathway had long-lasting changes after the ICP. This observation suggests that the TLR pathway has the most important role in enhanced immune protection against reinfection by *V. parahaemolyticus* and is involved in the process of immune priming of *S. paramamosain*. In addition, except for *Dscam*, there were complex interactions among the other six genes, which is worthy of more in-depth research in the future.

CONCLUSIONS

The present study provides evidence of the immune priming of *S. paramamosain* to *V. parahaemolyticus*. The differences between hemocytes and the hepatopancreas between the HkVp +Vp and the PS+Vp groups were studied by macroscopic survival rate and molecular-biology methods.

Our study elicits two main conclusions. First, our experiments indicate that immune priming is present in *S. paramamosain* when it was infected repeatedly by *V. parahaemolyticus* and that the related genes, which may have been involved in the immune priming of hemocytes and hepatopancreas of *S. paramamosain*, were identified. Second, the TLR signaling pathway, but not the classical style, was activated to participate in the immune priming of *S. paramamosain*. Our results provid further molecular insight into enhanced immune protection in *S. paramamosain*. Our data is valuable for understanding the mechanisms of enhanced immune protection in invertebrates.

DATA AVAILABILITY STATEMENT

The datasets presented in this article are not readily available because: The data will be available upon request. Requests to access the datasets should be directed to zhangziping@hotmail.com.

AUTHOR CONTRIBUTIONS

YW and ZZ conceived the study and designed the experiments. XZ conducted the experiments and wrote the manuscript. XYZ analyzed the data. YS conducted the experiments. YW and ZZ checked and modified the manuscript. All authors contributed to the article and approved the submitted version.

FUNDING

The work was supported by the Natural Science Foundation of China (No. 31672681), the Discipline Development Grant from College of Animal Sciences FAFU (712018R0404), Open fund project of Fujian Engineering Research Center of Aquatic Breeding and Healthy Aquaculture (DF20902), and the Startup Fund of Fujian Agriculture and Forestry University (61201401201) for ZZ.

SUPPLEMENTARY MATERIAL

The Supplementary Material for this article can be found online at: https://www.frontiersin.org/articles/10.3389/fimmu.2020.565958/full#supplementary-material

SUPPLEMENTARY FIGURE 1 | Expression of genes of members of the TLR signaling pathway in hemocytes after the IPP and ICP. The *x*-axis denotes hours after bacterial injection [IPP (6, 9, and 72 h) and the ICP (174, 177, and 240 h)]. The *y*-axis reflects expression of genes of members of the TLR signaling pathway. The significant difference between the challenged group and control group is indicated by * at $p < 0.05$. *EF1-α* served as a reference gene.

SUPPLEMENTARY FIGURE 2 | Expression of genes of members of the TLR signaling pathway in the hepatopancreas after IPP and ICP. The *x*-axis denotes

hours after bacterial injection [IPP (6, 9, and 72 h) and the ICP (174, 177, and 240 h)]. The *y*-axis reflects expression of genes of members of the TLR signaling pathway. The significant difference between the challenged group and control group is indicated by * at $p < 0.05$. *EF1-α* served as a reference gene.

SUPPLEMENTARY FIGURE 3 | Expression of AMP genes in hemocytes after the IPP and ICP. The *x*-axis denotes hours after bacterial injection [IPP (6, 9, and 72 h) and the ICP (174, 177, and 240 h)]. The *y*-axis reflects expression of genes of members of the TLR signaling pathway. The significant difference between the challenged group and control group is indicated by * at $p < 0.05$. *EF1-α* served as a reference gene.

SUPPLEMENTARY FIGURE 4 | Expression of AMP genes in the hepatopancreas after the IPP and ICP. The *x*- axis denotes hours after bacterial injection [IPP (6, 9, and 72 h) and the ICP (174, 177, and 240 h)]. The *y*-axis reflects expression of genes of members of the TLR signaling pathway. The significant difference between the challenged and control groups is indicated by * at $p < 0.05$. *EF1-α* served as a reference gene.

REFERENCES

1. Cohn M, Mitchison NA, Paul WE, Silverstein AM, Talmage DW, Weigert M. Reflections on the clonal-selection theory. *Nat Rev Immunol* (2007) 7 (10):823–30. doi: 10.1038/nri2177
2. Hodgkin PD, Heath WR, Baxter AG. The clonal selection theory: 50 years since the revolution. *Nat Immunol* (2007) 8(10):1019–26. doi: 10.1038/ni1007-1019
3. Netea MG, Quintin J, Der Meer JWMV. Trained immunity: a memory for innate host defense. *Cell Host Microbe* (2011) 9(5):355–61. doi: 10.1016/j.chom.2011.04.006
4. Criscitiello MF, De Figueiredo P. Fifty shades of immune defense. *PloS Pathog* (2013) 9(2):e1003110. doi: 10.1371/journal.ppat.1003110
5. Moser M, Leo O. Key concepts in immunology. *Vaccine* (2010) 28(3):12–3. doi: 10.1016/j.vaccine.2010.07.022
6. Kurtz J. Memory in the innate and adaptive immune systems. *Microbes Infect* (2004) 6(15):1410–7. doi: 10.1016/j.micinf.2004.10.002
7. Contrerasgarduno J, Lanzmendoza H, Franco B, Nava AP, Pedrazareyes M, Canaleslazcano J. Insect immune priming: ecology and experimental evidences. *Ecol Entomol* (2016) 41(4):351–66. doi: 10.1111/een.12300
8. Rowley AF, Powell A. Invertebrate immune systems–specific, quasi-specific, or nonspecific? *J Immunol* (2007) 179(11):7209–14. doi: 10.4049/jimmunol.179.11.7209
9. Futo M, Sell MP, Kutzer MAM, Kurtz J. Specificity of oral immune priming in the red flour beetle *Tribolium castaneum*. *Biol Lett* (2017) 13(12):20170632. doi: 10.1098/rsbl.2017.0632
10. Kurtz J. Specific memory within innate immune systems. *Trends Immunol* (2005) 26(4):186–92. doi: 10.1016/j.it.2005.02.001
11. Little TJ, Kraaijeveld AR. Ecological and evolutionary implications of immunological priming in invertebrates. *Trends Ecol Evol* (2004) 19(2):58–60. doi: 10.1016/j.tree.2003.11.011
12. Pham LN, Dionne MS, Shirasuhiza M, Schneider DS. A specific primed immune response in Drosophila is dependent on phagocytes. *PloS Pathog* (2007) 3(3):e26. doi: 10.1371/journal.ppat.0030026
13. Venegas CA, Nonaka L, Mushiake K, Nishizawa T, Muroga K. Quasi-immune response of *Penaeus japonicus* to penaeid rod-shaped DNA virus (PRDV). *Dis Aquat Organ* (2000) 42(2):83–9. doi: 10.3354/dao042083
14. Karp RD, Hildemann WH. Specific allograft reactivity in the sea star *Dermasterias imbricata*. *Transplantation* (1976) 22(5):434–9. doi: 10.1097/00007890-197611000-00004
15. Langlet C, Bierne J. Immune characteristics of graft rejection in nemerteans of the genus lineus. *Eur J Immunol* (1982) 12(9):705–8. doi: 10.1002/eji.1830120902
16. Cooper EL, Roar P. Second-set allograft responses in the earthworm Lumbricus terrestris Kinetics and characteristics. *Transplantation* (1986) 41 (4):514–20. doi: 10.1097/00007890-198604000-00019
17. George JF, Howcroft TK, Karp RD. Primary integumentary allograft reactivity in the american cockroach, *Periplaneta americana*. *Transplantation* (1984) 43 (4):514–9. doi: 10.1097/00007890-198704000-00012
18. Kurtz J, Franz K. Innate defence: evidence for memory in invertebrate immunity. *Nature* (2003) 425(6953):37–8. doi: 10.1038/425037a
19. Sadd BM, Schmidhempel P. Insect immunity shows specificity in protection upon secondary pathogen exposure. *Curr Biol* (2006) 16(12):1206–10. doi: 10.1016/j.cub.2006.04.047
20. Mctaggart SJ, Wilson P, Little TJ. Daphnia magna shows reduced infection upon secondary exposure to a pathogen. *Biol Lett* (2012) 8(6):972–5. doi: 10.1098/rsbl.2012.0581
21. Tate AT, Graham AL. Trans-generational priming of resistance in wild flour beetles reflects the primed phenotypes of laboratory populations and is inhibited by co-infection with a common parasite. *Funct Ecol* (2015) 29 (8):1059–69. doi: 10.1111/1365-2435.12411
22. Milutinovic B, Peus R, Ferro K, Kurtz J. Immune priming in arthropods: an update focusing on the red flour beetle. *Zoology* (2016) 119(4):254–61. doi: 10.1016/j.zool.2016.03.006
23. Hauton C, Smith VJ. Adaptive immunity in invertebrates: a straw house without a mechanistic foundation. *BioEssays* (2007) 29(11):1138–46. doi: 10.1002/bies.20650
24. Little TJ, Colegrave N, Sadd BM, Schmidhempel P. Studying immunity at the whole organism level. *BioEssays* (2008) 30(4):404–5. doi: 10.1002/bies.20738
25. Pancer Z. Dynamic expression of multiple scavenger receptor cysteine-rich genes in coelomocytes of the purple sea urchin. *Proc Natl Acad Sci U S A* (2000) 97(24):13156–61. doi: 10.1073/pnas.230096397
26. Dheilly NM, Nair SV, Smith LC, Raftos DA. Highly variable immune-response proteins (185/333) from the sea urchin, strongylocentrotus purpuratus: proteomic analysis identifies diversity within and between individuals. *J Immunol* (2009) 182(4):2203–12. doi: 10.4049/jimmunol.07012766
27. Smith LC. Innate immune complexity in the purple sea urchin: diversity of the Sp185/333 system. *Front Immunol* (2012) 3:70–0. doi: 10.3389/fimmu.2012.00070
28. Watson FL, Puttmannholgado R, Thomas F, Lamar DL, Hughes M, Kondo M, et al. Extensive diversity of Ig-superfamily proteins in the immune system of insects. *Science* (2005) 309(5742):1874–8. doi: 10.1126/science.1116887
29. Dong Y, Taylor HE, Dimopoulos G. AgDscam, a hypervariable immunoglobulin domain-containing receptor of the *Anopheles gambiae* innate immune system. *PloS Biol* (2006b) 4(7):1137–46. doi: 10.1371/journal.pbio.0040229
30. Armitage SAO, Peus R, Kurtz J. Dscam and pancrustacean immune memory – A review of the evidence. *Dev Comp Immunol* (2015) 48(2):315–23. doi: 10.1016/j.dci.2014.03.004
31. Ng TH, Kurtz J. Dscam in immunity: a question of diversity in insects and crustaceans. *Dev Comp Immunol* (2020) 105:103539. doi: 10.1016/j.dci.2019.103539
32. Dong Y, Dimopoulos G. Anopheles fibrinogen-related proteins provide expanded pattern recognition capacity against bacteria and malaria parasites. *J Biol Chem* (2009) 284(15):9835–44. doi: 10.1074/jbc.M807084200
33. Hanington PC, Forys MA, Dragoo JW, Zhang SM, Adema CM, Loker ES. Role for a somatically diversified lectin in resistance of an invertebrate to parasite infection. *Proc Natl Acad Sci* (2010) 107(49):21087–92. doi: 10.1073/pnas.1011242107
34. Portela J, Duval D, Rognon A, Galinier R, Boissier J, Coustau C, et al. Evidence for specific genotype-dependent immune priming in the lophotrochozoan *Biomphalaria glabrata* snail. *J Innate Immun* (2013) 5(3):261–76. doi: 10.1159/000345909
35. Mone Y, Gourbal B, Duval D, Du Pasquier L, Kiefferjaquinod S, Mitta G. A large repertoire of parasite epitopes matched by a large repertoire of host immune receptors in an invertebrate host/parasite model. *PloS Neglected Trop Dis* (2010) 4(9):e813. doi: 10.1371/journal.pntd.0000813
36. Coustau C, Gourbal B, Duval D, Yoshino TP, Adema CM, Mitta G. Advances in gastropod immunity from the study of the interaction between the snail *Biomphalaria glabrata* and its parasites: a review of research progress over the last decade. *Fish Shellfish Immunol* (2015) 46(1):5–16. doi: 10.1016/j.fsi.2015.01.036
37. Dubief B, Nunes FLD, Basuyaux O, Paillard C. Immune priming and portal of entry effectors improve response to vibrio infection in a resistant population of

the European abalone. *Fish Shellfish Immunol* (2017) 60:255–64. doi: 10.1016/j.fsi.2016.11.017
38. de Melo ES, Brayner FA, Junior NCP, França IRS, Alves LC. Investigation of defense response and immune priming in *Biomphalaria glabrata* and *Biomphalaria straminea*, two species with different susceptibility to *Schistosoma mansoni*. *Parasitol Res* (2020) 119(1):189–201. doi: 10.1007/s00436-019-06495-4
39. Wang J, Yang B, Wang W, Song X, Jiang Q, Qiu L, et al. The enhanced immune protection in Chinese mitten crab *Eriocheir sinensis* against the second exposure to bacteria *Aeromonas hydrophila*. *Front Immunol* (2019) 10:2041. doi: 10.3389/fimmu.2019.02041
40. Wang W, Wang L, Liu Z, Song X, Yi Q, Yang C, et al. The involvement of TLR signaling and anti-bacterial effectors in enhanced immune protection of oysters after *Vibrio splendidus* pre-exposure. *Dev Comp Immunol* (2020) 103:103498. doi: 10.1016/j.dci.2019.103498
41. Weng SP, Guo Z, Sun JJ, Chan SM, He J. A reovirus disease in cultured mud crab, *Scylla serrata*, in southern China. *J Fish Dis* (2007) 30(3):133–9. doi: 10.1111/j.1365-2761.2007.00794.x
42. Li S, Sun L, Wu H, Hu Z, Liu W, Li Y, et al. The intestinal microbial diversity in mud crab (*Scylla paramamosain*) as determined by PCR-DGGE and clone library analysis. *J Appl Microbiol* (2012) 113(6):1341–51. doi: 10.1111/jam.12008
43. Xie C, Chen YW, Sun W, Ding J, Zhou L, Wang S, et al. Transcriptome and expression profiling analysis of the hemocytes reveals a large number of immune-related genes in mud crab *Scylla paramamosain* during *Vibrio parahaemolyticus* infection. *PloS One* (2014) 9(12):e114500. doi: 10.1371/journal.pone.0114500
44. Zhang Z, Li S, Xie C, Zhou L, Li C, Liu W, et al. Innate immune response and gene expression of *Scylla paramamosain* under *Vibrio parahaemolyticus* infection. *Aquacult Res* (2015) 46(2):462–71. doi: 10.1111/are.12194
45. Imjongjirak C, Amparyup P, Tassanakajon A, Sittipraneed S. Antilipopolysaccharide factor (ALF) of mud crab *Scylla paramamosain*: molecular cloning, genomic organization and the antimicrobial activity of its synthetic LPS binding domain. *Mol Immunol* (2007) 44(12):3195–203. doi: 10.1016/j.molimm.2007.01.028
46. Imjongjirak C, Amparyup P, Tassanakajon A, Sittipraneed S. Molecular cloning and characterization of crustin from mud crab *Scylla paramamosain*. *Mol Biol Rep* (2009) 36(5):841–50. doi: 10.1007/s11033-008-9253-0
47. Shan Z, Zhu K, Peng H, Chen B, Liu J, Chen F, et al. The new antimicrobial peptide SpHyastatin from the mud crab *Scylla paramamosain* with multiple antimicrobial mechanisms and high effect on bacterial infection. *Front Microbiol* (2016) 7:1140–0. doi: 10.3389/fmicb.2016.01140
48. Lin Z, Qiao J, Zhang Y, Guo L, Huang H, Yan F, et al. Cloning and characterisation of the SpToll gene from green mud crab, *Scylla paramamosain*. *Dev Comp Immunol* (2012) 37(1):164–75. doi: 10.1016/j.dci.2011.09.003
49. Li X, Zhang X, Zhou J, Ma H, Liu Z, Zhu L, et al. Identification, characterization, and functional analysis of tube and pelle homologs in the mud crab *Scylla paramamosain*. *PloS One* (2013a) 8(10):e76728. doi: 10.1371/journal.pone.0076728
50. Li X, Zhu L, Li L, Ren Q, Huang Y, Lu J, et al. A novel myeloid differentiation factor 88 homolog, SpMyD88, exhibiting SpToll-binding activity in the mud crab *Scylla paramamosain*. *Dev Comp Immunol* (2013b) 39(4):313–22. doi: 10.1016/j.dci.2012.11.011
51. Livak KJ, Schmittgen TD. Analysis of relative gene expression data using real-time quantitative PCR and the 2– ΔΔCT method. *methods* (2001) 25(4):402–8. doi: 10.1006/meth.2001.1262
52. Quintin J, Cheng S, Der Meer JWMV, Netea MG. Innate immune memory: towards a better understanding of host defense mechanisms. *Curr Opin Immunol* (2014) 29:1–7. doi: 10.1016/j.coi.2014.02.006
53. Boehm T, Mccurley N, Sutoh Y, Schorpp M, Kasahara M, Cooper MD. VLR-based adaptive immunity. *Annu Rev Immunol* (2012) 30(1):203–20. doi: 10.1146/annurev-immunol-020711-075038
54. Wang G, Zhang S, Wang Z. Responses of alternative complement expression to challenge with different combinations of *Vibrio anguillarum*, *Escherichia coli* and *Staphylococcus aureus*: evidence for specific immune priming in amphioxus *Branchiostoma belcheri*. *Fish Shellfish Immunol* (2009a) 26(1):33–9. doi: 10.1016/j.fsi.2008.09.018
55. Zhang T, Qiu L, Sun Z, Wang L, Zhou Z, Liu R, et al. The specifically enhanced cellular immune responses in Pacific oyster (*Crassostrea gigas*) against secondary challenge with *Vibrio splendidus*. *Dev Comp Immunol* (2014) 45(1):141–50. doi: 10.1016/j.dci.2014.02.015
56. Zhu F, Du H, Miao ZG, Quan HZ, Xu ZR. Protection of *Procambarus clarkii* against white spot syndrome virus using inactivated WSSV. *Fish Shellfish Immunol* (2009a) 26(5):685–90. doi: 10.1016/j.fsi.2009.02.022
57. Milutinovic B, Kurtz J. Immune memory in invertebrates. *Semin Immunol* (2016) 28(4):328–42. doi: 10.1016/j.smim.2016.05.004
58. Pope EC, Powell A, Roberts EC, Shields RJ, Wardle R, Rowley AF. Enhanced cellular immunity in shrimp (*Litopenaeus vannamei*) after 'vaccination'. *PloS One* (2011) 6(6):e20960. doi: 10.1371/journal.pone.0020960
59. Little TJ, Hultmark D, Read AF. Invertebrate immunity and the limits of mechanistic immunology. *Nat Immunol* (2005) 6(7):651–4. doi: 10.1038/ni1219
60. Wang T, Sun Y, Jin L, Xu Y, Wang L, Ren T, et al. Enhancement of non-specific immune response in sea cucumber (*Apostichopus japonicus*) by *Astragalus membranaceus* and its polysaccharides. *Fish Shellfish Immunol* (2009b) 27(6):757–62. doi: 10.1016/j.fsi.2009.09.002
61. Sun W, Zhang X, Wan W, Wang S, Wen X, Zheng H, et al. Tumor necrosis factor receptor-associated factor 6 (TRAF6) participates in anti-lipopolysaccharide factors (ALFs) gene expression in mud crab. *Dev Comp Immunol* (2017) 67:361–76. doi: 10.1016/j.dci.2016.08.015
62. Sun H, Towb P, Chiem DN, Foster BA, Wasserman SA. Regulated assembly of the Toll signaling complex drives Drosophila dorsoventral patterning. *EMBO J* (2004) 23(1):100–10. doi: 10.1038/sj.emboj.7600033
63. Dong Y, Cirimotich CM, Pike A, Chandra R, Dimopoulos G. Anopheles NF-κB-regulated splicing factors direct pathogen-specific repertoires of the hypervariable pattern recognition receptor AgDscam. *Cell Host Microbe* (2012) 12(4):521–30. doi: 10.1016/j.chom.2012.09.004
64. Chou P, Chang H, Chen I, Lee C, Hung H, Wang KCH. Penaeus monodon Dscam (*PmDscam*) has a highly diverse cytoplasmic tail and is the first membrane-bound shrimp Dscam to be reported. *Fish Shellfish Immunol* (2011) 30(4):1109–23. doi: 10.1016/j.fsi.2011.02.009
65. Armitage S, Freiburg RY, Kurtz J, Bravo IG. The evolution of Dscam genes across the arthropods. *BMC Evolution Biol* (2012) 12(1):53–3. doi: 10.1186/1471-2148-12-53
66. Ng TH, Hung H, Chiang YA, Lin JH, Chen YN, Chuang YC, et al. WSSV-induced crayfish Dscam shows durable immune behavior. *Fish Shellfish Immunol* (2014) 40(1):78–90. doi: 10.1016/j.fsi.2014.06.023
67. Brites D, Mctaggart SJ, Morris K, Anderson JE, Thomas K, Colson I, et al. The Dscam homologue of the crustacean daphnia is diversified by alternative splicing like in insects. *Mol Biol Evol* (2008) 25(7):1429–39. doi: 10.1093/molbev/msn087
68. Wang J, Wang L, Gao Y, Jiang Q, Yi Q, Zhang H, et al. A tailless Dscam from *Eriocheir sinensis* diversified by alternative splicing. *Fish Shellfish Immunol* (2013) 35(2):249–61. doi: 10.1016/j.fsi.2013.04.029
69. Chen Y, Aweya JJ, Sun W, Wei X, Gong Y, Ma H, et al. SpToll1 and SpToll2 modulate the expression of antimicrobial peptides in *Scylla paramamosain*. *Dev Comp Immunol* (2018) 87:124–36. doi: 10.1016/j.dci.2018.06.008
70. Li W, Tang X, Chen Y, Sun W, Liu Y, Gong Y, et al. Characterize a typically Dscam with alternative splicing in mud crab *Scylla paramamosain*. *Fish Shellfish Immunol* (2017) 71:305–18. doi: 10.1016/j.fsi.2017.10.023

Conflict of Interest: The authors declare that the research was conducted in the absence of any commercial or financial relationships that could be construed as a potential conflict of interest.

Copyright © 2020 Zhang, Zeng, Sun, Wang and Zhang. This is an open-access article distributed under the terms of the Creative Commons Attribution License (CC BY). The use, distribution or reproduction in other forums is permitted, provided the original author(s) and the copyright owner(s) are credited and that the original publication in this journal is cited, in accordance with accepted academic practice. No use, distribution or reproduction is permitted which does not comply with these terms.

frontiers in Immunology

ORIGINAL RESEARCH
published: 28 October 2020
doi: 10.3389/fimmu.2020.567838

Transcriptomic Profiling of the Adaptive and Innate Immune Responses of Atlantic Salmon to *Renibacterium salmoninarum* Infection

Khalil Eslamloo[1], Albert Caballero-Solares[1], Sabrina M. Inkpen[1], Mohamed Emam[1], Surendra Kumar[1], Camila Bouniot[2], Ruben Avendaño-Herrera[3], Eva Jakob[2] and Matthew L. Rise[1]*

[1] Department of Ocean Sciences, Memorial University of Newfoundland, St. John's, NL, Canada, [2] Cargill Innovation Center—Colaco, Calbuco, Chile, [3] Facultad Ciencias de la Vida, Viña del Mar, and FONDAP Interdisciplinary Center for Aquaculture Research (INCAR), Universidad Andrés Bello, Santiago, Chile

OPEN ACCESS

Edited by:
Monica Hongroe Solbakken, University of Oslo, Norway

Reviewed by:
Nguyen T. K. Vo, McMaster University, Canada
Agustin Barria, The University of Edinburgh, United Kingdom

***Correspondence:**
Khalil Eslamloo
keslamloo@mun.ca

Specialty section:
This article was submitted to Comparative Immunology, a section of the journal Frontiers in Immunology

Received: 30 May 2020
Accepted: 07 September 2020
Published: 28 October 2020

Citation:
Eslamloo K, Caballero-Solares A, Inkpen SM, Emam M, Kumar S, Bouniot C, Avendaño-Herrera R, Jakob E and Rise ML (2020) Transcriptomic Profiling of the Adaptive and Innate Immune Responses of Atlantic Salmon to Renibacterium salmoninarum Infection. Front. Immunol. 11:567838. doi: 10.3389/fimmu.2020.567838

Bacterial Kidney Disease (BKD), which is caused by a Gram-positive, intracellular bacterial pathogen (*Renibacterium salmoninarum*), affects salmonids including Atlantic salmon (*Salmo salar*). However, the transcriptome response of Atlantic salmon to BKD remained unknown before the current study. We used a 44K salmonid microarray platform to characterise the global gene expression response of Atlantic salmon to BKD. Fish (~54 g) were injected with a dose of *R. salmoninarum* (H-2 strain, 2×10^8 CFU per fish) or sterile medium (control), and then head kidney samples were collected at 13 days post-infection/injection (dpi). Firstly, infection levels of individuals were determined through quantifying the *R. salmoninarum* level by RNA-based TaqMan qPCR assays. Thereafter, based on the qPCR results for infection level, fish ($n = 5$) that showed no (control), higher (H-BKD), or lower (L-BKD) infection level at 13 dpi were subjected to microarray analyses. We identified 6,766 and 7,729 differentially expressed probes in the H-BKD and L-BKD groups, respectively. There were 357 probes responsive to the infection level (H-BKD vs. L-BKD). Several adaptive and innate immune processes were dysregulated in *R. salmoninarum*-infected Atlantic salmon. Adaptive immune pathways associated with lymphocyte differentiation and activation (e.g., lymphocyte chemotaxis, T-cell activation, and immunoglobulin secretion), as well as antigen-presenting cell functions, were shown to be differentially regulated in response to BKD. The infection level-responsive transcripts were related to several mechanisms such as the JAK-STAT signalling pathway, B-cell differentiation and interleukin-1 responses. Sixty-five microarray-identified transcripts were subjected to qPCR validation, and they showed the same fold-change direction as microarray results. The qPCR-validated transcripts studied herein play putative roles in various immune processes including pathogen recognition (e.g., *tlr5*), antibacterial activity (e.g., *hamp* and *camp*), regulation of immune responses (e.g., *tnfrsf11b* and *socs1*), T-/B-cell differentiation (e.g., *ccl4*, *irf1* and *ccr5*), T-cell functions (e.g., *rnf144a*, *il13ra1b* and *tnfrsf6b*), and

antigen-presenting cell functions (e.g., *fcgr1*). The present study revealed diverse immune mechanisms dysregulated by *R. salmoninarum* in Atlantic salmon, and enhanced the current understanding of Atlantic salmon response to BKD. The identified biomarker genes can be used for future studies on improving the resistance of Atlantic salmon to BKD.

Keywords: Bacterial Kidney Disease (BKD), *Salmo salar*, microarray, antibacterial responses, teleost, infection level, transcriptome, individual-dependent immune response to pathogen

INTRODUCTION

Due to the limitation of naturally supplied aquatic stocks and a growing human population, fish aquaculture has become one of the main sources fulfilling the global demand for fish consumption (1, 2). However, aquaculture faces several health challenges (e.g., bacterial or viral diseases), and an enhanced understanding of the fish immune and physiological responses to pathogens may help combat epidemics in aquaculture environments. Atlantic salmon (*Salmo salar*) is one of the most economically important fish species prevalently farmed in marine aquaculture worldwide (1, 3), and is susceptible to several Gram-positive and Gram-negative bacterial pathogens causing high mortalities and economic losses (4, 5). *Renibacterium salmoninarum* is a Gram-positive intracellular pathogen that causes Bacterial Kidney Disease (BKD) in Atlantic salmon and other salmonids [e.g., sockeye salmon (*Oncorhynchus nerka*) and rainbow trout (*O. mykiss*)] (6). BKD has been reported in Canada, Chile and several other countries worldwide (6, 7), and can cause up to 40% cumulative mortality in farmed Atlantic salmon (8, 9).

R. salmoninarum infection begins in the fish head kidney through formation of granulomas, and then develops in other internal organs (e.g., posterior kidney and liver) of the fish (7–9). Mortalities caused by BKD may be associated with immunosuppressive effects of *R. salmoninarum* on the host (10). An enhanced understanding of the Atlantic salmon response to *R. salmoninarum* can aid in the development of preventive management tools for BKD (e.g., vaccines and therapeutic diets). Previous *in vivo* and *in vitro* studies examined gene expression responses to *R. salmoninarum* in rainbow trout (11) and Chinook salmon (*O. tshawytscha*) (12) kidney as well as rainbow trout macrophages (13) and Atlantic Salmon Kidney (ASK) cell line (14). A genomics-based study used Suppression Subtractive Hybridisation (SSH) to identify BKD-responsive genes in Chinook salmon (15). A recent study reported expression responses of 22 genes (e.g., transcripts encoding interleukins and interferons) in the head kidney of Atlantic salmon infected with *R. salmoninarum* at different temperatures (16). Since vaccination with formalin-killed *R. salmoninarum* was found to enhance the resistance of salmonids to BKD (9), microarrays were previously used to profile the transcriptome response of Atlantic salmon to formalin-killed *R. salmoninarum* bacterin (17). Although this previous study enhanced our understanding of the Atlantic salmon immune response to *R. salmoninarum*-derived antigens, the transcriptome response and molecular pathways underlying Atlantic salmon response to live *R. salmoninarum* pathogen remained uncharacterised before the current study. Considering the immunomodulatory effects of *R. salmoninarum* on its host, profiling the BKD-responsive genes in Atlantic salmon is of prominent importance for the development of methods for combating BKD.

Microarray analyses can determine the transcriptome profile of immunological responses in a species (18). In addition to the aforementioned *R. salmoninarum* bacterin study (17), microarrays were previously employed to profile the antibacterial responses of Atlantic salmon to other bacterial pathogens such as *Piscirickettsia salmonis* (19), and *Aeromonas salmonicida* (20, 21) as well as commercial vaccines (e.g., for immunisation against *Yersinia ruckeri* and *Vibrio* spp.) (22, 23).

The consortium for Genomic Research on All Salmonids Project (cGRASP)-designed Agilent 44K salmonid oligonucleotide microarray (24) was previously used in several immune-related studies in Atlantic salmon and rainbow trout (17, 25–29). In the present study, we used this powerful microarray platform to identify Atlantic salmon head kidney transcripts responsive to *R. salmoninarum* pathogen and determine if the level of *R. salmoninarum* infection [i.e., higher and lower susceptibility levels corresponding to higher and lower infection levels, respectively, at 13 days post-infection/injection (dpi) as determined by TaqMan assays] influenced the Atlantic salmon response to BKD. All the fish in the present study received the same dose of *R. salmoninarum*, but individuals with various levels of infection (i.e., higher and lower infection level groups) at 13 dpi, as shown by reverse transcription—quantitative polymerase chain reaction (qPCR) TaqMan assays, were used for transcriptome analyses. Complementary to our previous investigation (17), the present study identified the genes and molecular pathways associated with Atlantic salmon response to *R. salmoninarum* pathogen, and provided a set of valuable biomarkers for future BKD-related investigations. Furthermore, the infection level-responsive genes identified herein broaden horizons for the understanding of the correlations between *R. salmoninarum* level and Atlantic salmon antibacterial responses.

MATERIALS AND METHODS

Animals

Atlantic salmon parr [54 ± 6 g; (mean ± SE)] were purchased from a local salmon production hatchery and transferred to the Cargill Innovation Center—Colaco, Chile. Before transportation and by sanitary regulations, qPCR assays were used to monitor

Atlantic salmon diseases, and fish were certified to be free of pathogens previously reported in Chilean salmon farms [i.e., infectious salmon anaemia virus (ISAV), infectious pancreatic necrosis virus (IPNV), *P. salmonis* and *R. salmoninarum*; (30)]. Fish were distributed to seven circular tanks (200 L tanks; 68 fish per tank), using a freshwater [i.e., five practical salinity unit (psu)] flow-through system (4.3 L min^{-1}). Prior to the infection trial, fish were acclimatised to the experimental conditions for 2 weeks and held at 10–11°C water temperature under a 24 h light photoperiod. Fish were fed to satiation using a standard EWOS commercial diet. Water quality parameters were monitored daily (i.e., temperature, oxygen saturation, salinity, and pH). Fish were fasted 12 h before all experimental procedures (e.g., injection and sampling), and were anaesthetised using Benzocaine (150 μl L^{-1} BZ-20®, Veterquímica S.A., Maipú, Santiago, Chile) before handlings and injections. All procedures in this study were conducted following the guidelines of the Canadian Council on Animal Care (31).

R. salmoninarum Strain and Culture

The previously characterised Chilean strain of *R. salmoninarum* (H-2), obtained from cage-cultured Atlantic salmon in 2014, was used for the present study. This strain was isolated from fish with clinical signs of BKD in southern Chile. Previous studies showed that strain H-2 has high siderophore production, which can result in high virulence potential (14, 32, 33). The strain identification was confirmed as *R. salmoninarum* with nested PCR, as described by Chase and Pascho (34), and culture purity was confirmed by Gram-staining, cell morphology and colony morphology (33). Stock cultures were maintained frozen at −80°C in Cryobille tubes (AES Laboratoire, Combourg, France) or in KDM-2 with 15% glycerol. The bacteria were cultured in KDM-2 [1% tryptone (AES Laboratoire), 0.05% yeast extract (AES Laboratoire), 0.1% L-cysteine hydrochloride (US Biological, Salem, MA), 10% fetal bovine serum (Biological Industries, Cromwell, CT); Evelyn 1977] agar under aerobic conditions for 10–15 days at 15°C, and with not more than two subcultures grown from glycerol-amended stock cultures.

Pathogen Infection

For BKD challenge, inocula were prepared through collecting the bacterial cells from KDM-2 plates and re-suspending in KDM-2 broth (4 ml). After reaching the logarithmic phase, bacterial culture was re-inoculated in KDM-2 broth (400 ml) at 15°C with agitation (50 rpm) to achieve an initial bacterial concentration of 3×10^9 cells ml^{-1}, which was determined using direct microscopy count. All fish in the BKD treatment (i.e., five tanks) were intraperitoneally injected with 200 μl of *R. salmoninarum* to obtain a final dose of 2×10^8 colony-forming units (CFU) per fish, as determined by the direct plate count. Fish were challenged using a single high dose of *R. salmoninarum*, as we aimed to study Atlantic salmon response to a lethal level of this pathogen. There was no previous study on mortalities of Atlantic salmon challenged with *R. salmoninarum*, strain H-2. However, a previous study reported fast and high mortalities (i.e., 100% mortality within 15 days) of Atlantic salmon (i.e., 50–70 g) challenged with 10^8 cells of other strains of *R. salmoninarum* (35). Therefore, we selected a *R. salmoninarum* dose slightly higher than that used in Daly et al. (35) to ensure high mortalities and a strong immune response of Atlantic salmon to BKD. Three tanks in the BKD group were used for monitoring fish mortality, and 2 tanks were used for sampling. Fish in the control group (i.e., two tanks) were injected with 200 μl of sterile KDM-2 broth. Fish in both treatments were fed as described above and held in optimal conditions (i.e., temperature 10–11°C and oxygen saturation above 90%) during the infection trial. Mortalities were recorded daily. Mortalities started at 24 dpi and 100% mortality was seen at 38 dpi. **Supplementary Figure S1** shows the cumulative mortality in each tank. Considering mortality data and the objectives of the present study, we selected 13 dpi for sampling and transcriptome analyses. Our sampling time point (i.e., 13 dpi) was approximately at the mid-point of the infection challenge between the start of the infection and the onset of mortalities; we anticipated that it would provide understanding of both early and late immune responses to *R. salmoninarum*. Further, with respect to chronic development of BKD, 13 dpi was considered as the adequate time for pathogen accumulation and for the *R. salmoninarum*-infected fish to show the individual-dependent variations in immune response; correspondingly, it was a suitable time point for studying the differences between the response of fish with higher and lower detected infection levels (i.e., higher and lower susceptible individuals). All the fish in the current study were infected with the same dose of *R. salmoninarum*, and infection level represents the quantitative results of pathogen detection, determined by Taq-Man qPCR assays for each individual at 13 dpi.

Sampling and RNA Extraction

Ten fish in each experimental tank (i.e., two tanks per treatment; $n = 20$), were euthanized using an overdose of Benzocaine [i.e., initial anaesthesia using 150 μl L^{-1} BZ-20® followed by euthanasia using 300 μl L^{-1} BZ-20® (Veterquímica S.A.)] at 13 dpi. Thereafter, individuals were dissected, and head kidney samples were collected and stored in RNA*later* (Thermo Fisher Scientific, Waltham, MA) at 4°C for 24 h. Then, RNA*later* was removed, and samples were kept at −80°C until RNA extraction. **Supplementary Figure S2** illustrates the overall experimental design of the present study. The average (mean ± SE) fish weight was 56.7 ± 1.7 g and 50.96 ± 1.6 g for all sampled fish ($n = 20$) in the control and BKD group, respectively, at 13 dpi.

Total RNA was extracted using TRIzol® Reagent (Thermo Fisher Scientific) following the manufacturer's instructions. Head kidney samples (50–100 mg) were TRIzol-lysed using a tissue homogeniser (Precellys 24, Bertin Instruments, Montigny-Le-Bretonneux, France) before total RNA extraction. To remove residual genomic DNA and enhance RNA quality, total RNA samples were on-column DNase-treated and column-purified using PureLink™ RNA Mini Kit (Thermo Fisher Scientific) and PureLink™ DNAse set (Thermo Fisher Scientific), according to the manufacturer's protocol.

The column-purified RNAs were quantified using a NanoDrop spectrophotometer (ND-1000), and RNA integrity was assessed using 1% agarose gel electrophoresis. The RNA samples used in the microarray and qPCR analyses of the current

study showed high integrity (i.e., tight 18S and 28S ribosomal RNA bands) and purity (i.e., A260/230 > 1.7 and A260/280 ratios > 1.8).

TaqMan Assays for Infection Level Detection and Sample Selection

The reverse transcription—quantitative polymerase chain reaction is referred to as qPCR in the current study. TaqMan qPCR assays were used to assess the infection level in DNase-treated and column-purified RNA samples of Atlantic salmon from both BKD and control groups at 13 dpi. We aimed to test if individuals that were injected with the same dose of live *R. salmoninarum* showed different infection levels at 13 dpi. TaqMan primers and probe for *R. salmoninarum 16S ribosomal RNA* (in-house developed by Cargill Innovation) were used for BKD detection, and Atlantic salmon *elongation factor 1 alpha-1* (*ef1a1*) (36) was used as an internal control. **Supplementary Table S1** shows the sequence and quality control results of TaqMan primers and probes used in the current study. All TaqMan assays in the present study were conducted in duplicate using the ViiA 7 Real-Time PCR system (384-well format) (Applied Biosystems, Thermo Fisher Scientific) and AgPath-ID One-Step RT-PCR Reagents (Applied Biosystems, Thermo Fisher Scientific). The assays were performed using 13 μl reactions consisting of 6.5 μl 2X RT-PCR Buffer, 0.52 μl 25X RT-PCR Enzyme Mix, 0.88 μl Detection Enhancer, 0.39 μl (600 nM) forward primer, 0.59 μl (900 nM) reverse primer, 0.23 μl (175 nM) Probe, 0.89 μl DEPC-treated water and 3 μl RNA template (50–100 ng, see below). The TaqMan PCR program comprised one cycle of 45°C for 10 min (reverse transcription), one cycle of 95°C for 10 min, and 45 cycles of 95°C for 15 s and 60°C for 45 s. A pool consisting of equal amounts of RNA from five individuals in the BKD group was used as a template to test the performance and amplification efficiencies of primers. Primer quality control tests were performed using a 5-point, 3-fold serial dilution of the pool RNA template, starting with 100 ng of input total RNA per reaction and a no-template control. Then, the infection level assays for each sample were measured using 50 ng of RNA input in each TaqMan reaction. Also, no-template, positive (i.e., a pool of RNA from 10 fish in BKD group) and negative (i.e., DNase-treated and column-purified RNA from the skin of a non-infected Atlantic salmon) controls were included in all TaqMan assays (i.e., both *R. salmoninarum 16S ribosomal RNA* and Atlantic salmon *ef1a1*). Using QuantStudio™ Real-Time PCR Software (Version 1. 3) (Applied Biosystems, Thermo Fisher Scientific), the fluorescence threshold cycle (C_T) values and amplification efficiencies of primers were used to calculate the relative quantity (RQ; i.e., calibrated to the sample with the lowest normalised expression level) of *R. salmoninarum 16S ribosomal RNA* through normalisation to Atlantic salmon *ef1a1* (C_T range: 18.03–18.81). Five head kidney samples from the control group were included in the microarray and qPCR studies. In addition, five fish with *16S ribosomal RNA* C_T values above 25 were selected as samples with lower infection level at 13 dpi or lower susceptibility (L-BKD) for microarray and qPCR analyses (**Supplementary Figure S3**), and five fish showing C_T values below 22 were selected as samples with higher infection level at 13 dpi or higher susceptibility (H-BKD) and were included in the microarray and qPCR studies (**Supplementary Figure S3**). The level of *R. salmoninarum* infection, which can also reflect the susceptibility, at 13 dpi significantly varied between the H-BKD and L-BKD groups (**Supplementary Figure S3**); therefore, these samples were used to test if various levels of infection at 13 dpi can influence the transcript expression response of Atlantic salmon to *R. salmoninarum*. Moreover, there was no significant correlation ($p = 0.6$) between weight and the infection level of individuals at 13 dpi, and no significant difference among the weight of individuals in the control, H-BKD and L-BKD groups ($n = 5$). Correspondingly, the differences seen between the infection level of fish [i.e., individuals with higher (H-BKD) and lower (L-BKD) infection level, as detected by Taq-Man assays] at 13 dpi can be associated with the individual-dependent variations in immune response and susceptibility to BKD.

Microarray Experimental Design and Hybridisation

The selected head kidney samples of five individuals in the control group, five individuals showing higher level of *R. salmoninarum* infection (H-BKD) at 13 dpi and five individuals with lower level of *R. salmoninarum* infection (L-BKD) at 13 dpi were subjected to microarray analysis (i.e., 15 samples in total). The current microarray experiment was designed based upon the Minimum Information About a Microarray Experiment (MIAME) guidelines (37), and it was conducted using cGRASP-designed Agilent 44K salmonid oligonucleotide microarrays (24). Briefly, anti-sense amplified RNA (aRNA) for each sample was *in vitro* transcribed using 1 μg of DNase-treated and column-purified RNA and the Amino Allyl MessageAmp™ II aRNA Amplification Kit (Ambion, Thermo Fisher Scientific), following the manufacturer's instructions. Gel electrophoresis and NanoDrop spectrophotometry were utilised to quality-check and measure the concentration, respectively, of aRNAs. The common reference was composed of an aRNA pool of all 15 samples (i.e., 15 μg from each sample) in the study. Twenty micrograms of aRNA from each sample or common reference were precipitated through a standard ethanol precipitation method and re-suspended in coupling buffer (Ambion, Thermo Fisher Scientific). Thereafter, the experimental samples were labelled with Cy5 (GE Healthcare Life Sciences, Buckinghamshire, UK), whereas the common reference was labelled with Cy3 (GE Healthcare Life Sciences), according to the manufacturer's instructions. Labelling efficiency and labelled aRNA concentrations were assessed using NanoDrop spectrophotometry (i.e., the microarray feature). For each individual sample, 825 ng of its corresponding Cy5-labelled aRNA and 825 ng of Cy3-labelled common reference were pooled, fragmented and co-hybridised to a 44K microarray following the manufacturer's recommendation (Agilent, Santa Clara, CA). The hybridisation of arrays was performed at 65°C for 17 h with rotation (10 rpm) using an Agilent hybridisation oven. According to the manufacturer' instruction, the wash buffers were supplemented with 10% Triton X-102 (Agilent) at

the concentration of 0.5 μl ml^{-1}. Slides were washed with Gene Expression Wash Buffer 1 (Agilent) and then Gene Expression Wash Buffer 2 (Agilent), using 50 ml Conical Centrifuge Tubes and a rocker platform [VWR Rocker (Radnor, PA); speed 40, tilt 6], for 5 min at room temperature. Slides were dried by centrifuging at 200 × *g* for 5 min at room temperature prior to scanning.

Microarray Data Acquisition and Analyses

Microarray slides were scanned at 5 μm resolution using a SureScan Microarray Scanner System (Agilent) and Microarray Scan Control Software v.9.1 following the Agilent HD 2-color gene expression microarray scan protocol. The signal intensity data were extracted and Loess-normalised using Agilent Feature Extraction Software v12.0 (Agilent). In GeneSpring Software v14.9 (Agilent), probes of low or marginal quality as well as absent values in more than 25% of all 15 arrays were removed from the dataset, and the missing values were imputed. The final dataset, passing the quality control in GeneSpring and subjected to the statistical analyses, consisted of 33,780 probes for all arrays (GEO accession number: GSE150335). The statistical analyses of microarray data were conducted using GeneSpring Software v14.9. One-way ANOVA was used to determine if there were any significant differences among groups ($p \leq 0.01$). This analysis was followed by Tukey's multiple comparisons *post-hoc* test to identify significant differences ($p \leq 0.01$) between groups, and Multiple Testing Correction was performed using the Benjamini-Hochberg procedure.

The differentially expressed probes (DEPs) were re-annotated using the contigs (24) based on which the 60-mer oligonucleotide probes on the array were designed. The BLASTx searches of NCBI's non-redundant (nr) amino acid sequence and Swiss-Prot databases (E-value < 1e-05) were performed using Blast2GO software (BioBam Bioinformatics S.L., Valencia, Spain) (38, 39). Using R and gplots Package, the microarray $\log_2$ ratios of the identified DEPs were median-centred and subjected to Pearson correlation and complete linkage hierarchical clustering.

The pathway enrichment analyses of different transcript lists (i.e., *R. salmoninarum* infection-responsive transcripts shared between H-BKD and L-BKD groups, infection level-responsive transcripts as well as *R. salmoninarum* infection-responsive transcripts only identified in the H-BKD or L-BKD group) were determined using ClueGO (40) plugin in Cytoscape (v3.5.1) (41). Enrichment (i.e., Right-sided hypergeometric test) analyses were performed using the Gene Ontology database (UniProt: 27.02.2019) for Biological Processes (BPs) and Benjamini-Hochberg test for *p*-value corrections ($p < 0.05$). Furthermore, ClueGO linked the enriched BP GO terms using kappa statistics (42), thus generating networks of functionally-associated terms. Cohen's kappa coefficients are calculated for each term-term relationships based on the shared genes between them. The obtained term-term kappa coefficients were also used to define functional groups of highly-connected terms within the GO networks. The kappa coefficient threshold set for the analysis was 0.4, i.e., term-term relationships with lower coefficients were considered non-significant.

For the subsequent interpretation of the resultant networks, the enriched GO terms were classified, using Gene Ontology Browser (http://www.informatics.jax.org), into 6 functional themes: (1) adaptive immune response; (2) immune response; (3) response to stress; (4) development; (5) metabolic process; and (6) cellular process, localisation, and structure. The GO terms were classified based on the biological process to which they were related and/or their parent terms (especially for highly-specific terms). Briefly, GO terms of biological processes and pathways related to adaptive immunity were classified as "adaptive immune response". Those immune-related GO terms that could not be classified as "adaptive immune response" were annotated as "immune response". Other GO terms associated with responses to abiotic and biotic stimuli that are not necessarily involved in immune processes or pathways fell within the "response to stress" theme. GO terms related to tissue development and/or derived from the parent term GO:0032502 (i.e., developmental process) were classified as "development". GO terms associated with metabolism-related processes and pathways and/or that have the parent term GO:0008152 (i.e., metabolic process) were classified as "metabolic process". The theme "cellular process, localisation, and structure" grouped all those GO terms not classifiable in any of the previous and derived from either GO:0009987 (i.e., cellular process) or GO:0051179 (i.e., localisation). In a few instances, terms that were close to the root of the ontology could not be assigned to one of the themes (i.e., the term was too general). Finally, some functional groups comprise GO terms from different themes; in such cases, the functional group is coloured according to the theme with the highest number of GO terms.

qPCR Validation

A subset of microarray-identified transcripts was subjected to qPCR analysis to test the validity of the microarray results. We selected 35 (i.e., 23 up-regulated and 12 down-regulated) transcripts of interest (TOI) from the BKD-responsive list overlapping only between the L-BKD and H-BKD groups (i.e., 6,285 DEPs; see **Figure 1A**). Moreover, 10 TOI (i.e., five up-regulated and five down-regulated) were selected from the responsive transcript list specific to the H-BKD group (i.e., 289 DEPs; **Figure 1A**), whereas 9 TOI (i.e., six up-regulated and three down-regulated) were taken from the L-BKD-specific transcript list (i.e., 1,176 DEPs; **Figure 1A**). To validate the infection level-responsive gene list, 11 TOI (i.e., six up-regulated and five down-regulated) were selected from transcripts differentially expressed between the H-BKD and L-BKD groups (i.e., total of 357 DEPs; **Figure 1A**). Among these infection level-responsive transcripts, five TOI (i.e., three up-regulated and two down-regulated) were from the identified transcripts in all comparison (i.e., 123 DEPs), and one down-regulated transcript was selected from the infection level-specific gene list (i.e., 20 DEPs). Also, two (i.e., one up-regulated and one down-regulated) and three (i.e., two up-regulated and one down-regulated) TOI were from the infection level-responsive transcripts overlapping with only-L-BKD and only-H-BKD responsive lists, respectively. Levels of these TOI were measured in samples from all groups (i.e., Control, L-BKD and H-BKD; 15 samples in total). Primers used for qPCR analyses were either designed using Primer3web v4.0.0

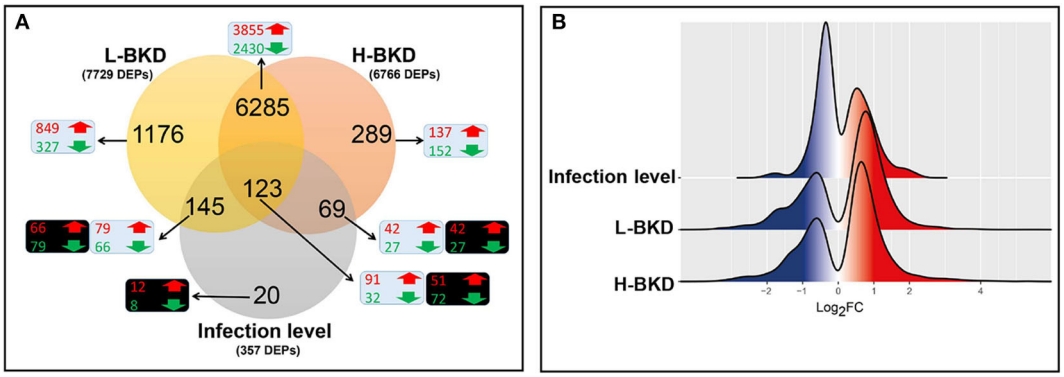

FIGURE 1 | Microarray results of Atlantic salmon head kidney in response to *R. salmoninarum* infection. Fish with no (Control), lower (L-BKD) or higher (H-BKD) level of *R. salmoninarum* infection at 13 dpi were used for microarray analyses ($n = 5$). Fish in the L-BKD and H-BKD groups were infected with the same dose of *R. salmoninarum*, but they showed different levels of infection at 13 dpi, as determined by RNA-based Taq-Man assays. H-BKD: H-BKD vs. Control. L-BKD: L-BKD vs. Control. Infection level: H-BKD vs. L-BKD. **(A)** Overview of microarray results. Differentially expressed probes (DEPs) identified by ANOVA ($p < 0.01$). The number of up-regulated (red) and down-regulated (green) probes in BKD- (L-BKD or H-BKD vs. Control) and infection level (H-BKD vs. L-BKD)-responsive lists are shown in blue and black boxes, respectively. **(B)** Histogram of the frequency density of $\log_2$-transformed fold-changes (FC) for the DEPs of the different comparisons. Red and blue colours indicate up-regulation and down-regulation, respectively.

(http://primer3.ut.ee/) or taken from previous studies (17, 28, 43–45) (see **Supplementary Table S1**).

First-strand cDNA templates were synthesised in 20 µl reactions using 1 µg of DNase-treated, column-purified total RNA, nuclease-free water (Invitrogen, Thermo Fisher Scientific), 1 µl of dNTPs (10 mM each; Invitrogen, Thermo Fisher Scientific), random primers (250 ng; Invitrogen, Thermo Fisher Scientific), DTT (10 mM final concentration), first-strand buffer (1X final concentration) and M-MLV reverse transcriptase (200 U; Invitrogen) according to the manufacturer's instructions.

The qPCR assays used in this study were performed following the Minimum Information for Publication of qPCR Experiments (MIQE) guidelines (46). All qPCR assays were conducted in triplicate using the ViiA 7 Real-Time PCR system (384-well format) (Applied Biosystems, Thermo Fisher Scientific), and the qPCR reactions (13 µl) consisted of 6.5 µl Power SYBR Green PCR Master Mix (Applied Biosystems, Thermo Fisher Scientific), 50 nM of each forward and reverse primers (0.52 µl of forward and 0.52 µl of reverse primers), 1.46 µl nuclease-free water (Invitrogen, Thermo Fisher Scientific) and 4 µl cDNA (see below for input total RNA quantity per reaction). The details of the PCR program are described in Eslamloo et al. (47). Two pools were generated using cDNA of all individuals from both BKD groups and control group for primer quality control of up- and down-regulated genes by BKD, respectively. For each primer set (i.e., TOI or normalisers), a 5-point, 3-fold serial dilution of the given cDNA template (i.e., standard curves; starting with cDNA representing 10 ng of input total RNA), as well as a no-template control were used to measure amplification efficiencies. The amplification efficiencies of 10 out of 67 primer pairs were calculated using 4-point serial dilutions of cDNA (see **Supplementary Table S1**).

Primer pairs used in the current study showed an amplification efficiency (48) ranging between 83 and 110%, an amplicon with a single melting peak and no primer-dimer present in the no-template control (**Supplementary Table S1**). Firstly, the expression of eight candidate normalisers [i.e., *60S ribosomal protein 32* (*rpl32*), *ef1a1*, *elongation factor 1 alpha-2* (*ef1a2*), *polyadenylate-binding protein, cytoplasmic 1* (*pabpc1*), *eukaryotic translation initiation factor 3 subunit D* (*eif3d*), *ATP binding cassette sub-family f member 2* (*abcf2*), *RNA polymerase 2* (*polr2*), and *NADH dehydrogenase (ubiquinone) iron-sulfur protein 7* (*ndufs7*)] was measured in all of the experimental samples (five fish per treatment) to determine the most suitable endogenous controls. Thereafter, in the qBase software (49), C_T values were analysed by geNorm to calculate the M-value, i.e., a measure of transcript expression stability. Two normaliser transcripts, *ef1a2* and *pabpc1*, showing low M-values ($M < 0.2$) and a comparable expression (i.e., C_T values) in all samples were selected for the qPCR assays. Then, the transcript (mRNA) levels of TOI and normalisers were assessed in all 15 samples using cDNA template representing 5 ng of input RNA per PCR reaction as well as a no-template control. The relative quantity (RQ) of each tested transcript was calculated through normalisation to both normaliser transcripts, as implemented by QuantStudio™ Real-Time PCR Software, Relative Quantification Study Application (Version 1.3; Applied Biosystems, Thermo Fisher Scientific). RQ calculations were conducted incorporating the amplification efficiencies of all genes, and RQ value of each transcript was calibrated to the sample that had the lowest normalised gene expression (i.e., assigned an RQ value = 1.0).

All statistical analyses were conducted using the Prism package v7.0 (GraphPad Software Inc., La Jolla, CA). The normality of data (i.e., RQ values) was analysed using the Kolmogorov-Smirnov normality test. Then, One-way ANOVA was applied to identify the differences among groups, followed by Tukey's multiple comparisons *post-hoc* test to determine significant differences ($p \leq 0.05$) between groups. Kruskal-Wallis test ($p < 0.05$) was used to determine the significant differences

between the groups for the transcripts that did not pass the normality test. Furthermore, Pearson's (r) correlation was used to test if the expression of transcripts correlated with infection level (RQ values of *R. salmoninarum 16S ribosomal RNA*).

PRIMER 7 (PRIMER-E Ltd., Auckland, New Zealand) was used to identify gene expression patterns among fish groups and TOI via principal coordinates analysis (PCoA) based on a Bray-Curtis similarity matrix generated using RQ values of TOI as well as infection level values (i.e., RQ values of *16S ribosomal RNA* of *R. salmoninarum* normalised to Atlantic salmon *ef1a1* and calibrated to the sample with the lowest normalised expression level).

RESULTS

Microarray Analyses

In this study, we used a 44K microarray platform to profile the response of Atlantic salmon head kidney to BKD. We compared the transcriptome profile of fish showing a lower (L-BKD) or a higher (H-BKD) level of the *R. salmoninarum* infection together and with a control group. The L-BKD and H-BKD fish were injected with the same dose of live *R. salmoninarum*, but they showed various infection levels, which also indicate the fish susceptibility to *R. salmoninarum,* at 13 dpi, as determined by TaqMan assays. **Figure 1A** illustrates the overall results of the microarray analyses in the present study. Using one-way ANOVA ($p \leq 0.01$), 6,766 DEPs were identified in the H-BKD group, whereas 7,729 DEPs were found in the L-BKD group compared to the control. When the H-BKD and L-BKD groups were compared, there were 357 DEPs significantly affected by the infection level (i.e., H-BKD vs. L-BKD; 171 up-regulated and 186 down-regulated). As shown by the Venn diagrams (**Figure 1A**), all three comparisons in the present study shared 123 DEPs. There were 6,408 DEPs (6,285 + 123 DEPs: 3,946 up-regulated and 2,462 down-regulated) overlapping between the H-BKD and L-BKD transcript lists. Among the infection level-responsive transcripts, 69 and 145 DEPs overlapped with BKD-responsive probes identified only in the H-BKD and L-BKD groups, respectively. **Supplementary Table S2** shows the complete list of the identified DEPs. As shown by **Figure 1A**,

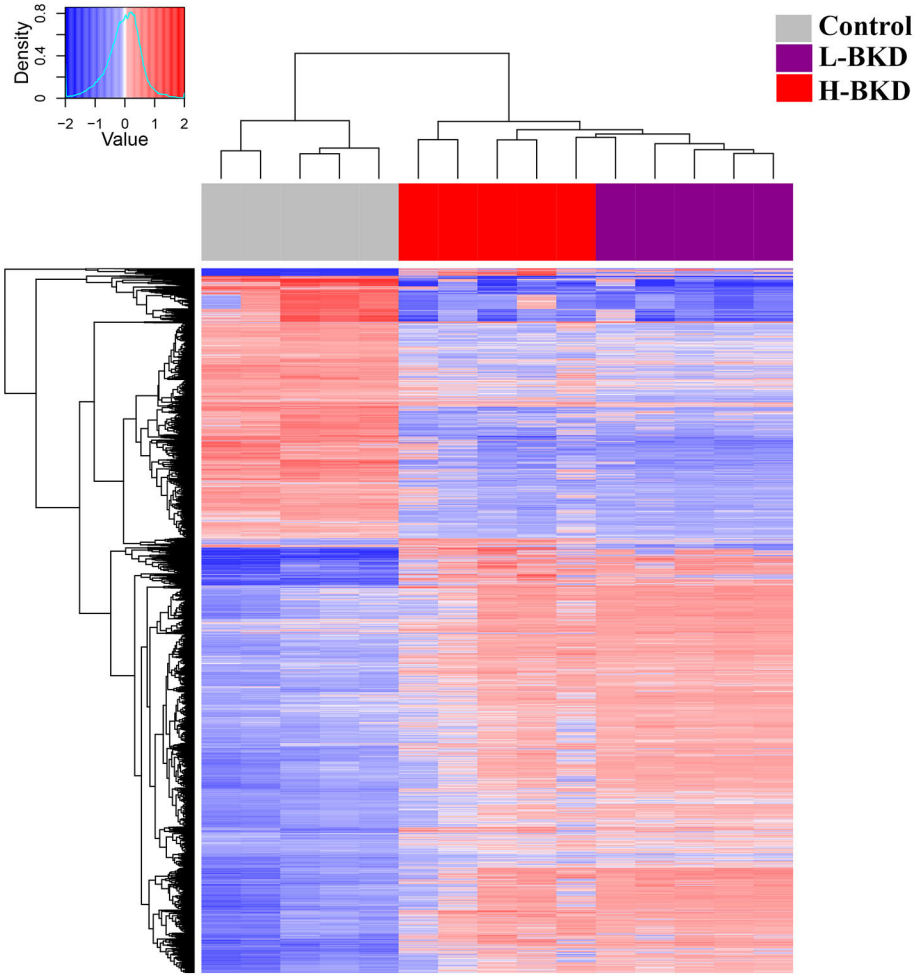

FIGURE 2 | Hierarchical clustering analyses of microarray results. Fish with no (Control), lower (L-BKD), or higher (H-BKD) level of *R. salmoninarum* infection at 13 dpi were used for microarray analyses ($n = 5$). All the differentially expressed probes (DEPs) identified by ANOVA ($p < 0.01$) were used for clustering analyses.

there was a larger number of BKD-responsive probes in the L-BKD group compared with the H-BKD group. Furthermore, the up-regulated probes in the L-BKD group were distributed slightly more frequently over higher $\log_2$ fold-changes compared with those in the H-BKD group (**Figure 1B**). Using all identified DEPs (ANOVA; $p \leq 0.01$) in hierarchical clustering analyses, samples associated with a given group were closely clustered (**Figure 2**), reflecting that samples in each group share an overall comparable gene expression response.

Pathway Enrichment Analyses

We used ClueGO to identify the BPs over-represented in BKD-responsive transcript lists compared to the whole microarray platform. First, we tested the BPs enriched in BKD-responsive transcripts overlapping between both treatments (6,408 DEPs). The enriched BPs by BKD (**Figure 3**) were associated with response to stress (8.6%), adaptive immunity (15.5%), immune responses (27.6%), cellular processes (23.8%) and metabolic process (24.3%).

Several pathways related to adaptive immunity were dysregulated by *R. salmoninarum* infection in Atlantic salmon (**Figure 3**; **Supplementary Table S3A**). This includes the induction of pathways linked to lymphocyte differentiation or activation (e.g., T-cell activation, regulation of lymphocyte activation and lymphocyte migration, immunoglobulin secretion), adaptive immunity-related cytokine responses (e.g., NIK/NF-kappaB signalling, interleukin-12 secretion, response to interferon-gamma, regulation of interleukin-6 production, T-cell cytokine production) and antigen presentation processes (e.g., antigen processing and presentation of peptide antigen via MHC class I). A large number of BPs involved in immune response (e.g., defence response, activation of the innate immune response, inflammatory response, response to molecule of bacterial origin, defence response to virus) and regulation of immune responses (e.g., regulation of NLRP3 inflammasome complex assembly, negative regulation of the viral process, immune response-regulating signalling pathway, regulation of innate immune response) were activated in response to BKD. Furthermore, we identified BKD-triggered dysregulation of several molecular (e.g., type I interferon production, cytokine production, response to cytokine, immune effector process) and cellular (e.g., leukocyte activation, granulocyte

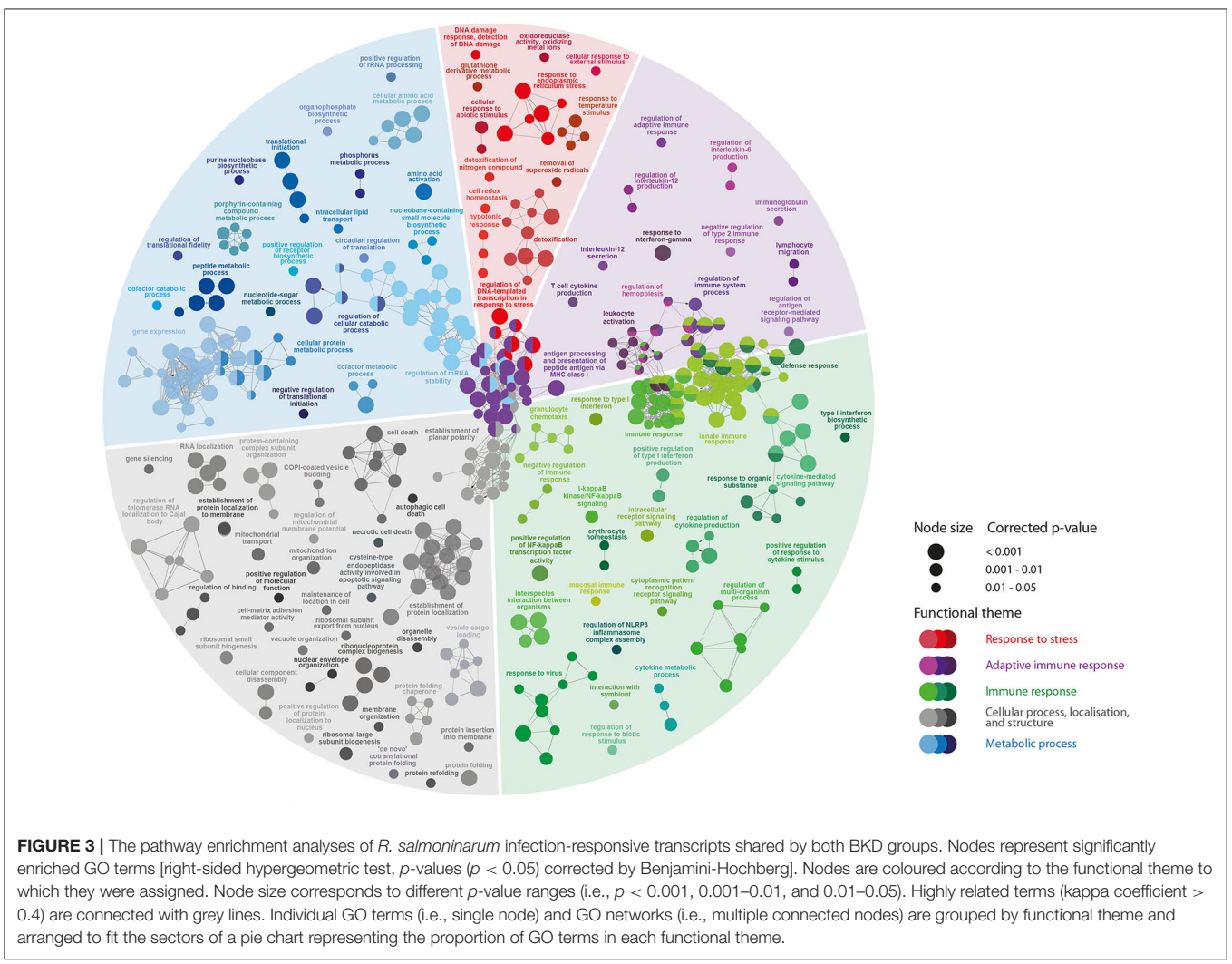

FIGURE 3 | The pathway enrichment analyses of *R. salmoninarum* infection-responsive transcripts shared by both BKD groups. Nodes represent significantly enriched GO terms [right-sided hypergeometric test, *p*-values ($p < 0.05$) corrected by Benjamini-Hochberg]. Nodes are coloured according to the functional theme to which they were assigned. Node size corresponds to different *p*-value ranges (i.e., $p < 0.001$, 0.001–0.01, and 0.01–0.05). Highly related terms (kappa coefficient > 0.4) are connected with grey lines. Individual GO terms (i.e., single node) and GO networks (i.e., multiple connected nodes) are grouped by functional theme and arranged to fit the sectors of a pie chart representing the proportion of GO terms in each functional theme.

activation, leukocyte chemotaxis, regulation of leukocyte migration) responses related to innate immunity (**Figure 3**; **Supplementary Table S3A**). There was extensive dysregulation of pathways related to cellular processes (e.g., necrotic cell death, negative regulation of cell death, programmed cell death, autophagic cell death) in *R. salmoninarum*-infected Atlantic salmon. Further, our findings show that BKD caused a massive metabolic dysregulation, such as nucleotide- (e.g., regulation of gene expression, regulation of mRNA stability, regulation of nucleotide metabolic process) and protein-related (e.g., cellular amino acid metabolic process, protein metabolic process, amino acid activation, translational initiation) processes, in the Atlantic salmon head kidney (**Figure 3**).

There were 357 DEPs by infection level (i.e., H-BKD vs. L-BKD), which were associated with several BPs including the regulation of Janus kinase (JAK)-Signal transducer and activator of transcription (STAT) signalling, activated downstream of the interferon (IFN) pathway (**Figure 4**; **Supplementary Table S3B**). Further, infection level-responsive transcripts were involved in humoral immune responses, B-cell differentiation, as well as response to interleukin-1 (**Figure 4**). Our findings showed that the infection level influenced multiple metabolic pathways in *R. salmoninarum*-infected Atlantic salmon.

There were 1,321 DEPs only identified in the L-BKD group (L-BKD vs. Control), and their over-represented BPs were associated with gene expression and its regulation, as well as metabolic processes. In addition, these DEPs were associated with viral process and activation of immune-related myeloid cells (**Supplementary Table S3C**). Several immune-related BPs were over-represented in the 358 DEPs only identified in the H-BKD group (H-BKD vs. Control; **Supplementary Table S3D**). Pathways involved in the regulation of immune processes, defence response, cell surface receptor signalling, cell communication and regulation of cell differentiation were enriched in the transcript list only identified in the H-BKD group (**Supplementary Table S3D**).

qPCR Validation

Sixty-five transcripts representing various molecular pathways (e.g., innate and adaptive immune responses) and dysregulations (i.e., up- and down-regulation, high and low fold-changes) were selected for qPCR validation. To have an acceptable representation of the microarray results, the transcripts contributing to qPCR assays were from different comparisons and gene lists, including the transcript lists overlapping between groups or specific to a given group. All the studied transcripts, except for *fc receptor-like protein 5* (*fcrl5*), showed the same fold-change direction as the microarray results of the differentially expressed transcripts (**Supplementary Table S4**); however, for some transcripts, the differences were not significant by qPCR. There were 35 (12 down-regulated and 23 up-regulated transcripts in response to BKD) qPCR-studied transcripts selected from the 6,285 DEPs overlapping only between L-BKD and H-BKD group transcript lists (**Figure 1A**), and except for *major histocompatibility class I* (*mh1*), the microarray results were confirmed ($p < 0.05$) by qPCR for all of the transcripts

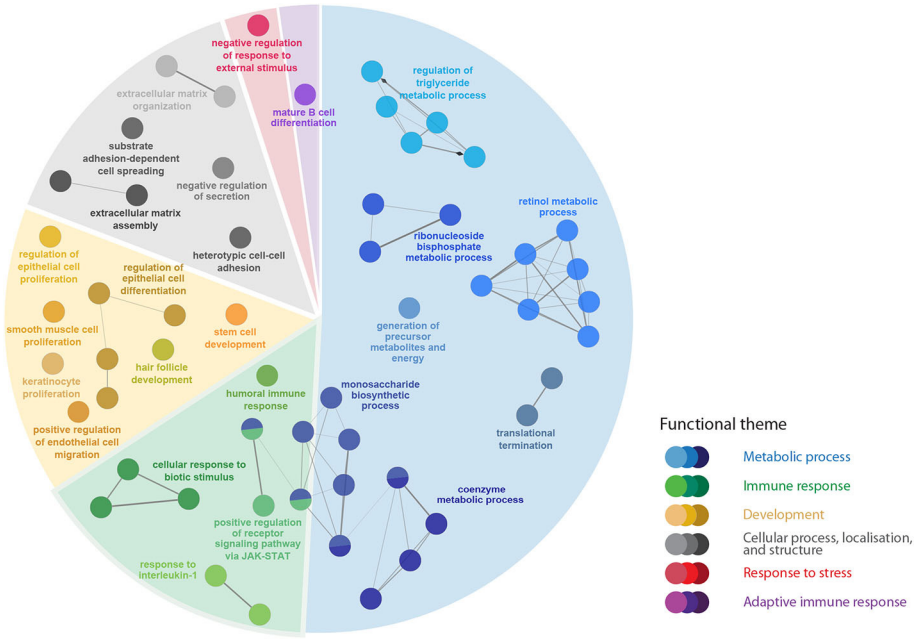

FIGURE 4 | The pathway enrichment analyses of transcripts responsive to the *R. salmoninarum* infection level (H-BKD vs. L-BKD). Nodes represent significantly enriched GO terms [right-sided hypergeometric test, *p*-values ($p < 0.05$) corrected by Benjamini-Hochberg]. Nodes are coloured according to the functional theme to which they were assigned. Highly related terms (kappa coefficient > 0.4) are connected with grey lines. Individual GO terms (i.e., single node) and GO networks (i.e., multiple connected nodes) are grouped by functional theme and arranged to fit the sectors of a pie chart representing the proportion of GO terms in each functional theme.

for at least one of the groups. Nine (4 down-regulated and 5 up-regulated) transcripts were from the L-BKD-specific transcript list (i.e., 1,176 DEPs; **Figure 1A**), and the microarray results of these transcripts were confirmed ($p < 0.05$) for all of them except for *fcrl5* and *dual specificity protein phosphatase 7* (*dusp7*). qPCR assays confirmed ($p < 0.05$) the results of 10 transcripts (5 down-regulated and 5 up-regulated) selected from the H-BKD-specific transcript list (i.e., 289 DEPs; **Figure 1A**). Despite showing the same direction of fold-changes (**Supplementary Table S4**), microarray results were only confirmed to be significantly different for 6 [i.e., *guanine deaminase* (*gda*), *granzyme a precursor* (*gzma*), *interferon-induced very large GTPase 1* (*gvinp1*), *leukemia inhibitory factor receptor* (*lifr*), *leucine-rich repeat transmembrane protein FLRT3* (*flrt3*), *interleukin 13 receptor alpha 1b* (*il13ra1b*)] out of 11 (5 down-regulated and 6 up-regulated) qPCR-studied transcripts selected from the infection level-responsive transcript list (i.e., H-BKD vs. L-BKD: 357 DEPs; **Figure 1A**). We categorised the qPCR-studied transcripts based on their putative function in immune responses.

qPCR results of 14 transcripts playing roles in innate immune responses are shown in **Figure 5**. There was significant up-regulation of *toll-like receptor 5* (*tlr5*), *radical s-adenosyl methionine domain containing* (*rsad2*; alias *viperin*), *complement factor D precursor* (*cfd*), and *hepcidin antimicrobial peptide* (*hamp*) in both L-BKD and H-BKD groups compared to the control (**Figures 5A–D**). Transcript expression of *CC chemokine* (*ccl*) increased in both L-BKD and H-BKD groups, but its level was significantly higher ($p < 0.05$) in the H-BKD group compared to the L-BKD group (**Figure 5E**). Despite

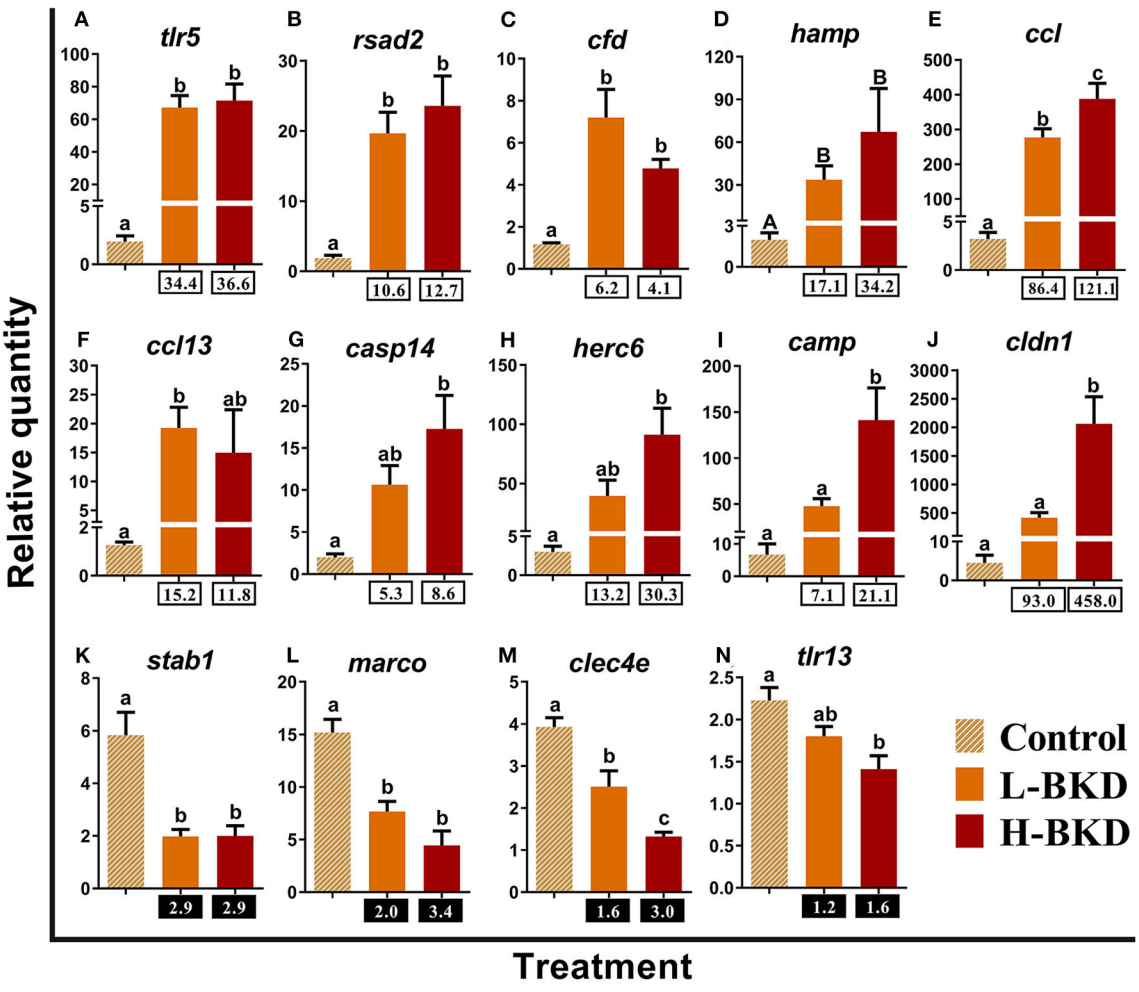

FIGURE 5 | (A–N) qPCR for *R. salmoninarum* infection-responsive transcripts playing putative roles in innate immune response. Fish with no (Control), lower (L-BKD) or higher (H-BKD) level of *R. salmoninarum* infection at 13 dpi were used for qPCR validation ($n = 5$). Fish in the L-BKD and H-BKD groups were infected with the same dose of *R. salmoninarum*, but they showed different levels of infection at 13 dpi, as determined by RNA-based Taq-Man assays. Data are presented as mean ± SE, with the lowest expressing sample as calibrator [i.e., set to relative quantity (RQ) 1.0]. Lower-case letters indicate significant differences between groups, as determined by one-way ANOVA with Tukey's *post-hoc* test ($p < 0.05$). Upper-case letters indicate significant differences between groups, as determined by Kruskal-Wallis test ($p < 0.05$). Fold-changes are shown below H-BKD and L-BKD groups, calculated as (mean H-BKD or L-BKD RQ)/(mean control RQ). Black boxes indicate the down-regulated or negative fold-changes, which were calculated as 1/fold-change for comparisons that yielded fold-change values <1.

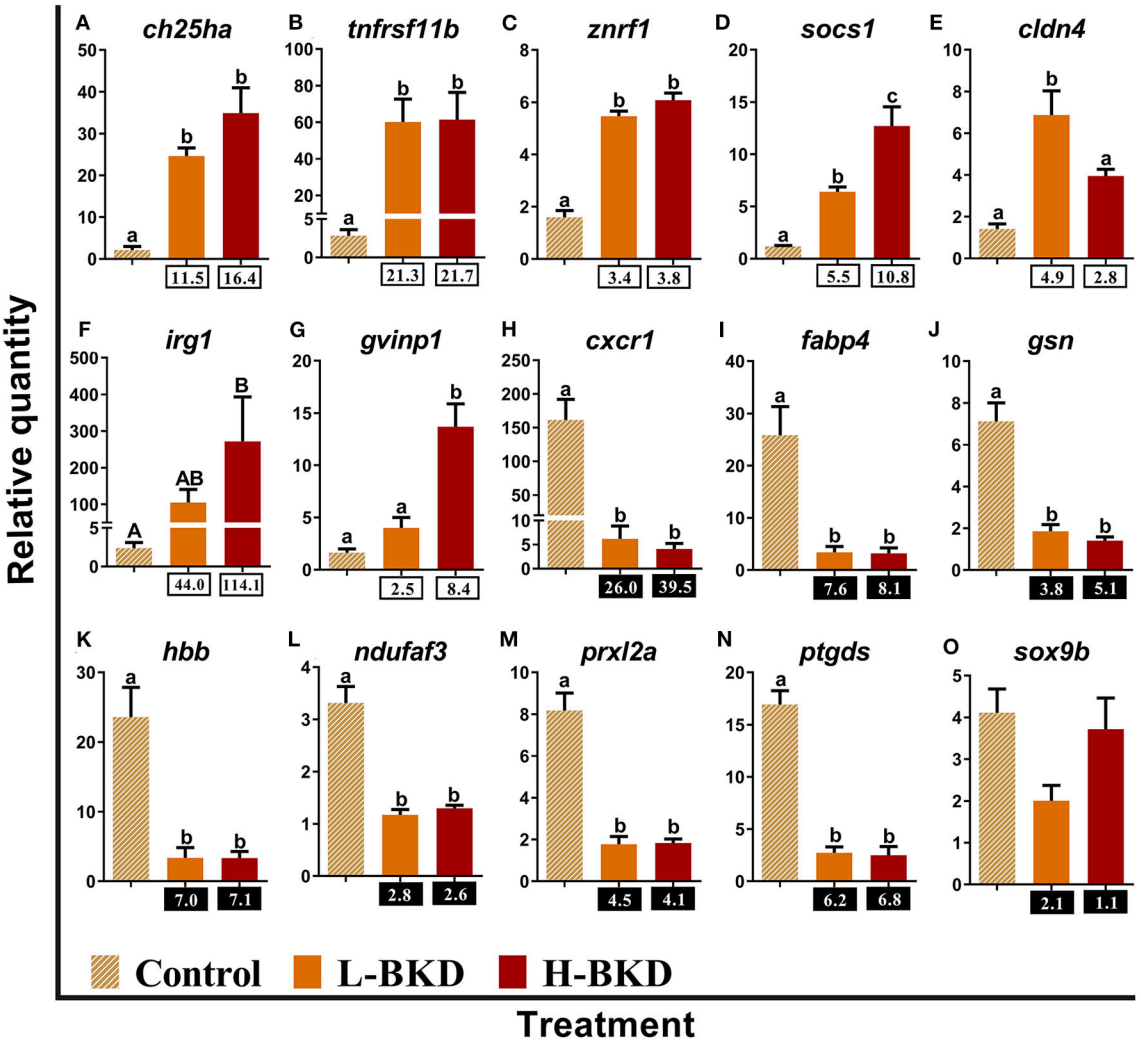

FIGURE 6 | (A–O) qPCR for *R. salmoninarum* infection-responsive transcripts involved in the regulation of innate immune and inflammatory responses. Fish with no (Control), lower (L-BKD) or higher (H-BKD) level of *R. salmoninarum* infection at 13 dpi were used for qPCR validation ($n = 5$). Data are presented as mean ± SE, with the lowest expressing sample as calibrator [i.e., set to relative quantity (RQ) 1.0]. Lower-case letters indicate significant differences between groups, as determined by one-way ANOVA with Tukey's *post-hoc* test ($p < 0.05$). Upper-case letters indicate significant differences between groups, as determined by Kruskal-Wallis test ($p < 0.05$). Fold-changes are shown below H-BKD and L-BKD groups, calculated as (mean H-BKD or L-BKD RQ)/(mean control RQ). Black boxes indicate the down-regulated or negative fold-changes, which were calculated as 1/fold-change for comparisons that yielded fold-change values <1.

up-regulation in both treatments, a significant difference for *C-C motif chemokine 13* (*ccl13*) expression was only seen between L-BKD compared with the control (**Figure 5F**). On the other hand, the significant up-regulation compared to the control for *caspase-14* (*casp14*), *E3 ubiquitin-protein ligase herc6* (*herc6*), *cathelicidin antimicrobial peptide* (*camp*), and *claudin-1* (*cldn1*) was only seen for the H-BKD, and *camp* and *cldn1* levels in the H-BKD group were significantly higher than those in the L-BKD group (**Figures 5G–J**). *R. salmoninarum* infection down-regulated the levels of *stabilin-1* (*stab1*), *macrophage receptor with collagenous structure* (*marco*), and *c-type lectin domain family 4 member e* (*clec4e*) in both H-BKD and L-BKD groups (**Figures 5K–M**). There was an infection level-dependent down-regulation for *clec4e*, with the lowest expression in the H-BKD group. Also, *toll-like receptor 13* (*tlr13*) was only down-regulated in the H-BKD group, compared to the control (**Figure 5N**).

Fifteen identified BKD-responsive transcripts involved in the regulation of innate immune and inflammatory responses were subjected to qPCR validation (**Figure 6**). The levels of *cholesterol 25-hydroxylase-like protein a* (*ch25ha*), *tumor necrosis factor receptor superfamily member 11b* (*tnfrsf11b*), *E3 ubiquitin-protein ligase znrf1* (*znrf1*), and *suppressor of cytokine signalling 1* (*socs1*) were significantly induced by *R. salmoninarum* infection in both H-BKD and L-BKD groups, and there was an infection level-dependent induction for *socs1*, with the highest level seen for the H-BKD group (**Figures 6A–D**). There was an up-regulation

of *claudin 4* (*cldn4*) in the L-BKD group compared to both H-BKD and control groups (**Figure 6E**). On the contrary, BKD-induced expression of *immune-responsive gene 1* (*irg1*) and *gvinp1* was only found in the H-BKD group, and *gvinp1* level was significantly higher in the H-BKD group, compared to the L-BKD group (**Figures 6F,G**). *R. salmoninarum* infection repressed the expression of *C-X-C chemokine receptor type 1* (*cxcr1*), *fatty acid-binding protein 4, adipocyte* (*fabp4*), *gelsolin* (*gsn*), *haemoglobin subunit beta* (*hbb*), *NADH dehydrogenase [ubiquinone] 1 alpha subcomplex assembly factor 3* (*ndufaf3*), *peroxiredoxin-like 2a* (*prxl2a*), and *prostaglandin D2 synthase* (*ptgds*) in both H-BKD and L-BKD groups (**Figures 6H–N**). Microarray results were not confirmed ($p > 0.05$) for *transcription factor Sox-9-b* (*sox9b*); its expression did not change among treatments (**Figure 6O**).

Eleven transcripts studied by qPCR in the current study play molecular roles as receptors or immune effectors in lymphocyte differentiation (**Figure 7**). Induction of *interleukin-1 beta* (*il1b*), *interferon regulatory factor 1* (*irf1*), *dedicator of cytokinesis protein 8* (*dock8*), and *C-C motif chemokine 4* (*ccl4*) occurred in both H-BKD and L-BKD groups, but *ccl4* level was significantly higher in the H-BKD compared to the L-BKD group (**Figures 7A–D**). However, significant up-regulation of *interferon gamma* (*ifng*) in response to *R. salmoninarum* infection was only seen in the H-BKD group (**Figure 7E**). Moreover, *lifr* and *matrix metallopeptidase-19* (*mmp19*) expression in the H-BKD group was significantly higher ($p < 0.05$) than that in the other groups, and there was not a significant difference between the L-BKD and control groups in expression of these transcripts (**Figures 7F,G**).

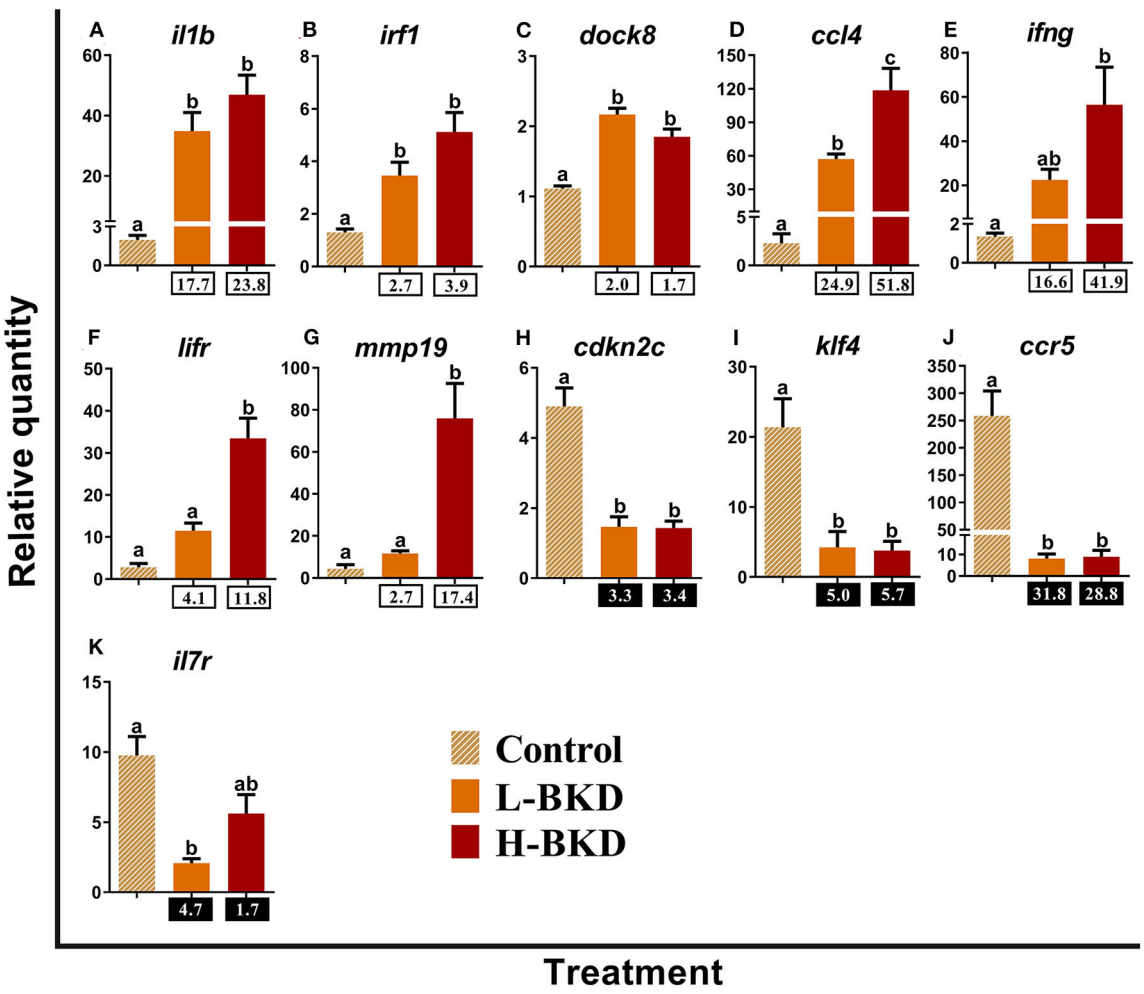

FIGURE 7 | (A–K) qPCR for *R. salmoninarum* infection-responsive transcripts playing molecular roles as receptors or immune effectors in lymphocyte differentiation. Fish with no (Control), lower (L-BKD) or higher (H-BKD) level of *R. salmoninarum* infection at 13 dpi were used for qPCR validation ($n = 5$). Data are presented as mean ± SE, with the lowest expressing sample as calibrator [i.e., set to relative quantity (RQ) 1.0]. Lower-case letters indicate significant differences between groups, as determined by one-way ANOVA with Tukey's *post-hoc* test ($p < 0.05$). Fold-changes are shown below H-BKD and L-BKD groups, calculated as (mean H-BKD or L-BKD RQ)/(mean control RQ). Black boxes indicate the down-regulated or negative fold-changes, which were calculated as 1/fold-change for comparisons that yielded fold-change values <1.

R. salmoninarum infection suppressed the expression of *cyclin-dependent kinase inhibitor 2c* (*cdkn2c*), *kruppel-like factor 4* (*klf4*), and *C-C chemokine receptor type 5* (*ccr5*) in both H-BKD and L-BKD groups (**Figures 7H–J**). As in the microarray results, BKD-dependent down-regulation of *interleukin-7 receptor subunit alpha* (*il7r*) was only observed in the L-BKD group; the difference between control and H-BKD groups for this transcript was not significant (**Figure 7K**).

We studied the expression levels of 11 transcripts encoding proteins that play putative roles in lymphocyte functions (**Figure 8**). Transcript levels of *matrix metallopeptidase-13* (*mmp13*) were up-regulated in response to *R. salmoninarum* infection in both L-BKD and H-BKD groups (**Figure 8A**). The expression levels of *protein kinase c delta type* (*prkcd*) and *dusp7* slightly but significantly increased ($p < 0.05$) only in the L-BKD and H-BKD groups, respectively (**Figures 8B,C**). Moreover, *E3 ubiquitin-protein ligase RNF144a-a* (*rnf144a*) and *tumor necrosis factor receptor superfamily member 6b* (*tnfrsf6b*) were strongly induced by *R. salmoninarum* infection only in the H-BKD group; the changes between the L-BKD and control groups were not significant (**Figures 8D,E**). Similar results were seen for *gzma* and *receptor-interacting serine/threonine-protein kinase 2* (*ripk2*), even though these transcripts showed significantly higher levels in the H-BKD compared with the L-BKD group (**Figures 8F,G**). The microarray results were not validated for *fcrl5*, as there was no difference among treatments for this transcript (**Figure 8H**). *R. salmoninarum* infection suppressed the levels of *receptor-type tyrosine-protein phosphatase kappa-like* (*ptprk*), *t-cell receptor alpha* (*tcra*) and *il13ra1b* in both L-BKD and H-BKD groups, although there was an infection level-dependent suppression for *il13ra1b,* with the maximum down-regulation in the H-BKD group (**Figures 8I–K**).

Figure 9 shows the qPCR results of the 6 transcripts involved in antigen-presenting cell (APC) functions. While *high affinity*

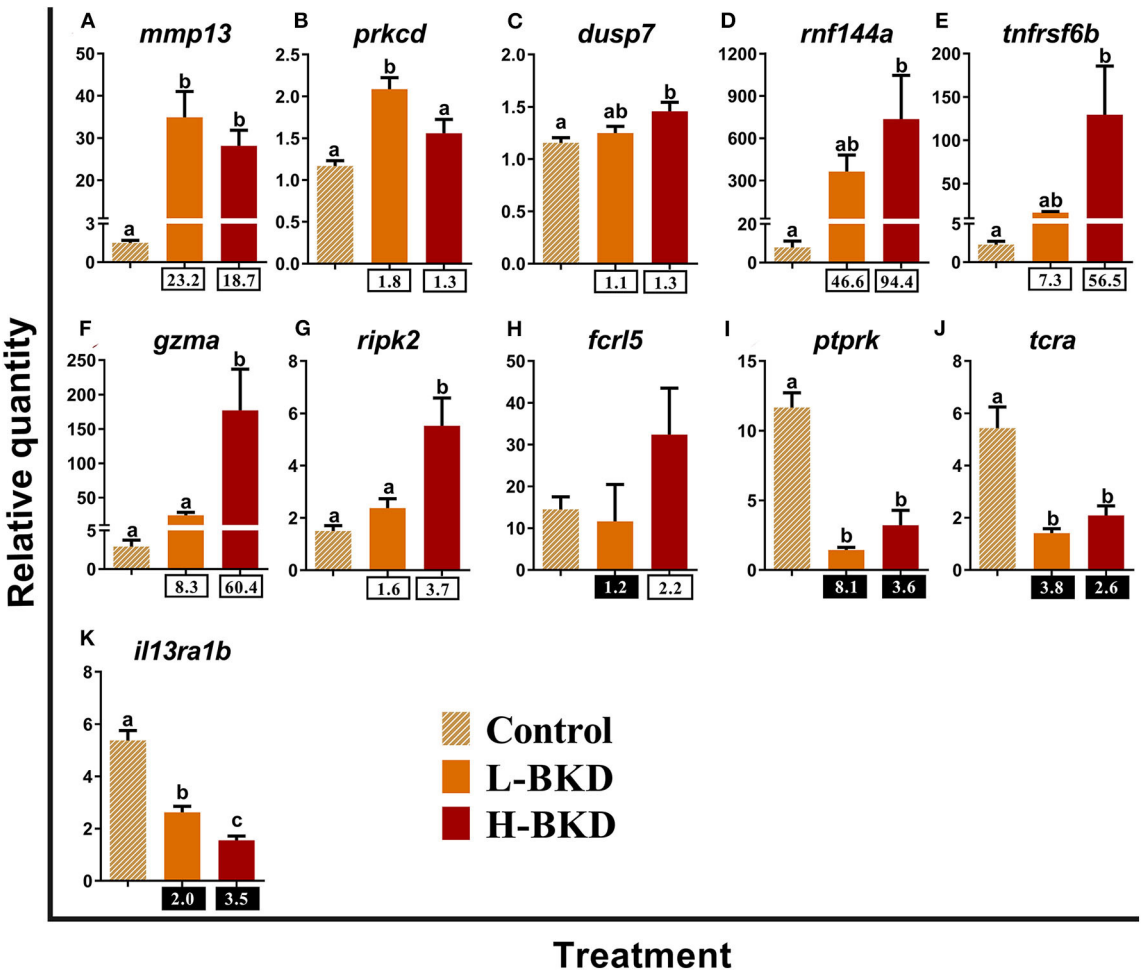

FIGURE 8 | (A–K) qPCR for *R. salmoninarum* infection-responsive transcripts playing putative roles in lymphocyte functions. Fish with no (Control), lower (L-BKD), or higher (H-BKD) level of *R. salmoninarum* infection at 13 dpi were used for qPCR validation ($n = 5$). Data are presented as mean ± SE, with the lowest expressing sample as calibrator [i.e., set to relative quantity (RQ) 1.0]. Lower-case letters indicate significant differences between groups, as determined by one-way ANOVA with Tukey's *post-hoc* test ($p < 0.05$). Fold-changes are shown below H-BKD and L-BKD groups, calculated as (mean H-BKD or L-BKD RQ)/(mean control RQ). Black boxes indicate the down-regulated or negative fold-changes, which were calculated as 1/fold-change for comparisons that yielded fold-change values <1.

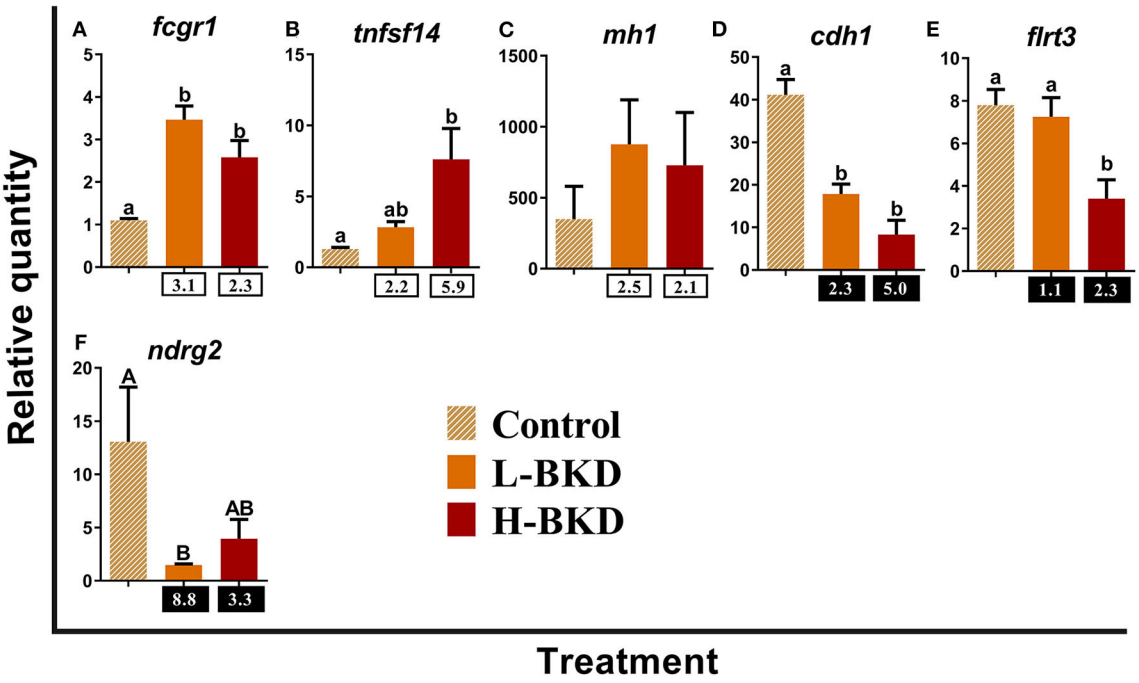

FIGURE 9 | (A–F) qPCR for *R. salmoninarum* infection-responsive transcripts involved in antigen-presenting cell functions. Fish with no (Control), lower (L-BKD) or higher (H-BKD) level of *R. salmoninarum* infection at 13 dpi were used for qPCR validation ($n = 5$). Data are presented as mean ± SE, with the lowest expressing sample as calibrator [i.e., set to relative quantity (RQ) 1.0]. Lower-case letters indicate significant differences between groups, as determined by one-way ANOVA with Tukey's *post-hoc* test ($p < 0.05$). Upper-case letters indicate significant differences between groups, as determined by Kruskal-Wallis test ($p < 0.05$). Fold-changes are shown below H-BKD and L-BKD groups, calculated as (mean H-BKD or L-BKD RQ)/(mean control RQ). Black boxes indicate the down-regulated or negative fold-changes, which were calculated as 1/fold-change for comparisons that yielded fold-change values <1.

immunoglobulin gamma Fc receptor I (*fcgr1*) was up-regulated in both L-BKD and H-BKD groups in response to *R. salmoninarum* infection, *tumor necrosis factor ligand superfamily member 14* (*tnfsf14*) induction was only seen in the H-BKD group (**Figures 9A,B**). Significant difference among treatments was not found for *mh1* (**Figure 9C**). *R. salmoninarum* infection down-regulated the expression of *B-cadherin-like* (*cdh1*) in both BKD conditions (**Figure 9D**). However, *R. salmoninarum* infection-suppressed expression of *flrt3* and *n-myc downstream-regulated gene* (*ndrg2*) was only seen in the H-BKD and L-BKD group, respectively (**Figures 9E,F**).

In addition to immune response-associated transcripts, we studied 8 transcripts with unknown function in immune responses of mammalian and fish species (**Figure 10**). The levels of *receptor-transporting protein 2* (*rtp2*), *receptor-transporting protein 3* (*rtp3*), *lipase maturation factor 2* (*lmf2*), and *MAP3K12-binding inhibitory protein 1* (*mbip*) were up-regulated by *R. salmoninarum* infection in both L-BKD and H-BKD treatments (**Figures 10A–D**). Up-regulation of *gda* was observed in the H-BKD group compared to both L-BKD and control groups (**Figure 10E**). On the other hand, *down syndrome cell adhesion molecule* (*dscam*), *tropomodulin-4-like* (*tmod4*), and *inactive carboxypeptidase-like protein X2* (*cpxm2*) expression was suppressed in response to *R. salmoninarum* infection in both L-BKD and H-BKD groups (**Figures 10F–H**).

Among all the qPCR-studied transcripts, 27 transcripts showed a significant correlation with the level of *R. salmoninarum* infection (**Supplementary Table S5**). The RQ values of *lifr*, *herc6*, *gzma*, *mmp19*, *gda*, *gvinp1*, *rtp3*, *socs1*, *casp14*, *dusp7*, *cldn1*, *camp*, *rsad2*, *ccl*, *irf1*, *ifng*, *ccl4*, *ripk2*, *rtp2*, *tnfsf14,* and *fcrl5* were positively correlated with the infection level (RQ value of *R. salmoninarum* expression), whereas *il13ra1b*, *dscam*, *cdh1*, *clec4e*, *marco,* and *flrt3* showed a significant negative correlation with the infection level. The significant correlations of these transcripts with the infection level suggest them as suitable biomarkers for assessing the *R. salmoninarum* level-dependent responses in Atlantic salmon.

The PCoA showed a clear separation among the experimental groups (**Figure 11**). PCO1 (i.e., 52.2% of total variation) and PCO2 (i.e., 34.3% of total variation) collectively explain 86.5% of the total variation. The control individuals were positively plotted on the PCO1, whereas individuals associated with both L-BKD and H-BKD groups negatively loaded on the PCO1. Samples were separated based on the infection level on PCO2, as the H-BKD and L-BKD individuals were loaded positively and negatively, respectively, on PCO2. Although all infected samples were associated with the left side vectors (e.g., *mmp19*, *gvinp1*, *cldn1*, *lifr*, *socs1*, *ccl4*, *ccl*, *ch25ha*, *il1b*, *znrf1*, *tlr5*, *mmp13*, *dock8*, *fcgr1,* and *rsad2*), varying levels of *R. salmoninarum* infection (i.e., H-BKD and L-BKD groups) showed different transcript-dependent association on the PCO2 (**Figure 11**). Fish in the H-BKD group were closely associated with vectors including *mmp19*, *gvinp1*, *gzma*, *cldn1*, *lifr*, *socs1*, *ccl4, ifng, tnfsf14, irf1, camp,* and *herc6* as well as *R. salmoninarum 16S ribosomal RNA*.

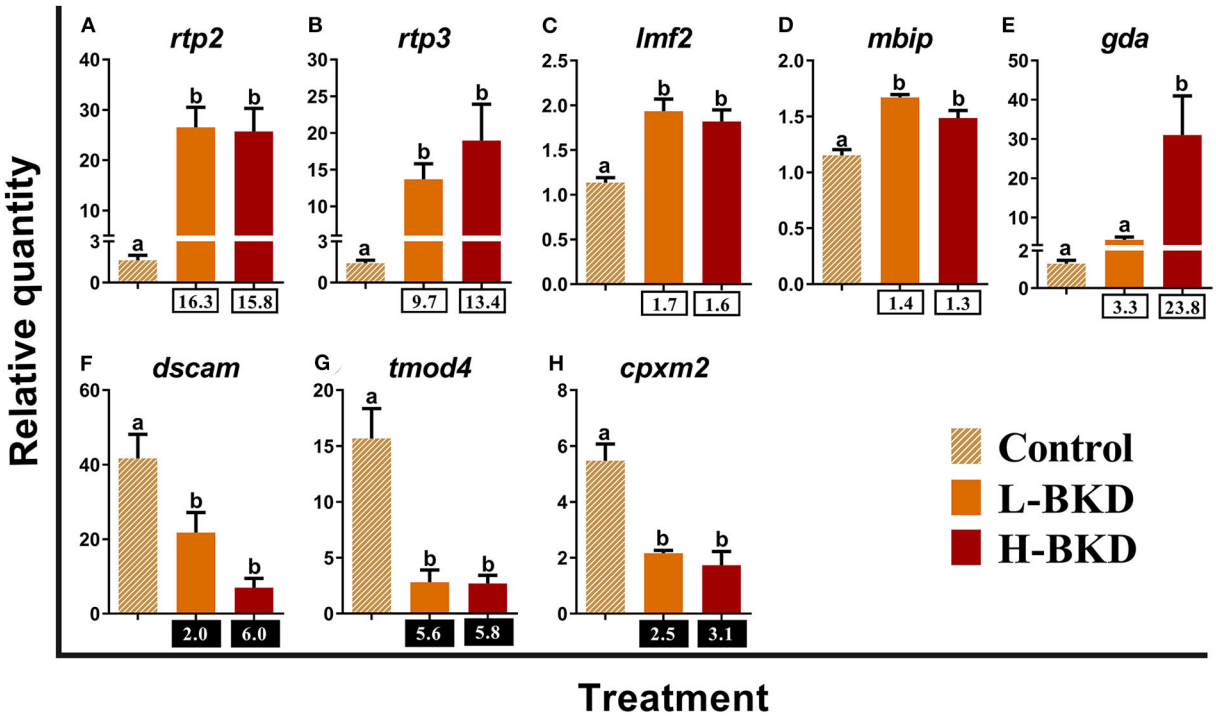

FIGURE 10 | (A–H) qPCR for *R. salmoninarum* infection-responsive transcripts with unknown function in immune responses of mammalian and fish species. Fish with no (Control), lower (L-BKD), or higher (H-BKD) level of *R. salmoninarum* infection at 13 dpi were used for qPCR validation ($n = 5$). Data are presented as mean ± SE, with the lowest expressing sample as calibrator [i.e., set to relative quantity (RQ) 1.0]. Lower-case letters indicate significant differences between groups, as determined by one-way ANOVA with Tukey's *post-hoc* test ($p < 0.05$). Fold-changes are shown below H-BKD and L-BKD groups, calculated as (mean H-BKD or L-BKD RQ)/(mean control RQ). Black boxes indicate the down-regulated or negative fold-changes, which were calculated as 1/fold-change for comparisons that yielded fold-change values <1.

Nonetheless, other vectors such as *prkcd*, *cldn4*, *cfd*, *fcgr1*, *dock8*, *mmp13*, and *lmf2* showed more association with the L-BKD samples (**Figure 11**).

DISCUSSION

The present study is the first report on the transcriptome response of Atlantic salmon head kidney to BKD. In addition to transcriptome profiling of BKD responses in Atlantic salmon, we aimed to test if different *R. salmoninarum* levels influence the Atlantic salmon responses to this disease. All the fish in the present study were infected with the same dose of *R. salmoninarum*, but Taq-Man qPCR assays revealed a significant difference between the levels of infection in selected individuals with a higher (H-BKD) and lower (L-BKD) detected *R. salmoninarum* level at 13 dpi (**Supplementary Figure S3**). In this study, mortalities started at 24 dpi and 100% mortality occurred at 38 dpi (**Supplementary Figure S1**). Also, we did not find a significant correlation between fish weight and infection level at 13 dpi, as well as any difference in fish weight among the groups (i.e., control, L-BKD and H-BKD) at 13 dpi. Therefore, variations in the detected *R. salmoninarum* level of individuals can be attributed to the susceptibility, and the higher (H-BKD) and lower (L-BKD) infection level groups in the present study can also be considered as higher and lower susceptible groups, respectively. Using microarray analyses, we identified 7,729 and 6,766 DEPs in the L-BKD and H-BKD groups, respectively, compared with the control fish. The majority of the identified transcripts overlapped between groups (6,408 DEPs: 3,946 up- and 2,462 down-regulated DEPs). Also, there were 357 probes (171 up- and 186 down-regulated DEPs) responsive to the infection level (i.e., H-BKD vs. L-BKD). Our previous 44K microarray-based study identified 379 DEPs in the head kidney of Atlantic salmon injected with formalin-killed *R. salmoninarum* bacterin compared with the saline-injected control fish at 24 h post-injection (17). In addition, a previous SSH-based study identified 132 expressed sequence tags (ESTs) differentially expressed in response to *R. salmoninarum* infection in Chinook salmon at 24 and 72 h post-infection (hpi) (15). The larger number of transcripts identified herein compared to the previous *R. salmoninarum*-related studies may be attributed to the differences in response to live vs. killed pathogen, the studied time point (e.g., 1 vs. 13 days), species-dependent responses, and fish age (e.g., ∼1,600 g fish in the bacterin study vs. ∼54 g fish in the current study). In addition, following 14 days of infection, microarray (i.e., ∼3.5K features) analysis identified 69 *P. salmonis*-responsive transcripts in the head kidney of Atlantic salmon (19). Using RNA-Seq, 825 and 412 transcripts were identified in Atlantic salmon spleen and head

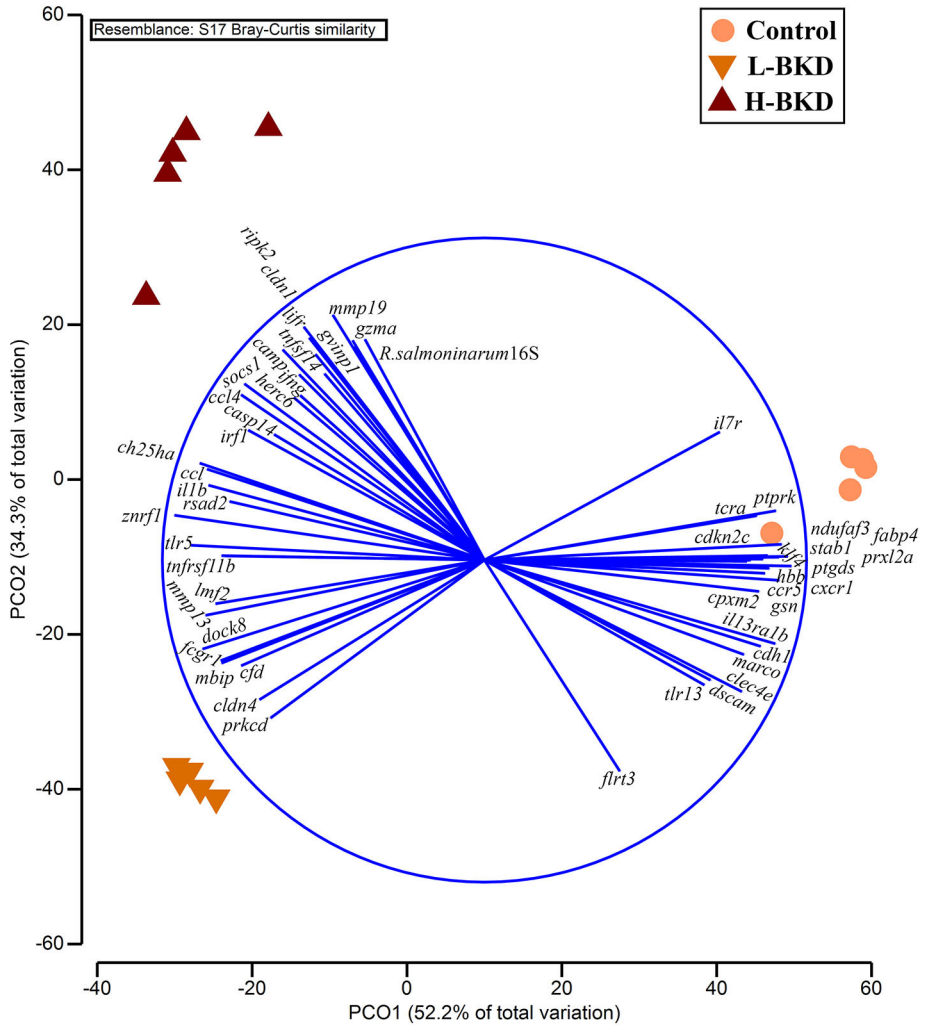

FIGURE 11 | Principal coordinate analysis using all qPCR-studied transcripts and *R. salmoninarum* infection level. Fish with no (Control), lower (L-BKD) or higher (H-BKD) level of *R. salmoninarum* infection at 13 dpi were used for qPCR validation ($n = 5$). Fish in the L-BKD and H-BKD groups were infected with the same dose of *R. salmoninarum*, but they showed different levels of infection at 13 dpi. The infection level indicates the expression of *R. salmoninarum 16S ribosomal RNA* as determined by RNA-based TaqMan assays. All vectors with Pearson's $r < 0.75$ are shown.

kidney, respectively, after 14 days *P. salmonis* infection (50). The differences in the numbers of responsive transcripts seen between the current and these previous studies may be caused by various factors such as experimental design, pathogen-dependent responses and the differences in transcriptome analyses (e.g., 3.5K vs. 44K microarray or RNA-Seq vs. microarray). The large number of *R. salmoninarum*-responsive transcripts compared to *P. salmonis*-responsive transcripts may also reflect the specific immune signalling triggered by different pathogen-associated molecular patterns (PAMPs) (e.g., Gram-positive vs. Gram-negative bacteria). The peptidoglycan of Gram-positive bacteria is recognised by TLR2, but TLR4 is the specific receptor for the lipopolysaccharides (LPS) of Gram-negative bacteria (51). Although they share some similarities, mammalian species were found to have distinct activated immune pathways in response to Gram-positive and Gram-negative bacteria (52, 53).

The present study used an IP challenge approach for profiling the transcriptome responses of Atlantic salmon to *R. salmoninarum* at 13 dpi. However, aspects such as route of infection, infection level, and patterns of disease spread in natural BKD outbreaks and saltwater environments may differ from the IP infection model used in the current study. Hence, *R. salmoninarum*-infected fish in aquaculture or natural environments may show some variations in dysregulation of the BKD-responsive biomarkers compared to the fish IP-challenged with *R. salmoninarum* in the present study. We studied the global gene expression response and discovered biomarkers for both lower and higher *R. salmoninarum* level/susceptible individuals, and the identified BKD-responsive biomarkers and pathways overlapping between lower and higher susceptible groups may represent the core immune response of Atlantic salmon to this pathogen. Nonetheless, further investigations

involving Atlantic salmon naturally infected or bath challenged with *R. salmoninarum* in freshwater and seawater are needed to have a better grasp of the regulatory patterns of the identified biomarkers in the face of BKD.

We used samples with a higher (H-BKD; C_T values below 22) or a lower (L-BKD; C_T values above 25) level of infection (**Supplementary Figure S3**) to test if different levels of infection affect the BKD-dependent immune responses. Close clustering of samples in a given treatment based on the expression of all DEPs (**Figure 2**) suggests the comparable global gene expression responses of the samples associated with each group. Further, this reveals that the BKD-dependent response in Atlantic salmon head kidney can be influenced by the level of infection, and fish with different *R. salmoninarum* levels may have distinct transcriptional response patterns. There was a larger number of DEPs in the L-BKD group (7,729 DEPs) compared to the H-BKD group (6,766 DEPs), and 357 differentially expressed between the H-BKD and L-BKD groups. Since *R. salmoninarum* has immunomodulatory effects on its host (10), the infection level-dependent BKD responses of Atlantic salmon in this study may be related to host-pathogen interactions. Variations in the infection level of fish seen herein may also be influenced by individual-based differences in immune response, and/or specific immune signalling potentially modulated by *R. salmoninarum*. The infection level-responsive transcript list identified herein provides a more comprehensive understanding of the putative immune pathways affected by *R. salmoninarum*.

To validate the microarray results, we subjected 65 transcripts to qPCR analyses. These transcripts were from different comparisons (e.g., H-BKD vs. L-BKD), with different regulation (e.g., down- and up-regulated by BKD) and putative roles in various immune processes. All of the qPCR-studied transcripts, except for *fcrl5*, showed the same fold-change direction as the microarray experiment (**Supplementary Table S4**), although some microarray-identified transcripts (i.e., 3 out of 52 H-BKD vs. control and 14 out of 49 L-BKD vs. control differentially expressed transcripts) were not shown to have significant differential expression by qPCR. There were 11 microarray-identified transcripts responsive to *R. salmoninarum* infection level that were subjected to qPCR, 6 of which were confirmed by qPCR to have significant differential expression. On the other hand, we found significant differences in qPCR for some comparisons that did not show significant changes in the microarray study (**Supplementary Table S4**). The differences seen between microarray and qPCR results may be attributed to the variations in the distribution of acquired values (i.e., normalised fluorescence ratios vs. RQ values, respectively) as well as stringency level and statistical methods used for data analyses.

The qPCR-studied transcripts were categorised based on their function in immune responses. Fourteen transcripts with putative roles in innate immune responses were included for qPCR validation (**Figure 5**). *R. salmoninarum* infection up-regulated the expression of the Atlantic salmon *tlr5, rsad2*, *cdf, hamp,* and *ccl* transcripts in both L-BKD and H-BKD groups compared with the control. While *ccl13* was only up-regulated in the L-BKD group, *casp14*, *herc6, camp,* and *cldn1* up-regulation was only seen in the H-BKD group. Further, *ccl, camp,* and *cldn1* were significantly up-regulated in the H-BKD compared with L-BKD group. Among innate immune relevant-studied transcripts, *cldn1* showed the strongest induction, i.e., 458-fold up-regulation in the H-BKD group compared with the control. *R. salmoninarum* infection down-regulated *stab1, marco,* and *clec4e* in both L-BKD and H-BKD groups, whereas *tlr13* down-regulation was only seen in the H-BKD group. Expression of *clec4e* negatively correlated with the infection level, as it was suppressed in the H-BKD group compared with the L-BKD fish. Our previous study (17) found the same fold-change direction in response to *R. salmoninarum* bacterin at 24 h post-injection for several of these transcripts (i.e., *tlr5, cdf, hamp*, *ccl, ccl13,* and *camp*), which indicates their importance in both early and late *R. salmoninarum*-related responses. **Figure 12** depicts the innate and adaptive immune pathways activated by BDK in Atlantic salmon head kidney. Our results show the activation of innate immune responses downstream of TLRs. In parallel, the pathway enrichment analyses showed the dysregulation of BPs associated with Nuclear factor kappa-B (NFKB) activation, thereby increasing cytokine production (**Figure 12**). TLR5 of mammals and teleosts [e.g., rainbow trout and Japanese flounder (*Paralichthys olivaceus*)] is a pattern recognition receptor (PRR) that recognises bacterial flagellin, and activates the Myeloid differentiation primary response 88 (MyD88)-dependent pathway, resulting in the production of pro-inflammatory cytokines (59, 60). On the other hand, mammalian TLR13 recognises bacterial rRNA (61). Besides TLR13, we found down-regulation of transcripts encoding C-type lectin receptors, such as *clec4e* (alias *mincle*), which activates the inflammatory responses by recognising pathogenic fungi (62). Furthermore, we observed the BKD-suppressed expression of scavenger receptor-encoding transcripts, i.e., *stab1* and *marco*. In mammals, STAB1 is an essential factor for receptor-mediated endocytosis in macrophages (63), and MARCO is a PRR playing roles in bacterial binding and removal (64). In agreement with our results, Atlantic salmon *marco* was suppressed in *P. salmonis*-infected macrophages (19). MARCO was reported to bind to bacteria and be induced by *Vibrio anguillarum* in Ayu (*Plecoglossus altivelis*), suggesting a conserved bacterial binding function for teleost MARCO (65). The BKD-suppressed expression of PRR-encoding transcripts in the current study may be caused by the negative feedback loop triggered by immune responses or host immunomodulation exerted by *R. salmoninarum*.

The innate immune pathways activated by *R. salmoninarum* infection increased the expression of *hamp*, *camp, cdf,* and *ccl13*, which are associated with antibacterial processes (**Figure 12**). Teleost HAMP and CAMP [e.g., rainbow trout and European seabass (*Dicentrarchus labrax*)] exhibited antibacterial activities against both Gram-positive and Gram-negative bacteria (66–69). Mammalian CDF is involved in the alternative complement pathway (70). Human CCL13 showed antibacterial activity against *Pseudomonas aeruginosa* (71). Interestingly, we found a strong up-regulation of some antiviral biomarkers (i.e., *rsad2*, *herc6,* and *cldn1*) in response to BKD. Atlantic salmon *rsad2* and *herc6* were found to be responsive to a viral mimic in macrophage-like cells (28). Mammalian RSAD2 and HERC6 are

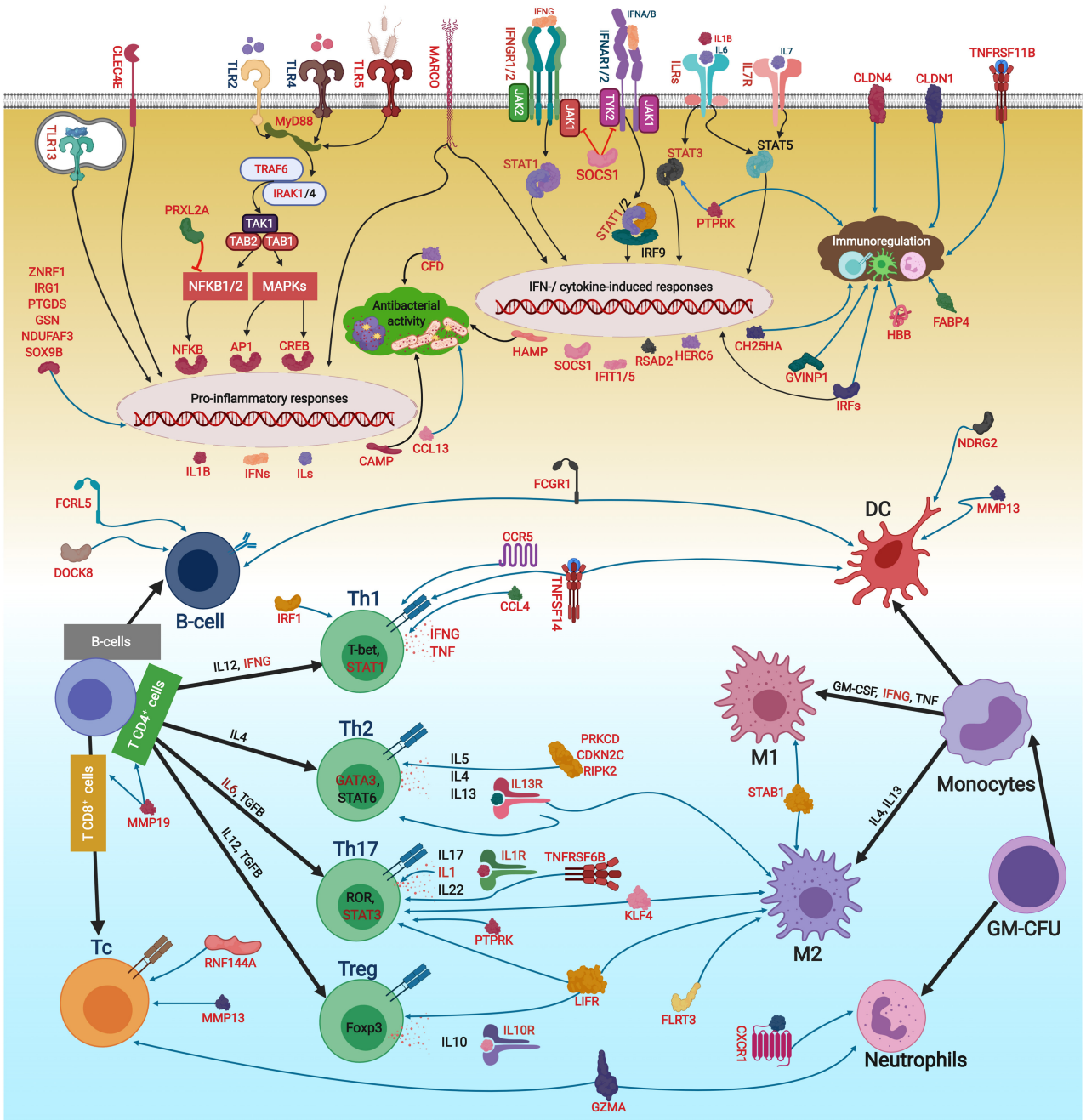

FIGURE 12 | The putative adaptive and innate immune pathways differentially regulated by *R. salmoninarum* infection in Atlantic salmon head kidney. This figure was developed using the identified genes in this study and their known functions and regulatory pathways in mammals (54–58) as explained in the discussion section. This figure was created in BioRender (https://biorender.com/). The BKD-responsive genes are shown in red font or red boxes. The microarray results were not confirmed by qPCR for *sox9b* and *fcrl5*. Black and blue arrows show activatory and regulatory effects, respectively, whereas red lines indicate inhibitory effects. Oval circles and clouds reflect gene expression activation and biological processes, respectively. TLR, Toll-like receptor; MyD88, Myeloid differentiation primary response 88; TNF, Tumor necrosis factor; TRAF, TNF receptor-associated factor; IRAK, Interleukin-1 receptor-associated kinase; TAK1, Transforming growth factor beta, (TGFB)-activated kinase 1; TAB, TAK1-binding protein; NFKB, Nuclear factor kappa-B; MAPK, Mitogen-activated protein kinase; AP1, Transcription factor AP1; CREB, cAMP response element-binding protein; ILs, interleukins) IFNs, Interferons; IFNRs, IFN receptors; ILRs, IL receptors; JAK, Janus kinase; TYK, Tyrosine kinase; STAT, Signal transducer and activator of transcription; IRF, Interferon regulatory factor; RSAD2, Radical S-adenosyl methionine domain containing 2; CFD, Complement factor D precursor; HAMP, Hepcidin antimicrobial peptide; CCL13, C-C motif chemokine 13; HERC6, E3 ubiquitin-protein ligase herc6; CAMP, Cathelicidin antimicrobial peptide; CLDN1, Claudin-1; CCL,CC chemokine; STAB1, Stabilin-1; MARCO, Macrophage receptor MARCO; CLEC4E, C-type lectin domain family 4 member E; CH25HA, Cholesterol

(Continued)

FIGURE 12 | 25-hydroxylase-like protein A; TNFR11B, Tumor necrosis factor receptor superfamily member 11B; ZNRF1, E3 ubiquitin-protein ligase znrf; IRG1, Immune-responsive gene 1; CLDN4, Claudin 4; GVINP1, Interferon-induced very large GTPase 1; SOCS1, Suppressor of cytokine signalling 1; CXCR1, C-X-C chemokine receptor type 1; FABP4, Fatty acid-binding protein 4, adipocyte; GSN, Gelsolin; HBB, Haemoglobin subunit beta; NDUFAF3, NADH dehydrogenase, ubiquinone, 1 alpha subcomplex assembly factor 3; PRXL2A, Peroxiredoxin-like 2A; PTGDS, Prostaglandin D2 synthase, lipocalin; DOCK8, Dedicator of cytokinesis protein 8; TNFSF14, Tumor necrosis factor ligand superfamily member 14; LIFR, Leukemia inhibitory factor receptor; MMP19, Matrix metallopeptidase-19; CCL4, C-C motif chemokine 4; CDKN2C, Cyclin-dependent kinase inhibitor 2C; KLF4, Kruppel-like factor 4; CCR5,C-C chemokine receptor type 5; MMP13, Matrix metallopeptidase 13; DUSP7, Dual specificity protein phosphatase 7; RNF144A, E3 ubiquitin-protein ligase RNF144A-A; TNFR6B, Tumor necrosis factor receptor superfamily member 6B; GZMA, Granzyme A precursor; RIPK2, Receptor-interacting serine/threonine-protein kinase 2; PRKCD, Protein kinase C delta type; FCRL5, Fc receptor-like protein 5; PTPRK, Receptor-type tyrosine-protein phosphatase kappa-like; IL13RA1B, Interleukin 13 receptor alpha 1B; FCGR1, High affinity immunoglobulin gamma Fc receptor I; SOX9B, Transcription factor Sox-9-B; FLRT3, Leucine-rich repeat transmembrane protein FLRT3; NDRG2, N-myc downstream-regulated gene; GM-CSF, Granulocyte-macrophage colony-stimulating factor; TGFB, Transforming growth factor beta; T-Bet, T-cell-specific T-box transcription factor; GATA3, GATA binding protein 3; ROR, RAR-related orphan receptor gamma; FOXP3, forkhead box P3; GM-CFU, Granulocyte-macrophage colony forming units; DC, dendritic cell; M1/2, macrophage M1/2; Th1/2/17, T helper 1/2/17 cell; Treg, regulatory T cells.

known as IFN-induced proteins involved in antiviral processes (72, 73). Besides antiviral responses, *rsad2* induction by bacterial pathogens or LPS was reported in several species, including fishes (73, 74). However, the antibacterial response of *rsad2* may be species-dependent (47). Moreover, mammalian CLDN1 plays a role in antiviral responses as a co-receptor for viral entry (75), but its function in the fish immune response remains unknown. Although our qPCR, microarray and pathway enrichment results (e.g., over-representation of response to viruses) reflect the importance of factors, with putative roles in antiviral responses, in the Atlantic salmon response to BKD, further investigations are needed to determine the role of these transcripts in Atlantic salmon antibacterial responses. Considering the enrichment of IFN-related processes as well as the positive correlation between *rsad2* and *herc6* with the infection level (**Supplementary Table S5**), the up-regulation of antiviral biomarkers in the current study may be caused by secondary immune responses or immunomodulatory functions of *R. salmoninarum.* Furthermore, *R. salmoninarum* is an intracellular pathogen (9), and an intracellular bacterium (i.e., *Listeria monocytogenes*) was reported to induce mammalian IFN type I through IRF3-dependent signalling (76). Accordingly, stimulation of antiviral response-relevant transcripts by *R. salmoninarum* may be caused by activation of factors involved in the entry of intracellular pathogen into host cells or receptors recognising the bacterial DNA. BKD induction of *casp14* as an apoptotic or inflammatory caspase (77), alongside over-representation of BPs related to cell death in the current study, suggests the activation of apoptotic pathways following the inflammatory response. The identified transcripts involved in innate immune responses that showed positive (i.e., *camp*, *casp14*, *ccl*, *cldn1*, *herc6,* and *rsad2)* or negative (i.e., *marco* and *clec4e*) correlation with *R. salmoninarum* level (**Supplementary Table S5**) can be suggested as suitable biomarkers for assessing the infection level-dependent responses of Atlantic salmon to BKD.

BKD influenced molecular pathways (e.g., regulation of leukocyte migration, negative regulation of immune response, regulation of NLRP3, inflammasome complex assembly and regulation of cytokine biosynthetic process) associated with regulation of immune responses, and several qPCR-studied transcripts in our study play putative immunoregulatory roles (**Figure 12**). For example, *R. salmoninarum* induced *ch25ha, tnfrsf11b, znrf1,* and *socs1* in both infection levels, whereas BKD induction of *cldn4, irg1,* and *gvinp1* occurred in either the L-BKD or the H-BKD group (**Figure 6**). IFN-induced CH25H shows antiviral activities and can positively and negatively regulate the inflammatory responses of mammals (78). Mammalian TNFRSF11B (alias Osteoprotegerin), ZNRF1 and CLDN4 regulate LPS-induced cytokine and/or inflammatory responses (79–81). GVINP1 is an IFN-induced GTPase, regulating oxidative and inflammasome-related antimicrobial activities of cells in mammals (82). Cytokine-activated IRG1 of zebrafish (*Danio rerio*) links cellular metabolism with immune defence through regulating mitochondrial reactive oxygen species (ROS) production (83). Moreover, *irg1* was up-regulated in *P. salmonis*-infected Atlantic salmon head kidney (19). The expression patterns of *irg1* and *gvinp1* were comparable with *socs1*, suggesting that these transcripts may share an activation pathway. Cytokine-inducible mammalian SOCS1 inhibits JAK/STAT signalling by binding to JAKs downstream of the cytokine receptors (**Figure 12**) (84). Significantly higher induction of *socs1* in the H-BKD group and its positive correlation with *R. salmoninarum* level (**Supplementary Table S5**) suggest this transcript as an important biomarker for infection level-dependent responses of Atlantic salmon to BKD. In agreement with *socs1* results, the JAK-STAT-related signalling pathway was found to be dysregulated in response to *R. salmoninarum* level. Taken together, the infection level-dependent response of *socs1* and other putative IFN-/Cytokine-inducible transcripts (*irg1* and *gvinp*), as well as pathway enrichment results, suggest that the JAK-STAT pathway may be an essential part of host-pathogen interactions between Atlantic salmon and *R. salmoninarum* (**Figure 12**).

In addition to these up-regulated transcripts, our qPCR results showed suppression of transcripts with putative immunoregulatory functions. *R. salmoninarum* infection down-regulated *cxcr1*, *fabp4, gsn, ndufaf3, prxl2a*, *ptgds,* and *hbb* in both H-BKD and L-BKD groups (**Figure 6**). Mammalian CXCR1 recruits neutrophils to the inflammation site and regulates their bactericidal activity (85). The same fold-change direction was seen for *cxcr1* in LPS-exposed peripheral blood leucocytes of fugu (*Takifugu rubripes*) (86) and *R. salmoninarum* bacterin-injected Atlantic salmon (17). Besides its fatty acid-related function, FABP4 of mammals regulates the Inhibitor of nuclear factor

kappa-B kinase (IKK) signalling pathway that activates the production of inflammatory cytokines (87). A previous study from our group found Atlantic salmon *fabp4* as a dietary fatty acid-responsive transcript (28). We found intracellular lipid transport process to be differentially regulated with BKD; further studies are needed to determine the association of Atlantic salmon antibacterial responses with *fabp4* and other lipid metabolism-relevant (e.g., *ch25ha)* transcripts identified herein. We also identified BKD-responsive transcripts involved in the regulation of inflammation. Recombinant GSN of mammals has been shown to inhibit LPS-induced cytokine responses (88). Mammalian NDUFAF3 is a factor associated with Mitochondrial Respiratory Complex I, which was found to modulate LPS-induced NFKB activation and pro-inflammatory responses (89). Similarly, PRXL2A inhibits Mitogen-activated protein kinase (MAPK) and NFKB signalling pathways in humans (90). Prostaglandins play immunoregulatory roles in teleosts (91), and PTGDS (aliases PGD2) was found to suppress *V. anguillarum* DNA-induced expression of *il1b* in gilthead seabream (*Sparus aurata*) granulocytes (92). *P. salmonis* repressed the expression of *ptgds* in Atlantic salmon head kidney (19). Considering that *P. salmonis* is an intracellular Gram-negative pathogen, the same gene expression regulation (e.g., *ptgds* suppression and *irg1* induction) of Atlantic salmon in response to *P. salmonis* (19) and *R. salmoninarum* may be linked to a common molecular pathway activated by intracellular bacteria. The suppressed expression of genes encoding putative immune modulators identified in the present study may be attributed to the host's need for boosting pro-inflammatory responses. Furthermore, haemoglobin-derived peptides of human and fish show antibacterial activities (93, 94), and HBB was reported to regulate the antiviral innate immune responses in humans (95). Additional studies are needed to develop a better understanding of the immunoregulatory functions of teleost *hbb* and other BKD-suppressed transcripts identified in this study.

There were several pathways (e.g., myeloid cell differentiation, regulation of stem cell differentiation, positive regulation of interleukin-12 production and interleukin-12 secretion) involved in the regulation of lymphocyte differentiation that were dysregulated in response to *R. salmoninarum* infection (**Figures 3**, **12**). Our qPCR results showed up-regulation of *il1b*, *irf1*, *dock8,* and *ccl4* in both BKD groups, whereas *ifng, mmp19,* and *lifr* induction was only significant in the H-BKD group (**Figure 7**). *R. salmoninarum* infection suppressed *cdkn2c, klf4,* and *ccr5* expression in both BKD groups, although *il7r* down-regulation only happened in the L-BKD group. These transcripts, except for *dock8,* are known to play roles in mammalian T-cell differentiation. DOCK8 is a crucial effector involved in TLR9-driven differentiation of B-cells (96). The pathway activated by IL1B provides a pro-survival signal for T-cells and triggers the differentiation of T helper 17 (Th17) cells from naïve T-cells (97). Besides its diverse immunoregulatory roles, IFNG is a necessary cytokine for differentiation of the naïve $CD4^+$ T-cells into Th1 cells (97). In addition to IL12, IFNG and STAT4, IRF1 is required for the differentiation of naïve T-cells into Th1, but not Th17 cells (98). MMP19 was also found to perform an essential function in T-cell differentiation (99). LIFR plays regulatory roles in the differentiation of the Th17 and regulatory T (Treg) cells (100). Our findings suggest the crucial role of Treg and Th differentiation-related processes in Atlantic salmon defence mechanisms against *R. salmoninarum.* In mammalian species, CCL4 is chiefly expressed by APCs and B-cells, and it can engage with CCR5 expressed on IFNG-producing Th1, thereby regulating polarisation and trafficking of Th1 cells (101). LPS-induced CCL4 of orange-spotted grouper (*Epinephelus coioides*) was reported to attract leukocytes and stimulate the Th1 differentiation pathway (102), suggesting the conserved function of mammalian and teleost CCL4. The opposite regulations of *ccl4* and *ccr5* in our study may be caused by negative feedback loops, or suggest that they can be regulated through different immune pathways. IL7R mediates T-cell and B-cell differentiation through activation of JAK1/3 and consequently STAT5 (103, 104). Besides its role in macrophage differentiation, KLF4 is a transcription factor required for Th17-cell differentiation and IL17 production (105). CDKN2C was found as an important factor associated with induction of GATA3-dependent Th2 cell proliferation (106). In agreement with *cdkn2c* expression, our microarray data showed down-regulation of Atlantic salmon *gata3* in response to *R. salmoninarum* infection, indicating the putative conserved roles of these genes in Atlantic salmon and mammals. Among identified lymphocyte differentiation biomarkers, *ccl4, mmp19,* and *lifr* showed *R. salmoninarum* level-dependent responses, suggesting them as suitable biomarkers assessing the Atlantic salmon response to BKD intensity. While our results suggested the putative role of these transcripts in antibacterial responses of Atlantic salmon, further studies are needed to functionally characterise these transcripts and their encoded proteins.

Our microarray data showed BKD-dependent dysregulation of pathways (e.g., T-cell activation, positive regulation of lymphocyte activation and lymphocyte chemotaxis) related to lymphocyte function (**Figures 3**, **12**). As shown by qPCR, *mmp13* was up-regulated in both BKD groups. Mammalian MMP13 is a Tumor necrosis factor alpha (TNFA)-induced protein mediating the conversion of the inactive form of Transforming growth factor beta 1 (TGFB1) to the active form, which facilitates TLR-driven immunoglobulin switching in B-cells (107). *R. salmoninarum* infection up-regulated *prkcd* only in the L-BKD group, whereas *dusp7*, *rnf144a*, *tnfrsf6b*, *gzma,* and *ripk2* were only significantly induced in the H-BKD group (**Figure 8**). Mammalian PRKCD plays a role in the up-regulation of IL10 (108). Mouse RIPK2 is a kinase involved in TLR2-activated IL10 production in response to Gram-positive *Streptococcus pneumoniae* (109). DUSPs may manage MAPK activation via negative feedback loops (110), and human DUSP7 was suggested to have an effector function associated with Th1 (111). Mammalian TNFRSF6B (alias DcR3) is an immunoregulator for Th17 cell activity and cytokine responses (112), and our previous study showed its transcriptional induction in Atlantic salmon stimulated with *R. salmoninarum* bacterin (17). In the current study, qPCR data showed the up-regulation of transcripts with putative roles in cytotoxic T-cell function. For example, *gzma* showed a *R. salmoninarum* level-dependent response in Atlantic salmon. Granzymes are cytolytic granules involved in the cell-mediated cytotoxic activity of $CD8^+$ T-cells (113). GZMA was

revealed as the main granzyme playing a role in cell-mediated cytotoxicity of teleosts (gilthead seabream and European seabass) (114). In addition, mammalian RNF144A is a key factor balancing IL2R-dependent responses of $CD8^+$ T-cells, thereby preventing severe inflammation (115). Although up-regulation of teleost [i.e., grass carp (*Ctenopharyngodon idellus*)] *rnf144a* in response to viral infection was previously reported (116), further studies are needed to characterise the function of this and other identified transcripts in fish antibacterial responses. In the current study, *ptprk, tcra,* and *il13ra1b* were suppressed in Atlantic salmon head kidney in response to *R. salmoninarum* infection. As reported in mammalian species (117), the BKD-suppressed response of *tcra* may be attributed to the negative feedback mechanism for managing pathogen elimination and minimising the inflammatory damages. PTPRK contributes to T-cell pathogenesis through STAT3 dephosphorylation, in which its under-expression results in STAT3 activation (118). As found by microarray, the slight up-regulation of STAT3 in our study may be associated with PTPRK regulatory function, but further studies are needed to determine if this function is conserved in fishes. IL13RA1 is a receptor expressed on various immune cells such as B-cells. Engagement of IL13RA1 with IL13, a regulatory cytokine produced by Th2 cells, elicits multiple immune processes such as STAT6 activation and promotion of IgE production in B-cells (119). Infection level-dependent dysregulation of *il13ra1b* and other identified lymphocyte-associated biomarkers (i.e., *prkcd*, *gzma,* and *ripk2*) suggests the importance of T-cell activated pathways in interactions between Atlantic salmon and *R. salmoninarum* (**Figure 12**).

APC-related processes (e.g., antigen processing and presentation of peptide antigen via MHC class I and antigen processing and presentation of exogenous antigen) were found to be dysregulated in *R. salmoninarum*-infected Atlantic salmon (**Figure 3**). As shown in **Figure 13**, our transcriptome profiling identified several *R. salmoninarum*-responsive transcripts involved in antigen-presenting and processing pathways. The teleost MH-I-dependent pathway exhibits several differences with their mammalian counterparts (123–128); for example, different paralogues (i.e., Calnexin) and splice variants (i.e., Tapasin) of molecules involved in the MH-I pathway were identified and suggested to play diverged or unique roles in salmonid antigen presentation (123–128). The qPCR results showed the *R. salmoninarum*-dependent up-regulation of *fcgr1* and *tnfsf14,* as well as down-regulation of *cdh1*, *flrt3,* and *ndrg2* (**Figure 9**). FCGR1 is a member of the Fc receptor protein family that links adaptive and innate immune responses through regulation of antibody activity and modulation of dendritic cell (DC) functions (e.g., antigen presentation and phagocytosis) (129). Mammalian TNFSF14 plays an essential role in the induction of DC maturation (130). CDH1 was described to be involved in cell-cell adhesion processes such as T-cell and DC interactions (131). Also, *flrt3* and *cdh1* were suggested to be associated with mammalian macrophage function, as they were strongly up-regulated in IL10-induced M2 macrophages and IL-4 + IL-10-stimulated bone marrow-derived macrophages, respectively (132). NDRG2 modulates the activation and differentiation of DCs as well as DC-mediated T-cell activation (133). The BKD-dependent induction of *mh1* was not confirmed by the qPCR, although our transcriptome data showed the activation of several co-receptors and immune effectors involved in antigen presentation pathways, reflecting the importance of MH-dependent pathways in Atlantic salmon response to BKD (**Figure 13**). Many pathogens employ strategies to evade MHC pathways (134). While bacterial immunoevasion of the MHC pathways were mainly associated with class II molecules, intracellular bacteria such as *Mycobacterium tuberculosis* and *Listeria monocytogenes* were found to suppress the expression of mammalian *mhc1* (134, 135). It remains unknown if *R. salmoninarum* possesses a mechanism for evading the antigen presentation pathway. Considering immunosuppressive features of *R. salmoninarum* (10), further studies are required to determine the interaction of this intracellular pathogen with the teleost MH-I pathway, test if its immunomodulatory features are related to MH-I molecule, and characterise the APC function-relevant transcripts identified herein.

R. salmoninarum induced the expression of *rtp2, rtp3, lmf2,* and *mbip,* and suppressed the expression of *dscam, tmod4,* and *cpxm2* in both H-BKD and L-BKD groups (**Figure 10**). In addition, there was an up-regulation of *gda* in the H-BKD group compared with both the L-BKD and control groups. The immune roles of these identified BKD-responsive transcripts in mammals remain undescribed. For example, while RTPs are established as odorant receptors in mammals (136), it is not known if mammalian RTPs play immune-relevant roles. GDA and TMOD4 are involved in the regulation of the neural response (137) and structural development (138), respectively. DSCAM is involved in the immune response of arthropods (139), and was found to be associated with zebrafish development (140). Further studies are needed to describe the immune function of vertebrate DSCAM. Nonetheless, since *dscam* suppression was correlated with a higher level of infection, our results suggest *dscam* as a suitable biomarker transcript for assessing the *R. salmoninarum* infection level-dependent response of Atlantic salmon.

In summary, the present study profiled the transcriptome of Atlantic salmon head kidney in response to different levels of *R. salmoninarum* infection. We developed a more complete picture of the genes and molecular pathways underlying the Atlantic salmon immune response to BKD. *R. salmoninarum* infection dysregulated transcripts encoding PRRs (e.g., *tlr5*), signal transducers (e.g., *traf6*), and transcription factors (e.g., *nfkb1*) associated with the MyD88-dependent pathway, resulting in activation of cytokines (e.g., *ifn*s and *il*s) and antimicrobial factors (e.g., *camp* and *hamp*). BKD also activated cytokine-dependent responses (e.g., JAK-STAT mediated pathway and IFN-induced transcripts) and immune regulators (e.g., *znrf1* and *irg1*). Furthermore, a large number of transcripts associated with adaptive immune responses such as T-/B-cell differentiation (e.g., *irf1*, *dock8,* and *ccl4*) and function (e.g., *rnf144a* and *tnfrsf6b*) as well as antigen presentation (e.g., *fcgr1* and *tnfsf14*), were identified as BKD-responsive in this study. The JAK-STAT signalling

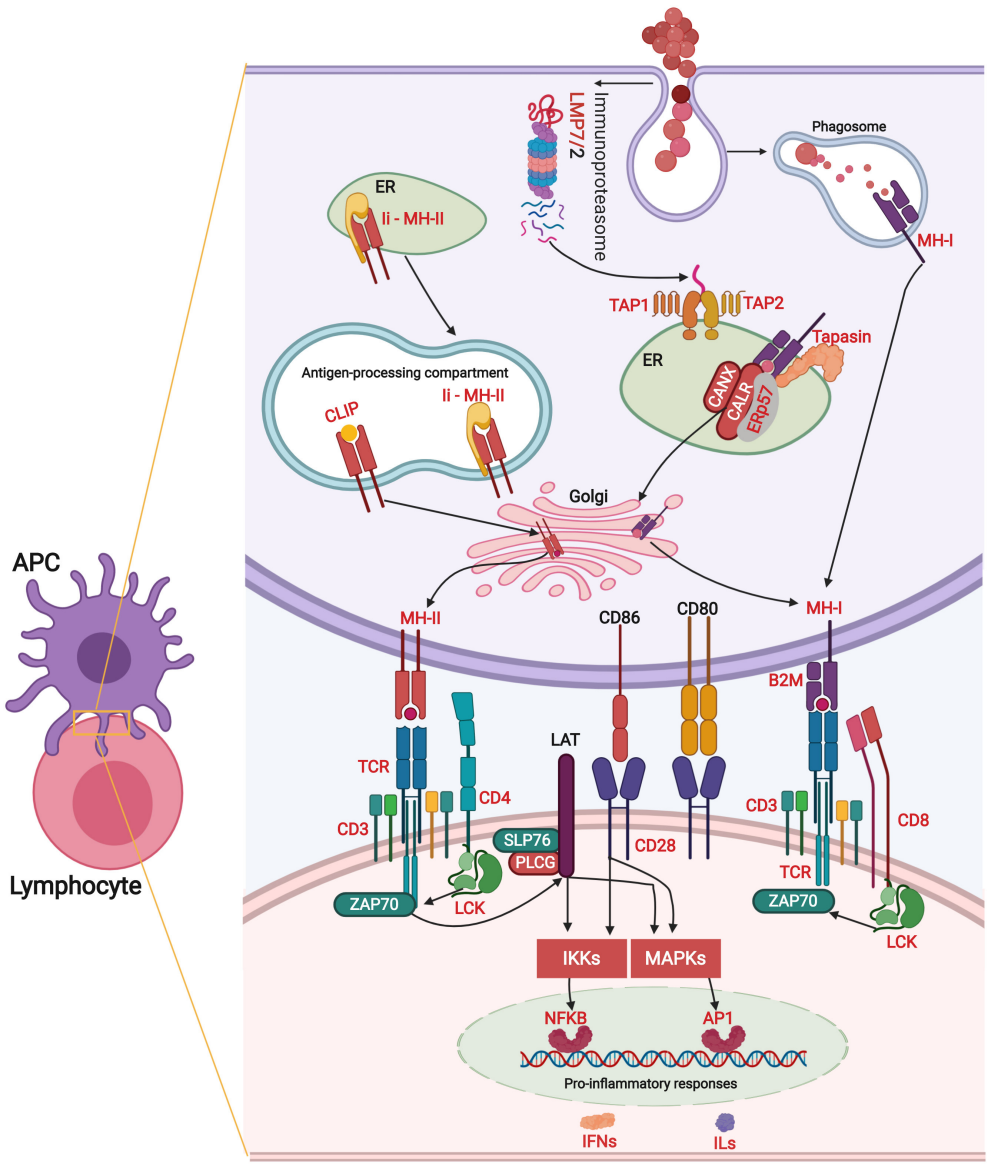

FIGURE 13 | The antigen-processing and presenting pathways differentially regulated by *R. salmoninarum* infection in Atlantic salmon head kidney. This figure was developed using the identified genes in this study and their known functions and regulatory pathways in mammals as explained in the discussion section (54, 120–122). This illustration was generated using BioRender (https://biorender.com/). The BKD-responsive genes are shown in red font or red boxes. The microarray results were not confirmed by qPCR for *mh1*. Black arrows show activatory effects. Oval circles reflect gene expression activation. APC, antigen-presenting cell; ER, endoplasmic reticulum; LMP2/7, Immunoproteasome subunits LMP2/7; Ii, Invariant chain Ii or CD74; MH-I/II, [Major histocompatibility I/II, known as Major histocompatibility complex I/II(MHC-I/II) in mammals]; CLIP, class II-associated invariant chain peptide; TAP, Protein associated with antigen processing; Tapasin, TAP-associated glycoprotein; ERp57, Endoplasmic reticulum protein of 57 KDa; CANX, Calnexin; CALR, Calreticulin; CD, Cluster of differentiation; B2M, Beta-2 microglobulin; TCR, T-cell receptor; SLP76, SH2 domain containing leukocyte protein of 76kd; LAT, Linker for activation of T-cells; PLCG, Phospholipase gamma; LCK, Lymphocyte -specific tyrosine kinase; ZAP70, Tyrosine kinase zeta chain-associated protein of 70 kD; IKK, NFKB1 inhibitor kinase; NFKB, Nuclear factor kappa-B; MAPK, Mitogen-activated protein kinase; AP1, Transcription factor AP1; ILs, Interleukins; IFNs, Interferons.

pathway was found to be influenced by *R. salmoninarum* level, suggesting the importance of IFN-dependent pathways in host-pathogen interactions. PCoA showed the significant correlation of BKD-responsive transcripts with a higher (e.g., *mmp19*, *gvinp1*, *cldn1*, *lifr*, *socs1*, *ccl4,* and *ccl*) or lower (e.g., *prkcd*, *cldn4,* and *cfd*) level of *R. salmoninarum.* These transcripts can be used as biomarkers to assess the infection level-dependent BKD responses of Atlantic salmon, and are suitable candidates for investigating the host component of interactions between Atlantic salmon and *R. salmoninarum.* We identified and qPCR validated *R. salmoninarum*- and infection level-responsive biomarker transcripts, which are valuable

tools for future research (e.g., development of therapeutic diets and vaccines) for improving the Atlantic salmon resistance to BKD. Further studies characterising the functions of transcripts identified herein can enhance the current understanding of molecular processes involved in BKD-related responses of Atlantic salmon.

DATA AVAILABILITY STATEMENT

The datasets generated for this study can be found in online repositories. The names of the repository/repositories and accession number(s) can be found at: https://www.ncbi.nlm.nih.gov/geo/, GSE150335.

ETHICS STATEMENT

All procedures in the present study were performed based upon the guidelines of the Canadian Council on Animal Care.

AUTHOR CONTRIBUTIONS

KE took a lead role in TaqMan assays, sample selection, microarray experimental design, microarray analyses, qPCR validation design, data analyses, data interpretation, and the writing of the manuscript draft. AC-S helped with enrichment analyses and writing a part of the manuscript. SMI helped with primer design and carried out the qPCR assays. ME helped with TaqMan assays and PCoA analysis. SK assisted with the annotation of the microarray results. CB helped with sampling and RNA extraction of the samples. RA-H was involved in the experimental design, bacterial culture and infection challenge, and reviewed the manuscript. EJ managed the experimental design, infection trial and samplings, and took a part in manuscript preparation. MLR was involved in experimental design, sample selection, microarray experimental design, data analyses and data interpretation, and took an active role in manuscript writing. All authors read and approved the final manuscript.

FUNDING

Research funding in the present study was provided by the Ocean Frontier Institute (OFI), through an award from the Canada First Research Excellence Fund. MLR's research program is also supported by a Natural Sciences and Engineering Research Council of Canada (NSERC) Discovery Grant, as well as the Integrated Pathogen Management of Co-infection in Atlantic salmon (IPMC) project which is funded by the Government of Canada through Genome Canada and Genome Atlantic, and Cargill Innovation (formerly EWOS Innovation). The IPMC project is also funded by the Government of Newfoundland and Labrador through the Department of Tourism, Culture, Industry and Innovation. The infection trial of the current study, conducted in Cargill Innovation Center—Colaco (Chile), was supported by Cargill Aqua Nutrition. The current study was also funded by FONDAP-INCAR 15110027 (ANID, Chile) to RA-H.

ACKNOWLEDGMENTS

We are thankful to Xi Xue for helping with microarray scanning, and Dr. Jennifer Hall (Aquatic Research Cluster, CREAIT Network, Memorial University) for providing us with primer sequences for *tcra*. We would like to thank the Cargill Innovation Center—Colaco (Chile) operational teams for conducting the infection trial and sampling, as well as the laboratory team for sample preparation. We would also like to thank Atlantic Computational Excellence Network (ACENET) and Compute Canada for providing computational resources in updating the annotation of the 44K array. We are also grateful to Magdalena S. Maeland for helping with RNA quality control and Tasha Harrold for helping as a Program Manager within the OFI.

SUPPLEMENTARY MATERIAL

The Supplementary Material for this article can be found online at: https://www.frontiersin.org/articles/10.3389/fimmu.2020.567838/full#supplementary-material

REFERENCES

1. FAO. *The State of World Fisheries and Aquaculture (SOFIA)*. Rome: FAO (2016).
2. FAO. *The State of World Fisheries and Aquaculture (SOFIA)*. Rome: FAO (2017).
3. FAO. *FAO Year Book, Fishery and Aquaculture Statistics*. Rome: FAO (2010).
4. Toranzo AE, Magarinos B, Romalde JL. A review of the main bacterial fish diseases in mariculture systems. *Aquaculture*. (2005) 246:37–61. doi: 10.1016/j.aquaculture.2005.01.002
5. Lafferty KD, Harvell CD, Conrad JM, Friedman CS, Kent ML, Kuris AM, et al. Infectious diseases affect marine fisheries and aquaculture economics. *Annu Rev Mar Sci*. (2015) 7:471–96. doi: 10.1146/annurev-marine-010814-015646
6. Austin B, Austin DA. Aerobic gram-positive rods and cocci. In: Austin B, Austin DA, editors. *Bacterial Fish Pathogens*. Cham: Springer. (2016). p. 83–160. doi: 10.1007/978-3-319-32674-0_3
7. Fryer J, Sanders J. Bacterial kidney disease of salmonid fish. *Annu Rev Microbiol*. (1981) 35:273–98. doi: 10.1146/annurev.mi.35.100181.001421
8. Elliott DG, Wiens GD, Hammell KL, Rhodes LD. Vaccination against bacterial kidney disease. In: Gudding R, Lillehaug A, Evensen Ø, editors. *Fish Vaccination*. Chichester: John Wiley & Sons, Ltd. (2014). p. 255–72. doi: 10.1002/9781118806913.ch22
9. Evenden A, Grayson T, Gilpin M, Munn C. *Renibacterium salmoninarum* and bacterial kidney disease—the unfinished jigsaw. *Annu Rev Fish Dis*. (1993) 3:87–104. doi: 10.1016/0959-8030(93)90030-F
10. Fredriksen Å, Endresen C, Wergeland H. Immunosuppressive effect of a low molecular weight surface protein from *Renibacterium salmoninarumon* lymphocytes from Atlantic salmon (*Salmo salar* L.). *Fish Shellfish Immunol*. (1997) 7:273–82. doi: 10.1006/fsim.1997.0082
11. Campos-Perez JJ, Ward M, Grabowski PS, Ellis AE, Secombes CJ. The gills are an important site of iNOS expression in rainbow trout *Oncorhynchus mykiss* after challenge with the Gram-positive pathogen *Renibacterium salmoninarum*. *Immunology*. (2000) 99:153–61. doi: 10.1046/j.1365-2567.2000.00914.x
12. Metzger DC, Elliott DG, Wargo A, Park LK, Purcell MK. Pathological and immunological responses associated with differential survival of Chinook

salmon following *Renibacterium salmoninarum* challenge. *Dis Aquat Org.* (2010) 90:31–41. doi: 10.3354/dao02214
13. Grayson TH, Cooper LF, Wrathmell AB, Evenden JR, Andrew J, Gilpin ML. Host responses to *Renibacterium salmoninarum* and specific components of the pathogen reveal the mechanisms of immune suppression and activation. *Immunology.* (2002) 106:273–83. doi: 10.1046/j.1365-2567.2002.01420.x
14. Bethke J, Arias-Muñoz E, Yáñez A, Avendaño-Herrera R. *Renibacterium salmoninarum* iron-acquisition mechanisms and ASK cell line infection: virulence and immune response. *J Fish Dis.* (2019) 42:1283–91. doi: 10.1111/jfd.13051
15. Rhodes LD, Wallis S, Demlow SE. Genes associated with an effective host response by Chinook salmon to *Renibacterium salmoninarum*. *Dev Comp Immunol.* (2009) 33:176–86. doi: 10.1016/j.dci.2008.08.006
16. Rozas-Serri M, Lobos C, Correa R, Ildefonso R, Vásquez J, Muñoz A, et al. Atlantic salmon pre-smolt survivors of *Renibacterium salmoninarum* infection show inhibited cell-mediated adaptive immune response and a higher risk of death during the late stage of infection at lower water temperatures. *Front Immunol.* (2020) 11:1378. doi: 10.3389/fimmu.2020.01378
17. Eslamloo K, Kumar S, Caballero-Solares A, Gnanagobal H, Santander J, Rise ML. Profiling the transcriptome response of Atlantic salmon head kidney to formalin-killed *Renibacterium salmoninarum*. *Fish Shellfish Immunol.* (2020) 98:937–49. doi: 10.1016/j.fsi.2019.11.057
18. Hyatt G, Melamed R, Park R, Seguritan R, Laplace C, Poirot L, et al. Gene expression microarrays: glimpses of the immunological genome. *Nat Immunol.* (2006) 7:686–91. doi: 10.1038/ni0706-686
19. Rise ML, Jones SR, Brown GD, von Schalburg KR, Davidson WS, Koop BF. Microarray analyses identify molecular biomarkers of Atlantic salmon macrophage and hematopoietic kidney response to *Piscirickettsia salmonis* infection. *Physiol Genomics.* (2004) 20:21–35. doi: 10.1152/physiolgenomics.00036.2004
20. Ewart KV, Belanger JC, Williams J, Karakach T, Penny S, Tsoi SC, et al. Identification of genes differentially expressed in Atlantic salmon (*Salmo salar*) in response to infection by *Aeromonas salmonicida* using cDNA microarray technology. *Dev Comp Immunol.* (2005) 29:333–47. doi: 10.1016/j.dci.2004.08.004
21. Martin SAM, Blaney SC, Houlihan D, Secombes CJ. Transcriptome response following administration of a live bacterial vaccine in Atlantic salmon (*Salmo salar*). *Mol Immunol.* (2006) 43:1900–11. doi: 10.1016/j.molimm.2005.10.007
22. Bridle AR, Koop BF, Nowak BF. Identification of surrogates of protection against yersiniosis in immersion vaccinated Atlantic salmon. *PLoS ONE.* (2012) 7:e40841. doi: 10.1371/journal.pone.0040841
23. Lund H, Bakke AF, Sommerset I, Afanasyev S, Schriwer G, Thorisdottir A, et al. A time-course study of gene expression and antibody repertoire at early time post vaccination of Atlantic salmon. *Mol Immunol.* (2019) 106:99–107. doi: 10.1016/j.molimm.2018.12.018
24. Jantzen SG, Sanderson DS, von Schalburg KR, Yasuike M, Marass F, Koop BF. A 44K microarray dataset of the changing transcriptome in developing Atlantic salmon (*Salmo salar* L.). *BMC Res Notes.* (2011) 4:88. doi: 10.1186/1756-0500-4-88
25. Müller A, Sutherland BJ, Koop BF, Johnson SC, Garver KA. Infectious hematopoietic necrosis virus (IHNV) persistence in Sockeye Salmon: influence on brain transcriptome and subsequent response to the viral mimic poly (I:C). *BMC Genomics.* (2015) 16:634. doi: 10.1186/s12864-015-1759-y
26. Sutherland BJ, Hanson KC, Jantzen JR, Koop BF, Smith CT. Divergent immunity and energetic programs in the gills of migratory and resident *Oncorhynchus mykiss*. *Mol Ecol.* (2014) 23:1952–64. doi: 10.1111/mec.12713
27. Sutherland BJ, Koczka KW, Yasuike M, Jantzen SG, Yazawa R, Koop BF, et al. Comparative transcriptomics of Atlantic *Salmo salar*, chum *Oncorhynchus keta* and pink salmon *O. gorbuscha* during infections with salmon lice *Lepeophtheirus salmonis*. *BMC Genomics.* (2014) 15:200. doi: 10.1186/1471-2164-15-200
28. Eslamloo K, Xue X, Hall JR, Smith NC, Caballero-Solares A, Parrish CC, et al. Transcriptome profiling of antiviral immune and dietary fatty acid dependent responses of Atlantic salmon macrophage-like cells. *BMC Genomics.* (2017) 18:706. doi: 10.1186/s12864-017-4099-2
29. Umasuthan N, Xue X, Caballero-Solares A, Kumar S, Westcott JD, Chen Z, et al. Transcriptomic profiling in fins of Atlantic salmon parasitized with sea lice: evidence for an early imbalance between chalimus-induced immunomodulation and the host's defense response. *Int J Mol Sci.* (2020) 21:2417. doi: 10.3390/ijms21072417
30. Avendaño-Herrera R. *Enfermedades infecciosas del cultivo de salmónidos en Chile y el mundo*. Puerto Varas: NIVA, Puerto Varas. (2011).
31. CCoA C. *Canadian Council on Animal Care Guidelines on: The Care and Use of Fish in Research, Teaching and Testing*. Ottawa. (2005).
32. Bethke J, Poblete-Morales M, Irgang R, Yáñez A, Avendaño-Herrera R. Iron acquisition and siderophore production in the fish pathogen *Renibacterium salmoninarum*. *J Fish Dis.* (2016) 39:1275–83. doi: 10.1111/jfd.12456
33. Bethke J, Quezada J, Poblete-Morales M, Irgang R, Yáñez A, Oliver C, et al. Biochemical, serological, and genetic characterisation of *Renibacterium salmoninarum* isolates recovered from salmonids in Chile. *Bull Eur Assoc Fish Pathol.* (2017) 37:169–80.
34. Chase DM, Pascho RJ. Development of a nested polymerase chain reaction for amplification of a sequence of the p57 gene of *Renibacterium salmoninarum* that provides a highly sensitive method for detection of the bacterium in salmonid kidney. *Dis Aquat Org.* (1998) 34:223–9. doi: 10.3354/dao034223
35. Daly J, Griffiths S, Kew A, Moore A, Olivier G. Characterization of attenuated *Renibacterium salmoninarum* strains and their use as live vaccines. *Dis Aquat Org.* (2001) 44:121–6. doi: 10.3354/dao044121
36. Lockhart K, McBeath A, Collet B, Snow M, Ellis A. Expression of Mx mRNA following infection with IPNV is greater in IPN-susceptible Atlantic salmon post-smolts than in IPN-resistant Atlantic salmon parr. *Fish Shellfish Immunol.* (2007) 22:151–6. doi: 10.1016/j.fsi.2006.04.002
37. Brazma A, Hingamp P, Quackenbush J, Sherlock G, Spellman P, Stoeckert C, et al. Minimum information about a microarray experiment (MIAME)—toward standards for microarray data. *Nat Genet.* (2001) 29:365–71. doi: 10.1038/ng1201-365
38. Götz S, García-Gómez JM, Terol J, Williams TD, Nagaraj SH, Nueda MJ, et al. High-throughput functional annotation and data mining with the Blast2GO suite. *Nucleic Acids Res.* (2008) 36:3420–35. doi: 10.1093/nar/gkn176
39. Conesa A, Götz S, García-Gómez JM, Terol J, Talón M, Robles M. Blast2GO: a universal tool for annotation, visualization and analysis in functional genomics research. *Bioinformatics.* (2005) 21:3674–6. doi: 10.1093/bioinformatics/bti610
40. Bindea G, Mlecnik B, Hackl H, Charoentong P, Tosolini M, Kirilovsky A, et al. ClueGO: a Cytoscape plug-in to decipher functionally grouped gene ontology and pathway annotation networks. *Bioinformatics.* (2009) 25:1091–3. doi: 10.1093/bioinformatics/btp101
41. Shannon P, Markiel A, Ozier O, Baliga NS, Wang JT, Ramage D, et al. Cytoscape: a software environment for integrated models of biomolecular interaction networks. *Genome Res.* (2003) 13:2498–504. doi: 10.1101/gr.1239303
42. Cohen J. Weighted kappa: nominal scale agreement provision for scaled disagreement or partial credit. *Psychol Bull.* (1968) 70:213. doi: 10.1037/h0026256
43. Katan T, Caballero-Solares A, Taylor RG, Rise ML, Parrish CC. Effect of plant-based diets with varying ratios of ω6 to ω3 fatty acids on growth performance, tissue composition, fatty acid biosynthesis and lipid-related gene expression in Atlantic salmon (*Salmo salar*). *Comp Biochem Physiol Part D Genomics Proteomics.* (2019) 30:290–304. doi: 10.1016/j.cbd.2019.03.004
44. Caballero-Solares A, Hall JR, Xue X, Eslamloo K, Taylor RG, Parrish CC, et al. The dietary replacement of marine ingredients by terrestrial animal and plant alternatives modulates the antiviral immune response of Atlantic salmon (*Salmo salar*). *Fish Shellfish Immunol.* (2017) 64:24–38. doi: 10.1016/j.fsi.2017.02.040
45. Zanuzzo F, Beemelmanns A, Hall J, Rise M, Gamperl A. The innate immune response of Atlantic salmon (*Salmo salar*) is not negatively affected by high temperature and moderate hypoxia. *Front Immunol.* (2020) 11:1009. doi: 10.3389/fimmu.2020.01009
46. Bustin SA, Benes V, Garson JA, Hellemans J, Huggett J, Kubista M, et al. The MIQE guidelines: minimum information for publication of quantitative real-time PCR experiments. *Clin Chem.* (2009) 55:611–22. doi: 10.1373/clinchem.2008.112797

47. Eslamloo K, Ghorbani A, Xue X, Inkpen SM, Larijani M, Rise ML. Characterisation and transcript expression analyses of Atlantic cod viperin. *Front Immunol.* (2019) 10:311. doi: 10.3389/fimmu.2019.00311
48. Pfaffl MW. A new mathematical model for relative quantification in real-time RT–PCR. *Nucleic Acids Res.* (2001) 29:2002–7. doi: 10.1093/nar/29.9.e45
49. Vandesompele J, De Preter K, Pattyn F, Poppe B, Van Roy N, De Paepe A, et al. Accurate normalization of real-time quantitative RT-PCR data by geometric averaging of multiple internal control genes. *Genome Biol.* (2002) 3:Research0034. doi: 10.1186/gb-2002-3-7-research0034
50. Valenzuela-Miranda D, Gallardo-Escárate C. Dual RNA-Seq uncovers metabolic amino acids dependency of the intracellular bacterium *Piscirickettsia salmonis* infecting Atlantic salmon. *Front Microbiol.* (2018) 9:2877. doi: 10.3389/fmicb.2018.02877
51. Mukherjee S, Karmakar S, Babu SPS. TLR2 and TLR4 mediated host immune responses in major infectious diseases: a review. *Braz J Infect Dis.* (2016) 20:193–204. doi: 10.1016/j.bjid.2015.10.011
52. Feezor RJ, Oberholzer C, Baker HV, Novick D, Rubinstein M, Moldawer LL, et al. Molecular characterization of the acute inflammatory response to infections with Gram-negative versus Gram-positive bacteria. *Infect Immun.* (2003) 71:5803–13. doi: 10.1128/IAI.71.10.5803-5813.2003
53. Tietze K, Dalpke A, Morath S, Mutters R, Heeg K, Nonnenmacher C. Differences in innate immune responses upon stimulation with Gram-positive and Gram-negative bacteria. *J Periodontal Res.* (2006) 41:447–54. doi: 10.1111/j.1600-0765.2006.00890.x
54. Gaud G, Lesourne R, Love PE. Regulatory mechanisms in T cell receptor signalling. *Nat Rev Immunol.* (2018) 18:485–97. doi: 10.1038/s41577-018-0020-8
55. O'Neill LA, Golenbock D, Bowie AG. The history of toll-like receptors—redefining innate immunity. *Nat Rev Immunol.* (2013) 13:453–60. doi: 10.1038/nri3446
56. Platanias LC. Mechanisms of type-I-and type-II-interferon-mediated signalling. *Nat Rev Immunol.* (2005) 5:375–86. doi: 10.1038/nri1604
57. Swain SL, McKinstry KK, Strutt TM. Expanding roles for $CD4^+$ T cells in immunity to viruses. *Nat Rev Immunol.* (2012) 12:136–48. doi: 10.1038/nri3152
58. Arango Duque G, Descoteaux A. Macrophage cytokines: involvement in immunity and infectious diseases. *Front Immunol.* (2014) 5:491. doi: 10.3389/fimmu.2014.00491
59. Moresco EMY, LaVine D, Beutler B. Toll-like receptors. *Curr Biol.* (2011) 21:R488–93. doi: 10.1016/j.cub.2011.05.039
60. Zhang J, Kong X, Zhou C, Li L, Nie G, Li X. Toll-like receptor recognition of bacteria in fish: ligand specificity and signal pathways. *Fish Shellfish Immunol.* (2014) 41:380–8. doi: 10.1016/j.fsi.2014.09.022
61. Vijay K. Toll-like receptors in immunity and inflammatory diseases: past, present, and future. *Int Immunopharmacol.* (2018) 59:391–412. doi: 10.1016/j.intimp.2018.03.002
62. Yabe R, Saijo S. Dectin-2 in antimicrobial immunity and homeostasis. In: Yamasaki S, editor. *C-Type Lectin Receptors in Immunity*. Tokyo: Springer. (2016). p. 3–13. doi: 10.1007/978-4-431-56015-9_1
63. Kzhyshkowska J, Gratchev A, Goerdt S. Stabilin-1, a homeostatic scavenger receptor with multiple functions. *J Cell Mol Med.* (2006) 10:635–49. doi: 10.1111/j.1582-4934.2006.tb00425.x
64. Kraal G, van der Laan LJ, Elomaa O, Tryggvason K. The macrophage receptor MARCO. *Microbes Infect.* (2000) 2:313–6. doi: 10.1016/S1286-4579(00)00296-3
65. Zhang L, Nie L, Cai S-Y, Chen J, Chen J. Role of a macrophage receptor with collagenous structure (MARCO) in regulating monocyte/macrophage functions in ayu, *Plecoglossus altivelis*. *Fish Shellfish Immunol.* (2018) 74:141–51. doi: 10.1016/j.fsi.2017.12.059
66. Álvarez CA, Acosta F, Montero D, Guzmán F, Torres E, Vega B, et al. Synthetic hepcidin from fish: uptake and protection against *Vibrio anguillarum* in sea bass (*Dicentrarchus labrax*). *Fish Shellfish Immunol.* (2016) 55:662–70. doi: 10.1016/j.fsi.2016.06.035
67. Cai L, Cai J-J, Liu H-P, Fan D-Q, Peng H, Wang K-J. Recombinant medaka (*Oryzias melastigmus*) pro-hepcidin: multifunctional characterization. *Comp Biochem Physiol B Biochem Mol Biol.* (2012) 161:140–7. doi: 10.1016/j.cbpb.2011.10.006
68. Álvarez CA, Guzmán F, Cárdenas C, Marshall SH, Mercado L. Antimicrobial activity of trout hepcidin. *Fish Shellfish Immunol.* (2014) 41:93–101. doi: 10.1016/j.fsi.2014.04.013
69. Zhang X-J, Zhang X-Y, Zhang N, Guo X, Peng K-S, Wu H, et al. Distinctive structural hallmarks and biological activities of the multiple cathelicidin antimicrobial peptides in a primitive teleost fish. *J Immunol.* (2015) 194:4974–87. doi: 10.4049/jimmunol.1500182
70. Harboe M, Ulvund G, Vien L, Fung M, Mollnes T. The quantitative role of alternative pathway amplification in classical pathway induced terminal complement activation. *Clin Exp Immunol.* (2004) 138:439–46. doi: 10.1111/j.1365-2249.2004.02627.x
71. Cossio-Ayala M, Domínguez-López M, Mendez-Enriquez E, del Carmen Portillo-Téllez M, García-Hernández E. *In vitro* and *in vivo* antimicrobial activity of a synthetic peptide derived from the C-terminal region of human chemokine CCL13 against *Pseudomonas aeruginosa*. *Peptides.* (2017) 94:49–55. doi: 10.1016/j.peptides.2017.06.006
72. Oudshoorn D, van Boheemen S, Sanchez-Aparicio MT, Rajsbaum R, García-Sastre A, Versteeg GA. HERC6 is the main E3 ligase for global ISG15 conjugation in mouse cells. *PLoS ONE.* (2012) 7:e0029870. doi: 10.1371/journal.pone.0029870
73. Fitzgerald KA. The interferon inducible gene: Viperin. *J Interferon Cytokine Res.* (2011) 31:131–5. doi: 10.1089/jir.2010.0127
74. Dang W, Zhang M, Hu Y-h, Sun L. Differential regulation of *Sciaenops ocellatus* viperin expression by intracellular and extracellular bacterial pathogens. *Fish Shellfish Immunol.* (2010) 29:264–70. doi: 10.1016/j.fsi.2010.04.015
75. Evans MJ, von Hahn T, Tscherne DM, Syder AJ, Panis M, Wölk B, et al. Claudin-1 is a hepatitis C virus co-receptor required for a late step in entry. *Nature.* (2007) 446:801–5. doi: 10.1038/nature05654
76. Stockinger S, Reutterer B, Schaljo B, Schellack C, Brunner S, Materna T, et al. IFN regulatory factor 3-dependent induction of type I IFNs by intracellular bacteria is mediated by a TLR-and Nod2-independent mechanism. *J Immunol.* (2004) 173:7416–25. doi: 10.4049/jimmunol.173.12.7416
77. Man SM, Kanneganti T-D. Converging roles of caspases in inflammasome activation, cell death and innate immunity. *Nat Rev Immunol.* (2016) 16:7–21. doi: 10.1038/nri.2015.7
78. Cyster JG, Dang EV, Reboldi A, Yi T. 25-Hydroxycholesterols in innate and adaptive immunity. *Nat Rev Immunol.* (2014) 14:731–43. doi: 10.1038/nri3755
79. Maruyama K, Takada Y, Ray N, Kishimoto Y, Penninger JM, Yasuda H, et al. Receptor activator of NF-κB ligand and osteoprotegerin regulate proinflammatory cytokine production in mice. *J Immunol.* (2006) 177:3799–805. doi: 10.4049/jimmunol.177.6.3799
80. Lee C-Y, Lai T-Y, Tsai M-K, Chang Y-C, Ho Y-H, Yu I-S, et al. The ubiquitin ligase ZNRF1 promotes caveolin-1 ubiquitination and degradation to modulate inflammation. *Nat Commun.* (2017) 8:15502. doi: 10.1038/ncomms15502
81. Lee P-H, Kim B-G, Lee S-H, Lee J-H, Park S-W, Kim D-J, et al. Alteration in claudin-4 contributes to airway inflammation and responsiveness in asthma. *Allergy Asthma Immunol.* (2018) 10:25–33. doi: 10.4168/aair.2018.10.1.25
82. Kim B-H, Shenoy AR, Kumar P, Bradfield CJ, MacMicking JD. IFN-inducible GTPases in host cell defense. *Cell Host Microbe.* (2012) 12:432–44. doi: 10.1016/j.chom.2012.09.007
83. Hall CJ, Boyle RH, Astin JW, Flores MV, Oehlers SH, Sanderson LE, et al. Immunoresponsive gene 1 augments bactericidal activity of macrophage-lineage cells by regulating β-oxidation-dependent mitochondrial ROS production. *Cell Metab.* (2013) 18:265–78. doi: 10.1016/j.cmet.2013.06.018
84. Kubo M, Hanada T, Yoshimura A. Suppressors of cytokine signaling and immunity. *Nat Immunol.* (2003) 4:1169–76. doi: 10.1038/ni1012
85. Hartl D, Latzin P, Hordijk P, Marcos V, Rudolph C, Woischnik M, et al. Cleavage of CXCR1 on neutrophils disables bacterial killing in cystic fibrosis lung disease. *Nat Med.* (2007) 13:1423–30. doi: 10.1038/nm1690
86. Saha NR, Bei J-X, Suetake H, Araki K, Kai W, Kikuchi K, et al. Description of a fugu CXC chemokine and two CXC receptor genes, and characterization of the effects of different stimulators on their expression. *Fish Shellfish Immunol.* (2007) 23:1324–32. doi: 10.1016/j.fsi.2007.06.008
87. Makowski L, Brittingham KC, Reynolds JM, Suttles J, Hotamisligil GS. The fatty acid-binding protein, aP2, coordinates macrophage cholesterol

trafficking and inflammatory activity macrophage expression of aP2 impacts peroxisome proliferator-activated receptor γ and IκB kinase activities. *J Biol Chem.* (2005) 280:12888–95. doi: 10.1074/jbc.M413788200
88. Cheng Y, Hu X, Liu C, Chen M, Wang J, Wang M, et al. Gelsolin inhibits the inflammatory process induced by lps. *Cell Physiol Biochem.* (2017) 41:205–12. doi: 10.1159/000456043
89. Zmijewski JW, Lorne E, Zhao X, Tsuruta Y, Sha Y, Liu G, et al. Mitochondrial respiratory complex I regulates neutrophil activation and severity of lung injury. *Am J Respir Crit Care Med.* (2008) 178:168–79. doi: 10.1164/rccm.200710-1602OC
90. He H, Guo F, Li Y, Saaoud F, Kimmis BD, Sandhu J, et al. Adiporedoxin suppresses endothelial activation via inhibiting MAPK and NF-κB signaling. *Sci Rep.* (2016) 6:1–10. doi: 10.1038/srep38975
91. Gómez-Abellán V, Sepulcre MP. The role of prostaglandins in the regulation of fish immunity. *Mol Immunol.* (2016) 69:139–45. doi: 10.1016/j.molimm.2015.09.022
92. Gómez-Abellán V, Montero J, López-Muñoz A, Figueras A, Arizcun M, Mulero V, et al. Professional phagocytic granulocyte-derived PGD_2 regulates the resolution of inflammation in fish. *Dev Comp Immunol.* (2015) 52:182–91. doi: 10.1016/j.dci.2015.04.017
93. Liepke C, Baxmann S, Heine C, Breithaupt N, Ständker L, Forssmann W-G. Human hemoglobin-derived peptides exhibit antimicrobial activity: a class of host defense peptides. *J Chromatogr B.* (2003) 791:345–56. doi: 10.1016/S1570-0232(03)00245-9
94. Ullal AJ, Litaker RW, Noga EJ. Antimicrobial peptides derived from hemoglobin are expressed in epithelium of channel catfish (*Ictalurus punctatus*, Rafinesque). *Dev Comp Immunol.* (2008) 32:1301–12. doi: 10.1016/j.dci.2008.04.005
95. Yang Q, Bai S-Y, Li L-F, Li S, Zhang Y, Munir M, et al. Human hemoglobin subunit beta functions as a pleiotropic regulator of RIG-I/MDA5-mediated antiviral innate immune responses. *J Virol.* (2019) 93:e00718–19. doi: 10.1128/JVI.00718-19
96. Jabara HH, McDonald DR, Janssen E, Massaad MJ, Ramesh N, Borzutzky A, et al. DOCK8 functions as an adaptor that links TLR-MyD88 signaling to B cell activation. *Nat Immunol.* (2012) 13:612–20. doi: 10.1038/ni.2305
97. Evavold CL, Kagan JC. How inflammasomes inform adaptive immunity. *J Mol Biol.* (2018) 430:217–37. doi: 10.1016/j.jmb.2017.09.019
98. Unutmaz D, Vilcek J. IRF1: a deus ex machina in TH 1 differentiation. *Nat Immunol.* (2008) 9:9–10. doi: 10.1038/ni0108-9
99. Beck IM, Rückert R, Brandt K, Mueller MS, Sadowski T, Brauer R, et al. MMP19 is essential for T cell development and T cell-mediated cutaneous immune responses. *PLoS ONE.* (2008) 3:e0002343. doi: 10.1371/journal.pone.0002343
100. Davis SM, Pennypacker KR. The role of the leukemia inhibitory factor receptor in neuroprotective signaling. *Pharmacol Ther.* (2018) 183:50–7. doi: 10.1016/j.pharmthera.2017.08.008
101. Esche C, Stellato C, Beck LA. Chemokines: key players in innate and adaptive immunity. *J Investig Dermatol.* (2005) 125:615–28. doi: 10.1111/j.0022-202X.2005.23841.x
102. Hsu Y-J, Hou C-Y, Lin S-J, Kuo W-C, Lin H-T, Lin JH-Y. The biofunction of orange-spotted grouper (*Epinephelus coioides*) CC chemokine ligand 4 (CCL4) in innate and adaptive immunity. *Fish Shellfish Immunol.* (2013) 35:1891–8. doi: 10.1016/j.fsi.2013.09.020
103. Kasai H, Kuwabara T, Matsui Y, Nakajima K, Kondo M. Identification of an essential cytoplasmic region of interleukin-7 receptor α subunit in B-cell development. *Int J Mol Sci.* (2018) 19:2522. doi: 10.3390/ijms19092522
104. Corcoran A, Smart F, Cowling R, Crompton T, Owen M, Venkitaraman A. The interleukin-7 receptor alpha chain transmits distinct signals for proliferation and differentiation during B lymphopoiesis. *EMBO J.* (1996) 15:1924–32. doi: 10.1002/j.1460-2075.1996.tb00543.x
105. Lebson L, Gocke A, Rosenzweig J, Alder J, Civin C, Calabresi PA, et al. Cutting edge: the transcription factor Kruppel-like factor 4 regulates the differentiation of Th17 cells independently of RORγt. *J Immunol.* (2010) 185:7161–4. doi: 10.4049/jimmunol.1002750
106. Hosokawa H, Tanaka T, Kato M, Shinoda K, Tohyama H, Hanazawa A, et al. Gata3/Ruvbl2 complex regulates T helper 2 cell proliferation via repression of Cdkn2c expression. *Proc Natl Acad Sci USA.* (2013) 110:18626–31. doi: 10.1073/pnas.1311100110
107. Fagarasan S, Kawamoto S, Kanagawa O, Suzuki K. Adaptive immune regulation in the gut: T cell–dependent and T cell–independent IgA synthesis. *Annu Rev Immunol.* (2009) 28:243–73. doi: 10.1146/annurev-immunol-030409-101314
108. Kawata J, Yamaguchi R, Yamamoto T, Ishimaru Y, Sakamoto A, Aoki M, et al. Human neutrophil elastase induce interleukin-10 expression in peripheral blood mononuclear cells through protein kinase C theta/delta and phospholipase pathways. *Cell J.* (2016) 17:692–700.
109. Moreira LO, El Kasmi KC, Smith AM, Finkelstein D, Fillon S, Kim Y-G, et al. The TLR2-MyD88-NOD2-RIPK2 signalling axis regulates a balanced pro-inflammatory and IL-10-mediated anti-inflammatory cytokine response to Gram-positive cell walls. *Cell Microbiol.* (2008) 10:2067–77. doi: 10.1111/j.1462-5822.2008.01189.x
110. Arthur JSC, Ley SC. Mitogen-activated protein kinases in innate immunity. *Nat Rev Immunol.* (2013) 13:679–92. doi: 10.1038/nri3495
111. Castro-Sánchez P, Ramirez-Munoz R, Roda-Navarro P. Gene expression profiles of human phosphotyrosine phosphatases consequent to Th1 polarisation and effector function. *J Immunol Res.* (2017) 2017:8701042. doi: 10.1155/2017/8701042
112. Mueller AM, Pedré X, Killian S, David M, Steinbrecher A. The decoy receptor 3 (DcR3, TNFRSF6B) suppresses Th17 immune responses and is abundant in human cerebrospinal fluid. *J Neuroimmunol.* (2009) 209:57–64. doi: 10.1016/j.jneuroim.2009.01.024
113. Ewen C, Kane K, Bleackley R. A quarter century of granzymes. *Cell Death Differ.* (2012) 19:28–35. doi: 10.1038/cdd.2011.153
114. Chaves-Pozo E, Valero Y, Lozano MT, Rodríguez-Cerezo P, Miao L, Campo V, et al. Fish Granzyme A shows a greater role than Granzyme B in fish innate cell-mediated cytotoxicity. *Front Immunol.* (2019) 10:2579. doi: 10.3389/fimmu.2019.02579
115. Afzali B, Kim S, West E, Nova-Lamperti E, Cheru N, Nagashima H, et al. RNF144A shapes the hierarchy of cytokine signaling to provide protective immunity against influenza. *bioRxiv [preprint].* (2019) 782680. doi: 10.1101/782680
116. Luo L, Zhu D, Huang R, Xiong L, Mehjabin R, He L, et al. Molecular cloning and preliminary functional analysis of six RING-between-ring (RBR) genes in grass carp (*Ctenopharyngodon idellus*). *Fish Shellfish Immunol.* (2019) 87:62–72. doi: 10.1016/j.fsi.2018.12.078
117. Gallegos AM, Xiong H, Leiner IM, Sušac B, Glickman MS, Pamer EG, et al. Control of T cell antigen reactivity via programmed TCR downregulation. *Nat Immunol.* (2016) 17:379–86. doi: 10.1038/ni.3386
118. Chen Y-W, Guo T, Shen L, Wong K-Y, Tao Q, Choi WW, et al. Receptor-type tyrosine-protein phosphatase κ directly targets STAT3 activation for tumor suppression in nasal NK/T-cell lymphoma. *Blood.* (2015) 125:1589–600. doi: 10.1182/blood-2014-07-588970
119. Hershey GKK. IL-13 receptors and signaling pathways: an evolving web. *J Allergy Clin Immunol.* (2003) 111:677–90. doi: 10.1067/mai.2003.1333
120. Roche PA, Furuta K. The ins and outs of MHC class II-mediated antigen processing and presentation. *Nat Rev Immunol.* (2015) 15:203–16. doi: 10.1038/nri3818
121. Hansen TH, Bouvier M. MHC class I antigen presentation: learning from viral evasion strategies. *Nat Rev Immunol.* (2009) 9:503–13. doi: 10.1038/nri2575
122. Joffre OP, Segura E, Savina A, Amigorena S. Cross-presentation by dendritic cells. *Nat Rev Immunol.* (2012) 12:557–69. doi: 10.1038/nri3254
123. Semple SL, Vo NTK, Li AR, Pham PH, Bols NC, Dixon B. Development and use of an Arctic charr cell line to study antiviral responses at extremely low temperatures. *J Fish Dis.* (2017) 40:1423–39. doi: 10.1111/jfd.12615
124. Sever L, Vo NT, Bols NC, Dixon B. Expression of tapasin in rainbow trout tissues and cell lines and up regulation in a monocyte/macrophage cell line (RTS11) by a viral mimic and viral infection. *Dev Comp Immunol.* (2014) 44:86–93. doi: 10.1016/j.dci.2013.11.019
125. Sever L, Vo NT, Bols NC, Dixon B. Rainbow trout (*Oncorhynchus mykiss*) contain two calnexin genes which encode distinct proteins. *Dev Comp Immunol.* (2014) 42:211–9. doi: 10.1016/j.dci.2013.09.005
126. Sever L, Vo NT, Lumsden J, Bols NC, Dixon B. Induction of rainbow trout MH class I and accessory proteins by viral haemorrhagic septicaemia virus. *Mol Immunol.* (2014) 59:154–62. doi: 10.1016/j.molimm.2014.02.001

127. Sever L, Vo NTK, Bols NC, Dixon B. Tapasin's protein interactions in the rainbow trout peptide-loading complex. *Dev Comp Immunol.* (2018) 81:262–70. doi: 10.1016/j.dci.2017.12.015
128. Stet RJ, Kruiswijk CP, Dixon B. Major histocompatibility lineages and immune gene function in teleost fishes: the road not taken. *Crit Rev Immunol.* (2003) 23:441–71. doi: 10.1615/CritRevImmunol.v23.i56.50
129. Nimmerjahn F, Ravetch JV. Fc-receptors as regulators of immunity. *Adv Immunol.* (2007) 96:179–204. doi: 10.1016/S0065-2776(07)96005-8
130. Holmes TD, Wilson EB, Black EV, Benest AV, Vaz C, Tan B, et al. Licensed human natural killer cells aid dendritic cell maturation via TNFSF14/LIGHT. *Proc Natl Acad Sci USA.* (2014) 111:E5688–96. doi: 10.1073/pnas.1411072112
131. Banh C, Brossay L. Immune receptors, cadherins and their interactions. *Curr Immunol Rev.* (2009) 5:2–9. doi: 10.2174/157339509787314440
132. Makita N, Hizukuri Y, Yamashiro K, Murakawa M, Hayashi Y. IL-10 enhances the phenotype of M2 macrophages induced by IL-4 and confers the ability to increase eosinophil migration. *Int Immunol.* (2015) 27:131–41. doi: 10.1093/intimm/dxu090
133. Melotte V, Qu X, Ongenaert M, Van Criekinge W, de Bruïne AP, Baldwin HS, et al. The N-myc downstream regulated gene (NDRG) family: diverse functions, multiple applications. *FASEB J.* (2010) 24:4153–66. doi: 10.1096/fj.09-151464
134. Antoniou AN, Powis SJ. Pathogen evasion strategies for the major histocompatibility complex class I assembly pathway. *Immunology.* (2008) 124:1–12. doi: 10.1111/j.1365-2567.2008.02804.x
135. Schüller S, Kügler S, Goebel W. Suppression of major histocompatibility complex class I and class II gene expression in *Listeria monocytogenes*-infected murine macrophages. *FEMS Immunol Med Microbiol.* (1998) 20:289–99. doi: 10.1016/S0928-8244(98)00024-8
136. Mainland J, Matsunami H. Ramp like proteins. In: Spielman WS, Parameswaran N, editors. *RAMPs*. New York, NY: Springer. (2012). p. 75-86. doi: 10.1007/978-1-4614-2364-5_7
137. Akum BF, Chen M, Gunderson SI, Riefler GM, Scerri-Hansen MM, Firestein BL. Cypin regulates dendrite patterning in hippocampal neurons by promoting microtubule assembly. *Nat Neurosci.* (2004) 7:145–52. doi: 10.1038/nn1179
138. Zhao X, Huang Z, Liu X, Chen Y, Gong W, Yu K, et al. The switch role of the Tmod4 in the regulation of balanced development between myogenesis and adipogenesis. *Gene.* (2013) 532:263–71. doi: 10.1016/j.gene.2013.08.088
139. Ng TH, Chiang Y-A, Yeh Y-C, Wang H-C. Review of Dscam-mediated immunity in shrimp and other arthropods. *Dev Comp Immunol.* (2014) 46:129–38. doi: 10.1016/j.dci.2014.04.002
140. Galicia CA, Sukeena JM, Stenkamp DL, Fuerst PG. Expression patterns of dscam and sdk gene paralogs in developing zebrafish retina. *Mol Vis.* (2018) 24:443–58.

Conflict of Interest: EJ and CB are employed by Cargill Aqua Nutrition.

EJ, in the representation of Cargill Innovation, designed the fish infection trial and oversaw the fish trial execution. CB was the lead technician for the experimental fish trial as well as RNA extraction.

The remaining authors declare that the research was conducted in the absence of any commercial or financial relationships that could be construed as a potential conflict of interest.

The handling editor declared a past co-authorship with several of the authors SI, KE, and MR.

Copyright © 2020 Eslamloo, Caballero-Solares, Inkpen, Emam, Kumar, Bouniot, Avendaño-Herrera, Jakob and Rise. This is an open-access article distributed under the terms of the Creative Commons Attribution License (CC BY). The use, distribution or reproduction in other forums is permitted, provided the original author(s) and the copyright owner(s) are credited and that the original publication in this journal is cited, in accordance with accepted academic practice. No use, distribution or reproduction is permitted which does not comply with these terms.

frontiers in Immunology

ORIGINAL RESEARCH
published: 20 November 2020
doi: 10.3389/fimmu.2020.576897

CD10$^+$ Cells and IgM in Pathogen Response in Lumpfish (*Cyclopterus lumpus*) Eye Tissues

Robert L. Gendron[1], Hélène Paradis[1], Raahyma Ahmad[1], Kenneth Kao[1], Danny Boyce[2], William V. Good[3], Surendra Kumar[2], Ignacio Vasquez[2], Trung Cao[2], Ahmed Hossain[2], Setu Chakraborty[2], Katherinne Valderrama[2] and Javier Santander[2]*

[1] Division of Biomedical Sciences, Faculty of Medicine, Memorial University, St. John's, NL, Canada, [2] Marine Microbial Pathogenesis and Vaccinology Lab, Department of Ocean Sciences, Memorial University, St. John's, NL, Canada, [3] Smith Kettlewell Eye Research Institute, San Francisco, CA, United States

OPEN ACCESS

Edited by:
Gyri T. Haugland, University of Bergen, Norway

Reviewed by:
Zhen Xu, Huazhong Agricultural University, China
Neil Ruane, Marine Institute, Ireland

***Correspondence:**
Robert L. Gendron
rgendron@mun.ca

Specialty section:
This article was submitted to Comparative Immunology, a section of the journal Frontiers in Immunology

Received: *27 June 2020*
Accepted: *22 October 2020*
Published: *20 November 2020*

Citation:
Gendron RL, Paradis H, Ahmad R, Kao K, Boyce D, Good WV, Kumar S, Vasquez I, Cao T, Hossain A, Chakraborty S, Valderrama K and Santander J (2020) CD10$^+$ Cells and IgM in Pathogen Response in Lumpfish (Cyclopterus lumpus) Eye Tissues. Front. Immunol. 11:576897. doi: 10.3389/fimmu.2020.576897

Lumpfish (*Cyclopterus lumpus*), a North Atlantic "cleaner" fish, is utilized to biocontrol salmon louse (*Lepeophtheirus salmonis*) in Atlantic salmon (*Salmo salar*) farms. Lumpfish require excellent vision to scan for and eat louse on salmon skin. The lumpfish eye immune response to infectious diseases has not been explored. We examined the ocular response to a natural parasite infection in wild lumpfish and to an experimental bacterial infection in cultured lumpfish. Cysts associated with natural myxozoan infection in the ocular scleral cartilage of wild adult lumpfish harbored cells expressing cluster of differentiation 10 (CD10) and immunoglobulin M (IgM). Experimental *Vibrio anguillarum* infection, which led to exophthalmos and disorganization of the retinal tissues was associated with disruption of normal CD10 expression, CD10$^+$ cellular infiltration and IgM expression. We further describe the lumpfish CD10 orthologue and characterize the lumpfish scleral skeleton in the context of myxozoan scleral cysts. We propose that lumpfish develop an intraocular response to pathogens, exemplified herein by myxozoan and *V. anguillarum* infection involving novel CD10$^+$ cells and IgM$^+$ cells to contain and mitigate damage to eye structures. This work is the first demonstration of CD10 and IgM expressing cells in a novel ocular immune system component in response to disease in a teleost.

Keywords: lumpfish (*Cyclopterus lumpus* L.), eye, immune response, infection, cluster of differentiation 10, immunoglobulin M

INTRODUCTION

The aquaculture and utilization of lumpfish as cleaner fish to control sea-lice infestation in the Atlantic salmon (*Salmo salar*) industry has become commercially relevant in the last 10 years (1–5), making the study and protection of this species increasingly important. Sea-lice are copepod ectoparasites that immune compromise the fish host, increasing susceptibility to infections (6), resulting in significant losses and high treatment costs (7–9).

The literature on disease causing infection in lumpfish has been growing over the past decade (10–12), indicating the significant environmental threats that lumpfish encounter in the wild. Lumpfish recently have been designated as near-threatened on a global basis and as threatened in the Northwest Atlantic in Canada (13); Committee on the Status of Endangered Wildlife in Canada [COSEWIC], Government of Canada). New knowledge of inherent features that participate in response to exogenous threats to the eyes of lumpfish is required to better understand their survival in the wild and/or use as a cleaner fish.

Pelagic trawl records and videos suggest that, while lumpfish reside mainly in the upper 60 m of the ocean, they can also be frequently found up to 498 m with daily vertical migrations greater than 100 m (14–18). The range in habitat across depths containing large variations in light levels, temperature and hydrostatic pressure might have forced evolution of novel morphological changes, ostensibly offering survival advantages to this species.

Lumpfish have a scan-and-pick sea-lice feeding behavior that requires sophisticated anatomical and functional features in their visual system. We have described novel accessory retinal tissues harbored by lumpfish (19). These tissues represent one example of how these animals' visual system might have adapted to their widely ranging habitat (20). Since our initial study (19), our group has continued to further characterize the eyes of cultured and wild lumpfish at the histological level. We have observed that otherwise healthy wild caught lumpfish without exophthalmos harbor cystic-like structures containing what appears to be leukocyte-like cellular elements in their scleral cartilage. Lumpfish possess scleral skeletal tissue associated with their eye globes similar to those described in other teleosts (21). Pathological cases of chondritis, an inflammatory reaction within cartilage structures, have been previously described in domesticated mammals, experimental animal models and humans (22–24), but we are not aware of previous reports of leukocytic tissue within teleost scleral skeletal tissues.

It has been described that *Myxobolus albi*, a metazoan parasite, infects the scleral cartilage and causes mild to severe exophthalmos in lumpfish (25). In addition, *Vibrio anguillarum*, a Gram-negative bacterium and the causative agent of vibriosis, is a frequent pathogen of lumpfish and causes exophthalmos (26). The rationale of our study was to explore any intraocular immune response in wild lumpfish harboring scleral cysts and cultured lumpfish infected with *V. anguillarum*.

Gross anatomy, histology, immunohistochemistry, genetic and bioinformatic approaches have been utilized to explore the cellular characteristics of scleral cartilage infected with *M. albi* cysts and *V. anguillarum*. Herein, we report here that the intraocular immune response to myxozoan cysts and *V. anguillarum* infection are associated with a host response involving IgM+ cells and CD10+ cells, which, in the context of the immune system, is a marker for hematopoietic cells (27, 28). These results indicate a novel ocular immune system component in response to infection in a teleost.

MATERIALS AND METHODS

Lumpfish Samples, Histology, and Whole Mounts

The work described herein was performed on specimens of lumpfish obtained at the Dr. Joe Brown Aquatic Research Building (JBARB), Department of Ocean Sciences, Memorial University, under approval by the Institutional Animal Care Committee (protocol #17-03-RG). Lumpfish eyes were collected from wild male adults of unknown age and approximately 0.5 kg (n=2), wild female adults of unknown age and approximately 3–4 kg (n=3) and wild female adults that were domesticated for 4 years (n=4) in the JBARB lumpfish culture facility. The wild male animals were collected from Harbour Main of the Newfoundland Avalon Peninsula in 2019. The wild female animals were collected from Newfoundland coastal waters in two different years (two from 2018 from several different geographical locations around the Avalon Peninsula Newfoundland and one from the Champney's area of Trinity Bay, Newfoundland in 2019). All wild fish were considered as overtly healthy. None showed clinical signs of illness or exophthalmos. Fish were euthanized by a lethal dose of TMS/MS-222 (400 mg/L). Eyes were carefully excised, either fixed in 4% paraformaldehyde and processed for paraffin embedding or freshly dissected for tissue collection and whole mount Alcian blue (cartilage)/Alizarin red (bone) staining. Dissections were performed under a stereomicroscope fitted with an eyepiece adapter facilitating photography.

Paraffin blocks were sectioned and slides stained with hematoxylin and eosin (H&E) or the following special stains. Giemsa stain is commonly utilized to visualize white blood cells, Van Gieson stain is commonly used to detect matrix components such as elastin, Masson's Trichrome stain is useful for differentially staining elements of bone, cartilage, extracellular matrix and leukocytic features, and basic fuchsin/toluidine blue stain can be used to detect cellular elements (29).

To visualize the lumpfish ocular skeleton, whole mounts of scleral cups or were stained with Alcian blue (to stain cartilage blue) and Alizarin red (to stain ossified bone elements red) as previously described (30). Bony fin tissue from the same animals was used as a positive control tissue. Differential histological stains and whole mount stains were performed by the Histology Core Facility in the Faculty of Medicine, Memorial University.

Detection of *M. albi* DNA in Lumpfish Scleral Cartilage Tissue

Scleral cartilage cup tissues with or without grossly visible white scleral cartilage tissue pockets were collected from freshly euthanized wild adult lumpfish. Additionally, similar size scleral cartilage cups were collected from cultured lumpfish. Tissues were snap frozen, after which DNA was then isolated from the tissues. Specific primer sets included 538MyxFw and 540MyxRv targeting a 1.5 kb fragment of genomic *M. albi* DNA encoding for the 18S ribosomal RNA (EU420055.2) were generated and used in polymerase chain reaction (PCR) as previously reported (25). Mouse (*Mus musculus*) DNA and naïve cultured lumpfish DNA were used for negative controls.

Lumpfish Holding, Immunization, and *V. anguillarum* Challenge

V. anguillarum infected lumpfish eye tissues were sourced from ongoing vaccination studies. The immunization and challenge experiments were performed in accordance with the guidelines of the Canadian Council on Animal Care and approved by Memorial University of Newfoundland's Institutional Animal Care Committee (protocols #18-01-JS; #18-02-JS). Juvenile specimens of lumpfish 50 ± 0.2 g (mean ± SE) were obtained from the JBARB at the Department of Ocean Sciences, Memorial University of Newfoundland, Canada. The animals were kept according to established conditions (28), 10°C in 500 l tanks supplied with 95%–110% air saturated and UV treated filtered flow-through seawater, and an ambient photoperiod. The fish were fasted during 48 h pre-vaccination. The fish were intraperitoneally (IP) vaccinated with formalin inactivated *V. anguillarum* J360 (Chromosome I, NCBI accession number: CP034572.1; chromosome II, NCBI accession number: CP034573.1) and PBS-mock control. After 8 weeks-post vaccination the animals were challenged with *V. anguillarum* J360 ($6.7x10^6$ CFU/dose; for fish numbers and vaccinology results see (28). Lumpfish ocular tissues were collected at 7 days post-challenge and processed for paraffin sectioning, histology and CD10 immunostaining described below.

Lumpfish IgM Purification and Chicken IgY Anti-Lumpfish IgM Production

To assess the presence of lumpfish IgM expression, an anti-lumpfish IgM antibody was produced in chicken. Lumpfish IgM was purified according to protocols described previously for other Teleosts (31) with modifications. Briefly, IgM was purified from pooled lumpfish fresh serum (250 ml) using an immobilized mannan binding protein (MBP) column kit (Pierce Biotechnology) according to manufacturer´s instructions, except that 250 ml of serum were used instead of 1 ml. The integrity and purity of the lumpfish IgM was evaluated by 10% SDS-PAGE (**Figure S1**). Chicken IgY anti-lumpfish IgM antibody was produced and biotinylated commercially at Somru BioScience Inc. (Charlottetown, PEI, Canada). Briefly, chickens were immunized *via* intramuscular injection into breast muscle with a maximum volume of 500 µl/injection and a maximum immunogen concentration of 0.4 mg/ml (200 µg/500 µl). Two chickens were immunized with lumpfish IgM in combination with Freund's complete and incomplete adjuvant. The immunization series was initiated when chickens were 14 weeks of age. The initial immunization was 400 µg of lumpfish IgM in Freund's Complete adjuvant in a total volume of 1 ml. Four subsequent immunizations of 200 ug of lumpfish IgM in Freund's incomplete adjuvant in a total volume of 1 ml were delivered at 14 day intervals. For all immunizations, 0.5 ml of immunogen preparation was delivered per breast muscle. Serum titers were monitored every 14 days using direct ELISA. Western blot of purified lumpfish IgM was performed using the chicken IgY anti-lumpfish IgM primary antibody and goat anti-IgY-HRP (horseradish peroxidase; Promega) secondary antibody (**Figure S1**).

Immunohistochemistry

Immunohistochemistry (IHC) for CD10 was performed using a Ventana Benchmark Ultra automated immunostainer (Roche) in the Department of Anatomical Pathology, General Hospital, Eastern Health, St. John's NL, on sections from lumpfish eyes, lumpfish head kidney and human tonsil applied to positively charged slides using rabbit monoclonal IgG antibody clone SP67 directed against human CD10. Sections were processed on the automated immunostainer using citrate-based (10 mM, pH 6) and tris-based buffer CC1 (Roche, Switzerland) for antigen retrieval at 100°C for 64 min followed by 32 min of incubation at room temperature with either rabbit monoclonal IgG antibody clone SP67 anti-human CD10 (Roche, Diagnostic 790-4506) or a rabbit IgG (Roche, Diagnostics 790-4795) as negative control using a 1:200 dilution and detected using Ultraview (Roche) and counterstained with hematoxylin. Anti-alpha smooth muscle actin (ASMA) IHC was performed as previously described (19). Double anti-CD10/ASMA IHC was performed on a Leica Bond automated immunostainer using parameters similar to those used for automated CD10 staining. For IgM IHC, we used the anti-lumpfish-IgM IgY antibody custom produced in collaboration with Somru BioScience described above. Anti-lumpfish-IgM IgY was applied at a 1/500 dilution of a 2.7 mg/ml stock concentration using IHC procedures previously described (19) except that an alkaline phosphatase-conjugated anti-IgY secondary antibody was used at 1/250 dilution to develop the IgM staining reaction. As a specificity control, the anti-lumpfish-IgM IgY antibody was pre-absorbed for 1 h with a 100-fold excess concentration of purified lumpfish-IgM prior to being applied to the sections for IHC (32).

Sequence Analysis

Nucleotide Basic Local Alignment Search Tool (BLAST) 2.7.1 (33) was performed based on the sequences of the putative lumpfish CD10 present in the public genome sequence of *C. lumpus* (34), and *Homo sapiens* CD10 (EAW78758.1) gene sequence. Amino acid sequence alignments were performed using the CLC Workbench 20 (Qiagen). For phylogenic analysis, the bootstrap consensus tree inferred from 100 replicates were taken to represent the evolutionary history of the taxa analyzed (35). Branches corresponding to partitions reproduced in less than 50% bootstrap replicates were collapsed. Initial tree(s) for the heuristic search were obtained automatically by applying Neighbor-Joining and BioNJ algorithms to a matrix of pairwise distances estimated using a JTT model, and then selecting the topology with superior log likelihood value. The analysis involved 34 amino acid sequences. All positions containing gaps and missing data were eliminated. There was a total of 704 positions in the final dataset. Evolutionary analyses were conducted in MEGA7 (36). Protein structural-based alignments were performed by using the web-based interface for ESPript v.2.2 located at http://espript.ibcp.fr/ESPript/cgi-bin/ESPript.cgi (37). The 3D structure of *C. lumpus* CD10 protein was predicted using position specific iterative-BLAST (PSI-BLAST) alignment and HHpred (https://toolkit.tuebingen.mpg.de/#/) (38, 39).

RESULTS

Gross Anatomical and Histological Characteristics of the Scleral Skeleton of Wild Lumpfish in the Context of Myxozoan Cysts

All of the wild lumpfish studied herein were otherwise overtly healthy showing no signs of illness or exophthalmos (**Figure 1**). We observed, histologically, pockets of densely packed cellular tissue within their eye scleral cartilage (described below in **Figure 3**). Such structures were similar to myxozoan cysts previously described in diseased aquaria lumpfish (25). Sequential anterior to posterior anatomical dissection of the lens, retina, and *rete mirabile* vascular tissues (40) of wild adult lumpfish eye revealed the cysts in the semi-transparent scleral skeletal tissue (**Figures 2A–E**). Soft clumps of cystic material can be easily pulled out from the scleral skeletal tissue with ophthalmologic forceps (**Figure 2F**) and were confirmed to be myxozoan positive (see 3.2).

These cysts in scleral cartilage were seen in three out of five independent healthy wild specimens. Two of these specimens were harvested in 2018 and one in 2019 from separate geographical locations near St. John's NL. We did not observe scleral cartilage cysts in any of 4 wild lumpfish specimens of comparable size that were domesticated in the JBARB lumpfish culture facility for 4 years.

Further characterization of the ocular cysts was performed. Whole mount staining with Alcian blue and Alizarin red, of the scleral cups from two of the healthy wild caught adult lumpfish, revealed that one animal harbored grossly visible, posteriorly protruding, scleral skeletal cysts clearly embedded within the blue staining scleral skeletal tissue, resembling tubercles (**Figures 2G–I**). Alcian blue cartilage staining displayed the expected general shape and configuration of the scleral cartilage cup, including a posterior window of non-cartilaginous, non-ossified sclera to accommodate the optic nerve and *rete mirabile* tracts (**Figure 2J**).

Whole mount staining of a scleral cup from a cultured lumpfish specimen revealed no scleral cartilage cysts but did show the same general shape and configuration of the scleral cartilage cup with posterior scleral optic tract window as with the wild specimen (**Figure 2K**). Absence of Alizarin Red staining in either the wild or the cultured lumpfish scleral cups indicated no ossification to bone tissue, as compared with the positive control fin (see red staining tissue in **Figure 2L**).

Histological sections of the otherwise healthy wild adult lumpfish eyes displayed extensive densely packed cystic structures with what appeared to be myxozoan spores (25) present in the scleral cartilage (**Figures 3A–F** and **4A, B**). Histologically, the cystic tissue was strikingly similarity to mammalian active bone marrow, a tissue containing high numbers of leukocytes and little or no fat tissue (29), but also contained hallmarks of scleral myxozoan cysts with spores previously described as being associated with exophthalmos in *M. albi* infection in scleral cartilage of clinically ill captive lumpfish (25).

FIGURE 1 | Normal wild adult lumpfish. Head and eye regions of several approximately 3 kg wild adult female North Atlantic lumpfish, representative of most of those studied herein, are shown immediately following sacrifice. As exemplified in the image, the wild specimens studied herein appeared overtly healthy and did not show any overt signs of clinical eye disease or exophthalmos.

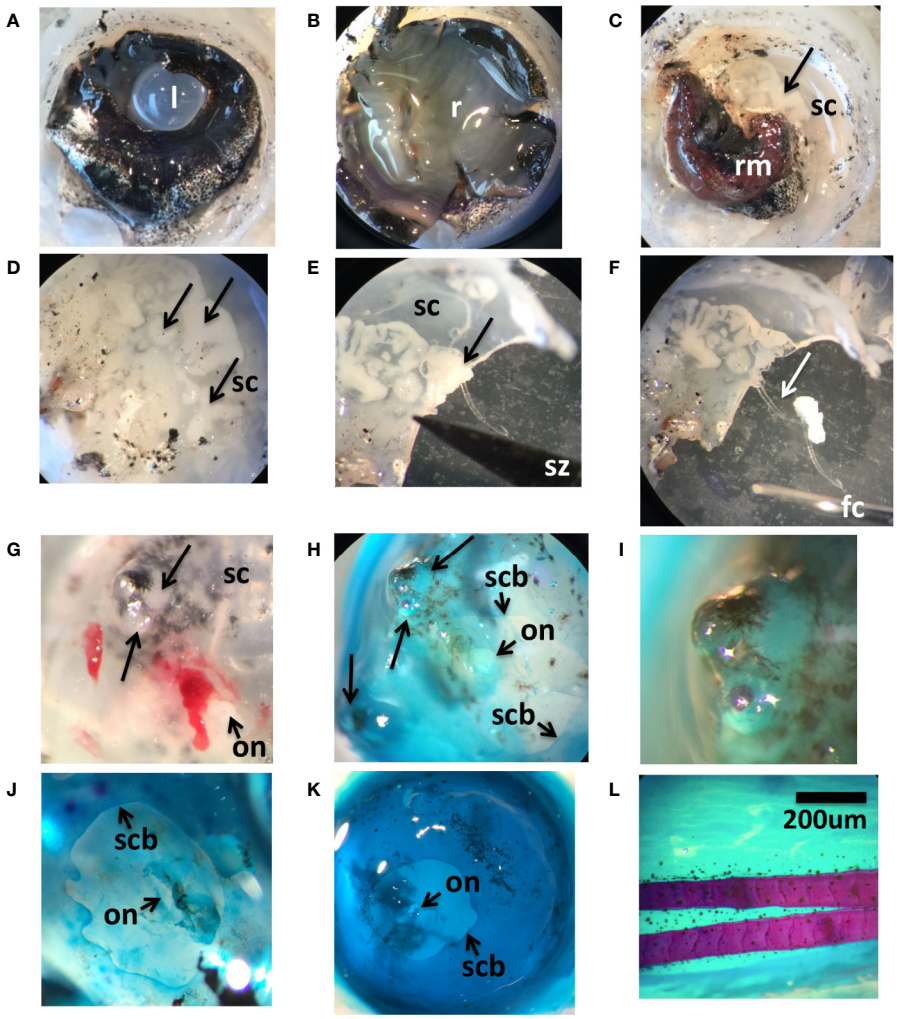

FIGURE 2 | Anatomical characteristics of wild adult lumpfish scleral cartilage. Panels **(A–F)** show an anterior-posterior sequential dissection of an eye from a ~3 kg North Atlantic wild adult lumpfish revealing, first, lens (l) set in middle of pigmented iris **(A)**, next, retina (r) **(B)**, next, the *rete mirabile* vascular organ (rm) **(C)** and finally the semi-transparent scleral cartilage (sc) **(C–E)**; arrows show the cysts. Panel **(E)** shows scleral cartilage cut in half through a cystic structure (arrow) with the tip of the scissors (sz) visible in the image. Panel **(F)** shows the soft white clump of tissue (arrow) pulled out of the scleral pocket with ophthalmologic forceps (fc) of which one metal tip is visible in the image. Panels **(G–I)** show an eye from a ~0.5 kg adult North Atlantic wild adult lumpfish. Panel **(G)** shows freshly dissected scleral cartilage (sc) with protruding lesions (large arrows) next to the optic nerve head (on). Panels **(H, I)** show the same region after Alcian blue/Alizarin red whole mount staining, panel **(I)** magnified twice as much. Alcian blue/Alizarin red staining of scleral cup from another ~0.5 kg adult North Atlantic wild adult lumpfish **(J)** and from a similar size adult North Atlantic cultured lumpfish **(K)**. In panels **(J, K)**, the boundary of the scleral cartilage and sclera are indicated (scb), as is the position of the optic nerve head (on). Panels **(G–K)** are from an ocular posterior viewpoint. Panel **(L)** shows fin tissue from one of the same adult North Atlantic cultured lumpfishes, stained with Alcian blue/Alizarin red, and which was used as a positive control for fully ossified bone tissue as seen by red fin bone staining. Dissected and whole mounted eyes were previously fixed in 4% paraformaldehyde which slightly opacifies the lens. Magnification: 65X. Scale bar in **(L)** applies to all panels.

The scleral cartilage cystic structures were found in central portions of the eye globe, in close proximity to the most robust portions of the *rete mirabile* (as shown in **Figures 2** and **3A–F**). Giemsa stain, which differentially stains most leukocytes blue and erythrocytes pink, revealed small blue staining white blood cell-like cells with basophilic nuclei and larger blue staining stromal-like cells in the cysts of the scleral cartilage (**Figures 3C** and **4A**). Giemsa staining of the *rete mirabile* revealed a more prominent pink staining than the scleral cartilage cysts by virtue of the larger proportion of red blood cells within the *rete mirabile* (**Figure 3C**).

Van Gieson stain which is classically used to define matrix components such as elastin staining all blood cells gold, revealed a staining pattern of the scleral cartilage cysts similar to the blood cell elements in the *rete mirabile* (**Figure 3D**). The scleral cartilage matrix material stained a typical blueish green color with Masson's Trichrome (blue staining of bone, cartilage and extracellular matrix and eosin staining of

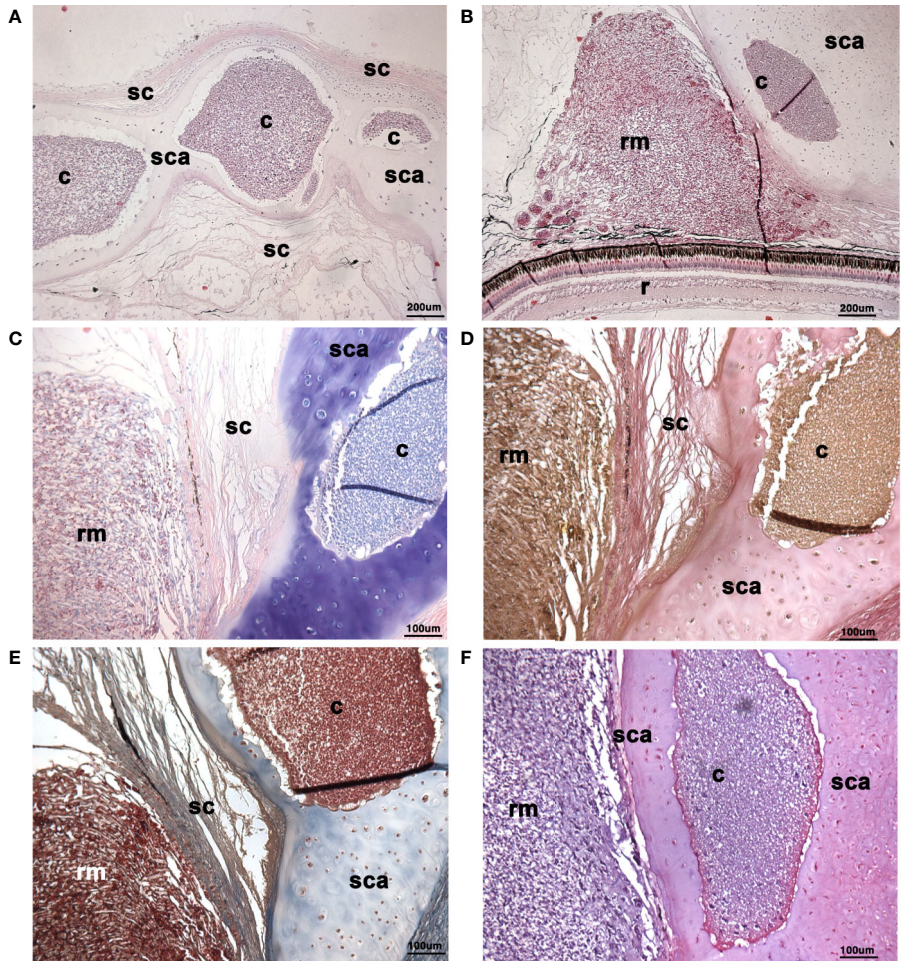

FIGURE 3 | Histological morphology of cysts in scleral cartilage of wild adult lumpfish eyes. Histology of wild lumpfish eye displays extensive cystic structures containing densely packed cellular tissue present in spaces of the scleral cartilage when stained with Hematoxylin & eosin **(A, B)**, Giemsa **(C)**, Van Gieson **(D)**, Masson's Trichrome **(E)**, and basic fuchsin/toluidine blue **(F)**. The scleral cartilage cysts were located in central portions of the eye globe, in close proximity to the most robust portions of the *rete mirabile* vascular tissue (rm). Consistent with the differential staining utility of Giemsa staining **(C)** which differentially stains white blood cells (blue) versus red blood cells (pink), the scleral cartilage cysts stained mainly blue with Giemsa versus the more pink Giemsa staining observed in the *rete mirabile* which is rich in red blood cells. Van Gieson **(D)**, which stains all blood cells gold, and basic fuchsin/toluidine blue **(F)** which stains all blood cells purple, revealed a histological staining pattern for the scleral cartilage cysts that was similar to the blood cell elements in the *rete mirabile* (rm). The scleral cartilage matrix material stained a typical blueish green with Masson's Trichrome while the cysts contained highly eosinophilic staining **(E)**. r, retina; rm, *rete mirabile*; scl, sclera; sca, scleral cartilage; c, cyst. Magnification: **(A, B)** 100X; **(C–F)** 200X. Representative images are shown.

granulated cells), while the leukocytic-like elements stained red similarly to the blood cells in the *rete mirabile* (**Figure 3E**). Both H&E and basic fuchsin/toluidine blue stains also revealed a similar staining pattern for the blood cell-like elements of the scleral cartilage cysts and the blood cells in the *rete mirabile* (**Figures 3B, F**).

Closer examination of the basic fuchsin/toluidine blue stain indicated the presence of the myxozoan spores, and, in some cases at different planes of section, revealing the spore polar bodies previously described for the *M. albi genus of* these myxozoans (25), (**Figure 4B**). The Masson's trichrome stain of the scleral cartilage cysts also revealed, at high magnification (400x), highly eosinophilic cells similar to those which were also present in leukocytic rich regions of head kidney (**Figure 5**).

The presence of lymphocytic-like cells (small round cells with a large nucleus and little cytoplasm) and larger cells were observed in tissue stained with Giemsa or basic fuchsin / toluidine blue differential histological staining (**Figure 4**). These results suggest that at least some of the cells in the scleral cartilage cysts could be leukocytes.

The scleral cartilage cysts do not appear to be lined by perichondrium, a connective tissue layer that overlies surfaces of normally developing scleral cartilage tissue in teleosts (41). Although a thin but histologically distinct layer of material is

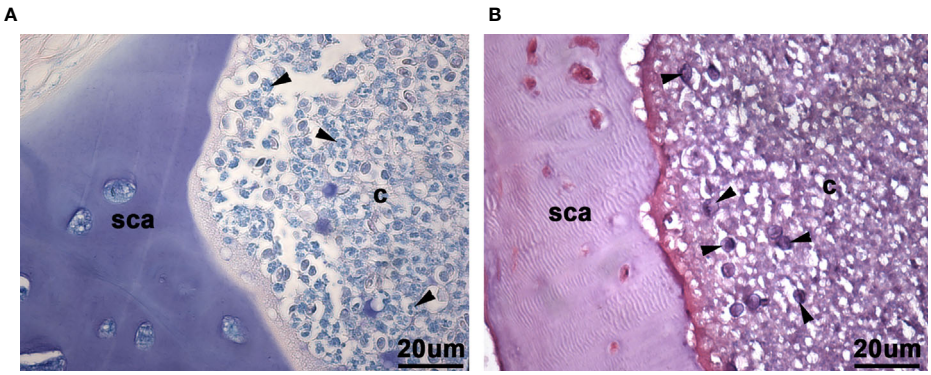

FIGURE 4 | Higher power view of leukocyte-like cells and myxozoan spores in Giemsa and basic fuchsin/toluidine blue histological stains of scleral cartilage cysts of wild adult lumpfish eyes. Giemsa **(A)** which stains blood cell nuclei deep blue, revealed a polymorphonuclear histological staining pattern of some cells (arrowheads in **(A)**) reminiscent of granulocytes in the scleral cartilage cysts. Basic fuchsin/toluidine blue stains **(B)** revealed myxozoan spores with or without polar bodies, depending on plane of section (arrowheads in **(B)**). sca, scleral cartilage; c, cyst. Magnification: 400X. Representative images are shown.

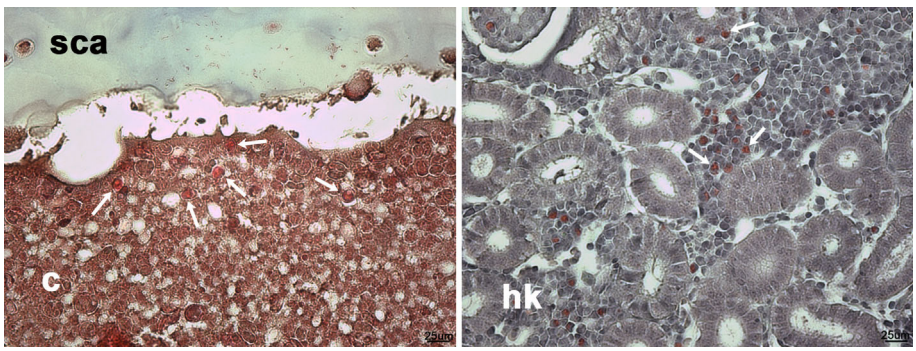

FIGURE 5 | Eosinophilic leukocyte-like cells in Masson's trichrome histological stains of scleral cartilage cysts of wild adult lumpfish eyes. Masson's trichrome (left) revealed intense eosinophilia of some cyst cells (arrows), similar to eosinophilic cells (arrows in right) in leukocyte rich regions of head kidney. c, cyst; hk, head kidney. Magnification: 400X. Representative images are shown.

observable lining the cysts in specimens stained with Masson's trichrome (**Figure 3E**) and basic fuchsin/toluidine blue (**Figures 3F** and **4**), it did not appear to contain nucleated cells and therefore does not resemble true perichondrium.

Myxozoan Presence in Wild Lumpfish Scleral Cartilage

PCR analyses for *M. albi* 18S ribosomal DNA of wild lumpfish specimens with scleral cartilage cysts revealed amplification of the expected 1.5 kb DNA fragment (**Figure 6A**). The 1.5 kb DNA amplicon was not detected in PCR analyses for *M. albi* 18S ribosomal DNA of scleral cartilage cup tissues collected from freshly euthanized, similarly sized cultured lumpfish, or of DNA samples prepared from mouse tissues (**Figure 6A**). Restriction digests of the PCR reaction amplicons with *Bgl*II were next performed to verify the specificity of the 1.5 kb amplicon for *M. albi* 18S ribosomal DNA (**Figure 6B**). *Bgl*II digestion resulted in digestion of the 1.5 kb amplicon into the expected two fragments of ~910 bp and ~605 bp (**Figure 6B**).

IgM Expression in Wild Lumpfish Scleral Cartilage Cysts

Histological staining suggested that the scleral cartilage cysts contained cells of the immune system. High levels of expression of IgM (42, 43) were detected by IHC mainly in the center of the scleral cartilage cysts while more diffuse lower levels were observed at the edges of the cysts. Mainly diffuse, lower levels of IgM staining with occasional densely focused expression pattern on individual cells was also present within the lumens of blood vessels of the *rete mirabile* as expected, serving as a positive internal control for IgM staining (**Figure 7C**). IgM expression was not observed in neural retinal tissue (not shown) or in the cartilage tissue surrounding the scleral cartilage cysts (**Figure 7A**). Furthermore, using the anti-lumpfish IgM IgY antibody pre-absorbed for 1 h with a 100-fold excess concentration of

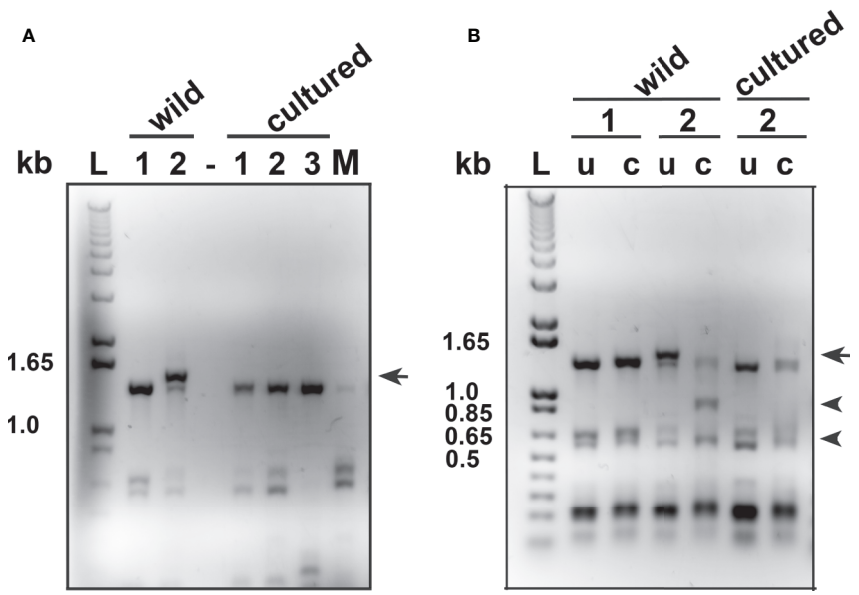

FIGURE 6 | Polymerase chain reaction (PCR) analysis of *M. albi* 18S ribosomal DNA in lumpfish specimens. **(A)** Representatives PCR analyses for *M. albi* 18S ribosomal DNA of wild lumpfish specimens with (wild #2 lane) and without (wild #1 lane) white scleral cartilage cysts revealed amplification of an expected 1.5 kb DNA fragment (arrow) only in the wild specimen with visible scleral cartilage cysts. The 1.5 kb DNA amplicon was not detected in PCR analyses for *M. albi* 18S ribosomal DNA of scleral cartilage cup tissues collected from freshly euthanized, similarly sized cultured lumpfish (cultured #1, 2 and 3 lanes) or, of DNA samples prepared from mouse tissues (M lane) and in the absence of DNA (lane -). **(B)** BglII digestion of PCR reactions for *M. albi* 18S ribosomal DNA (lanes c) resulted in the cut of the 1.5 kb amplicon into the expected two fragments of ~910 bp and ~605 bp (arrowheads: wild #2 lane, c). These two fragments were not detected in BglII digests of PCR reactions from lumpfish without visible scleral cartilage cysts (wild #1 lane and cultured #2 lane). Lanes u: uncut PCR reactions; lane L: 1 kb plus DNA ladder.

purified lumpfish IgM resulted in no staining of the scleral cartilage tissue (**Figure 7B**). Western blot of purified lumpfish IgM further confirmed the specificity of the anti-lumpfish IgM antibody for the 75 kDa heavy and 25 kDa light chains of lumpfish IgM and for the various dimers formed by these chains (**Figure S1**).

CD10 Expression in Normal Lumpfish Tissues

In addition to IgM, we searched for potential molecular homologs expressed in cells of the mammalian immune system to confirm the leukocyte identity of the cyst cells. CD10 is a cell surface endopeptidase expressed in cells involved in the immune response in mammals (44). We found that the sequence of human CD10 protein is overall 60% identical with the putative lumpfish CD10 protein sequence (**Figure 8**). The secondary structure domains, including the conserved cysteine residues that form a disulfide-bound partner, the essential residues for proteolytic activity and the ligand binding-residues are all identical between lumpfish and *H. sapiens* CD10 (**Figure 8**) (45). Although the protein sequence of lumpfish CD10 presented in **Figure 8** requires further verification, our analysis showed a highly conserved neprilysin active site (45) required for proteolytic activity (**Figure 8**). In addition, the essential residues for protein folding and functional conformation were found conserved in lumpfish CD10 (**Figures 8** and **9A, B**).

The lumpfish CD10 structural prediction analysis supported the presence of the residues required for correct folding of the protein (**Figures 9A, B**). Two of the three glycosylation sites present in human CD10 were found present in lumpfish CD10. However, these glycosylation sites are not well conserved in the sequences of other vertebrate CD10 (**Figure 8**). Phylogenetic analysis of lumpfish CD10 revealed that it is closely related to other Teleosts but distantly related to *Danio rerio*, *Mus musculus*, and *Homo sapiens* (**Figure 10**).

We utilized a rabbit anti-human CD10 monoclonal antibody (validated using clinical reference standard at NordiQC https://www.nordiqc.org/epitope.php?id=23), raised against amino acids 450–550 of human CD10 which, as shown in **Figure 8**, has 68% identical matches and 80% positive matches with the putative lumpfish CD10 protein sequence. In addition, amino acids 450–550 of the human CD10 protein sequence share 22 regions of 100% identity with the lumpfish CD10 orthologue. Moreover, we have recently successfully utilized this anti-CD10 antibody to stain CD10 positive cells in an experimental infection scenario in various tissues of other teleosts (47). Using this antibody we identified specific and distinctive CD10 expression in lumpfish head kidney, a tissue rich in lymphoid cells (48), and in the lumpfish eye (**Figure 11**). CD10 was expressed in numerous small leukocytic-like cells in follicular regions of the head kidney and in basal cells of the renal tubules

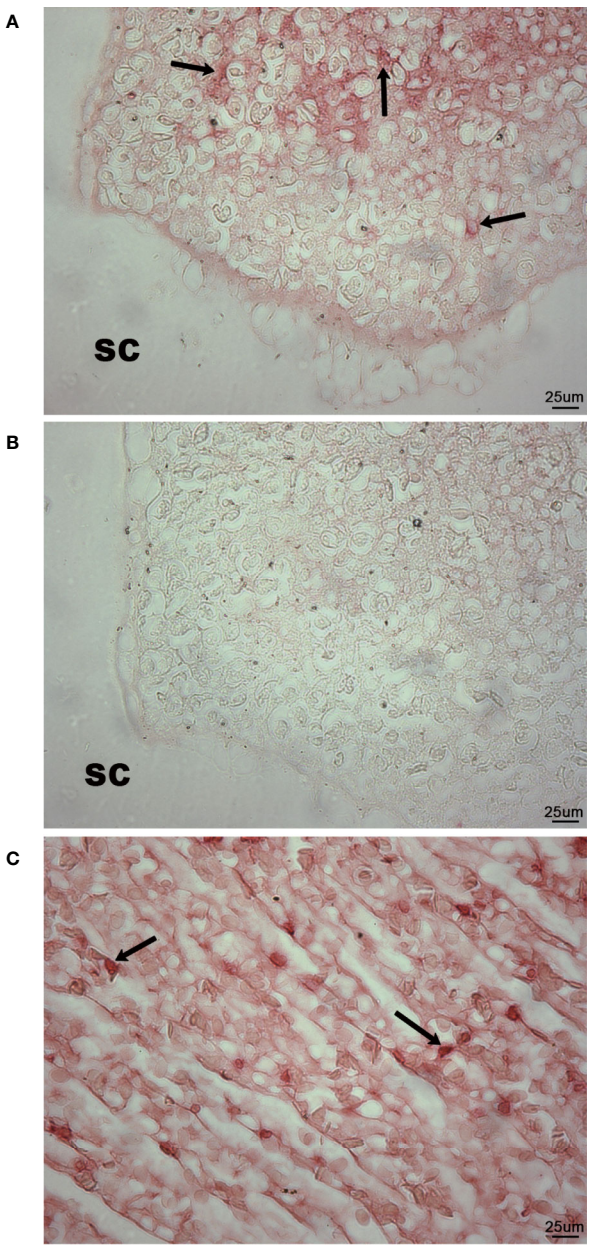

FIGURE 7 | Immunohistochemistry for IgM in wild adult lumpfish eyes. IgM staining in scleral cartilage cysts **(A)** and blood vessels of the *rete mirabile* **(C)** appeared as a bright red staining reaction. No counterstain was applied in order to emphasize both the densely focused cellular IgM and the sometimes diffusely distributed IgM expression. IgM expression was observed within blood vessels of the *rete mirabile* (used as positive control) **(C)** but not in the cartilaginous portions (sc) of the scleral cartilage **(A)**. Arrows in **(A, C)** indicate examples of individual cells expressing high levels of IgM. Further negative control using the anti-lumpfish IgM IgY antibody pre-absorbed for 1 h with a 100-fold excess concentration of purified lumpfish IgM resulted in no staining of the scleral cartilage cyst **(B)**. Magnification: 400X; scale bars 50 um. We observed scleral cartilage cysts harboring IgM^+ cells in scleral cartilage of three out of five independent healthy wild specimens. Representative images are shown.

of the head kidney (**Figures 11A, B**). We also found CD10 expression in a well-defined peri-photoreceptor pattern in the outer layers of the retina and in well defined bands in the inner layers of the retina (**Figures 11C, D**), both of which largely colocalize with expression of alpha smooth muscle actin (**Figures 11E, F**) (ASMA), a marker we have previously described to be expressed in lumpfish retina (19).

CD10 Expression in Wild Lumpfish Scleral Cartilage Cysts

Immunohistochemistry revealed the presence of a $CD10^+$ cell population in the scleral cartilage cysts of wild adult lumpfish eyes (**Figures 12A, B**). The $CD10^+$ cells in the scleral cartilage cysts were relatively small round cells and expressed CD10 intensely. $CD10^+$ cells were infrequently observed within blood spaces of the eye (*rete mirabile*, choroidal blood vessels and other vascular compartments) encompassing ocular peripheral blood compartment (not shown). The $CD10^+$ cells were located in more peripheral or cortical regions of the scleral cartilage cysts (**Figure 12A**). Negative controls, in which the anti-CD10 primary antibody was substituted with a species-matched IgG antibody using the same CD10 staining protocol, showed only light brown background (**Figures 12C, D**). Human tonsil, a lymphoid tissue, was used as a positive control and this tissue showed numerous $CD10^+$ leukocytic cells as expected (**Figure 12E**).

CD10 Expression in *V. anguillarum* Challenged Lumpfish Ocular Tissue

In order to assess the role of lumpfish ocular CD10 expression in a separate pathogen infection scenario, histomorphology, CD10 and IgM expression were analyzed in ocular tissues of lumpfish infected with *V. anguillarum*, in vaccinated and naïve lumpfish (non-vaccinated fish). Giemsa staining revealed that the scleral cartilage, the *rete mirabile* vascular elements and the retinal layers, were relatively undisturbed in vaccinated and challenged animals (**Figure 13A**). CD10 expression (**Figure 13C**) was localized mainly in the distinctive retinal banding pattern found in healthy animals as shown in **Figure 11**.

Naïve infected lumpfish developed exophthalmos, and showed various levels of retinal and subretinal tissue disorganization (see lesion portions of retinal tissue arrowed in **Figure 13D** compared to the surrounding, less disturbed retinal tissues visible in **Figures 13B, D**). Most of the naïve infected lumpfish were severely affected, retinal layers structure was lost and retinal tissue became thickened and disorganized (**Figures 13B, E**). $CD10^+$ cells were highly present in tissue severely damaged and disorganized (**Figures 13D, F, G**). Patches of what appears to be chondrogenesis were present in one of naïve infected lumpfish (**Figure 13E**). Tissue areas with high density of CD10+ cells closely coincided with these areas of putative chondrogenesis (**Figure 13F**). Also, intraretinal IgM expression was present at high levels in the choroidal vasculature and in specific layers in both thickened lesioned retinal areas (**Figure 13J**) and non-thickened areas of retinal tissues of all naïve infected lumpfish.

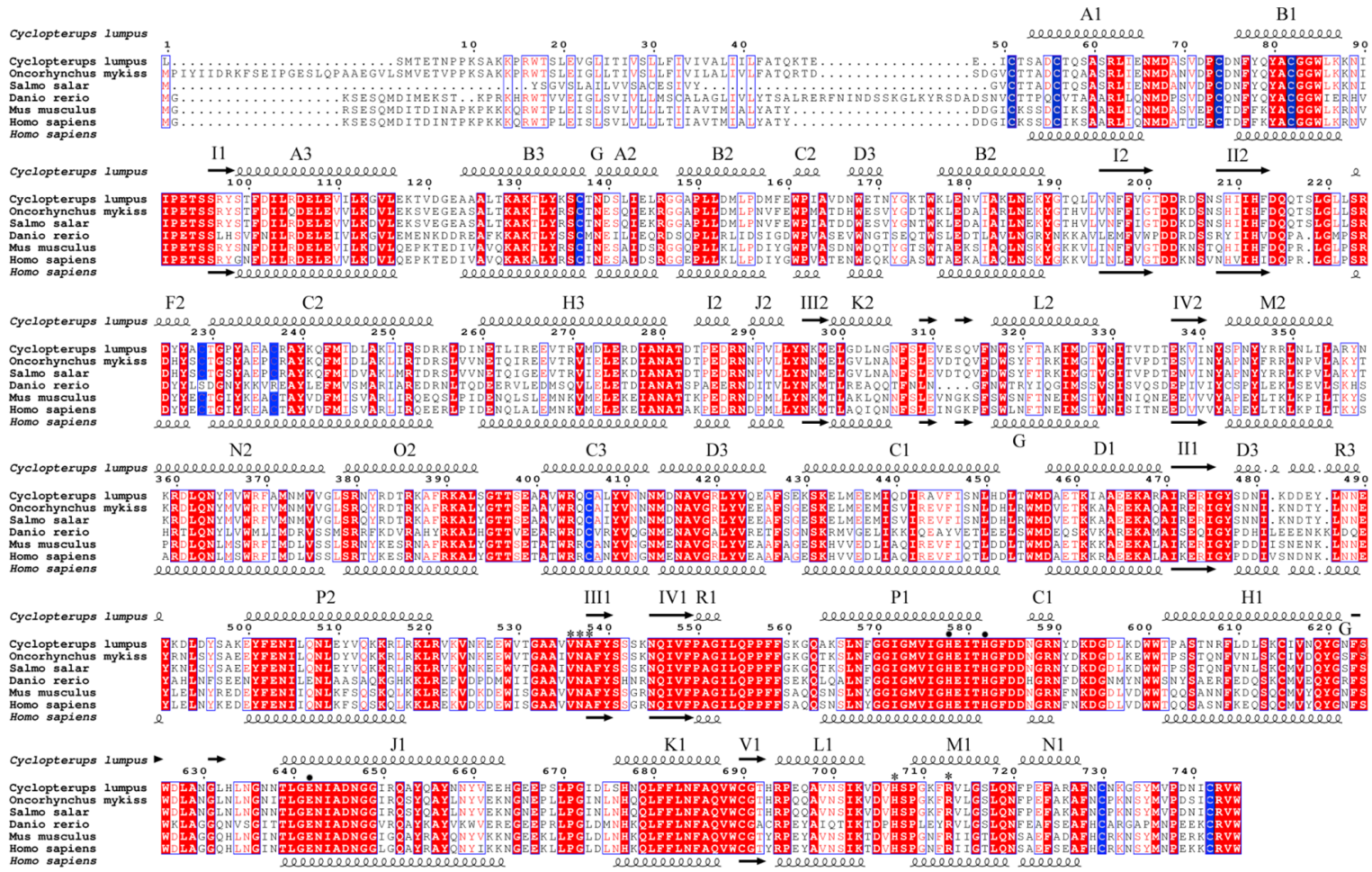

FIGURE 8 | Lumpfish CD10 alignment and secondary protein structure. The blue boxed regions indicate the conserved cysteine residues that form a disulfide-bound partner. The black dots indicate the essential residues for proteolytic activity. The asterisk regions (*) indicate the ligand binding-residues.

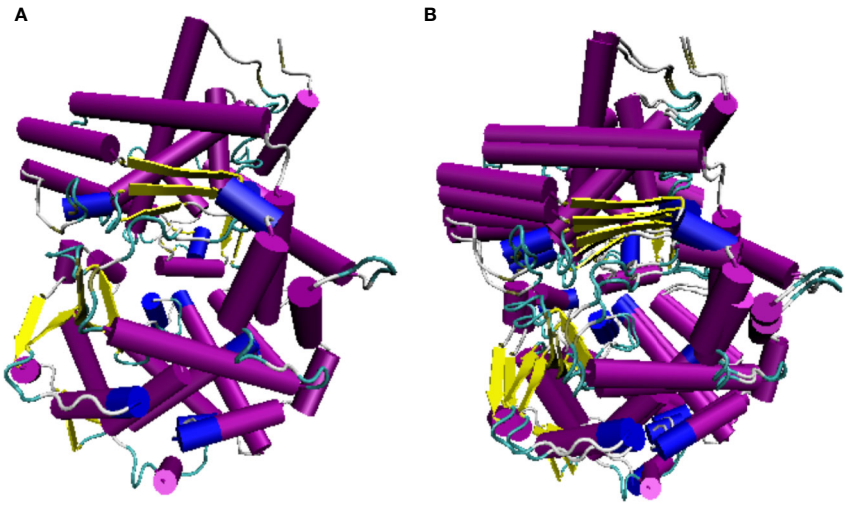

FIGURE 9 | Lumpfish CD10 3D predicted protein structure. **(A)** Lumpfish CD10 protein, **(B)** Lumpfish and human CD10 protein overlap. The purple and blue cylinders represent α-helix structures and the yellow arrows represent the β-sheet structures. *H. sapiens* CD10 accession number: NP_000893.2; *C. lumpus* CD10 accession numbers: MT978157, MT978158, MT978159, MT978160, MT978161, MT978162, MT978163, and MT978164.

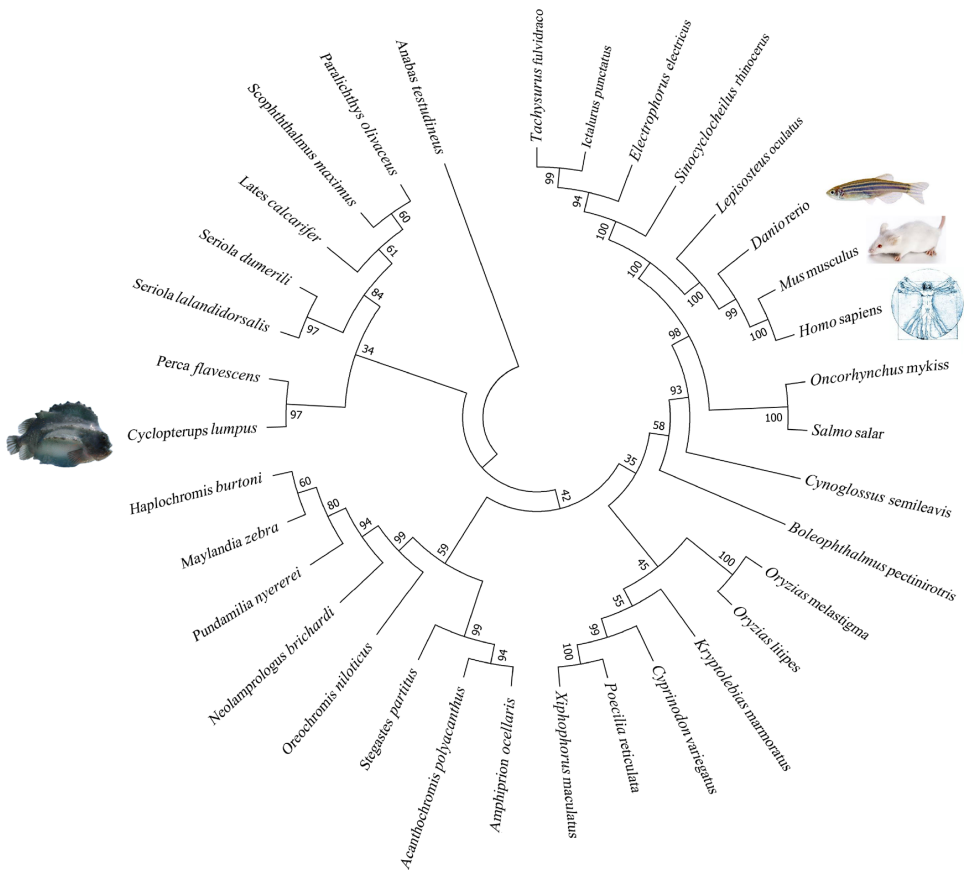

FIGURE 10 | Lumpfish CD10 molecular phylogenetic analysis. The evolutionary history of CD10 was inferred by using the Maximum Likelihood method based on the JTT matrix-based model (46).

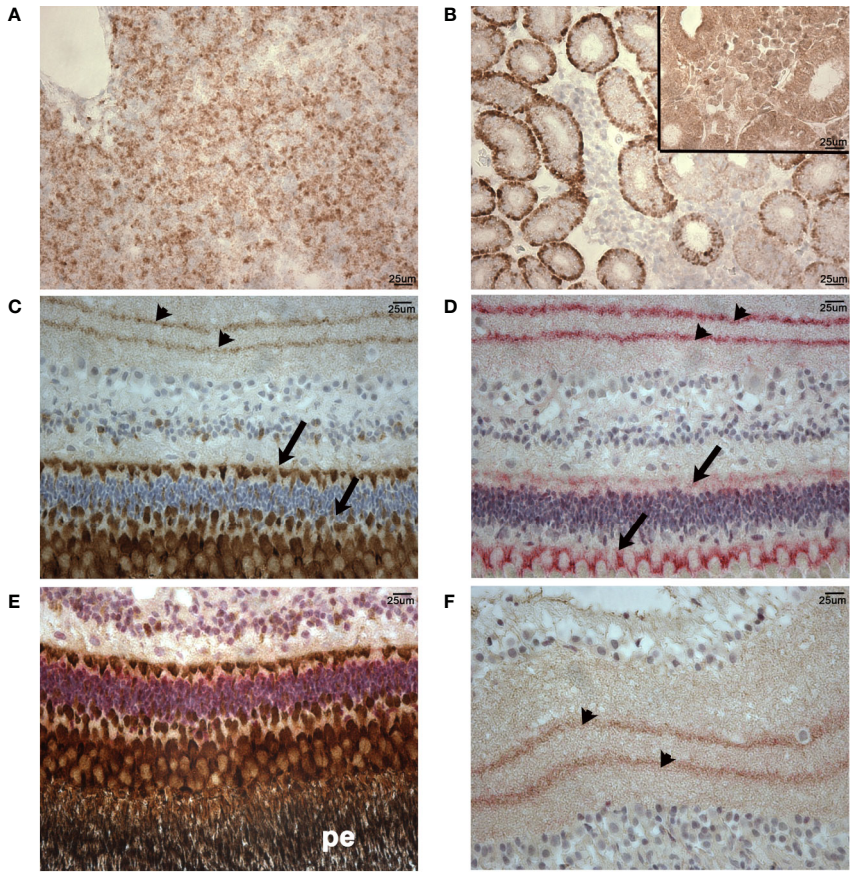

FIGURE 11 | Normal patterns of CD10 and ASMA expression in lumpfish tissues. CD10 expression (brown staining) was detected in numerous small cells in follicular regions of the head kidney **(A)** and basal cells of the renal tubules **(B).** Inset in **(B)** is a negative control of an adjacent section of those used in **(A, B)** stained using no primary antibody. **(C)**, CD10 expression (brown staining) was detected in a well-defined peri-photoreceptor pattern in the outer layers of the retina (arrows) and in well-defined bands in the inner layers of the retina (arrowheads). **(D)**, ASMA expression (red staining) pattern in the retina was highly similar to CD10 pattern of expression. CD10 and ASMA double staining in peri-photoreceptor pattern in the outer layers of the retina **(E)** and inner layers of the retina **(F)**. The pigmented epithelial layer (pe) in panel **(E)** is black due to the endogenous pigment in these cells. Double stained sections show overlap of stain and a blended magenta staining color in areas of expression overlap (arrowheads in **(F)**). Magnification: 400X. Scale bars in **(A, B)** are also representative of scale in **(C–F)**. Representative images are shown.

DISCUSSION

Teleosts use soft tissue organs such as head kidney for hematopoiesis (48–50). Since CD10 is known as a marker for hematopoiesis progenitor and stem cells (44, 51), the presence of CD10 cells in ocular tissue raises the possibility that wild lumpfish might utilize a form of ocular extramedullary hematopoiesis, which has been described in mammals (52, 53) for specific adaptations such as during response to ocular infection by pathogens. Teleosts are known to utilize plasmablast and plasma cell derived IgM in response to pathogens (43) and IgM has been demonstrated to play a role in response to inflammatory reaction in lumpfish (54).

Molecular biological studies of species such as lumpfish are impeded by the lack of genetics and antibody reagents specific to the organism under study. Although we were fortunate to be able to assess the expression of lumpfish IgM, among the several antibody reagents raised against mammalian leukocytic markers (CD3, CD45, CD34) that we tested against the scleral cartilage cysts in lumpfish, only CD10 antibodies demonstrated true positive staining, supported by genetic and bioinformatic results confirming a lumpfish CD10 orthologue. Moreover, CD10 immunoreactivity was detected in normal noninfected lumpfish head kidney and retinal tissue as well as in tissue from animals infected with *V. anguillarum*, a pathogen completely different from myxozoans. These results strongly support that the anti-CD10 monoclonal antibody is indeed staining a lumpfish CD10 orthologue epitope.

Here, we provide evidence supporting the presence of a host immune response in association with subclinical myxozoan infection of scleral cartilage of otherwise healthy wild lumpfish of different ages sourced from different geographical locations of the Northwest Atlantic. Whole mount staining confirmed that the scleral skeletal cysts, which are observable at a gross

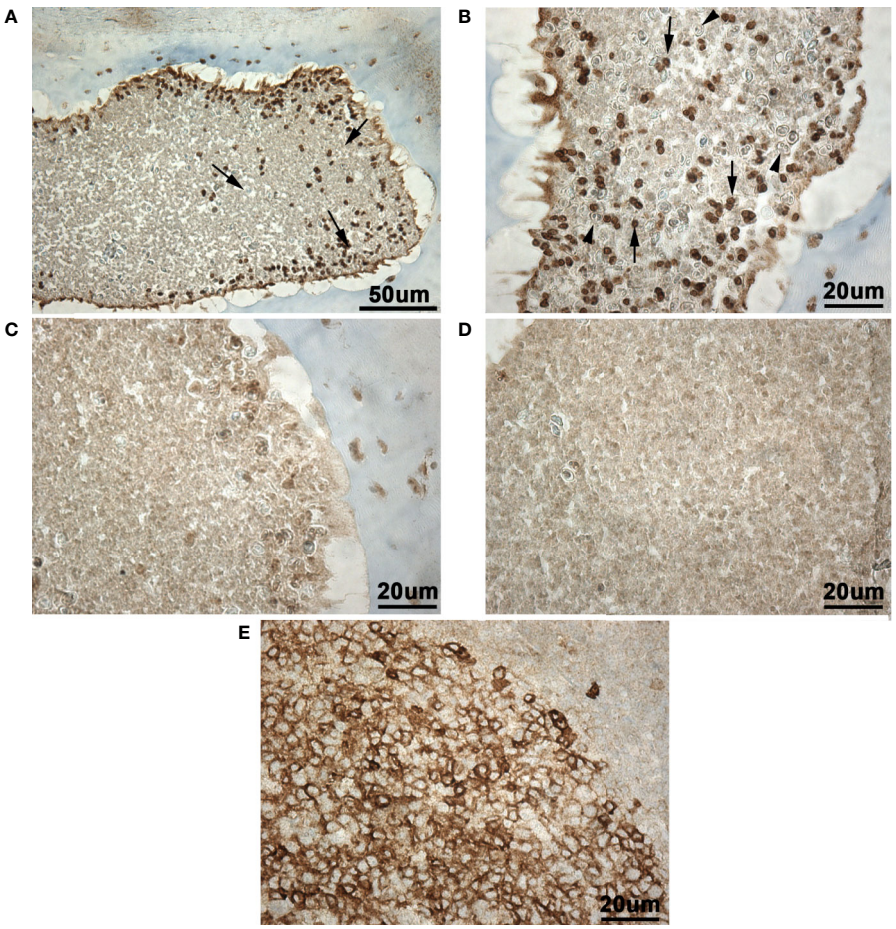

FIGURE 12 | Immunohistochemistry for CD10 in wild adult lumpfish scleral cartilage cysts. CD10 stain of cysts present in the scleral cartilage appeared as dark brown staining [arrows in **(A, B)**] against light brown background staining seen in **(C, D)** and a light blue hematoxylin counterstain. Sections adjacent to those used for anti-CD10 staining but instead stained with negative control [rabbit IgG **(C, D)**] show a similar level of background staining reaction to that seen in the background of the anti-CD10 preparations. The cysts present in the scleral cartilage contained numerous small round leukocyte-like cells expressing CD10 well above the background staining seen in **(C, D)**. In higher power view **(B)**, polymorphonuclear cells reminiscent of granulocytes and negative for CD10 were observed in the scleral cartilage cysts (arrowheads). **(E)**, Positive control human tonsil section serves as a positive staining control for CD10 (dark brown staining). Magnification: **(A)**, 200X; **(B-E)**, 400X. We observed scleral cartilage cysts harboring $CD10^{+}$ cells in scleral cartilage of three out of five independent healthy wild specimens. Representative images are shown.

anatomical level as multiple discrete pockets of densely packed soft cellular like material in the scleral skeleton (**Figures 2A–G**) are embedded in cartilage rather than bone since these areas do not stain with the Alizarin red bone stain (**Figures 2H, I**). Neither wild or cultured lumpfish scleral cups showed any appreciable histological staining with Alizarin red for bone, indicating that lumpfish in general likely lack scleral ossicles. Franz-Odendaal has proposed a relationship between the configuration of the scleral skeleton and swimming depth of teleosts in which deep sea animals are more likely to lack scleral ossicles (21, 30, 55). Previous studies showing that lumpfish are known to frequent deeper water (14–18) as well as our results herein showing no evidence of scleral ossicle development in lumpfish are consistent with the proposals of Franz-Odendaal.

Our results provide four lines of evidence that wild lumpfish *M. albi* cysts contain host immune components. First, our results using Giemsa and basic fuchsin / toluidine blue differential histochemical staining (**Figures 3–5**) suggest the presence of leukocytic cells within the scleral cartilage cysts of wild lumpfish where we detected *M. albi* (**Figure 6**). The cells we observed in the cyst tissue resembled the leukocytes described in previously published histochemical studies by Boomker et al., and Mumford et al. (56, 57). Second, we detected the *M. albi* 18S ribosomal RNA [as previously reported by Cavin *et al.*, 2012 (25)] in scleral cartilage cup tissues collected from wild but not in cultured lumpfish, the latter of which do not harbor scleral cartilage cysts. This result supports the notion that an immune response to pathogen invasion, presumably involving host immune cells such as leukocytes, is occurring in the *M. albi* cysts. Third, CD10, which is known to be a marker for hematopoietic progenitor cells in mammalian bone marrow (51), is present in lumpfish (**Figures 8–11**) and is expressed in small round cells in the

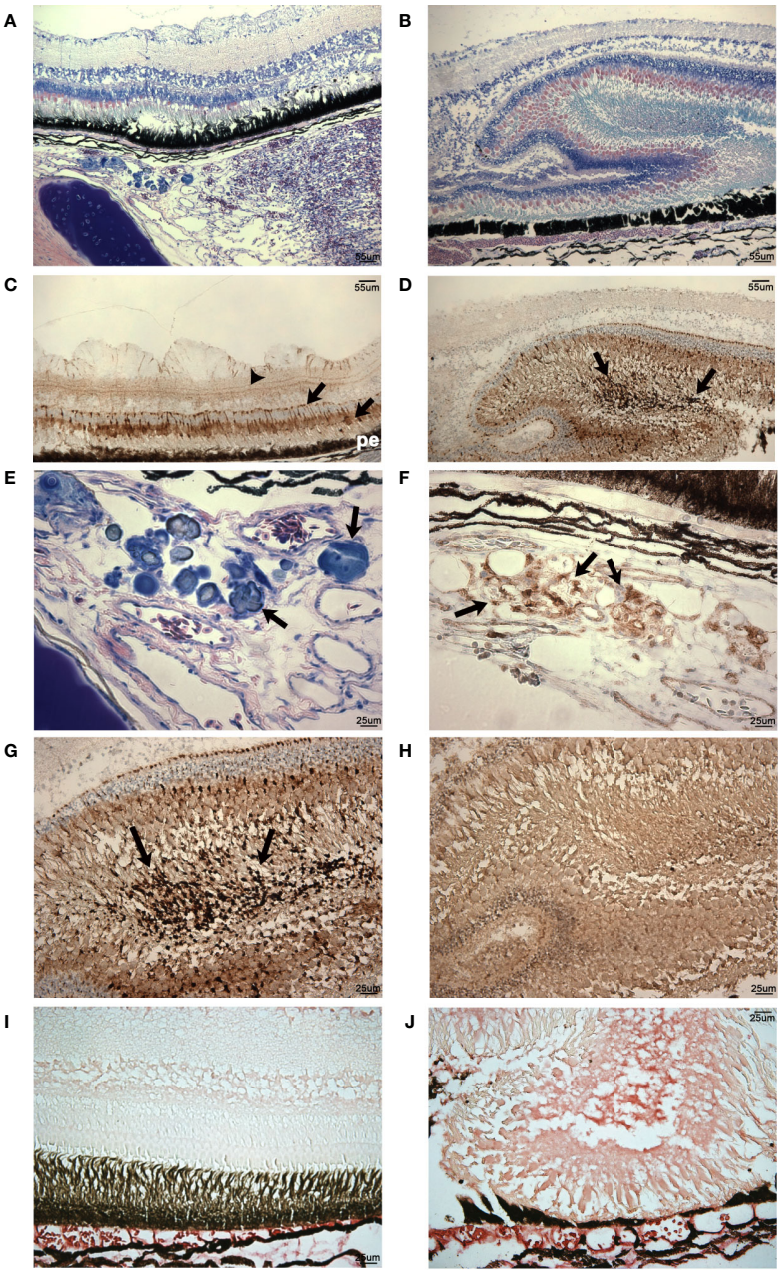

FIGURE 13 | Analysis of histomorphology and CD10 expression in vaccinated and nonvaccinated *V. anguillarum* challenged lumpfish ocular tissues. **(A, B)**, Giemsa staining of retinal regions of vaccinated **(A)** and nonvaccinated **(B)** *V. anguillarum* challenged lumpfish ocular tissues. **(A)**, in the vaccinated challenged animal the scleral cartilage (sc) visible in the lower left corner of the image (dark blue staining), the *rete mirabile* (rm) vascular elements visible in the bottom right quadrant of image and the retinal layers (r) located in the top half of image all appeared relatively undisturbed. **(B)**, in the nonvaccinated challenged animal, the normal retinal layers were lost, retinal tissue, which took up most of the image area, became thickened and disorganized. **(C, D, F, G)**, CD10 expression (dark brown) in retinal regions of vaccinated (C: 100X, F: 400X) and nonvaccinated (D: 100X, G: 400X) *V. anguillarum* challenged lumpfish ocular tissues. **(E)**, magnified view (400X) of a subretinal region of the Giemsa staining shown in **(A)** of a vaccinated *V. anguillarum* challenged lumpfish displaying areas of putative chondrogenesis staining dark blue (arrows). **(F)**, CD10 expression (dark brown, arrows) in a section adjacent to that shown in **(E)** of the same vaccinated *V. anguillarum* challenged lumpfish revealed areas of CD10 expression closely coinciding with the areas of putative chondrogenesis visible in **(E)**. Arrows in **(C, D, F, G)** indicate the CD10 stain appeared as deep dark brown staining reaction against the lighter brown background. Sections adjacent to those used for anti-CD10 staining but instead stained with no primary antibody **(H)** show only a similar level of background staining reaction to that seen in the background of the anti-CD10 preparations. IgM expression (bright red stain) is elevated in thickened retinal regions of nonvaccinated animals **(J)** but only in choroidal vasculature (cv) areas of vaccinated animals **(I)** *V. anguillarum* challenged lumpfish. r, retina; rm, *rete mirabile*; sc, scleral cartilage; cv, choroidal vasculature; pe, pigmented epithelium. Magnification: (**A–D**, 100X), **(E–H)**, 400X. Scale bars in **(A, B)** are also representative of scale in **(C, D)**. For these studies, three individual previously vaccinated *V. anguillarum* challenged lumpfish and 4 individual non-vaccinated *V. anguillarum* challenged lumpfish were assessed. Representative images are shown.

scleral cartilage cysts of wild lumpfish (**Figure 12**). Forth, specific staining for IgM was found in both cell-focused and more diffuse staining patterns in the scleral cartilage cysts (**Figure 7**). The IgM staining was specific since pre-absorption of the anti-lumpfish IgM antibody with purified lumpfish IgM abrogated the staining. Furthermore, western blot of purified lumpfish IgM using this antibody (**Figure S1**) revealed the expected heavy and light chains and the various dimers formed by lumpfish IgM, further confirming the specificity of the anti-lumpfish IgM antibody. These results are consistent with those obtained using an anti-lumpfish IgM antibody described by Bilal et al. (58).

Future studies will be needed to explore and define if the CD10+ cells in lumpfish scleral cartilage cysts are indeed hematopoietic or express other leukocyte characteristics. However, taken together, our collective evidence supports the hypothesis that scleral cartilage cysts commonly develop within the scleral cartilage of wild lumpfish and are composed of a mixture of different host cells of leukocytic lineages and spores or other life cycle material related to a subclinical myxozoan infection. The high number of CD10+ cells in myxozoan infected ocular cartilage tissue raises questions about the level of specificity of this immune response. While lumpfish are known to express genes coding for components of specific immune responses (i.e., as mediated by T and B lymphocytes) and have been demonstrated to mount measurable specific immune responses (42, 47, 59, 60), less is known about innate immune responses in lumpfish. However, lumpfish B lymphocytes are known to be phagocytic (60), suggesting that unique forms of innate immunity could exist in lumpfish. It remains possible that the large CD10+ cell presence in *M. albi* cysts represents a component of a nonspecific innate immune response. Future studies will be needed to explore this.

The absence of scleral cartilage cysts with leukocytic-like tissue and CD10 expression in lumpfish cultured under aseptic conditions at JBARB suggests that CD10 might be useful as a biomarker for myxozoan infection in lumpfish. Since none of the wild animals we analyzed in this study had exophthalmos or other overtly detectable clinical grade disease, our results suggest that lumpfish might uniquely develop an intra-ocular host response to stabilize or contain myxozoan damage to scleral cartilage and other eye structures.

As mentioned previously, *V. anguillarum* infects the eyes of lumpfish and causes exophthalmia. Therefore, we also evaluated the presence of CD10+ cells and IgM in the ocular tissues of lumpfish vaccinated and non-vaccinated after challenge and infection, respectively. While scleral cartilage, *rete mirabile* vascular elements and retinal layers appear relatively undisturbed in vaccinated and *V. anguillarum* challenged animals (**Figures 13A, C**), non-vaccinated infected animals show non-artifactual loss of normal retinal layers, thickening and disorganization of retinal tissues (**Figures 13B, D**) and large numbers of $CD10^+$ cells associated with these retinal lesions (**Figures 13D, G**), similar to those we described previously as various forms of retinopathy (61–63). Moreover, areas of putative chondrogenesis or dystrophic mineralization observed in one of the non-vaccinated infected animals (**Figure 13E**) closely coincide with areas of CD10 expression (**Figure 13F**) reminiscent of the leukocytic infiltration comprised of mast cells, macrophages, T and B lymphocytes and neutrophils during auricular chondritis in cat (*Felis catus*) cartilage regeneration as described by Wilson and colleagues (22). An increased level of IgM expression was present in the retinal lesions in the non-vaccinated infected animals compared to the vaccinated challenged animals (**Figures 13J, I**, respectively)). Our results suggest that the immune interaction with the pathogen, either bacterial or myxozoan, increases CD10+ cells, IgM+ cells and IgM in the ocular tissue. Our results support the idea that normal lumpfish ocular CD10 expression changes in response to pathogens and that CD10+ cells are recruited to regions of intraocular disease in an ocular immune response to pathogens.

The expression of CD10 and its co-expression with other markers such as ASMA in lumpfish tissues prompts additional questions. CD10 marks hematopoietic progenitor cells in mammalian bone marrow (51) and is considered to play a functional role in development of stem cells (44). Other studies have shown that CD10 expression by stromal cells is involved in maturation niches mediating B lymphocyte development in bone marrow (64). There is also evidence that CD10 plays a role in chondrogenesis (65, 66). Herein we observed specific CD10 expression in numerous small cells in follicular regions of the head kidney (**Figure 11A**) and in basal cells of the renal tubules (67) of the head kidney (**Figure 11B**). Zebrafish renal tubule tissue contains stem cells that can act to regenerate kidney throughout life (68) but we do not know if these cells express CD10 or if the $CD10^+$ cells that we observed in lumpfish renal tubules are stem cells. In normal adult lumpfish eye, CD10 is expressed in a well-defined peri-photoreceptor pattern in the outer layers of the retina and in well-defined bands in the inner layers of the retina which, upon double IHC, is observed to largely colocalize with ASMA (**Figures 11C–F**). The colocalization of CD10 and ASMA in normal lumpfish retina is intriguing but requires further study. The CD10 expression in normal retina is also reminiscent of the expression of CD10 in sable fish brain (47). Since ASMA is known to be expressed by neural crest cell derived lineages (69, 70), further work could explore if ASMA-like expression in *C. lumpus* retina is functionally related to CD10 or other properties of retinal nervous tissue in health and disease states. The size and shape of the $CD10^+$ cells in the scleral cartilage cysts best matches the phenotype of "possible precursor cells" but could also represent lymphocytes, macrophages or granulocytes previously described in lumpfish (42). Another CD10 expression pattern that we observed in the lumpfish eye was in cells of a more stromal or dendritic morphology (64). Beyond its well-known classical role in hematopoiesis, the dysregulated expression of CD10 (otherwise known as neprilysin, membrane metallo-endopeptidase, neutral endopeptidase, common acute lymphoblastic leukemia antigen), is known to be associated not only with leukemia but also with ocular and neurological diseases in mammal (44, 71–73). Much remains to be discovered about the characteristics and roles of CD10 in both normal and pathogen-bearing lumpfish tissues.

To conclude, we propose that lumpfish possess a novel IgM and $CD10^+$ cell-related intraocular response to pathogens in

order to mitigate damage to eye structures. Recent studies have demonstrated that IgT-B cells play a key role in fish mucosal immune responses to parasitic and bacterial pathogens (63). Future studies could assess if IgT-B cells contribute to a putative ocular specific immune response to infection by pathogens. A recent national level analysis of cleaner fish use on salmon farms in Norway concluded that, while benefits of the use of cleaner fish on some farms is clear, suboptimal usage of cleaner fish remains in some settings (74). Our results raise the possibility that pathogen mediated visual disruption might impact cleaner fish visual health in such settings. While our results provide some examples whereby subclinical opportunistic disease might be manageable by wild lumpfish, they also raise the more broadly important questions of how subclinical disease processes impact normal visual function and survival of lumpfish in the wild or efficacy as pest biocontrol.

DATA AVAILABILITY STATEMENT

The datasets presented in this study can be found in online repositories. The names of the repository/repositories and accession number(s) can be found in the article/**Supplementary Material**.

ETHICS STATEMENT

The animal study was reviewed and approved by Institutional Animal Care Committee Memorial University.

AUTHOR CONTRIBUTIONS

Conceptualization: RG, JS, HP, RA, WG, KK, SK, IV. Methodology: RG, JS, HP, RA, SK, IV, TC, AH, SC, KV, DB. Investigation: RG, HP, RA, IV, TC, KK. Writing—original draft: RG, JS, HP, KK, WG, SK. Resources: RG, HP, JS, DB, KK, DB. Writing—Review and Editing: RG, JS, HP, KK, WG, SK, IV, TC, AH, SC, KV. Visualization: JS, RG. Supervision: RG, HP, JS. Funding acquisition: RG, JS, HP. All authors contributed to the article and approved the submitted version.

FUNDING

This work was funded through grants from the Vitamin Research Fund, Ocean Frontier Institute (2017), Canada First – Ocean Frontier Institute (Module J3), Medical Research Foundation of the Faculty of Medicine (2016), through leverage funds from School of Graduate Studies, Memorial University, NSERC-Discovery (RGPIN-2018-05942), and through support from the Dr. Joe Brown Aquatic Research Building (JBARB). Canada Foundation for Innovation.

ACKNOWLEDGMENTS

We thank the Department of Ocean Sciences staff members Stephen Hill and Nicole Smith of Cold-ocean Deep-sea Research Facility (CDRF) and JBARB staff members Jessica Fry, Jennifer Monk, Kelsie Jeannot, Denise Tucker and Jillian Porter for expert technical assistance. We thank staff at the IHC lab, Eastern Health, for expert assistance with CD10 immunohistochemistry and Iliana Dimitrova and Danielle Gardiner of the Histology Core Facility, Faculty of Medicine, for expert technical assistance with special stains histology and whole mount staining. We thank Adrianna Warren for help with manuscript editing. We thank Jeremy Langburt and Fatima Zouanat of Leica Biosystems for expert assistance with the ASMA-CD10 double immunohistochemistry. We thank Somru BioScience, Charlottetown PEI, for help with production of the chicken IgY anti-lumpfish IgM antibody. We thank Giuseppe Scapigliati, of University of Tuscia, Viterbi, Italy, for discussions, advice and expert assistance with expression of teleost leukocytic markers. We thank the reviewers of the manuscript for their thoughtful comments which improved the manuscript.

SUPPLEMENTARY MATERIAL

The Supplementary Material for this article can be found online at: https://www.frontiersin.org/articles/10.3389/fimmu.2020.576897/full#supplementary-material

REFERENCES

1. Imsland AK, Reynolds P, Eliassen G, Hangstad TA, Foss A, Vikingstad E, et al. The use of Lumpfish (*Cyclopterus lumpus* L.) to control sea lice (*Lepeophtheirus salmonis Krøyer*) infestations in intensively farmed Atlantic salmon (*Salmo salar* L.). *Aquaculture* (2014) s424–425:18–23. doi: 10.1016/j.aquaculture.2013.12.033
2. Scott WB, Scott MG. Atlantic Fishes of Canada. *Can Bull Fish Aquat Sci* (1988) 219:518–9.
3. Powell A, Treasurer JW, Pooley CL, Keay AJ, Lloyd R, Imsland AK, et al. Use of lumpfish for sea-lice control in salmon farming: challenges and opportunities. *Rev Aquacult* (2018) 10:683–702. doi: 10.1111/raq.12194
4. Boyce D, Ang KP, Prickett R. Cunner and lumpfish as cleaner fish species in Canada. In: JW Treasurer, editor. *Cleaner fish biology and aquaculture applications*. Sheffield, UK: 5m Publishing Ltd. (2018). p. 451 pp.
5. Whittaker BA, Consuegra S, Garcia de Leaniz C. Genetic and phenotypic differentiation of lumpfish (*Cyclopterus lumpus*) across the North Atlantic: implications for conservation and aquaculture. *Peer J* (2018) 6:e5974. doi: 10.7717/peerj.5974
6. Hamre LA, Eichner C, Caipang CM, Dalvin ST, Bron JE, Nilsen F, et al. The Salmon Louse *Lepeophtheirus salmonis* (Copepoda: Caligidae) life cycle has only two Chalimus stages. *PloS One* (2013) 8:e73539. doi: 10.1371/journal.pone.0073539
7. *Fisheries and Oceans Canada. Managing disease and parasites*. Government of Canada (2017). Available at: http://www.dfo-mpo.gc.ca/aquaculture/protect-protege/parasites-eng.html.
8. Costello MJ. How sea lice from salmon farms may cause wild salmonid declines in Europe and North America and be a threat to fishes elsewhere. *Proc Biolog Sci* (2009) 276:3385–94. doi: 10.1098/rspb.2009.0771
9. Costello MJ. The global economic cost of sea lice to the salmonid farming industry. *J Fish Dis* (2009) 32:115–8. doi: 10.1111/j.1365-2761.2008.01011.x
10. Freeman MA, Kasper JM, Kristmundsson Á. Nucleospora cyclopteri n. sp., an intranuclear microsporidian infecting wild lumpfish, Cyclopterus lumpus L. In: *Icelandic waters*. Springer: Paras Vectors (2013). doi: 10.1186/1756-3305-6-49

11. Scholz F, Fringuelli E, Bolton-Warberg M, Marcos-López M, Mitchell S, Prodhol P, et al. First record of Tetramicra brevifilum in lumpfish (Cyclopterus lumpus, L.). *J Fish Dis* (2017) 40:757–71. doi: 10.1111/jfd.12554
12. Pietrak M, Rosser TG. Morphologic and molecular characterization of Gyrodactylus cyclopteri Scyborskaja,1948, from Cyclopterus lumpus L., 1758. *Parasitol Res* (2020) 119:879–84. doi: 10.1007/s00436-019-06542-0
13. Lorance P, Cook R, Herrera J, de Sola L, Florin A, Papaconstantinou C. *Cyclopterus lumpus. The IUCN Red List of Threatened Species* (2015), e.T18237406A45078284.
14. Department of Fisheries and Aquaculture and Government of Newfoundland and Labrador. *Lumpfish Emerging Species Profile Sheet*. Government of Newfoundland and Labrador.
15. Davenport J., vol. 147. United Nations: FAO Fisheries Synopsis (1985). p. 31.
16. Blacker RW. Pelagic records of the lumpsucker, Cyclopterus lumpus L. *J Fish Biol* (1983) 23:405–17. doi: 10.1111/j.1095-8649.1983.tb02921.x
17. Rosen S, Holst JC. Deep Vision in-trawl imaging: sampling the water column in four dimensions. *Fisher Res* (2013) 148:64–73. doi: 10.1016/j.fishres.2013.08.002
18. Kennedy J, Jónsson SP, Ólafsson HG, Kasper JM. Observations of vertical movements and depth distribution of migrating female lumpfish (*Cyclopterus lumpus*) in Iceland from data storage tags and trawl surveys. *ICES J Marine Sci* (2016) 73:1160–9. doi: 10.1093/icesjms/fsv244
19. Ahmad R, Paradis H, Boyce D, McDonald J, Gendron RL. Novel characteristics of the cultured Lumpfish *Cyclopterus lumpus* eye during post-hatch larval and juvenile developmental stages. *J Fish Biol* (2019) 94:297–312. doi: 10.1111/jfb.13892
20. Cronin TW, Douglas RH. Seeing and doing: how vision shapes animal behaviour. *Phil Trans R Soc London Biol Sci* (2014) 369:1–3. doi: 10.1098/rstb.2013.0030
21. Franz-Odendaal TA. Scleral ossicles of teleostei: evolutionary and developmental trends. *Anat Rec (Hoboken)* (2008) 291:161–8. doi: 10.1002/ar.20639
22. Wilson TM, Machado M, De Sousa DER, Braúna T, Torres Neto R, Laufer-Amorim R, et al. Immunopathological findings in a cat with auricular chondritis. *Acta Vet Hung* (2019) 67:81–6. doi: 10.1556/004.2019.009
23. Kitagaki M, Hirota M. Auricular chondritis caused by metal ear tagging in C57BL/6 mice. *Vet Pathol* (2007) 44:458–66. doi: 10.1354/vp.44-4-458
24. Hansson AS, Holmdahl R. Cartilage-specific autoimmunity in animal models and clinical aspects in patients - focus on relapsing polychondritis. *Arthritis Res* (2002) 4:296–301. Review. doi: 10.1186/ar425
25. Cavin JM, Donahoe SL, Frasca S, Innis CJ, Kinsel MJ, Kurobe T, et al. Myxobolus albi infection in cartilage of captive lumpfish (Cyclopterus lumpus). *J Veter Diagnost Invest* (2012) 24:516–24. doi: 10.1177/1040638712440990
26. Chakraborty S, Cao T, Hossain A, Ganangobal H, Vasquez I, Boyce D, et al. Vibrogen-2 Vaccine Trial in Lumpfish (*Cyclopterus lumpus*) Against. *Vibrio anguillarum J Fish Dis* (2019) 42:1057–64.
27. Béné MC. Immunophenotyping of acute leukaemias. *Immunol Lett* (2005) 98:9–21. doi: 10.1016/j.imlet.2004.10.008
28. Shipp MA, Stefano GB, Switzer SN, Griffin JD, Reinherz EL. CD10 (CALLA)/neutral endopeptidase 24.11 modulates inflammatory peptide-induced changes in neutrophil morphology, migration, and adhesion proteins and is itself regulated by neutrophil activation. *Blood* (1991) 78:1834–41. doi: 10.1182/blood.V78.7.1834.bloodjournal7871834
29. Wheater PR, Burkitt HG, Daniels VG. *Functional Histology*. Churchill Livingston (1979).
30. Franz-Odendaal TA. Intramembranous ossification of scleral ossicles in Chelydra serpentina. *Zool* (2006) 109:75–81. doi: 10.1016/j.zool.2005.10.001
31. Santander J, Mitra A, Curtiss RII. Phenotype, virulence, and immunogenicity of Edwardsiella ictaluri cyclic adenosine 3',5'-monophosphate receptor protein (Crp) mutants in catfish host. *Fish Shellf Immunol* (2011) 31:1142–53. doi: 10.1016/j.fsi.2011.10.009
32. Gendron RL, Adams LC, Paradis H. Tubedown-1, a novel acetyltransferase associated with blood vessel development. *Dev Dyn* (2000) 218(2):300–15. doi: 10.1002/(SICI)1097-0177(200006)218:2<300::AID-DVDY5>3.0.CO;2-K
33. Zhang Z, Schwartz S, Wagner L, Miller W. A greedy algorithm for aligning DNA sequences. *J Comput Biol* (2000) 7:203–14. doi: 10.1089/10665270050081478
34. Knutsen TM. *Lumpfish (Cyclopterus lumpus) draft genome assembly. figshare. Dataset*. (2018). Available at: https://figshare.com/articles/Lumpfish_Cyclopterus_lumpus_draft_genome_assembly/7301546.
35. Felsenstein J. Confidence limits on phylogenies: An approach using the bootstrap. *Evolution* (1985) 39:783–91. doi: 10.1111/j.1558-5646.1985.tb00420.x
36. Kumar S, Stecher S. Tamura K. MEGA7: Molecular Evolutionary Genetics Analysis version 7.0 for bigger datasets. *Mol Biol Evolut* (2016) 33:1870–4. doi: 10.1093/molbev/msw054
37. Robert X, Gouet P. Deciphering key features in protein structures with the new ENDscript server. *Nuc Acids Res* (2014) 42:W320–4. doi: 10.1093/nar/gku316
38. Altschul SF, Madden TL, Schäffer AA, Zhang J, Zhang Z, Miller W, et al. and PSI-BLAST: a new generation of protein database search programs. *Nuc Acids Res* (1997) 25:3389–402. doi: 10.1093/nar/25.17.3389
39. Soding J, Biegert A, Lupas AN. The HHpred interactive server for protein homology detection and structure prediction. *Nuc Acids Res* (2007) 33:W244–8. doi: 10.1093/nar/gki408
40. Wittenberg JB, Haedrich RL. The choroid *rete mirabile* of the fish eye. II. Distribution and relation to the pseudobranch and to the swimbladder. *rete mirabile Biol Bullit* (1974) 146:137–56. doi: 10.2307/1540403
41. Franz-Odendaal TA, Ryan K, Hall BK. Developmental and morphological variation in the teleost craniofacial skeleton reveals an unusual mode of ossification. *J Exp Zool Part B Mol Dev Evolut* (2007) 308:709–21. doi: 10.1002/jez.b.21185
42. Rønneseth A, Ghebretnsae DB, Wergeland HI, Haugland GT. Functional characterization of IgM+ B cells and adaptive immunity in lumpfish (*Cyclopterus lumpus* L.). *Dev Compar Immunol* (2015) 52:132–43. doi: 10.1016/j.dci.2015.05.010
43. Salinas I, Zhang YA, Sunyer JO. Mucosal immunoglobulins and B cells of teleost fish. *Dev Compar Immunol* (2011) 35:1346–65. doi: 10.1016/j.dci.2011.11.009
44. Maguer-Satta V, Besançon R, Bachelard-Cascales E. Concise review: neutral endopeptidase (CD10): a multifaceted environment actor in stem cells, physiological mechanisms, and cancer. *Stem Cells* (2011) 29:389–96. doi: 10.1002/stem.592
45. Oefner C, D'Arcy A, Hennig M, Winkler FK, Dale GE. Structure of Human Neutral Endopeptidase (Neprilysin) Complexed with Phosphoramidon. *J Mol Biol* (2000) 296:341–9. doi: 10.1006/jmbi.1999.3492
46. Jones DT, Taylor WR, Thornton JM. The rapid generation of mutation data matrices from protein sequences. *Comput Appl Biosci* (1992) 8:275–82. doi: 10.1093/bioinformatics/8.3.275
47. Vasquez I, Cao T, Hossain A, Valderrama K, Gnanagobal H, Dang M, et al. *Aeromonas salmonicida* Infection Kinetics and Protective Immune Response to Vaccination in Sablefish (*Anopoploma fimbria*). *Fish Shellf Immunol* (2020) 104:557 566. doi: 10.1016/j.fsi.2020.06.005
48. Geven EJW, Klaren PHM. The teleost head kidney: Integrating thyroid and immune signalling. *Dev Compar Immunol* (2017) 66:73–83. doi: 10.1016/j.dci.2016.06.025
49. Witten PE, Huysseune A. A comparative view on mechanisms and functions of skeletal remodelling in teleost fish, with special emphasis on osteoclasts and their function. *Biol Rev Cambridge Phil Soc* (2009) 84:315–46. doi: 10.1111/j.1469-185X.2009.00077.x
50. Kobayashi I, Katakura F, Moritomo T. Isolation and characterization of hematopoietic stem cells in teleost fish. *Dev Compar Immunol* (2016) 58:86–94. Review. doi: 10.1016/j.dci.2016.01.003
51. Hollander Z, Shah VO, Civin CI, Loken MR. Assessment of proliferation during maturation of the B lymphoid lineage in normal human bone marrow. *Blood* (1988) 71:528–31. doi: 10.1182/blood.V71.2.528.528
52. Arredondo JL, Fernandes JR, Rao C. Ocular findings in pediatric deaths under 2 years of age (1994-2004). *J Forens Sci* (2008) 53:928–34. doi: 10.1111/j.1556-4029.2008.00757.x
53. Kim DD, Memmen JE, Sharpe RW, Bethel KJ, Keefe KS, Hall W, et al. Choroidal hematopoiesis in an adult. *Arch Ophthalmol* (1996) 114:1421–2. doi: 10.1001/archopht.1996.01100140621022
54. Yu YY, Kong W, Yin YX, Dong F, Huang ZY, Yin GM, et al. Mucosal immunoglobulins protect the olfactory organ of teleost fish against parasitic infection. *PloS Pathog* (2018) 114(11):e1007251. doi: 10.1371/journal.ppat.1007251

55. Franz-Odendaal TA, Vickaryous MK. Skeletal elements in the vertebrate eye and adnexa: morphological and developmental perspectives. *Dev Dynam* (2006) 235:1244–55. Review. doi: 10.1002/dvdy.20718
56. Boomker J. The haemocytology and histology of the haemopoietic organs of south African freshwater fish. III. The leukocytes, plasma cells and macrophages of clarias gariepinus and sarotherodon mossambicus. Onderstepoort. *J Veter Res* (1981) 48:185–93.
57. Mumford S, Heidel J, Smith C, Morrison J, MacConnell B, Blazer V. *Fish Histology and Histopathology. Department of Fish and Wildlife Service, US Government*. (2007). Available at: https://training.fws.gov/resources/course-resources/fish-histology/Fish_Histology_Manual_v4.pdf.
58. Bilal S, Lie KK, Karlsen OA, Hordvik I. Characterization of IgM in Norwegian cleaner fish (lumpfish and wrasses). *Fish Shellfish Immunol* (2016) 56:9–17.
59. Erkinharju T, Strandskog G, Vågnes Ø, Hordvik I, Dalmo RA, Seternes T. Intramuscular vaccination of Atlantic lumpfish (*Cyclopterus lumpus* L.) induces inflammatory reactions and local immunoglobulin M production at the vaccine administration site. *J Fish Dis* (2019) 42(12):1731–43. doi: 10.1111/jfd.13101
60. Haugland GT, Rønneseth A, Wergeland HI. Immunology and vaccinology of lumpfish and wrasse. In: J Treasurer, editor. *Cleaner fish biology and aquaculture applications, 1st ed.* Sheffield, UK: 5M Publishing Ltd (2018). p. 258–64.
61. Gendron RL, Good WV, Miskiewicz E, Tucker S, Phelps DL, Paradis H. Tubedown-1 (Tbdn-1) suppression in oxygen-induced retinopathy and in retinopathy of prematurity. *Mol Vis* (2006) 12:108–16.
62. Gendron RL, Laver NV, Good WV, Grossniklaus HE, Miskiewicz EM, Whelan A, et al. Loss of tubedown expression as a contributing factor in the development of age-related retinopathy. *Invest Ophthalmol Vis Sci* (2010) 51:5267–77. doi: 10.1167/iovs.09-4527
63. Wall DS, Gendron RL, Good WV, Miskiewicz E, Woodland M, Leblanc K, et al. Conditional knockdown of tubedown-1 in endothelial cells leads to neovascular retinopathy. *Invest Ophthalmol Vis Sci* (2004) 45:3704–12. doi: 10.1167/iovs.03-1410
64. Torlakovic E, Tenstad E, Funderud S, Rian E. CD10+ stromal cells form B-lymphocyte maturation niches in the human bone marrow. *J Pathol* (2005) 205(3):311–7. doi: 10.1002/path.1705
65. Sekiya I, Vuoristo JT, Larson BL, Prockop DJ. In vitro cartilage formation by human adult stem cells from bone marrow stroma defines the sequence of cellular and molecular events during chondrogenesis. *Proc Nat Acad Sci USA* (2002) 99(7):4397–402. doi: 10.1073/pnas.052716199
66. Ding L, Vezzani B, Khan N, Su J, Xu L, Yan G, et al. CD10 expression identifies a subset of human perivascular progenitor cells with high proliferation and calcification potentials. *Stem Cells* (2020) 38(2):261–75. doi: 10.1002/stem.3112
67. Calderwood WL. The head kidney of teleostean fishes. *J Marine Biolog Assoc U K* (1891) 2:43–6. N. S., Volume ii. No 1. doi: 10.1017/S0025315400049456
68. Diep CQ, Ma D, Deo RC, Holm TM, Naylor RW, Arora N, et al. Identification of adult nephron progenitors capable of kidney regeneration in zebrafish. *Nature* (2011) 470(7332):95–100. doi: 10.1038/nature09669
69. Sugimoto T, Ueyama H, Hosoi H, Inazawa J, Kato T, Kemshead JT, et al. Alpha-smooth-muscle actin and desmin expressions in human neuroblastoma cell lines. *Int J Cancer* (1991) 48(2):277–83. doi: 10.1002/ijc.2910480221
70. Jahed A, Rowland JW, McDonald T, Boyd JG, Doucette R, Kawaja MD. Olfactory ensheathing cells express smooth muscle alpha-actin in vitro and in vivo. *J Comp Neurol* (2007) 503(2):209–23. doi: 10.1002/cne.21385
71. Auer-Grumbach M, Toegel S, Schabhüttl M, Weinmann D, Chiari C, Bennett DLH, et al. Rare Variants in MME, Encoding Metalloprotease Neprilysin, Are Linked to Late-Onset Autosomal-Dominant Axonal Polyneuropathies. *Amer J Hum Genet* (2016) 99(3):607–23. doi: 10.1016/j.ajhg.2016.07.008
72. Hara H, Oh-hashi K, Yoneda S, Shimazawa M, Inatani M, Tanihara H, et al. Elevated neprilysin activity in vitreous of patients with proliferative diabetic retinopathy. *Mol Vis* (2006) 12:977–82.
73. Hasby EA, Saad HA. Immunohistochemical expression of Fas ligand (FasL) and neprilysin (neutral endopeptidase/CD10) in keratoconus. *Int Ophthalmol* (2013) 33(2):125–31. doi: 10.1007/s10792-012-9651-0
74. Barrett LT, Overton K, Stien LH, Oppedal F, Dempster T. Effect of cleaner fish on sea lice in Norwegian salmon aquaculture: a national scale data analysis. *Int J Parasitol* (2020) 50(10-11):787–96. doi: 10.1016/j.ijpara.2019.12.005

Conflict of Interest: The authors declare that the research was conducted in the absence of any commercial or financial relationships that could be construed as a potential conflict of interest.

Copyright © 2020 Gendron, Paradis, Ahmad, Kao, Boyce, Good, Kumar, Vasquez, Cao, Hossain, Chakraborty, Valderrama and Santander. This is an open-access article distributed under the terms of the Creative Commons Attribution License (CC BY). The use, distribution or reproduction in other forums is permitted, provided the original author(s) and the copyright owner(s) are credited and that the original publication in this journal is cited, in accordance with accepted academic practice. No use, distribution or reproduction is permitted which does not comply with these terms.

frontiers in Immunology

ORIGINAL RESEARCH
published: 26 February 2021
doi: 10.3389/fimmu.2021.568729

Evolution and Expression of the Immune System of a Facultatively Anadromous Salmonid

Thomas J. Colgan [1†‡], Peter A. Moran [1,2†‡], Louise C. Archer [1,2], Robert Wynne [1,2], Stephen A. Hutton [1,2], Philip McGinnity [1,3] and Thomas E. Reed [1,2†]*

[1] School of Biological, Earth and Environmental Sciences, University College Cork, Cork, Ireland, [2] Environmental Research Institute, University College Cork, Cork, Ireland, [3] Marine Institute, Newport, Ireland

OPEN ACCESS

Edited by:
Sissel Jentoft,
University of Oslo, Norway

Reviewed by:
Daniel J. Macqueen,
University of Edinburgh,
United Kingdom
Simen Sandve,
Norwegian University of Life Sciences,
Norway

***Correspondence:**
Thomas J. Colgan
joe.colgan@ucc.ie

†ORCID:
Thomas J. Colgan
orcid.org/0000-0002-0547-8228
Peter A. Moran
orcid.org/0000-0002-2206-4721
Thomas E. Reed
orcid.org/0000-0002-2993-0477

‡Present address:
Thomas J. Colgan,
Institute of Organismic and Molecular Evolution, Johannes Gutenberg University Mainz, Mainz, Germany
Peter A. Moran,
Department of Ecological Science—Animal Ecology, Vrije Universiteit Amsterdam, Amsterdam, Netherlands

Specialty section:
This article was submitted to Comparative Immunology, a section of the journal Frontiers in Immunology

Received: 02 June 2020
Accepted: 07 January 2021
Published: 26 February 2021

Citation:
Colgan TJ, Moran PA, Archer LC, Wynne R, Hutton SA, McGinnity P and Reed TE (2021) Evolution and Expression of the Immune System of a Facultatively Anadromous Salmonid. Front. Immunol. 12:568729. doi: 10.3389/fimmu.2021.568729

Vertebrates have evolved a complex immune system required for the identification of and coordinated response to harmful pathogens. Migratory species spend periods of their life-cycle in more than one environment, and their immune system consequently faces a greater diversity of pathogens residing in different environments. In facultatively anadromous salmonids, individuals may spend parts of their life-cycle in freshwater and marine environments. For species such as the brown trout *Salmo trutta*, sexes differ in their life-histories with females more likely to migrate to sea while males are more likely to stay and complete their life-cycle in their natal river. Salmonids have also undergone a lineage-specific whole genome duplication event, which may provide novel immune innovations but our current understanding of the differences in salmonid immune expression between the sexes is limited. We characterized the brown trout immune gene repertoire, identifying a number of canonical immune genes in non-salmonid teleosts to be duplicated in *S. trutta*, with genes involved in innate and adaptive immunity. Through genome-wide transcriptional profiling ("RNA-seq") of male and female livers to investigate sex differences in gene expression amplitude and alternative splicing, we identified immune genes as being generally male-biased in expression. Our study provides important insights into the evolutionary consequences of whole genome duplication events on the salmonid immune gene repertoire and how the sexes differ in constitutive immune expression.

Keywords: facultatively anadromous, immunity, gene expression, gene duplications, sexual dimorphism, salmonids

INTRODUCTION

Species that migrate face a range of challenges. First, the physical act of migration can be metabolically and energetically demanding, resulting in trade-offs with other metabolically intensive physiological processes, such as immunity, when resources are limiting (1–3). Second, migratory species move through different environments and hence may be exposed to different pathogens and parasites (4, 5). For aquatic species that exhibit diadromy—the ability to move between marine and freshwater environments—an efficient immune system is required to cope with

the challenges imposed by living in, and moving between, different osmotic environments with different pathogen and parasite communities.

In vertebrates, a sophisticated immune system has evolved that performs two vital functions: 1) the recognition and distinction of invasive pathogenic organisms from normal cells ("self"), and 2) coordinating an appropriate response through triggering pathways responsible for the synthesis of effector molecules that directly or indirectly reduce or remove the pathogenic threat (6, 7). Aside from detection of non-self-pathogenic organisms, the immune system also functions in the removal of abnormal cells and thus provides an important role in reducing the development and onset of disease.

Given the importance of the immune system in preventing infection and establishment of disease, there is strong selection pressure acting on immune genes. In response to these pressures, immune genes are generally fast evolving (8, 9). Additional innovations in immune potential can also arise through tandem duplication, retrotransposition, larger scale duplication of chromosomal regions or entire chromosomes, as well as whole genome duplication events (WGD). For example, two rounds of WGD events are suggested to have contributed to the genesis of the adaptive immune system in vertebrates (10). Indeed, WGD events produce duplicated copies of all genes, which selection can act on resulting in retention or removal of one or both copies. In terms of removal, as with general duplication events, gene loss can occur through reduced purifying selection resulting in functional divergence between the copies. Accumulation of deleterious mutations may eventually lead to one copy becoming non-functional (11). Gene loss may also be adaptive. For example, loss of gene function in a duplicated copy may be adaptive in response to environmental challenges (12, 13), including pathogens (14, 15). Alternatively, after duplication of a gene, functional divergence can occur whereby one copy evolves a slightly different or entirely novel function relative to the other copy. Functional divergence can result in subfunctionalization, whereby individual copies specialize on different components of the same function originally performed by the ancestral gene pre-duplication (i.e., "division of labor"), or neofunctionalization, whereby one copy may evolve a novel function (16).

As stated previously, the continuous expression and activation of immunity can be metabolically costly, resulting in trade-offs with fecundity and longevity (17). In particular, the sexes can differ in their levels of immune function with greater immunocompetence generally evident in females in comparison to males (18–23). Lower immunocompetence in males has been attributed in proximate terms to differences in circulating levels of hormones and their effects, such as androgen, and in ultimate terms to differences in life-history strategies, with males investing more in reproduction and associated secondary sexual characters while females invest in immune function and longevity (24). Moreover, in facultatively migratory species, differences are often evident between the sexes in the rate or timing of migration (25–28), which in turn has implications for exposure to pathogens and parasites and investment in immune defense. Differences in the level of immunity between the sexes can be detected at the transcriptional level (22, 29–31), whereby genes associated with the immune system may differ in their expression between the sexes. Approaches such as genome-wide transcriptomics ("RNA-seq") are important tools for high-resolution detection and profiling of genes that differ in expression amplitude, as well as splicing, between the sexes. Such approaches have been applied to improve our understanding of genes underlying sexually dimorphic traits in a variety of taxa (32–35), including immunity (36).

An interesting study system for understanding the evolution and expression of the immune system and how it differs between the sexes are the salmonids, a group of culturally, economically and ecologically important teleost fish (37). The salmonids consist of approximately 70 species across 11 genera that have evolved flexible life-histories with a diversity of ecological adaptations that allow for migration to, and survival in, a range of freshwater and marine aquatic environments (38). There is a gradient from entirely non-anadromous species (which complete their entire life cycles in fresh water) through facultatively anadromous species to species that are almost entirely anadromous (39–44). Within facultatively anadromous species, rates of anadromy and other migratory tactics can vary between populations, and even among individuals within populations, particularly between the sexes with females more likely to undergo migration than males (42, 43, 45, 46).

Survival for prolonged periods in different aquatic environments, which contain different pathogenic threats, requires an immune system that can detect and respond to a diverse array of immune challenges. These factors likely placed strong selection pressures that shaped immune system evolution but additional immune novelty in salmonids may be the result of the salmonid-specific WGD event. The common ancestor of salmonids underwent an autotetraploidization event approximately 80–100 mya (47–49), which is believed to have contributed to genomic and phenotypic innovation as well as speciation within the salmonids (50). While the timing of the WGD event and first appearance of the anadromy during salmonid evolution are highly temporally detached, speciation rates were shown to be elevated within anadromous salmonids compared to non-anadromous salmonids with ecological factors, such as climate cooling, rather than the WGD suggested as the primary drivers of anadromy-linked diversification (47). The sequencing of the Atlantic salmon (*Salmo salar*) genome revealed that approximately 25% of the genome is undergoing delayed rediploidization, which is associated with major chromosomal rearrangements (48). Delayed rediploidization has been ongoing in parallel with speciation events, which has led to the proposal of 'lineage-specific ohnolog resolution' (LORe) as a mechanism to understand the impact of delayed rediploidization on the functional divergence of ohnologs across lineages that share a common ancestral WGD event (50). Under LORe, species divergence occurs before the rediploidization process is complete resulting in functional divergence of ohnologs independently within each lineage. The alternative model predicts rediploidization is completed prior to species

diversification resulting in functional divergence of ohnologs within a shared ancestor ("Ancestral Ohnologue Resolution" or "AORe" model).

Due to shared selection pressures acting on ohnologs within a common ancestor, ohnologs that diverged in an ancestor are predicted to possess conserved functions across modern lineages (50). Recent genomic studies on salmonids have found evidence of relatively high rates of retention of duplicated genes arising from this most recent WGD (>50% of genes being found in functional ohnolog pairs), as well as evidence of neofunctionalization, whereby copies may diverge and are suggested to perform novel functions (48, 51, 52). Indeed, the evolutionary consequences of such events have served as impetus to examine functional divergence among ohnologous genes with putative immunological roles in salmonids (53–56). Despite these advances in our fundamental understanding of salmonid immunology, we understand less for species, such as the facultatively anadromous, brown trout (*Salmo trutta*). Recent declines in sea migration of *S. trutta* populations in Ireland and Scotland have raised concerns over the impact of disease and parasites, such as sea lice, on brown trout health and population performance (57–59). Given the enormous selection pressures exerted by parasites on their hosts, host defenses, including components of the host immune system, would be required to adapt to tolerate or resist so as to increase host survival and fitness (60). Therefore, increasing our understanding of brown trout immunity is warranted.

Here we had three main aims: Firstly, to characterize predicted immune genes found in the brown trout genome. For this, we used comparative genomic approaches to identify these genes in *S. trutta* based on homology with immune genes annotated in model organisms, such as zebrafish (*Danio rerio*), mouse (*Mus musculus*) and human (*Homo sapiens*). Given the overall enlarged gene repertoire in salmonids due to the salmonid-specific WGD event, as well as the strong selection pressures placed on immune genes by pathogens from both marine and freshwater environments, we would expect retention of most canonical immune genes, as well as the potential expansion of beneficial immune gene families. Secondly, we aimed to investigate evolutionary patterns of functional conservation and divergence, including gene loss in *S. trutta* immune ohnologs. Our final aim was to identify immune genes with sex-biased expression profiles. For this approach, we performed transcriptomic analyses on the liver, an important immunocompetent organ (61, 62), and quantified differences between males and females in gene expression amplitude, as well as alternative splicing, to identify molecular processes underlying sex differences in immune transcription and regulation.

MATERIALS AND METHODS

Identification of Putative Brown Trout Immune Homologs

To identify genes in brown trout with putative immune function, we obtained gene lists for annotated immune genes in the zebrafish, *Danio rerio* [obtained from Zebrafish Information Network (ZFIN) database; (63)], as well as for the mouse, *Mus musculus* (obtained from Mouse Genome Informatics (MFI) database (64) and human, *Homo sapiens* [obtained from ImmPort (65)]. Using biomaRt [v. 2.45.8; (66)], we parsed the Ensembl BioMart database to identify "high confidence" orthologs found in the brown trout genome based on homology (phylogenetic protein trees), as well as conserved synteny (gene order conservation score and whole genome alignment scores). The threshold for classification of a brown trout gene as a 'high confidence' ortholog included: 1) a minimum gene conservation score of 50, which indicates the percentage of how many of the four closest neighbors of a gene match been orthologous pairs (i.e., at least two (50%) of neighboring genes match); 2) a minimum whole genome alignment score of 50; and 3) a minimum protein percentage identity of 50%. This approach identified 2,275 brown trout genes with homology to immune genes in three model organisms (**Supplemental Information Table 1**).

Identification of Putative Immune Genes Across Salmonids

As a preliminary measure to understand immune gene repertoires across salmonids, we investigated the presence of homologues of putative brown trout immune genes in other salmonid species. To identify homology relationships, we first followed the approach outlined by Gillard et al. (51), and obtained protein sequences for the predicted proteomes from Ensembl [release 101; (67)] for twelve teleost fish, including the zebrafish (*Danio rerio*; GRCz11: GCA_000002035.4), three-spined stickleback (*Gasterosteus aculeatus*; BROAD S1), Japanese medaka (*Oryzias latipes*; ASM223467v1: GCA_002234715.1), Northern pike (*Esox Lucius*; Eluc_v4: GCA_004634155.1), Atlantic herring (*Clupea harengus*; Ch_v2.02: GCA_900700415.1), Atlantic cod (*Gadus morhua*; gadMor1), and guppy (*Poecilia reticulata*; GCA_000633615.2), and the salmonids, rainbow trout (*Oncorhynchus mykiss*; Omyk_1.0: GCA_002163495.1), Coho salmon (*Oncorhynchus kisutch*; Okis_V2: GCA_002021735.2), Chinook salmon (*Oncorhynchus tshawytscha*; Otsh_v1.0: GCA_002872995.1), Atlantic salmon (*Salmo salar*; ICSASG_v2: GCA_000233375.4), and brown trout (*Salmo trutta*; fSalTru1.1: GCA_901001165.1). From Ensembl, we also obtained two mammalian outgroups, human, *Homo sapiens* (GRCh38.p13: GCA_000001405.28), and mouse, *Mus musculus* (GRCm38.p6: GCA_000001635.8). For protein FASTA files downloaded from Ensembl, we extracted the longest protein isoform per gene per species using the OrthoFinder script "primary_transcripts.py" [v.2.3.11; (68, 69)]. We used OrthoFinder to assign groups of orthologs based on protein sequence similarity. Multiple sequence alignment was performed for protein sequences within each orthogroup using MAFFT. Maximum-likelihood trees were estimated using FastTree as implemented within OrthoFinder. OrthoFinder constructed a total of 47,752 orthogroups of which 22,101 were species-specific groups (**Supplemental Information Table 2**). The percentage of genes per species represented in the orthogroups was high (92%–97.5%). We parsed these

orthogroups using the putative brown trout immune genes identified through the Ensembl-based analysis (n = 2,275 genes) and identified putative immune homologs present in 1,227 orthogroups (**Supplemental Information Table 3**). As a secondary measure to understand immune gene expansions and losses within the salmonids, we ran OrthoFinder using only the five salmonid proteomes, as well as Northern pike, the closest related species that did not undergo a fourth WGD event (70). While other salmonid genomes are publicly available, we restricted our analysis to Ensembl-generated datasets to account for gene models being predicted using a similar annotation pipeline (**Supplemental Information Table 4**). The presence of single copy orthologs in both Northern pike and all sequenced salmonids suggests that gene loss occurred in a common ancestor of modern salmonids soon after the WGD event or multiple independent losses have occurred across the salmonids.

Expression of Brown Trout Immune Genes

To examine the functional expression of putative immune genes of *S. trutta*, we obtained available RNA-seq libraries for eight tissues from the NCBI (National Center for Biotechnology Information) Short Read Archive (SRA) database (BioProject: PRJEB33055). For each sample, we quantified transcript abundance using the quasialigner, Salmon [v.0.12.0; (71)]. Using these transcript abundances, we calculated gene-level counts using tximport [v.1.14.2; (72); **Supplemental Information Table 5**] and corrected for library-sizes using DESeq2 [v.1.26.0; (73)]. For each tissue, we quantified the total number of immune genes expressed per tissue, as well as compared relative abundance of immune gene expression for each tissue against non-immune genes.

Identification of Putative Immune Ohnologs

To identify putative immune ohnologs, we first extracted within-species paralogs for brown trout using the Ensembl BioMart database (filter: "with_strutta_paralog"). Ensembl employs a pipeline that through protein trees can time and predict the last common ancestor for paralogs. We then subsetted putative immune genes identifying putative species-specific paralogs (n = 456), genus-specific (n = 344), as well as paralogs predicted to have arisen in the Salmoninae ancestor, which may represent paralogs generated as a result of the Salmonid-specific WGD. For each of these "Salmoninae" paralogs present in the brown trout genome, we subsetted and retained paralogs that shared at least 85% protein sequence similarity. We then obtained the Northern pike ortholog of each putative paralog. We extracted paralog pairs where only a single non-duplicated pike ortholog was evident, which matched only two paralogs in brown trout. For this, we kept only Northern pike orthologs that shared at least 85% sequence similarity to each of the brown trout paralogs. We also investigated the physical genomic coordinates of each ohnolog identifying that collinearity among putative immune ohnolog pairs is a global feature of the data, consistent with these genes being ohnologs. We therefore consider these brown trout paralogs as putative ohnologs. We found no significant difference (paired two sample t-test; $p > 0.05$) in predicted protein length between each ohnolog pair or their respective non-duplicated ortholog in Northern pike. This approach resulted in the identification of 434 ohnolog pairs (n = 868 genes) with potential immune function. We also extracted Atlantic salmon homologs of putative immune ohnolog pairs in brown trout and compared overlap with the *S. salar* ohnolog pairs described by Bertolotti et al. (74). Of the 434 brown trout immune ohnolog pairs, 408 pairs shared homologs in Atlantic salmon. Of this number, 88% (n = 362) were also identified as ohnolog pairs within the analysis of Bertolotti et al. providing independent evidence for the classification of such immune genes as ohnologs.

Ohnolog Analysis of Immune Genes

Assessment of Putative Functional Conservation and Divergence

For each ohnolog pair, we estimated the evolutionary distance between each pair and the non-duplicated ortholog in Northern pike using distmat from EMBOSS [v.6.6.0; (75)] (in terms of amino acid substitutions per 100 amino acids; **Supplemental Information Table 6**). This allowed for the determination of copies that were more conserved or diverged in terms of protein sequence while accounting for variation in predicted amino acid length. To explore variation in functional domain architecture, we obtained InterPro functional domains assigned to predicted proteins for each pair from Ensembl BioMart (67). We then counted and compared the number of assigned domains for each ohnolog pair to identify any differences, which may be consistent with the genes performing different functions. As variation in protein length may explain variation in protein domains, we also compared predicted protein lengths between ohnologs identifying no significant difference in length (paired two sample t-test; $p = 0.6$).

Assessment of Variation in Expression Profiles Between Ohnologs

Using the gene-level counts generated by eight tissues, we generated co-expression clusters for putative immune ohnologs using Clust [v.1.10.8; (76)]. Here differences in expression profiles between ohnologs may reflect functional divergence, which has been determined in other salmonid species (48, 49, 51, 77). To determine divergence, we extracted ohnolog pairs that were assigned to different co-expression clusters and used corrected counts per sample generated by Clust for visualization purposes. Gene assignments to clusters are provided in **Supplemental Information Table 7**.

Assessment of Variation in Selection Patterns Acting on Ohnologs

To understand differences in selection acting on each pair, we calculated *dN/dS* ratios between each brown trout ohnolog and their respective non-duplicated Northern pike ortholog (**Supplemental Information Table 6**). We first aligned predicted protein sequences using clustal Omega [v.1.2.4; (78)] and converted the aligned sequences to nucleic acids using

pal2nal [v.14; (79)] to obtain codon-based nucleic acid alignments. We then ran codeML as part of PAML [v.4.9; (80)] to estimate *dN/dS* ratios.

Sampling of Laboratory-Based Brown Trout

To provide additional functional information on brown trout immune genes, and to examine potential sex differences in immune expression, we sampled livers from mature male and female *S. trutta* for transcriptomic analyses (**Supplemental Information Table 8**). For the present study, the fish used originated from a larger experimental aquaculture project that explored the expression of alternative life history tactics in brown trout (81, 82). This wider set-up involved 18 different tanks all connected within a recirculating aquaculture system (RAS), but in the current analysis, all our sampled fish came from two independent tanks (with each tank comprising fish from a different genetic background). Full details on the origins of the fish, fish husbandry procedures and other general information are given in Archer et al. (81, 82).

Tissue Collection for Gene Expression Analysis

All fish were dissected between May and June 2018 (the endpoint of the larger experiment) when the fish were between two and three calendar years old. We collected livers from each individual fish and transferred the tissues to fresh 2 ml Eppendorf tubes containing RNALater solution. Samples were kept for 24 h at room temperature, and then stored at -80°C for later analysis. Samples during dissection were visually checked for mature testes or ovaries. For confirmation of genetic sex, we also obtained caudal fin clips from each fish during dissection and stored in 100% ethanol before subsequent genotyping.

RNA Extraction, Purification, and Quality Assessment

Total RNA was extracted from a total of 37 tissues using TRIzol. Specifically, we extracted RNA from fifteen livers from males and from 22 livers from females. For RNA extractions, we removed each sample from -80°C long-term storage and incubated them on ice to thaw. Using a pipette, the RNALater solution was removed. We added 1ml of autoclaved phosphate-buffered saline to each tissue to briefly wash them before using sterilized forceps to transfer each washed tissue to an individual 2ml screw-cap homogenization tube. To each sample, 200ul of TRIzol was added and the sample was transferred to -80°C storage. Tissue disruption was performed using a 2 mm steel bead and a Tissuslyer II (Qiagen, UK). To each sample, a 2 mm steel bead was added and samples were homogenized at 30 Hz for 30 s. Post-homogenization, samples were visually inspected to ensure thorough disruption. Total RNA was extracted using chloroform followed by isopropanol precipitation. Precipitated RNA was washed using three washes of ethanol before elution in the elution buffer (Sigma, UK). Total RNA was purified using the Sigma GenElute Mammalian Total RNA kit. Quality assessment was initially performed using a NanoDrop ND-1000 (ThermoFisher, UK) while an accurate assessment of quantity was estimated using the Qubit fluorometer, followed by a TapeStation 2200 (Agilent, UK).

Library Preparation and Sequencing

mRNA-enriched library preparation was performed for each individual sample using the NEBNext® Ultra™ RNA Library Preparation kit and sequencing performed on an Illumina NovaSeq6000. Library preparation and sequencing was performed by NovoGene, Hong Kong. Sequencing resulted in a median of 26.1 million paired-end (PE) reads (2*150 bp) per individual (min. 20.1 million PE reads; max. 34.2 million PE reads). A combined total of 980 million PE reads were generated. Summary of sample information is provided in **Supplemental Information Table 8**.

Quality Assessment of Raw Sequences

We quality assessed raw FASTQ sequences using FastQC [v.0.11.8; (83)] to identify adaptor contamination and sequences of low quality. Raw reads were aligned against the reference genome assembly (GCA_901001164.1) for *Salmo trutta* using STAR [v.2.7.0a; (84)]. Alignment statistics were calculated using samtools flagstat [v.1.9; (85)]. Summary statistics of alignments were compiled using Qualimap [v.2.2.1; (86)] and the output visualized using MultiQC [v.1.7; (87)].

Transcript Abundance, Gene-Level Estimates, and Differential Expression Analysis

We quantified transcript abundance using two complementary approaches. Similar to the approach outlined above, using Salmon, we quasialigned raw reads against cDNA sequences for coding and non-coding genes available for *S. trutta* from Ensembl. We calculated gene-level counts using tximport and loaded these values into a DESeq2 object using DESeq2. Raw gene-level counts are provided in **Supplemental Information Table 9**. We performed a Wald test implemented by DESeq2 to identify significantly differentially expressed genes between males and females (Benjamini-Hochberg (BH) adjusted $p < 0.05$; **Supplemental Information Table 10**). To explore similarities in expression profiles across all samples, a principal component analysis was performed with DESeq2 for all samples using gene-level counts for 33,228 genes expressed in the liver following a variance stabilization transformation implemented by DESeq2. As a complementary measure, for each individual, we examined gene expression using a traditional aligner-based approach. We aligned reads against the brown trout reference genome assembly using STAR and extracted gene-level counts from the resultant BAM files using HTSeq [v. 0.11.2; (88); **Supplemental Information Table 11**]. We found an extremely high correlation (Pearson's correlation: r=0.9, $p < 2.2e^{-16}$) between the mean gene-level counts for both this approach, as well as the Salmon approach outlined above. This is also true for comparisons for individual samples across both approaches (lowest r=0.83, highest r=0.97). As an additional measure, we analyzed and compared the number of differentially expressed

genes identified with DESeq2 when using the output of either transcript quantification approach (**Supplemental Information Table 12**). We found that >85% of genes identified as significantly differentially expressed between the sexes by Salmon were also identified as significant by the STAR-HTSeq approach. As quasi- and pseudoaligners, such as Salmon and kallisto, have higher accuracy and consistency in transcript quantification compared to traditional aligners (89), we report only the findings of our Salmon analysis.

Differential Intron Usage Between the Sexes

While the sexes may express genes at different amplitudes, they may also express different isoforms of the same gene. We used the intron-splice analyzer leafcutter [v.0.2.8; (90)] to investigate differences between the sexes. Briefly, for each sample, we aligned raw reads against the brown trout genome assembly (GCA_901001165.1) using STAR (–outSAMstrandField intronMotif, –twopassMode Basic). We extracted splice junctions using bam2junc.sh and generated intron clusters using leafcutter.py (parameters: –minclureads 50, –maxintronlen 500000, –minreads 5). We then performed differential intron analysis using leafcutter_ds.R whereby for a cluster to be included it must be identified within at least five individuals within each sex (parameters: –min_samples_per_intron 5, –min_samples_per_group 5) to allow for investigation of genes with signatures of differential intron usage between the sexes. Leafcutter implements a log likelihood ratio test comparing a null model that assumes there is no difference between groups and an alternative model, which does. We adjusted resulting p values for multiple testing (False Discovery Rate < 0.05; **Supplemental Information Table 13**).

Gene Ontology Term Enrichment Analysis of Immune and Sex-Biased Genes

Gene Ontology term enrichment analysis and visualization of outputs were performed using modified scripts generated by Colgan et al. (91). As the zebrafish is a model organism with extensive functional annotation of genes, we assigned GO terms for genes in the *Danio rerio* genome to putative *S. trutta* orthologs using biomaRt. We performed GO term enrichment analysis using topGO [v.2.34; (92)] with the 'weight01' algorithm and a node size of 20. The background universe consisted of all genes (n = 29,527) annotated with a Gene Ontology term.

For functional annotation of putative *S. trutta* immune genes, we performed a Fisher's Exact test to identify enrichment of GO terms for species-specific duplications, genus-specific and putative immune ohnologs (**Figure 1**). For sex-biased immune genes, we performed Gene Ontology term enrichment analysis using a Kolmogorov-Smirnov (K-S) test. For all tests, we corrected for multiple testing using the Benjamini-Hochberg procedure and only reported terms as significant with an adjusted $p < 0.05$.

Statistical Tests

For comparison between metrics associated with ohnologs, including variation in raw gene expression, predicted amino acid length, *dN/dS* ratios and evolutionary distance to non-duplicated ortholog outgroup, we used base statistical functions in R (v. 3.5.1). For pairwise comparison of means, we used Welch Two sample t-tests or Wilcoxon rank sum test. We tested for correlations using Pearson's product moment correlation coefficient.

RESULTS

Functional Annotation of *Salmo trutta* Immune Genes

Through comparison with annotated immune genes in zebrafish, mouse and human, we identified 2,275 putative homologs encoded by the brown trout genome (**Supplemental Information Table 1**). As expected, due to the salmonid-specific WGD event, the number of genes with putative roles in the immune system were elevated in salmonids in comparison to non-salmonid fishes (**Figure 2**) with the analysis by OrthoFinder indicating an additional 1,132 homologous sequences based on sequence similarity alone. However, as the immune orthologs identified by Ensembl are assigned based on additional synteny-based information, we consider the 2,275 of higher confidence and therefore, we based the rest of our analyses on these genes.

To identify if putative *S. trutta* immune genes are transcribed and therefore can be considered functional, we first investigated gene expression of all potential immune genes across eight available tissues (PRJEB33055). Collectively, we identified evidence of expression for 2,233 genes out of 2,275 (98.1% of immune genes) with 1,587 genes (69.8% of putative immune genes) expressed across all tissue types (**Figure 3**; **Supplemental Information Table 5**). We identified significantly higher expression (Wilcoxon test: $p < 0.05$) of immune genes in comparison to non-immune genes for all tissues examined, including immunocompetent organs, such as the spleen, kidney and liver, as well as the gills, which are an entry point for infection.

Functional Conservation and Divergence in Immune Genes

To understand the evolutionary consequences for the immune system post salmonid-specific WGD, we compared the predicted brown trout gene complement to that of the Northern pike, *E. lucius*. Using the 2,275 putative immune genes in the brown trout genome, we obtained 2,000 'high-confidence' orthologs in Northern pike. Of this number, 1,444 were present as 2:1 orthologs of Northern pike genes with 868 genes (434 pairs; **Supplemental Information Table 6**) annotated by Ensembl as paralogs with the time of duplication estimated within the Salmoninae, suggesting that these genes may be produced by the salmonid-specific WGD and represent ohnologs. Of the other 2:1 duplicate pairs, 30 (n = 60 genes) and 27 (n = 54 genes) were estimated to have duplicated within the genus *Salmo* and within *S. trutta*, respectively. The remainder may represent older duplication events, form part of expanded gene families in brown trout or represent gene losses in Northern pike. In terms of potential immune gene loss, we identified 253 immune genes

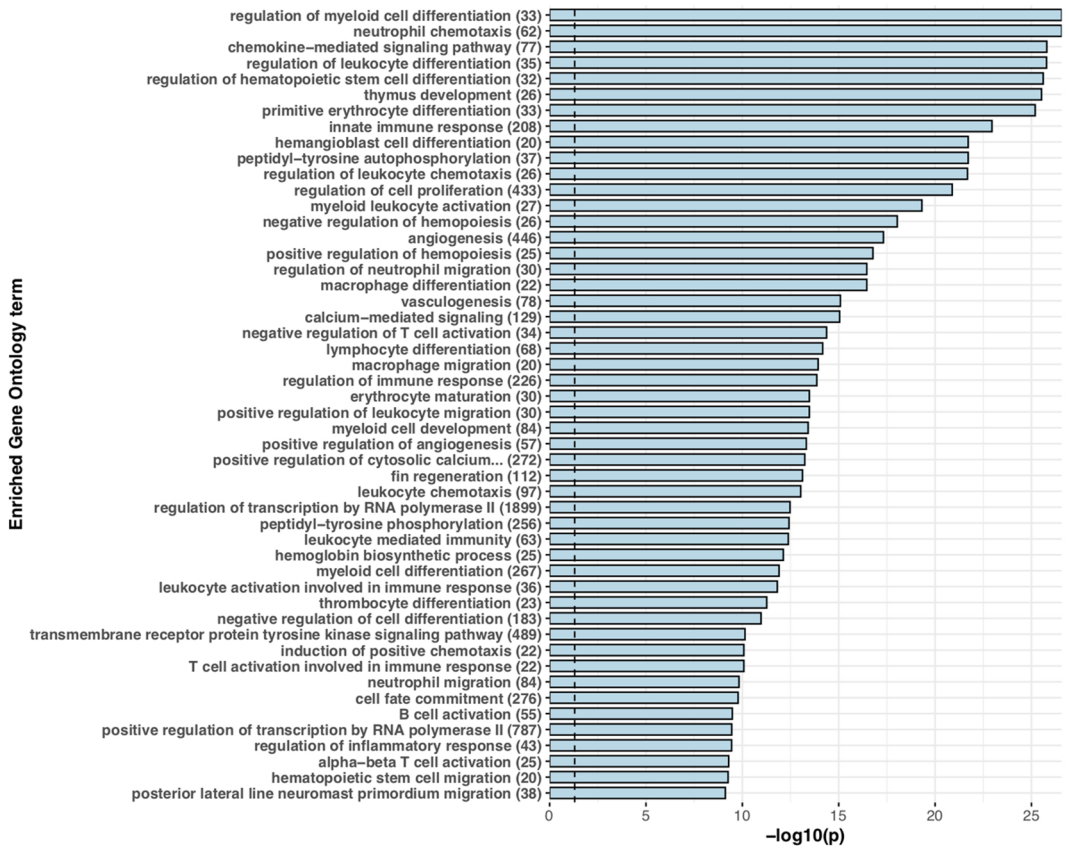

FIGURE 1 | Expanded immune gene repertoire in the brown trout genome. Barchart displaying the top 50 significantly enriched 'biological process' associated Gene Ontology terms for putative immune genes with more than one copy in the brown trout genome in comparison to non-duplicated single copies in the Northern pike genome. For each significantly enriched term (Benjamini-Hochberg adjusted $p < 0.05$), the -log10 transformed p value is provided. For each term, the number of genes annotated with that specific term in the predicted *S. trutta* proteome is provided. The blue dotted vertical line represents threshold of significance (-log10 transformed p = 0.05).

with 1:1 copies in both *S. trutta* and Northern pike. Of these 253 genes, OrthoFinder also identified 127 as single copy across salmonids.

To investigate patterns of functional conservation and divergence among immune ohnolog pairs, we first examined structural variation between ohnolog pairs in terms of the number of functional domains. Of the 434 immune ohnolog pairs, all proteins were annotated with at least one functional domain with 42 pairs differing in the number of functional domains with the more diverged copy generally having fewer domains suggestive that predicted proteins for at least ~11% of immune ohnolog have the potential to perform different functions. Overall, however, there was no significant difference in the number of predicted functional domains that each copy had (Wilcoxon test: $p > 0.05$; **Figure 4**). Similarly, there were no significant differences (Wilcoxon test: $p > 0.05$) in the mean gene, CDS or predicted protein length of ohnolog pairs. We also investigated variation between the pairs in terms of divergence from the single copy ortholog in Northern pike. Here, the more diverged copies based on evolutionary distance had significantly higher *dN/dS* ratios (paired two-sample t-test: $p < 0.05$; **Figure 4**) in comparison to more conserved copies but overall indicated that both copies for those pairs analyzed were under strong purifying selection ($dN/dS < 0.25$).

To understand differences in gene expression profiles between immune ohnolog pairs, we performed a hierarchical clustering analysis to explore patterns of functional divergence. As a provisional measure, we first constructed co-expression networks using all putative immune genes identifying eight clusters consisting of 823 genes (smallest cluster = 20 genes; largest cluster = 257 genes). For immune ohnologs (n = 434 pairs), our analysis clustered 302 immune ohnologs into seven respective co-expression clusters (**Figure 5**). Of this number, 152 assigned genes belonged to ohnolog pairs (i.e., 76 pairs), where both ohnologs could be assigned to a co-expression network. The majority of these pairs (n = 55 pairs) were assigned to the same co-expression network indicating that both copies have conserved expression profiles across tissues suggestive that functions may also be conserved. Twenty one immune ohnolog pairs showed divergent co-expression profiles (**Figure 5**). For the remainder of the genes (n = 150) assigned to a cluster, they represent only one ohnolog from a pair where the other copy was unassigned due to lack of variation in expression or lack of expression across tissues.

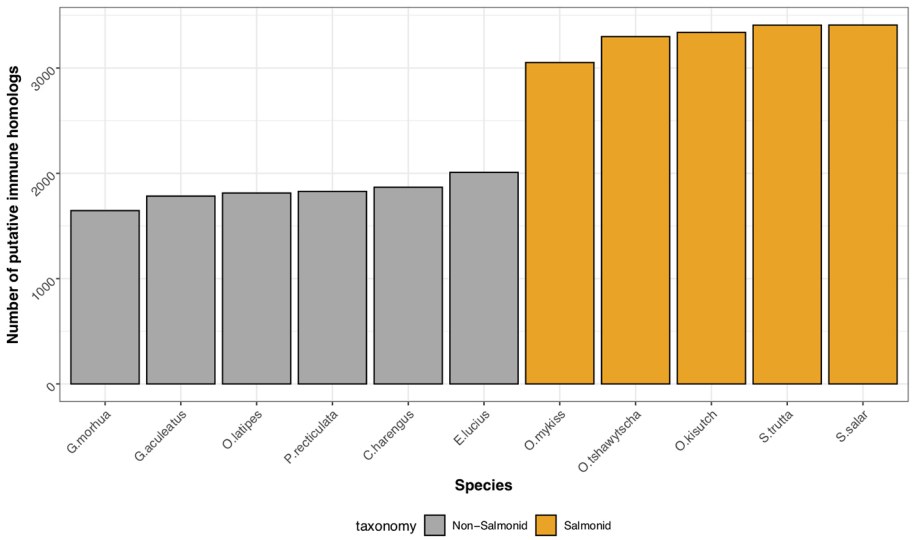

FIGURE 2 | Conservation of immune gene repertoire in salmonid genomes. Histogram displaying the number of putative immune genes found within representative genomes of salmonid (Atlantic salmon, *S. salar*; Brown trout, *S. trutta*, Rainbow trout, *O. mykiss*, Coho salmon, *O. kisutch*, Chinook salmon, *O. tshawytscha*), and non-salmonid teleost fish (Northern pike, *E. lucius*; Atlantic herring, *C. harengus*; guppy, *P. reticulata*; Japanese medaka, *O. latipes*; three-spined stickleback, *G. aculeatus*; Atlantic cod, *G. morhua*).

Assessment of Gene Loss in Brown Trout Immune Genes

Single copy genes present in salmonid genomes may be the result of adaptive loss or loss of a duplicated copy through neutral processes. First, using the reduced comparative dataset, we identified 4,297 single copy orthologs (SCOs) shared across the genomes of these six species. Of this number, 223 genes were annotated as putative immune genes but there was no evidence of significant enrichment of immune genes among all single copy orthologs ($X^2_{df=1} = 0.54, p = 0.46$) . We identified these genes as significantly enriched for the Gene Ontology term 'toll-like receptor signaling pathway' (GO:0002224). In total, these genes were identified as being significantly enriched (BH adjusted $p <$ 0.05) for 26 terms with the most significant terms per GO category being 'erythrocyte differentiation', 'immune response', 'complement activation' and 'cell chemotaxis'.

Sexual Dimorphic Immune Expression Evident Within Brown Trout Liver

Differences in Gene Expression Amplitude Between the Sexes

To investigate overall differences in gene expression between the sexes, we first performed a principal component analysis. Principal component 1 (PC1) accounted for 23% of the variance in the dataset with PC1 largely separating males and females providing evidence of sex-biased expression profiles evident in the brown trout liver (**Figure 6**). We also find additional variation within PC2, which is likely attributed to differences in genetic background between tanks. Second, through differential expression analysis, we identified 3,689 genes as significantly differentially expressed (BH adjusted p-value < 0.05) between the sexes (**Supplemental Information Table 10**). Of this number, the majority (n = 1,969) had a female-biased expression profile, which was a significant trend (binomial test, $p < 10^{-4}$). Differentially expressed genes between the sexes were significantly enriched for 12 Gene Ontology terms with the most significant per GO category being "nucleobase catabolic process" (GO:0046113), "phosphatidylethanolamine binding" (GO:0008429) and "nucleolus" (GO:0005730) (**Supplemental Information Tables 14-16**).

In relation to immune expression, we detected 83% of putative immune genes (n = 1,936 of 2,275) expressed in the liver. Of this number, we identified 269 genes as significantly differentially expressed (BH $p<$ 0.05, **Figure 7**, **Supplementary Information Table 10**) between the sexes. Thirty-five of these 269 genes were annotated as single copy immune orthologs in the brown trout genome. In contrast to the entire transcriptome, which generally demonstrated female-biased expression, we detected more immune genes with higher gene expression in males (n = 158), which was more than expected by chance (binomial test, $p < 0.03$). Male-biased immune genes were significantly enriched (Fisher's exact test; BH-adjusted $p < 0.05$) for 18 biological process-associated Gene Ontology terms, including 'erythrocyte development' (GO:0048821), 'hemopoiesis' (GO:0030097), and 'response to cytokine' (GO:0034097). For female-biased immune genes, we identified seven significantly enriched Gene Ontology terms associated with hemopoiesis and neutrophil differentiation.

Evidence of Alternative Splicing Between Sexes

We identified 218 intron clusters corresponding to 176 genes with evidence of significant alternative splicing (BH adjusted p-value < 0.05; **Supplemental Information Table 13**) between males and

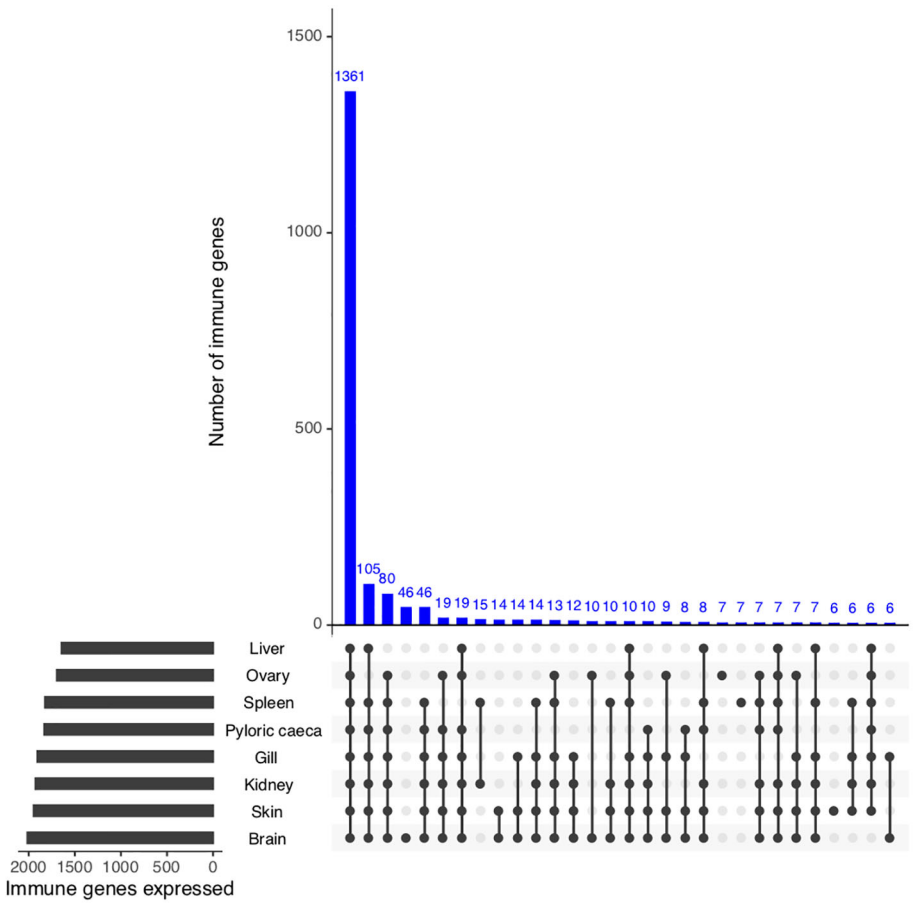

FIGURE 3 | Functional validation of *S. trutta* immune expression across tissues. UpSet plot of immune gene expression across eight tissue types in brown trout. For each tissue, the plot contains a bar chart displaying the total number of immune genes expressed per tissue, as well as a histogram displaying the number of genes identified as expressed across tissues.

females. Of this number, 55 were also significantly differentially expressed between the two sexes. We detected 15 alternatively spliced genes with roles in the salmonid immune system. Four of these genes were also differentially expressed between the sexes.

Conserved Sex-Biased Ohnolog Expression Among Immune Genes

We investigated if ohnologs demonstrated sex-biased gene expression and found 98 unique genes with sex-biased gene expression of which 12 ohnolog pairs exhibited significant differential expression for both genes (BH adjusted $p < 0.05$) between the sexes. For the majority (n = 10) of these ohnolog pairs, the ohnolog pairs have conserved differential expression whereby expression in both copies was elevated in the same sex compared to the other (n = 6 male-biased; n = 4 female-biased). Only for two ohnolog pairs did we identify differences in expression profiles between the ohnologs whereby the more conserved copies were all increased in males compared to females, but the less conserved copy had the opposite expression profile i.e., significantly reduced in males compared to females.

DISCUSSION

Migratory species, such as anadromous salmonids, require efficacious and adaptable immune systems to survive in a diversity of environments. Here we provide an important insight into the immune gene repertoire, as well as conservation and differences in gene expression across tissue types, for the facultatively anadromous brown trout *S. trutta*. Our findings indicate duplications and expansions of genes involved in immunological functions, such as chemotaxis and immune cell differentiation. Second, we assessed immune ohnologs for evidence of functional divergence in terms of domain architecture and gene expression profiles, identifying the majority to have conserved functional expression across tissue types in brown trout, while, surprisingly, only a few immune ohnolog pairs differed in terms of gene expression or the number of functional domains. We also identify evidence of immune gene loss in the salmonids. Lastly, we quantified sex-biased differences in immune gene expression in the brown trout liver, identifying the majority of differentially expressed immune

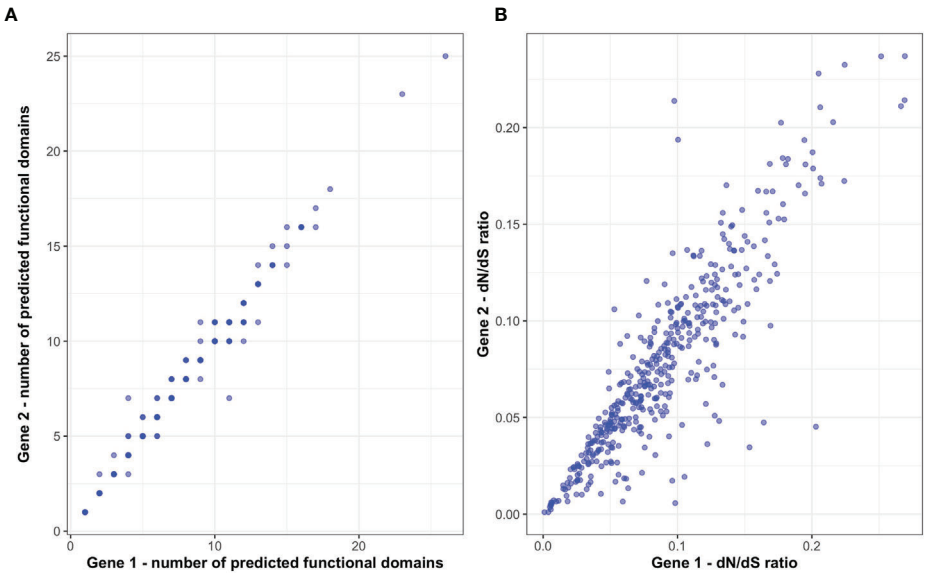

FIGURE 4 | Assessment of functional divergence between *S. trutta* immune ohnolog pairs. **(A)** The number of predicted functional domains within the predicted protein coded for by each immune ohnolog. **(B)** For each ohnolog, *dN/dS* ratios were calculated for each and their respective non-duplicated ortholog in Northern pike.

genes to have male-biased expression. Our findings provide a novel insight into the immune complement of an ecologically and commercially important salmonid.

Immune Gene Repertoire in Brown Trout: Retention and Expansion of Canonical Immune Genes

For teleost species that have undergone more recent whole genome duplication events, such as the salmonids, retention of duplicated genes may increase immune potential. In the brown trout genome, we identified high confidence orthologs for known canonical immune genes demonstrating that brown trout have essential genetic components of both innate and adaptive immune systems, as well as expansions (**Figures 1** and **2**). This number increases if we include protein homologs identified by OrthoFinder but additional synteny-based analyses would be required to confirm these genes as putative immune homologs. As our comparative analysis was mainly restricted to model species with well annotated immune repertoires, novel immune genes or genes highly diverged within the salmonids or restricted to *Salmo trutta* will not be reported. Gene expression analysis using eight available tissues indicates the vast majority of predicted immune genes as functional with expression evident across tissues (**Figure 3**). Retained duplicate copies were enriched for Gene Ontology terms associated with both innate and adaptive immunity. Among the most significantly enriched terms was neutrophil chemotaxis (**Figure 1**). Neutrophils are innate immune cells that are among the first responders to pathogen infection and inflammation and are a key aspect of the salmonid immune system. The response of these cells to chemical stimuli, known as chemotaxis, is important for the rapid response and subsequent migration of neutrophils to the site of signal origin (93). Neutrophils possess antimicrobial and phagocytic activity with the latter differing across teleost species (94). The expansion in brown trout of genes involved in chemotaxis may allow for the increased recognition of more diverse chemical stimulants, which may be beneficial for their migratory life-history that involves use of freshwater, brackish and marine environments.

Due to the complexity of the life-histories expressed by brown trout, immune repertoires are required for regulation and maintenance of immune expression during migration, an energetically stressful period, as well as to survive in both freshwater and marine environments, which can contain unique pathogenic threats (95). Variation in the strength of selection acting on duplicated genes can result in amino acid and/or regulatory divergence leading to the evolution of new functions or indeed, the process of pseudogenization and gene loss. Here, we found no significant difference in the overall number of functional domains between immune ohnologs in brown trout (**Figure 4**), as well as differences in expression profiles across tissues (**Figure 5**). However, for certain pairs, we did find evidence of domain architecture variation, as well as differences in expression profiles across tissues. We find variation in terms of functional domains for 42 pairs, and while future experimental validation is required, such pairs represent interesting candidates for investigating functional divergence in immune ohnologs. Similarly, 21 ohnolog pairs demonstrate divergence in gene expression profiles across eight tissues examined (**Figure 5**). As our analysis involved eight tissues rather than 15, which were previously used for Atlantic salmon (48) and rainbow trout (49), our power to detect divergent

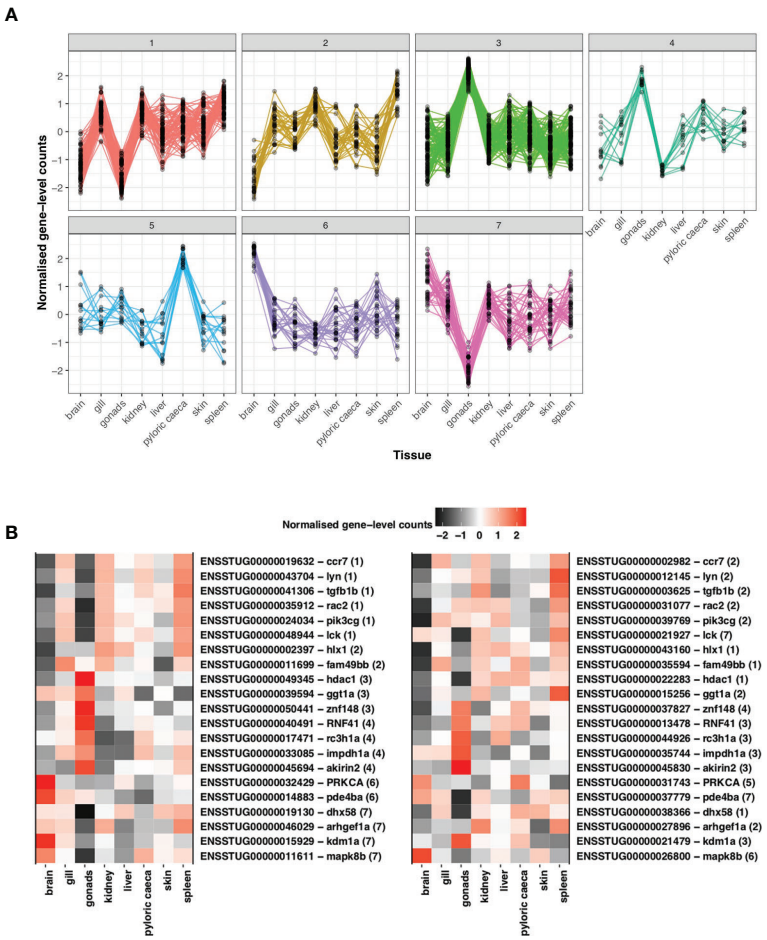

FIGURE 5 | Assessment of divergence in *S. trutta* immune ohnolog expression profiles. **(A)** Clustering based on gene-level counts assigned 302 immune genes, which consist of one member of an ohnolog pair, to seven co-expression networks assigned based on the expression profile of each gene across eight tissue types. Each co-expression cluster is represented by a single line graph whereby the y-axis consists of gene-level counts normalized by Clust and the x-axis consists of eight tissues obtained from a single double haploid female. **(B)** Heatmap of expression profiles for ohnolog pairs where both ohnologs were assigned to different co-expression networks based on expression profiles across eight tissue types. Ensembl gene ID and description (separated by hyphen) are provided on the y-axis with number in parentheses indicating the cluster the gene was assigned to. The x-axis represents the eight tissues used to construct the co-expression networks.

expression profiles may be reduced. Similarly, previous studies on salmonids explored conservation of ancestral function ohnologs through the construction of genome-wide co-expression networks, where one salmonid copy clustered by expression profile with that of a non-duplicated ortholog in the closely related, Northern pike, suggestive that one copy may retain and perform a conserved function across taxa. We did not explore such patterns in our analysis for brown trout due to the limited tissues available for both brown trout, of which only five were also available for Northern pike.

Of the ohnolog pairs with evidence of divergent gene expression profiles, such genes were annotated with a range of immunological function, including antiviral defense (*DHX58*, *zinc finger protein 148*), apoptosis (*RAC2*), inflammation regulation (*MAPK8*, *PDE4B, Roquin-1*), anti-microbial response (Akirin-2, *ARHGEF2*), T-cell activation (*LCK*, *HLX*) as well as tumor suppression (*PRKCA*, *FAM49B*, *IMPDH1*). Specific ohnolog pairs of interest included pairs where both genes were annotated as chemokine receptor type 7. In mammals, CC-chemokine receptor 7 (CCR7) is part of the G protein-coupled receptor family and can function in the activation of naive B and T lymphocytes with additional research suggesting the receptor may function in antiviral defense (96). In teleosts, the functions of chemokine receptors are less well understood but a CCR7 homolog has been previously characterized in the rainbow trout, *O. mykiss*, where based on sequence similarity, the predicted protein is suggested to perform a similar function to that of mammalian homologs (97, 98). The second ohnolog pair of interest were annotated as tyrosine-protein kinase Lyn. Lyn belongs to a Src- family of

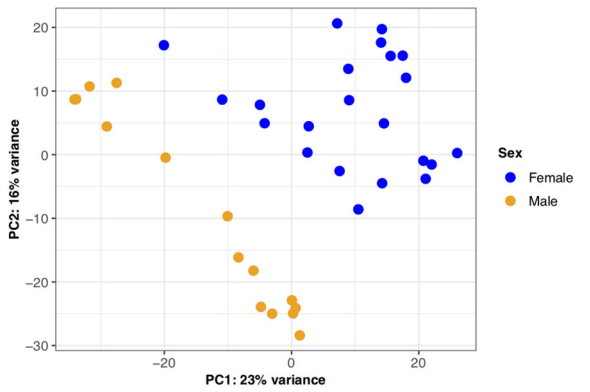

FIGURE 6 | Sexually dimorphic gene expression in *S. trutta* liver. Principal component analysis for gene-level counts revealed sexually dimorphic gene expression in *S. trutta* liver. Principal component (PC1) explained 23% of variance with males and females clearly separating. Each dot on the scatterplot represent a single individual sample and are color-coded by sex (female = blue; male = orange).

tyrosine kinases found in immune cells that can negatively regulate important signaling pathways (99). The gene is also a key mediator of pathways involved in B cell activation (99, 100) a function suggested as conserved in teleosts (101).

While extensive retention and functional divergence of ohnologs have been characterized in other salmonids, gene loss can also occur. Two primary molecular processes can lead to gene loss: as a consequence of an abrupt mutational event, such as an error in crossing over during meiosis, or through the slow accumulation of mutations during pseudogenization after an initial loss-of-function mutation (12). Comparative genomic studies have revealed biased patterns in gene loss in terms of functional bias with genes involved in certain cellular processes, such as DNA repair and transcription, more likely to be represented among genes where a copy has been lost (102, 103). In relation to WGD events, there is also evidence of genomic positional biases in terms of gene loss (104). Clusters of single copies may be due to reliance on similar transcriptional regulation machinery or architecture. Here through comparative analyses, we find gene loss conserved across salmonids. The conservation of synteny across salmonid genomes would suggest that loss of putative immune genes is non-random, as has been shown for other species (12). Future work will benefit from understanding the molecular, cellular and evolutionary consequences of gene loss in these species.

Sexual Dimorphism in Trout Immune Expression

Sexes share largely the same genome but express it differently giving rise to different morphological and behavioral phenotypes. Here we investigated differences in gene expression in the liver, an organ

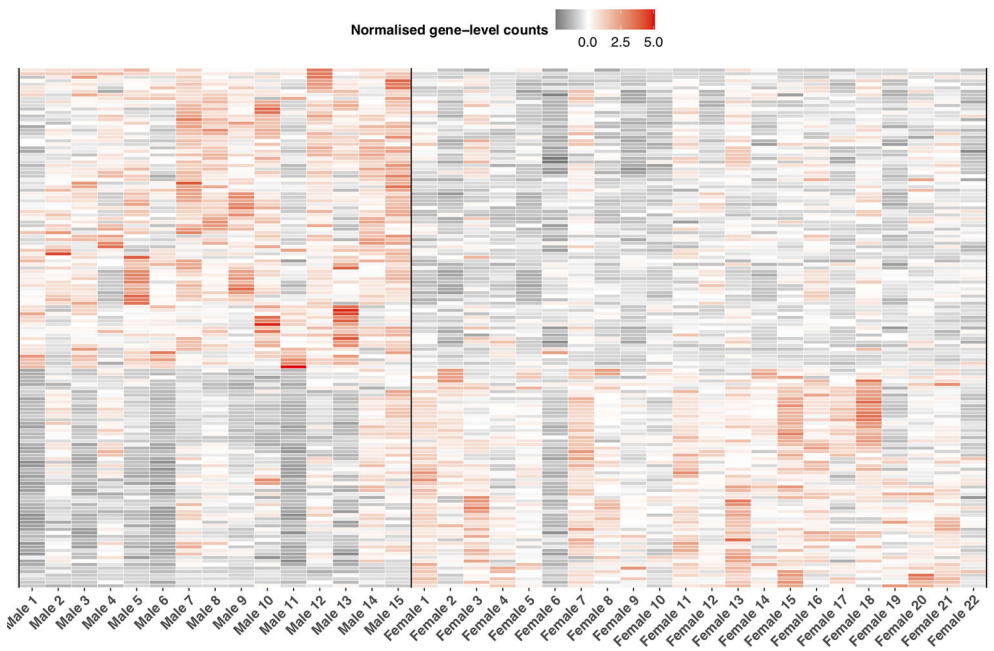

FIGURE 7 | Sexually dimorphic immune expression in *S. trutta* liver. Heatmap displaying significantly differentially expressed immune genes between the sexes. Relative variation in immune gene expression is represented by a color gradient (gray = low, white = medium, red = high). Each column represents an individual trout with a vertical black line separating male from female samples. Each row represents expression level for an individual immune gene.

previously used to understand salmonid metabolism gene expression (51), response to environmental stressors (105), as well as genes underlying sexual dimorphism (106). While the liver may have traditional roles in metabolism and antioxidant activity, a growing body of literature on mammalian and teleost immunology has provided important insights into the role of the liver in the innate immune response, immune tolerance and hematopoiesis (74, 107–112), as well as creating hostile molecular environments for parasites to migrate through (113, 114). Here we identified differential immune gene expression both in terms of expression amplitude (**Figures 6, 7**) and splicing between the sexes. Immune genes exhibited a general male-bias in expression, which was in contrast to overall gene expression in the liver being female-biased. Immunological studies on sex differences in immune function in brown trout have suggested reduced immune function in mature males (115, 116), and therefore, females would have been expected to have higher immune gene expression compared to males. While our fish were laboratory reared and not directly immune challenged, they were maintained in normal lab environments (i.e., clean but not sterile) and therefore, we would expect a background level of immune gene expression. Sex-biased differences in expression could be due to anticipation of immune challenge. As male brown trout are less likely to undergo sea migration, remaining resident and completing their life-cycle in freshwater environments, pathogens present in freshwater environments are more likely to encounter males than females and therefore, parasite-mediated selection in brown trout may result in variation in environment-dependent immune expression between sexes. Indeed, males do suffer more severe infestations by freshwater ectoparasites in comparison to females (117), yet our understanding of immune potential and function is lacking.

An interesting finding among the genes with sex-biased differences was the presence of putative single copy orthologs. As sexes largely share the same genome but have different fitness optima and may express some genes differently, this can result in sexually antagonistic loci, which increase fitness when expressed in one sex but are detrimental in the other. Sex-biased gene expression has been suggested as a mechanism to resolve such conflict (118, 119). Aside from transcriptional regulation, modifications in genomic architecture, such as sex-dependent dominance (120), maintenance of sexually antagonistic loci on sex chromosomes (121) or duplication events (122, 123) may also resolve conflict. It is interesting therefore that since the salmonid WGD, duplicate copies of immune genes have been lost either through adaptive or neutral processes that may now be sexually antagonistic. The application of population genetic approaches, in combination with sex-biased gene expression, have been used to reveal genomic signatures of loci associated with sexual conflict (118, 124), which could be applied to future studies in brown trout and other salmonids to provide important insights into the evolutionary processes shaping sex differences.

CONCLUSION

Salmonid genomics is a rapidly advancing field and is providing comprehensive insights into genes underlying phenotypically plastic traits, such as sea age at maturity, as well as genomic structures resolving sexually antagonistic loci (28, 120). Here we explore the consequences of a salmonid-specific WGD on immune gene repertoire in brown trout, finding that brown trout has an enlarged immune gene complement relative to non-salmonids, with many immune ohnologs retained that have conserved immune expression profiles between the pairs. We find preliminary signatures of some ohnologs coding for proteins that may have potential divergent functions between the pairs, but functional validation is required to determine the exact role these genes may play in the brown trout immune system. Lastly, we add to a growing body of research that explores key physiological differences among the sexes through the identification of differences in immune expression.

Our findings provide important insights into immune gene evolution and expression in a culturally, economically and ecologically important species. Like many species, brown trout face an uncertain future due to changing climates with increasing temperatures potentially leading to reduced sea migration rates (82) as well as potentially impacting immune function (125) while pathogens, such as sea lice, associated with increasing aquaculture, are also suggested to contribute to migratory declines (126). Improved understanding of immune potential, expression and function may benefit management strategies and conservation schemes for wild populations to assist in the maintenance of at-risk facultatively anadromous populations.

DATA AVAILABILITY STATEMENT

Raw sequence data files are deposited in the NCBI short read archive (BioProject ID: PRJNA667168). Scripts underpinning the data analysis are archived on GitHub (https://github.com/Joscolgan/salmonid_immune_study). Raw read counts used in the present analyses are provided as tables in **Supplementary Information**.

ETHICS STATEMENT

The animal study was reviewed and approved by This study was carried out in accordance with the recommendations of the Health Products Regulatory Authority (HPRA) Ireland, under HPRA project license AE19130/P034, and HPRA individual licenses AE19130/I087, AE19130/I200, AE19130/I201, and AE19130/I202.

AUTHOR CONTRIBUTIONS

TC, PAM, PMcG, and TR designed the experiment. LA, RW, and SH harvested the liver samples. TC performed the RNA extractions and quality checks. TC performed the majority of analyses. All authors contributed to the article and approved the submitted version.

FUNDING

This research was supported by an ERC Starting Grant (639192-ALH) and an SFI ERC Support Award awarded to TR. PMcG was funded by an SFI-DEL grant (2015 15/IA/3028) and the Marine Research Programme 2014–2020 RESPI/FS/16/01 (Marine Institute).

ACKNOWLEDGMENTS

The authors would like to thank Brian Clarke, Dr. Deirdre Cotter, members of the FishEyE team at UCC, and the staff of Inland Fisheries Ireland (in particular Dr. Paddy Gargan) and the Marine Institute (in particular Dr. Russell Poole) for obtaining brood stock and for assistance in fish rearing. We also thank Luke Harman in particular for his invaluable role in designing and building a recirculating aquaculture system, and Ronan O'Sullivan and Dr. Adam Kane for assistance in fish maintenance. We thank Dr. Jamie Coughlan for genotyping fish, Dr. Eileen Dillane with assistance in logistics and Profs Tom Cross and Paulo Prodöhl for discussion on brown trout genomics. We also thank the editor and two reviewers for the beneficial and insightful comments that have greatly improved this manuscript.

SUPPLEMENTARY MATERIAL

The Supplementary Material for this article can be found online at: https://www.frontiersin.org/articles/10.3389/fimmu.2021.568729/full#supplementary-material

REFERENCES

1. Altizer S, Bartel R, Han BA. Animal migration and infectious disease risk. *Science* (2011) 331:296–302. doi: 10.1126/science.1194694
2. Eikenaar C, Hegemann A, Packmor F, Kleudgen I, Isaksson C. Not just fuel: energy stores are correlated with immune function and oxidative damage in a long-distance migrant. *Curr Zool* (2020) 66:21–8. doi: 10.1093/cz/zoz009
3. Eikenaar C, Hegemann A. Migratory common blackbirds have lower innate immune function during autumn migration than resident conspecifics. *Biol Lett* (2016) 12:20160078. doi: 10.1098/rsbl.2016.0078
4. Waldenström J, Bensch S, Kiboi S, Hasselquist D, Ottosson U. Cross-species infection of blood parasites between resident and migratory songbirds in Africa. *Mol Ecol* (2002) 11:1545–54. doi: 10.1046/j.1365-294X.2002.01523.x
5. MacKenzie K. Parasites as biological tags in population studies of marine organisms: an update. *Parasitology* (2002) 124:153–63. doi: 10.1017/S0031182002001518
6. Renshaw SA, Trede NS. A model 450 million years in the making: zebrafish and vertebrateimmunity. *Dis Model Mech* (2012) 5:38–47. doi: 10.1242/dmm.007138
7. Pancer Z, Cooper MD. The evolution of adaptive immunity. *Annu RevImmunol* (2006) 24:497–518. doi: 10.1146/annurev.immunol.24.021605.090542
8. Shultz AJ, Sackton TB. Immune genes are hotspots of shared positive selection across birds and mammals. *Elife* (2019) 8:e41815. doi: 10.7554/eLife.41815
9. Kosiol C, Vinar T, da Fonseca RR, Hubisz MJ, Bustamante CD, Nielsen R, et al. Patterns of positive selection in six mammaliangenomes. *PLoS Genet* (2008) 4:e1000144. doi: 10.1371/journal.pgen.1000144
10. Flajnik MF, Kasahara M. Origin and evolution of the adaptive immune system: genetic eventsand selective pressures. *Nat Rev Genet* (2010) 11:47–59. doi: 10.1038/nrg2703
11. Balakirev ES, Ayala FJ. Pseudogenes: Are they "junk" or functional DNA? *Annu Rev Genet* (2003) 37:123–51. doi: 10.1146/annurev.genet.37.040103.103949
12. Albalat R, Cañestro C. Evolution by gene loss. *Nat Rev Genet* (2016) 17:379–91. doi: 10.1038/nrg.2016.39
13. Sharma V, Hecker N, Roscito JG, Foerster L, Langer BE, Hiller M. A genomics approach reveals insights into the importance of genelosses for mammalian adaptations. *Nat Commun* (2018) 9:1215. doi: 10.1038/s41467-018-03667-1
14. Solbakken MH, Rise ML, Jakobsen KS, Jentoft S. Successive losses of central immune genes characterize the Gadiformes' alternate immunity. *Genome Biol Evol* (2016) 8:3508–15. doi: 10.1093/gbe/evw250
15. Wang X, Grus WE, Zhang J. Gene losses during human origins. *PLoS Biol* (2006) 4:e52. doi: 10.1371/journal.pbio.0040052
16. Glasauer SMK, Neuhauss SCF. Whole-genome duplication in teleost fishes and its evolutionaryconsequences. *Mol Genet Genomics* (2014) 289:1045–60. doi: 10.1007/s00438-014-0889-2
17. Sadd BM, Schmid-Hempel P. Principles of ecological immunology. *EvolAppl* (2008) 2:113–21. doi: 10.1111/j.1752-4571.2008.00057.x
18. Nunn CL, Lindenfors P, Pursall ER, Rolff J. On sexual dimorphism in immune function. *Philos Trans R Soc Lond B Biol Sci* (2009) 364:61–9. doi: 10.1098/rstb.2008.0148
19. Zuk M, Stoehr AM. Immune defense and host life history. *Am Nat* (2002) 160 Suppl4:S9–S22. doi: 10.1086/342131
20. Møller AP, Sorci G, Erritzøe J. Sexual dimorphism in immune defense. *Am Nat* (1998) 152:605–19. doi: 10.1086/286193
21. Rolff J, Armitage SAO, Coltman DW. Genetic constraints and sexual dimorphism in immune defense. *Evolution* (2005) 59:1844–50. doi: 10.1111/j.0014-3820.2005.tb01831.x
22. Gal-Oz ST, Maier B, Yoshida H, Seddu K, Elbaz N, Czysz C, et al. ImmGen report: sexual dimorphism in the immune system transcriptome. *Nat Commun* (2019) 10:4295. doi: 10.1038/s41467-019-12348-6
23. Lawniczak MKN, Barnes AI, Linklater JR, Boone JM, Wigby S, Chapman T. Mating and immunity in invertebrates. *Trends Ecol Evol* (2007) 22:48–55. doi: 10.1016/j.tree.2006.09.012
24. Vincent CM, Gwynne DT. Sex-biased immunity is driven by relative differences in reproductive investment. *Proc R Soc B Biol Sci* (2014) 281:20140333. doi: 10.1098/rspb.2014.0333
25. Chapman BB, Brönmark C, Nilsson J-Å, Hansson L-A. The ecology and evolution of partial migration. *Oikos* (2011) 120:1764–75. doi: 10.1111/j.1600-0706.2011.20131.x
26. Morbey YE, Ydenberg RC. Protandrous arrival timing to breeding areas: areview. *Ecol Lett* (2001) 4:663–73. doi: 10.1046/j.1461-0248.2001.00265.x
27. Quinn TP, McGinnity P, Reed TE. The paradox of "premature migration" by adult anadromoussalmonid fishes: patterns and hypotheses. *Can J Fish Aquat Sci* (2016) 73:1015–30. doi: 10.1139/cjfas-2015-0345
28. Pearse DE, Barson NJ, Nome T, Gao G, Campbell MA, Abadía-Cardoso A, et al. Sex-dependent dominance maintains migration supergene in rainbowtrout. *Nat Ecol Evol* (2019) 3:1731–42. doi: 10.1038/s41559-019-1044-6
29. Fish EN. The X-files in immunity: sex-based differences predispose immuneresponses. *Nat Rev Immunol* (2008) 8:737–44. doi: 10.1038/nri2394
30. Rinn JL, Snyder M. Sexual dimorphism in mammalian gene expression.*Trends Genet* (2005) 21:298–305. doi: 10.1016/j.tig.2005.03.005
31. Krasnov A, Wesmajervi Breiland MS, Hatlen B, Afanasyev S, Skugor S. Sexual maturation and administration of 17β-estradiol and testosterone induce complex gene expression changes in skin and increase resistance of Atlantic salmon to ectoparasite salmon louse. *Gen Comp Endocrinol* (2015) 212:34–43. doi: 10.1016/j.ygcen.2015.01.002
32. Zheng W, Xu H, Lam SH, Luo H, Karuturi RKM, Gong Z. Transcriptomic analyses of sexual dimorphism of the zebrafish liver and the effect of sex hormones. *PLoS One* (2013) 8:e53562. doi: 10.1371/journal.pone.0053562
33. Melé M, Ferreira PG, Reverter F, DeLuca DS. The human transcriptome across tissues and individuals. *Science* (2015) 348:660–5. doi: 10.1126/science.aaa0355

34. Yang X, Schadt EE, Wang S, Wang H, Arnold AP, Ingram-Drake L, et al. Tissue-specific expression and regulation of sexually dimorphic genes in mice. *Genome Res* (2006) 16:995–1004. doi: 10.1101/gr.5217506
35. Kopp A, Duncan I, Godt D, Carroll SB. Genetic control and evolution of sexually dimorphic characters in *Drosophila*. *Nature* (2000) 408:553–9. doi: 10.1038/35046017
36. Markle JG, Fish EN. SeXX matters in immunity. *Trends Immunol* (2014) 35:97–104. doi: 10.1016/j.it.2013.10.006
37. Waples RS, Naish KA, Primmer CR. Conservation and management of salmon in the age of genomics. *Annu Rev Anim Biosci* (2020) 8:117–43. doi: 10.1146/annurev-animal-021419-083617
38. Nelson JS, Grande TC, Wilson MVH. *Fishes of the world*. Hoboken, New Jersey, USA: John Wiley & Sons (2016).
39. Quinn TP, Myers KW. Anadromy and the marine migrations of Pacific salmon and trout: Rounsefell revisited. *Rev Fish Biol Fish* (2004) 14:421–42. doi: 10.1007/s11160-005-0802-5
40. Curry RA, Bernatchez L, Whoriskey F, Audet C. The origins and persistence of anadromy in brook charr. *Rev Fish Biol Fish* (2010) 20:557–70. doi: 10.1007/s11160-010-9160-z
41. Dodson JJ, Aubin-Horth N, Thériault V, Páez DJ. The evolutionary ecology of alternative migratory tactics in salmonid fishes. *Biol Rev Camb Philos Soc* (2013) 88:602–25. doi: 10.1111/brv.12019
42. Ferguson A, Reed TE, Cross TF, McGinnity P, Prodöhl PA. Anadromy, potamodromy and residency in brown trout *Salmotrutta*: the role of genes and the environment. *J Fish Biol* (2019) 95:692–718. doi: 10.1111/jfb.14005
43. Kendall NW, McMillan JR, Sloat MR, Buehrens TW, Quinn TP, Pess GR, et al. Anadromy and residency in steelhead and rainbow trout (*Oncorhynchus mykiss*): a review of the processes and patterns. *Can J Fish Aquat Sci* (2015) 72:319–42. doi: 10.1139/cjfas-2014-0192
44. Hutchings JA, Jones MEB. Life history variation and growth rate thresholds for maturity in Atlantic salmon, Salmo salar. *Can J Fish Aquat Sci* (1998) 55:22–47. doi: 10.1139/d98-004
45. Ohms HA, Sloat MR, Reeves GH, Jordan CE, Dunham JB. Influence of sex, migration distance, and latitude on life historyexpression in steelhead and rainbow trout (*Oncorhynchus mykiss*). *Can J Fish Aquat Sci* (2014) 71:70–80. doi: 10.1139/cjfas-2013-0274
46. Morita K, Tamate T, Kuroki M, Nagasawa T. Temperature-dependent variation in alternative migratory tactics andits implications for fitness and population dynamics in a salmonid fish. *J Anim Ecol* (2014) 83:1268–78. doi: 10.1111/1365-2656.12240
47. Macqueen DJ, Johnston IA. A well-constrained estimate for the timing of the salmonid whole genome duplication reveals major decoupling from species diversification. *Proc Biol Sci* (2014) 281:20132881. doi: 10.1098/rspb.2013.2881
48. Lien S, Koop BF, Sandve SR, Miller JR, Kent MP, Nome T, et al. The Atlantic salmon genome provides insights into rediploidization. *Nature* (2016) 533:200–5. doi: 10.1038/nature17164
49. Berthelot C, Brunet F, Chalopin D, Juanchich A, Bernard M, Noël B, et al. The rainbow trout genome provides novel insights into evolution after whole-genome duplication in vertebrates. *Nat Commun* (2014) 5:3657. doi: 10.1038/ncomms4657
50. Robertson FM, Gundappa MK, Grammes F, Hvidsten TR, Redmond AK, Lien S, et al. Lineage-specific rediploidization is a mechanism to explain time-lags between genome duplication and evolutionary diversification. *Genome Biol* (2017) 18:111. doi: 10.1186/s13059-017-1241-z
51. Gillard G, Harvey TN, Gjuvsland A, Jin Y, Thomassen M, Lien S, et al. Life-stage-associated remodelling of lipid metabolism regulation in Atlantic salmon. *Mol Ecol* (2018) 27:1200–13. doi: 10.1111/mec.14533
52. Macqueen DJ, Primmer CR, Houston RD, Nowak BF, Bernatchez L, Bergseth S, et al. Functional Annotation of All Salmonid Genomes (FAASG): an international initiative supporting future salmonid research, conservation and aquaculture. *BMC Genomics* (2017) 18:484. doi: 10.1101/095737
53. Wang T, Hu Y, Wangkahart E, Liu F, Wang A, Zahran E, et al. Interleukin (IL)-2 Is a key regulator of T Helper 1 and T Helper 2 cytokine expression in fish: Functional characterization of two divergent IL2 paralogs in salmonids. *Front Immunol* (2018) 9:1683. doi: 10.3389/fimmu.2018.01683
54. Wang J, Liu M, Wu Y, Yoon S, Alnabulsi A, Liu F, et al. Immune-modulation of two BATF3 paralogues in rainbow trout *Oncorhynchus mykiss*. *Mol Immunol* (2018) 99:104–14. doi: 10.1016/j.molimm.2018.04.016
55. Lee PT, Zou J, Holland JW, Martin SAM, Kanellos T, Secombes CJ. Identification and characterization of TLR7, TLR8a2, TLR8b1 and TLR8b2 genes in Atlantic salmon (*Salmo salar*). *Dev Comp Immunol* (2013) 41:295–305. doi: 10.1016/j.dci.2013.05.013
56. Xu Q, Li R, Monte MM, Jiang Y, Nie P, Holland JW, et al. Sequence and expression analysis of rainbow trout CXCR2, CXCR3a and CXCR3b aids interpretation of lineage-specific conversion, loss and expansion of these receptors during vertebrate evolution. *Dev Comp Immunol* (2014) 45:201–13. doi: 10.1016/j.dci.2014.03.002
57. Penston MJ, McKibben MA, Hay DW, Gillibrand PA. Observations on open-water densities of sea lice larvae in LochShieldaig, Western Scotland. *Aquac Res* (2004) 35:793–805. doi: 10.1111/j.1365-2109.2004.01102.x
58. McVicar AH, Sharp LA, Walker AF, Pike AW. Diseases of wild sea trout in Scotland in relation to fishpopulation decline. *Fish Res* (1993)17:175–85. doi: 10.1016/0165-7836(93)90017-2
59. Poole WR, Whelan KF, Dillane MG, Cooke DJ, Matthews M. The performance of sea trout, *Salmo trutta* L.,stocks from the Burrishoole system western Ireland, 1970–1994. *FishManag Ecol* (1996) 3:73–92. doi: 10.1111/j.1365-2400.1996.tb00131.x
60. Schmid-Hempel P. Variation in immune defence as a question of evolutionaryecology. *Proc Biol Sci* (2003) 270:357–66. doi: 10.1098/rspb.2002.2265
61. Heymann F, Tacke F. Immunology in the liver—from homeostasis todisease. *Nat Rev Gastroenterol Hepatol* (2016) 13:88. doi: 10.1038/nrgastro.2015.200
62. Magnadottir B, Lange S, Gudmundsdottir S, Bøgwald J, Dalmo RA. Ontogeny of humoral immune parameters in fish. *Fish Shellfish Immunol* (2005) 19:429–39. doi: 10.1016/j.fsi.2005.03.010
63. Ruzicka L, Howe DG, Ramachandran S, Toro S, Van Slyke CE, Bradford YM, et al. The Zebrafish Information Network: new support for non-coding genes, richer Gene Ontology annotations and the Alliance of Genome Resources. *Nucleic Acids Res* (2019) 47:D867–73. doi: 10.1093/nar/gky1090
64. Bult CJ, Blake JA, Smith CL, Kadin JA, Richardson JE. Mouse Genome Database Group. Mouse Genome Database (MGD) 2019. *Nucleic Acids Res* (2019) 47:D801–6. doi: 10.1093/nar/gky1056
65. Bhattacharya S, Dunn P, Thomas CG, Smith B, Schaefer H, Chen J, et al. ImmPort, toward repurposing of open access immunological assay data for translational and clinical research. *Sci Data* (2018) 5:180015.a. doi: 10.1038/sdata.2018.15
66. Durinck S, Spellman PT, Birney E, Huber W. Mapping identifiers for the integration of genomic datasets with the R/Bioconductor package biomaRt. *Nat Protoc* (2009) 4:1184–91. doi: 10.1038/nprot.2009.97
67. Kinsella RJ, Kähäri A, Haider S, Zamora J, Proctor G, Spudich G, et al. Ensembl BioMarts: a hub for data retrieval across taxonomic space. *Database* (2011) 2011:bar030. doi: 10.1093/database/bar030
68. Emms DM, Kelly S. OrthoFinder: solving fundamental biases in whole genome comparisons dramatically improves orthogroup inference accuracy. *Genome Biol* (2015) 16:157. doi: 10.1186/s13059-015-0721-2
69. Emms DM, Kelly S. OrthoFinder: phylogenetic orthology inference for comparative genomics. *Genome Biol* (2019) 20:238. doi: 10.1186/s13059-019-1832-y
70. Rondeau EB, Minkley DR, Leong JS, Messmer AM, Jantzen JR, von Schalburg KR, et al. The genome and linkage map of the Northern pike (*Esox lucius*): Conserved synteny revealed between the salmonid sister group and the Neoteleostei. *PLoS One* (2014) 9:e102089. doi: 10.1371/journal.pone.0102089
71. Patro R, Duggal G, Love MI, Irizarry RA, Kingsford C. Salmon provides fast and bias-aware quantification of transcript expression. *Nat Methods* (2017) 14:417–9. doi: 10.1038/nmeth.4197
72. Soneson C, Love MI, Robinson MD. Differential analyses for RNA-seq: transcript-level estimates improve gene-level inferences. *F1000Res* (2015) 4:1521. doi: 10.12688/f1000research.7563.1
73. Love MI, Huber W, Anders S. Moderated estimation of fold change and dispersion for RNA-seq data with DESeq2. *Genome Biol* (2014) 15:550. doi: 10.1186/s13059-014-0550-8
74. Bertolotti AC, Layer RM, Gundappa MK, Gallagher MD, Pehlivanoglu E, Nome T, et al. The structural variation landscape in 492 Atlantic salmon genomes. *Nat Commun* (2020) 11:1–16. doi: 10.1038/s41467-020-18972-x
75. Rice P, Longden I, Bleasby A. EMBOSS: the European Molecular Biology Open Software Suite. *Trends Genet* (2000) 16:276–7. doi: 10.1016/S0168-9525(00)02024-2

76. Abu-Jamous B, Kelly S. Clust: automatic extraction of optimal co-expressed gene clusters from gene expression data. *Genome Biol* (2018) 19:172. doi: 10.1186/s13059-018-1536-8
77. Campbell MA, Hale MC, McKinney GJ, Nichols KM, Pearse DE. Long-term conservation of ohnologs through partial tetrasomy following whole-genome duplication in Salmonidae. *G3* (2019) 9(6):2017–28. doi: 10.1534/g3.119.400070
78. Sievers F, Wilm A, Dineen D, Gibson TJ, Karplus K, Li W, et al. Fast, scalable generation of high-quality protein multiple sequence alignments using Clustal Omega. *Mol Syst Biol* (2011) 7:539. doi: 10.1038/msb.2011.75
79. Suyama M, Torrents D, Bork P. PAL2NAL: robust conversion of protein sequence alignments into the corresponding codon alignments. *Nucleic Acids Res* (2006) 34:W609–12. doi: 10.1093/nar/gkl315
80. Yang Z. PAML 4: phylogenetic analysis by maximum likelihood. *Mol Biol Evol* (2007) 24:1586–91. doi: 10.1093/molbev/msm088
81. Archer LC, Hutton SA, Harman L, O'Grady MN, Kerry JP, Russell Poole W, et al. The interplay between extrinsic and intrinsic factors in determining migration decisions in brown trout (*Salmo trutta*): An experimental study. *Front Ecol Evol* (2019) 7:222. doi: 10.3389/fevo.2019.00222
82. Archer LC, Hutton SA, Harman L, McCormick SD, O'Grady MN, Kerry JP, et al. Food and temperature stressors have opposing effects in determining flexible migration decisions in brown trout (*Salmo trutta*). *Glob Chang Biol* (2020) 26:2878–96. doi: 10.1111/gcb.14990
83. Andrews S. FastQC: a quality control tool for high throughput sequence data. In: *Reference Source* (2010). Available at: http://www.bioinformatics.babraham.ac.uk/projects/fastqc/.
84. Dobin A, Davis CA, Schlesinger F, Drenkow J, Zaleski C, Jha S, et al. STAR: ultrafast universal RNA-seq aligner. *Bioinformatics* (2013) 29:15–21. doi: 10.1093/bioinformatics/bts635
85. Li H, Handsaker B, Wysoker A, Fennell T, Ruan J, Homer N, et al. 1000 Genome Project Data Processing Subgroup. The Sequence Alignment/Map format and SAMtools. *Bioinformatics* (2009) 25:2078–9. doi: 10.1093/bioinformatics/btp352
86. García-Alcalde F, Okonechnikov K, Carbonell J, Cruz LM, Götz S, Tarazona S, et al. Qualimap: evaluating next-generation sequencing alignment data. *Bioinformatics* (2012) 28:2678–9. doi: 10.1093/bioinformatics/bts503
87. Ewels P, Magnusson M, Lundin S, Käller M. MultiQC: summarize analysis results for multiple tools and samples in a single report. *Bioinformatics* (2016) 32:3047–8. doi: 10.1093/bioinformatics/btw354
88. Anders S, Pyl PT, Huber W. HTSeq–a Python framework to work with high-throughput sequencing data. *Bioinformatics* (2015) 31:166–9. doi: 10.1093/bioinformatics/btu638
89. Sahraeian SME, Mohiyuddin M, Sebra R, Tilgner H, Afshar PT, Au KF, et al. Gaining comprehensive biological insight into the transcriptome by performing a broad-spectrum RNA-seq analysis. *Nat Commun* (2017) 8:59. doi: 10.1038/s41467-017-00050-4
90. Li YI, Knowles DA, Humphrey J, Barbeira AN, Dickinson SP, Im HK, et al. Annotation-free quantification of RNA splicing using LeafCutter. *Nat Genet* (2018) 50:151–8. doi: 10.1038/s41588-017-0004-9
91. Colgan TJ, Fletcher IK, Arce AN, Gill RJ, Rodrigues AR, Stolle E, et al. Caste- and pesticide-specific effects of neonicotinoid pesticide exposure on gene expression in bumblebees. *Mol Ecol* (2019) 28(8):1964–74. doi: 10.1111/mec.15047
92. Alexa A, Rahnenfuhrer J. "topGO: Enrichment analysis for Gene Ontology. R package version 2.28. 0". In: *Cranio* (2016).
93. Nuzzi PA, Lokuta MA, Huttenlocher A. Analysis of neutrophil chemotaxis. *Methods Mol Biol* (2007) 370:23–36. doi: 10.1385/1-59745-353-6:23
94. Øverland HS, Pettersen EF, Rønneseth A, Wergeland HI. Phagocytosis by B-cells and neutrophils in Atlantic salmon (*Salmo salar* L.) and Atlantic cod (*Gadus morhua* L.). *Fish Shellfish Immunol* (2010) 28:193–204. doi: 10.1016/j.fsi.2009.10.021
95. Molloy S, Holland C, Poole R. Helminth parasites of brown and sea trout *Salmo trutta* L. from the west coast of Ireland. *Biol Environ Proc R Ir Acad* (1993) 93B:137–42.
96. Yoshida R, Imai T, Hieshima K, Kusuda J, Baba M, Kitaura M, et al. Molecular cloning of a novel human CC chemokine EBI1-ligand chemokine that is a specific functional ligand for EBI1, CCR7. *J Biol Chem* (1997) 272:13803–9. doi: 10.1074/jbc.272.21.13803
97. Bird S, Tafalla C. Teleost chemokines and their receptors. *Biology* (2015) 4:756–84. doi: 10.3390/biology4040756
98. Daniels GD, Zou J, Charlemagne J, Partula S, Cunningham C, Secombes CJ. Cloning of two chemokine receptor homologs (CXC-R4 andCC-R7) in rainbow trout *Oncorhynchus mykiss*. *J Leukoc Biol* (1999) 65:684–90. doi: 10.1002/jlb.65.5.684
99. Xu Y, Harder KW, Huntington ND, Hibbs ML, Tarlinton DM. Lyn tyrosine kinase: accentuating the positive and the negative. *Immunity* (2005) 22:9–18. doi: 10.1016/S1074-7613(04)00381-4
100. Hibbs ML, Tarlinton DM, Armes J, Grail D, Hodgson G, Maglitto R, et al. Multiple defects in the immune system of Lyn-deficient mice, culminating in autoimmune disease. *Cell* (1995) 83:301–11. doi: 10.1016/0092-8674(95)90171-X
101. Wu L, Kong L, Yang Y, Bian X, Wu S, Li B, et al. Effects of cell differentiation on the phagocytic activities of IgM+ B cells in a teleost fish. *Front Immunol* (2019) 10:2225. doi: 10.3389/fimmu.2019.02225
102. De Smet R, Adams KL, Vandepoele K, Van Montagu MCE, Maere S, Van de Peer Y. Convergent gene loss following gene and genome duplications creates single-copy families in flowering plants. *Proc Natl Acad Sci U S A* (2013) 110:2898–903. doi: 10.1073/pnas.1300127110
103. Librado P, Vieira FG, Sánchez-Gracia A, Kolokotronis S-O, Rozas J. Mycobacterial phylogenomics: An enhanced method for gene turnover analysis reveals uneven levels of gene gain and loss among species and gene families. *Genome Biol Evol* (2014) 6:1454–65. doi: 10.1093/gbe/evu117
104. Liu S, Liu Y, Yang X, Tong C, Edwards D, Parkin IAP, et al. The *Brassica oleracea* genome reveals theasymmetrical evolution of polyploid genomes. *Nat Commun* (2014) 5:3930. doi: 10.1038/ncomms4930
105. Webster TMU, Uren Webster TM, Santos EM. Global transcriptomic profiling demonstrates induction of oxidative stress and of compensatory cellular stress responses in brown trout exposed to glyphosate and Roundup. *BMC Genomics* (2015) 16:32. doi: 10.1186/s12864-015-1254-5
106. Sutherland BJG, Prokkola JM, Audet C, Bernatchez L. Sex-specific co-expression networks and sex-biased gene expression in the salmonid Brook Charr *Salvelinus fontinalis*. *G3* (2019) 9:955–68. doi: 10.1534/g3.118.200910
107. Sheth K, Bankey P. The liver as an immune organ. *Curr Opin Crit Care* (2001) 7:99–104. doi: 10.1097/00075198-200104000-00008
108. Gao B, Jeong W-I, Tian Z. Liver: An organ with predominant innate immunity. *Hepatology* (2008) 47:729–36. doi: 10.1002/hep.22034
109. Deslyper G, Colgan TJ, Cooper AJR, Holland CV, Carolan JC. A proteomic investigation of hepatic resistance to *Ascaris* in a murine model. *PLoS Negl Trop Dis* (2016) 10:e0004837. doi: 10.1371/journal.pntd.0004837
110. Deslyper G, Holland CV, Colgan TJ, Carolan JC. The liver proteome in a mouse model for *Ascarissuum* resistance and susceptibility: evidence for an altered innate immuneresponse. *Parasit Vectors* (2019) 12:402. doi: 10.1186/s13071-019-3655-9
111. Kim J-H, Macqueen DJ, Winton JR, Hansen JD, Park H, Devlin RH. Effect of growth rate on transcriptomic responses to immunestimulation in wild-type, domesticated, and GH-transgenic coho salmon. *BMC Genomics* (2019) 20:1024. doi: 10.1186/s12864-019-6408-4
112. Skugor S, Jørgensen SM, Gjerde B, Krasnov A. Hepatic gene expression profiling reveals protective responses inAtlantic salmon vaccinated against furunculosis. *BMC Genomics* (2009) 10:503. doi: 10.1186/1471-2164-10-503
113. Martin SAM, Blaney SC, Houlihan DF, Secombes CJ. Transcriptome response following administration of a live bacterial vaccine in Atlantic salmon (*Salmo salar*). *Mol Immunol* (2006) 43:1900–11. doi: 10.1016/j.molimm.2005.10.007
114. Causey DR, Pohl MAN, Stead DA, Martin SAM, Secombes CJ, Macqueen DJ. High-throughput proteomic profiling of the fish liver following bacterial infection. *BMC Genomics* (2018) 19:719. doi: 10.1186/s12864-018-5092-0
115. Pickering AD. Cortisol-induced lymphocytopenia in brown trout, *Salmo trutta* L. *Gen Comp Endocrinol* (1984) 53:252–9. doi: 10.1016/0016-6480(84)90250-8
116. Pickering AD, Duston J. Administration of cortisol to brown trout, *Salmo trutta* L., and its effects on the susceptibility to *Saprolegnia* infection and furunculosis. *J Fish Biol* (1983) 23:163–75. doi: 10.1111/j.1095-8649.1983.tb02891.x
117. Pickering AD, Christie P. Sexual differences in the incidence and severity of ectoparasitic infestation of the brown trout, *Salmo trutta* L. *J Fish Biol* (1980) 16:669–83. doi: 10.1111/j.1095-8649.1980.tb03746.x
118. Chen CY, Lopes-Ramos CM, Kuijjer ML, Paulson JN. Sex differences in gene expression and regulatory networks across 29 human tissues. *Cell Reports* (2020) 31:107795. doi: 10.1016/j.celrep.2020.107795

119. Wright AE, Fumagalli M, Cooney CR, Bloch NI, Vieira FG, Buechel SD, et al. Male-biased gene expression resolves sexual conflict through the evolution of sex-specific genetic architecture. *Evol Lett* (2018) 2:52–61. doi: 10.1002/evl3.39
120. Barson NJ, Aykanat T, Hindar K, Baranski M, Bolstad GH, Fiske P, et al. Sex-dependent dominance at a single locus maintains variation in ageat maturity in salmon. *Nature* (2015) 528:405–8. doi: 10.1038/nature16062
121. Mank JE. Population genetics of sexual conflict in the genomicera. *Nat Rev Genet* (2017) 18:721–30. doi: 10.1038/nrg.2017.83
122. Gallach M, Betrán E. Intralocus sexual conflict resolved through geneduplication. *Trends Ecol Evol* (2011) 26:222–8. doi: 10.1016/j.tree.2011.02.004
123. VanKuren NW, Long M. Gene duplicates resolving sexual conflict rapidly evolved essentialgametogenesis functions. *Nat Ecol Evol* (2018) 2:705–12. doi: 10.1038/s41559-018-0471-0
124. Cheng C, Kirkpatrick M. Sex-specific selection and sex-biased gene expression in humans andflies. *PLoS Genet* (2016) 12:e1006170. doi: 10.1371/journal.pgen.1006170
125. Coughlan J, McGinnity P, O'Farrell B, Dillane E, Diserud O, de Eyto E, et al. Temporal variation in an immune response gene (MHC I) in anadromous*Salmo trutta* in an Irish river before and during aquacultureactivities. *ICES J Mar Sci* (2006) 63:1248–55. doi: 10.1016/j.icesjms.2006.03.025
126. Limburg KE, Waldman JR. Dramatic declines in North Atlantic diadromousfishes. *Bioscience* (2009) 59:955–65. doi: 10.1525/bio.2009.59.11.7

Conflict of Interest: The authors declare that the research was conducted in the absence of any commercial or financial relationships that could be construed as a potential conflict of interest.

Copyright © 2021 Colgan, Moran, Archer, Wynne, Hutton, McGinnity and Reed. This is an open-access article distributed under the terms of the Creative Commons Attribution License (CC BY). The use, distribution or reproduction in other forums is permitted, provided the original author(s) and the copyright owner(s) are credited and that the original publication in this journal is cited, in accordance with accepted academic practice. No use, distribution or reproduction is permitted which does not comply with these terms.

frontiers in Immunology

REVIEW
published: 31 May 2021
doi: 10.3389/fimmu.2021.642343

Evolutionary Comparative Analyses of DNA-Editing Enzymes of the Immune System: From 5-Dimensional Description of Protein Structures to Immunological Insights and Applications to Protein Engineering

Atefeh Ghorbani[1,2*†], *Emma M. Quinlan*[1*†] *and Mani Larijani*[1,2*]

[1] *Program in Immunology and Infectious Diseases, Department of Biomedical Sciences, Faculty of Medicine, Memorial University of Newfoundland, St. John's, NL, Canada,* [2] *Department of Molecular Biology and Biochemistry, Faculty of Science, Simon Fraser University, Burnaby, BC, Canada*

The immune system is unique among all biological sub-systems in its usage of DNA-editing enzymes to introduce targeted gene mutations and double-strand DNA breaks to diversify antigen receptor genes and combat viral infections. These processes, initiated by specific DNA-editing enzymes, often result in mistargeted induction of genome lesions that initiate and drive cancers. Like other molecules involved in human health and disease, the DNA-editing enzymes of the immune system have been intensively studied in humans and mice, with little attention paid (< 1% of published studies) to the same enzymes in evolutionarily distant species. Here, we present a systematic review of the literature on the characterization of one such DNA-editing enzyme, activation-induced cytidine deaminase (AID), from an evolutionary comparative perspective. The central thesis of this review is that although the evolutionary comparative approach represents a minuscule fraction of published works on this and other DNA-editing enzymes, this approach has made significant impacts across the fields of structural biology, immunology, and cancer research. Using AID as an example, we highlight the value of the evolutionary comparative approach in discoveries already made, and in the context of emerging directions in immunology and protein engineering. We introduce the concept of 5-dimensional (5D) description of protein structures, a more nuanced view of a structure that is made possible by evolutionary comparative studies. In this higher dimensional view of a protein's structure, the classical 3-dimensional (3D) structure is integrated in the context of real-time conformations and evolutionary time shifts (4th dimension) and the relevance of these dynamics to its biological function (5th dimension).

Keywords: DNA-editing enzyme, immune response, cancer, gene mutations, cytidine deaminase, AID/APOBEC and ADAR deaminases, protein structure/folding, evolutionary immunology

OPEN ACCESS

Edited by:
Gyri T. Haugland, University of Bergen, Norway

Reviewed by:
Hao-Ching Wang, Taipei Medical University, Taiwan
Kazuo Kinoshita, Shizuoka General Hospital, Japan
Jeroen E. J. Guikema, Academic Medical Center, Netherlands

***Correspondence:**
Atefeh Ghorbani
Atefeh_Ghorbani@sfu.ca
Emma M. Quinlan
mq630@mon.ca
Mani Larijani
mani_larijani@sfu.ca

†*These authors have contributed equally to this work*

Specialty section:
This article was submitted to Comparative Immunology, a section of the journal Frontiers in Immunology

Received: *15 December 2020*
Accepted: *06 April 2021*
Published: *31 May 2021*

Citation:
Ghorbani A, Quinlan EM and Larijani M (2021) Evolutionary Comparative Analyses of DNA-Editing Enzymes of the Immune System: From 5-Dimensional Description of Protein Structures to Immunological Insights and Applications to Protein Engineering. Front. Immunol. 12:642343. doi: 10.3389/fimmu.2021.642343

INTRODUCTION

The adaptive immune system in its classical mammalian form first appeared in the common ancestor of all jawed vertebrates (gnathostomes), with the cartilaginous fish being the first extant animals to evolve somatically diversified lymphocyte (B and T cell) receptors (BCR or antibodies, and TCR, respectively) (1). However, further study of the earlier-evolved jawless vertebrates revealed that these animals too were capable of adaptive immunity. Instead of B and T cell lymphocytes, their respective humoral and cellular adaptive immune responses are mediated by lymphocyte-like cells with Variable Lymphocyte Receptors (VLRs). Interestingly, these VLRs also appeared to be somatically diversified, highlighting the importance of lymphocyte receptor diversification in the adaptive immune response (2).

Lymphocyte receptors are diversified *via* purposeful induction of DNA damage in the form of recombination and gene mutation (3). Unlike other genes, in jawed vertebrates, the genes encoding the adaptive immune antigen receptors are segmented. To encode a functional receptor, the variable (V), diversity (D; only in the case of the heavy chain), and joining (J) fragments are assembled by V(D)J recombination, a site-specific recombination process that is lymphocyte-specific and mediated by the recombination-activating gene products 1 and 2 (RAG1/2) co-enzyme complex (4–7). Following binding to recombination signal sequences (RSS) at the ends of V, D, or J gene segments, the RAG1/2 complex introduces double strand breaks (DSBs) at the RSS-coding juncture. Non-homologous end joining (NHEJ) is initiated to repair the DSBs, resulting in ligation and forming the V(D)J-encoding gene.

This primary diversification process that occurs during B and T cell development in the bone marrow and thymus respectively, gives rise to the initial antibody (BCR) or TCR repertoire in B and T lymphocytes. In the case of B lymphocytes, further secondary diversification rounds of the BCR are initiated when a mature peripheral B lymphocytes bind its cognate antigen (8). As a result of secondary diversification, activated B cells, expressing low affinity IgM, give rise to B cells secreting high affinity antibodies of switched isotopes including IgA, IgG and IgE. Secondary antibody diversification in jawed vertebrates includes two processes: affinity maturation (AM) and isotype switching (IS), driven by somatic hypermutation (SHM) and Class Switch Recombination (CSR), respectively. SHM in the antibody V region genes, followed by cellular selection leads to antibodies of higher affinity to the cognate antigen. CSR changes the class of antibody from IgM into other isotypes (i.e., IgA, IgG, or IgE). CSR is mediated by DSBs in the switch (S) regions flanking the heavy chain constant genes (C_H) which initiate a NHEJ event resulting in the replacement of $C_H\mu$ with other C_H isotypes, changing the antibody's effector function (9–11). The outcome of secondary antibody diversification is the production of more effective isotypes of antibodies which also have as much as 1000-fold higher affinity for the antigen. The mutations and DSBs that underlie SHM and CSR are both caused by the enzyme activation-induced cytidine deaminase (AID) (12, 13). AID is a member of the AID/APOBEC (apolipoprotein B mRNA editing enzyme, catalytic polypeptide-like) family of cytidine deaminase enzymes that carry out cytidine (dC) to uridine (dU) conversion in single stranded DNA or cytidine (C) to uridine (U) conversion in RNA (14, 15).

The AID/APOBEC family includes 11 family members in humans: AID, APOBEC1, APOBEC2, APOBEC3 (A-H, excluding E), and APOBEC4. APOBEC4 and related enzymes have been found as early as Cnidarian invertebrates but are frequently absent in actinopterygians and present again in all mammals (14, 16) (**Figure 1A**). The APOBEC3 sub-branch emerged in mammals followed by rapid expansion and diversification in primates (16, 64) (**Figure 1A**). APOBEC3s function in immune response by acting as restriction factors against viruses. They do so through mediating mutagenesis of viral genomes, or interference with the reverse transcription and integration of the viral DNA (65–68). In addition the adenosine deaminases acting on double-stranded RNA (ADARs) are enzymes that mediate cellular mRNA processing through Adenosine (A) to Inosine (I) conversion; however, they have also been demonstrated to mutate viral RNA and carry out a range of cytoplasmic innate anti-viral functions (69–73).

In contrast to jawed vertebrates, the jawless vertebrate lamprey lacks a classical antibody and TCR, and their antibody structure is grossly different, both at the genetic and protein levels. Rather than the classical V(D)J recombination-based Ig system of jawed vertebrates, lampreys employ a presumed gene conversion-like process to assemble 8-10 variable leucine rich repeat motifs in between conserved genes that encode N- and C-terminal ends of their antibody protein. Although the jawless vertebrates lack the classical RAG and AID/APOBEC enzymes, the proposed lymphocytes antigen receptor diversification process is thought to be mediated by AID/APOBEC-like cytidine deaminase enzymes denoted CDA (cytosine deaminase) of which there are two sub-types, CDA1 and CDA2, the former group appearing to have multiple enzyme members (2, 17, 74–78).

Though essential for immunity, the DNA-editing enzymes used to diversify antigen receptors also mediate significant off-target genome damage. There are several mechanisms in place to ensure targeting of RAG1/2 to the *Ig* and T cell receptor (*TCR)* genes. These mechanisms include precursor lymphocyte-restricted RAG expression, *CTCF*-binding elements flanking paired RSS sequences, active chromatin markers, active transcription, and stalled RNA polymerase II (79–82). Despite these regulatory mechanisms, RAG is known to cause chromosomal translocation, deletion, and insertions leading to different types of T cell and B cell lymphoid malignancies, and many of these off-target RAG cleavage events are believed to occur through recognition of RSS-like sequences at non-*Ig* loci, termed cryptic RSSs (83, 84). It has also been shown that the excised signal circle can play the role of RSS and cause RAG-mediated DSBs at a cryptic RSSs in a process termed "cut-and-run" (85). RAG-mediated chromosomal translocations, presumably as a form of mis-targeting of V(D)J recombination are implicated in the etiology of chronic myeloid leukemia (CML), leukemias and lymphomas (79, 86, 87).

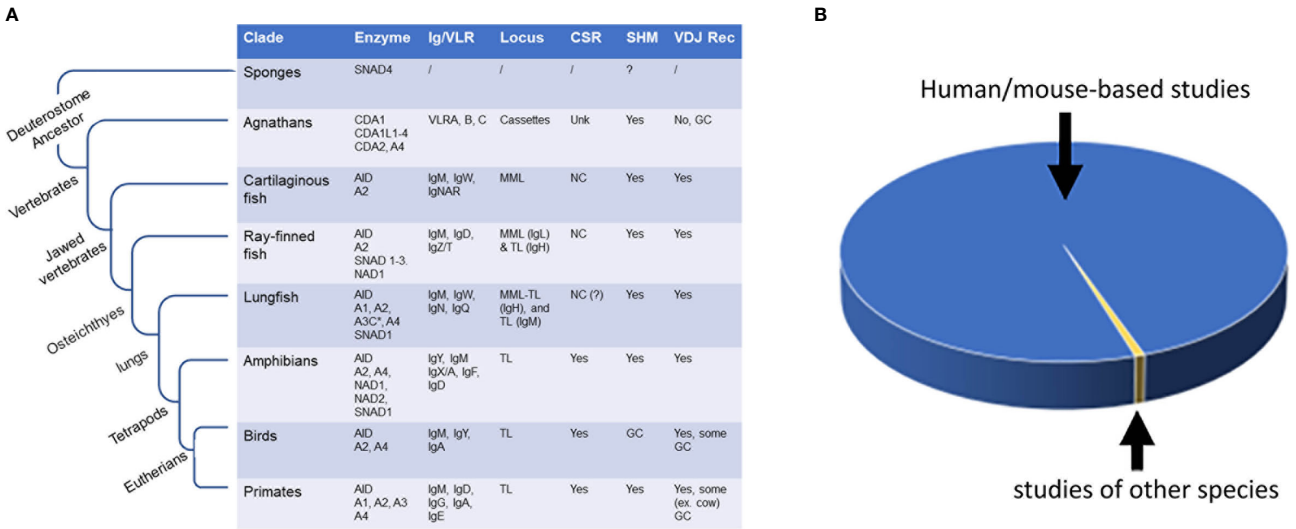

FIGURE 1 | Evolutionary and evolutionary comparative studies of AID/APOBEC and AID/APOBEC-like enzymes. **(A)** The emergence of AID/APOBEC and AID/APOBEC-like enzymes during evolution and the evolution of antibody genes (Ig/VLR), and occurrence of secondary antibody diversification (i.e., antibody maturation; SHM and CSR) and primary antibody diversification (i.e., V[D]J recombination) within and outside of vertebrate class. **(B)** Comparison of number of reports examining AID in human and mouse (blue; > 99%) and studies done on other species (yellow; < 0.7%). The total number of published peer-reviewed studies on AID as measured by AID being a keyword in title/abstract (pubmed/scopus search) is 2368. Of these, 49 discussed the topic of AID in species other than human or mice (15–63) and 17 (0.7%) presented experimental data examining evolutionary divergent AID orthologs (17, 20, 21 26, 30–33, 39, 42, 45, 47, 52, 56, 61–63). NC, noncanonical; MML, multiple mini loci; TL, translocon; GC, Gene conversion (or Gene conversion-like); unk, unknown.

Mis-targeted activity of AID also causes genome instability and mutations in B cells (88). For example, in patients with chronic myeloid leukemia (CML), AID-mediated hypermutation of tumor repressor and DNA repair genes have been associated with progression into B lymphoid blast crisis and Imatinib-resistance phenotype (89). In diffuse large B cell lymphomas (DLBCL), somatic hypermutation off-targeting has been reported in proto-oncogenes (90). The IGH/MYC translocation that is signature of Burkitt lymphoma (BL) has a frequency that is correlated with AID activity level (91). AID-induced hypermutations have also been observed in chronic lymphoid leukemia (CLL) (92). There has also been evidence of AID-mediated carcinogenesis in germinal center (GC) B cells as the result of Epstein-Barr virus (EBV)-induced AID expression (93). Interestingly, under strong inflammatory stimuli, the premature expression of AID during B cell development creates an opportunity for cooperation between RAG and AID to drive the clonal evolution of childhood B cell acute lymphoblastic leukemia (B-ALL) (94). The role of AID in tumorigenesis has been conclusively established in several mouse models. In mouse models of IgH/MYC translocation-driven BL, AID has been shown to be directly responsible for this tumor-driving chromosomal translocation (95), and AID transgenic mice are also prone to AID-driven tumorigenesis (96).

In addition to AID, its APOBEC relatives, the APOBEC3 sub-branch of enzymes (A3A, A3B, A3H), which have antiviral properties, are also a significant source of genome damage and mutations implicated in many types of cancers, such as breast, ovarian, and lung cancers, as the driving mutation and cancer progression associated signatures (68, 97–108). Their mutagenic activity in tumors is often the most prevalent mutational signature, and overall, only second to aging-related mutations signatures. In addition to AID/APOBEC cytidine deaminases, recent evidence also implicates ADARs as sources of mRNA mutations in cancer (109–112). Like AID, the role of APOBEC enzymes in tumor initiation has also recently been established in APOBEC-transgenic mouse models (113).

The diversification of the adaptive immune antigen receptors is the only vertebrate example of controlled self-DNA editing and damage in the form of purposeful mutation and rearrangement. The RAG, AID/APOBEC, and ADAR DNA-editing enzymes play important roles in adaptive and innate immunity through the mutagenesis and recombination of the endogenous *Ig* genes, and the response to viral infection. The importance of these enzymes is underscored by the immunodeficiency disorders caused by their deficiency: severe combined immunodeficiency (SCID) and Hyper IgM syndrome in the case of dysfunctional RAG and AID, respectively (114–121). On the other hand, these enzymes also mediate considerable disease-driving collateral damage to the genome. Given their importance to immunity, infection, and cancer, it is not surprising that the DNA-editing enzymes of the immune system have been the topic of intense study in various fields including immunology, virology, cancer, DNA damage/repair and structural biology. In the next section, we provide an overview of the methodological and model organism landscape of this research area. The central thesis of this review is that the evolutionary aspect of these enzymes, despite being an understudied area, has provided key insights from the basic biological and applied biomedical perspectives.

CENTRAL THESIS: DESPITE THE OVERWHELMINGLY ANTHRO- AND MURINE-CENTRIC APPROACHES TO STUDY DNA-EDITING ENZYMES, EVOLUTIONARY COMPARATIVE STUDIES FOCUSING ON DIVERGENT SPECIES HAVE PROVIDED SIGNIFICANT INSIGHTS

A survey of published literature on PubMed/Scopus reveals ~5000 articles focusing on the DNA-editing and DNA-damaging enzymes of the immune system (RAGs: 729, AID: 2368, APOBECs: 2628, wherein these enzymes are in the title/abstract), published over the last 3 decades of work on RAGs and 1-2 decades of work on AID/APOBEC/ADARs. In the remainder of this article, because our work has mostly focused on AID, we will use this enzyme as a representative example of a genome-editing enzyme that has been extensively studied for 20 years [since its discovery in 1999 – (12, 13)] in the fields of immunity, cancer, DNA damage/repair, and epigenetics. In the following paragraphs, we examine the themes, experimental approaches and model systems used to study AID. The principles discussed and the conclusions reached at the end of this review in the context of AID apply equally and in the same manner to other DNA/RNA-editing enzymes involved in immunity (APOBECs, RAGs, and others, discussed below), and, for that matter, to the study of all other molecules that play roles in human health and disease.

First, in terms of study themes, topics of investigation include: understanding (1) functions, including "normal" immune functions (antibody diversification), non-immune biological functions (epigenetic regulation of the genome), and deleterious functions as a result of mis-expression or mis-targeted activity (initiation and progression of cancers), (2) regulation, including regulation of expression, interacting partners (protein, DNA or RNA), and regulation of the targeting of these enzymes to specific genes or genomic loci, (3) networks of cellular processes including for instance the DNA repair and damage response pathways activated downstream of these enzymes' mutational activities, (4) molecular mechanisms, including biochemical analyses, and (5) 3D structure determination.

Second, in terms of methodological approaches, studies fall into several categories: (1) whole animal *in vivo*, (2) mechanistic experiments using primary cells *or* model cell line *ex vivo*, (3) genomics or bioinformatics studies examining genome-altering signatures of these enzymes, and association with immunity or cancer, (4) structure determination by crystallography or nucleic magnetic resonance (NMR) or emerging computational methods, (5) "simple" cellular experimental systems such as bacteria or yeast in which the enzyme is exogenously expressed followed by reporter assays, (6) biochemical reductionist cell-free studies of the enzymes as purified molecules, *in vitro*.

Third, in terms of model organisms, which will be the focus of this review, for DNA/RNA-editing enzymes involved in immunity and cancer, and indeed for most molecules that play roles in human health and disease, the vast majority of research has been focused on human and, to a lesser extent, mice. For the past several decades, cellular and molecular biology approaches for studying molecules involved in human health focused almost entirely on a handful of well-characterized model species, including the fruit fly *D. Melanogaster*, the worm *C. elegans*, and rodents, most notably lab mice. There are several reasons for this: first, many disease-related molecules function in similar pathways in humans and these model organisms and their dysfunction in the model species closely mirrors the resulting human condition; second, many of these disease-causing molecular pathways are well understood within the model organisms due to decades of research; and third, the model organisms are easy to grow, observe and manipulate at the cellular and genetic levels. Therefore, the concept of studying a handful of model organisms to glean mechanisms of human disease is logical. Indeed, studying molecular mechanisms of human health/disease-related processes in great depth but in a limited number of model organisms is what has led to an unprecedented pace of generating insights into the molecular basis of human diseases.

The total number of studies with AID as the main, or one of the main topics of study, as of the time of preparing this article, is 2368, of which 49 have discussed the topic of AID in species other than human or mice (15–63). Of these, 14 are literature reviews, and of the remaining 35, only 17 studies have presented primary experimental data wherein activities or functional properties of evolutionary divergent AID orthologs were compared (17, 20, 21, 26, 30–33, 39, 42, 45, 47, 52, 56, 61–63). And, among these 17, only less than a handful of studies had an evolutionary comparison as a main conceptual thrust. Therefore, in terms of effort, this area makes up a minuscule (0.7%) subset of the research devoted to the AID enzyme, with > 99% of studies being restricted to human or mouse AID (**Figure 1B**).

The goal of this review is two-fold: Our first aim is to make the case that despite this underrepresentation of effort, several important discoveries have been contributed by working on evolutionary distant AID orthologs, with implications across the fields of cancer, immunity, and genetics. Using the example of AID, we aim to highlight the concept that despite being a road infrequently taken, the evolutionary comparative approach to molecules involved in human health and disease provides immense value for fundamental biological discovery, with emerging practical applications in therapeutics and biotechnology. Our second aim is to suggest that considering the scale of the evolutionary diversity of species, there is an immense knowledge gap in our understanding of DNA/RNA-editing enzymes from species other than human and mouse. In the sections below, we first review the evolution of AID and related enzymes, followed by a review of the contributions made by examining AID through a species-comparative and evolutionary lens, and the future potential of such avenues of inquiry.

EVOLUTION OF AID IN THE CONTEXT OF RELATED DEAMINASE ENZYMES

The AID/APOBEC family is thought to have originated from tRNA adenosine deaminase (Tad)/adenosine deaminase acting on tRNA (ADAT2), the latter of which forms a heterodimer with ADAT3 to deaminate adenosine (A) to inosine (I) in 34 tRNA. These mutated tRNAs can recognize multiple mRNA codons, as I pairs with U, C, or A in the wobble (3^{rd}) position (15, 16). Interestingly, ADAT2 may be able to deaminate cytidine in DNA as well (122) indicating the substrate promiscuity of the AID/APOBEC family may have evolved before the APOBEC family divided into the multiple family members. Other enzymes related to Tad/ADAT2, but not to the AID/APOBEC family, include Tad1p/ADAT1, which deaminates tRNA, adenosine deaminases acting on pre-mRNA (ADARs 1, 2, and 3), which is involved in post-translational modifications of RNA (123–125); and cytosine deaminase, cytidine deaminase, and deoxycytidine monophosphate deaminase (dCMP), members of the pyrimidine salvage pathway which recycles nucleotides (126). These enzymes are found throughout the metazoa phylum (16).

Members of the classical AID/APOBEC family (APOBECs 1, 2, 3, and 4) and their newly discovered sister clades and members are discussed below, in the order in which they likely evolved. It is suggested that the AID/APOBEC family has evolved from the tRNA adenosine deaminases containing the consensus motif (C/H)xEx_nPCxxC (x is any given amino acid) as their catalytic domain (14, 127). The shift in substrate specificity from adenine to cytidine during the divergence of the AID/APOBEC family from Tad2/TadA deaminases has been attributed to the expansion of the α4-β4 loop (i.e., Loop8) and a conserved tyrosine in this loop. The larger L8 decreases the size of the substrate-binding pocket, and the conserved tyrosine could participate in base-stacking interactions (128). Moreover, the $HxEx_nPCxxC$ motif is the conserved catalytic domain shared by the AID/APOBEC family in which the glutamate (E) acts as a proton donor and the histidine (H) with two cysteines (C) coordinate a Zn^{2+} ion with the help of a water molecule (39, 52, 129, 130).

The secreted novel AID/APOBEC-like (SNAD) enzymes belong to a sister clade to the classical AID/APOBEC family, evolving in the first animals to diverge from fungi (sponges, SNAD4) and appearing throughout the vertebrate phylum (SNAD1). SNAD2 and 3 found only in the ray-finned fishes are likely the result of whole genome duplication event and/or subsequent expansion of this class. SNAD enzymes are the only AID-like enzymes in multicellular eukaryotes with a characteristic predicted secretion sequence and have therefore been proposed to be secreted potentially for delivery to virus-infected cells or extracellular parasites; however, their catalytic activity and other biochemical characteristics remain unknown. They may have originated from bacterial toxin proteins (16).

APOBEC4 (A4), a member of the classical AID/APOBEC family, was likely next to evolve, first appearing in the cnidarians (corals), which diverged after sponges (16). The lack of introns in the A4 gene indicates it may be the result of early retrotranspositional events. A4 is present in the first vertebrates, the jawless fish (agnathans), the lobe-finned fish (sarcopterygians), and tetrapods, but is lost in sharks and often lost in ray-finned fishes (actinopterygians). It is expressed in human testes, but its biological role and catalytic activity are unknown. Unlike the other members of the AID/APOBEC family which are known to deaminate polynucleotides, critical amino acids required for polynucleotide deamination (SWS and F in the middle of the deaminase motif HXE….PCXXC) are missing from A4, indicating it may act on other substrates (15, 16, 131).

The next-evolved branch of AID-like enzymes include cytidine deaminase-like 1 (CDA1), CDA1L1, 2, 3, and 4, and CDA2 found in the jawless vertebrates (agnathans). Lampreys lack many canonical "pillars" of the adaptive immune system, such as RAGs and MHC; however, they do have antibody-like proteins (VLRs) that are diversified somatically, which led to the discovery of CDA1-like, and CDA1 and 2 in the freshwater and sea lampreys, respectively. These enzymes will be discussed in detail in a following section (16, 17, 20).

This was followed by the emergence of AID and APOBEC2 (A2) in the common ancestor(s) of jawed vertebrate classes of cartilaginous and bony fish. Hence, A2 and AID are considered the ancestral family members of the classical APOBEC family due to being present in most jawed vertebrates tested to date. They appeared at the same evolutionary juncture where the classical V(D)J-based *Ig* recombination and canonical heavy/light-chain based antibody structures emerged (16, 57). Interestingly, the involvement of CDA1 in diversifying the lamprey's immune receptors and the continuing of a similar role for AID in the jawed vertebrate may be an example of convergent evolution in that the acquisition of the lymphocyte receptor diversification role by the AID-like branch had already occurred before the further divergence of this branch within vertebrates. A2 may be the result of early retrotranspositional events, which used AID as a scaffold. Like A4, human A2 does not appear to edit RNA, DNA, or free cytidine *in vitro*. Its ortholog in zebrafish, which has been implicated in retina and muscle generation, also lacks deaminase activity (132–134). Additionally, A2 seems to inhibit transforming growth factor (TGF)-β in *Xenopus* (frog, amphibian) and zebrafish (135).

The so-called novel AID/APOBEC-like Deaminases 1 and 2 (NAD1/2), while not being original members of the classical AID/APOBEC family, are closer in sequence to A1, A2, A3 than A4. NAD1 is found in ray-finned fishes, the coelacanth (sarcopterygian), amphibians, lizards, and marsupials; NAD2 is found only in amphibians. Neither NAD has been characterized and their biological relevance remains unknown (16).

APOBEC1 (A1) is the founding member of the AID/APOBEC family (136–138). It was originally thought to be first evolved in mammals due to duplication of AID; however, this duplication likely occurred in or before the lungfish. A1 deaminates the cytosine at position 6666 of Apolipoprotein B mRNA, creating a premature stop codon at this position, altering ApoB100 to ApoB48, which is essential for secretion of triglyceride-rich chylomicrons (139). It was later discovered

that like AID and A3s (below), A1 is also quite promiscuous, acting on retroviral substrates and ssDNA (140, 141). As A1 is among the later AID/APOBEC family members to evolve, the RNA-editing capabilities seen in other members of this family may be a late-evolved characteristic. On the other hand, due to the progenitors of the AID/APOBEC family acting on RNA and, in some cases, both RNA and DNA (142), substrate promiscuity may be an original characteristic of the many family members, whose activity has just not yet been fully elucidated. In support of this, changes in substrate binding surface regions of the AID and APOBEC-related deaminases appear to be the most rapidly evolving structural feature of these enzymes, and AID certainly appears to recognize RNA and DNA/RNA hybrids with very high affinity though its catalytic activity is restricted to the ssDNA strand (143).

APOBEC3 (A3) is the last group of AID/APOBEC enzymes to have emerged, likely the result of AID's gene duplication events. A pronounced expansion has occurred most recently in primates leading to 7 unique primate-specific A3 genes (A3A, A3B, A3C, A3DE, A3F, A3G, and A3H) (64, 144). The expansion of these enzymes has been proposed to be due to an arms race between mammals and the targets of A3, retroviruses. The origin of A3 is not fully clear: the initiating duplication event was thought to take place in the first placental mammal where no A3 ortholog were found in animals that diverged before placental mammals. It is thought that in rodents, pigs, and cattle, two AID-like genes fused to form a single gene; in horses, bats, and felines, one of the two genes repeatedly duplicated leading to an expansion of A3 genes. However, the sequenced lungfish genome appeared to contain a putative A3C gene (145). It is possible that the A3C found in the lungfish was a novel APOBEC-like gene representative of convergent evolution.

THE EVOLUTION OF IMMUNOGLOBULIN LOCI AND DIVERSIFICATION

Pre-vertebrates (protochordates) lack AID but have AID-like enzymes such as the aforementioned SNADs. While also lacking B cell receptors, these animals have immune receptors belonging to the immunoglobulin superfamily (146–149). It is believed that a type of proto-AID (or AID ortholog) was present in the first vertebrate ancestor, which then diverged to CDA in the lamprey and to AID in the early jawed vertebrates, the shark (17, 18). Similarly, it is hypothesized that the targets of this proto-AID (somatically diversified lymphocyte receptors) diverged into three unique receptors with three different lymphocyte cell lineages: a secreted form (VLRB in the lamprey and BCR in jawed vertebrates in B cell-like cells) and two membrane-bound receptors (VLRA/C in the lamprey and TCR αβ/γδ in jawed vertebrates in T cell-like cells) (18, 150). Due to CDA1/1L genes lacking introns, it has been posited that CDA2 was the original enzyme in all three lamprey lineages, with the ability to somatically diversify all three VLRs, and that CDA1/1L genes were the result of retrotransposon events after which CDA2 was subsequentially silenced in CDA1/1L$^+$ cell lineages. This idea is supported by the fact that in the first-diverged subsequent jawed vertebrate, the shark, AID appears to initiate somatic hypermutation of both B and T cell receptors (19, 35, 151, 152). This suggests that perhaps this broader dual role of AID was lost in subsequent vertebrate lineages and the role became focused on antibody diversification in B cells only but the dual role appears again in limited later-diverged species, such as the Ballan Rasse (ray-finned fish) and in camels (36, 153). Lamprey CDAs have been relatively understudied after their discovery, with their VLR antibodies garnering the most attention as novel non-classical antibody structures that may hold biotechnological and therapeutic potential (154–156).

The first immunoglobulin loci to evolve were those in the elasmobranchs (sharks and skates) that are organized quite differently from the most-studied mammal *Ig* loci. Shark *Ig* loci are organized into multiple mini loci (MML) (149, 157), with a mini locus or "cluster" equating to one V region placed next to one or more D regions, followed by one J segment and a single constant region $(V\text{-}DDD\text{-}J\text{-}C)_n$ (158). Some MML are rearranged in the germline, while most are rearranged by the RAG recombinase. Shark *Ig* undergo SHM, with long, tandem substitutions unique to these species and presumed to be due to AID-initiated mutations (57, 158–162). It was initially believed that shark *Ig* did not undergo CSR; however, though shark Ig sequences lack the conventional switch regions which first appeared in amphibians, recombined VDJ of one cluster can be "switched" with that of another, leading to a different constant region attached to the recombined VDJ region, possibly initiated by AID acting on recombination hotspots in a process that is concomitant with SHM rather than separated as in after the appearance of distinct switch regions (24, 163, 164). The studied Sharks have three types of Ig: IgM, present in almost all vertebrates, IgW (may be a counterpart to IgD), and IgNAR, which is unique to sharks, being made up of only heavy chains (165).

Outside of humans and mice, SHM and CSR have been studied most in ray-finned fish. Poikilotherms such as ray-finned fish have modest changes in antibody affinity, which has been reported in several species to be initiated by SHM (40, 41, 43, 49, 57, 166–168). This is likely due to inefficiencies caused by a lack of organized GCs; instead, ray-finned fish appear to have GC-like clusters of melanomacrophages with AID-producing cells in the centre (41, 169). Teleost fish (ray- and lobe-finned fish) appear to have *Ig* loci made up of both MML and translocon-type organizations, the latter of which is how most tetrapod *Ig* loci are arranged. In ray-finned fish, the V, D, and J segments are arranged as in mammalian *Ig* loci, with the IgM and IgD constant regions at the 3' end, one after the other. However, the teleost-unique IgZ/T constant region is located further upstream, separated from the IgM and IgD constant regions by D segments ($V_n\text{-}D_n\text{-}J_n\text{-}C_{Z\text{-}}D_n\text{-}C_\mu C_\delta$) (57, 157, 170–172). Lungfish also have IgW and the lungfish-specific IgN and IgQ (173). Though bony fish *Ig* loci do not undergo CSR which appears first in amphibians, the IgM and IgD isotopes are "switched" *via* alternative mRNA splicing, while IgZ/T can be expressed after alternative V(D)J rearrangement.

COMPARATIVE EVOLUTIONARY STUDIES OF AID IN CELL-BASED FUNCTIONAL ASSAYS

The most emphasis outside human and mouse AID has been on fish, because of the expected level of divergence in the primary sequence, and unique features found in fish AID's primary structure compared to the very well conserved mammalian counterparts. Due to evidence of SHM in the early-diverging vertebrate fish lineages as discussed in the above section, it was hypothesized that an AID ortholog could be found in bony fish, and it was indeed found in channel catfish (Ip-AID) (40). This was the first non-human/mouse AID ortholog to be identified followed by detailed work on tissue expression patterns and possible roles in SHM. Shortly thereafter, it was determined that zebrafish also has a *bona fide* AID gene (Dr-AID) and noted that it, along with the predicted AID genes from other ray-finned fish, encodes an additional 9 amino acids (aa) in the cytidine deaminase motif, along with a different N terminal motif compared to tetrapod AIDs (44). In 2004-2006, a series of early studies looked at the functionality of a small number of fish AID alongside *Xenopus* AID using exogenous expression in bacteria or yeast and measuring mutagenic activity in colony formation reversion assays, or expression in murine or human AID-deficient B cells followed by assaying for CSR (31–33, 49). Even though canonical CSR only occurs in tetrapods (37), multiple fish AID orthologs were able to initiate both mutations in *E. coli*, *S. cerevisiae*, and murine cells and CSR when exogenously expressed in AID-deficient B cells, albeit less effectively than mammalian AID (31–33, 49). This suggested that CSR as it occurs in mammals evolved due to the emergence of switch regions within immunoglobulin loci, and not due to adaptations of the different AID orthologs, and that the poikilotherm AID itself is fully capable of mediating CSR. In depth analyses of the regions of human AID required for CSR pointed to the C-terminus raising the possibility that this region of AID may be important in other biological roles prior to the evolutionary emergence of Ig CSR (174). Importantly, these studies also provide strong opposition to the view that CSR mediation by AID requires a specific set of protein co-factors, because early fish AID are presumably not co-evolved with such presumed co-factors required to chaperone AID to switch regions of the *Ig* genes in mouse cells. These findings are in line with later findings that the role of AID in mediating CSR is simple dC mutation and DSB generation, and that likely AID is targeted to these regions through the abundance of ssDNA structures such as R-loops and DNA/RNA hybrids that are inherently favored by AID (143, 175, 176).

In experiments wherein fish AIDs were exogenously expressed in murine AID-deficient B cells, zebrafish AID and mouse AID could mediate equally efficient CSR, with fugu AID and catfish AID being respectively 4- and 7-fold less efficient than these. Nuclear cytoplasmic shuttling of AID has been shown to be a key regulator of its activity and catfish and fugu AIDs appear to have nuclear export and localization domains conserved with other non-mammalian vertebrate domains with expectant results upon their mutation and it was shown that removal of this domain results in accumulation of AID in the nucleus, confirming its functionality. However, generation of hybrid AID with interchanged NES domains demonstrated that the aforementioned difference in their ability to mediate CSR was not due to different NES sequences, suggesting that fish AIDs may have different inherent catalytic robustness (31, 32, 49, 177). In the same set of experiments, the functionality of *Xenopus* AID was also confirmed for the first time.

Another property of fish AID that was examined in these early studies was temperature sensitivity. It was found that incubating the cells in which the fish AID are being expressed at lower temperatures than the typical 37°C (18°C for bacteria, 30°C for yeast, and 26°C for mammalian cell lines), yielded generally more AID activity in the bacterial colony count, yeast-null mutation, and GFP reversion based assays employed in bacteria, yeast, and cell lines, respectively (15, 31, 32, 49). The lamprey CDA1-class deaminases were also shown in bacterial and yeast-based expression assays to be active cytidine deaminases. Another example of a structure:function insight was the example of using zebrafish AID to propose a role for S38 phosphorylation-dependent interaction of AID with replication protein A (RPA) and its role in mediating CSR. Since zebrafish AID lacks this residue but contains D44 which can act as a phosphomimetic residue, it was proposed that S38 phosphorylation dependent Replication protein A (PRA) interaction is essential for CSR, though another study using a zebrafish AID with a D44 mutation found that this residue is not critical for CSR (30, 42, 62, 178); therefore the importance of this axis of S38 phosphorylation-AID-RPA remains uncertain, as the early view that specific cofactors chaperone AID to the *Ig* locus ought to be considered in balance with the various explanations that it may be the process of transcription and its unique features at the *Ig* loci including robust and bidirectional transcription, and unique DNA or RNA secondary structures (e.g. G quadruplexes) are the determinants that recruit AID to the Ig loci to carry out SHM and CSR (179–182).

As the first tetrapods, amphibian (*Xenopus*) antibodies undergo SHM and CSR; however, the switch regions in *Xenopus* are AT-rich compared to GC-rich, which may affect switching efficiency (183, 184). *Xenopus* AID has been shown to demonstrate CSR activity, and is expressed in hematopoietic tissues, hinting at a role in ontogeny (31, 51). Neither *Xenopus* nor other amphibian AIDs have been biochemically characterized. Avian *Ig* loci, at least the ones sequenced (duck, chicken, and ostrich) are unique among the higher vertebrates in that there is a single functional germline locus (V-D_n-J or V-J) that is recombined *via* V(D)J recombination; further diversification occurs *via* AID-mediated gene recombination (similar to how VLRs are recombined), initiated by avian AID (185–188). Aside from experiments demonstrating that bovine AID can demethylate DNA *via* deaminase activity (61), no other non-human, non-mouse AID has been characterized in the higher vertebrates, and its targets (*Ig*) and activity (SHM and CSR) in many non-human animals remain unstudied.

COMPARATIVE EVOLUTIONARY ANALYSES OF AID IN CELL-FREE BIOCHEMICAL ASSAYS

Over the last decade, we have pursued a comparative enzymology approach to study the biochemical properties and structure:function aspects of purified AID from divergent orthologs. The initial goal of this effort was to gain insights into the 3D structure of human AID. Given AID/APOBECs' involvement in immunity and cancer, intense research has been dedicated to solving their 3D structures. Unfortunately, AID/APOBECs proved to be problematic subjects for X-ray or NMR because they are difficult to make in large quantities due to host cell toxicity, and they form extensive non-specific interactions with other molecules making them hard to purify and insoluble. Hence, > 90% of the 40 reported AID/APOBEC structures are of partial or significantly altered versions, quite a few with < 50% identity to the native protein (PDB databank: https://www.rcsb.org/) (53). These alterations were necessary to enable crystal formation for X-ray crystallography or enhance solubility for NMR. AID is a small (only 198 aa) protein but it has by far the most positively charged surface amongst the AID/APOBEC family, which underlies its exceptionally high binding affinity (~nM-range) for its negatively charged ss-DNA substrate (189). Partially because of this, it has not been possible to obtain a native AID crystal or NMR structure despite intense attempts for 20 years since its discovery in 1999.

Based on the initial insights from the cell-based assays that revealed differences in functional efficiencies of orthologous AIDs and the relatively high divergence among mammalian and fish AID, we posited that AID from more distantly evolved species, might have distinct properties and that discovering the basis of their differences would shed light on AID's inner workings. We began studying AID from key evolutionary points. Fish were of great interest because they are the most evolutionarily divergent species known to have AID, and their AID sequences exhibit the highest degree of primary sequence divergence. Parallel to the evolutionary approach, several partial X-ray or NMR structures of APOBECs were utilized in computational modelling to generate thousands of predicted AID 3D structures. Through this computational modelling and evolutionary approach, hereafter referred to as the "computational-biochemical-evolutionary" method, parts of AID were predicted to have a specific function. A library of different AID versions (mutants, chimeras with exchanged domains, fish orthologs) was generated, purified, and subjected to functional biochemical enzyme assays (e.g., enzyme kinetics, substrate binding, and optimal temperature determination) to verify whether a motif predicted by the modelling indeed mediated the supposed function. The experimental results were cross-referenced with the evolutionary/computational predictions, in order to refine a functional map of AID's structure, first published in 2015 through this approach (52). This functional map of AID was later confirmed independently by an X-ray crystal of a near-native AID in 2017 containing 20 aa truncations and a handful of residues mutations which altered the surface charge of AID from ~+10 to +3 (52, 129). In the following paragraphs, we review the insights gained through the computational-biochemical-evolutionary method.

In 2012, by comparing the enzymatic activity and predicted structure of Hs-AID with bony fish AIDs (i.e., zebrafish [Dr-AID] and catfish AID [Ip-AID]), we demonstrated that different AID orthologs present diverse biochemical properties, such as catalytic rate and optimal temperature, which are governed by a single amino acid in their C terminus (26). The difference in the optimal temperature mirrored the ambient temperature of each organism. We observed that Dr-AID was several fold more active than Hs-AID while Ip-AID was significantly less active than Hs-AID, in line with the previous observations of its lesser ability to mediate CSR when deployed in an AID-deficient B cell (26). The different catalytic rates amongst AID orthologs may reflect the different evolutionary paths taken by each species' immune system. The computational modelling of the surface charge and topology, and functional ssDNA binding assays of bony fish and human AIDs, also led to an early picture of AID's ssDNA binding grooves. The width of this groove is ~ 10 Å. Given the width of ds-DNA helix (~ 20 Å), the identified DNA binding groove on AID explained its substrate specificity for acting only on ssDNA and not dsDNA (190–193). The presence of this DNA binding groove has been confirmed upon crystallization of Hs-AID with ssDNA (129, 194).

In 2013, we demonstrated that zebrafish AID, unlike its human counterpart and several other bony fish AIDs had the unique enzymatic ability to mutate 5-methyl dC (5mC) in addition to regular dC (39). Soon after its discovery, a possible role of AID in genome methylation and epigenetic reprogramming was suggested where AID demethylation activity in the CpG motifs would convert 5mC to deoxythymidine (dT) (195). Supporting evidence came from the fact that the AICDA gene is located in a cluster with other pluripotency genes and is expressed in oocytes and primordial germ cells (196). Soon after this initial report, AID-mediated deamination of 5-mC was reported in induced pluripotent stem (iPS) cells, primordial germ cells, B cells, cancerous cell lines, and bovine and zebrafish embryo (60, 61, 197–201). Regarding the enzymatic activity of AID on 5-mC, initially, it was claimed that Hs-AID has comparable activity on 5-mC as well (196). However, soon after, several reports showed that although Hs-AID can indeed deaminate 5-mC, its activity on this substrate and on other cytidine derivatives with bulky adducts is many folds less than on dC (39, 202–204). This is a key aspect of AID activity since AID-mediated CpG demethylation through a C to T mutation could be a mutagenic process. Given the importance of CpG motifs in gene expression and epigenetics, one would expect to avoid efficient activity of AID on 5-mC. In fact, methylation has been proposed as a protective mechanism against undesirable AID activity (202). We then used our comparative computational approach and reported that unlike Hs-AID, Ip-AID, medaka AID (Ol-AID), and tetraodon AID (Tn-AID), the zebrafish AID exhibits more efficient activity on 5m-C, deaminating it more efficiently than many other orthologs deaminate regular dC and significantly more efficient as

normalized to its own activity on dC (39). From a biological standpoint, these results explained why in zebrafish, AID was uniquely involved in embryonic development and its knockdown resulted in genomes with hypermethylated CpG motifs. From an AID structure:function standpoint, modeling predictions of human and zebrafish AID catalytic pockets docked with dC showed that both AIDs are predicted to form catalytic pockets with the classical triad of Zn-coordinating residues (C87, C92, and H56 in human AID) and catalytic glutamic acid (E58 in human AID) that can accommodate a dC residue in orientations that support the 4-stage deamination chemistry common to cytidine and cytosine deaminase. Importantly, the catalytic pocket of zebrafish AID was predicted to have one of its composing loops extended and more flexible as compared to that of human AID, thus providing more space for a 5mC substrate that is bulkier than a dC (204). In this manner, the computational-biochemical-evolutionary method not only solved a biological puzzle about the role of AID in zebrafish, but it also made a key structural biology contribution by providing the first detailed maps of AID's catalytic pocket through predictive modelling corroborated with functional enzymology.

In 2015, using our computational-biochemical-evolutionary method, we mapped a network of primary and secondary catalytic residues that either contact and/or stabilize the dC in a catalytic pocket (52). This network of amino acids consists of G23, R24, R25, E26, T27, L29, N51, K52, N53, G54, C55, V57, T82, W84, S85, P86, D89, Y114, F115, C116, and E122 in human AID (52). These residues form the "walls" and "floors" of the catalytic pocket and interact with substrate dC in several predicted protein conformations through hydrogen bonding, electrostatic interactions, and aromatic base stacking. The importance of direct interactions between some of the secondary catalytic residues and substrate DNA was validated when the crystal structure of a partially truncated and mutated but relatively near native AID was published (129). Given the importance of proper positioning of dC inside the active site for efficient deamination activity, defining the secondary catalytic pocket residues was a step forward in solving the functional structure of AID. In the same work, we also described a novel structural regulatory mechanism of AID/APOBEC activity in that the majority of Hs-AID conformations at any given time contain catalytic pockets that are closed and inaccessible for accommodating a dC for deamination (194). Furthermore, we observed that the majority of ssDNA:AID binding events result in ssDNA bound non-productively on the surface in conformations that do not pass over the catalytic pocket, presumably due to the highly positively charged surface of AID (+11, the highest surface positive charge amongst AID/APOBECs) (52, 194). Taken together, the frequent catalytic closure and sporadic ssDNA binding are significant bottlenecks for AID activity such that < 1% of all ssDNA:AID binding events translate into a cytidine deamination event. We then proposed that due to the potential danger of AID/APOBEC activity for genomic DNA, this inherent structural regulatory mechanism is in place as a safe-guard mechanism in AID and in the tumorigenic A3 family members; the main pillar of this hypothesis was that the open:closed dynamic ratio in AID, A3A and A3B correlated with their catalytic rates and with their relative responsibility for mediating tumorigenic mutations in cancers. We termed this novel mechanism Schrödinger's CATalytic Pocket (53). Here again, the computational-biochemical-evolutionary method was key in providing the functional proof for the existence and regulatory role of Schrödinger's CATalytic Pocket. A panel of chimeric AID enzymes, including bony fish-human chimeras, was generated since certain fish AID (e.g., the aforementioned zebrafish AID) have catalytic pockets are composed of loops of different lengths and hence different breathing dynamics compared to human AID. The demonstration that the AID chimeras (*e.g.*, human/zebrafish catalytic pocket chimera AID, or AID/A3 chimera) predicted to spend more time in the open conformation also have higher catalytic rates, provided functional proof of the concept for Schrödinger's CATalytic Pocket. First revealed by the computational-biochemical-evolutionary method, the pocket dynamic has since been independently confirmed by structural analyses of A3s.

In a study in 2017, to examine whether Hs-AID's unique biochemical properties (i.e., low catalytic rate and high affinity for its substrate) were conserved across vertebrates, we compared the enzymatic activity of Hs-AID to that of sea lamprey, nurse shark, and coelacanth. These species were chosen to represent key points of evolution, lamprey being a jawless vertebrate, shark being the first jawed vertebrate with the classical Ig system, and coelacanth being the "fossil fish" lobe fined fish thought to be the closest fish ancestor of tetrapods (21). We found that despite the biochemical variability amongst these enzymes in substrate sequence preference (WRC *vs.* non-WRC motifs) and optimal temperatures, the key defining enzymatic characteristics of AID (lethargic catalytic rate and high nM range affinity for ssDNA binding) were maintained (205). This finding suggests that these unique biochemical regulatory features of low catalytic rate and high ssDNA binding affinity in AID are evolutionary conserved and thus important for its function, for instance the balance between making SHM and CSR mutations while protecting the genome from rampant promiscuous mutagenesis. Furthermore, using computational modelling, we showed that all of the above-mentioned AIDs are predicted to exhibit the Schrödinger's CATalytic Pocket phenomenon, revealing the importance of this intrinsic structural regulatory mechanism for AID activity throughout the vertebrate class (205). Importantly, this was also the first study to show that two species, key in the evolution of adaptive immunity in its classical mammalian form, the shark and the coelacanth, do indeed have a functional AID enzyme.

In a more recent study, colleagues and we turned our focus to the extant agnathan the sea lamprey, in which thus far two AID-like cytidine deaminases (CDA1 and CDA2) have been found (20). Genetic analyses revealed that CDA1 and CDA2 were found in both the sea and freshwater lampreys, along with, unexpectedly, multiple CDA1-like genes that could be divided into two distinct groups (CDA1L1_1, _2, _3, _4 and CDA1L2_1, _2). Genomic DNA from other individuals were searched for homologs of these new

CDA1-like genes, which were found, along with splice variants of CDA1L1_1 and CDA1L1_3. When their amino acid sequences were compared with those of other AID orthologs, these novel CDA-like proteins were found to contain the conserved deaminase core catalytic motif ($HxEx_nPCxxC$), suggesting they could be active cytidine deaminase. *In silico* modeling of each CDA ortholog also demonstrated the high likelihood of catalytic cytidine deaminase activity, as each protein formed a putative cytidine deaminase catalytic site, and catalytic activity was demonstrated by expressing these enzymes in 293T cells and assaying the extracts for cytidine deaminase activity. The enzymes exhibited cold adaptation, with optimal temperatures being between 14-22°C, and most had an acid pH-adapted activity profile, reminiscent of the human A3 branch enzymes (A3A, A3B, A3G, A3F) rather than human AID, and commensurate with structural modeling showing that these proteins have a lower surface charge than human AID. These results showed for the first time that lamprey has more than just one version of a CDA1 enzyme, and remarkably, that these are variably expressed in individuals of the same species, a novel biological phenomenon the mechanism and importance of which is yet to be discovered.

DISCUSSION

In the above sections, we reviewed the insights relevant to structural biology, immunology, and cancer research that have been brought forth by comparative studies of AID from non-human/mouse species. This section highlights the future potential of comparative evolutionary studies for impacting emerging approaches in structural biology, base-editing, and protein engineering. The concept of how evolutionary studies illuminate each of these three arenas is illustrated in **Figure 2**.

First, with respect to structural biology (**Figure 2** arrow 3, bottom panel, and **Figure 3**), the significance of this computational-biochemical-evolutionary approach for AID is evident by its track record of providing the first 3D map of AID structure and revealing the concept of Schrödinger's CATalytic Pocket in the AID/APOBEC family, both of which have subsequently been confirmed by independent studies employing the traditional structure solution methods of crystallography and NMR. Thus, in the case of AID, not only did the evolutionary-biochemical-computational approach for solving its structure prove to be quicker, it was also the only approach able to deal with AID in an unaltered native state, as the only way to crystalize AID has been to alter it, with the most near-native crystal structure still containing 20 aa truncation and multiple surface mutations that change the charge of native AID drastically (from +11 to +3) (52, 129). Furthermore, the evolutionary-biochemical-computational method also revealed additional time/space dimensions of the structure that are not normally probed through the traditional methodologies (53). For this reason, we termed this type of computational-biochemical-evolutionary structure a five-dimensional (5D) description of a 3D structure. In the 5D structure of a protein, as opposed to the classical protein structure which has always been viewed as a 3D shape, the structure's dynamics are further explored through time (4^{th} dimension) dimensions of '*tempus*' and '*aevum*'. The '*tempus*' analysis is the studying of a protein structure in a real time manner where one can examine/predict the 'protein breathing' on the time scale of fractions of a second, while the '*aevum*' sub-dimension is one wherein dynamic change is compared throughout ortholog evolution from both closely- and remotely-related species, on the time scale of hundreds of millions of years. The 5^{th} dimension, which is "function", then explores the understanding of how these dynamic 3D and 4D structures relate to the biological function of the protein, including functions in human health/disease. **Figure 3** illustrates the concept of how a 5D structure description contains orders of magnitude more information than the conventional 3D picture.

Others and we have shown that AID orthologs exhibit a vast diversity in many of their biochemical properties such as catalytic rate, optimal temperature, optimal pH, and substrate sequence specificity. Indeed, the catalytic rate varies over 3 orders of magnitude, temperature optima vary from very cold to human body temperature, and pH optima vary over a range of nearly 2 units. Firstly, this is indeed a remarkable range of variation for evolutionary closely related versions of the same enzyme, given that a large portion of the enzyme's primary sequence and its overall 3D structural architecture are conserved. Secondly, each of these biochemical characteristics is an indicator of a specific structural aspect of a protein. For instance, variations in catalytic rate can be due to differences in substrate binding or differential dynamics of the catalytic pocket as dictated by breathing loops that compose the catalytic pocket. Variations in optimal pH are largely owing to the surface charge of the protein, which in AID can vary from only slight positive in some bony fish (e.g., +3 in *Salmo Salar*) to extremely positive (e.g., +11 in human and mouse). Substrate specificity differences are mediated by a well-defined substrate specificity loop which is one of the more variable structural regions among the AID/APOBEC family members, causing different surface binding pockets next to the catalytic pocket that underlie differential preference for the -2 and -1 base positions next to the target dC that is positioned in the catalytic pocket. For temperature sensitivity, proteins may increase their thermoresistance using several strategies. In the first mechanism, the enthalpy change (ΔH_s) measured at the temperature of maximum stability (T_s) becomes more negative, causing ΔG for all temperatures to decrease. This strategy can be seen as a stability curve to be shifted downward. The second strategy is to increase (less negative) the change in the heat capacity upon folding (ΔC_p) which causes T_m to increase. In this case, the stability curve would broaden. The last approach is to increase T_s which shifts the curve to the right. Proteins may apply one, two, or all of these strategies to improve their thermal resistance, and this is dictated by differences in the secondary structures employed in various parts of the protein and/or overall flexibility of the structure. Thus, not only is each of an enzyme's biochemical properties reflective of a structural trait in terms of the 3D folding of the structure, but the relationship between properties (e.g., between catalytic rate and optimal temperature)

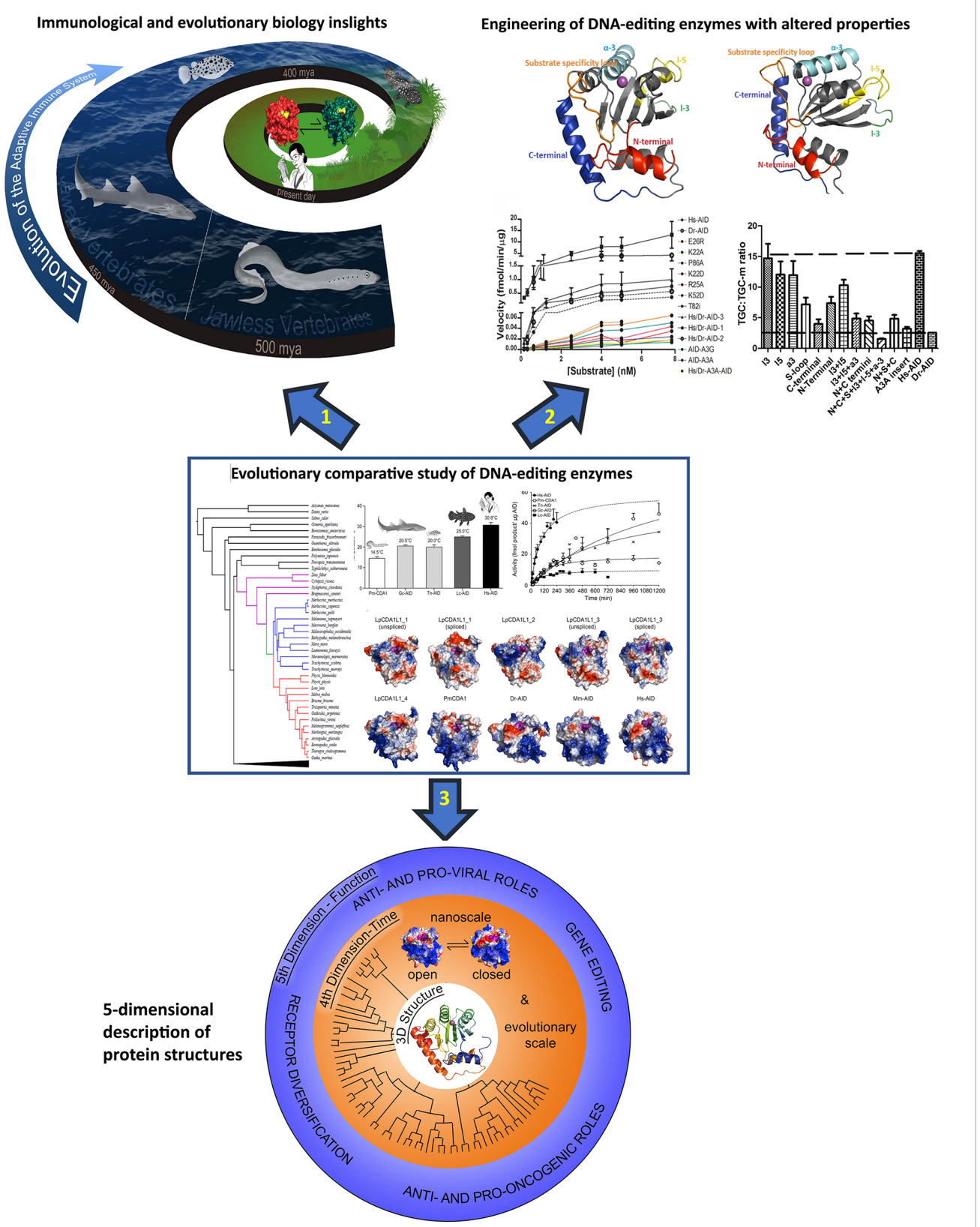

FIGURE 2 | Continued

FIGURE 2 | The concept and three main applications of the evolutionary-biochemical-computational approach to studying DNA-editing enzymes. The evolutionary comparative approach is shown in the middle with 3 arrows each pointing to an area wherein this approach can make significant impact. The evolutionary comparative approach shown in the middle panel consists of comparing biochemical properties (Michaelis-Menten kinetics, substrate binding kinetics, optimal temperature, optimal pH, substrate sequence or shape specificity, etc.) of the enzymes using enzyme assays and considering insights in the context of their 3D solved structures or computational predicted models as shown in this figure. Due to vast biochemical diversity observed amongst various AID orthologs, examining the biochemical properties of divergent AID orthologs has shed light on many structure:function aspects of AID/APOBEC enzymes. Arrow 1: the evolutionary comparative study of DNA-editing enzymes can provide insights into the evolution of the immune system, for instance on whether the immune systems use active deaminases and how/if they have gene sequences or other immune genes that have co-evolved with their deaminases. Arrow 2: using different orthologs allows for generation of libraries of mutants and chimeric enzymes which can have diverse biochemical properties such as DNA/RNA-targeting profiles and sequence specificities, and these can be used for applications such as base editing. Arrow 3: the most important highlight of the evolutionary-biochemical-computational approach is the birth of the concept of 5-dimentional (5D) structural description, proposed in this article. The 5D description integrates the classical 3D structure of a protein with dynamic changes in time (4th dimension) and the relevance of these to function (5th dimension). The middle panel contains reproduced figures from previous publications. The thermosensitivity and enzyme velocity plots are from our previous work Quinlan EM et al. (21). Biochemical regulatory features of activation-induced cytidine deaminase remain conserved from lampreys to humans. Mol Cell Biol 37:e00077-17. https://doi.org/10.1128/MCB.00077-17. Copyright © 2017 American Society for Microbiology. The computational models are adapted from our previous work Holland et al. (20). Expansions, diversification, and interindividual copy number variations of AID/APOBEC family cytidine deaminase genes in lampreys. 2018 Apr 3;115(14):E3211-E3220. doi: 10.1073/pnas.1720871115 Copyright (2018) National Academy of Sciences.

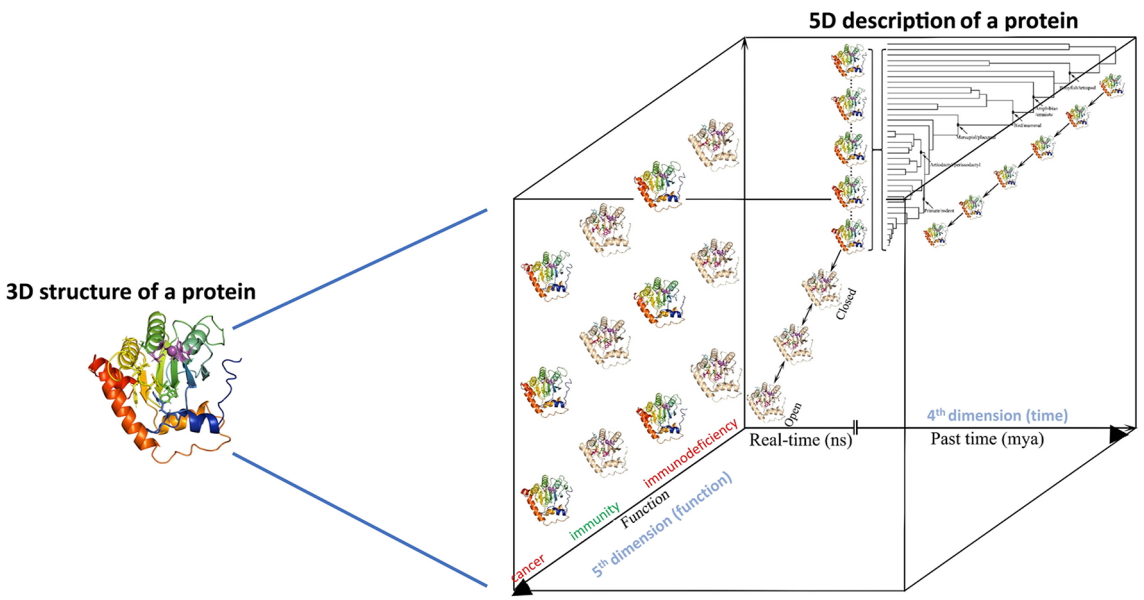

FIGURE 3 | 5-dimensional description of biological molecules. In the 5D structure description proposed here, the information from the traditional 3D structure is combined with the structure dynamics in time (4th dimension = time, in real time measured in fractions of a second, and evolutionary time measured in millions of years) and integrated with how these real-time and evolutionary dynamic structural changes impact the biological function of the protein (5th dimension = biological function as dependent on 3D and 4D descriptions of a protein's structure).

itself can also provide finer level information into the subtle differences of 3D folding of the enzyme's protein structure.

Modelling of proteins with no known related structure is a long-standing challenge in the field of structural biology where the recent breakthrough of AlpahFold has gained considerable attention (206). The AlphaFold algorithm, a learned-based method in contrast to knowledge- and physics-based ones, uses co-evolution methods and deep convolutional neural networks. Remarkably, combining the deep-learning methods such as AlphaFold with molecular dynamics stimulations has improved the accuracy of protein structural prediction even further (207). However, to achieve an accurate result using learned-based methods, access to a large dataset (e.g., multiple sequence alignment [MSA] of 10^5 to 10^6 sequences) of evolutionarily diverse sequences is necessary (208). Co-evolution-derived contact methods are based on the idea that the residues in close contact (< 8 Å considering the Cα) in the 3D structure, which define the local secondary structural features, co-evolve while the residues with medium- and long-range contact specify the overall 3D structure of a protein. In fact, the evolutionarily conserved dynamical/functional domains (termed evolutionary domains [ED]) have been predicted by coevolutionary coupling analysis of co-evolving residues (209). The contact map of the protein can be retrieved either through the evolutionary coupling analysis (ECA) or supervised machine learning (SML). ECA relies on a high-quality large MSA (with at least 64 times the square root of the

length of the target protein) while SML methods are capable of retrieving the contact map even in the case of smaller MSA by combining the sequence-dependent and independent information (210). Therefore, the approach of studying a family of proteins from many orthologs that cover a large range of biochemical properties, coupled with artificial intelligence (AI) learning, will pave the road for even more refinement of such AI-based computational approaches to protein folding, and especially so in the field of enzymology. Given that this methodology may be nearing the accuracy of experimental structure determination, as announced recently, and the applicability of enzyme (e.g., virus polymerases) structure prediction and engineering for treatment of emerging pathogens, the evolutionary comparative study of enzymes can make a critical contribution in this domain.

From a basic evolutionary immunology perspective (**Figure 2**, arrow 1, top left), the comparative enzymology approach also has brought forth meaningful insights and points for further research. For instance, the discovery that AID's catalytic pocket has evolved in one fish species to be significant more active, or capable of carrying out genome demethylation, speaks to issues of DNA-repair and genome demethylation that provide hints that in some instances in evolution, AID may indeed have had a significantly higher weight of non-immune based physiological functions as compared to the case in mammals where it plays a strictly immune role. Though other roles such as epigenetic remodelling have been proposed for human and mouse AID, the fact that AID-deficient mice appear only to suffer from Hyper IgM and no other perturbations suggest that any non-immune functions of AID in mammals are either marginal or highly redundant. This in turn suggests that perhaps AID initially emerged for other functions in the fish and was later co-opted by the immune system, a familiar pattern, that has already been shown for other DNA-damaging enzymes used by the immune system, namely the RAG recombinases. Demonstrating that AID is an active deaminase in species like sharks and coelacanth, which are key fishes in the evolution of vertebrates, also shed light on AID's role in earlier-evolved immune systems. Lastly, the unexpected and novel expansion and inter-individual copy number variation of the AID-like CDA1 enzymes in the lamprey speaks to the intriguing possibility that somehow the enzymes themselves may be the subject of an as-yet-undiscovered type of genetic diversification or environmental response.

From the perspective of protein biotechnological advancements in protein engineering (**Figure 2**, arrow 2, top right), the comparative evolutionary enzymology method is also of value for emerging biotechnological applications, such as in the emerging field of base-editing. DNA base editing is a new genome editing tool, introduced in 2016, based on the clustered regularly interspaced short palindromic repeats (CRISPR) associated (Cas) system of bacterial adaptive immunity, where a point mutation is precisely introduced into the genomic DNA (211–214). This tool is comprised of a guide RNA, a catalytically impaired Cas nuclease coupled to a ssDNA mutating enzyme. There are two different classes of ssDNA base editors, the cytidine base editors (CBEs) and adenine base editors (ABEs), where different deaminases are used as the ssDNA mutating enzyme (215). CBEs accomplish the conversion of C:G to T:A using cytidine deaminases (i.e., AID/APOBEC family members) while ABEs perform the reverse mutation using adenine deaminases (e.g., TadA). The specificity of the CBE complexes is defined by the protospacer adjacent motif (PAM) which is recognized by the Cas enzyme, the activity-window which is defined by the target sequence incorporated into the single-guide RNA (sg-RNA), and the substrate specificity of the ssDNA mutating enzyme. Since the sequence content of the target dC is defined by the target genomic regions, diversifying the substrate specificity of the ssDNA editing enzymes are of a great interest. To accomplish this goal, different members of the AID/APOBEC family, such as AID, APOBEC1, A3A, 3B, 3C, 3D, 3F, 3G, 3H, and CDA1 from human, rat, and sea lamprey, and their variants have been tethered to Cas. Deamination of methylated dC was also accomplished by using A3A variants as the ssDNA editing enzyme (216). Given the observed diversity in the biochemical properties of AID orthologs, using AID from different species, especially bony fish, would assist in expanding the specificity of the CBEs arsenal. A recent study acts as evidence for this; the study did a screen of 153 *in vitro*-evolved cytidine deaminases (APOBECs, AIDs, CDAs, etc.), led to ones that exhibited the lowest unguided off-target DNA and cellular RNA deamination events along with the highest on-target deamination events. Using this screening approach to choosing a ssDNA editing enzyme, it became possible to reduce the unguided off-target DNA deamination events by 45-fold and transcriptome-wide deamination events by 12- to 69-fold, all while maintaining a similar DNA on-target editing frequency (212). Others and we who have been studying cytidine deaminase structure:function and evolution have also generated libraries of chimeric and mutant enzymes, bearing different motifs exchanged between orthologs in order to pinpoint enzyme functionality to structural parts (**Figure 2**, arrow 2, top right). In so doing, these libraries often contain engineered enzymes with variable targeting and substrate specificity profiles that could also prove as useful tools in the field of base-editing.

In conclusion, molecules involved in human health and disease are typically studied in only a handful of well-characterized model species. Here, using the example AID, a DNA-editing enzyme involved in immunity and cancer, we have reviewed how the few studies that have examined this molecule in evolutionarily distant species have brought forth important and unexpected insights in structural biology, immunology, and cancer research. For other DNA-damaging enzymes involved in immunity and cancer, such as RAGs, the case is parallel, with less than a handful of hundreds of studies probing non-mouse/human species; however, the studies that have ventured into the evolutionary past have brought forth intriguing ideas that have changed our understanding of RAG function and evolution (217–221). This, taken together with the fact that by far the greatest window of evolutionary diversity in these DNA-editing proteins, and indeed in all proteins, lies in earlier-evolved species that have remained unstudied, would make it reasonable to conclude that much fundamental and applicable biological insights can be uncovered by large-scale evolutionary studies. The case of understudied orthologs discussed here (**Figure 1B**) is made even more glaring considering that unlike

the field of evolutionary immunology which is a recognized subfield of immunology with its own research groups, journals and scientific meetings, other disciplines such as DNA repair, cancer research, neurodegenerative diseases, and many others do not have a formal evolutionary sub-discipline. We have also discussed how, in addition to generating novel fundamental knowledge on biology, the evolutionary comparative approach for studying protein structure:function is a valuable tool to complement the emerging AI-guided protein folding methodologies as well as protein engineering in the field of base-editing and beyond.

AUTHOR CONTRIBUTIONS

All authors contributed to the preparation of the text and figures. All authors contributed to the article and approved the submitted version.

FUNDING

Natural Sciences and Engineering Research Council of Canada (NSERC), Grant/Award Number: 2015-047960.

REFERENCES

1. Flajnik MF, Kasahara M. Origin and Evolution of the Adaptive Immune System: Genetic Events and Selective Pressures. *Nat Rev Genet* (2010) 11 (1):47–59. doi: 10.1038/nrg2703
2. Pancer Z, Amemiya CT, Ehrhardt GR, Ceitlin J, Gartland GL, Cooper MD, et al. Somatic Diversification of Variable Lymphocyte Receptors in the Agnathan Sea Lamprey. *Nature* (2004) 430(6996):174–80. doi: 10.1038/nature02740
3. Lewis SM, Wu GE. The Origins of V(D)J Recombination. *Cell* (1997) 88 (2):159–62. doi: 10.1016/S0092-8674(00)81833-4
4. Oettinger MA, Schatz DG, Gorka C, Baltimore D. RAG-1 and RAG-2, Adjacent Genes That Synergistically Activate V(D)J Recombination. *Science* (1990) 248(4962):1517–23. doi: 10.1126/science.2360047
5. Schatz DG, Oettinger MA, Baltimore D. The V(D)J Recombination Activating Gene, RAG-1. *Cell* (1989) 59(6):1035–48. doi: 10.1016/0092-8674(89)90760-5
6. Gellert M. V(D)J Recombination: RAG Proteins, Repair Factors, and Regulation. *Annu Rev Biochem* (2002) 71:101–32. doi: 10.1146/annurev.biochem.71.090501.150203
7. Schatz DG, Swanson PC. V(D)J Recombination: Mechanisms of Initiation. *Annu Rev Genet* (2011) 45:167–202. doi: 10.1146/annurev-genet-110410-132552
8. Honjo T, Kinoshita K, Muramatsu M. Molecular Mechanisms of Class Switch Recombination: Linkage With Somatic Hypermutation. *Annu Rev Immunol* (2002) 20:165–96. doi: 10.1146/annurev.immunol.20.090501.112049
9. Methot SP, Di Noia JM. Molecular Mechanisms of Somatic Hypermutation and Class Switch Recombination. *Adv Immunol* (2017) 133:37–87. doi: 10.1016/bs.ai.2016.11.002
10. Min IM, Selsing E. Antibody Class Switch Recombination: Roles for Switch Sequences and Mismatch Repair Proteins. *Adv Immunol* (2005) 87:297–328. doi: 10.1016/S0065-2776(05)87008-7
11. Stavnezer J, Guikema JE, Schrader CE. Mechanism and Regulation of Class Switch Recombination. *Annu Rev Immunol* (2008) 26:261–92. doi: 10.1146/annurev.immunol.26.021607.090248
12. Muramatsu M, Kinoshita K, Fagarasan S, Yamada S, Shinkai Y, Honjo T, et al. Class Switch Recombination and Hypermutation Require Activation-Induced Cytidine Deaminase (AID), a Potential RNA Editing Enzyme. *Cell* (2000) 102(5):553–63. doi: 10.1016/S0092-8674(00)00078-7
13. Revy P, Muto T, Levy Y, Geissmann F, Plebani A, Sanal O, et al. Activation-Induced Cytidine Deaminase (AID) Deficiency Causes the Autosomal Recessive Form of the Hyper-IgM Syndrome (HIGM2). *Cell* (2000) 102 (5):565–75. doi: 10.1016/S0092-8674(00)00079-9
14. Conticello SG. The AID/APOBEC Family of Nucleic Acid Mutators. *Genome Biol* (2008) 9(6):229. doi: 10.1186/gb-2008-9-6-229
15. Conticello SG, Thomas CJ, Petersen-Mahrt SK, Neuberger MS. Evolution of the AID/APOBEC Family of Polynucleotide (Deoxy)Cytidine Deaminases. *Mol Biol Evol* (2005) 22(2):367–77. doi: 10.1093/molbev/msi026
16. Krishnan A, Iyer A, Holland SJ, Boehm T, Aravind L. Diversification of AID/APOBEC-like Deaminases in Metazoa: Multiplicity of Clades and Widespread Roles in Immunity. *Proc Natl Acad Sci USA* (2018) 115(14): E3201–10. doi: 10.1073/pnas.1720897115
17. Rogozin IB, Iyer LM, Liang L, Glazko GV, Liston VG, Pavlov YI, et al. Evolution and Diversification of Lamprey Antigen Receptors: Evidence for Involvement of an AID-APOBEC Family Cytosine Deaminase. *Nat Immunol* (2007) 8(6):647–56. doi: 10.1038/ni1463
18. Trancoso I, Morimoto R, Boehm T. Co-Evolution of Mutagenic Genome Editors and Vertebrate Adaptive Immunity. *Curr Opin Immunol* (2020) 65:32–41. doi: 10.1016/j.coi.2020.03.001
19. Ott JA, Castro CD, Deiss TC, Ohta Y, Flajnik MF, Criscitiello MF. Somatic Hypermutation of T Cell Receptor Alpha Chain Contributes to Selection in Nurse Shark Thymus. *Elife* (2018) 7. doi: 10.7554/eLife.28477
20. Holland SJ, Berghuis LM, King JJ, Iyer LM, Sikora K, Fifield H, et al. Expansions, Diversification, and Interindividual Copy Number Variations of AID/APOBEC Family Cytidine Deaminase Genes in Lampreys. *Proc Natl Acad Sci USA* (2018) 115(14):E3211–20. doi: 10.1073/pnas.1720871115
21. Quinlan EM, King JJ, Amemiya CT, Hsu E, Larijan M. Biochemical Regulatory Features of Activation-Induced Cytidine Deaminase Remain Conserved From Lampreys to Humans. *Mol Cell Biol* (2017) 37 (20):00077–17. doi: 10.1128/MCB.00077-17
22. Zhang ZZ, Pannunzio NR, Lu Z, Hsu E, Yu K, Lieber MR. The Repetitive Portion of the Xenopus Igh Mu Switch Region Mediates Orientation-Dependent Class Switch Recombination. *Mol Immunol* (2015) 67(2 Pt B): 524–31. doi: 10.1016/j.molimm.2015.07.039
23. Hirano M, Das S, Guo P, Cooper MD. The Evolution of Adaptive Immunity in Vertebrates. *Adv Immunol* (2015) 109:125–57. doi: 10.1016/B978-0-12-387664-5.00004-2
24. Magor BG. Antibody Affinity Maturation in Fishes-Our Current Understanding. *Biol (Basel)* (2015) 4(3):512–24. doi: 10.3390/biology 4030512
25. Kato L, Stanlie A, Begum NA, Kobayashi M, Aida M, Honjo T, et al. An Evolutionary View of the Mechanism for Immune and Genome Diversity. *J Immunol* (2012) 188(8):3559–66. doi: 10.4049/jimmunol.1102397
26. Dancyger AM, King JJ, Quinlan MJ, Fifield H, Tucker S, Sauders HL. Differences in the Enzymatic Efficiency of Human and Bony Fish AID are Mediated by a Single Residue in the C Terminus Modulating Single-Stranded DNA Binding. *FASEB J* (2012) 26(4):1517–25. doi: 10.1096/fj.11-198135
27. Zhu C, Hsu E. Error-Prone DNA Repair Activity During Somatic Hypermutation in Shark B Lymphocytes. *J Immunol* (2010) 185(9):5336–47. doi: 10.4049/jimmunol.1000779
28. Basu U, Chaudhuri J, Phan RT, Datta A. Regulation of Activation Induced Deaminase Via Phosphorylation. *Adv Exp Med Biol* (2007) 596:129–37. doi: 10.1007/0-387-46530-8_11
29. Arakawa H, Buerstedde JM. Activation-Induced Cytidine Deaminase-Mediated Hypermutation in the DT40 Cell Line. *Philos Trans R Soc Lond B Biol Sci* (2009) 364(1517):639–44. doi: 10.1098/rstb.2008.0202
30. Basu U, Wang Y, Alt FW. Evolution of Phosphorylation-Dependent Regulation of Activation-Induced Cytidine Deaminase. *Mol Cell* (2008) 32 (2):285–91. doi: 10.1016/j.molcel.2008.08.019

31. Ichikawa HT, Sowden MP, Torelli AT, Bachl J, Huang P, Dance GS, et al. Structural Phylogenetic Analysis of Activation-Induced Deaminase Function. *J Immunol* (2006) 177(1):355–61. doi: 10.4049/jimmunol.177.1.355
32. Wakae K, Magor BG, Saunders H, Nagaoka H, Kawamura A, Kinoshita K, et al. Evolution of Class Switch Recombination Function in Fish Activation-Induced Cytidine Deaminase, AID. *Int Immunol* (2006) 18(1):41–7. doi: 10.1093/intimm/dxh347
33. Barreto VM, Pan-Hammarstrom Q, Zhao Y, Hammarstrom L, Misulovin Z, Nussenzweig MC. AID From Bony Fish Catalyzes Class Switch Recombination. *J Exp Med* (2005) 202(6):733–8. doi: 10.1084/jem.20051378
34. Stavnezer J, Amemiya CT. Evolution of Isotype Switching. *Semin Immunol* (2004) 16(4):257–75. doi: 10.1016/j.smim.2004.08.005
35. Ott JA, Harrison J, Flajnik MF, Criscitiello MF. Nurse Shark T-cell Receptors Employ Somatic Hypermutation Preferentially to Alter Alpha/Delta Variable Segments Associated With Alpha Constant Region. *Eur J Immunol* (2020) 50(9):1307–20. doi: 10.1002/eji.201948495
36. Bilal S, Lie KK, Saele O, Hord I. T Cell Receptor Alpha Chain Genes in the Teleost Ballan Wrasse (Labrus Bergylta) Are Subjected to Somatic Hypermutation. *Front Immunol* (2018) 9:1101. doi: 10.3389/fimmu.2018.01101
37. Zhu C, Lee V, Finn A, Senger KT, Zarrin AA, Du Pasquier L, et al. Origin of Immunoglobulin Isotype Switching. *Curr Biol* (2012) 22(10):872–80. doi: 10.1016/j.cub.2012.03.060
38. Zhu C, Feng W, Weedon J, Hua P, Stefanov D, Ohta Y, et al. The Multiple Shark Ig H Chain Genes Rearrange and Hypermutate Autonomously. *J Immunol* (2011) 187(5):2492–501. doi: 10.4049/jimmunol.1101671
39. Abdouni H, King JJ, Suliman M, Quinlan M, Fifield H, Larijani M. Zebrafish AID is Capable of Deaminating Methylated Deoxycytidines. *Nucleic Acids Res* (2013) 41(10):5457–68. doi: 10.1093/nar/gkt212
40. Saunders HL, Magor BG. Cloning and Expression of the AID Gene in the Channel Catfish. *Dev Comp Immunol* (2004) 28(7–8):657–63. doi: 10.1016/j.dci.2004.01.002
41. Saunders HL, Oko AL, Scott AN, Fan CW, Magor BG. The Cellular Context of AID Expressing Cells in Fish Lymphoid Tissues. *Dev Comp Immunol* (2010) 34(6):669–76. doi: 10.1016/j.dci.2010.01.013
42. Chatterji M, Unniraman S, McBride KM, Schatz DG. Role of Activation-Induced Deaminase Protein Kinase A Phosphorylation Sites in Ig Gene Conversion and Somatic Hypermutation. *J Immunol* (2007) 179(8):5274–80. doi: 10.4049/jimmunol.179.8.5274
43. Yang F, Waldbieser GC, Lobb CJ. The Nucleotide Targets of Somatic Mutation and the Role of Selection in Immunoglobulin Heavy Chains of a Teleost Fish. *J Immunol* (2006) 176(3):1655–67. doi: 10.4049/jimmunol.176.3.1655
44. Zhao Y, Pan-Hammarstr√∂m Q, Zhao Z, Hammarstr√∂m L. Identification of the Activation-Induced Cytidine Deaminase Gene From Zebrafish: An Evolutionary Analysis. *Dev Comp Immunol* (2005) 29(1):61–71. doi: 10.1016/j.dci.2004.05.005
45. Lada AG, Dhar A, Boissy RJ, Hirano M, Rubel AA, Rogozin IB, et al. AID/APOBEC Cytosine Deaminase Induces Genome-Wide Kataegis. *Biol Direct* (2012) 7:47. doi: 10.1186/1745-6150-7-47
46. Kasahara M. Variable Lymphocyte Receptors: A Current Overview. *Results Probl Cell Differ* (2015) 57:175–92. doi: 10.1007/978-3-319-20819-0_8
47. Lada AG, Stepchenkova EI, Waisertreiger IS, Noskov VN, Dhar A, Eudy JD, et al. Genome-Wide Mutation Avalanches Induced in Diploid Yeast Cells by a Base Analog or an APOBEC Deaminase. *PloS Genet* (2013) 9(9):e1003736. doi: 10.1371/journal.pgen.1003736
48. Bajoghli B, et al. A Thymus Candidate in Lampreys. *Nature* (2011) 470 (7332):90–4. doi: 10.1038/nature09655
49. Barreto VM, Magor BG. Activation-Induced Cytidine Deaminase Structure and Functions: A Species Comparative View. *Dev Comp Immunol* (2011) 35 (9):991–1007. doi: 10.1016/j.dci.2011.02.005
50. Bascove M, Frippiat JP. Molecular Characterization of Pleurodeles Waltl Activation-Induced Cytidine Deaminase. *Mol Immunol* (2010) 47(7-8):1640–9. doi: 10.1016/j.molimm.2010.01.005
51. Marr S, Morales H, Bottaro A, Cooper M, Flajnik M, Robert J, et al. Localization and Differential Expression of Activation-Induced Cytidine Deaminase in the Amphibian Xenopus Upon Antigen Stimulation and During Early Development. *J Immunol* (2007) 179(10):6783–9. doi: 10.4049/jimmunol.179.10.6783
52. King JJ, Manuel CA, Barrett CV, Raber S, Lucas H, Sutter P, et al. Catalytic Pocket Inaccessibility of Activation-Induced Cytidine Deaminase is a Safeguard Against Excessive Mutagenic Activity. *Structure* (2015) 23 (4):615–27. doi: 10.1016/j.str.2015.01.016
53. King JJ LM. A Novel Intrinsic Regulator of AID/APOBECs: Schrödinger's CATalytic Pocket. *Front Immunol* (2017) 8:351. doi: 10.3389/fimmu.2017.00351
54. Morimoto R, O'Meara CP, Holland SJ, Trancoso I, Souissi A, Schorpp M, et al. Cytidine Deaminase 2 is Required for VLRB Antibody Gene Assembly in Lampreys. *Sci Immunol* (2020) 5(45). doi: 10.1126/sciimmunol.aba0925
55. Costello R, Cantillo JF, Kenter AL. Chicken MBD4 Regulates Immunoglobulin Diversification by Somatic Hypermutation. *Front Immunol* (2019) 10:2540. doi: 10.3389/fimmu.2019.02540
56. Liu MC, Liao WY, Buckley KM, Yang SY, Rast JP, Fugmann SD. AID/APOBEC-Like Cytidine Deaminases are Ancient Innate Immune Mediators in Invertebrates. *Nat Commun* (2018) 9(1):1948. doi: 10.1038/s41467-018-04273-x
57. Patel B, Banerjee R, Samanta M, Das S. Diversity of Immunoglobulin (Ig) Isotypes and the Role of Activation-Induced Cytidine Deaminase (AID) in Fish. *Mol Biotechnol* (2018) 60(6):435–53. doi: 10.1007/s12033-018-0081-8
58. Villota-Herdoiza D, Pila EA, Quiniou S, Waldbieser GC, Magor BG. Transcriptional Regulation of Teleost Aicda Genes. Part 1 - Suppressors of Promiscuous Promoters. *Fish Shellfish Immunol* (2013) 35(6):1981–7. doi: 10.1016/j.fsi.2013.09.035
59. Verma S, Goldammer T, Aitken R. Cloning and Expression of Activation Induced Cytidine Deaminase From Bos Taurus. *Vet Immunol Immunopathol* 134(3-4):151–9. doi: 10.1016/j.vetimm.2009.08.016
60. Rai K, Huggins IJ, James SR, Karpf AR, Jones DA, Cairns BR, et al. DNA Demethylation in Zebrafish Involves the Coupling of a Deaminase, a Glycosylase, and Gadd45. *Cell* (2008) 135(7):1201–12. doi: 10.1016/j.cell.2008.11.042
61. Moon SY, Eun HJ, Baek SK, Jin SJ, Kim TS, Kim SW, et al. Activation-Induced Cytidine Deaminase Induces Dna Demethylation of Pluripotency Genes in Bovine Differentiated Cells. *Cell Reprogram* (2016) 18(5):298–308. doi: 10.1089/cell.2015.0076
62. Basu U, Franklin A, Schwer B, Cheng HL, Chaudhuri J, Alt FW. Regulation of Activation-Induced Cytidine Deaminase DNA Deamination Activity in B-cells by Ser38 Phosphorylation. *Biochem Soc Trans* (2009) 37(Pt 3):561–8. doi: 10.1042/BST0370561
63. Methot SP, et al. Consecutive Interactions With HSP90 and eEF1A Underlie a Functional Maturation and Storage Pathway of AID in the Cytoplasm. *J Exp Med* (2015) 212(4):581–96. doi: 10.1084/jem.20141157
64. Zhang J, Webb DM. Rapid Evolution of Primate Antiviral Enzyme APOBEC3G. *Hum Mol Genet* (2004) 13(16):1785–91. doi: 10.1093/hmg/ddh183
65. Harris RS, Liddament MT. Retroviral Restriction by APOBEC Proteins. *Nat Rev Immunol* (2004) 4(11):868–77. doi: 10.1038/nri1489
66. Smith HC. APOBEC3G: A Double Agent in Defense. *Trends Biochem Sci* (2011) 36(5):239–44. doi: 10.1016/j.tibs.2010.12.003
67. Monajemi M, Woodworth CF, Benkaroun J, Grant M, Larijani M. Emerging Complexities of APOBEC3G Action on Immunity and Viral Fitness During HIV Infection and Treatment. *Retrovirology* (2012) 9:35. doi: 10.1186/1742-4690-9-35
68. Borzooee F, Asgharpour M, Quinlan E, Grant MD, Larijani M. Viral Subversion of APOBEC3s: Lessons for Anti-Tumor Immunity and Tumor Immunotherapy. *Int Rev Immunol* (2018) 37(3):151–64. doi: 10.1080/08830185.2017.1403596
69. Pujantell M, Riveira-Munoz E, Badia R, Castellvi M, Garcia-Vidal E, Sirera G, et al. RNA Editing by ADAR1 Regulates Innate and Antiviral Immune Functions in Primary Macrophages. *Sci Rep* (2017) 7(1):13339. doi: 10.1038/s41598-017-13580-0
70. Lamers MM, van den Hoogen BG, Haagmans BL. Adar1: "Editor-in-Chief" of Cytoplasmic Innate Immunity. *Front Immunol* (2019) 10:1763. doi: 10.3389/fimmu.2019.01763

71. Sabag O, Zamir A, Keshet I, Hecht M, Ludwig G, Tabib A, et al. Establishment of Methylation Patterns in ES Cells. *Nat Struct Mol Biol* (2014) 21(1):110–2. doi: 10.1038/nsmb.2734
72. Samuel CE. Adenosine Deaminases Acting on RNA (Adars) are Both Antiviral and Proviral. *Virology* (2011) 411(2):180–93. doi: 10.1016/j.virol.2010.12.004
73. Samuel CE. Adars: Viruses and Innate Immunity. *Curr Top Microbiol Immunol* (2012) 353:163–95. doi: 10.1007/82_2011_148
74. Alder MN, et al. Antibody Responses of Variable Lymphocyte Receptors in the Lamprey. *Nat Immunol* (2008) 9(3):319–27. doi: 10.1038/ni1562
75. Das S, Sutoh Y, Hirano M, Han Q, Li J, Cooper MD, et al. Characterization of Lamprey BAFF-Like Gene: Evolutionary Implications. *J Immunol* (2016) 197(7):2695–703. doi: 10.4049/jimmunol.1600799
76. Holland SJ, Gao M, Hirano M, Iyer LM, Luo M, Schorpp M, et al. Selection of the Lamprey VLRC Antigen Receptor Repertoire. *Proc Natl Acad Sci USA* (2014) 111(41):14834–9. doi: 10.1073/pnas.1415655111
77. Pancer Z, Amemiya CT, Ehrhardt GRA, Ceitlin J, Gartland GL, Cooper MD. Pillars Article: Somatic Diversification of Variable Lymphocyte Receptors in the Agnathan Sea Lamprey. Nature. *2004. 430: 174-180. J Immunol* (2018) 201(5):1336–42. doi: 10.1038/nature02740
78. Pancer Z, Mayer WE, Klein J, Cooper MD. Prototypic T Cell Receptor and CD4-like Coreceptor are Expressed by Lymphocytes in the Agnathan Sea Lamprey. *Proc Natl Acad Sci USA* (2004) 101(36):13273–8. doi: 10.1073/pnas.0405529101
79. Thomson DW, Shahrin NH, Wang PPS, Wadham C, Shanmuganathan N, Scott HS, et al. Aberrant RAG-mediated Recombination Contributes to Multiple Structural Rearrangements in Lymphoid Blast Crisis of Chronic Myeloid Leukemia. *Leukemia* (2020). doi: 10.1038/s41375-020-0751-y
80. Hu J, Zhang Y, Zhao L, Frock RL, Du Z, Meyers RM, et al. Chromosomal Loop Domains Direct the Recombination of Antigen Receptor Genes. *Cell* (2015) 163(4):947–59. doi: 10.1016/j.cell.2015.10.016
81. Heinaniemi M, Vuorenmaa T, Teppo S, Kaikkonen MU, Bouvy-Liivrand M, Mehtonen J, et al. Transcription-Coupled Genetic Instability Marks Acute Lymphoblastic Leukemia Structural Variation Hotspots. *Elife* (2016) 5. doi: 10.7554/eLife.13087
82. Shimazaki N, Tsai AG, Lieber MR. H3k4me3 Stimulates the V(D)J RAG Complex for Both Nicking and Hairpinning in Trans in Addition to Tethering in Cis: Implications for Translocations. *Mol Cell* (2009) 34 (5):535–44. doi: 10.1016/j.molcel.2009.05.011
83. Mijuskovic M, Chou YF, Gigi V, Lindsay CR, Shestova O, Lewis SM, et al. Off-Target V(D)J Recombination Drives Lymphomagenesis and Is Escalated by Loss of the Rag2 C Terminus. *Cell Rep* (2015) 12(11):1842–52. doi: 10.1016/j.celrep.2015.08.034
84. Schlissel MS, Kaffer CR, Curry JD. Leukemia and Lymphoma: A Cost of Doing Business for Adaptive Immunity. *Genes Dev* (2006) 20(12):1539–44. doi: 10.1101/gad.1446506
85. Kirkham CM, Scott JNF, Wang X, Smith AL, Kupinski AP, Ford AM, et al. Cut-and-Run: A Distinct Mechanism by Which V(D)J Recombination Causes Genome Instability. *Mol Cell* (2019) 74(3):584–97.e9. doi: 10.1016/j.molcel.2019.02.025
86. Walker BA, Wardell CP, Johnson DC, Kaiser MF, Begum DB, Dahir NB, et al. Characterization of IGH Locus Breakpoints in Multiple Myeloma Indicates a Subset of Translocations Appear to Occur in Pregerminal Center B Cells. *Blood* (2013) 121(17):3413–9. doi: 10.1182/blood-2012-12-471888
87. Vaandrager JW, Schuuring E, Philippo K, Kluin PM. V(D)J Recombinase-Mediated Transposition of the BCL2 Gene to the IGH Locus in Follicular Lymphoma. *Blood* (2000) 96(5):1947–52. doi: 10.1182/blood.V96.5.1947
88. Choudhary M, Tamrakar A, Singh AK, Jain M, Jaiswal A, Kodgire P. Aid Biology: A Pathological and Clinical Perspective. *Int Rev Immunol* (2018) 37 (1):37–56. doi: 10.1080/08830185.2017.1369980
89. Klemm L, Duy C, Iacobucci I, Kuchen S, von Levetzow G, Feldhahn N, et al. The B Cell Mutator AID Promotes B Lymphoid Blast Crisis and Drug Resistance in Chronic Myeloid Leukemia. *Cancer Cell* (2009) 16(3):232–45. doi: 10.1016/j.ccr.2009.07.030
90. Seifert M, Scholtysik R, Kuppers R. Origin and Pathogenesis of B Cell Lymphomas. *Methods Mol Biol* (2019) 1956:1–33. doi: 10.1007/978-1-4939-9151-8_1
91. Takizawa M, Tolarova H, Li Z, Dubois W, Lim S, Callen E, et al. AID Expression Levels Determine the Extent of cMyc Oncogenic Translocations and the Incidence of B Cell Tumor Development. *J Exp Med* (2008) 205 (9):1949–57. doi: 10.1084/jem.20081007
92. Burns A, Alsolami R, Becq J, Timbs A, Bruce D, Robbe P, et al. Whole-Genome Sequencing of Chronic Lymphocytic Leukaemia Reveals Distinct Differences in the Mutational Landscape Between IgHVmut and IgHVunmut Subgroups. *Leukemia* (2017). doi: 10.1038/leu.2017.311
93. Mohri T, Nagata K, Kuwamoto S, Matsushita M, Sugihara H, Kato M, et al. Aberrant Expression of AID and AID Activators of NF-kappaB and PAX5 is Irrelevant to EBV-associated Gastric Cancers, But is Associated With Carcinogenesis in Certain EBV-non-associated Gastric Cancers. *Oncol Lett* (2017) 13(6):4133–40. doi: 10.3892/ol.2017.5978
94. Swaminathan S, Klemm L, Park E, Papaemmanuil E, Ford A, Kweon SM, et al. Mechanisms of Clonal Evolution in Childhood Acute Lymphoblastic Leukemia. *Nat Immunol* (2015) 16(7):766–74. doi: 10.1038/ni.3160
95. Pasqualucci L, Bhagat G, Jankovic M, Compagno M, Smith P, Muramatsu M, et al. AID is Required for Germinal Center-Derived Lymphomagenesis. *Nat Genet* (2008) 40(1):108–12. doi: 10.1038/ng.2007.35
96. Kotani A, Kakazu N, Tsuruyama T, Okazaki IM, Muramatsu M, Kinoshita K, et al. Activation-Induced Cytidine Deaminase (AID) Promotes B Cell Lymphomagenesis in Emu-cmyc Transgenic Mice. *Proc Natl Acad Sci USA* (2007) 104(5):1616–20. doi: 10.1073/pnas.0610732104
97. Lindley RA, Humbert P, Larner C, Akmeemana EH, Pendlebury CR. Association Between Targeted Somatic Mutation (TSM) Signatures and HGS-OvCa Progression. *Cancer Med* (2016) 5(9):2629–40. doi: 10.1002/cam4.825
98. Leonard B, Hart SN, Burns MB, Carpenter MA, Temiz NA, Rathore A, et al. APOBEC3B Upregulation and Genomic Mutation Patterns in Serous Ovarian Carcinoma. *Cancer Res* (2013) 73(24):7222–31. doi: 10.1158/0008-5472.CAN-13-1753
99. Ruder U, Denkert C, Kunze CA, Jank P, Lindner J, Johrens K, et al. APOBEC3B Protein Expression and mRNA Analyses in Patients With High-Grade Serous Ovarian Carcinoma. *Histol Histopathol* (2019) 34(4):405–17.
100. Zou J, Wang C, Ma X, Wang E, Peng G. APOBEC3B, a Molecular Driver of Mutagenesis in Human Cancers. *Cell Biosci* (2017) 7:29. doi: 10.1186/s13578-017-0156-4
101. Sasaki H, Suzuki A, Tatematsu T, Shitara M, Hikosaka Y, Okud K, et al. APOBEC3B Gene Overexpression in non-Small-Cell Lung Cancer. *BioMed Rep* (2014) 2(3):392–5. doi: 10.3892/br.2014.256
102. Swanton C, McGranahan N, Starrett GJ, Harris RS. Apobec Enzymes: Mutagenic Fuel for Cancer Evolution and Heterogeneity. *Cancer Discovery* (2015) 5(7):704–12. doi: 10.1158/2159-8290.CD-15-0344
103. Siriwardena SU, Chen K, Bhagwat AS. Functions and Malfunctions of Mammalian Dna-Cytosine Deaminases. *Chem Rev* (2016) 116(20):12688–710. doi: 10.1021/acs.chemrev.6b00296
104. Burns MB, et al. APOBEC3B is an Enzymatic Source of Mutation in Breast Cancer. *Nature* (2013) 494(7437):366–70. doi: 10.1038/nature11881
105. Roberts SA, Gordenin DA. Hypermutation in Human Cancer Genomes: Footprints and Mechanisms. *Nat Rev Cancer* (2014) 14(12):786–800. doi: 10.1038/nrc3816
106. Alexandrov LB, Nik-Zainal S, Wedge DC, Aparicio SA, Behjati S, Biankin AV, et al. Signatures of Mutational Processes in Human Cancer. *Nature* (2013) 500(7463):415–21.
107. Starrett GJ, Luengas EM, McCann JL, Ebrahimi D, Temiz NA, Love RP, et al. The DNA Cytosine Deaminase APOBEC3H Haplotype I Likely Contributes to Breast and Lung Cancer Mutagenesis. *Nat Commun* (2016) 7:12918. doi: 10.1038/ncomms12918
108. Nik-Zainal S, Davies H, Staaf J, Ramakrishna M, Glodzik D, Zou X, et al. Landscape of Somatic Mutations in 560 Breast Cancer Whole-Genome Sequences. *Nature* (2016) 534(7605):47–54.
109. Chan TH, Qamra A, Tan KT, Guo J, Yang H, Qi L, et al. Adar-Mediated RNA Editing Predicts Progression and Prognosis of Gastric Cancer. *Gastroenterology* (2016) 151(4):637–50.e10. doi: 10.1053/j.gastro.2016.06.043
110. Wang C, Zou J, Ma X, Wang E, Peng G. Mechanisms and Implications of ADAR-mediated RNA Editing in Cancer. *Cancer Lett* (2017) 411:27–34. doi: 10.1016/j.canlet.2017.09.036
111. Roberts JT, Patterson DG, King VM, Amin SV, Polska CJ, Houserova D, et al. Adar Mediated Rna Editing Modulates MicroRNA Targeting in Human Breast Cancer. *Processes (Basel)* (2018) 6(5). doi: 10.3390/pr6050042

112. Jiang Q, Isquith J, Ladel L, Mark A, Holm F, Mason C, et al. Inflammation-Driven Deaminase Deregulation Fuels Human Pre-Leukemia Stem Cell Evolution. *Cell Rep* (2021) 34(4):108670. doi: 10.1016/j.celrep.2020.108670
113. Law EK, Levin-Klein R, Jarvis MC, Kim H, Argyris PP, Carpenter MA, et al. APOBEC3A Catalyzes Mutation and Drives Carcinogenesis in Vivo. *J Exp Med* (2020) 217(12). doi: 10.1084/jem.20200261
114. Durandy A. Mini-Review Activation-induced Cytidine Deaminase: A Dual Role in Class-Switch Recombination and Somatic Hypermutation. *Eur J Immunol* (2003) 33(8):2069–73. doi: 10.1002/eji.200324133
115. Durandy A. Activation-Induced Cytidine Deaminase: A Dual Role in Class-Switch Recombination and Somatic Hypermutation. *Eur J Immunol* (2003) 33(8):2069–73. doi: 10.1002/eji.200324133
116. Durandy A, Peron S, Fischer A. Hyper-IgM Syndromes. *Curr Opin Rheumatol* (2006) 18(4):369–76. doi: 10.1097/01.bor.0000231905.12172.b5
117. Gennery A. Recent Advances in Understanding RAG Deficiencies. *F1000Res* (2019) 8. doi: 10.12688/f1000research.17056.1
118. Schwarz K, Gauss GH, Ludwig L, Pannicke U, Li Z, Lindner D, et al. RAG Mutations in Human B Cell-Negative SCID. *Science* (1996) 274(5284):97–9. doi: 10.1126/science.274.5284.97
119. Shinkai Y, Rathbun G, Lam KP, Oltz EM, Stewart V, Mendelsohn M, et al. Rag-2-deficient Mice Lack Mature Lymphocytes Owing to Inability to Initiate V(D)J Rearrangement. *Cell* (1992) 68(5):855–67. doi: 10.1016/0092-8674(92)90029-C
120. Mombaerts P, Iacomini J, Johnson RS, Herrup K, Tonegawa S, Papaioannou VE, et al. Rag-1-deficient Mice Have No Mature B and T Lymphocytes. *Cell* (1992) 68(5):869–77. doi: 10.1016/0092-8674(92)90030-G
121. Lada AG, Iyer LM, Rogozin IB, Aravind L, Pavlov Iu I. Vertebrate Immunity: Mutator Proteins and Their Evolution. *Genetika* (2007) 43(10):1311–27.
122. Rubio MA, Pastar I, Gaston KW, Ragone FL, Janzen CJ, Cross GA, et al. An Adenosine-to-Inosine tRNA-editing Enzyme That can Perform C-to-U Deamination of DNA. *Proc Natl Acad Sci USA* (2007) 104(19):7821–6. doi: 10.1073/pnas.0702394104
123. Gerber A, Grosjean A, Melcher T, Keller W. Tad1p, a Yeast tRNA-specific Adenosine Deaminase, is Related to the Mammalian pre-mRNA Editing Enzymes ADAR1 and ADAR2. *EMBO J* (1998) 17(16):4780–9. doi: 10.1093/emboj/17.16.4780
124. Gerber AP, Keller W. An Adenosine Deaminase That Generates Inosine At the Wobble Position of Trnas. *Science* (1999) 286(5442):1146–9. doi: 10.1126/science.286.5442.1146
125. Zhou W, Karcher D, Bock R. Importance of Adenosine-to-Inosine Editing Adjacent to the Anticodon in an Arabidopsis Alanine tRNA Under Environmental Stress. *Nucleic Acids Res* (2013) 41(5):3362–72. doi: 10.1093/nar/gkt013
126. Conticello SG, Langlois MA, Yang Z, Neuberger MS. DNA Deamination in Immunity: AID in the Context of its APOBEC Relatives. *Adv Immunol* (2007) 94:37–73. doi: 10.1016/S0065-2776(06)94002-4
127. Torres AG, Pineyro D, Filonava L, Stracker TH, Batlle E, Ribas de Pouplana L. A-to-I Editing on tRNAs: Biochemical, Biological and Evolutionary Implications. *FEBS Lett* (2014) 588(23):4279–86. doi: 10.1016/j.febslet.2014.09.025
128. Iyer LM, Zhang D, Rogozin IB, Aravind L. Evolution of the Deaminase Fold and Multiple Origins of Eukaryotic Editing and Mutagenic Nucleic Acid Deaminases From Bacterial Toxin Systems. *Nucleic Acids Res* (2011) 39(22):9473–97. doi: 10.1093/nar/gkr691
129. Qiao Q, Wang L, Meng FL, Hwang JK, Alt FW, Wu H. Aid Recognizes Structured DNA for Class Switch Recombination. *Mol Cell* (2017) 67(3):361–73.e4. doi: 10.1016/j.molcel.2017.06.034
130. Silvas TV, Schiffer CA. Apobec3s: DNA-editing Human Cytidine Deaminases. *Protein Sci* (2019) 28(9):1552–66. doi: 10.1002/pro.3670
131. Rogozin IB, Basu MK, Jordan IK, Pavlov YI, Koonin EV. APOBEC4, a New Member of the AID/APOBEC Family of Polynucleotide (Deoxy)Cytidine Deaminases Predicted by Computational Analysis. *Cell Cycle* (2005) 4(9):1281–5. doi: 10.4161/cc.4.9.1994
132. Liao W, Hong SH, Chan BH, Rudolph FB, Clark SC, Chan L. Apobec-2, a Cardiac- and Skeletal Muscle-Specific Member of the Cytidine Deaminase Supergene Family. *Biochem Biophys Res Commun* (1999) 260(2):398–404. doi: 10.1006/bbrc.1999.0925
133. Mikl MC, Watt IN, Lu M, Reik W, Davies SL, Neuberger MS, et al. Mice Deficient in APOBEC2 and APOBEC3. *Mol Cell Biol* (2005) 25(16):7270–7. doi: 10.1128/MCB.25.16.7270-7277.2005
134. Sato Y, Probst HC, Tatsumi R, Ikeuchi Y, Neuberger MS, Rad C. Deficiency in APOBEC2 Leads to a Shift in Muscle Fiber Type, Diminished Body Mass, and Myopathy. *J Biol Chem* (2010) 285(10):7111–8. doi: 10.1074/jbc.M109.052977
135. Vonica A, Rosa A, Arduini BL, Brivanlou AH. APOBEC2, a Selective Inhibitor of TGFbeta Signaling, Regulates Left-Right Axis Specification During Early Embryogenesis. *Dev Biol* (2011) 350(1):13–23. doi: 10.1016/j.ydbio.2010.09.016
136. Fujino T, Navaratnam N, Scott J. Human Apolipoprotein B RNA Editing Deaminase Gene (APOBEC1). *Genomics* (1998) 47(2):266–75. doi: 10.1006/geno.1997.5110
137. Harris RS, Petersen-Mahrt SK, Neuberger MS. RNA Editing Enzyme APOBEC1 and Some of its Homologs can Act as DNA Mutators. *Mol Cell* (2002) 10(5):1247–53. doi: 10.1016/S1097-2765(02)00742-6
138. Nakamuta M, Oka K, Krushkal J, Kobayashi K, Yamamoto M, Li WH, et al. Alternative mRNA Splicing and Differential Promoter Utilization Determine Tissue-Specific Expression of the Apolipoprotein B mRNA-editing Protein (Apobec1) Gene in Mice. Structure and Evolution of Apobec1 and Related Nucleoside/Nucleotide Deaminases. *J Biol Chem* (1995) 270(22):13042–56. doi: 10.1074/jbc.270.22.13042
139. Nakamuta M, Chang BH, Zsigmond E, Kobayashi K, Lei H, Ishida BY, et al. Complete Phenotypic Characterization of Apobec-1 Knockout Mice With a Wild-Type Genetic Background and a Human Apolipoprotein B Transgenic Background, and Restoration of Apolipoprotein B mRNA Editing by Somatic Gene Transfer of Apobec-1. *J Biol Chem* (1996) 271(42):25981–8. doi: 10.1074/jbc.271.42.25981
140. Petersen-Mahrt SK, Neuberger MS. In Vitro Deamination of Cytosine to Uracil in Single-Stranded DNA by Apolipoprotein B Editing Complex Catalytic Subunit 1 (APOBEC1). *J Biol Chem* (2003) 278(22):19583–6. doi: 10.1074/jbc.C300114200
141. Petit V, Guetard D, Renard M, Keriel A, Sitbon M, Wain-Hobson S, et al. Murine APOBEC1 is a Powerful Mutator of Retroviral and Cellular RNA In Vitro and In Vivo. *J Mol Biol* (2009) 385(1):65–78. doi: 10.1016/j.jmb.2008.10.043
142. Sharma S, Patnaik SK, Taggart RT, Kannisto ED, Enriquez SM, Gollnick P, et al. APOBEC3A Cytidine Deaminase Induces RNA Editing in Monocytes and Macrophages. *Nat Commun* (2015) 6:6881. doi: 10.1038/ncomms7881
143. Abdouni HS, King JJ, Ghorbani A, Fifield H, Berghuis L, Larijani M. DNA/RNA Hybrid Substrates Modulate the Catalytic Activity of Purified AID. *Mol Immunol* (2018) 93:94–106. doi: 10.1016/j.molimm.2017.11.012
144. Sawyer SL, Emerman M, Malik HS. Ancient Adaptive Evolution of the Primate Antiviral DNA-editing Enzyme APOBEC3G. *PloS Biol* (2004) 2(9):E275. doi: 10.1371/journal.pbio.0020275
145. Tacchi L, Larragoite ET, Munoz P, Amemiya CT, Salinas I. African Lungfish Reveal the Evolutionary Origins of Organized Mucosal Lymphoid Tissue in Vertebrates. *Curr Biol* (2015) 25(18):2417–24. doi: 10.1016/j.cub.2015.07.066
146. Flajnik MF. Primitive Vertebrate Immunity: What is the Evolutionary Derivative of Molecules That Define the Adaptive Immune System? *Ciba Found Symp* (1994) 186:224–32; discussion 233-6. doi: 10.1002/9780470514658.ch13
147. Flajnik MF. The Immune System of Ectothermic Vertebrates. *Vet Immunol Immunopathol* (1996) 54(1-4):145–50. doi: 10.1016/S0165-2427(96)05685-1
148. Du Pasquier L. The Phylogenetic Origin of Antigen-Specific Receptors. *Curr Top Microbiol Immunol* (2000) 248:160–85. doi: 10.1007/978-3-642-59674-2_8
149. Hsu E, Pulham N, Rumfelt LL, Flajnik MF. The Plasticity of Immunoglobulin Gene Systems in Evolution. *Immunol Rev* (2006) 210:8–26. doi: 10.1111/j.0105-2896.2006.00366.x
150. Hirano M, Guo P, McCurley N, Schorpp M, Das S, Boehm T, et al. Evolutionary Implications of a Third Lymphocyte Lineage in Lampreys. *Nature* (2013) 501(7467):435–8. doi: 10.1038/nature12467
151. Chen H, Kshirsagar S, Jensen I, Lau K, Covarrubias R, Schluter SF, et al. Characterization of Arrangement and Expression of the T Cell Receptor Gamma Locus in the Sandbar Shark. *Proc Natl Acad Sci USA* (2009) 106(21):8591–6. doi: 10.1073/pnas.0811283106
152. Chen H, Kshirsagar S, Jensen I, Lau K, Simonson C, Schluter SF, et al. Characterization of Arrangement and Expression of the Beta-2

Microglobulin Locus in the Sandbar and Nurse Shark. *Dev Comp Immunol* (2010) 34(2):189–95. doi: 10.1016/j.dci.2009.09.008
153. Ciccarese S, Vaccarelli G, Lefranc MP, Tasco G, Consiglio A, Casadio R, et al. Characteristics of the Somatic Hypermutation in the Camelus Dromedarius T Cell Receptor Gamma (TRG) and Delta (TRD) Variable Domains. *Dev Comp Immunol* (2014) 46(2):300–13. doi: 10.1016/j.dci.2014.05.001
154. Tasumi S, Velikovsky CA, Xu G, Gai SA, Wittrup KD, Flajnik MF, et al. High-Affinity Lamprey VLRA and VLRB Monoclonal Antibodies. *Proc Natl Acad Sci USA* (2009) 106(31):12891–6. doi: 10.1073/pnas.0904443106
155. Waters EA, Shusta EV. The Variable Lymphocyte Receptor as an Antibody Alternative. *Curr Opin Biotechnol* (2018) 52:74–9. doi: 10.1016/j.copbio.2018.02.016
156. Moot R, Moot SS, Moot L, Moot M, Moot DE, Moot H, et al. Genetic Engineering of Chimeric Antigen Receptors Using Lamprey Derived Variable Lymphocyte Receptors. *Mol Ther Oncolytics* (2016) 3:16026. doi: 10.1038/mto.2016.26
157. Ghaffari SH, Lobb CJ. Structure and Genomic Organization of a Second Cluster of Immunoglobulin Heavy Chain Gene Segments in the Channel Catfish. *J Immunol* (1999) 162(3):1519–29.
158. Dooley H, Flajnik MF. Antibody Repertoire Development in Cartilaginous Fish. *Dev Comp Immunol* (2006) 30(1-2):43–56. doi: 10.1016/j.dci.2005.06.022
159. Hinds-Frey KR, Nishikata H, Litman RT, Litman GW, et al. Somatic Variation Precedes Extensive Diversification of Germline Sequences and Combinatorial Joining in the Evolution of Immunoglobulin Heavy Chain Diversity. *J Exp Med* (1993) 178(3):815–24. doi: 10.1084/jem.178.3.815
160. Malecek K, Brandman J, Brodsky JE, Ohta Y, Flajnik MF, Hsu E, et al. Somatic Hypermutation and Junctional Diversification At Ig Heavy Chain Loci in the Nurse Shark. *J Immunol* (2005) 175(12):8105–15. doi: 10.4049/jimmunol.175.12.8105
161. Dooley H, Flajnik MF. Shark Immunity Bites Back: Affinity Maturation and Memory Response in the Nurse Shark, Ginglymostoma Cirratum. *Eur J Immunol* (2005) 35(3):936–45. doi: 10.1002/eji.200425760
162. Diaz M, Greenberg AS, Flajnik MF. Somatic Hypermutation of the New Antigen Receptor Gene (NAR) in the Nurse Shark Does Not Generate the Repertoire: Possible Role in Antigen-Driven Reactions in the Absence of Germinal Centers. *Proc Natl Acad Sci USA* (1998) 95(24):14343–8. doi: 10.1073/pnas.95.24.14343
163. Eason DD, Cannon JP, Haire RN, Rast JP, Ostrov DA, Litman GW, et al. Mechanisms of Antigen Receptor Evolution. *Semin Immunol* (2004) 16(4):215–26. doi: 10.1016/j.smim.2004.08.001
164. Eason DD, Litman RT, Luer CA, Kerr W, Litman GW, et al. Expression of Individual Immunoglobulin Genes Occurs in an Unusual System Consisting of Multiple Independent Loci. *Eur J Immunol* (2004) 34(9):2551–8. doi: 10.1002/eji.200425224
165. Greenberg AS, Avila D, Hughes M, Hughes A, McKinney EC, Flajnik MF, et al. A New Antigen Receptor Gene Family That Undergoes Rearrangement and Extensive Somatic Diversification in Sharks. *Nature* (1995) 374(6518):168–73. doi: 10.1038/374168a0
166. Kaattari SL, Zhang HL, Khor IW, Kaattari IM, Shapiro DA, et al. Affinity Maturation in Trout: Clonal Dominance of High Affinity Antibodies Late in the Immune Response. *Dev Comp Immunol* (2002) 26(2):191–200. doi: 10.1016/S0145-305X(01)00064-7
167. Cain KD, Jones DR, Raison RL. Antibody-Antigen Kinetics Following Immunization of Rainbow Trout (Oncorhynchus Mykiss) With a T-cell Dependent Antigen. *Dev Comp Immunol* (2002) 26(2):181–90. doi: 10.1016/S0145-305X(01)00063-5
168. Marianes AE, Zimmerman AM. Targets of Somatic Hypermutation Within Immunoglobulin Light Chain Genes in Zebrafish. *Immunology* (2011) 132(2):240–55. doi: 10.1111/j.1365-2567.2010.03358.x
169. Neely HR, Flajnik MF. Emergence and Evolution of Secondary Lymphoid Organs. *Annu Rev Cell Dev Biol* (2016) 32:693–711. doi: 10.1146/annurev-cellbio-111315-125306
170. Bengten E, Clem LW, Miller NW, Warr GW, Wilson M, et al. Channel Catfish Immunoglobulins: Repertoire and Expression. *Dev Comp Immunol* (2006) 30(1-2):77–92. doi: 10.1016/j.dci.2005.06.016
171. Danilova N, Bussmann J, Jekosch K, Steiner LA, et al. The Immunoglobulin Heavy-Chain Locus in Zebrafish: Identification and Expression of a Previously Unknown Isotype, Immunoglobulin Z. *Nat Immunol* (2005) 6(3):295–302. doi: 10.1038/ni1166
172. Hansen JD, Landis ED, Phillips RB. Discovery of a Unique Ig Heavy-Chain Isotype (IgT) in Rainbow Trout: Implications for a Distinctive B Cell Developmental Pathway in Teleost Fish. *Proc Natl Acad Sci USA* (2005) 102(19):6919–24. doi: 10.1073/pnas.0500027102
173. Zhang T, Tacchi L, Wei Z, Zhao Y, Salinas I, et al. Intraclass Diversification of Immunoglobulin Heavy Chain Genes in the African Lungfish. *Immunogenetics* (2014) 66(5):335–51. doi: 10.1007/s00251-014-0769-2
174. Zahn A, Eranki AK, Patenaude AM, Methot SP, Fifield H, Cortizas EM, et al. Activation Induced Deaminase C-terminal Domain Links DNA Breaks to End Protection and Repair During Class Switch Recombination. *Proc Natl Acad Sci USA* (2014) 111(11):E988–97. doi: 10.1073/pnas.1320486111
175. Yu K, Chedin F, Hsieh CL, Wilson TE, Lieber MR, et al. R-Loops At Immunoglobulin Class Switch Regions in the Chromosomes of Stimulated B Cells. *Nat Immunol* (2003) 4(5):442–51. doi: 10.1038/ni919
176. Zarrin AA, Del Vecchio C, Tseng E, Gleason M, Zarin P, Tian M, et al. Antibody Class Switching Mediated by Yeast Endonuclease-Generated DNA Breaks. *Science* (2007) 315(5810):377–81. doi: 10.1126/science.1136386
177. Patenaude AM, Orthwein A, Hu Y, Campo VA, Kavli B, Buschiazzo A, et al. Active Nuclear Import and Cytoplasmic Retention of Activation-Induced Deaminase. *Nat Struct Mol Biol* (2009) 16(5):517–27. doi: 10.1038/nsmb.1598
178. Basu U, Chaudhuri J, Alpert C, Dutt S, Ranganath G, et al. The AID Antibody Diversification Enzyme is Regulated by Protein Kinase A Phosphorylation. *Nature* (2005) 438(7067):508–11. doi: 10.1038/nature04255
179. Qian J, Wang Q, Dose M, Pruett N, Kieffer-Kwon KR, Resch W, et al. B Cell Super-Enhancers and Regulatory Clusters Recruit AID Tumorigenic Activity. *Cell* (2014) 159(7):1524–37. doi: 10.1016/j.cell.2014.11.013
180. Meng FL, Du Z, Federation A, Hu J, Wang Q, Kieffer-Kwon KR, et al. Convergent Transcription At Intragenic Super-Enhancers Targets AID-initiated Genomic Instability. *Cell* (2014) 159(7):1538–48.
181. Branton SA, Ghorbani A, Bolt BN, Fifield H, Berghuis LM, Larijani M, et al. Activation-Induced Cytidine Deaminase can Target Multiple Topologies of Double-Stranded DNA in a Transcription-Independent Manner. *FASEB J* (2020) 34(7):9245–68. doi: 10.1096/fj.201903036RR
182. Zheng S, Vuong BQ, Vaidyanathan B, Lin JY, Huang FT, Chaudhuri J, et al. Non-Coding RNA Generated Following Lariat Debranching Mediates Targeting of AID to DNA. *Cell* (2015) 161(4):762–73. doi: 10.1016/j.cell.2015.03.020
183. Zarrin AA, Alt FW, Chaudhuri J, Stokes N, Kaushal D, Du Pasquier L, et al. An Evolutionarily Conserved Target Motif for Immunoglobulin Class-Switch Recombination. *Nat Immunol* (2004) 5(12):1275–81. doi: 10.1038/ni1137
184. Mussmann R, Courtet M, Schwager J, Du Pasquier L, et al. Microsites for Immunoglobulin Switch Recombination Breakpoints From Xenopus to Mammals. *Eur J Immunol* (1997) 27(10):2610–9. doi: 10.1002/eji.1830271021
185. Lundqvist ML, Middleton DL, Radford C, Warr GW, Magor KE, et al. Immunoglobulins of the non-Galliform Birds: Antibody Expression and Repertoire in the Duck. *Dev Comp Immunol* (2006) 30(1-2):93–100. doi: 10.1016/j.dci.2005.06.019
186. Huang T, Zhang M, Wei Z, Wang P, Sun Y, Hu X, et al. Analysis of Immunoglobulin Transcripts in the Ostrich Struthio Camelus, a Primitive Avian Species. *PloS One* (2012) 7(3):e34346. doi: 10.1371/journal.pone.0034346
187. Reynaud CA, Anquez V, Dahan A, Weill JC, et al. A Single Rearrangement Event Generates Most of the Chicken Immunoglobulin Light Chain Diversity. *Cell* (1985) 40(2):283–91. doi: 10.1016/0092-8674(85)90142-4
188. Arakawa H, Hauschild J, Buerstedde JM. Requirement of the Activation-Induced Deaminase (Aid) Gene for Immunoglobulin Gene Conversion. *Science* (2002) 295(5558):1301–6. doi: 10.1126/science.1067308
189. Larijani M, Petrov AP, Kolenchenko O, Berru M, Krylov SN, Martin A, et al. AID Associates With Single-Stranded DNA With High Affinity and a Long Complex Half-Life in a Sequence-Independent Manner. *Mol Cell Biol* (2007) 27(1):20–30. doi: 10.1128/MCB.00824-06
190. Bransteitter R, Pham P, Scharff MD, Goodman MF, et al. Activation-Induced Cytidine Deaminase Deaminates Deoxycytidine on Single-Stranded DNA

But Requires the Action of Rnase. *Proc Natl Acad Sci USA* (2003) 100 (7):4102–7. doi: 10.1073/pnas.0730835100
191. Dickerson SK, Market E, Besmer E, Papavasiliou FN, et al. Aid Mediates Hypermutation by Deaminating Single Stranded Dna. *J Exp Med* (2003) 197 (10):1291–6. doi: 10.1084/jem.20030481
192. Sohail A, Klapacz J, Samaranayake M, Ullah A, Bhagwat AS, et al. Human Activation-Induced Cytidine Deaminase Causes Transcription-Dependent, Strand-Biased C to U Deaminations. *Nucleic Acids Res* (2003) 31(12):2990–4. doi: 10.1093/nar/gkg464
193. Larijani M, Martin A. Single-Stranded DNA Structure and Positional Context of the Target Cytidine Determine the Enzymatic Efficiency of AID. *Mol Cell Biol* (2007) 27(23):8038–48. doi: 10.1128/MCB.01046-07
194. King JJ, Larijani M. Structural Plasticity of Substrate Selection by Activation-Induced Cytidine Deaminase as a Regulator of its Genome-Wide Mutagenic Activity. *FEBS Lett* (2020) 595(1):3–13. doi: 10.1002/1873-3468.13962
195. Ramiro AR, Barreto VM. Activation-Induced Cytidine Deaminase and Active Cytidine Demethylation. *Trends Biochem Sci* (2015) 40(3):172–81. doi: 10.1016/j.tibs.2015.01.006
196. Morgan HD, Dean W, Coker HA, Reik W, Petersen-Mahrt SK. Activation-Induced Cytidine Deaminase Deaminates 5-Methylcytosine in DNA and is Expressed in Pluripotent Tissues: Implications for Epigenetic Reprogramming. *J Biol Chem* (2004) 279(50):52353–60. doi: 10.1074/jbc.M407695200
197. Bhutani N, Brady JJ, Damian M, Sacco A, Corbel SY, Blau HM, et al. Reprogramming Towards Pluripotency Requires AID-dependent DNA Demethylation. *Nature* (2010) 463(7284):1042–7. doi: 10.1038/nature08752
198. Dominguez PM, Teater M, Chambwe N, Kormaksson M, Redmond D, Ishii J, et al. Dna Methylation Dynamics of Germinal Center B Cells Are Mediated by AID. *Cell Rep* (2015) 12(12):2086–98. doi: 10.1016/j.celrep.2015.08.036
199. Munoz DP, Lee EL, Takayama S, Coppe JP, Heo SJ, Boffelli D, et al. Activation-Induced Cytidine Deaminase (AID) is Necessary for the Epithelial-Mesenchymal Transition in Mammary Epithelial Cells. *Proc Natl Acad Sci USA* (2013) 110(32):E2977–86. doi: 10.1073/pnas.1301021110
200. Popp C, Dean W, Feng S, Cokus SJ, Andrews S, Pellegrini M, et al. Genome-Wide Erasure of DNA Methylation in Mouse Primordial Germ Cells is Affected by AID Deficiency. *Nature* (2010) 463(7284):1101–5. doi: 10.1038/nature08829
201. Kumar R, DiMenna L, Schrode N, Liu TC, Franck P, Munoz-Descalzo S, et al. AID Stabilizes Stem-Cell Phenotype by Removing Epigenetic Memory of Pluripotency Genes. *Nature* (2013) 500(7460):89–92. doi: 10.1038/nature12299
202. Larijani M, Frieder D, Sonbuchner TM, Bransteitter R, Goodman MF, Bouhassira EE, et al. Methylation Protects Cytidines From AID-mediated Deamination. *Mol Immunol* (2005) 42(5):599–604. doi: 10.1016/j.molimm.2004.09.007
203. Wijesinghe P, Bhagwat AS. Efficient Deamination of 5-Methylcytosines in DNA by Human APOBEC3A, But Not by AID or APOBEC3G. *Nucleic Acids Res* (2012) 40(18):9206–17. doi: 10.1093/nar/gks685
204. Nabel CS, Jia H, Ye Y, Shen L, Goldschmidt HL, Stivers JT, et al. AID/APOBEC Deaminases Disfavor Modified Cytosines Implicated in DNA Demethylation. *Nat Chem Biol* (2012) 8(9):751–8. doi: 10.1038/nchembio.1042
205. Quinlan EM, King JJ, Amemiya CT, Hsu E, Larijani M. Biochemical Regulatory Features of AID Remain Conserved From Lamprey to Humans. *Mol Cell Biol* (2017) 37(15). doi: 10.1128/MCB.00077-17
206. Senior AW, Evans R, Jumper J, Kirkpatrick J, Sifre L, Green T, et al. Improved Protein Structure Prediction Using Potentials From Deep Learning. *Nature* (2020) 577(7792):706–10. doi: 10.1038/s41586-019-1923-7
207. Heo L, Feig M. High-Accuracy Protein Structures by Combining Machine-Learning With Physics-Based Refinement. *Proteins* (2020) 88(5):637–42. doi: 10.1002/prot.25847
208. AlQuraishi M. AlphaFold At CASP13. *Bioinformatics* (2019) 35(22):4862–5. doi: 10.1093/bioinformatics/btz422
209. Granata D, Ponzoni L, Micheletti C, Carnevale V, et al. Patterns of Coevolving Amino Acids Unveil Structural and Dynamical Domains. *Proc Natl Acad Sci USA* (2017) 114(50):E10612–21. doi: 10.1073/pnas.1712021114
210. Feng J, Shukla D. Fingerprintcontacts: Predicting Alternative Conformations of Proteins From Coevolution. *J Phys Chem B* (2020) 124(18):3605–15. doi: 10.1021/acs.jpcb.9b11869
211. Komor AC, Kim YB, Packer MS, Zuris JA, Liu DR, et al. Programmable Editing of a Target Base in Genomic DNA Without Double-Stranded DNA Cleavage. *Nature* (2016) 533(7603):420–4. doi: 10.1038/nature17946
212. Yu Y, Leete TC, Born DA, Young L, Barrera LA, Lee SJ, et al. Cytosine Base Editors With Minimized Unguided DNA and RNA Off-Target Events and High on-Target Activity. *Nat Commun* (2020) 11(1):2052. doi: 10.1038/s41467-020-15887-5
213. Shimatani Z, Kashojiya S, Takayama M, Terada R, Arazoe T, Ishii H, et al. Targeted Base Editing in Rice and Tomato Using a CRISPR-Cas9 Cytidine Deaminase Fusion. *Nat Biotechnol* (2017) 35(5):441–3. doi: 10.1038/nbt.3833
214. Nishida K, Arazoe T, Yachie N, Banno S, Kakimoto M, Tabata M, et al. Targeted Nucleotide Editing Using Hybrid Prokaryotic and Vertebrate Adaptive Immune Systems. *Science* (2016) 353(6305). doi: 10.1126/science.aaf8729
215. Rees HA, Liu DR. Base Editing: Precision Chemistry on the Genome and Transcriptome of Living Cells. *Nat Rev Genet* (2018) 19(12):770–88. doi: 10.1038/s41576-018-0059-1
216. Wang X, Li J, Wang Y, Yang B, Wei J, Wu J, et al. Efficient Base Editing in Methylated Regions With a Human APOBEC3A-Cas9 Fusion. *Nat Biotechnol* (2018) 36(10):946–9. doi: 10.1038/nbt.4198
217. Fugmann SD, Messier C, Novack LA, Cameron RA, Rast JP, et al. An Ancient Evolutionary Origin of the Rag1/2 Gene Locus. *Proc Natl Acad Sci USA* (2006) 103(10):3728–33. doi: 10.1073/pnas.0509720103
218. Martin EC, Vicari C, Tsakou-Ngouafo L, Pontarotti P, Petrescu AJ, Schatz DG, et al. Identification of RAG-like Transposons in Protostomes Suggests Their Ancient Bilaterian Origin. *Mob DNA* (2020) 11:17. doi: 10.1186/s13100-020-00214-y
219. Teng G, Schatz DG. Regulation and Evolution of the RAG Recombinase. *Adv Immunol* (2015) 128:1–39. doi: 10.1016/bs.ai.2015.07.002
220. Zhang Y, Cheng TC, Huang G, Lu Q, Surleac MD, Mandell JD, et al. Transposon Molecular Domestication and the Evolution of the RAG Recombinase. *Nature* (2019) 569(7754):79–84. doi: 10.1038/s41586-019-1093-7
221. Zhang Y, Corbett E, Wu S, Schatz D.G., et al. Structural Basis for the Activation and Suppression of Transposition During Evolution of the RAG Recombinase. *EMBO J* (2020) 39(21):e105857. doi: 10.15252/embj.2020105857

Conflict of Interest: The authors declare that the research was conducted in the absence of any commercial or financial relationships that could be construed as a potential conflict of interest.

Copyright © 2021 Ghorbani, Quinlan and Larijani. This is an open-access article distributed under the terms of the Creative Commons Attribution License (CC BY). The use, distribution or reproduction in other forums is permitted, provided the original author(s) and the copyright owner(s) are credited and that the original publication in this journal is cited, in accordance with accepted academic practice. No use, distribution or reproduction is permitted which does not comply with these terms.

frontiers in Immunology

ORIGINAL RESEARCH
published: 29 June 2021
doi: 10.3389/fimmu.2021.626895

Expression and Function Analysis of Interleukin-17A/F1, 2, and 3 Genes in Yellow Catfish (*Pelteobagrus fulvidraco*): Distinct Bioactivity of Recombinant IL-17A/F1, 2, and 3

Xu Zhou[1,2,3], *Gui-Rong Zhang*[2,3], *Wei Ji*[2,3], *Ze-Chao Shi*[4], *Xu-Fa Ma*[2,3], *Zun-Lan Luo*[1*] *and Kai-Jian Wei*[2,3*]

[1] State Key Laboratory of Environmental Criteria and Risk Assessment, Chinese Research Academy of Environmental Sciences, Beijing, China, [2] National Demonstration Center for Experimental Aquaculture Education, Huazhong Agricultural University, Wuhan, China, [3] Key Laboratory of Freshwater Animal Breeding, Ministry of Agriculture and Rural Affairs, College of Fisheries, Huazhong Agricultural University, Wuhan, China, [4] Key Laboratory of Freshwater Biodiversity Conservation, Ministry of Agriculture and Rural Affairs, Yangtze River Fisheries Research Institute, Chinese Academy of Fishery Sciences, Wuhan, China

In mammals, Interleukin-17 cytokine family plays critical roles in both acute and chronic inflammatory responses. In fish species, three Interleukin-17A/F (IL-17A/F) genes have been identified to be homologous to mammalian IL-17A and IL-17F, but little is known about their functional activity. In this study, *Pf*_IL-17A/F1, 2 and 3 genes were cloned from yellow catfish (*Pelteobagrus fulvidraco*) and they differed in protein structure and exon length, implying that they may have divergent bioactivity. Real-time quantitative PCR analyses revealed that three *Pf*_IL-17A/F genes were highly expressed in blood and mucosal tissues (skin+mucus and gill) from healthy adult fish. The mRNA expressions of *Pf*_IL-17A/F1, 2 and 3 genes were significantly up-regulated in the gill, skin+mucus, head kidney and spleen after challenge with *Edwardsiella ictaluri* and in the isolated peripheral blood leucocytes (PBLs) of yellow catfish after stimulation with phytohaemagglutinin (PHA), lipopolysaccharides (LPS), peptidoglycan (PGN) and polyinosinic-polycytidylic acid (Poly I:C). These results indicate that *Pf*_IL-17A/F1, 2 and 3 genes may play a vital role in the regulation of immune against pathogens. Additionally, the recombinant (r) *Pf*_IL-17A/F1, 2 and 3 proteins significantly induced the mRNA expressions of proinflammatory cytokines, chemokines and antibacterial peptides genes, and the r*Pf*_IL-17A/F 2 and 3 proteins promoted phagocytosis of PBLs more powerfully than the r*Pf*_IL-17A/F1. Furthermore, the r*Pf*_IL-17A/F1, 2 and 3 proteins might activate the NF-κB and MAPK signal pathways by IL-17RA, ACT1, TRAF6, TRAF2, TRAF5 and TAK1, indicating that the three *Pf*_IL-17A/F proteins may play different roles in promoting inflammatory response.

Keywords: yellow catfish, IL-17A/Fs, expression, bioactivity, phagocytosis, downstream pathway

OPEN ACCESS

Edited by:
Monica Hongroe Solbakken, University of Oslo, Norway

Reviewed by:
Masahiro Sakai, University of Miyazaki, Japan
Kun Wu, South China Agricultural University, China
Zhi Luo, Huazhong Agricultural University, China

***Correspondence:**
Kai-Jian Wei
kjwei@mail.hzau.edu.cn
Zun-Lan Luo
luozunlan@163.com

Specialty section:
This article was submitted to Comparative Immunology, a section of the journal Frontiers in Immunology

Received: *07 November 2020*
Accepted: *14 June 2021*
Published: *29 June 2021*

Citation:
Zhou X, Zhang G-R, Ji W, Shi Z-C, Ma X-F, Luo Z-L and Wei K-J (2021) Expression and Function Analysis of Interleukin-17A/F1, 2, and 3 Genes in Yellow Catfish (Pelteobagrus fulvidraco): Distinct Bioactivity of Recombinant IL-17A/F1, 2, and 3. Front. Immunol. 12:626895. doi: 10.3389/fimmu.2021.626895

INTRODUCTION

Water quality is one of the most critical factors of healthy aquaculture. The deterioration of the water environment can reduce fish growth rate and lower fish immunity, which may lead to the invasion of pathogens and the occurrence of fish diseases. Inflammation is broadly defined as a protective response of the organism to stimulation by invading pathogens or endogenous signals such as damaged cells (1). Moderate inflammation can accelerate the clearance of pathogens and tissue repair. Cytokine, as the medium of communication between cells, plays an important regulative role in the development of inflammation (2). As an important cytokine family, the interleukin-17 family can promote inflammation by activating downstream pathways to induce the expression of antimicrobial peptides, inflammatory cytokines, and chemokines (3).

In mammals, the interleukin-17 (IL-17) cytokine family comprises six members based on the structure similarity: IL-17A, IL-17B, IL-17C, IL-17D, IL-17E, and IL-17F. IL-17A, originally called cytotoxic T-lymphocyte antigen 8 (CTLA8) (4), is a symbolic cytokine that plays a redundant role in inflammation, host defense, and tumorigenesis (5). IL-17A and IL-17F are most similar in amino acid sequences, and they are co-expressed and play overlapping roles in the inflammatory response (6). IL-17A and IL-17F were considered to be released by the activated $CD4^+$ T cell. In 2005, IL-17-producing T cells were classified as a new distinct $CD4^+$ T cell subset, T helper 17 cells (Th17) (7). In mouse, the naïve $CD4^+$ T cells can differentiate into Th17 cells under the control of a set of cytokines including TGF-β, IL-6, IL-1β, IL-23, and IL-21, which lead to the activation of retinoid-related orphan nuclear receptor γt (ROR-γt) and signal transducer and activators of transcription 3 (STAT3) pathways (8–12). IL-2, interferon-γ (IFN-γ), IL-4 or IL-12 on these pathways can suppress the differentiation of Th17 cells (7, 13, 14). Though Th17 cells were thought as a major source of IL-17A and IL-17F, IL-17A and IL-17F can also be produced by T cells (Tc-17, γδ-17, NKT-17), innate lymphoid cells (monocyte, neutrophils, NK), and other non-immune cells (paneth cells, epithelial cells) (15, 16). Upon infection and wounding, IL-17A and IL-17F are rapidly produced by immune and non-immune cells or later by adaptive Th17 cells, subsequently these two released cytokines can induce the expression of host defense genes, such as cytokines (IL-1β, TNF, IL-6, and GM-CSF), chemokines (CXCL1, CXCL2, and CXCL8) and antibacterial peptides (β-defensin and S100 proteins) in targeting cells (epithelial cells, keratinocytes, endothelial cells, fibroblasts, and muscle cells), which will further activate NFκB, MAPKs and C/EBPs downstream pathways to protect the host from harmful pathogens (17, 18). Though the roles of IL-17A and IL-17F overlap, they exist in distinct roles in host defense mechanisms. In the colon, IL-17A was produced mainly in T cells, whereas IL-17F was produced in T cells, immune cells and epithelial cells. Furthermore, IL-17A induced inflammatory cytokines more strongly than IL-17F in the autoimmunity, but IL-17F has more critical roles than IL-17A in protecting colonic epithelial cells against the invasion of bacteria (19, 20).

In teleosts, five members of IL-17 family genes have been identified except IL-17E. Three IL-17A or IL-17F homologous genes have been found in zebrafish (*Danio rerio*) and named IL-17A/F1, IL-17A/F2 and IL-17A/F3, because it is difficult to distinguish IL-17A and IL-17F genes (21). Besides, IL-17A/F1, 2 and 3 genes have been identified in medaka (*Oryzias latipes*), Japanese pufferfish (*Takifugu rubripes*), rainbow trout (*Oncorhynchus mykiss*), Atlantic salmon (*Salmo salar*), channel catfish (*Ictalurus punctatus*), sea bass (*Dicentrarchus labrax*), large yellow croaker (*Larimichthys crocea*) and miiuy croaker (*Miichthys miiuy*) (22–28). Zebrafish IL-17A/F1 and 2 genes are localized on the same chromosome and are different from zebrafish IL-17A/F3 (22). Moreover, fish IL-17A/F1 and 3 were clustered in a branch on the phylogenetic trees, showing that fish IL-17A/F1 and 3 share the greatest structural homology (28). There have been many studies on tissue expression and immunoregulation of teleost IL-17A/F genes. Teleost IL-17A/F genes are mainly expressed in immune-related tissues (e.g. kidney, head kidney, and spleen) and mucosal tissues (e.g. gills, skin, and intestine) (23–28), and their gene expression can be modulated following bacterial infection and *in vitro* or *in vivo* stimulation of lipopolysaccharides (LPS), phytohaemagglutinin (PHA) and other immune stimuli (25–28). However, there have been limited researches on the bioactivity of IL-17A/Fs in teleosts, such as rainbow trout, common carp, grass carp and large yellow croaker. Recombinant rainbow trout IL-17A/F2 can induce the expression of chemokines (IL-6 and CXCL8) and antibacterial peptide (β-defensin3) in splenocytes (29). Common carp rIL-17A/F2a can induce the expression of pro-inflammatory cytokine (IL-1β) and antimicrobial peptides (S100A1, S100A10a, and S100A10b) in the primary kidney (30). Grass carp rIL-17A/F1 can enhance the expression of some pro-inflammatory cytokines genes (IL-1β, TNF, IL-6, and CXCL-8), possibly by activating the NF-kB and MAPKs pathways (31). Large yellow croaker rIL-17A/Fs can promote the expression of pro-inflammatory cytokines (IL-1β, IL-6, and TNF-α), two chemokines (CXCL8 and CXCL13) and antimicrobial peptide (hepcidin), potentially *via* the NF-κB pathway (28). These results illustrate that fish IL-17A/F genes are involved in host defense by inducing cytokines, chemokines and antimicrobial peptide. But so far limited researches have been reported to compare the similarities and differences among three IL-17A/F genes, and the unique roles of IL-17A/F genes in fish immunity are still unclear.

Yellow catfish (*Pelteobagrus fulvidraco*) is an important commercial freshwater fish in China. With the rapid development of the aquaculture industry in recent years, yellow catfish suffers from several kinds of bacterial diseases such as ascites disease, enteric septicemia, and crack-head disease (32, 33). Inflammation can effectively prevent and eliminate invaded pathogens, and IL-17A and F could produce strong inflammatory responses by inducing other pro-inflammatory cytokines, chemokines, and antimicrobial peptides (19, 34). Although three genes of IL-17A/F have been found in various fishes, there is no research to compare their distinct function in fish. In this study, we identified three IL-17A/F homologous genes (*Pf*_IL-17A/F1, 2, and 3) in yellow catfish and investigated

the mRNA expression of *Pf*_IL-17A/F1, 2 and 3 genes in various tissues. Subsequently, we detected the expression changes of three *Pf*_IL-17A/F genes in gill, skin+mucus, head kidney and spleen after challenge of *Edwardsiella ictaluri*, and analyzed the expression modulation of three *Pf*_IL-17A/F genes in isolated peripheral blood leucocytes (PBLs) of yellow catfish after stimulation with PHA, LPS, PGN and Poly I:C. Moreover, recombinant *Pf*_IL-17A/F1, 2 and 3 proteins were produced and used to compare their bioactivity in PBLs to modulate the mRNA expression of proinflammatory cytokines, chemokines and antimicrobial peptides genes, promote phagocytosis, and activate the downstream signal pathways. The results will provide useful information to better understand the expression patterns and potential functions of three IL-17A/F genes against pathogenic microbes in teleosts.

MATERIALS AND METHODS

Fish Collection

Healthy adult yellow catfish (one year old, ~50 g) were collected from the Liangzi Lake, Hubei Province, and were transported to the fish breeding base of Huazhong Agricultural University (HZAU). Before artificial reproduction, gene cloning and mRNA tissue distribution experiments, the fishes were acclimatized to laboratory conditions in two circulating water tanks (water temperature at ~26°C, dissolved oxygen at ~6.5 mg/L, and pH at ~8.5) and were fed a commercial diet (Hubei Haid Feeds Company, Wuhan, China) twice a day (09:00 and 16:00). The offsprings from artificial reproduction were cultivated in the circulating water tanks to provide fish samples for bacterial challenge and isolation of PBLs.

Cloning of cDNA Sequences for Three Genes

Three gene-specific primer pairs (IL-17A/F1-F1/IL-17A/F1-R1, IL-17A/F2-F1/IL-17A/F2-R1, and IL-17A/F3-F1/IL-17A/F3-R1) and three 3'-untranslated region (UTR)-specific primers were designed based on the previous transcriptome data of yellow catfish to obtain the core cDNA sequences of the *Pf*_IL-17AF1, 2 and 3 genes (**Supplemental Table 1**). The open reading frame (ORF) and 3' UTR of three *Pf*_IL-17A/F genes were obtained using PCR and 3' nested rapid amplification of cDNA ends (RACE) PCR, respectively. The PCR product was cloned into the pMD18-T vector (TaKaRa, China) and sequenced as described previously (35).

The completed sequence of the ORF of the target gene was found using the ORF Finder (http://www.ncbi.nlm.nih.gov/projects/gorf/). The theoretical isoelectric point and molecular weight of the amino acid were predicted using the ExPASy (https://web.expasy.org/compute_pi/). The protein structure of the target gene was predicted by the Simple Modular Architecture Research Tool (SMART) (http://smart.embl-heidelberg.de/). Homologous sequences of the *Pf*_IL-17A/F1, *Pf*_IL-17A/F2 and *Pf*_IL-17A/F3 genes were searched in GenBank with the BLAST program (https://blast.ncbi.nlm.nih.gov/Blast.cgi). Amino acid sequence similarity and identity were computed using the Sequence Manipulation Suite (http://www.bio-soft.net/sms/index.html). A neighbor-joining (NJ) phylogenetic tree was constructed for three *Pf*_IL-17A/F genes and their homologues from other vertebrates based on the amino acid sequences using the MEGA 6.06. Protein secondary structure was predicted using Jpred4 program (http://www.compbio.dundee.ac.uk/jpred/). Disulfide bonding and cysteine connectivity were predicted using the DISULFIND program (http://disulfind.dsi.unifi.it/). The synteny of IL-17A/Fs loci was analyzed using Genomicus (https://www.genomicus.biologie.ens.fr/genomicus-91.01/cgi-bin/search.pl).

Tissue Distribution

Fifteen adult yellow catfish (~50 g) were anesthetized with tricaine methanesulfonate (MS-222, 300 mg/L), and 15 different tissues, including blood, swim bladder, skin+mucus, hindgut, liver, stomach, brain, gill, spleen, head kidney, muscle, heart, testis, fin and trunk kidney, were rapidly collected for RNA isolation. Every five fishes were as a group of biological duplication. All tissues were immediately frozen in liquid nitrogen and stored at −80°C until RNA extraction.

Modulation of *Pf*_IL-17AF1, 2 and 3 Gene Expression *In Vivo* and *In Vitro*

To examine the immune responses of the *Pf*_IL-17A/F1, 2 and 3 genes after bacterial challenge, juvenile individuals of yellow catfish (~14 g) were collected at the fish breeding base of HZAU. The bacteria (*E. ictaluri*) for immune challenge experiments were obtained from the fish immunology laboratory of HZAU, and were cultured on brain-heart infusion (BHI) and incubated 12 h at 28°C in the incubator. Fish were injected intraperitoneally with 200 μL of suspended *E. ictaluri* in phosphate-buffered saline (PBS, pH 7.2) with a concentration of 1.5×10^7 CFU/mL as the experimental group or with the same volume of PBS as the control group. Fifteen fish were randomly sampled from the experimental group at 3, 6, 12, 24, 48, 72 and 120 hours post-injection and from the control group at 0 hours, and every five fishes at each time point were as a group of biological duplication. The sampled fish were anesthetized with 300 mg/L MS-222, and then the gill, skin+mucus, spleen and head kidney tissues were collected for RNA extraction. All tissues were immediately frozen in liquid nitrogen and stored at −80°C until RNA extraction.

To examine the immune responses of the *Pf*_IL-17A/F1, 2 and 3 genes in isolated peripheral blood leucocytes (PBLs) of yellow catfish after stimulation with LPS, PHA and Poly I:C, the blood sample was collected from adult individuals of yellow catfish (~35 g), and PBLs were isolated by density gradient centrifugation as described (35). 5×10^6 cells were incubated in RPMI (RPMI with L-glutamine, penicillin, streptomycin and 20% fetal bovine serum (FBS); Solarbio, Beijing, China) with 30 μg/mL PHA (Yuanye, Shanghai, China), 15 μg/mL LPS (Sigma, USA), 15 μg/mL PGN (Ryon, Shanghai, China), and 15 μg/mL Poly I:C (Ryon, Shanghai, China), respectively. The cells were gathered by centrifugation at 3, 6, 12 and 24 h after treatment with PHA, LPS, PGN and Poly I:C. Non-treated cells were used

as the negative control. All cells were immediately frozen in liquid nitrogen and stored at −80°C until RNA extraction.

Production and Purification of r*Pf*_IL-17A/F1, r*Pf*_IL-17A/F2 and r*Pf*_IL-17A/F3 Proteins

The ORF sequence of *Pf*_IL-17A/F1, *Pf*_IL-17A/F2 and *Pf*_IL-17A/F3 genes after removal of the signal peptide sequence was amplified with gene-specific primers (**Table 1**) for prokaryotic expression. After digested with *Sal I* and *EcoR I*, the amplicon was inserted into the multiple cloning sites (MCS) of the pET-32a vector. The recombinant plasmid pET-32a-IL-17A/F1, pET-32a-IL-17A/F2 and pET-32a-IL-17A/F3 were then transformed into *E. coli* BL21 (DE3) competent cells, respectively, and the recombinant IL-17A/F (rIL-17A/F) expression was induced at 37°C for 4 h with IPTG at a final concentration of 1.0 mM. Subsequently, the r*Pf*_IL-17A/F protein was purified by Ni-NTA (nitrilotriacetic acid) affinity chromatography (Sangon, Shanghai, China) according to the manufacturer's instructions. The identity of the recombinant protein was confirmed by SDS-PAGE as a band with the correct molecular weight. The purified protein was quantitated using the Bradford protein quantitation assay by Nanodrop 2000 (Thermo Electron Corporation, USA).

Modulation of Gene Expression in Yellow Catfish PBLs by Recombinant IL-17A/F Isoforms

The blood sample was collected from adult individuals of yellow catfish (~35 g), and PBLs were isolated by density gradient centrifugation as described (35). 5×10^6 cells were incubated in RPMI1640 (RPMI1640 with L-glutamine, penicillin, streptomycin, and 10% fetal bovine serum (FBS); Solarbio, Beijing, China) with different doses of r*Pf*_IL-17A/F1, 2 and 3 proteins (5, 50, and 500 ng/mL) for 6 h, and then the mRNA expressions of IL-1β and CXCL8 genes were detected to compare their changes after different treatments and to screen an appropriate dose for bioactivity analysis of three r*Pf*_IL-17A/F proteins in the yellow catfish PBLs. In the bioactivity experiment of three r*Pf*_IL-17A/F proteins, a dose of 500 ng/mL was used for each r*Pf*_IL-17A/F because the IL-1β and CXCL8 genes had good responses in the yellow catfish PBLs at this treatment dose. Freshly prepared PBLs were stimulated with r*Pf*_IL-17A/F1, 2 and 3 proteins (500 ng/mL) for 3 h, 6 h and 12 h. Medium-treated cells were used as a negative control. Also, the PBLs were treated by r*Pf*_IL-17A/F1, 2 and 3 proteins (500 ng/mL) or NF-κB inhibitor PDTC (0.5 μM, Sigma-Aldrich) and p38 MAPK inhibitor SB203580 (20 μM, Calbiochem, San Diego, USA) for 6 h. All cells were immediately frozen in liquid nitrogen and stored at -80°C until RNA extraction. Afterwards, the mRNA expressions of proinflammatory cytokines (IL-1β, TNF-α, IL-6, IL-11, IL-22, and IFN-γ), chemokine (CXCL1, CXCL8, CXCL11, CCL3, and CCL4), antimicrobial peptide (β-defensin, S100A1, and LEAP) and IL-17A/Fs downstream pathway genes (IL-17RA, ACT1, TRAF6, TRAF5, TRAF2, and TAK1) in the PBLs were examined by qPCR to detect the effects of three recombinant *Pf*_IL-17A/F proteins (**Supplemental Table 1**).

Phagocytic Assay

PBLs in complete cell culture medium prepared above (2×10^6 cells/mL) were added to 6-well suspension cell culture plates

TABLE 1 | Transcriptional fold changes of inflammatory cytokines, chemokines, antibacterial peptides and downstream signaling-related genes in yellow catfish PBLs after treatment with the r*Pf*_IL-17A/F1, 2 and 3 proteins (500 ng/mL) for 3 h, 6 h and 12 h.

Gene category	Gene name	r*Pf*_IL-17A/F1			r*Pf*_IL-17A/F2			r*Pf*_IL-17A/F3		
		3 h	6 h	12 h	3 h	6 h	12 h	3 h	6 h	12 h
Inflammatory cytokine	IL-1β	1.39**	1.86**	1.32	3.69**	3.55**	0.70	142.39**	122.19**	58.63**
	IL-6	2.83*	1.55	1.75	1.71*	2.40**	1.85**	4.35**	4.84**	3.69*
	IL-11	1.09	0.79	1.24	1.47	3.64*	3.21*	9.16**	11.94**	5.81**
	IL-22	1.29	0.55	0.78	1.62	4.15**	1.44	4.31*	0.86	0.30
	TNFα	1.16	1.75*	0.99	2.50*	1.58*	0.75	7.08**	3.95**	1.25
	IFNγ1	0.85	0.83	0.60*	1.13	1.10	1.33*	0.75*	0.78**	0.63**
Chemokine	CXCL1	1.95*	1.26	1.52*	0.79	1.23	1.16	1.02	1.35	1.67*
	CXCL8	2.43*	2.00*	24.79**	2.76*	2.23**	1.35	0.50**	0.46*	2.11
	CXCL11	5.46**	8.79**	2.03**	1.51*	1.46*	1.85**	2.68**	4.40**	8.95**
	CCL3	1.72*	1.24	0.90	1.36	1.04	0.77	6.92**	0.84	0.82
	CCL4	0.73	1.76*	2.09*	0.80	1.69*	2.09**	1.90**	9.91**	3.02*
Antibacterial peptide	S100A	2.95**	1.90**	0.37**	3.04*	2.76**	0.85	2.55**	1.19	0.61*
	LEAP	2.44*	1.05	0.29*	0.11**	3.53*	0.16*	1.38	4.61*	0.10*
	β-defensins	1.51	0.97	0.74	0.22*	4.23*	0.71	2.47*	2.16*	0.54**
Downstream signaling-related gene	IL-17RA	1.72	3.50**	0.12**	0.82	1.24	0.86	3.75*	2.77**	0.79
	ACT1	1.26	4.88**	0.09**	4.21*	1.05	0.52	3.13*	2.41*	0.10**
	TRAF6	3.54*	1.72*	0.19**	1.49	1.44	0.56**	6.07*	6.08**	0.45**
	TRAF2	1.22	4.94**	0.09**	0.79	2.90*	0.21**	5.07*	5.70**	0.48**
	TRAF5	3.44*	2.34*	4.08**	1.10	2.42*	0.37*	24.53**	40.63**	1.52
	TAK1	1.71	1.75*	0.61	1.32	2.00*	0.41**	4.78**	8.58**	1.04

*Data are the average transcriptional fold changes of 20 genes at each time point after treatment with three rPf_IL-17A/Fs, which were calculated compared to the control group at the same time point (*controls = 1, n = 3*). The PBLs were isolated from five individuals of yellow catfish and were mixed equally, and the pooled sample was further divided into 12 experiment units for different experimental treatments. Significant difference at each time point compared to the control is indicated by asterisks (*P < 0.05, **P < 0.01).*

(Corning) and incubated at 28°C with 5% CO_2. The fresh PBLs were stimulated with r*Pf*_IL-17A/F1, r*Pf*_IL-17A/F2, r*Pf*_IL-17A/F3 proteins (500 ng/mL), and also treated by medium alone as a control. Fluorescent latex beads (Fluoresbrite Yellow Green Microspheres, 1.0 μm in diameter; Polysciences) were added 18 h later at a cell/bead ratio of 1:25, and then the PBLs were incubated for a further 2 h. The cells were harvested using PBS and the supernatant was removed by centrifugation at 400 g for 3 min. Non-ingested beads were removed by centrifugation (at 100 g for 10 min at 4°C) over a 3% BSA and 4.5% d-glucose buffer solution prepared with PBS. The cells were washed with PBS and analyzed with Beckman cytoflex Flow Cytometer, measuring at least 50,000 cells after live cell gating according to the forward scatter (FSC)/side scatter (SSC).

RNA Extraction and cDNA Synthesis

Total RNA was extracted from various tissues and cells using Trizol Reagent (Invitrogen, USA) according to the manufacturer's instruction. The quality of total RNA was checked by 1% agarose gel electrophoresis. The concentration of total RNA was determined using a Nanodrop ND-2000 spectrophotometer (Thermo Electron Corporation, USA). The first-strand cDNA was generated using the Revert Aid™ M-MLV Reverse Transcriptase Kit (Promega, USA) following the manufacturer's instructions. The cDNA products were stored at –20°C.

qPCR

qPCR was used to detect mRNA expression levels of *Pf*_IL-17A/F1, *Pf*_IL-17A/F2 and *Pf*_IL-17A/F3 genes in various tissues and cells of yellow catfish using a 7300 RT-PCR system (Applied Biosystems, USA). The gene-specific primer pairs for qPCR were designed based on the cloned cDNA sequences of *Pf*_IL-17A/F1, *Pf*_IL-17A/F2 and *Pf*_IL-17A/F3 genes (**Supplemental Table 1**). The β-actin gene (XM_027148463.1) was used as an internal control gene. The PCR reaction mixture consisted of 10 μL LightCycler® 480 SYBR Green I Master (Roche, Germany), 7 μL ddH_2O, 2 mL cDNA (5 times dilution of a template) and 0.5 μL of either gene-specific primer (10 μM) in a total volume of 20 μL. The qPCR of each sample was performed in triplicate according to the following conditions: 95°C for 10 min, followed by 40 cycles at 95°C for 15 s, annealing temperature for 30 s and 72°C for 30 s respectively. At the end of each PCR reaction, amplification curve and melting curve analyses were performed to check the integrity of the reaction and the quality of the product, respectively. To compare mRNA expressions of *Pf*_IL-17A/F1, *Pf*_IL-17A/F2 and *Pf*_IL-17A/F3 genes, the $2^{-\Delta\Delta Ct}$ method (36) was adopted to calculate the relative expression levels of the target genes.

Statistical Analyses

All data from the qPCRs were expressed as the mean ± standard error (SEM). One-way analysis of variance (ANOVA) and Duncan's *post hoc* test (α = 0.05) were used to examine the differences of mRNA expression levels among different treatments using STATISTICA 8.0 software. A *t*-test was performed to examine the differences of mRNA expression levels between the control group and the experimental group after different treatments (α = 0.05, 0.01). All histograms were plotted using GraphPad Prism 5.0 software.

RESULTS

Characterization of *Pf*_IL-17A/F1, *Pf*_IL-17A/F2 and *Pf*_IL-17A/F3 cDNA Sequences

The partial cDNA sequences of the *Pf*_IL-17A/F1, *Pf*_IL-17A/F2 and *Pf*_IL-17A/F3 genes were cloned from yellow catfish. The *Pf*_IL-17A/F1 cDNA consisted of an ORF of 483 bp and a 3'-untranslated region (UTR) of 236 bp. The ORF encoded a protein of 161 amino acids (aa) with a predicted signal peptide (1–27 aa), a typical IL-17 superfamily domain (74–153 aa) and one N-glycosylation site (NDS^{73-75}). The 3'-UTR contained three mRNA instability motifs (ATTTA) (**Supplemental Figure 1A**). The estimated theoretical isoelectric point (IP) and molecular weight (MW) of *Pf*_IL-17A/F1 protein were 5.18 and 18.42 kDa, respectively. The *Pf*_IL-17A/F2 cDNA was 816 bp in length, including an ORF of 420 bp and a 3'-UTR of 396 bp. The ORF encoded a protein of 139 aa with a predicted signal peptide (1–20 aa), IL-17 superfamily domain (55–132 aa), and one N-glycosylation site (NRS^{55-57}). The 3'-UTR contained two mRNA instability motifs (ATTTA) and three putative polyadenylation signal sequences (AATAAA) (**Supplemental Figure 1B**). The estimated theoretical IP and MW of *Pf*_IL-17A/F2 protein were 5.2 and 15.81 kDa, respectively. The *Pf*_IL-17A/F3 cDNA contained an ORF of 483 bp and a 3'-UTR of 44 bp. The ORF encoded a protein of 160 aa with a predicted signal peptide (1–16 aa) and IL-17 superfamily domain (73–152 aa) (**Supplemental Figure 1C**). The estimated theoretical IP and MW of *Pf*_IL-17A/F3 protein were 5.21 and 18.05 kDa, respectively.

Sequence and Organization Analysis of *Pf*_IL-17A/F1, *Pf*_IL-17A/F2 and *Pf*_IL-17A/F3 Genes

Multiple alignment of amino acid sequences showed that eight cysteine residues were highly conserved in different IL-17A/F genes of vertebrates (**Supplemental Figure 2**). Four conserved cysteine residues of fish IL-17A/F1 and IL-17A/F3 were expected to form two intrachain disulphide bridges (C3/C7 and C4/C8), fish IL-17A/F2 and tetrapod IL-17A and IL-17F possessed six conserved cysteine residues forming three intrachain disulphide bridges, respectively: fish IL-17A/F2 (C2/C6, C3/C7, and C4/C8), tetrapod IL-17A and IL-17F (C1/C5, C3/C7, and C4/C8) (**Figure 1A**). The secondary structures of *Pf*_IL-17A/F1, *Pf*_IL-17A/F2 and *Pf*_IL-17A/F3 proteins all possessed four β-strands as those of human IL-17A and IL-17F, while the length of the fourth β-strand of *Pf*_IL-17A/F2 was shorter than those of *Pf*_IL-17A/F1, *Pf*_IL-17A/F3 and human IL-17A and IL-17F (**Supplemental Figure 2**).

The DNA sequences of *Pf*_IL-17A/F1, *Pf*_IL-17A/F2 and *Pf*_IL-17A/F3 genes all had three exons and two introns as

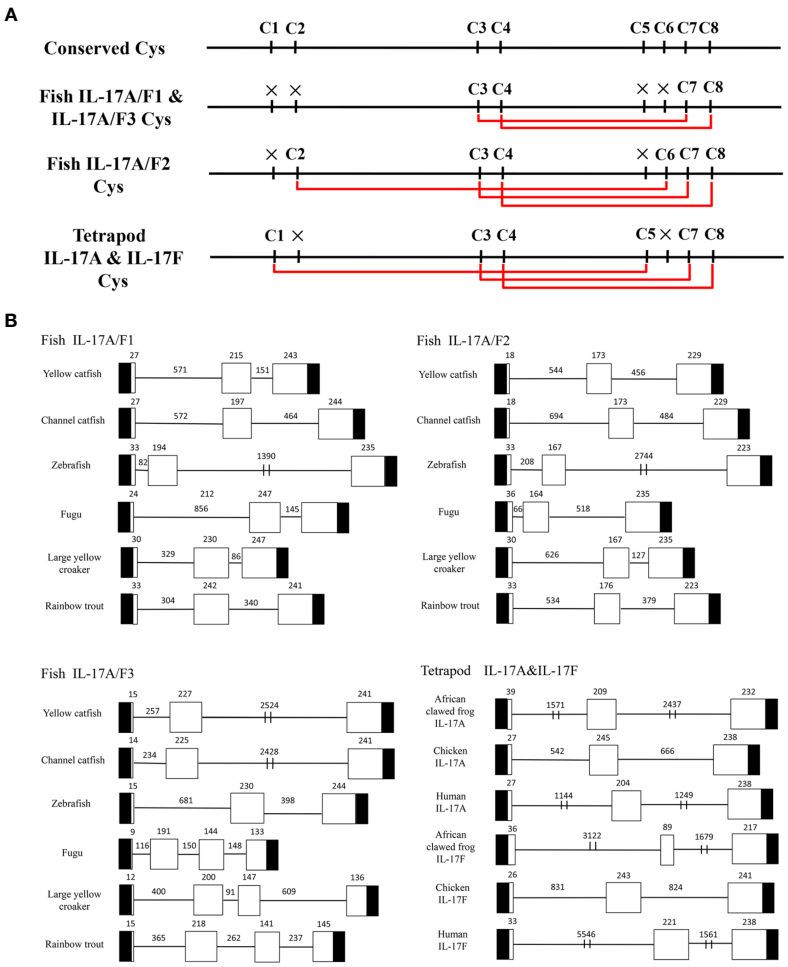

FIGURE 1 | Conserved cysteine residues and predicted potential intra-molecular disulfide bonds in the deduced amino acid sequences of fish IL-17A/F1, 2 and 3 genes and tetrapod IL-17A and F genes **(A)** and comparison of the gene organization of these genes **(B)**. **(A)** Cysteine residues potentially forming disulfide bonds are linked by red lines in tetrapod IL-17A and F, and fish IL-17A/F1, 2 and 3. The disulfide bonds were predicted using DISULFIND. **(B)** The black boxes represent untranslated region, the white boxes represent exons, and the lines represent introns. The genomic sequences are taken from the NCBI database: Yellow catfish, GCF_003724035.1; Channel catfish, GCF_001660625.1; Zebrafish, GCF_000002035.6; Medaka, GCF_002234675.1; Rainbow trout, GCF_002163495; African clawed frog: GCF_001663975.11; Chicken: GCF_000002315.6; human, GCF_000001405.39.

those of other fishes and tetrapod except for the IL-17A/F3 gene organization (four exons and three introns) of fugu, large yellow croaker and rainbow trout (**Figure 1B**). The first exon of IL-17A/F2 in yellow catfish and channel catfish and fish IL-17A/F3 was shorter in length (9–18 bp) than that of other vertebrate IL-17A/F genes (24–39 bp). The second exon of fish IL-17A/F2 (164–176 bp) and African clawed frog IL-17F (89 bp) was very shorter than that of other vertebrate IL-17A/F genes (191–245 bp). The IL-17A/F3 gene of fugu, large yellow croaker and rainbow trout possessed a shorter length of the third exon (144 bp, 147 bp, and 141 bp) and the fourth exon (133 bp, 136 bp, and 145 bp), whereas the IL-17A/F genes of other fishes and tetrapod had a longer length of the third exon (217–247 bp) (**Figure 1B**). Moreover, the introns of IL-17A/F genes were distinctly different in length among various fishes and tetrapod (**Figure 1B**).

Homology and Phylogenetic Analysis of *Pf*_IL-17A/F1, *Pf*_IL-17A/F2 and *Pf*_IL-17A/F3 Genes

Homology analysis of amino acids sequences showed that the *Pf*_IL-17A/F1, *Pf*_IL-17A/F2 and *Pf*_IL-17A/F3 had the highest similarity (69.2%, 79.1%, 83.8%) with the homologues in channel catfish, followed by moderate similarity (51.0%, 55.6%, 57.4%) with zebrafish, and low similarity (44.3%, 41.3%, 42.8%) with medaka. In addition, the three *Pf*_IL-17A/Fs had very lower sequence similarity (27.2%–37.8%) to IL-17A or IL-17F in human, chicken, and western clawed frog (**Supplemental Table 2**). The NJ phylogenetic tree of deduced IL-17A/F amino acid sequences showed that the *Pf*_IL-17A/F1, *Pf*_IL-17A/F2 and *Pf*_IL-17A/F3 of yellow catfish were clustered respectively with those of other teleost IL-17A/Fs into three

branches (IL-17A/F1, IL-17A/F2, and IL-17A/F3), of which the IL-17A/F1 and IL-17A/F3 branches were further clustered into a group (**Figure 2**). However the IL-17A and IL-17F of mammals, birds and amphibians were grouped into another branch (**Figure 2**).

Synteny Analysis of *Pf*_IL-17A/F1, 2, and 3 Genes

Syntenic analysis of IL-17A/F genes showed the synteny arrangements of three IL-17A/F genes were conserved across teleosts, which were different from that of tetrapod IL-17A and

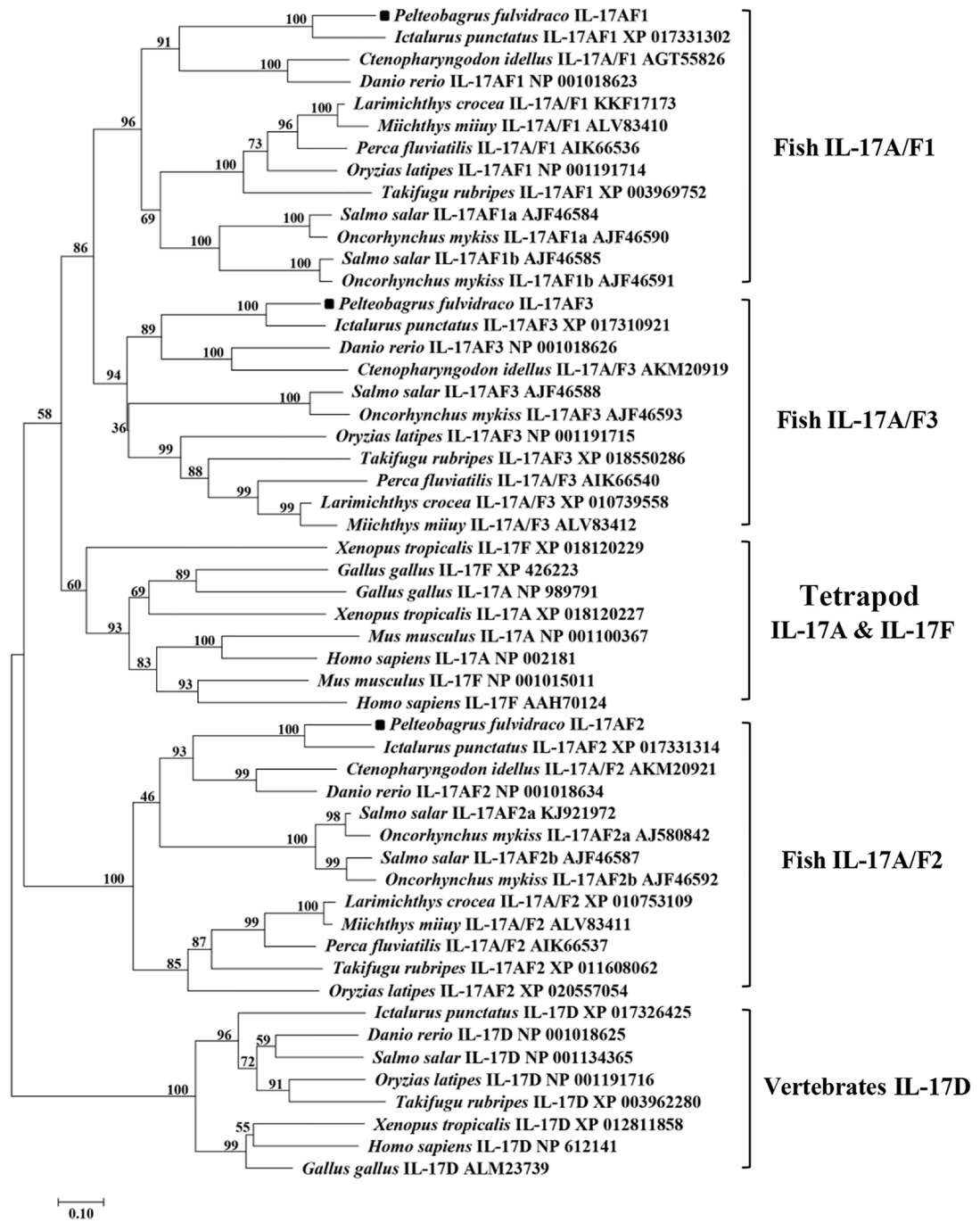

FIGURE 2 | Neighbor-joining (NJ) phylogenetic tree constructed based on deduced amino acid sequences of vertebrate IL-17A/F using MEGA 6.06. A bootstrap analysis is performed using 1000 replicates to test the relative support for particular clades. GenBank accession number for each sequence is given after the species name and molecular type.

IL-17F genes (**Figure 3**). Unlike tetrapod IL-17A and IL-17F genes, fish IL-17A/F1 and IL-17A/F2 genes were adjacent and localized on the same chromosome, whereas fish IL-17A/F3 gene was localized on another chromosome (**Figure 3**). The membrane progestin receptor beta-like (paqr8) gene was conserved across vertebrates. In addition, seven genes (mcm3, stmn4l, gpn1, elp3, pnoc, znf395, and stmn4) were conserved across teleosts, and eight genes (nfkbia, insm2, ralgapa1, brms1, irrc57, emilin1, khk, and ankef) were only conserved across yellow catfish, channel catfish and zebrafish.

Expression Pattern of *Pf*_IL-17A/F1, 2 and 3 Genes in Various Tissues From Healthy Adults

The tissue distributions of *Pf*_IL-17A/F1, *Pf*_IL-17A/F2 and *Pf*_IL-17A/F3 mRNA expressions were detected by qPCR in various tissues of adult yellow catfish (**Figure 4**). The results showed that *Pf*_IL-17A/F1, 2 and 3 genes were constitutively expressed in all 15 examined tissues, with an extremely high expression level in the blood. *Pf*_IL-17A/F1 and *Pf*_IL-17A/F2 mRNAs were expressed with a high level in the skin+mucus, gill,

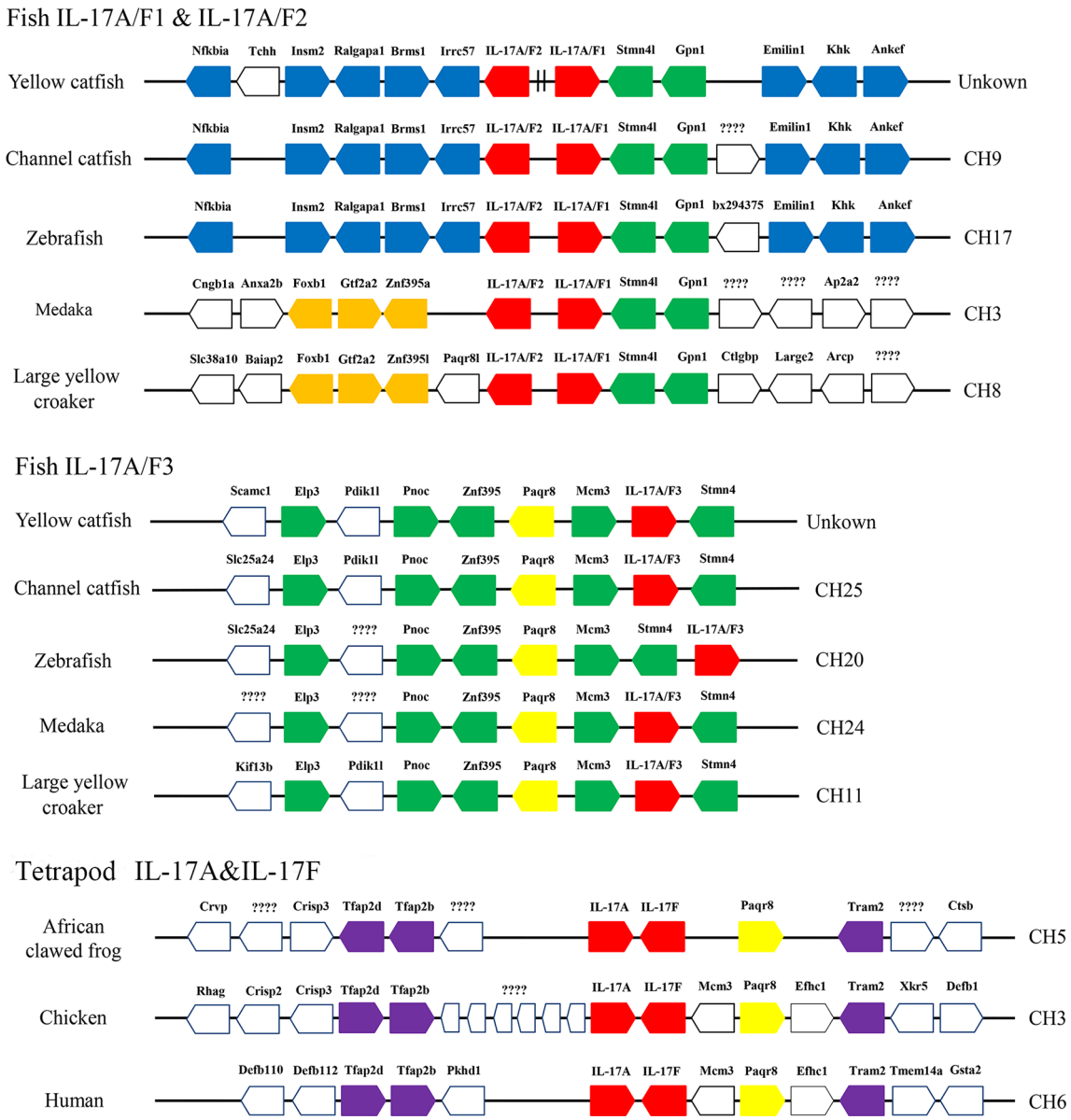

FIGURE 3 | Schematic representation of gene synteny at the IL-17A/Fs loci in teleosts and the IL-17A and IL-17F loci in African clawed frog, chicken and human. The IL-17A/Fs, IL-17A and IL-17F genes are shown in red, the other syntenic genes are shown to be conserved across vertebrates (yellow), only across teleosts (green), only in yellow catfish, channel catfish and zebrafish (blue), only in medaka and large yellow croaker (orange), and only across tetrapod (purple).

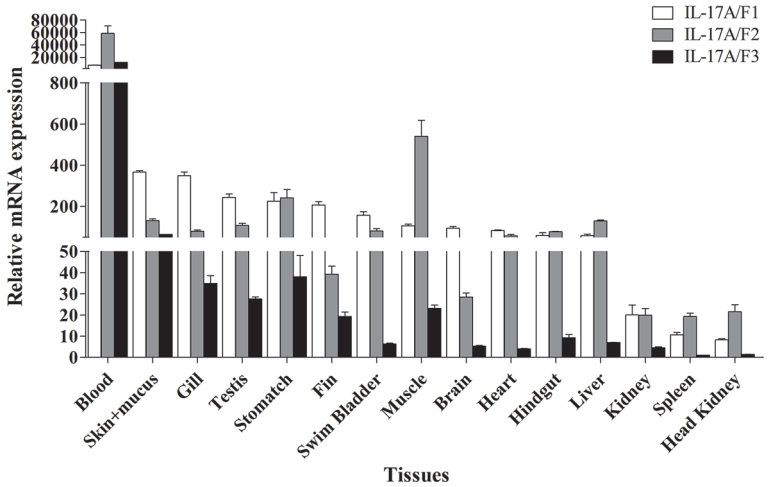

FIGURE 4 | Tissues expression levels of *Pf*_IL-17A/F1, *Pf*_IL-17A/F2 and *Pf*_IL-17A/F3 mRNAs in adult yellow catfish blood, swim bladder, skin+mucus, hindgut, liver, stomach, brain, gill, spleen, head kidney, muscle, heart, testis, fin and trunk kidney. The mRNA expressions of three IL-17A/F genes were detected using qPCR and normalized to the internal gene β-actin. Columns represent the means for each treatment (n = 3). Error bars represent standard error of the means.

testis, stomach, swim bladder, muscle, heart, hindgut and liver, and a relatively low level in other tissues. *Pf*_IL-17A/F3 gene was expressed with a high level in the skin+mucus, and a relatively low level in other tissues. Three *Pf*_IL-17A/F genes were expressed at a low level in the kidney, spleen and head kidney. Overall, the expressions of *Pf*_IL-17A/F1 and *Pf*_IL-17A/F2 mRNAs were higher than those of *Pf*_IL-17A/F3 mRNA in almost all tissues (**Figure 4**).

Expression of *Pf*_IL-17A/F1, 2 and 3 Genes After Challenge of *Edwardsiella ictaluri* and Stimulation With Stimulators

The expression levels of *Pf*_IL-17A/F1, 2 and 3 mRNAs were detected in the gill, skin+mucus, head kidney and spleen tissues of yellow catfish after challenge with *E. ictaluri* (**Figure 5A**). In the gill, the expression of *Pf*_IL-17A/F1 mRNA was significantly up-regulated from 3 h to 120 h with the peak level at 48 h ($P < 0.01$) except for returning to the control level at 72 h, the expression of *Pf*_IL-17A/F2 mRNA was significantly up-regulated from 3 h to 120 h with the highest value at 120 h ($P < 0.01$), and the expression of *Pf*_IL-17A/F3 mRNA was significantly up-regulated from 3 h to 120 h with the peak at 72 h except for a decline to the control level at 24 h (**Figure 5A**). In the skin+mucus, the expression of *Pf*_IL-17A/F1 mRNA was significantly up-regulated from 6 h to 120 h and reached the peak at 24 h ($P < 0.01$), and the expression of *Pf*_IL-17A/F2 and *Pf*_IL-17A/F3 mRNAs was significantly up-regulated from 3 h to 120 h with the peak level at 6 h ($P < 0.01$) except that the *Pf*_IL-17A/F2 mRNA expression declined to the control level at 24 h (**Figure 5A**). In the head kidney, the expression of *Pf*_IL-17A/F1 mRNA was significantly up-regulated from 3 h to 120 h with the highest level at 6 h ($P < 0.01$) except for a decline to a moderate level at 48 h ($P < 0.05$), the expression of *Pf*_IL-17A/F2 mRNA was significantly up-regulated from 3 h and 120 h ($P < 0.01$ or 0.05) except for a significant down-regulation at 72 h ($P < 0.01$), and the expression of *Pf*_IL-17A/F3 mRNA was significantly up-regulated from 3 h and 120 h ($P < 0.01$) except a decrease to the control level at 72 h (**Figure 5A**). In the spleen, the expression of *Pf*_IL-17A/F1 mRNA was significantly up-regulated from 24 h to 120 h with the peak at 72 h ($P < 0.01$) after a fluctuation from 3 h to 12 h, the expression of *Pf*_IL-17A/F2 and 3 mRNAs was significantly up-regulated from 3 h to 48 h with the peak at 3 h ($P < 0.01$ or 0.05), afterwards it was significantly down-regulated to a low level at 72 h ($P < 0.01$) and returned to the control level at 120 h (**Figure 5A**).

To further explore the immunoregulation of *Pf*_IL-17A/F1, 2 and 3 genes, the expressions of *Pf*_IL-17A/F1, *Pf*_IL-17A/F2 and *Pf*_IL-17A/F3 mRNAs in isolated peripheral blood leucocytes (PBLs) of yellow catfish were detected after stimulation with LPS, PGN, poly I:C and PHA (**Figure 5B**). After LPS and PGN stimulation, the expression of *Pf*_IL-17A/F1 mRNA was significantly up-regulated at 3 h and 6 h ($P < 0.01$), and then it was significantly down-regulated at 12 h ($P < 0.01$ or 0.05) and returned to a moderate level at 24 h, while the expression of *Pf*_IL-17A/F1 mRNA was significantly up-regulated from 3 h to 24 h with the peak at 12 h after poly I:C stimulation (**Figure 5B**). The expression of *Pf*_IL-17A/F2 mRNA was significantly up-regulated at 3 h and 6 h, and it was significantly down-regulated at 12 h after PGN stimulation ($P < 0.01$); while the expression of *Pf*_IL-17A/F1 mRNA was only significantly up-regulated at 6 h and the *Pf*_IL-17A/F3 mRNA was significantly up-regulated at 6 h and 24 h, and they were significantly down-regulated at 12 h after LPS and Poly I:C stimulation ($P < 0.01$) (**Figure 5B**). After LPS, PGN and Poly I:C stimulation, the expression levels of *Pf*_IL-17A/F1, 2 and 3 mRNAs were significantly up-regulated at 3 h, 6 h and 24 h with the highest values at 3 h, and they decreased to a level lower or close to the control at 12 h (**Figure 5B**). After PHA stimulation, the expression levels of *Pf*_IL-17A/F1 and 2 mRNAs were up-regulated at 3 h and 6 h with the peak value at 6 h ($P < 0.01$

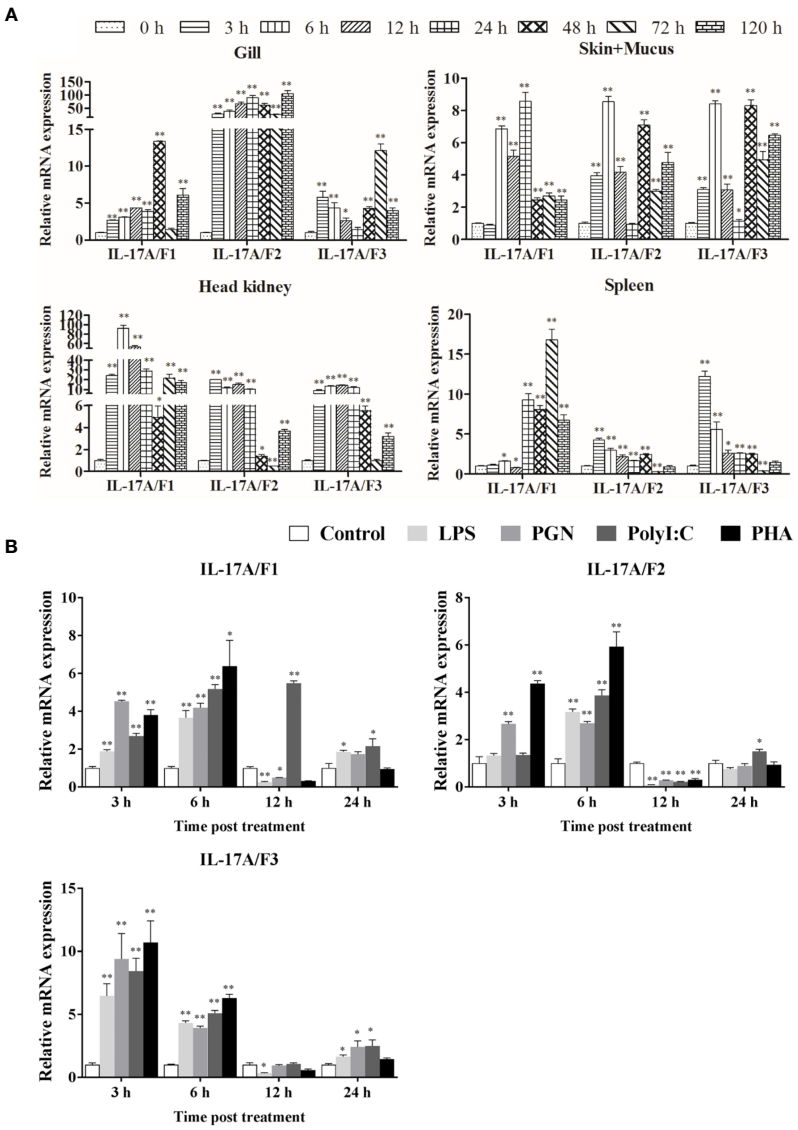

FIGURE 5 | *Pf*_IL-17A/F1, 2 and 3 mRNAs can be induced after the infection of bacteria and the stimulation with stimulators. **(A)** The changes of relative expression levels in the gill, skin+mucus, head kidney and spleen of yellow catfish after challenge of *Edwardsiella ictaluri*. Columns and deviation bars represent the means for each treatment (n = 3) and the standard errors of the means, respectively. **(B)** The changes of expression levels in PBLs of yellow catfish after stimulation with LPS, PGN, Poly I:C and PHA. The PBLs were isolated from five individuals of yellow catfish and were mixed equally, and the pooled sample was further divided into 20 experiment units for different experimental treatments. Columns and deviation bars represent the means for each treatment (n = 3) and the standard errors of the means, respectively. Significant differences at different time points after challenge compared to the control are indicated by asterisks (*P < 0.05, **P < 0.01).

or 0.05), subsequently they were significantly down-regulated at 12 h (P < 0.01) and increased to the control level at 24 h, while the expression of *Pf*_IL-17A/F3 mRNA was up-regulated at 3 h and 6 h with the peak at 3 h (P < 0.01) and decreased to a level close to the control at 12 h and 24 h (**Figure 5B**).

Production, Purification, and Dose Screening of Three Recombinant *Pf*_IL-17A/F Proteins

To determine the biological function of *Pf*_IL-17A/F 1, 2 and 3, three recombinant (r) *Pf*_IL-17A/F proteins were expressed as an N-terminal 6-histidine-tagged fusion protein in *E. coli* and purified with nickel-nitrilotriacetic acid (Ni-NTA) metal affinity chromatography. SDS-PAGE analysis showed that the molecular mass of r*Pf*_IL-17A/F1, 2 and 3 proteins including His-tag was roughly 33.6, 30.67 and 34.3 kDa, respectively (**Figure 6**). Yellow catfish PBLs were treated with the different concentrations (5, 50, and 500 ng/mL) of r*Pf*_IL-17A/F1, 2 and 3 proteins for 6 h. The dose-course experiments showed that the mRNA expression of IL-1β gene was significantly induced at 500 ng/mL of three r*Pf*_IL-17A/F proteins (P < 0.01), and the mRNA expression of CXCL8 gene was notably induced at 500 ng/mL of

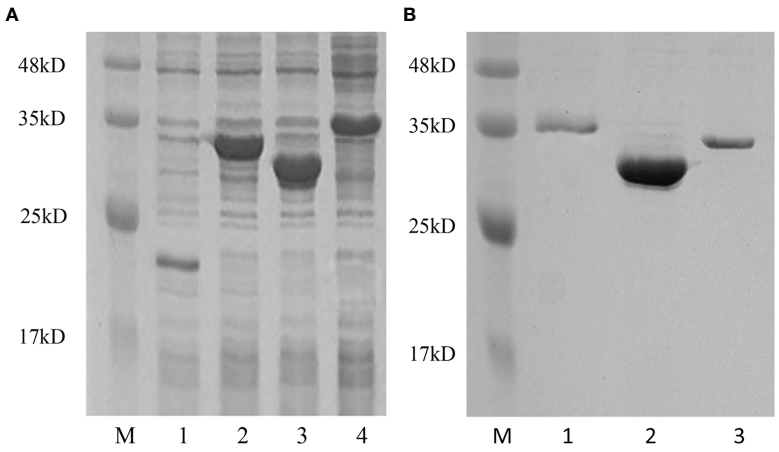

FIGURE 6 | Production and purification of recombinant *Pf*_IL-17A/F1, 2 and 3 proteins by SDS-PAGE. **(A)** Production of r*Pf*_IL-17A/F1, 2 and 3 proteins. Lane 1: Tag protein; Lane 2: r*Pf*_IL-17A/F1 protein; Lane 3: r*Pf*_IL-17A/F2 protein; Lane 4: r*Pf*_IL-17A/F3 protein. **(B)** Purification of three r*Pf*_IL-17A/Fs proteins. Lane 1: r*Pf*_IL-17A/F3 protein; Lane 2: r*Pf*_IL-17A/F2 protein; Lane 3: r*Pf*_IL-17A/F1 protein.

r*Pf*_IL-17A/F1 and 2 proteins ($P < 0.01$) (**Figure 7**). Therefore yellow catfish PBLs were sensitive to the r*Pf*_IL-17A/F1, 2 and 3 proteins at a dose of 500 ng/mL.

Modulation of Inflammatory Cytokines, Chemokines, Antimicrobial Peptides and Downstream Signaling-Related Genes' Expression by Three r*Pf*_IL-17A/F Proteins in Yellow Catfish PBLs

After yellow catfish PBLs were stimulated with the r*Pf*_IL-17A/F1, 2 and 3 proteins (500 ng/mL) for 3 h, 6 h and 12 h, the mRNA expression of inflammatory cytokines, chemokines, antimicrobial peptides and downstream signaling-related genes were detected by qPCR (**Table 1**). IL-1β, TNFα and IL-6 mRNAs were notably induced in yellow catfish PBLs by the r*Pf*_IL-17A/F1, 2 and 3 proteins at some time points ($P < 0.01$ or $P < 0.05$). IL-11 and IL-22 mRNAs were significantly induced in the PBLs by the r*Pf*_IL-17A/F2 and 3 proteins at some time points ($P < 0.01$ or $P < 0.05$). Interestingly, the mRNA expression of IFNγ1 was notably inhibited in the PBLs by the r*Pf*_IL-17A/F1 and 3 proteins at some time points ($P < 0.05$ or 0.01), whereas it was significantly induced by the r*Pf*_IL-17A/F1 protein at 12 h in the PBLs ($P < 0.05$). CXCL11 and CCL4 mRNAs were significantly induced in the PBLs by the r*Pf*_IL-17A/F1, 2 and 3 proteins at some time points ($P < 0.01$ or $P < 0.05$). CXCL1 and CCL3 mRNAs were notably induced in the PBLs by the r*Pf*_IL-17A/F1

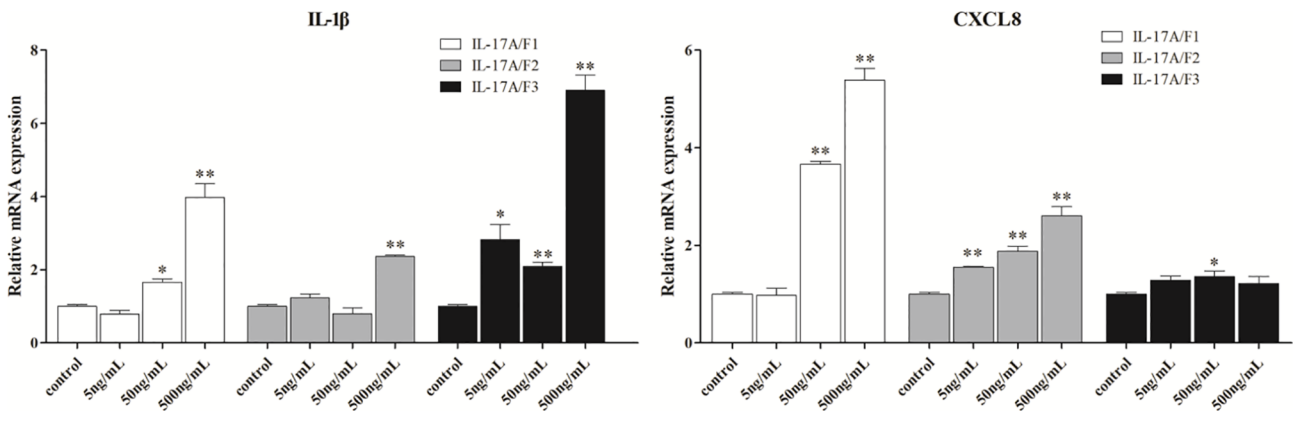

FIGURE 7 | Effects of recombinant *Pf*_IL-17A/F1, 2 and 3 dose course on the expressions of IL-1β and CXCL8 mRNAs in PBLs of yellow catfish. PBLs were treated with different doses of r*Pf*_IL-17A/F1, 2 and 3 proteins (5, 50, 500 ng/mL) for 6 h. Transcriptional fold changes of the IL-1β and CXCL8 genes at different treatment doses were calculated compared to the control group. The PBLs were isolated from four individuals of yellow catfish and were mixed equally, and the pooled sample was further divided into 12 experiment units for different experimental treatments. Columns and deviation bars represent the means and standard errors for each treatment ($n = 3$), respectively. Significant difference at different treatment doses compared to the control is indicated by asterisks (*$P < 0.05$, **$P < 0.01$).

and 3 at some time points ($P < 0.01$ or $P < 0.05$). The expression of CXCL8 mRNA was only distinctly induced in the PBLs by the r*Pf*_IL-17A/F1 and 2 proteins at some time points ($P < 0.05$ or 0.01). S100A1 and LEAP mRNAs were distinctly induced in the PBLs by the r*Pf*_IL-17A/F1, 2 and 3 at some time points ($P < 0.01$ or $P < 0.05$). β-defensins mRNA was distinctly induced in the PBLs by the r*Pf*_IL-17A/F2 and 3 proteins at some time points ($P < 0.05$). The mRNA expressions of IL-17RA, ACT1, TRAF6, TRAF2, TRAF5 and TAK1 were distinctly induced in the PBLs by the r*Pf*_IL-17A/F1 and 3 at some time points ($P < 0.01$ or $P < 0.05$). The r*Pf*_IL-17A/F2 proteins can significantly up-regulated the mRNA expressions of ACT1, TRAF2, TRAF5 and TAK1 at some time points ($P < 0.05$) (**Table 1**). On the whole, the r*Pf*_IL-17A/F2 and 3 proteins could induce the mRNA expressions of pro-inflammatory cytokine genes more powerfully than the r*Pf*_IL-17A/F1 protein, the mRNA expression levels of chemokine genes induced by the r*Pf*_IL-17A/F1 and 3 proteins were higher than those by the r*Pf*_IL-17A/F2 protein, and the r*Pf*_IL-17A/F1, 2 and 3 proteins all could induce the mRNA expression of antimicrobial peptides and downstream signaling-related genes in the PBLs of yellow catfish (**Table 1**).

Three r*Pf*_IL-17A/F Proteins Promote Phagocytosis of Yellow Catfish PBLs

To investigate the effect of three r*Pf*_IL-17A/F proteins on the phagocytosis of yellow catfish PBLs, the PBLs stimulated with three r*Pf*_IL-17A/F proteins (500 ng/mL) and incubated with fluorescent beads were analyzed by flow cytometry. Lymphocytes (Lym) and myeloid cells (Mye) were gated in the PBLs (**Figure 8A**). The r*Pf*_IL-17A/F2 and 3 proteins significantly

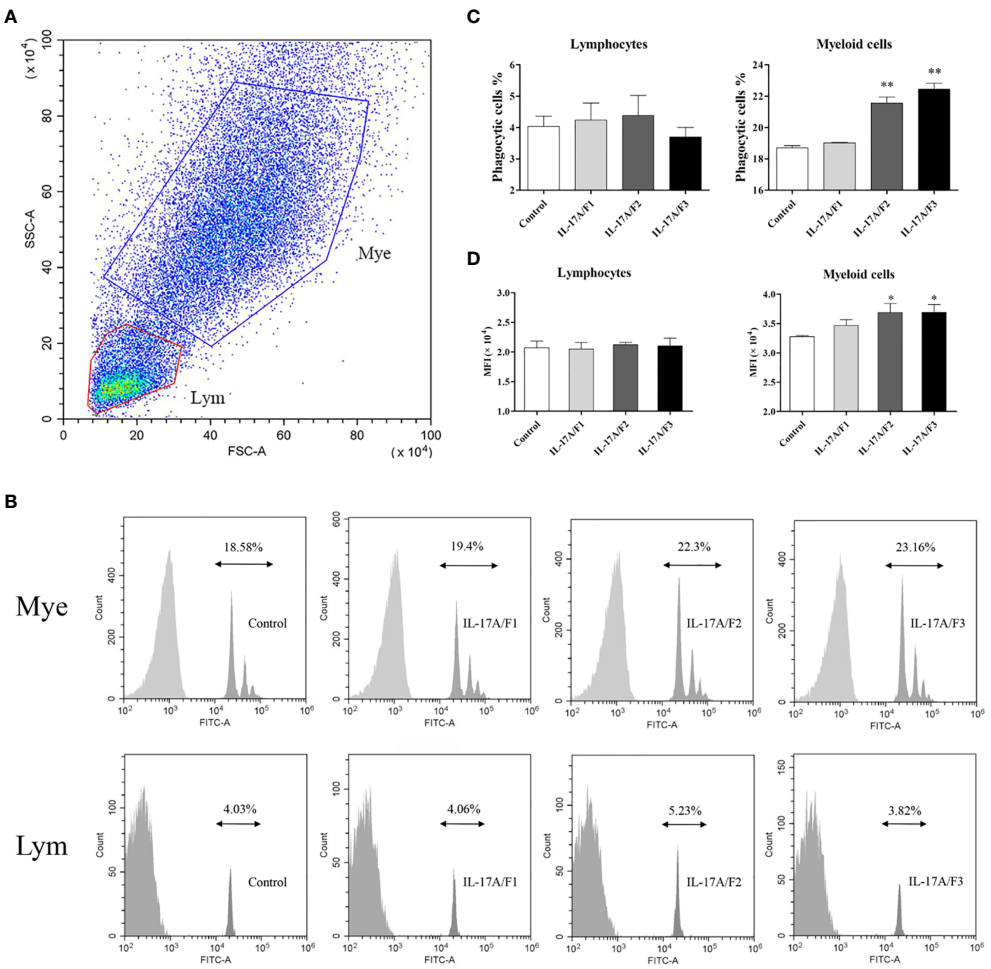

FIGURE 8 | The r*Pf*_IL-17A/F1, 2 and 3 promote phagocytosis of PBLs in yellow catfish. **(A)** Cell typing of PBLs by flow cytometry analysis. Yellow catfish PBLs were incubated with r*Pf*_IL-17A/F1, IL-17A/F2 and IL-17A/F3 proteins (500 ng/mL) or medium alone as a control for 18 h. The PBLs were then incubated with 1.0 μm fluorescent beads for 2 h and analyzed by flow cytometry. Mye: myeloid cells, Lym: lymphocytes. **(B)** The phagocytic activity of PBLs detected by flow cytometry. Typical results from a biological replication experiment are shown. **(C)** The percentage of phagocytic leukocytes in lymphocytes and myeloid cells. **(D)** The mean fluorescence intensity (MFI) of phagocytic cells. The PBLs were isolated from three individuals of yellow catfish and were mixed equally, and the pooled sample was further divided into four experiment units for different experimental treatments. Columns and deviation bars represent the means and standard errors for each treatment ($n = 3$), respectively. Significant difference in different protein treatments compared to the control is indicated by asterisks (*$P < 0.05$, **$P < 0.01$).

promoted the phagocytic activity of myeloid cells in the PBLs ($P < 0.01$), whereas the r*Pf*_IL-17A/F1 protein just slightly increased the phagocytic activity of myeloid cells, and the three r*Pf*_IL-17A/Fs proteins had no obvious effect on the phagocytic activity of lymphocytes in the PBLs (**Figures 8B, C**). Simultaneously, the mean fluorescence intensity (MFI) of myeloid cells was significantly up-regulated in the PBLs after stimulation with the r*Pf*_IL-17A/F2 and 3 proteins ($P < 0.05$), whereas the MFI of lymphoid cells was not altered after three r*Pf*_IL-17A/F proteins treatment (**Figure 8D**).

Recombinant *Pf*_IL-17A/F1, 2, and 3 Proteins Promoted IL-1β and CXCL11 mRNA Expression in PBLs *via* MAPK and NF-κB Pathway

After the yellow catfish PBLs were exposed to the r*Pf*_IL-17A/F1, 2 and 3 (500 ng/mL) for 6 h in the presence of NF-κB inhibitor PDTC (0.5 μM) and p38 MAPK inhibitor SB203580 (20 μM), the IL-1β and CXCL-11 mRNA expressions triggered by the r*Pf*_IL-17A/F1, 2 and 3 were differently blocked by the PDTC and SB203580 (**Figure 9**).

DISCUSSION

In this study, partial cDNA sequences of three IL-17A/F genes were cloned from yellow catfish. The deduced *Pf*_IL-17A/F1, 2 and 3 amino sequences contained a signal peptide and an IL-17 superfamily domain as the human IL-17A and IL-17F, and their isoelectric points were acidic and close in size (5.18–5.21), indicating that *Pf*_IL-17A/F 1, 2 and 3 genes may have some similar biological functions or signal pathways as the human IL-17A and IL-17F genes (28, 29, 31, 37). Moreover, the *Pf*_IL-17A/F1 and *Pf*_IL-17A/F2 cDNAs possessed several copies of mRNA instability motif (ATTTA), which might regulate the degradation of mRNA in their 3'-UTR (38).

During biological evolution, the two rounds of whole genome duplication (WGD) event dated from 520–550 million year ago in vertebrates (39, 40). Moreover, a teleosts-specific third WGD event happened 226–316 million year ago, and approximately 50% of duplicated genes were retained that may have important roles (41). Therefore, some teleosts may have more homologues in some duplicated genes than mammals. In mammals, IL-17A and IL-17F genes have high amino acid sequence similarity, whereas there have been three or five IL-17A or F homologue genes (IL-17A/F) found in teleosts (22, 26). Fish IL-17A/F1, 2 and 3 had the same genome organization with those of tetrapods (three exons and two introns) except for IL-17A/F3 in fugu, large yellow croaker and rainbow trout (four exons and three introns). In terms of exon length, we inferred that the third exon of IL-17A/F3 in fugu, large yellow croaker and rainbow trout might have been split into two small exons in fish evolution process (22). Mammalian and avian IL-17A and IL-17F are adjacently located on the same chromosomes (22). In fish, IL-17A/F1 and IL-17A/F2 were adjacently located on the same

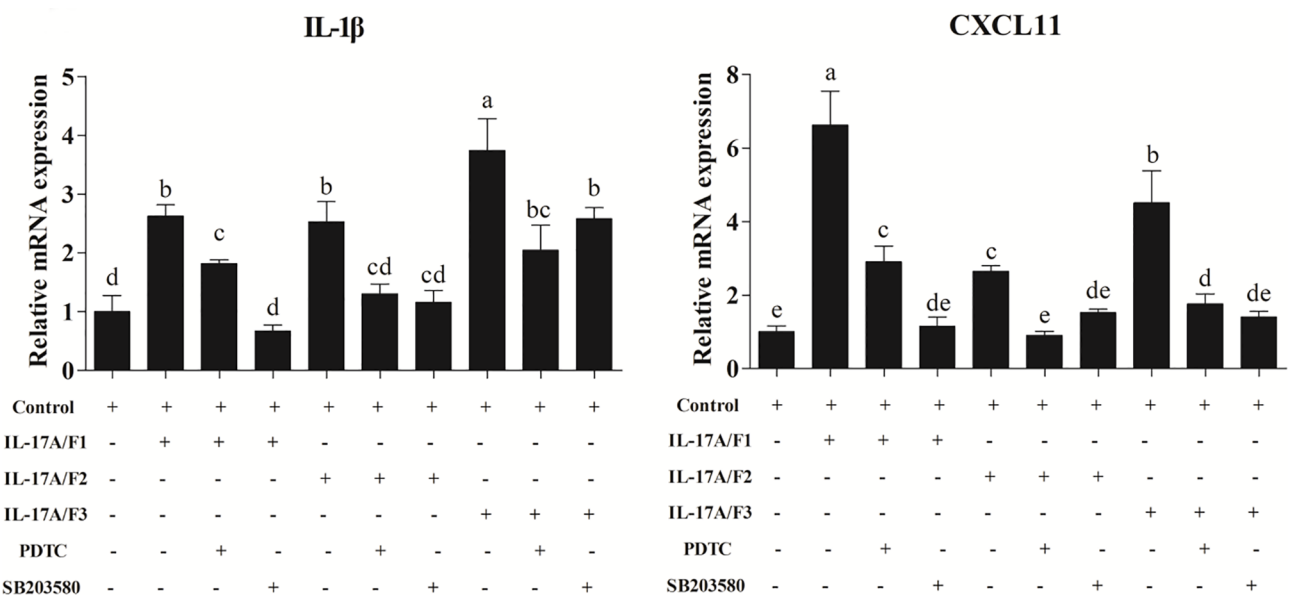

FIGURE 9 | Recombinant *Pf*_IL-17A/F1, 2 and 3 proteins promoted IL-1β and CXCL11 mRNA expression in PBLs *via* MAPK and NF-κB pathway. PBLs were treated with 500 ng/mL r*Pf*_IL-17A/F1, 2 and 3 for 6 h in the presence (+) or absence (-) of different inhibitors (PDTC and SB203580). The mRNA levels of IL-1β and CXCL11 were determined by qPCR. The PBLs were isolated from four individuals of yellow catfish and were mixed equally, and the pooled sample was further divided into ten experiment units for different experimental treatments. Columns represent the means for each treatment ($n = 3$). Error bars represent standard error of the means. Different letters above the bars indicate significant difference among/between the means (One-way ANOVA and Duncan test, $P < 0.05$).

chromosome, but IL-17A/F3 was located on another chromosome, indicating that fish have more IL-17A/F homologue genes than tetrapods because of genome duplication and chromosomal rearrangement in fish biological evolution (22).

Although mammalian IL-17A and IL-17F play important and similar roles in inflammation, IL-17A can induce inflammatory cytokines more strongly than IL-17F in the autoimmunity, and IL-17F plays a more critical role than IL-17A in protecting colonic epithelial cells from bacterial invasion (19, 20). In fish, IL-17A/F1, 2 and 3 are vital pro-inflammatory cytokines through which can promote the mRNA expressions of other pro-inflammatory cytokines, chemokines and antimicrobial peptides, but little is known about the functional difference of fish IL-17A/F1, 2 and 3. Both human IL-17A and IL-17F monomers have two pairs of anti-parallel β-sheets (strands 1–4), with the second and fourth strands connected by two disulfide bonds (6, 42). Similarly, *Pf*_IL-17A/F1, 2 and 3 were predicted to possess four inferred β-strands, the second and fourth strands were linked by two disulfide bonds, while the fourth β-strand of *Pf*_IL-17A/F2 was shorter than those of *Pf*_IL-17A/F1, *Pf*_IL-17A/F3, human IL-17A and IL-17 F. Moreover, *Pf*_IL-17A/F2 also formed another disulfide bond similar to human IL-17A and IL-17F that is not bound by the receptor (42). The IL-17 superfamily domain was encoded by the second and third exons, but the second exon of fish IL-17A/F2 is shorter than those of fish IL-17A/F1 and 3. Furthermore, phylogenetic and homological analysis showed that teleost IL-17A/F1 is more similar to IL-17A/F3 than IL-17A/F2 in amino acid sequence. Different amino acid sequences will construct distinct secondary and tertiary structures and result in functional diversification. These results imply that fish IL-17A/F genes may exist distinct functional diversification due to the impact of their structure difference on receptor-binding affinity/signaling.

In mammals, IL-17A and IL-17F are mainly secreted by Th17 cells (15). Here, the highest expression levels of *Pf*_IL-17A/F1, 2 and 3 mRNAs were detected in blood of healthy yellow catfish. Moreover, PHA, as a stimulator of accelerating T cell proliferation (43), was able to significantly induce the mRNA expressions of *Pf*_IL-17A/F1, 2 and 3 genes in PBLs, indicating that the production of IL-17A/F1, 2 and 3 in yellow catfish is similar to that in mammals by T cells. In mammals, Th17 cytokines can protect the host from pathogens at epithelial and mucosal tissues including the skin, lung and intestine (44). IL-17A is produced by intestinal paneth cells (45). IL-17F mRNA is expressed in colonic epithelial cells (20). Similarly, fish IL-17A/F1, 2 and 3 mRNAs are highly expressed in mucosal tissues (skin, gill, and intestine) and have low expressions in the head kidney in channel catfish, Japanese pufferfish, and large yellow croaker (23, 25, 28). Skin, gill and intestine are all part of the mucosal surface, which is the first barrier exposed to a complicated environment to prevent and eliminate invasive pathogens through recruiting neutrophils and lymphocytes (46). In this study, higher expression levels of *Pf*_IL-17A/F1, 2 and 3 mRNAs were detected in skin+mucus, and low expressions of *Pf*_IL-17A/F1, 2 and 3 mRNAs were present in the kidney, head kidney and spleen. Furthermore, in teleosts, after stimulation of stimulators (LPS or Poly I:C) in PBLs, IL-17A/F1, 2 and 3 mRNAs were notably induced in zebrafish and grass carp (21, 31). After bacterial challenge (*A. hydrophila* or *E. ictaluri*), IL-17A/F1, 2 and 3 transcripts were distinctly up-regulated in the head kidney or mucosal tissues in channel catfish and large yellow croaker (25, 28). Here, the expression levels of *Pf*_IL-17A/F1, 2 and 3 mRNAs were significantly up-regulated in all four detected tissues after challenge of *E. ictaluri* and in yellow catfish PBLs after stimulation of LPS, PGN and Poly I:C. These data suggest that *Pf*_IL-17A/F1, 2 and 3 genes may play a crucial role in the host defense against pathogens infection.

Interestingly, although the expression levels of *Pf*_IL-17A/F1, 2 and 3 mRNAs were low in the head kidney and spleen of healthy yellow catfish, they were rapidly and dramatically up-regulated in the head kidney and spleen after challenge of *E. ictaluri*, indicating that fish IL-17A/F1, 2 and 3 genes need to be modulated strictly like human IL-17A and IL-17F as their persistent and excess expression is harmful for the host (34). In mammals, IL-17A is mainly produced in T cells, whereas IL- 17F is produced in T cells, innate immune cells and epithelial cells (20). The mRNA expression of *Pf*_IL-17A/F3 gene is relatively lower than that of *Pf*_IL-17A/F1 and 2 genes in healthy yellow catfish, but it is more induced after stimulation of stimulators and *E. ictaluri* infection, implying that *Pf*_IL-17A/F1, 2 and 3 genes might have functional diversification.

Although mammalian IL-17A and IL-17F have many overlapping functions, they play different roles in host defense against bacterial infection. IL-17A is more effective to induce pro-inflammatory cytokines than IL-17F (18, 47). In fish, IL-17A/F1, 2 and 3 genes can induce the mRNA expressions of IL-1β, TNFα, IL-6, CXCL8 and antimicrobial peptides (28–31), but little is known about the different roles of IL-17A/F1, 2 and 3 in the immune response.

The pro-inflammatory cytokines can directly activate the immune cells to eliminate invading pathogens. In mammals, IL-1β, TNFα, IL-6, IL-11 and IFNγ can directly activate macrophages and neutrophils (1, 48–50), and IL-22, which is derived from Th17 cells and innate lymphoid cells, acts on epithelial cells (1). In large yellow croaker, three rIL-17A/Fs induced the mRNA expressions of IL-1β, IL-6 and TNF-α in the head kidney (28). In this study, the r*Pf*_IL-17A/F2 and 3 proteins notably induced the mRNA expressions of IL-1β, IL-6, IL-11, IL-22 and TNFα in PBLs at certain time points, while the r*Pf*_IL-17A/F1 protein only significantly induced the mRNA expressions of IL-1β, IL-6 and TNFα at 3 h and/or 6 h. Furthermore, r*Pf*_IL-17A/F2 and 3 proteins enhanced the phagocytosis of myeloid cells except for r*Pf*_IL-17A/F1 protein, whereas three r*Pf*_IL-17A/F proteins were ineffective to promote the phagocytosis of lymphocytes in yellow catfish PBLs. These results indicate that the r*Pf*_IL-17A/F2 and 3 proteins can more significantly induce the expression of pro-inflammation cytokines and contribute to the phagocytosis of myeloid cells compared with the r*Pf*_IL-17A/F1 protein. In mammals, IFNγ, as the symbolic cytokine, can inhibit the development of Th17 cells from naive precursor cells (7). Similarly, the r*Pf*_IL-17A/F2

protein only distinctly up-regulated the mRNA expression of IFNγ in PBLs at 12 h, and the r*Pf*_IL-17A/F1 and 3 proteins notably inhibited the mRNA expression of IFNγ, indicating that fish IL-17A/Fs might control the development of fish T cells whose functions like mammalian Th1 cells.

In mammals, both IL-17A and IL-17F can stimulate the release of CXCL1, CXCL2 and CXCL8, and IL-17A can also recruit and activate neutrophils under certain conditions (3, 47, 51). In grass carp, rIL-17A/F1 enhanced the mRNA expression of CXCL8 in head kidney cells to stimulate PBLs migration (31). Large yellow croaker rIL-17A/Fs could promote the mRNA expressions of CXCL8 and CXCL13 in the head kidney (28). In the present study, three r*Pf*_IL-17A/Fs proteins notably induced the mRNA expressions of CXCL11 and CCL4 in PBLs at 6 h and 12 h, the r*Pf*_IL-17A/F1 and 3 proteins significantly up-regulated the mRNA expressions of CXCL1 and CCL3 at a certain time point, and CXCL8 mRNA was induced by the r*Pf*_IL-17A/F1 and 2 proteins. These results showed that fish IL-17A/Fs can promote the expression of chemokines to recruit and activate immune cells.

In humans, IL-17A can more significantly induce the mRNA expressions of β-defensins-2, S100A7, S100A8 and S100A9 compared with IL-17F in primary human keratinocytes (18). Common carp rIL-17A/F2a could induce the mRNA expressions of S100A1, S100A10a and S100A10b in the primary kidney (30). Rainbow trout IL-17A/F2 promoted the mRNA expression of β-defensins-3 in splenocytes (29). Three large yellow croaker IL-17A/Fs proteins could enhance the mRNA expression of hepcidin in the head kidney (28). In this study, three r*Pf*_IL-17A/F proteins were able to stimulate the mRNA expressions of S100A1 in PBLs at certain time points, and only the r*Pf*_IL-17A/F2 and 3 proteins induced the mRNA expression of β-defensins. Moreover, mammalian LEAP2 is not only highly expressed in hepatocytes, but also is blood-derived antimicrobial peptide and expressed in gastro-intestinal epithelial tissues and monocytes (52, 53). But there is no literature that shows that the expression of the LEAP2 gene is regulated by IL-17 at present. Here, three r*Pf*_IL-17A/F proteins were able to stimulate the mRNA expression of LEAP in PBLs at certain time points. These results uncover that, like mammalian IL-17A and IL-17F, fish IL-17A/Fs can facilitate the expressions of antibacterial peptides to eliminate the invading pathogens.

In mammals, IL-17A and IL-17F combine with IL-17RA and IL-17RC to bind ACT1. Subsequently, ACT1 mediates TRAF6 ubiquitination to activate NF-kB and MAPK pathways, or ACT1 recruits TRAF2 and TRAF5 to enhance mRNA stability (3, 44, 47). In large yellow croaker, three rIL-17A/Fs proteins could activate the NF-kB pathway (28). In yellow catfish, the r*Pf*_IL-17A/F1 and 3 proteins notably induced the mRNA expressions of IL-17RA, ACT1, TRAF6, TRAF2, TRAF5 and TAK1 in PBLs, whereas the r*Pf*_IL-17A/F2 protein only enhanced the mRNA expressions of ACT1, TRAF2, TRAF5 and TAK1 at 3 h or 6 h. Furthermore, the IL-1β and CXCL11 mRNA expressions triggered by the r*Pf*_IL-17A/F1, 2 and 3 were blocked by the NF-κB inhibitor PDTC and the p38 MAPK inhibitor SB203580. These results indicate that compared with mammalian IL-17A and IL-17F, fish IL-17A/F1 and 3 may have similar downstream signal pathways, while the downstream signal pathway of fish IL-17A/F2 may be somewhat different.

The individual variability of fish such as body size and physiological status may have potential effects on immuno-related gene expressions and phagocytosis of PBLs. In this study, to reduce the potential effects of fish individual variability, the randomized block design (3 blocks × *M* experimental treatments) was used to control the test error. The PBLs were isolated from several individuals of yellow catfish and were mixed equally, and the pooled sample was further divided into a certain number of experiment units (*M*) as a block for being dealt with different experimental treatments such as the control and other experiment conditions. The second and the third pooled samples were also divided and treated as above. Therefore, in each experimental treatment (i.e. experimental group), three experiment units were from three different pooled samples; in each block, *M* experiment units were from the same pooled sample, and they are homogeneous. Therefore we used dependent t-test to compare the difference between the control group and each other treatment group, this will help to eliminate or reduce the effect of three pooled samples' difference on statistical analysis. Additionally, pooling a PBLs sample from several fish individuals might produce leucocyte activation to make graft rejection. However, in this study, the death phenomenon of PBLs was not observed in the pooled PBLs samples during the whole experiment. Even if the pooling produces leucocyte activation, this activation will occur both in the treatment groups by IL-17A/Fs and in the control group without IL-17A/Fs. Through analysis of dependent t-test, the effect of this potential leucocyte activation will be eliminated, and the t-test results will mainly reflect the effect of IL-17A/Fs treatments.

In conclusion, we cloned partial cDNA sequences of three IL-17A/F homologous genes (*Pf*_IL-17A/F1, 2, and 3) from yellow catfish. *Pf*_IL-17A/F1, 2 and 3 genes displayed distinct structural characteristics. *Pf*_IL-17A/F1, 2 and 3 mRNAs were ubiquitously expressed in fifteen examined adult tissues and preferentially expressed in the blood, gill, and skin+mucus. The expressions of *Pf*_IL-17A/F1, 2 and 3 mRNAs were all rapidly and significantly up-regulated in the gill, skin+mucus, head kidney and spleen after *E. ictaluri* challenge and in yellow catfish PBLs after stimulation with PHA, LPS, PGN and poly I:C. Moreover, the r*Pf*_IL-17A/F1, 2 and 3 proteins showed divergent bioactivity in PBLs. The r*Pf*_IL-17A/F1, 2 and 3 proteins significantly induced the mRNA expressions of proinflammatory cytokines, chemokines and antibacterial peptides genes, and the r*Pf*_IL-17A/F 2 and 3 proteins promoted more powerful phagocytosis of PBLs than the r*Pf*_IL-17A/F1 protein. Furthermore, the r*Pf*_IL-17A/F1, 2 and 3 proteins could activate the NF-κB and MAPK signal pathways by IL-17RA, ACT1, TRAF6, TRAF2, TRAF5 and TAK1. The results indicate that *Pf*_IL-17A/F1, 2 and 3 play different roles in promoting the inflammatory response and host defense against bacterial infection. These data will help to better understand the potential function of three IL-17A/F genes in fish immune responses towards pathogen infections.

DATA AVAILABILITY STATEMENT

The original contributions presented in the study are included in the article/**Supplementary Material**. Further inquiries can be directed to the corresponding authors.

ETHICS STATEMENT

The animal study was reviewed and approved by Institutional Animal Care and Use Committees (IACUC) of HZAU, Wuhan, P. R. China.

AUTHOR CONTRIBUTIONS

XZ performed the experiments, analyzed the data, and wrote the manuscript. G-RZ, WJ, X-FM, Z-LL, and K-JW conceived and designed the study. Z-CS helped with the preparation of experimental fishes. XZ, Z-LL, and K-JW revised the manuscript. All authors contributed to the article and approved the submitted version.

FUNDING

This study was supported by the Biodiversity Survey and Assessment Project of the Ministry of Ecology and Environment, China (Grant No. 2019HJ2096001006), and the National Natural Science Foundation of China (Grant No. 31772851).

SUPPLEMENTARY MATERIAL

The Supplementary Material for this article can be found online at: https://www.frontiersin.org/articles/10.3389/fimmu.2021.626895/full#supplementary-material

REFERENCES

1. Netea MG, Balkwill F, Chonchol M, Cominelli F, Donath MY, Giamarellos-Bourboulis EJ, et al. A Guiding Map for Inflammation. *Nat Immunol* (2017) 18:826–31. doi: 10.1038/ni.3790
2. McInnes IB, Schett G. Cytokines in the Pathogenesis of Rheumatoid Arthritis. *Nat Rev Immunol* (2007) 7:429–42. doi: 10.1038/nri2094
3. Gu C, Wu L, Li X. IL-17 Family: Cytokines, Receptors and Signaling. *Cytokine* (2013) 64:477–85. doi: 10.1016/j.cyto.2013.07.022
4. Moseley TA, Haudenschild DR, Rose L, Reddi AH. Interleukin-17 Family and IL-17 Receptors. *Cytokine Growth Factor Rev* (2003) 14:155–74. doi: 10.1016/s1359-6101(03)00002-9
5. Song X, Qian Y. IL-17 Family Cytokines Mediated Signaling in the Pathogenesis of Inflammatory Diseases. *Cell Signal* (2013) 25:2335–47. doi: 10.1016/j.cellsig.2013.07.021
6. Hymowitz SG, Filvaroff EH, Yin JP, Lee J, Cai L, Risser P, et al. IL-17s Adopt a Cystine Knot Fold: Structure and Activity of a Novel Cytokine, IL-17F, and Implications for Receptor Binding. *EMBO J* (2001) 20(19):5332–41. doi: 10.1093/emboj/20.19.5332
7. Harrington LE, Hatton RD, Mangan PR, Turner H, Murphy TL, Murphy KM, et al. Interleukin 17-Producing CD4+ Effector T Cells Develop *Via* a Lineage Distinct From the T Helper Type 1 and 2 Lineages. *Nat Immunol* (2005) 6 (11):1123–32. doi: 10.1038/ni1254
8. Mangan PR, Harrington LE, O'Quinn DB, Helms WS, Bullard DC, Elson CO, et al. Transforming Growth Factor-Beta Induces Development of the T(H)17 Lineage. *Nature* (2006) 441:231–4. doi: 10.1038/nature04754
9. Yang XO, Panopoulos AD, Nurieva R, Chang SH, Wang D, Watowich SS, et al. STAT3 Regulates Cytokine-Mediated Generation of Inflammatory Helper T Cells. *J Biol Chem* (2007) 282:9358–63. doi: 10.1074/jbc.C600321200
10. Acosta-Rodriguez EV, Napolitani G, Lanzavecchia A, Sallusto F. Interleukins 1beta and 6 But Not Transforming Growth Factor-Beta Are Essential for the Differentiation of Interleukin 17-Producing Human T Helper Cells. *Nat Immunol* (2007) 8:942–9. doi: 10.1038/ni1496
11. Nurieva R, Yang XO, Martinez G, Zhang Y, Panopoulos AD, Ma L, et al. Essential Autocrine Regulation by IL-21 in the Generation of Inflammatory T Cells. *Nature* (2007) 448:480–3. doi: 10.1038/nature05969
12. Chung Y, Chang SH, Martinez GJ, Yang XO, Nurieva R, Kang HS, et al. Critical Regulation of Early Th17 Cell Differentiation by Interleukin-1 Signaling. *Immunity* (2009) 30:576–87. doi: 10.1016/j.immuni.2009.02.007
13. Veldhoen M, Hocking RJ, Atkins CJ, Locksley RM, Stockinger B. TGFbeta in the Context of an Inflammatory Cytokine Milieu Supports *De Novo* Differentiation of IL-17-Producing T Cells. *Immunity* (2006) 24:179–89. doi: 10.1016/j.immuni.2006.01.001
14. Laurence A, Tato CM, Davidson TS, Kanno Y, Chen Z, Yao Z, et al. Interleukin-2 Signaling *Via* STAT5 Constrains T Helper 17 Cell Generation. *Immunity* (2007) 26:371–81. doi: 10.1016/j.immuni.2007.02.009
15. Cua DJ, Tato CM. Innate IL-17-Producing Cells: The Sentinels of the Immune System. *Nat Rev Immunol* (2010) 10:479–89. doi: 10.1038/nri2800
16. Gaffen SL, Jain R, Garg AV, Cua DJ. The IL-23-IL-17 Immune Axis: From Mechanisms to Therapeutic Testing. *Nat Rev Immunol* (2014) 14:585–600. doi: 10.1038/nri3707
17. Shen F, Ruddy MJ, Plamondon P, Gaffen SL. Cytokines Link Osteoblasts and Inflammation: Microarray Analysis of Interleukin-17- and TNF-Alpha-Induced Genes in Bone Cells. *J Leukoc Biol* (2005) 77:388–99. doi: 10.1189/jlb.0904490
18. Liang SC, Tan XY, Luxenberg DP, Karim R, Dunussi-Joannopoulos K, Collins M, et al. Interleukin (IL)-22 and IL-17 Are Coexpressed by Th17 Cells and Cooperatively Enhance Expression of Antimicrobial Peptides. *J Exp Med* (2006) 203:2271–9. doi: 10.1084/jem.20061308
19. Dubin PJ, Kolls JK. Interleukin-17A and Interleukin-17F: A Tale of Two Cytokines. *Immunity* (2009) 30:9–11. doi: 10.1016/j.immuni.2008.12.010
20. Ishigame H, Kakuta S, Nagai T, Kadoki M, Nambu A, Komiyama Y, et al. Differential Roles of Interleukin-17A and -17F in Host Defense Against Mucoepithelial Bacterial Infection and Allergic Responses. *Immunity* (2009) 30:108–19. doi: 10.1016/j.immuni.2008.11.009
21. Gunimaladevi I, Savan R, Sakai M. Identification, Cloning and Characterization of Interleukin-17 and Its Family From Zebrafish. *Fish Shellfish Immunol* (2006) 21:393–403. doi: 10.1016/j.fsi.2006.01.004
22. Kono T, Korenaga H, Sakai M. Genomics of Fish IL-17 Ligand and Receptors: A Review. *Fish Shellfish Immunol* (2011) 31:635–43. doi: 10.1016/j.fsi.2010.11.028
23. Korenaga H, Kono T, Sakai M. Isolation of Seven IL-17 Family Genes From the Japanese Pufferfish *Takifugu Rubripes*. *Fish Shellfish Immunol* (2010) 28:809–18. doi: 10.1016/j.fsi.2010.01.016
24. Nuñez Ortiz N, Gerdol M, Stocchi V, Marozzi C, Randelli E, Bernini C, et al. T Cell Transcripts and T Cell Activities in the Gills of the Teleost Fish Sea Bass (*Dicentrarchus Labrax*). *Dev Comp Immunol* (2014) 47:309–18. doi: 10.1016/j.dci.2014.07.015
25. Wang X, Li C, Thongda W, Luo Y, Beck B, Peatman E. Characterization and Mucosal Responses of Interleukin 17 Family Ligand and Receptor Genes in Channel Catfish *Ictalurus Punctatus*. *Fish Shellfish Immunol* (2014) 38:47–55. doi: 10.1016/j.fsi.2014.02.020
26. Wang T, Jiang Y, Wang A, Husain M, Xu Q, Secombes CJ. Identification of the Salmonid IL-17A/F1a/b, IL-17A/F2b, IL-17A/F3 and IL-17N Genes and Analysis of Their Expression Following *In Vitro* Stimulation and Infection. *Immunogenetics* (2015) 67:395–412. doi: 10.1007/s00251-015-0838-1

27. Yang Q, Sun Y, Su X, Li T, Xu T. Characterization of Six IL-17 Family Genes in Miiuy Croaker and Evolution Analysis of Vertebrate IL-17 Family. *Fish Shellfish Immunol* (2016) 49:243–51. doi: 10.1016/j.fsi.2015.12.031
28. Ding Y, Ao J, Ai C, Chen X. Molecular and Functional Identification of Three Interleukin-17A/F (IL-17A/F) Homologues in Large Yellow Croaker (*Larimichthys Crocea*). *Dev Comp Immunol* (2016) 55:221–32. doi: 10.1016/j.dci.2015.09.010
29. Monte MM, Wang T, Holland JW, Zou J, Secombes CJ. Cloning and Characterization of Rainbow Trout Interleukin-17A/F2 (IL-17A/F2) and IL-17 Receptor A: Expression During Infection and Bioactivity of Recombinant IL-17A/F2. *Infect Immun* (2013) 81:340–53. doi: 10.1128/IAI.00599-12
30. Li H, Yu J, Li J, Tang Y, Yu F, Zhou J, et al. Cloning and Characterization of Two Duplicated Interleukin-17A/F2 Genes in Common Carp (*Cyprinus Carpio* L.): Transcripts Expression and Bioactivity of Recombinant IL-17A/F2. *Fish Shellfish Immunol* (2016) 51:303–12. doi: 10.1016/j.fsi.2016.01.042
31. Du L, Feng S, Yin L, Wang X, Zhang A, Yang K, et al. Identification and Functional Characterization of Grass Carp IL-17A/F1: An Evaluation of the Immunoregulatory Role of Teleost IL-17A/F1. *Dev Comp Immunol* (2015) 51:202–11. doi: 10.1016/j.dci.2015.03.014
32. Geng Y, Wang KY, Chen DF, Fan FL, Huang YD. Isolation and Characterization of *Edwardsiella Ictaluri* From Cultured Yellow Catfish (*Pelteobagrus Fulvidraco*). *Oceanol Limnol Sin* (2010) 62:105–15. doi: 10.3724/SP.J.1238.2010.00453
33. Ye S, Li H, Qiao G, Li Z. First Case of *Edwardsiella Ictaluri* Infection in China Farmed Yellow Catfish *Pelteobagrus Fulvidraco*. *Aquaculture* (2009) 292:6–10. doi: 10.1016/j.aquaculture.2009.03.036
34. Cooper AM. IL-17 and Anti-Bacterial Immunity: Protection Versus Tissue Damage. *Eur J Immunol* (2009) 39:649–52. doi: 10.1002/eji.200839090
35. Wang KL, Ji W, Zhang GR, Wei KJ, Shi ZC, Zhang XT, et al. Molecular Characterization and Expression Analysis of Three TLR Genes in Yellow Catfish (*Pelteobagrus Fulvidraco*): Responses to Stimulation of *Aeromonas Hydrophila* and TLR Ligands. *Fish Shellfish Immunol* (2017) 66:466–79. doi: 10.1016/j.fsi.2017.05.056
36. Livak KJ, Schmittgen TD. Analysis of Relative Gene Expression Data Using Real-Time Quantitative PCR and the $2^{(-\text{Delta Delta C(T)})}$ Method. *Methods* (2001) 25:402–8. doi: 10.1006/meth.2001.1262
37. Chang SH, Dong C. A Novel Heterodimeric Cytokine Consisting of IL-17 and IL-17F Regulates Inflammatory Responses. *Cell Res* (2007) 17:435–40. doi: 10.1038/cr.2007.35
38. Sachs AB. Messenger RNA Degradation in Eukaryotes. *Cell* (1993) 74:413. doi: 10.1016/0092-8674(93)80043-E
39. Macqueen DJ, Johnston IA. A Well-Constrained Estimate for the Timing of the Salmonid Whole Genome Duplication Reveals Major Decoupling From Species Diversification. *Proc Biol Sci* (2014) 281:20132881. doi: 10.1098/rspb.2013.2881
40. Van de Peer Y, Maere S, Meyer A. The Evolutionary Significance of Ancient Genome Duplication. *Nat Rev Genet* (2006) 10:725–32. doi: 10.1038/nrg2600
41. Pasquier J, Cabau C, Nguyen T, Jouanno E, Severac D, Braasch I, et al. Gene Evolution and Gene Expression After Whole Genome Duplication in Fish: The PhyloFish Database. *BMC Genomics* (2016) 17:368. doi: 10.1186/s12864-016-2709-z
42. Liu S, Song X, Chrunyk BA, Shanker S, Hoth LR, Marr ES, et al. Crystal Structures of Interleukin 17A and Its Complex With IL-17 Receptor A. *Nat Commun* (2013) 4:1888. doi: 10.1038/ncomms2880
43. Yang M, Wang Y, Wang X, Chen C, Zhou H. Characterization of Grass Carp (*Ctenopharyngodon Idellus*) Foxp1a/1b/2: Evidence for Their Involvement in the Activation of Peripheral Blood Lymphocyte Subpopulations. *Fish Shellfish Immunol* (2010) 28:289–95. doi: 10.1016/j.fsi.2009.11.007
44. Iwakura Y, Ishigame H, Saijo S, Nakae S. Functional Specialization of Interleukin-17 Family Members. *Immunity* (2011) 34:149–62. doi: 10.1016/j.immuni.2011.02.012
45. Takahashi N, Vanlaere I, de Rycke R, Cauwels A, Joosten LA, Lubberts E, et al. IL-17 Produced by Paneth Cells Drives TNF-Induced Shock. *J Exp Med* (2008) 205:1755–61. doi: 10.1084/jem.20080588
46. Salinas I. The Mucosal Immune System of Teleost Fish. *Biology (Basel)* (2015) 4:525–39. doi: 10.3390/biology4030525
47. Kolls JK, Linden A. Interleukin-17 Family Members and Inflammation. *Immunity* (2004) 21:467–76. doi: 10.1016/j.immuni.2004.08.018
48. Dinarello CA. Overview of the IL-1 Family in Innate Inflammation and Acquired Immunity. *Immunol Rev* (2018) 281:8–27. doi: 10.1111/imr.12621
49. Dostert C, Grusdat M, Letellier E, Brenner D. The TNF Family of Ligands and Receptors: Communication Modules in the Immune System and Beyond. *Physiol Rev* (2019) 99:115–60. doi: 10.1152/physrev.00045.2017
50. Jones SA, Jenkins BJ. Recent Insights Into Targeting the IL-6 Cytokine Family in Inflammatory Diseases and Cancer. *Nat Rev Immunol* (2018) 18:773–89. doi: 10.1038/s41577-018-0066-7
51. Hartupee J, Liu C, Novotny M, Li X, Hamilton T. IL-17 Enhances Chemokine Gene Expression Through mRNA Stabilization. *J Immunol* (2007) 179:4135–41. doi: 10.4049/jimmunol.179.6.4135
52. Krause A, Sillard R, Kleemeier B, Klüver E, Maronde E, Conejo-García JR, et al. Isolation and Biochemical Characterization of LEAP-2, a Novel Blood Peptide Expressed in the Liver. *Protein Sci* (2003) 12:143–52. doi: 10.1110/ps.0213603
53. Howard A, Townes C, Milona P, Nile CJ, Michailidis G, Hall J. Expression and Functional Analyses of Liver Expressed Antimicrobial Peptide-2 (LEAP-2) Variant Forms in Human Tissues. *Cell Immunol* (2010) 261:128–33. doi: 10.1016/j.cellimm.2009.11.010

Conflict of Interest: The authors declare that the research was conducted in the absence of any commercial or financial relationships that could be construed as a potential conflict of interest.

The reviewer (ZL) has declared an institutional affiliation, with no other collaboration, with some of the authors (XZ, G-RZ, WJ, X-FM, K-JW) to the handling editor during the time of review.

Copyright © 2021 Zhou, Zhang, Ji, Shi, Ma, Luo and Wei. This is an open-access article distributed under the terms of the Creative Commons Attribution License (CC BY). The use, distribution or reproduction in other forums is permitted, provided the original author(s) and the copyright owner(s) are credited and that the original publication in this journal is cited, in accordance with accepted academic practice. No use, distribution or reproduction is permitted which does not comply with these terms.

Advantages of publishing in Frontiers

OPEN ACCESS
Articles are free to read for greatest visibility and readership

FAST PUBLICATION
Around 90 days from submission to decision

HIGH QUALITY PEER-REVIEW
Rigorous, collaborative, and constructive peer-review

TRANSPARENT PEER-REVIEW
Editors and reviewers acknowledged by name on published articles

Frontiers
Avenue du Tribunal-Fédéral 34
1005 Lausanne | Switzerland

Visit us: www.frontiersin.org
Contact us: frontiersin.org/about/contact

REPRODUCIBILITY OF RESEARCH
Support open data and methods to enhance research reproducibility

DIGITAL PUBLISHING
Articles designed for optimal readership across devices

FOLLOW US
@frontiersin

IMPACT METRICS
Advanced article metrics track visibility across digital media

EXTENSIVE PROMOTION
Marketing and promotion of impactful research

LOOP RESEARCH NETWORK
Our network increases your article's readership